Accessing chemically robust amide cages via the Pinnick oxidation

Avinash Shashidhar Bhat

Dissertation

Heidelberg

2021

Inaugural-Dissertation

zur Erlangung der Doktorwürde der

Naturwissenschaftlichen-Mathematischen Gesamtfakultät

der Ruprecht-Karls-Universität Heidelberg

vorgelegt von

Avinash Shashidhar Bhat, M.Sc.

aus Mysore, Indien

April 2021

Tag der mündlichen Prüfung: 28.05.2021

Accessing chemically robust amide cages via the Pinnick oxidation

Gutachter: Prof. Dr. Michael Mastalerz

Jun.-Prof. Dr. Franziska Thomas

Eidesstattliche Versicherung gemäß § 8 der Promotionsordnung der Naturwissenschaftlich-Mathematischen Gesamtfakultät der Universität Heidelberg

1. Bei der eingereichten Dissertation zu dem Thema „Accessing chemically robust amide cages via the Pinnick oxidation" handelt es sich um meine eigenständig erbrachte Leistung.

2. Ich habe nur die angegebenen Quellen und Hilfsmittel benutzt und mich keiner unzulässigen Hilfe Dritter bedient. Insbesondere habe ich wörtlich oder sinngemäß aus anderen Werken übernommene Inhalte als solche kenntlich gemacht.

3. Die Arbeit oder Teile davon habe ich bislang nicht an einer Hochschule des In- oder Auslands als Bestandteil einer Prüfungs- oder Qualifikationsleistung vorgelegt.

4. Die Richtigkeit der vorstehenden Erklärungen bestätige ich.

5. Die Bedeutung der eidesstattlichen Versicherung und die strafrechtlichen Folgen einer unrichtigen oder unvollständigen eidesstattlichen Versicherung sind mir bekannt.

Ich versichere an Eides statt, dass ich nach bestem Wissen die reine Wahrheit erklärt und nichts verschwiegen habe.

_____   _____

Ort, Datum   Unterschrift

Die vorliegende Arbeit wurde von März 2017 bis Dezember 2020 im Arbeitskreis von Prof. Dr. Michael Mastalerz an der Ruprecht-Karls-Universität zu Heidelberg angefertigt.

Teile dieser Arbeit wurden bereits veröffentlicht:

Avinash Shashidhar Bhat, Sven M. Elbert, Wen-Shan Zhang, Frank Rominger, Michael Dieckmann, Rasmus R. Schröder, Michael Mastalerz, *Angew. Chem. Int. Ed.* **2019**, 58, 8819-8823: "***Transformation of a [4+6] Salicylbisimine Cage to Chemically Robust Amide Cages***".

Poster:

Avinash S. Bhat, Sven M. Elbert, Wen-Shan Zhang, Frank Rominger, Michael Dieckmann, Rasmus R. Schröder, and Michael Mastalerz, *2nd International Symposium on Porous Organic Polymer* (POPs 2019), **09.09.2019 – 12.09.2019,** Heidelberg: "***Chemically Robust Amide Cages***".

Avinash S. Bhat, Sven M. Elbert, Wen-Shan Zhang, Frank Rominger, Michael Dieckmann, Rasmus R. Schröder, and Michael Mastalerz, *International Symposium on Confinement Controlled Chemistry*, **16.09.2019- 18.09.2019,** Bochum: "***Chemically Robust Amide Cages***".

Kurzzusammenfassung

Poröse organische Käfigmoleküle sind eine aufstrebende Klasse von funktionalen Materialien, die Kavitäten enthalten, die groß genug sind, um Gastmoleküle aufzunehmen. In den letzten Jahren hat die Verwendung der dynamischen Bildung kovalenter Bindungen zu einer Vielzahl von Käfigverbindungen mit unterschiedlichen Geometrien und Größen geführt. Eine solche häufig verwendete Reaktion ist die Iminkondensation, die Käfigverbindungen in hervorragenden Ausbeuten bildet, jedoch mit ihrer chemischen Labilität einen großen Nachteil aufweist.

Diese Arbeit befasst sich mit der Umwandlung von Iminkäfigen in chemisch robuste Amidkäfige mithilfe der Pinnick-Oxidation. In der Vergangenheit wurden Amidkäfige durch einfaches Kuppeln von Säurechloriden und Aminen synthetisiert. Dieses Verfahren ist jedoch für die Bildung größere Käfigmoleküle mit komplexen Geometrien nicht anwendbar. Unter Verwendung der Pinnick-Oxidation wurde ein Triptycen-basierter [4+6]-Salicyldiamid-Käfig synthetisiert, der nicht über eine irreversible Amidkupplung erzeugt werden konnte. Der neue Amidkäfig zeigte eine ausgezeichnete chemische und thermische Stabilität sowie eine spezifische Oberfläche von $S_A(\text{BET}) = 370$ m²/g. Die Vielseitigkeit dieser Methode zur Gewinnung von Amidkäfigen wurde durch die Durchführung einer Studie mittels Variation verschiedener Parameter wie elektronischen Effekten, Löslichkeit, Hydrolysestabilität des Iminkäfigs und sterischen Effekten nachgewiesen. Darüber hinaus war es möglich, die Pinnick-Oxidation erfolgreich auf Iminkäfige anzuwenden, die durch Einsatz von aromatischen Aminen sowie aliphatischen Aminen hergestellt wurden.

Zusätzlich bot die verbesserte chemische Stabilität der Amidkäfige eine einzigartige Gelegenheit, die Käfigverbindungen durch bekannte Reaktionen wie Bromierung, Nitrierung, Suzuki-Kupplung und CH-aktivierte Borylierung zu funktionalisieren. Folglich konnten funktionelle Amidkäfige erhalten werden, die ein großes Potenzial bei der Aufnahme kleiner Moleküle sowie beim Aufbau hierarchischer Strukturen (wie COFs oder Polymere) bieten.
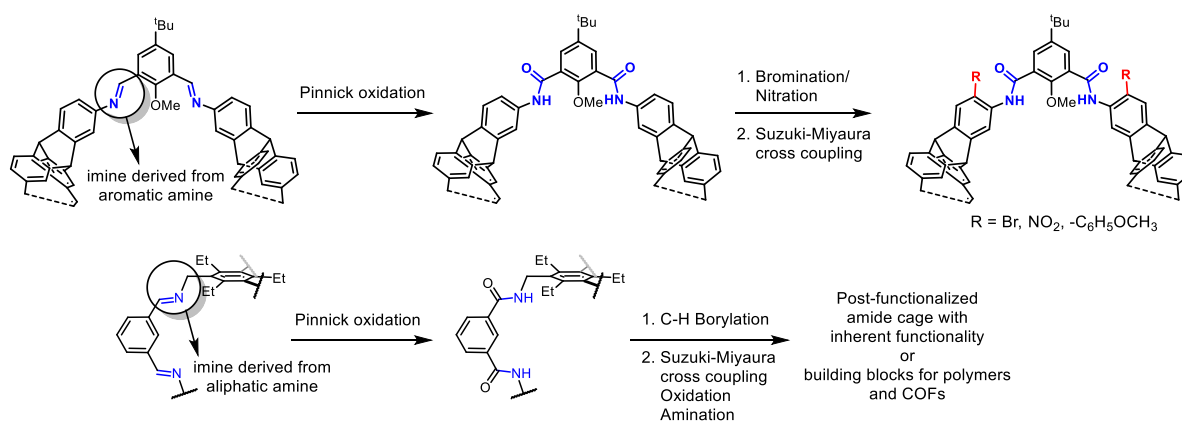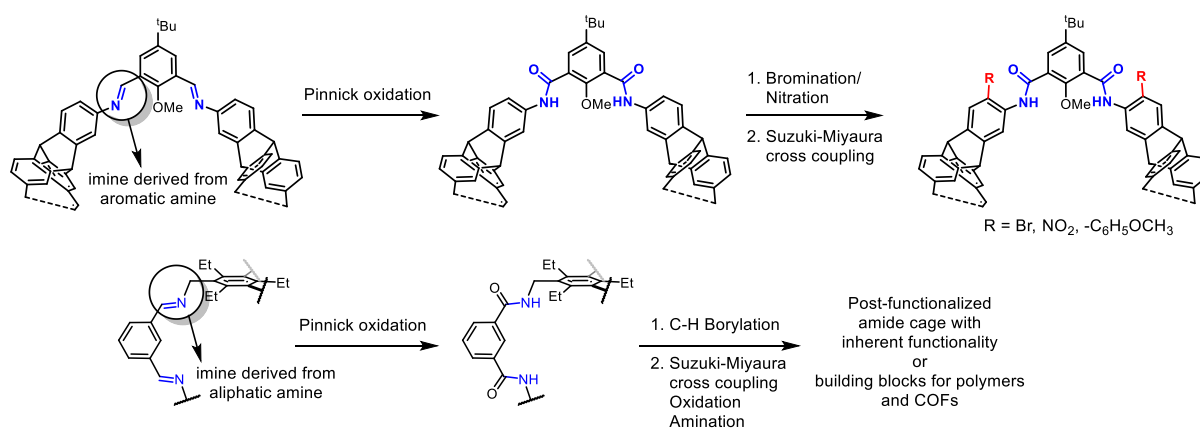
Abstract

Porous organic cages (POC) are an emerging class of functional materials containing cavities large enough to host guest molecules. In recent years, the use of dynamic covalent bond formation has resulted in a vast array of cage compounds with different geometries and sizes. One such commonly used reaction is the imine condensation, which forms cage compounds in excellent yields but has a major disadvantage due its chemically labile nature.

This thesis deals with the transformation of imine cages to chemically robust amide cages via the Pinnick oxidation. Historically, amide cages have been synthesized by simply coupling acid chlorides and amines, however, this method is ineffective in accessing larger cage molecules with complex geometries. Using the Pinnick oxidation, a triptycene-based [4+6] salicylbisamide cage was synthesized, which could not be generated via an irreversible amide bond forming reaction. The novel amide cage exhibited excellent chemical and thermal stability, as well as a specific surface area of S_A (BET) $= 370$ m^2/g. The versatility of this method to obtain amide cages was established by carrying out a 'scope and limitation' study by varying parameters such as electronic effects, solubility, hydrolytic stability of the imine cage, and steric effects. Moreover, it was possible to successfully apply the Pinnick oxidation on imine cages derived from aromatic amines as well as aliphatic amines.

Furthermore, the enhanced chemical stability of the amide cages offered a unique opportunity to post-functionalize the cage compounds by well-known reactions such as bromination, nitration, Suzuki coupling, C-H activated borylation, etc. Consequently, functional amide cages could be obtained which have great potential in the encapsulation of small molecules as well as construction of hierarchical structures (such as COFs or polymers).

Table of Contents

I. Introduction

1. Organic cage compounds

IUPAC defines 'cage compounds' as "polycyclic molecules that have the shape of a cage".[1] While this may include platonic bodies which have a 'cage-like' structure,[2] or 'coordination cages' which have metal atoms in the cage backbone,[3] this thesis focuses on 'organic cage compounds'. Organic cage compounds are comprised of fundamental units having features typical of organic molecules, but with a three-dimensional structure exhibiting a cavity large enough to accommodate molecular guests.[4] The synthesis of "two-dimensional" crown ethers reported by Charles Pederson[5], was extended to a "three-dimensional" cryptand by Jean-Marie Lehn which was probably the first reported synthesis of an 'organic cage compound'.[6] Taking inspiration from this work, Donald Cram went on to synthesize carcerands in 1985 (in Latin: *carcer* ; in English: prison) which were large molecular structures with a cavity capable of trapping guest molecules (see Figure 1).[7] This series of advances in the synthesis of 'cage-like' molecules to encapsulate guests resulted in the three pioneers (Pedersen, Lehn and Cram) to receive the Nobel Prize in Chemistry in 1987.

18-Crown-6
(Charles Pedersen)

[2.2.2] Cryptand
(Jean-Marie Lehn)

Solvent molecules

Carcerand
(Donald Cram)
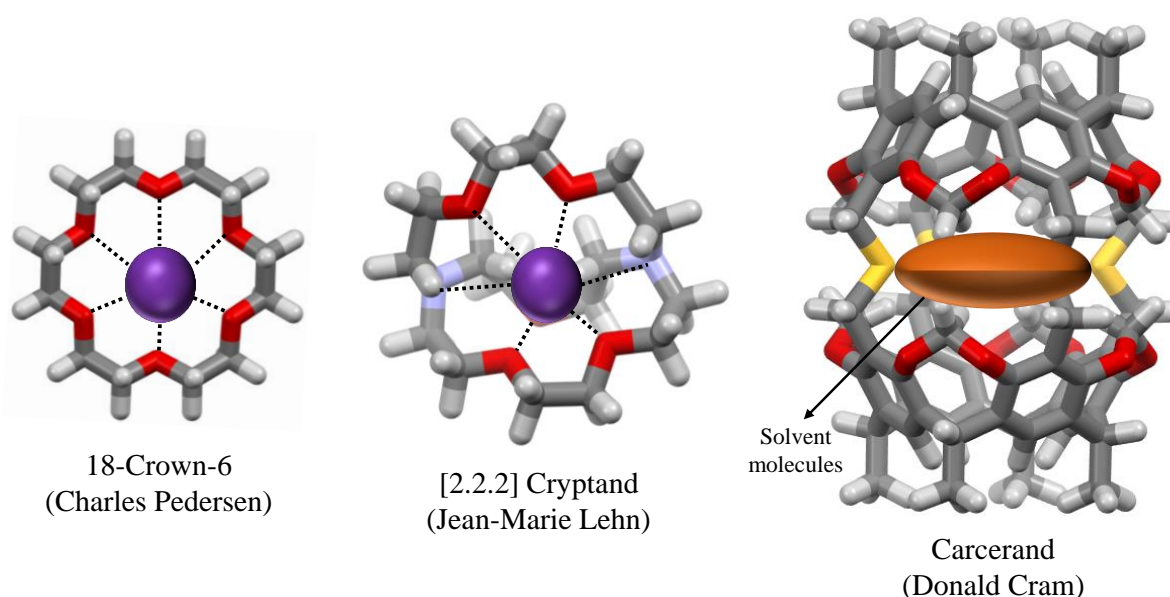
Figure 1. Structures of (from left) 18-crown-6 (by Charles Pederson),[5] cryptand (by Jean-Marie Lehn)[6] and carcerand (by Donald Cram).[7a] Purple spheres indicate encapsulated potassium cation. Grey = carbon, white = hydrogen, blue = nitrogen, red = oxygen and yellow = sulphur.

The field of 'organic cage compounds' was advanced by the teams led by Vögtle,[8] Moore[9] and Sessler,[10] among several others. However, the synthesis of the reported cage compounds involved long and tedious synthetic pathways, usually resulting in low overall yields. Vögtle

et al. showed that cage **3** formed in higher yields (13%) using a pre-organized building block **2** compared to reacting the monomeric units directly (1.5%).[11] As described in the same report, cage **4** was also observed to bind to ferric ions stronger than ethylenediaminetetraacetic acid (EDTA). Employing a ferric ion as a template to form a similar cage compound **9**, Raymond et al. achieved a remarkable yield of 70% for the final cyclization step (as shown in Scheme 1).[12] In contrast, the absence of a template ion resulted in a mere yield of 3.5% for the cyclization step. Although pre-organization and template effect provides a solution to the low yield, access to a diverse array of cage compounds of larger sizes and complex geometries was still a challenge.
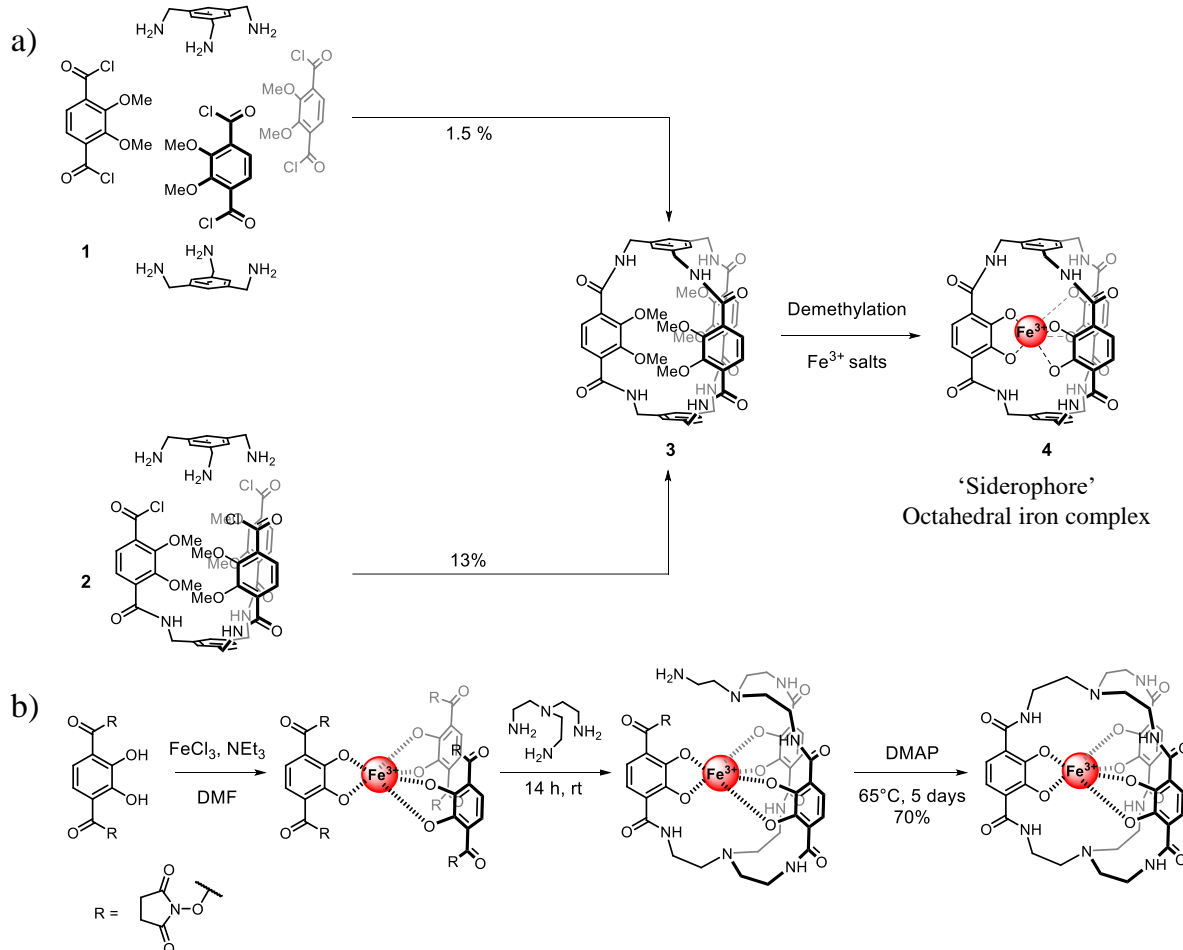
Scheme 1. a) Synthesis of cage **3** with and without a pre-organized building block, followed by modification to cage **4** to bind ferric ions;[11] b) Use of ferric ions as templates for the synthesis of cage **9**.[12]

In 1987, Lehn and co-workers first used the reversible imine condensation reaction to synthesize a series of TREN-based cage molecules with different aryl moieties as spacers, achieving yields of up to 80%.[13] Later in 1991, Donald Cram used the same strategy to synthesize larger cage structures, e.g. hemicarcerands.[14] This was followed by Lehn proposing the idea of dynamic covalent chemistry (DCC) for the synthesis of organic cage compounds by

utilizing the 'self-healing' process of reversible reactions.[15] The underlying concept is the making and breaking of imine bonds until the connections lead to a thermodynamically favourable product. The reaction outcome can be controlled by varying certain key parameters, such as; solvent polarity,[16] temperature,[17] properties of the building blocks,[18] and template effects[19].

In contrast to extended frameworks (e.g., covalent organic frameworks) which are also obtained by DCC,[20] solution-processibility is a key advantage offered by discrete cage compounds over the former. Although several reversible reactions exist which have been used in DCC, only a few have been made use of to prepare organic cage compounds; imine condensation,[21] boronic ester condensation,[22] alkyne metathesis[23] and disufide formation[24] (as shown below in Scheme 2). However, with the focus of this thesis being the synthesis of imine cages and subsequent transformation, the following sections will be focused on presenting a background only on organic cage compounds formed by imine condensation reaction and not the others.
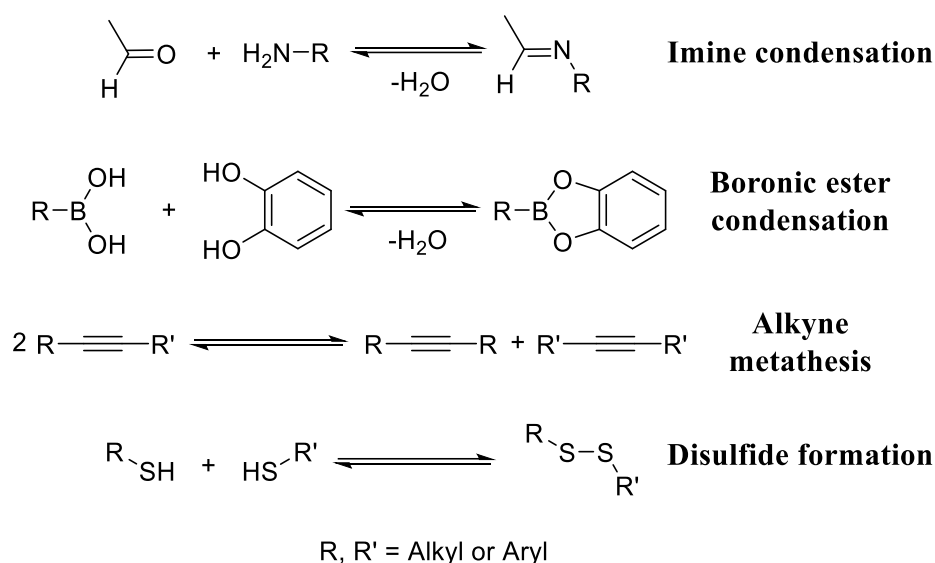
Scheme 2. Reversible reactions used to synthesize organic cage compounds.

1.1. Imine cage compounds

The field of imine organic cage compounds advanced greatly from a collaboration by Donald Cram and Fraser Stoddart in 1991, wherein a nearly-quantitative formation of a hemicarcerand was achieved by using catalytic amounts of TFA.[25] This was a big milestone because the dynamic nature of imine bonds was exploited not only to achieve quantitative yields but also to provide a novel mechanism for an inclusion-exclusion cycle of a trapped guest (ferrocene in this case). Eventually, a substantial expansion of the accessible shapes and sizes of the cage

structures was brought about for various applications like anion/cation binding,[26] molecular containers,[27] sensing[28] and gas adsorption[29]. The imine cage compounds that followed had geometries with trigonal symmetry,[26] cubic symmetry,[30] tetrahedral symmetry,[29a] etc., having cavities varying from 0.8 nm[26] to 3 nm[31] in size depending on the precursors (as shown in Figure 2). It is worth noting that the required properties of the building blocks for rational design of organic cage compound are far from being understood. While pure *in silico* methods have been unable to handle the complexity of these systems,[32] a deeper understanding of the geometrical and physicochemical requirements to effectively form cage molecules is being pursued by several research teams.[33]
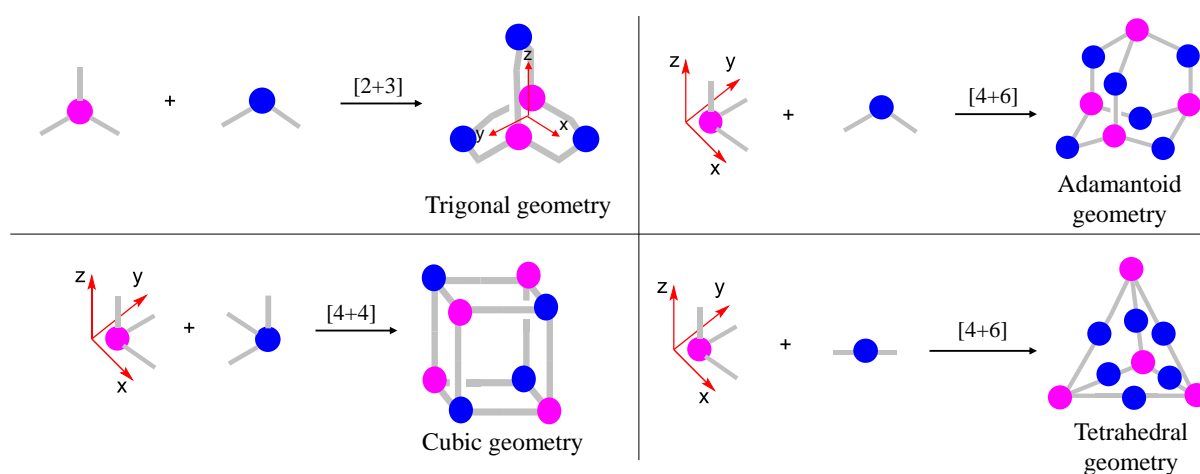
Figure 2. Examples of generating cage compounds of varying geometry.

A commonly used precursor is the tripodal 1,3,5-trisubstituted benzene (**10a** and **10b** from Scheme 3) exhibiting pre-organization, where the R-groups are positioned such that they are located in a plane opposite to the amine/aldehyde groups with respect to the aromatic system. Cage **11** was synthesized by Mateus et al. in 2009 with an excellent yield of 90% and its reduced form (amine cage) was used as a selective receptor for tetrahedral dianions.[26] Synthesis of imine cages **14** and **15** was achieved in moderate yields by the Gawronski group in 2008 and Cooper group in 2009 respectively,[29a, 34] but a scalable synthesis was later optimized, making them the first imine cage compounds to be commercially available.[35] These cages (named CC3) and their analogues (and derivatives) have been shown to have several interesting applications like selective uptake of gases[36] and chiral gas chromatography,[37]. Later in 2015, a large chemically stable porphyrin-based imine cage **12** with a rhombicuboctahedron structure was formed in quantitative yields, and was further shown to selectively adsorb CO_2 over CH_4 by Kim et al.[38] Another Archimedean solid, a

truncated tetrahedron, was generated by Mastalerz et al. in 2018, wherein imine cage **13** and a series of analogues with different side chains were obtained by a kinetically driven process.[39]
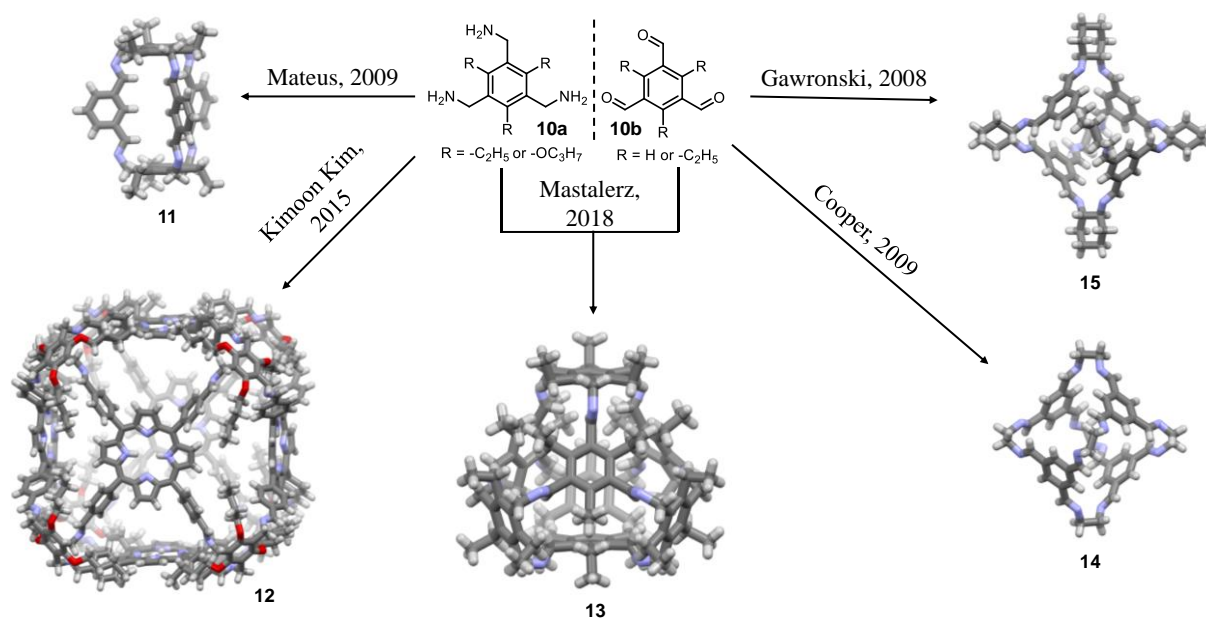
Scheme 3. SCXRD structures of imine cages reported by various groups starting from the 1,3,5-substituted tripodal precursors **10a** and **10b**: [2+3] imine cage **11** (CCDC 1827878),[26] the porphyrin-based cage **12** (CCDC 1405313),[38] [4+4] truncated tetrahedron cage **13** (CCDC 1588272)[39] and, the CC3 cages **14** (CCDC 707056)[29a] and **15** (CCDC 720851)[34]. The crystal structures were acquired from the CCDC database. Grey = carbon, white = hydrogen, blue = nitrogen and red = oxygen.

Mastalerz et al. synthesized a series of imine cages introducing a new C_3 symmetric triaminotriptycene **16** that is pre-organised to react along a single axis and generate a cage (as shown in Scheme 4).[40] When maintaining the same triamine, the outcome of the reaction and the geometry of the cage is determined by the specific choice of aldehyde co-reactant. In the case of dialdehyde **17** a [2+3] imine cage with trigonal geometry **18** is obtained, exhibiting exo-functionality due to the external phenolic groups.[41] Alternatively, dialdehyde **19** also provides an exo-functionalized cage compound but with an adamantoid T_d-symmetry **20**.[42] On the other hand, using dialdehyde **23** an imine cage with endo-functionality **24** could be achieved while retaining the adamantoid geometry.[40] This imine cage held the record for the highest specific surface area for imine cage compounds until it was surpassed by a resorcin[4]arene-based cage compound in 2020.[43] Moreover, the hydrogen bond donors present inside the large cavity of the cage compound makes it possible to selectively bind γ-butyrolactone.[44] Hence, this thesis encompasses further work on this imine cage compound, discussed in a later chapter. Finally, combining the C_3-symmetric triamine **21** with another C_3-symmetric building block **16** generated a cubic cage **22**.[30] These large complex cage structures were not only isolated in good yields but also showed permanent shape-persistence, due to

rigidity of the precursors and also the stabilizing effect of the hydrogen bonding between the hydroxy groups and the neighbouring imine bonds.[4]
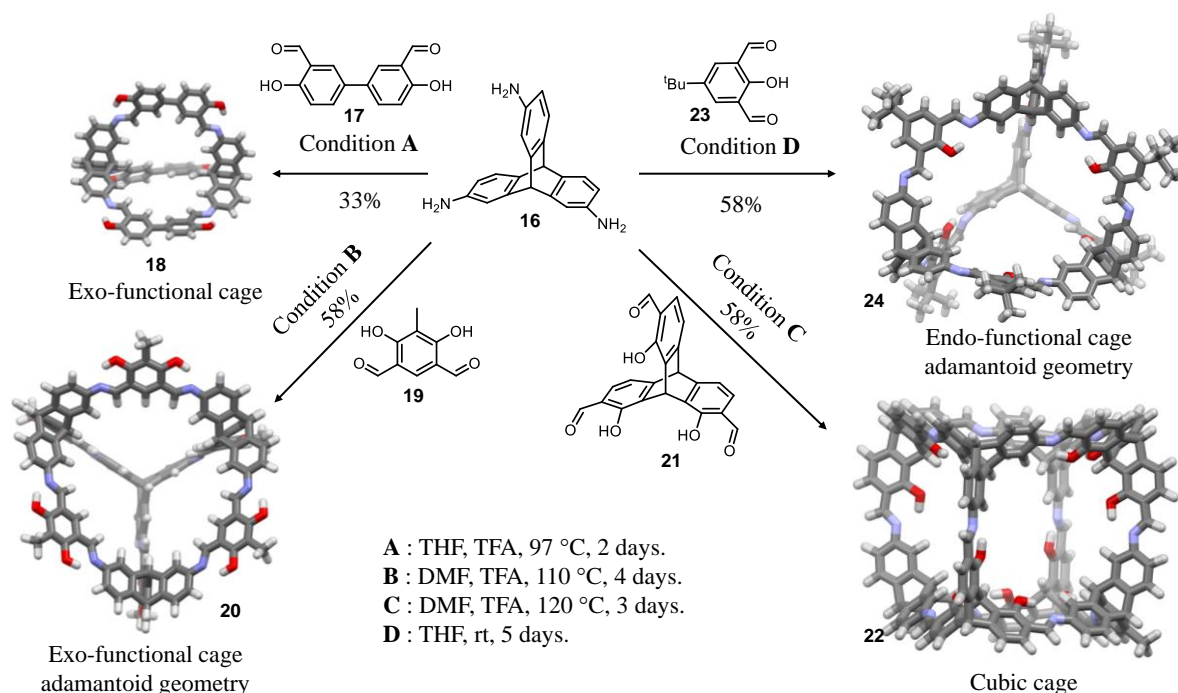
Scheme 4. Imine cages reported by the Mastalerz group: SCXRD structures of **18** (CCDC 860485)[41] and **24** (CCDC 789520)[43b] and, MM2 optimized structures of imine cages **20**[42] and **22**[30], starting from the C_3 symmetric triaminotriptycene **16**. The crystal structures were acquired from the CCDC database. Grey = carbon, white = hydrogen, blue = nitrogen and red = oxygen.

By carefully choosing the geometry and chemical properties of the building blocks, a diverse range of cage structures can be acquired, hence showing the potential of using DCC for the synthesis of organic cage compounds.

1.2. Transformation of imine cage compounds to more chemically stable structures

The use of DCC to obtain cage compound has been both a bane and a boon. While this method allows for the facile synthesis of cage compounds in excellent yields, the resulting cage molecules contain chemically labile groups which are highly susceptible to decomposition. This has driven researchers to pursue the transformation of these feasibly accessible dynamic cages into chemically robust systems that would otherwise be challenging to produce directly (as discussed previously).

Imines are rich in chemistry and the reduction of imine bonds to amine bonds is probably the simplest transformation strategy to obtain chemically stable cage compounds. While there exist some applications of such amine bond-based cage compounds in solution,[26, 45] it has been found that the cage compound loses its shape-persistence in solid state.[43b] The greater degree

of flexibility inherent to an sp^3 hybridised amine in comparison to its sp^2 hybridised imine leads to a collapse of the cage structure and a loss of inherent porosity. A noteworthy step forward was reported by Cooper et al. with the synthesis of a dodecaamide cage **26**. Although a flexible sp^3-hybridised amine was still present (in **26**), microporous dendrimers could be generated by choosing the right R-groups (Scheme 5a).[46] Furthermore, in 2019, Mastalerz et al. reported by transformation of an imine cage **11** (Note: only applicable to imines derived from aliphatic amines) into a fully hydrocarbon cage **28**, which offers chemical stability but not shape-persistence due to flexible methylene groups (Scheme 5b).[47]
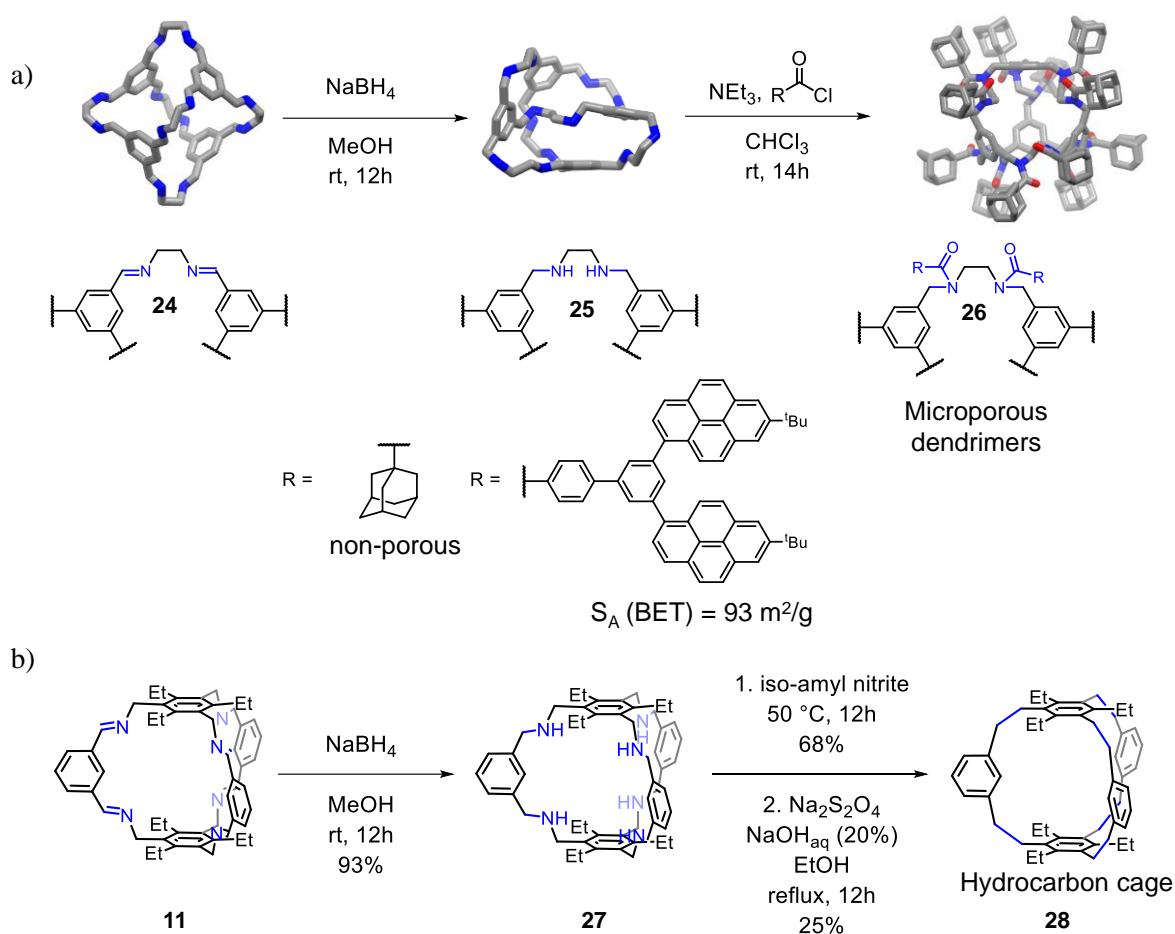
Scheme 5. a) Modification of a collapsed amine cage to a dodecaamide cage **26** containing appropriate R groups generating microporous dendrimers. Crystal structures of **24** (CCDC 707056) and **26** (CCDC 955294)[46] were obtained from the CCDC database; b) Conversion of a [2+3] imine cage **11** to a fully hydrocarbon cage **28** over three steps.[47]

On the other hand, two novel approaches were presented to solve the problem of the loss of shape-persistence: 1. Subsequent reaction after imine reduction to recover the shape persistence; 2. Direct transformation of the imine bond to alternative structurally and chemically stable groups (as shown in Scheme 7b). The first approach was realized by Cooper group, wherein an amine cage **30** with a collapsed structure in solid state, was seen to regain

porosity by a "tying" step. Using paraformaldehyde, an aminal-based cage compound **31** could be formed which exhibited chemical stability in a pH range of 2-12.[48] The "tying" step requires the amine groups to be in the 1,2-arrangement to form the 5-membered aminal ring (as seen in Scheme 6).

29
Imine cage – porous

30
Amine – collapsed
non-porous

31
Aminal – porous
stable from pH 2-12
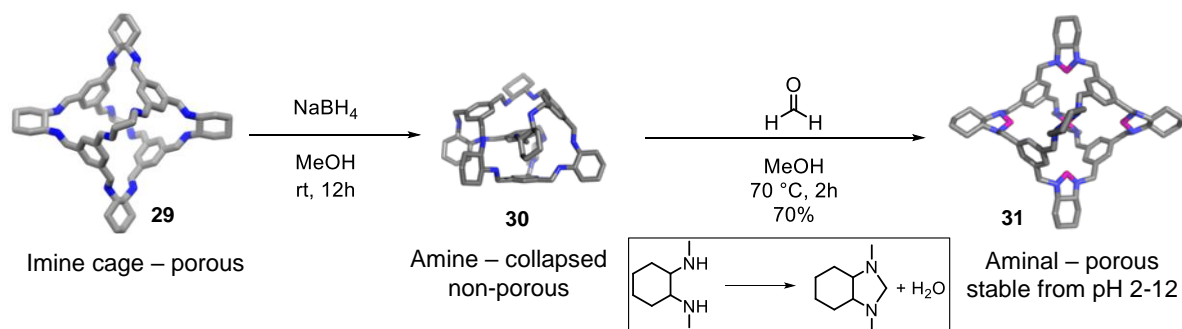
Scheme 6. Synthesis of a chemically and structurally stable organic cage via the "tying" of the flexible amine bonds to form a rigid aminal-cage **31**.[48]

Alternatively, Mastalerz and co-workers, reported another method by forming a carbamate-based cage, where a similar "tying" step is used as above, however at the exterior of the cage molecule (compared to the aminal formation at the interior cavity of the cage in cage **31**). By making use of an -OH group in the *ortho*-position to the imine/amine bond (as shown in Scheme 7a), the structure flexible amine-based cage could be converted to a chemically and structurally stable carbamate cage **33**.[49] The resulting cage **33** not only exhibited exceptional chemical stability over a pH range of -1 to 14 but also shape-persistence in solid state, with a specific surface area of S_A (BET) = 113 m^2/g. The second approach was carried out by directly transforming the imine bonds (in cage **24**) to a quinoline ring (in cage **34**) via the Povarov reaction (Scheme 7b).[50] The quinoline-based cage **34** displayed an even greater chemical stability showing no decomposition even in concentrated sulphuric acid, as well as a higher surface area of S_A (BET) = 698 m^2/g.

Each approach requires the presence of specific functionality apart from the imine bond, whether it be an -OH group in the ortho-position or an exclusively aromatic imine derivative. It would however be very preferable to utilize a method in which imine cages can be directly converted to a chemically and structurally stable cage not requiring additional functional groups and that may be applied on aromatic and aliphatic imines.
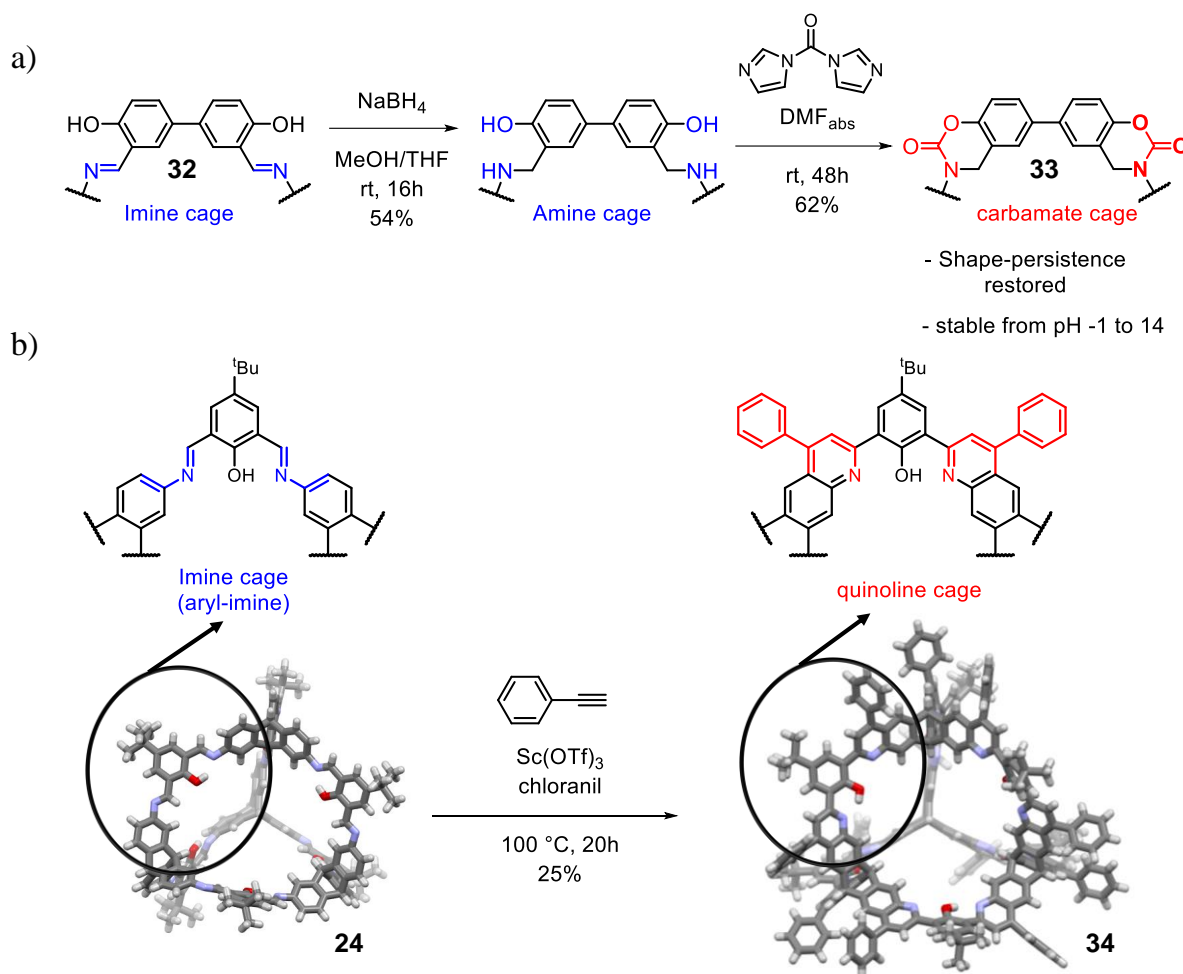
Scheme 7. a) Conversion of the [2+3] imine cage **32** to an exceptionally stable carbamate cage **33** over two steps;[49] b) Transformation of an imine cage **34** (CCDC 789520) to a quinoline-cage **35** (CCDC 2002767) via the Povarov reaction.[50] The crystal structures were acquired from the CCDC database.

With this in mind, attempts have been made to synthesis highly stable amide cages, which are the focus of this thesis and shall be discussed in more detail in a following section.
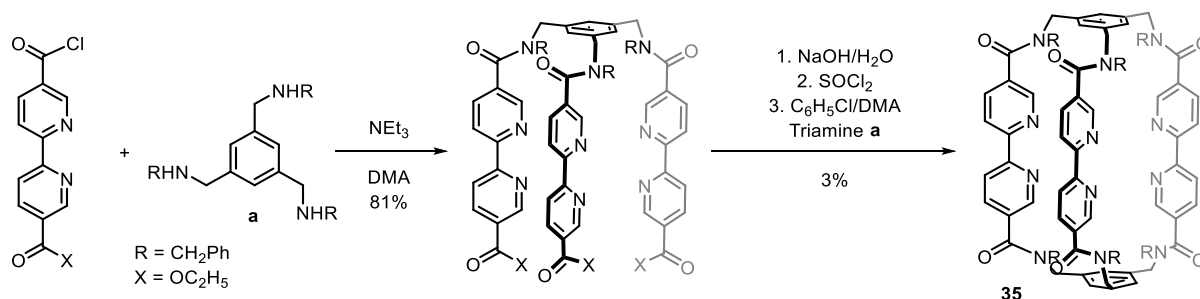
2. Amide cages

2.1. Synthesis by irreversible amide coupling reaction

Amides are abundant in the world around us, as peptides, synthetic polymers such as Nylon and Kevlar, and in small molecule agrochemicals and pharmaceuticals, indeed, over 54% of marketed active pharmaceutical ingredients contain one or more amide bond.[51] A useful characteristic of amide bonds is the high carbon-nitrogen bond strength of up to 90-100 kcal/mol.[52] Unfortunately, this high bond strength doesn't facilitate an equilibrating "make and break" process which has hindered its use in dynamic covalent chemistry. Although there exist a few examples of transamidation reactions, most of these methods are not reversible.[53] One exception is the use of Zirconium and Hafnium-amido complexes as catalysts for

equilibrium controlled transamidation reactions, but the use of such expensive metals renders the method unsustainable on a larger scale.[54] Dynamic transamidation was also achieved in peptide chemistry, where enzymes initiate the transamidation reaction or thiol-tethered amides were used to create a dynamic equilibrium,[55] both of which could only be applied in aqueous media.

Therefore, amide cages or macrocycles have always been prepared via an irreversible amide bond forming reaction, the first of which was reported by Vögtle et al. in 1984 using high-dilution conditions (as shown previously in Scheme 1).[11] This was later expanded by incorporating bipyridyl-units as spacers which offers a larger cavity and forms an extremely stable octahedral complex with Fe (II).[56] This bipyridyl-based amide cage was promising in the complexation of Ru (II) to form photoluminescent cage-metal complexes;[57] however, the final cyclization step to afford the amide cage **35** was achieved in yield of just 3% (as shown in Scheme 8).[56a]

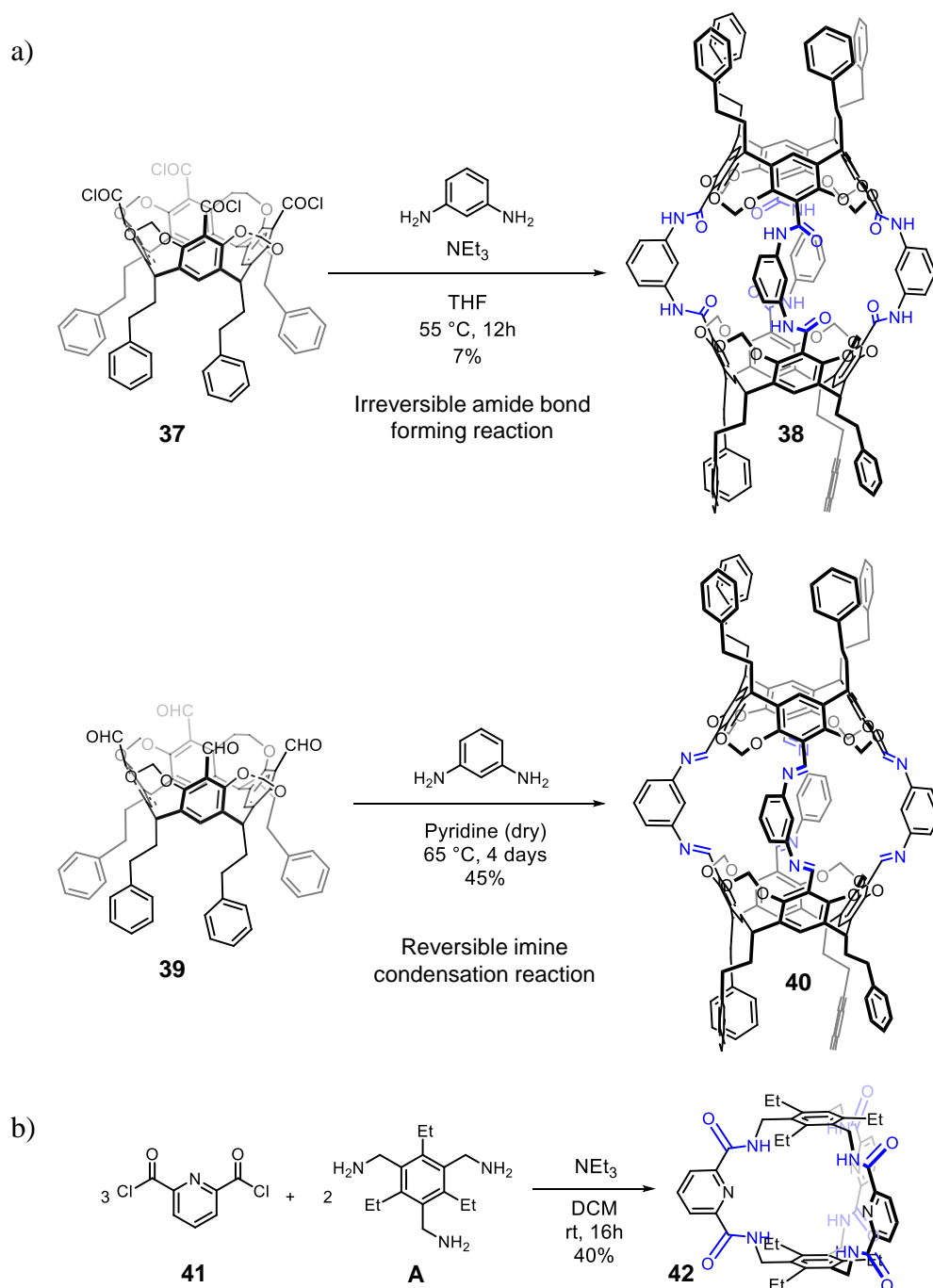**Scheme 8**. Synthesis of amide cage **35** containing bipyridyl units.[56a]

Between 1984 and 1991, several reports were published which used similar strategies to synthesize amide-based cage compounds.[58] Many of these publications exhibited the same issue, with the final cyclization step usually delivering low yields. An exception was the step-wise synthesis of a chiral spherical amide macrocycle **36**, where the final cyclization step gave a yield of 56%, and the overall yield of the final product from commercially available starting materials was 18% over 4 steps (as shown in Scheme 9).[59]
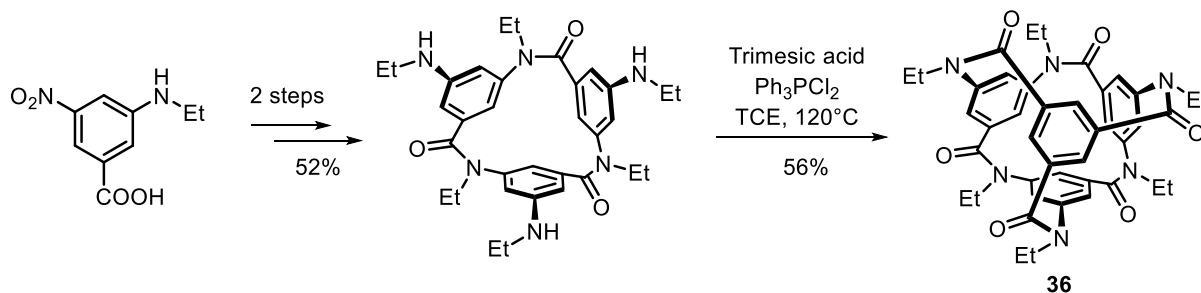
**Scheme 9**. Synthesis of a chiral spherical amide capsule.

One solution to this problem was the use of a template Fe(III) ion to drive the formation of the desired cage structure following which yields as high as 70% was achieved (as discussed previously in Scheme 1).[12, 56b] However, the use of template effect combined with multiple steps proved to be highly inefficient while synthesizing larger cage compounds, and hence could never be achieved.

In 1992, the group of Donald Cram synthesized an 'octaamide hemicarcerand' **38** which was large enough to host molecules such as 1,4-diacetoxybenzene.[60] Indeed, the synthesis of such large amide cages led to a significant decrease in yield (to 7%) because of the irreversible nature of the acid chloride mediated amide bond formation, and a greater number of amide bonds being formed. A stark difference could be seen during the synthesis of an imine hemicarcerand **40**, which was achieved in a much better yield of 45%, owing to the DCC of imine bonds (as shown in Scheme 10a).[14] Meanwhile, Anslyn and co-workers synthesized cage **42** from acid chloride **41** and triamine **A** in a surprisingly high yield of 40% (as shown in Scheme 10b). It was hypothesized that the pre-organization of the triamine precursor, and the hydrogen bonding interactions between the amide -NH groups and the nitrogen atom of the pyridine drive the formation of this cage structure.[61]

a)

37 → **38**

H2N—⟨⟩—NH2

NEt3

THF
55 °C, 12h
7%

Irreversible amide bond
forming reaction

39 → **40**

H2N—⟨⟩—NH2

Pyridine (dry)
65 °C, 4 days
45%

Reversible imine
condensation reaction

b)

41 + **A** → **42**

NEt3

DCM
rt, 16h
40%

Scheme 10. a) Synthesis of the octaamide hemicarerand **38** from acid chloride **37**, and the synthesis of an imine hemicarcerand **40** with aldehyde **39**;[14, 60] b) Synthesis of a C_3 symmetric amide cage **42** in a surprisingly high yield.[61]

Around the same time, the group of Anthony Davis reported a five-step synthesis of a tricyclic polyamide **43** (see Scheme 11) which enabled the extraction of carbohydrates into organic media.[28] Several variations of such a tricyclic polyamide were synthesized where the final cyclization step gave yields of around 55%.[62] Synthesis of these cages was realized in a step-wise manner over multiple steps leading to low overall yields.
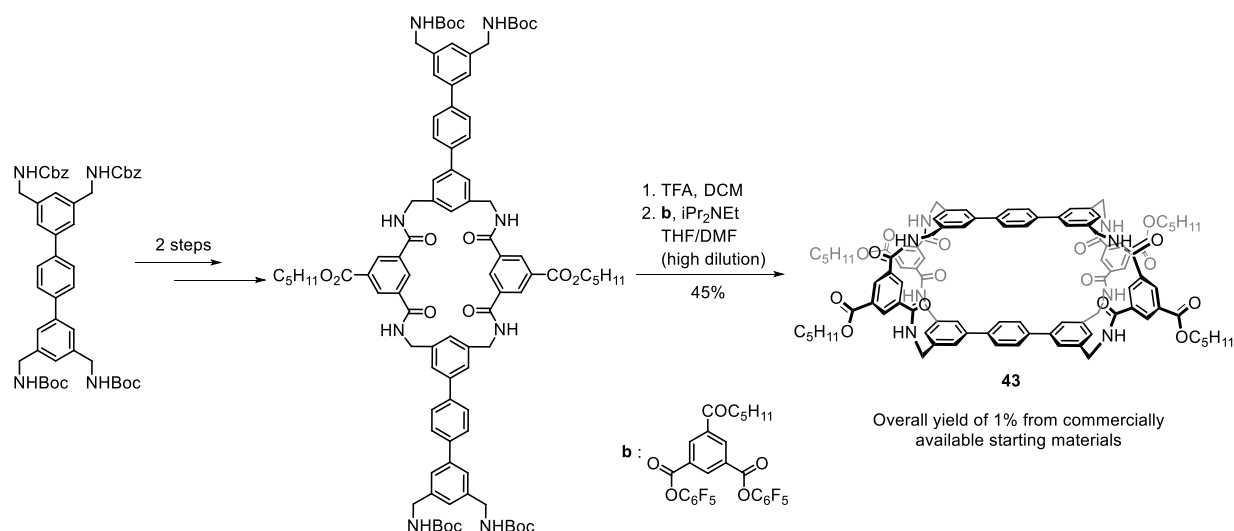
Scheme 11. Synthesis of a carbohydrate receptor **43** by Davis et al.[28]

Finally, a result that draws attention was published by Arndtsen and co-workers in 2020. The reversibility of the coupling of acid chlorides and imines to form α-chloroamides was demonstrated, and could indeed be exploited by DCC to generate amide-based cages/macrocycles (as shown in Scheme 12).[63] This method shows great promise as a competition to the idea behind the work encompassing this thesis; however, the scope of this method for constructing large and complex cages is yet to be investigated.
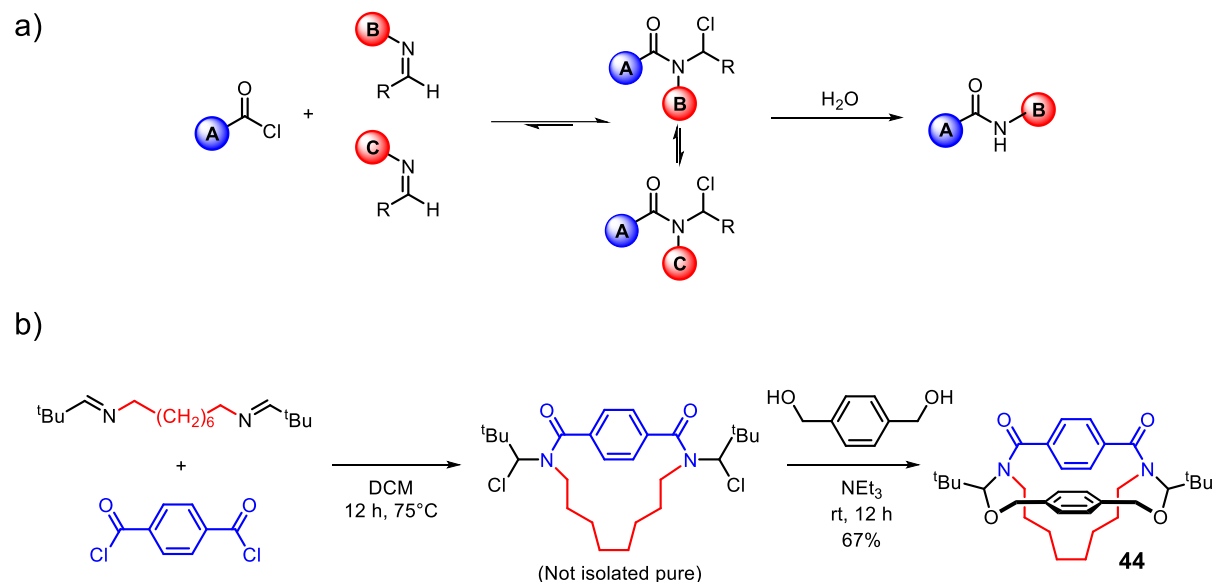

Scheme 12. Dynamic amide bond formation: a) General scheme for the dynamic formation of amides via a reversible coupling of acid chlorides and imines; b) Generation of a cage **44** using the approach shown in a).[63]

A few important points can be summarized from the above reports: 1. Synthesis of larger amide cages via an irreversible amide bond forming reaction results in low yields. 2. Pre-organization of the building blocks drives cage formation. 3. Templates can help to bring cage constituents

together in the correct alignment. However, the use of these methods to obtain larger amide cage compounds in good yields has not been realized to date.

2.2. Applications of amide-based macrocycles, cages, polymers and frameworks

Amide bonds, apart from their very good chemical stability, are capable of forming hydrogen bonding interactions and is a key aspect behind their applications. The efficiency of this interaction is modulated by the surrounding functional groups, for example electron donating substituents may increase electron density on the carbonyl oxygen and thus improve the inherent acceptor properties. Likewise, withdrawing substituents on the nitrogen increase the relative acidity of the N-H bond thus improve the hydrogen bond donor capability. The strength of the amide bonds and the complementary hydrogen bonds make them excellent candidates for use as mechanically strong materials such as Nylon and Kevlar (as mentioned previously). Apart from these well-known applications, amide-based compounds and materials have been reported to have several novel applications, a few of which are highlighted in Figure 3 and elaborated in the following subsections.
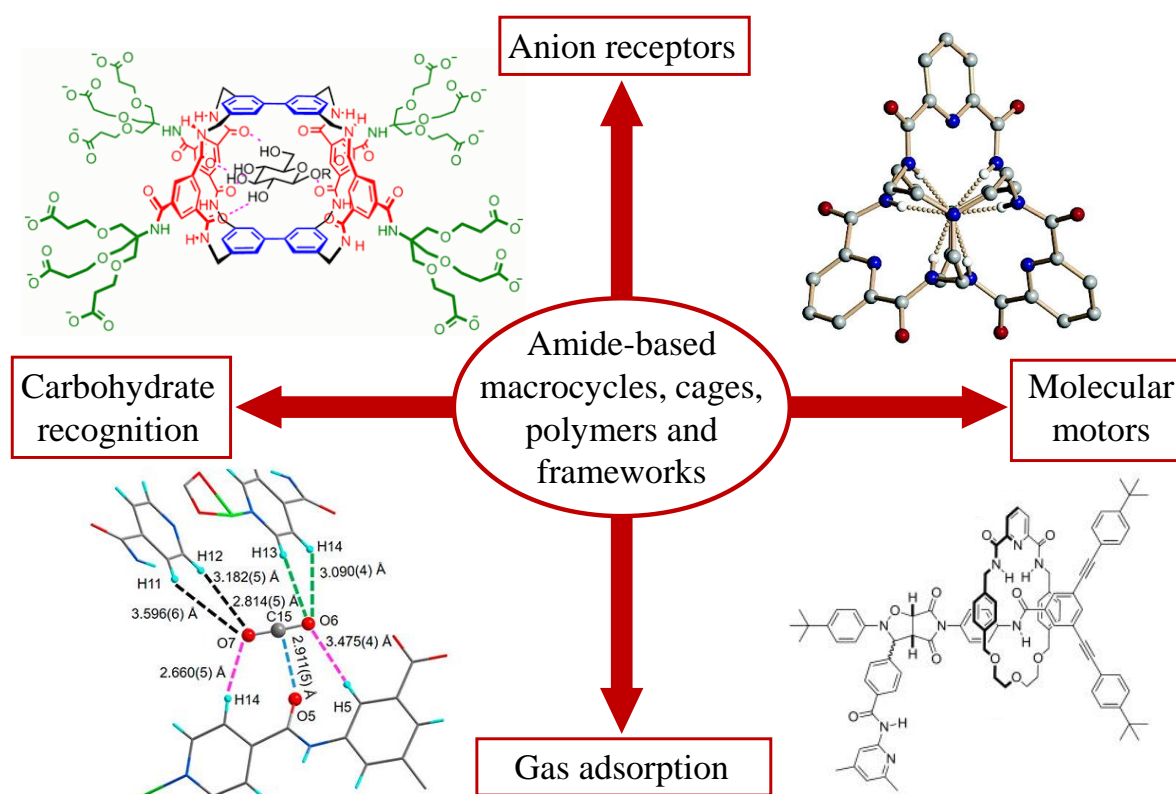
Figure 3. Schematic representation of the four main applications of amide-based macrocycles, cages, polymers and frameworks. The images on the top left,[64] top right,[65] bottom left[66] and bottom right[67] are used with permission, Copyright ACS Publications as well as licence under creative commons (CC BY 4.0).

2.2.1. Anion receptors

The design of anion receptors is particularly challenging because anions are inherently larger than the isoelectronic cations and therefore have a lower charge to size ratio.[68] This means that the electrostatic binding interactions would be less effective in comparison to the smaller cations. Furthermore, anions are often protonated in acidic media and vary widely in geometry and shape.[69] Although anion recognition occurs due to multiple non-covalent interaction such as anion-π,[70] C_{sp^2}-H-anion,[71] halogen bonding,[72] etc., amide macrocycles/cages are dominated by hydrogen bonding interactions.[73] One of the earliest examples of such amide-based receptors was reported by Pascal et al. where a cyclophane containing three amide bonds with the N-H groups directed towards the central cavity, having affinity to a fluoride anion.[74]
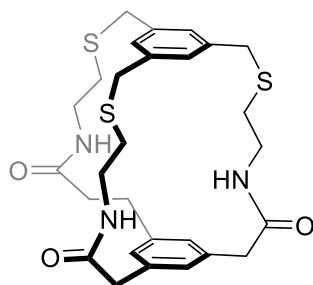

Scheme 13. Amide-based cyclophane synthesized by Pascal et al. in 1986.[74]

Therefore, an ideal anion receptor must work by a concerted action of multiple hydrogen bond donors in a specific pH range, and have a geometry such that the hydrogen bond donors are arranged very precisely within the guest molecule to achieve perfect complementarity to the guest.[73, 75] This requires the preparation of a vast array of amide-based macrocycles or cages having different geometries, electronic properties and solubilities. This synthetic challenge has been taken up by several pioneers in the field. Anslyn et al. first reported the synthesis of a C_3 symmetric receptor **43** (see Figure 4) which was able to sense nitrate anions and also signal the anion binding using colourimetric dyes.[76]
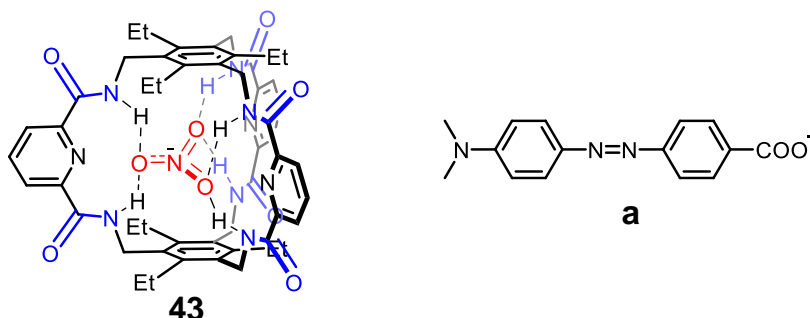

Figure 4. Recognition of a trigonal nitrate anion by a trigonal amide cage receptor **43**. Methyl red **a** used as a colourimetric dye to signal the binding of nitrate anions.[76]

In 2001, Kubik and co-workers designed the first cyclic peptide containing proline units for anion recognition.[77] Several others like Philip Gale[78] and Jonathan Sessler[79] made great advances in the synthesis of amide-based macrocycles for anion recognition. Bowman-James and co-workers synthesized an amide cryptand which selectively binds to fluoride anion, and further showed that cryptands with pyridine spacers show superior fluoride binding compared to the analogous isophthaloyl spacer (as shown in Figure 5).[80] This observation has been attributed to the preorganization effect of the pyridine N atoms on the nearby amide H atom.[73, 81] Although the thioamide showed a slightly lower affinity for a fluoride anion (compared to its amide analogues), it was shown that the selectivity for fluoride anion was more pronounced when screened against a series of other anions like $H_2PO_4^-$, HSO_4^-, Cl^-, Br^- and I^-.[82]

$K_a = 3.3 \times 10^4$ $K_a = 8.1 \times 10^5$ $K_a = 3.2 \times 10^4$
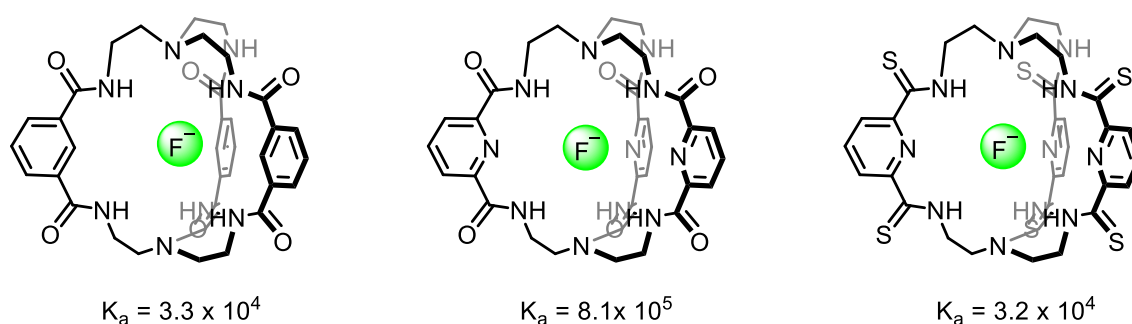
Figure 5. Fluoride anion binding with amides (containing different spacers) and a thioamide.[80]

Generation and stabilization of a soluble peroxide species has been a challenge and usually involved expensive transition metals.[83] Lopez et al. used a hexacarboxamide cryptand (similar to the one in Figure 5, on the left) to generate and stabilize a peroxide anion (O_2^{2-}) in solution utilizing the multiple hydrogen bond donors in the cryptand (Figure 6a).[84] Furthermore, Sessler and co-workers synthesized a pyrrol-based cage compound containing both hydrogen bond acceptors (imine bonds) and hydrogen bond donors (amide bonds) which showed a high affinity ($K_a = 10^6$ M^{-1}) for tetrahedral oxyanions such as $H_2PO_4^-$, HSO_4^- and SO_4^{2-} (Figure 6b).[85]
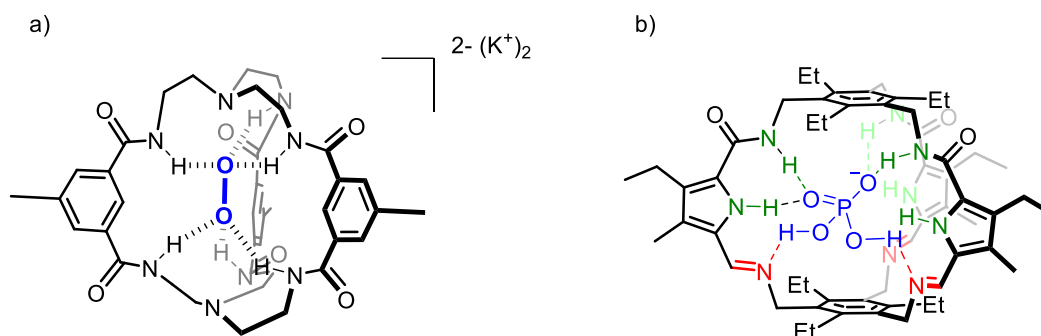

Figure 6. a) Stabilization of a peroxide anion using an amide cage;[84] b) recognition of a tetrahedral dihydrogen photosphate anion using a cage containing both hydrogen bond donors (in green) and acceptors (in red).[85]

Therefore, an improved synthesis protocol for such amide cages (or cryptands) followed by post-functionalization that allows for tuning of its properties would be highly beneficial.

2.3.2. Rotaxanes and molecular motors

Since the first amide-based hydrogen bond templated catenanes synthesized by Hunter and then Vögtle in 1992,[86] the field was led by David Leigh after the serendipitous synthesis of a benzylic amide macrocycle-based catenane.[87] However, the most influential advance in this field came with the synthesis of rotaxanes.[88] Building upon this work, a series of rotaxane switches were prepared that could be switched by light/heat.[89] One such example is shown below in Scheme 14, where the photo-isomerism of a C=C is utilized to shift the macrocycle from one end of the axle to another. This work on switches subsequently progressed to produce directional rotation in catenane systems to result in molecular motors. Since their first discovery the preparation and application of rotaxanes has grown expediently but lies outside the purview of this thesis; however, Evans et al. published an excellent review that covers the topic in detail.[67]
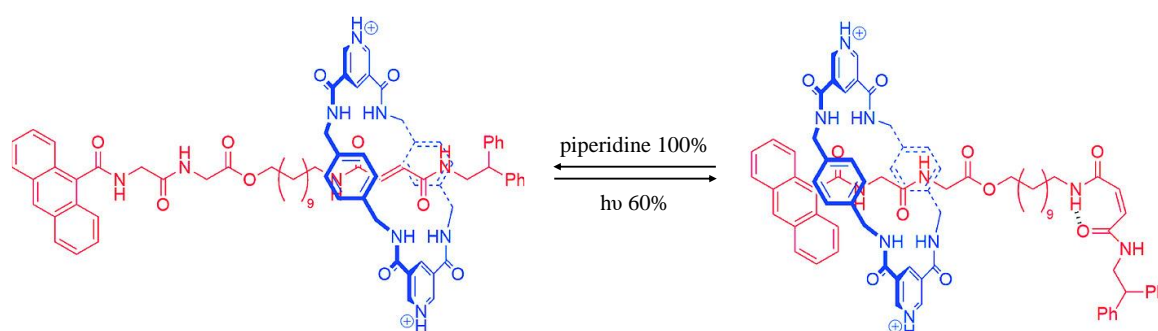

Scheme 14. An example of a Leigh-type light-operated molecular switch. The image is used with permission,[67] Wiley-VCH, licensed under creative commons (CC BY 4.0).

2.3.3. Carbohydrate recognition

The synthesis of amide-based cage molecules for carbohydrate recognition has advanced considerably by the likes of Davis and co-workers.[64] With so many polar groups, carbohydrate recognition in non-polar organic media is more feasible since the solvent molecules neither supress H-bonding nor are competing species for complexation. For carbohydrate recognition in water, the saccharide -OH group must replace water molecules to bind to the guest, which is enthalpically demanding. Moreover, there is also a synthetic challenge in designing such molecules to exhibit solubility in water, which was addressed by the Davis group by attaching tricarboxylate solubilizing groups to a "temple-type" receptor (as shown in Figure 7). These

cage compounds possess parallel aromatic surfaces as the roof/floor of the "temple" which are able to form CH-π interactions with the substrates (carbohydrates), [90] and these are held apart by rigid isophthalamide spacers that assists in binding to carbohydrates through hydrogen bonds. However, the affinity for glucose was found to be quite low (K_a = 9 M^{-1} in water) with receptor **46a**. Keeping the rotational flexibility of biphenyl units in hindsight, a more rigid aromatic moiety was chosen for the roof/floor of the receptors with pyrene units (cage **46b**), resulting in an enhanced binding of glucose (K_a = 120 M^{-1} in water).[91] Achieving water solubility with pyrene-containing receptors proved to be a challenge and hence required the use of longer solubilizing groups (as shown in Figure 7). Finally, with the chiral receptor **46c**, an even greater binding (K_a = 250 M^{-1} in water) could be achieved for glucose, while also offering enantioselectivity.[92] Lastly, it is worth mentioning that with receptor **46b**, a much higher affinity was observed with all-equatorial oligosaccharides such as cellotetraose (K_a = 12000 M^{-1}).[91]
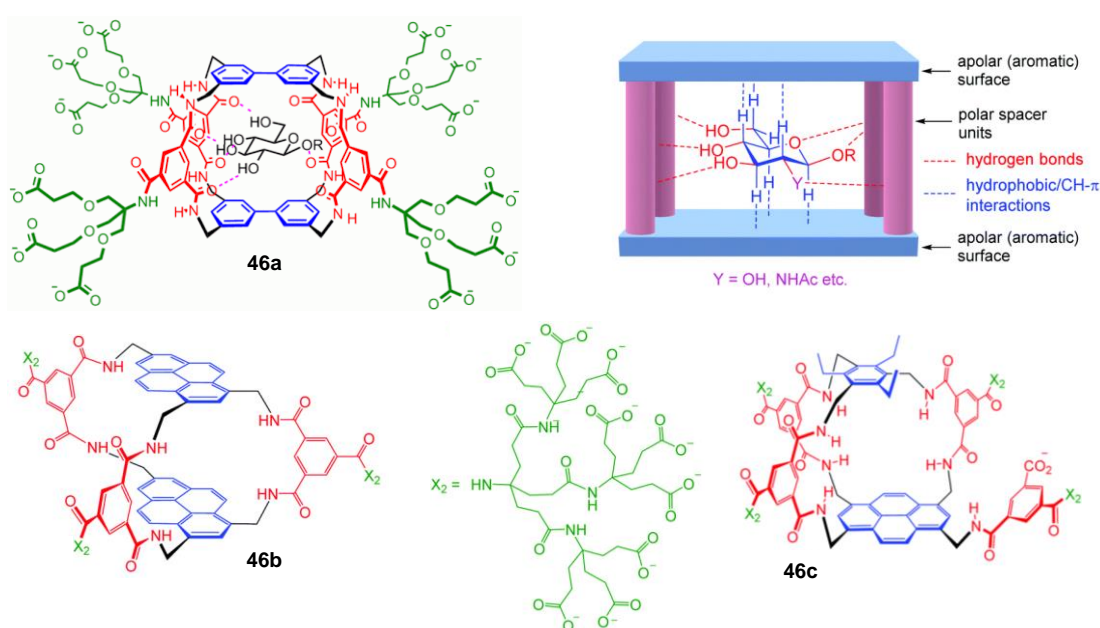
Figure 7. Design of "temple-like" hosts for carbohydrate recognition. Edited image used with permission,[64] Copyright Royal Society of Chemistry.

The synthetic access to such cage compounds has been a bottleneck in conducting further studies to improve the binding to carbohydrates. Therefore, a new approach to synthesize larger amide cages having such a 'temple-type' geometry is imperative.

2.3.4. Gas adsorption

Although cage compounds have exhibited several applications as mentioned previously, utilization of their porosity in solid-state has only developed in the last decade. Application of

cage compounds as porous materials has been well documented by Cooper and co-workers in an extensive review.[93] Although the use of amide macrocycles for binding CO_2 was suggested back in 1995 by David Leigh through computational studies, it was never realized experimentally.[87] With the advent of metal organic frameworks (MOFs) and an improved understanding of porous materials, reports of using amide-based MOFs and organic polymers for selective adsorption of CO_2 emerged, where interactions between amide groups and CO_2 molecules were also studied.[66, 74, 94] In 2016, Yaghi and co-workers prepared amide-based COFs via the Pinnick oxidation (discussed again in the next section) which showed remarkable chemical stability but the specific surface area of the amide COF (S_A(BET) = 655 m^2/g) was consistently lower than that of the imine COF (S_A(BET) = 1250 m^2/g).[95] Nevertheless, there is only one example of a discrete amide-based cage compound being used as a porous material, wherein the amide cage by itself was found to be non-porous but instead porosity was realized by constructing microporous dendrimers using appropriate substituents (as illustrated previously in Scheme 5a).

Although a variety of applications have been exhibited by amide-based cages, macrocycles, frameworks and polymers, preparation of such compounds is limited by inefficient synthetic routes usually resulting in multiple steps and/or low yields. With a growing need to develop new ways to access such amide compounds, this thesis encompasses the first attempt at the synthesizing a series of amide cages by exploiting the advantages of DCC (high yields) to first obtain imine cages followed by subsequent oxidation of the imine bonds.

2.3. Accessing amide compounds via an imine

There are several well-known methods of oxidizing imine bonds to amide bonds, namely, using KMnO$_4$,[96] transition metal catalysis,[97] *m*-CPBA,[98] and Oxone.[99] Despite an array of methods to oxidize imines to amides that are useful with simple small molecules, these methods are inefficient to apply to cage compounds because of the following reasons:

a) extremely harsh reaction conditions – e.g., with KMnO$_4$ alkyl side chains would also get oxidized.

b) Moderate yields – e.g., with transition metal catalysis and Oxone. The yield observed with transformation of one imine bond to an amide bond is around 50-60% which would prove inefficient for cage compounds that contain multiple imine bonds.

c) Side products – e.g., with *m*-CPBA. The reaction has been proposed to form side products due to rearrangement of the intermediate species. This would result in a complex crude mixture with cage compounds.

d) Sensitive reagents – e.g., with *m*-CPBA. This method requires the use of $BF_3 \cdot OEt_2$ which is highly sensitive to air and moisture making the synthesis procedure tedious.

On the other hand, Pinnick oxidation, originally developed by Lindgren in 1973[100] and later advanced by Pinnick in 1981,[101] is a mild and low-cost oxidation method having an exceptionally good functional group tolerance.[101-102] This reaction was initially used to oxidize aldehydes to carboxylic acids but was later extended to oxidize imines to amides.[103] This reaction not only offers excellent yields (> 90% in most cases) but also involves no sensitive reagents. Hence, this provides a new route to obtain amide bond-based organic cage compounds, which is the focus of this thesis.

2.3.1 Pinnick oxidation

The Pinnick oxidation, due to its low-cost reagents and excellent functional group tolerance, has been used extensively in natural product synthesis to oxidize aldehydes to carboxylic acids.[104] The use of $NaClO_2$ for the oxidation of aldehydes dates back to 1952 where Pearl and Barton reported the oxidation of vanillin using sodium chlorite in an acidic solution (as shown in Scheme 15).[105] They report that the product of the oxidation was 2,4-furandicarboxylic acid wherein a six-membered benzene ring was converted to a 5-member furan ring.
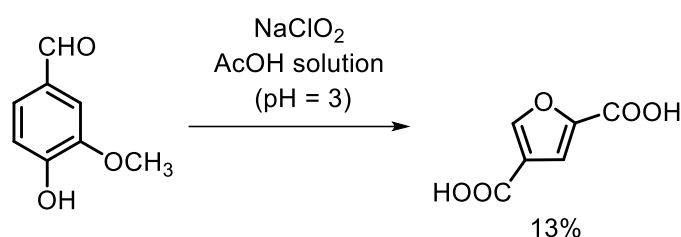

Scheme 15. The use of $NaClO_2$ to oxidize vanillin by Pearl and Barton in 1952.[105]

Similar attempts by Purves and co-workers in 1955 observed large amounts of chlorinated products chlorinated products (with 17% 5-chlorovanillin being isolated) along with the desired carboxylic acid which could not be isolated.[106] In pursuit of oxidative delignification, Sarkanen et al. in 1962 [107] and Ishikawa et al. in 1969[108] also observed unexplained (ring opening, ring oxidation) products isolated in low yields (as shown in Scheme 16).
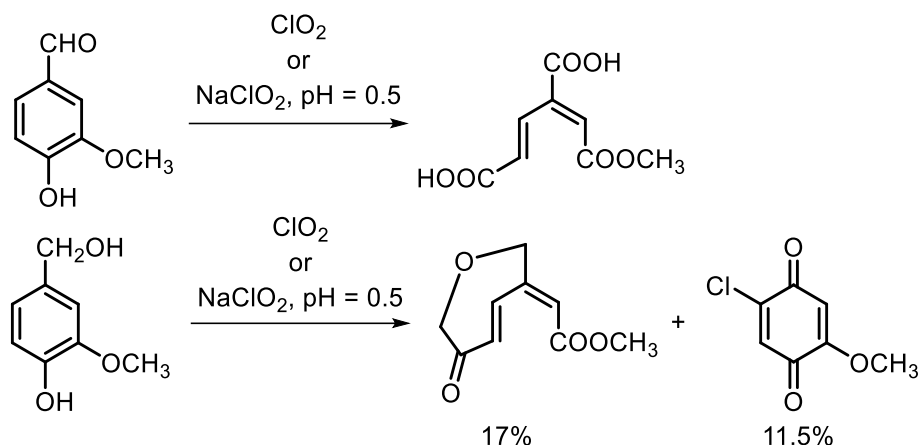
Scheme 16. Isolated side products of the $NaClO_2$ oxidation without a scavenger as reported by Husband et al. and Sarkanen et al. in the 1950s and 1960s.[106-107]

In 1973, Lindgren and Nilsson showed that the use of a 'chlorine scavenger' like sulphamic acid/resorcinol (in the oxidation of vanillin using $NaClO_2$) prevents the formation of undesired products, and instead only leads to the oxidation of the aldehyde group to a carboxylic acid.[100] They recognized that hypochlorite (ClO^-), a by-product of the reaction, is a stronger oxidation agent than chlorite (ClO_2^-) and in fact the former oxidizes the latter to chlorine dioxide, hence quenching the reaction. During further efforts to rectify this, Kraus and co-workers used 2-methyl-2-butene as the hypochlorite scavenger,[109] followed by the work of Pinnick et al. who applied this method to a series of α,β-unsaturated aldehydes (as shown in Scheme 17), also demonstrating the scope and the excellent functional group tolerance of this reaction.[101]
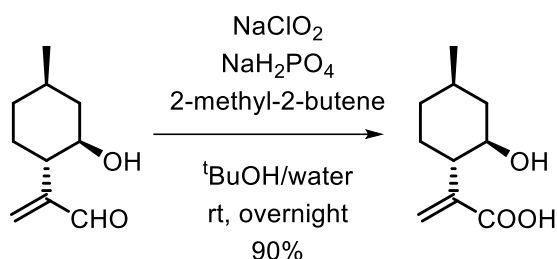
Scheme 17. Oxidation of α,β-unsaturated aldehyde using sodium chlorite by Pinnick and co-workers.[110]

The proposed mechanism for the Pinnick oxidation is as displayed below in Scheme 18.[100] The reaction is initiated by protonation of the carbonyl moiety, thus activating it to a nucleophilic attack of the chlorite oxidant. Subsequent pericyclic decomposition of this unstable acetal, results in the extrusion of hypochlorous acid and the product carboxylic acid. Finally, the hypochlorous acid undergoes addition across the 2-methyl-2-butene scavenger generating a halohydrin that is inert towards the reactants.
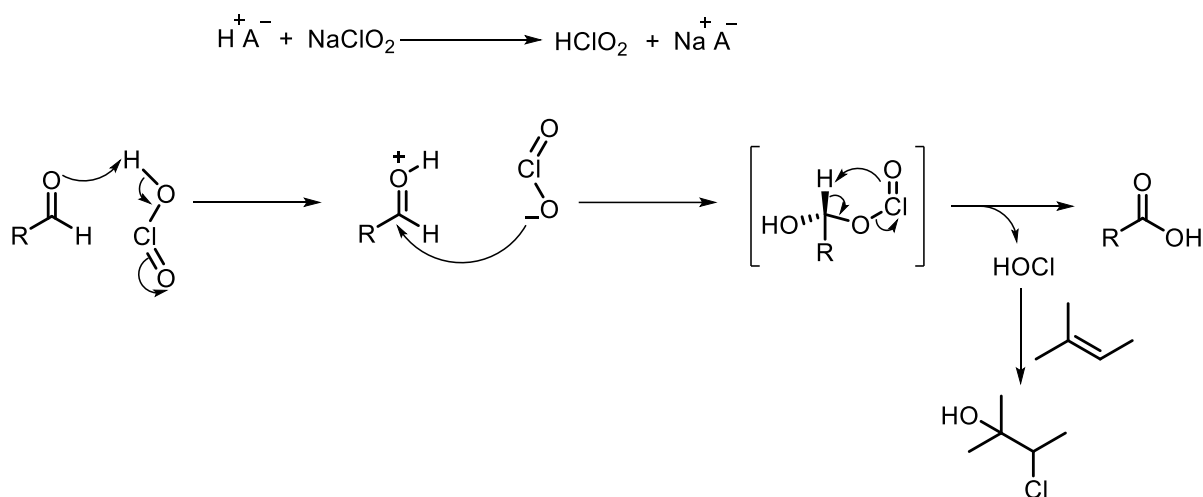
Scheme 18. Proposed mechanism of the Pinnick oxidation by Lindgren and Nilsson.

An extensive study of the substrate scope accompanied by the use of H_2O_2 as the scavenger was reported by Dalcanale et al. in 1986.[102] This method offers a huge advantage because the by-products formed after the scavenging step would be water, oxygen and hydrochloric acid (as shown in equation 1) instead of organic impurities. Nonetheless, this method is limited in more complex substrates that maybe unstable towards hydrogen peroxide and strong acids such as HCl.

$$HOCl + H_2O_2 \longrightarrow HCl + H_2O + O_2 \qquad (1)$$
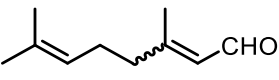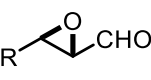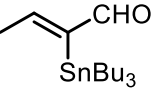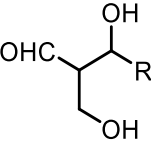
A major problem encountered while carrying out a substrate scope study was that the highly reactive hypochlorous acid (HOCl) reacted with the substrate faster than the scavenger necessitating the use of different scavengers in some cases. Employing DMSO as a scavenger enabled a feasible oxidation of electron rich aldehydes and aldehydes containing unconjugated alkenes and alkynes. Furthermore, several labile functional groups that wouldn't survive other harsh oxidation conditions like tert-butyldimethyl silyl group,[101] iodides,[111] stannanes,[112] N-formyl groups,[113] Boc protective group,[113] epoxides,[114] and to a certain extent non-conjugated alkene groups were found to withstand the Pinnick oxidation reaction. Table 1 summarizes the scope and limitation of the Pinnick oxidation compiled from previous publications.
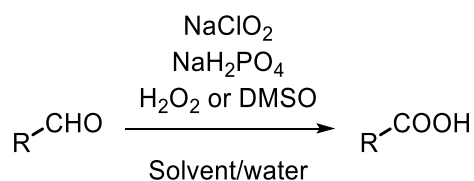

Scheme 19. General scheme for the Pinnick oxidation for the results in Table 1.

Table 1. Substrate scope of the Pinnick oxidation as shown in Scheme 19.

| Aldehyde	Isolated yield of carboxylic acid (in %)	Remarks
⟨benzaldehyde, Ph–CHO⟩	93[102]	-
⟨pyridine-4-carbaldehyde, N⟩–CHO	100[102]	Generally works better with EWG
H₃CO–⟨phenyl⟩–CHO	86[102]	Generally works worse with EDG
HO–⟨phenyl⟩–CHO	7/83[102]	H₂O₂ as scavenger: 7% DMSO as scavenger: 83%
H₂N–⟨phenyl⟩–CHO	0[102]	Only tars observed
⟨cinnamaldehyde, Ph–CH=CH–CHO⟩	95[102]	Works with α,β-unsaturated aldehydes
OHC–⟨X⟩	X = NH: 0[102] X = O: 82[102] X = S: 94[102]	X = NH: only tars observed X = O: Maleic acid formed
⟨o-tolualdehyde, CH₃-phenyl⟩–CHO	91[102]	No significant effect of steric hindrance
⟨citral⟩–CHO	46[102]	H₂O₂ as scavenger: No product DMSO as scavenger: 46%
R–⟨epoxide, O⟩–CHO	76[114]	No ring opening of epoxides observed
⟨CHO, SnBu₃ alkene⟩	71[112]	Stannanes stable during reaction
OHC–⟨OH, R, OH⟩	88[115]	Protection of hydroxyl groups not necessary
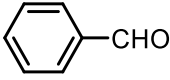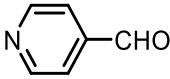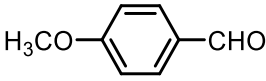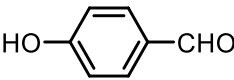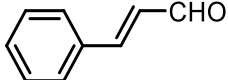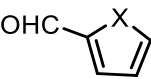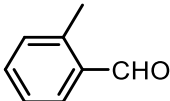
A mechanistic study of the Pinnick oxidation using DFT calculations was reported recently, where solvent effects and the electronic effects of substituents were studied.[116] Firstly, it was found that the addition of the $HClO_2$ species to the carbonyl occurs in a concerted manner due to the more stable cis-conformation of the $HClO_2$ species (as seen in Figure 8). Polar protic solvents were seen to have a deleterious effect (due to their hydrogen bonding ability) on the reaction since it raises the energy of the first transition state (**FTS**) from 20.2 kcal/mol to 28.7 kcal/mol. Although it is necessary to use polar solvents (in particular solvents that are miscible with water), Pinnick oxidations were expected to work better in aprotic solvents like acetonitrile and THF. Furthermore, it was found that electron withdrawing groups were found to decrease the electron density on the oxygen of the aldehyde, hence reducing its basicity which leads to an increased energy barrier of the FTS. On the other hand, the electron donating groups (e.g. $-CH_3$ and $-OCH_3$) were found to reduce the energy barrier for the FTS.
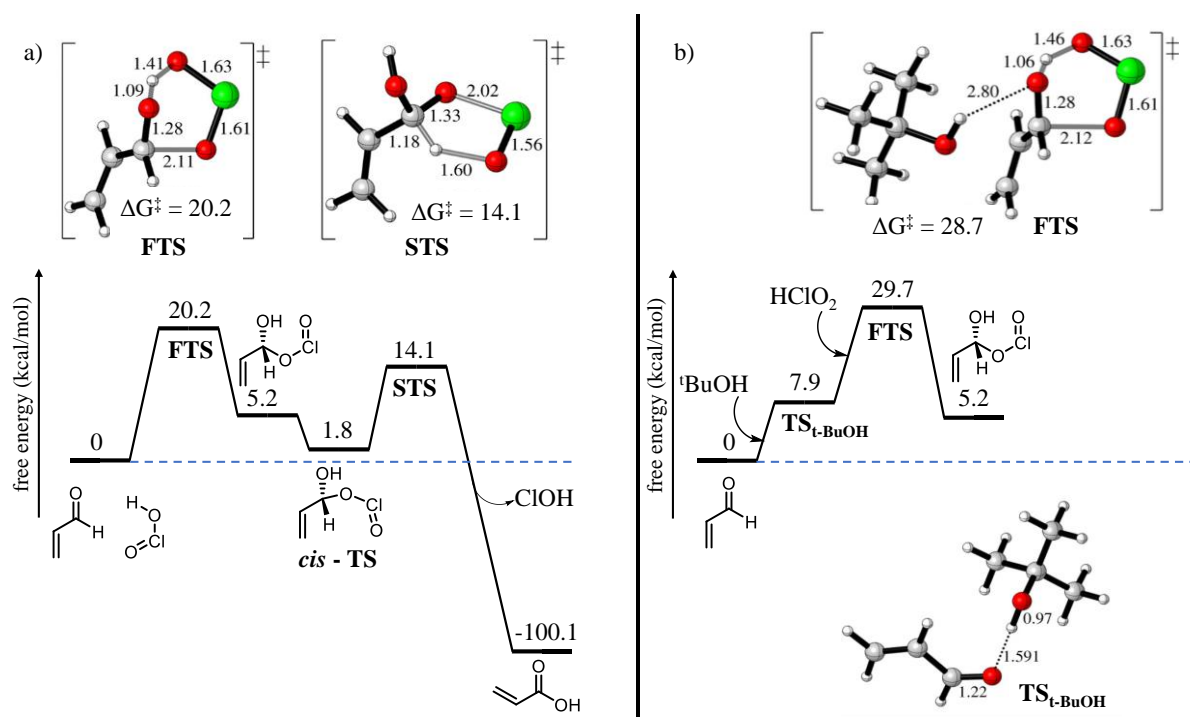
Figure 8. Energy profile (DFT- calculated) of the Pinnick oxidation. a) Energy profile for the oxidation of acrylaldehyde to acrylic acid in the absence of ^tBuOH; b) in the presence of ^tBuOH; Green: chlorine, red: oxygen, white: hydrogen, grey: carbon. **FTS**, **STS** and **TS$_{t-BuOH}$** images are adopted directly from literature, and the energy profile is reproduced with permission,[116] Copyright Royal Society Publishing, licensed under creative commons (CC BY 4.0).

2.3.2. Pinnick oxidation to convert imines to amides

The application of the Pinnick oxidation to oxidize imines to amides was first reported in 2009 by Mohamed et al. (as shown in Scheme 20).[103] It was also proposed that the oxidation of imines follows a similar mechanistic pathway as exhibited by oxidation of aldehydes.
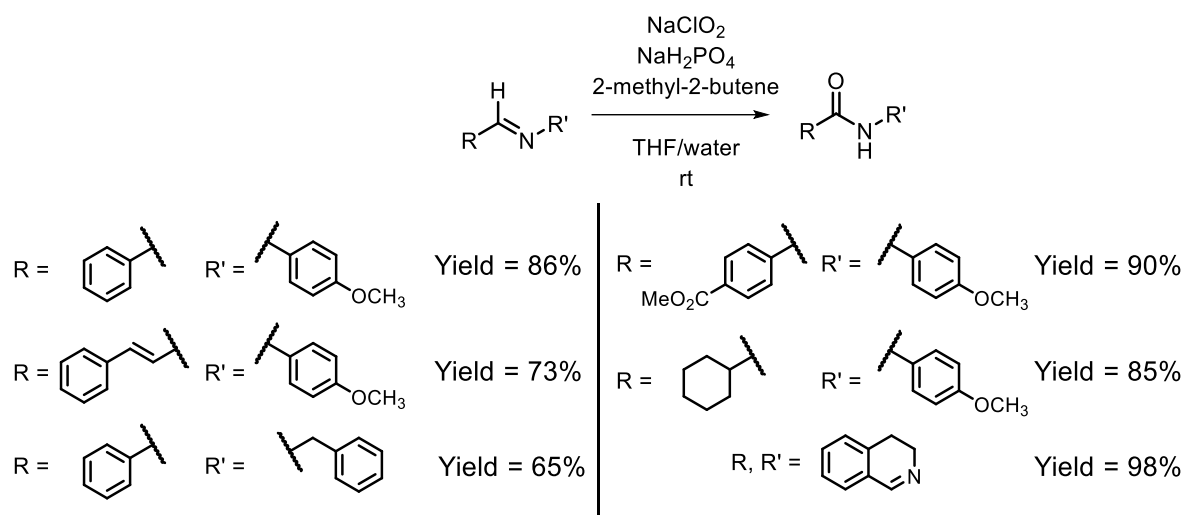
**Scheme 20**. Pinnick oxidation on imines by Mohamed et al.[103]

This method to access amides was applicable to both aromatic and aliphatic imines, although a relatively lower yield (85% and 65% respectively) was obtained for aliphatic imines. Oxidation of 3,4-dihydroisoquinoline gave the best outcome, probably due to the fact that it was the most stable imine among all the substrates.

An additional substrate scope was published by Goh and Tan, where the imine condensation and the Pinnick oxidation was done as a one-pot reaction (Scheme 21), allowing for an efficient scale-up.[117] They studied the effect of different acids on the yield of the reaction and also an extensive substrate scope with various aliphatic chains and substituted aromatic rings.
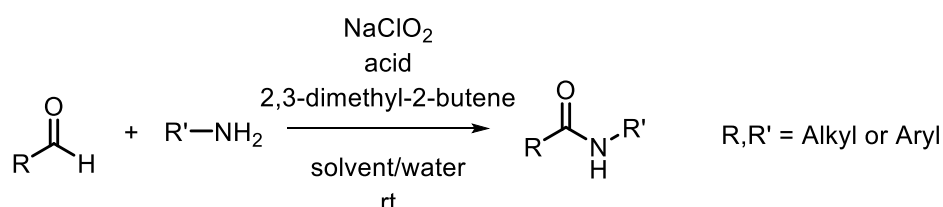

Scheme 21. One-pot reaction to generate amides from aldehydes via the Pinnick oxidation. R,R'-groups correspond to aliphatic chains with varying lengths, saturation and substituents as well as aromatic rings containing various substituents.[117]

The method to obtain amides from imines via Pinnick oxidation was finally used in materials chemistry by Yaghi et al. in 2016 where an imine-based COF was converted to an amide-based COF showing enhanced stability (Scheme 22).[95]
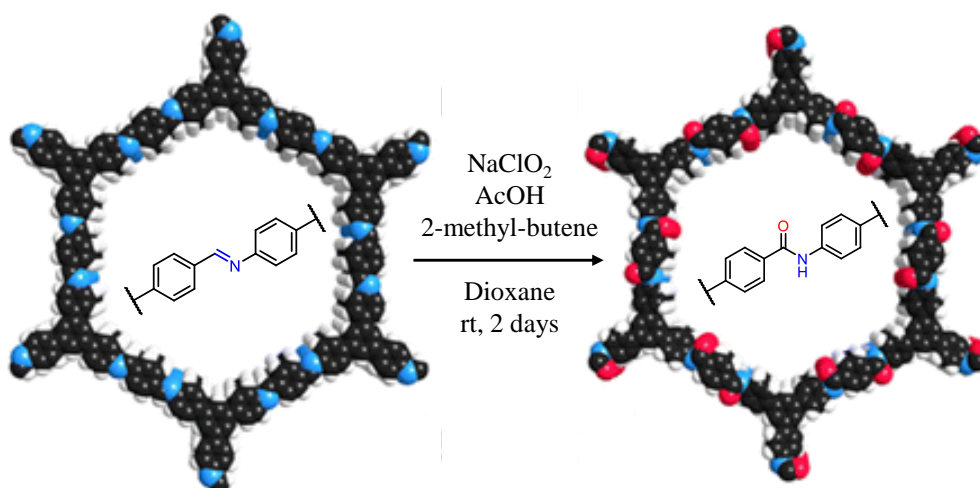
Scheme 22. Accessing amide-based COFs via the Pinnick oxidation. Edited image used with permission,[95] Copyrights ACS publications.

Additionally, Pinnick oxidation was also used by Han et al to obtain an amide-based COF, which was used as a stationary phase for enantiomeric separation (as shown in Figure 9).[118]
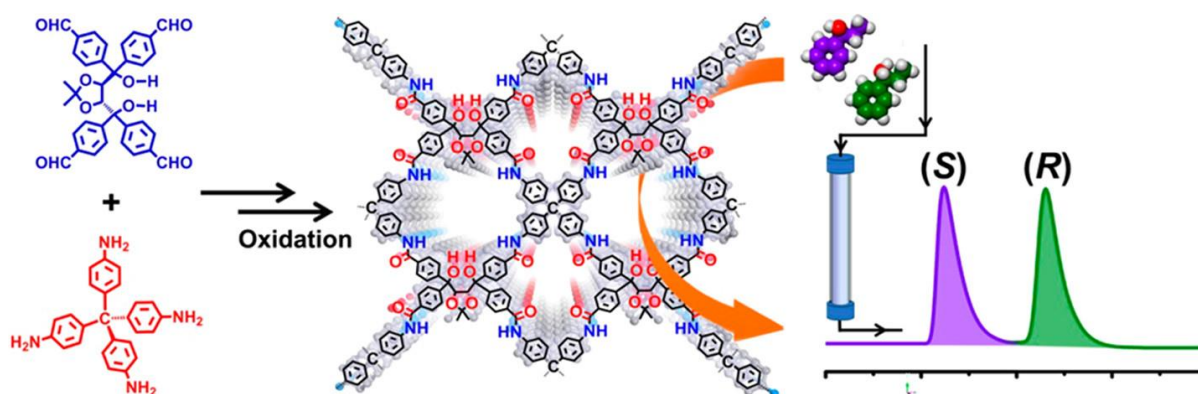
Figure 9. Schematic representation of synthesising amide-based COFs via the Pinnick oxidation and its use as a stationary phase for enantiomeric separation. Image used with permission,[118] Copyright ACS Publications.

The facile synthesis of amide-based materials utilizing the benefits of DCC followed by the Pinnick oxidation is a very promising approach but there has only been one report of this method being applied on organic cage compounds.[119] Preliminary results for the transformation of a [4+6] triptycene-based imine cage to an amide cage via the Pinnick oxidation was realized as part of the PhD work of Dr. Sven Elbert (Mastalerz group, Heidelberg University), wherein a crystal structure of amide cage **48** was reported after purification by reversed phase-HPLC, albeit in a yield of 5% (as shown in Scheme 23).
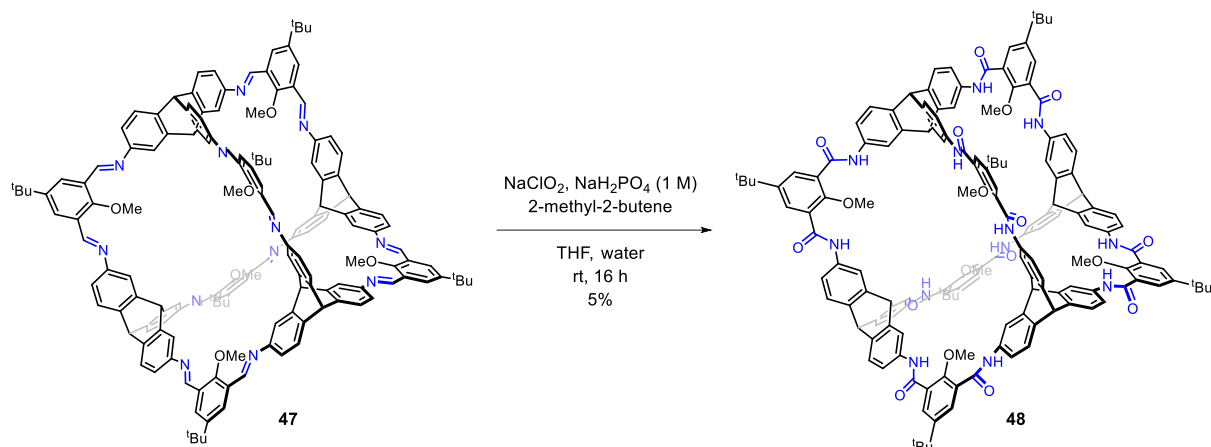
Scheme 23. Conversion of a triptycene-based [4+6] imine cage to an amide cage via the Pinnick oxidation, as presented by Dr. Sven Elbert (Mastalerz group, Heidelberg University) in his doctoral dissertation.[119]

Using this result as a starting point, this thesis entails the synthesis of a series of amide cage compounds followed by strategies to post-functionalize the chemically robust amide cages, resulting in promising materials for future applications.

II. Objective

The primary goal of this thesis is to develop a method to access amide-based organic cage compounds that are chemically robust and exhibit permanent shape-persistence. Using a rigid triptycene building block, shape-persistent [4+6] imine cages offering record breaking porosity was reported by the Mastalerz group.[29b, 43b] Furthermore, the group also demonstrated the post-modification strategy which not only alters the cage cavity but also acts as a protecting group for phenols which may hinder the Pinnick oxidation.[120] Following the doctoral work of Dr. Sven Elbert (as mentioned previously),[119] the first task involved reproduction of the existing procedure while looking for possibilities to improve. The main aim behind the improvement being the isolation of significant quantities of the amide cage **48** in a single batch via the synthetic route shown in Scheme 24.
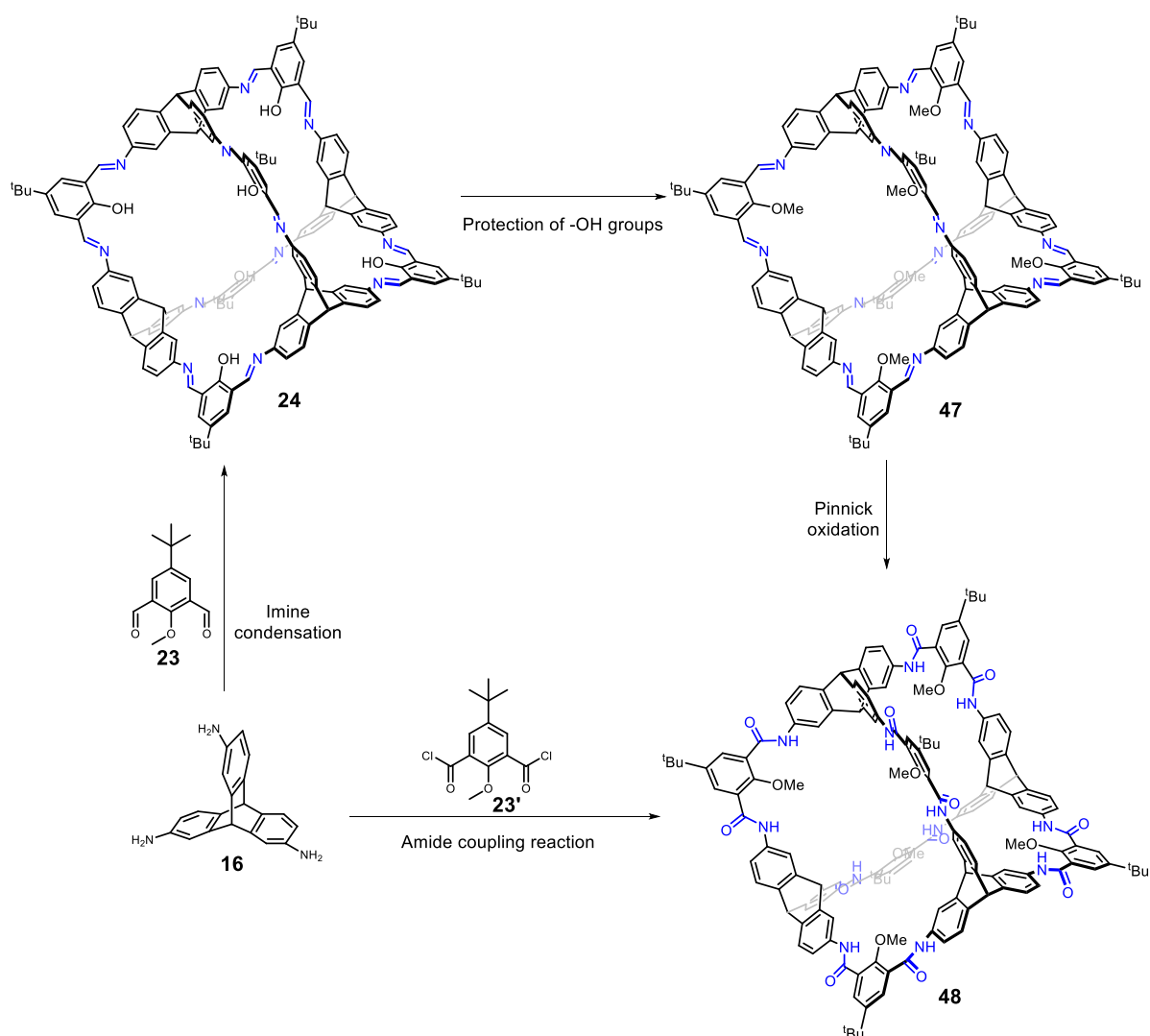
Scheme 24. Two different synthetic routes to prepare the triptycene-based [4+6] amide cage **48**.

Imine cage **47** contains imines derived from an aromatic amine, but however, the versatility of this method to obtain amide cages was to be extended by applying the method on imine cages derived from aliphatic amines. This could be realized by preparing a series of imine cages using a commonly used aliphatic amine precursor (triamine **A** in Scheme 25).
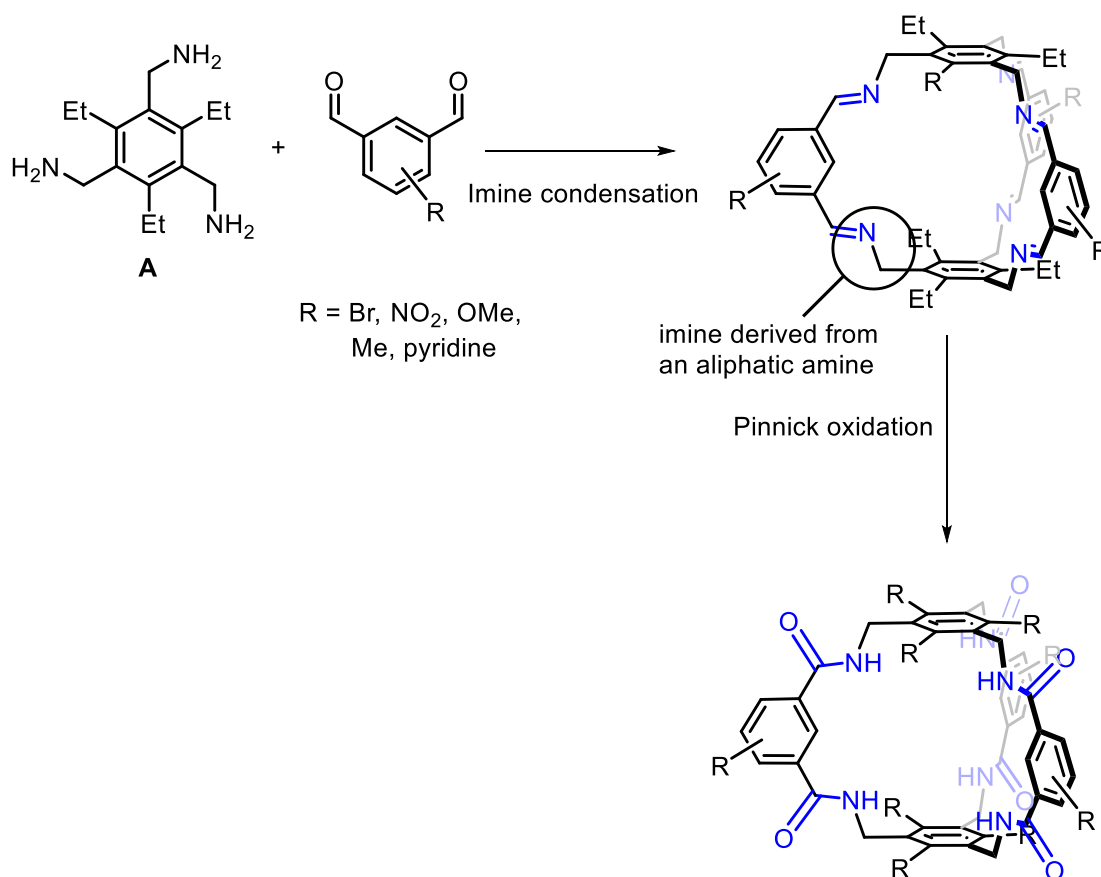
Scheme 25. Synthesis of an imine cage derived from aliphatic an amine, followed by subsequent Pinnick oxidation.

Alternatively, it was necessary to determine if the amide cages could also be synthesized directly via an irreversible amide coupling reaction (for example as shown in Scheme 24), as performed previously to prepare other amide cages (see Introduction section 2.1). Finally, the most important characteristic of amide cages being their chemical robustness, offers the possibility to post-functionalize. Therefore, developing strategies to decorate the exterior of the cage molecules with chemically rich moieties would result in promising functional materials.

III. Results and discussion

1. [4+6] triptycene-based cage compounds

1.1. Synthesis of the [4+6] triptycene-based salicylbisamide cage

In this section, the synthesis of the [4+6] salicylbisimine cage followed by post-modification to protect the hydroxy groups will be discussed. This will be followed by optimization of the Pinnick oxidation procedure to obtain the [4+6] amide cage. Finally, there will be a detailed description on how the amide cage was isolated and characterized.

1.1.1. Pinnick oxidation on model compounds

The Pinnick oxidation reaction, before being conducted on the [4+6] salicylbisimine cage, was tested with two model compounds that contain functionality and substitution patterns comparable to the full cage motif. Using the published procedure to convert imines to amides,[103] the following reactions were conducted:
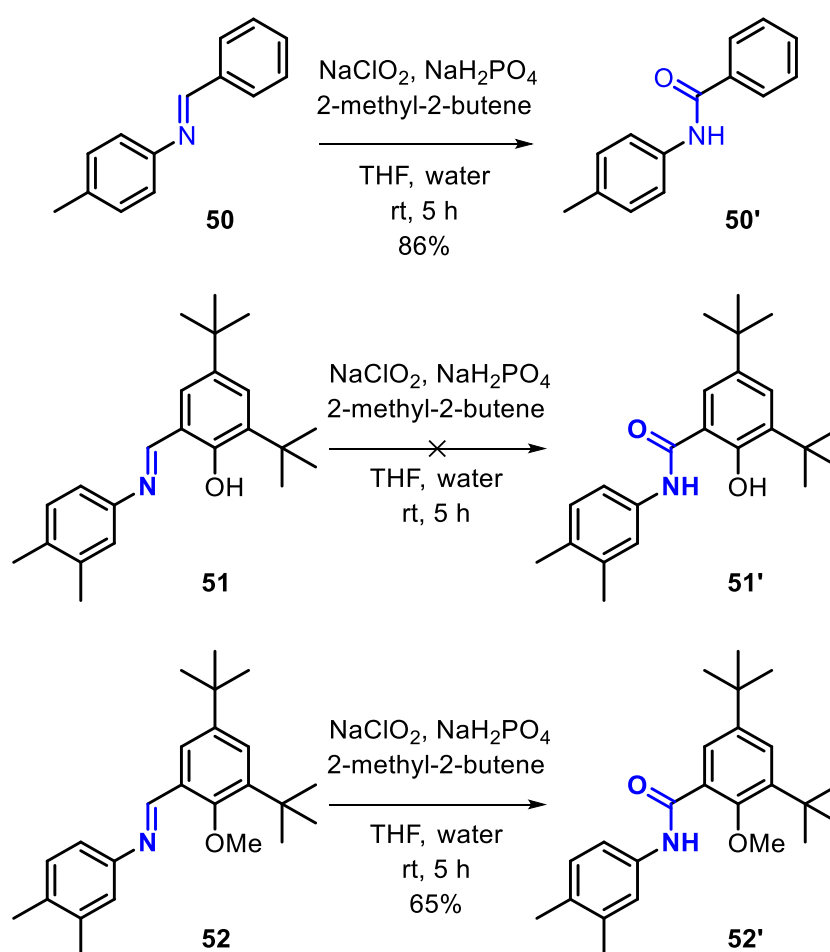

Scheme 26. Pinnick oxidation on model compounds **50, 51** and **52**.

Model imine compound **50** was converted to an amide **50'** by Pinnick oxidation with a good yield of 85% (as shown in Scheme 26). Subsequently, the model imine compound **52** was subjected to the Pinnick oxidation to get the amide **52'** in a moderate yield of 65%. Imine **52** has a methoxy group in the *ortho* position, which when unprotected (imine **51**), does not form the desired amide compound. Instead, the Pinnick oxidation delivered the starting material (imine **51**) with a yield of only 70%, suggesting partial hydrolysis. The Pinnick oxidation procedure was used as described in literature, using 5 equivalents of the oxidant (NaClO$_2$), 1.5 equivalents of NaH$_2$PO$_4$ and 10 equivalents of the scavenger (2-methyl-2-butene).[103] These conditions were then applied to convert the [4+6] salicylbisimine cage.
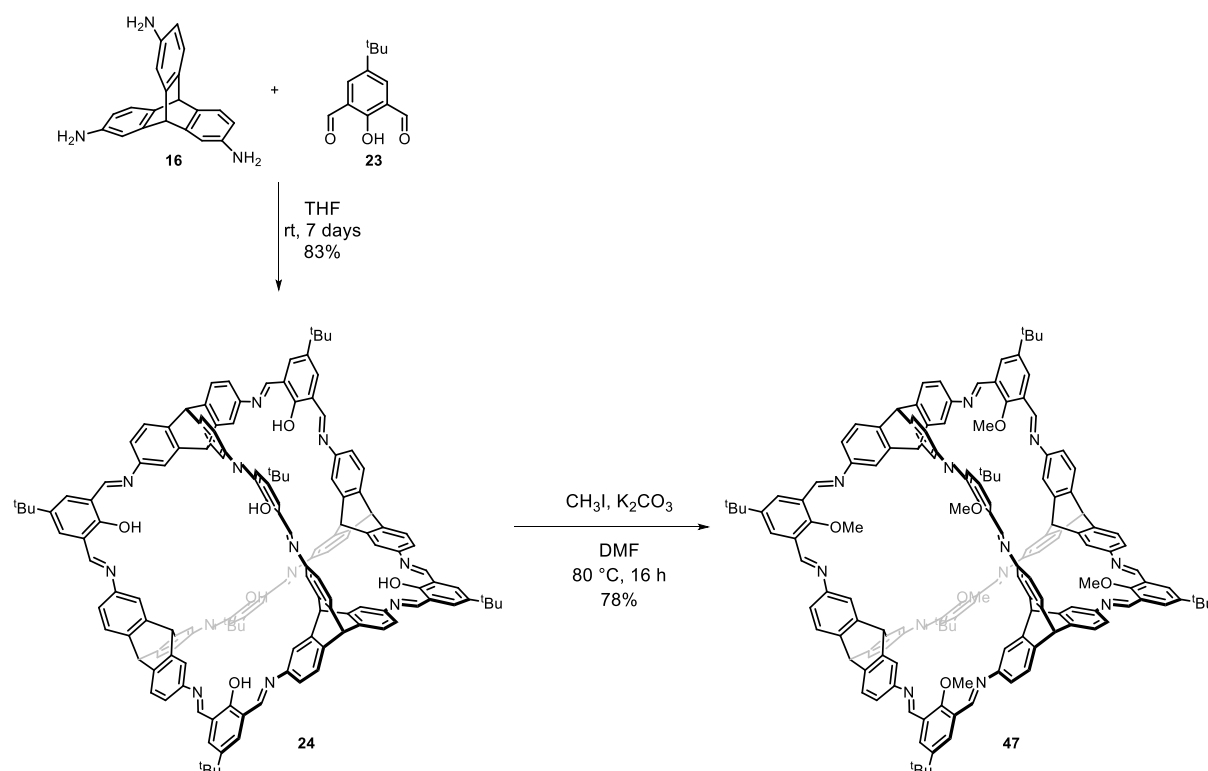
1.1.2. Synthesis of the [4+6] salicylbisimine cage

The unsubstituted triptycene **53** was synthesized via the Diels-Alder reaction (as shown in Scheme 27),[121] which was followed by nitration using fuming nitric acid. The minor product (isomer **55a**) was isolated by column chromatography and reduced using hydrazine hydrate catalysed by Palladium on charcoal, to obtain the 2,7,14-triaminotriptycene.[122]
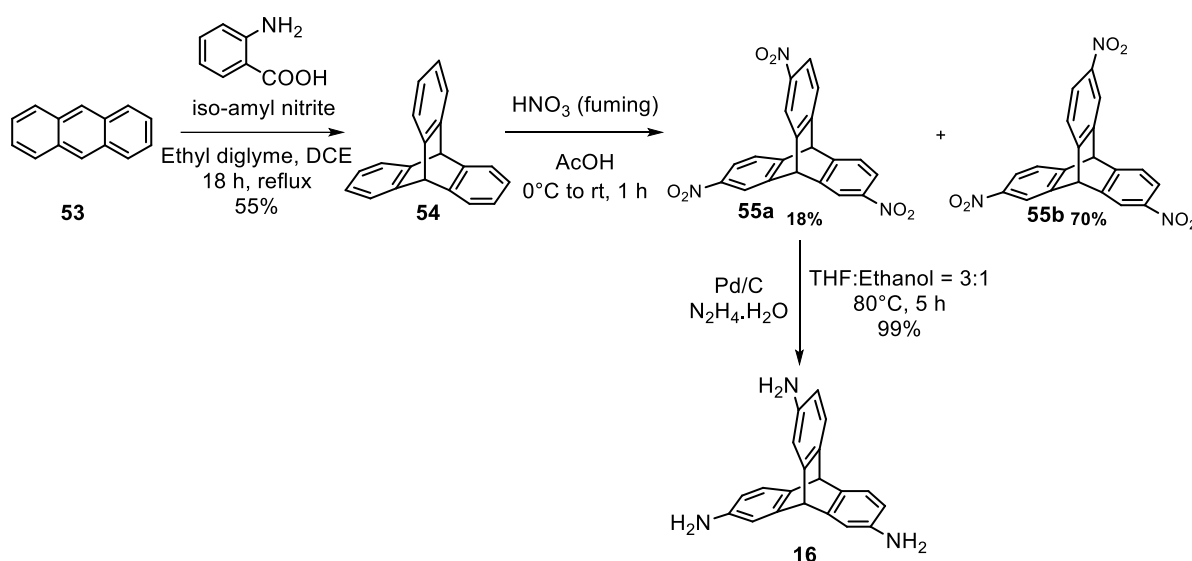
Scheme 27. Synthesis of 2,7,14-triaminotriptycene **16**.

Using precursor **16** and commercially available dialdehyde **23**, the [4+6] salicylbisimine cage **24** was synthesized by a 12-fold imine condensation,[40] and subsequent protection of the hydroxy groups inside the cavity of the cage afforded cage **47** (as shown in Scheme 28).[120] This step proved to be the bottleneck in the synthetic pathway as scale up beyond a 100 mg scale proved unsuccessful, resulting in incomplete protection. Adding excess methyl iodide to

force the reaction to completion proved ineffective since it resulted in a solid that was insoluble in all organic solvents, possibly due to the formation of the iminium salt.
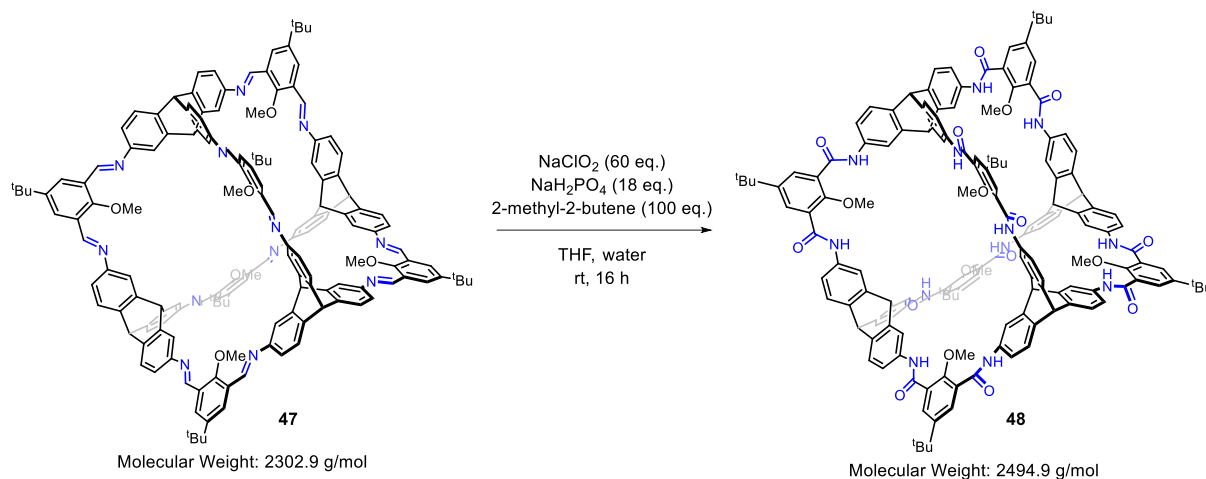

Scheme 28. Synthesis of the [4+6] Salicylbisimine cage **24** followed by protection of hydroxy groups.

Protection of the hydroxy groups was absolutely necessary to transform the imine cage to an amide cage via the Pinnick oxidation since it was shown that unprotected -OH groups, especially next to the aldehyde/imine, greatly hinder the Pinnick oxidation (as described in the section 2.2).[102]

1.1.3. Synthesis, isolation and characterization of the [4+6] Salicylbisamide cage

The 12-fold oxidation of imine cage **47** was done under typical Pinnick oxidation conditions with $NaClO_2$ as the oxidant, NaH_2PO_4 as the source of proton (to generate the active species, $HClO_2$) and 2-methyl-2-butene as the scavenger (in a large excess). The reaction was conducted in a THF-water mixture (water used to dissolve the inorganic salts) at room temperature as shown below in Scheme 29.

Scheme 29. Transformation of the [4+6] Salicylbisimine cage **47** to a [4+6] amide cage **48**. The recognizable change in molecular mass is also shown, which was used to indicate the formation of the product.

Formation of amide cage **48** was initially confirmed by MALDI-MS, where the peak corresponding to **48** was observed as the $[M]^+$ peak at $m/z = 2495$ (Calc. MW = 2494.9, Scheme 29). On removal of THF, a thick yellow gel was obtained which exhibits an NMR spectrum (Spectrum a, Figure 10) clearly showing large amounts of impurities in the aliphatic region, likely formed by subsequent reaction of 2-methyl-2-butene and its principal halohydrin by-product. Assuming the impurities were non-polar in nature, the crude substance was suspended in petroleum ether, at which point a yellow solid precipitated. This crude material exhibited reduced levels of impurities; however further purification was still required (Spectrum b, Figure 10). The remaining impurities were washed off using methanol (Spectrum c, Figure 10). The peak observed at 11.75 ppm shown in the red box could be assigned to a carboxylic acid species that could be formed by oxidation of an aldehyde species (formed after the hydrolysis of imine bonds). Carboxylic acids being highly polar do not get washed away in the PE washing step, and are instead washed away when washed with a polar solvent like methanol. Furthermore, the peak at 3.75 ppm in the blue box is another noticeable broad peak that could likely correspond to free amine groups (formed after hydrolysis of the imine bonds). Finally this crude substance was dissolved in DMSO and purified by reverse phase HPCL (C-18 column, MeCN:THF = 100:0 to 80:20, 10 mL/min flow rate) to obtain the amide cage with a yield of 11% (Spectrum d, Figure 10).
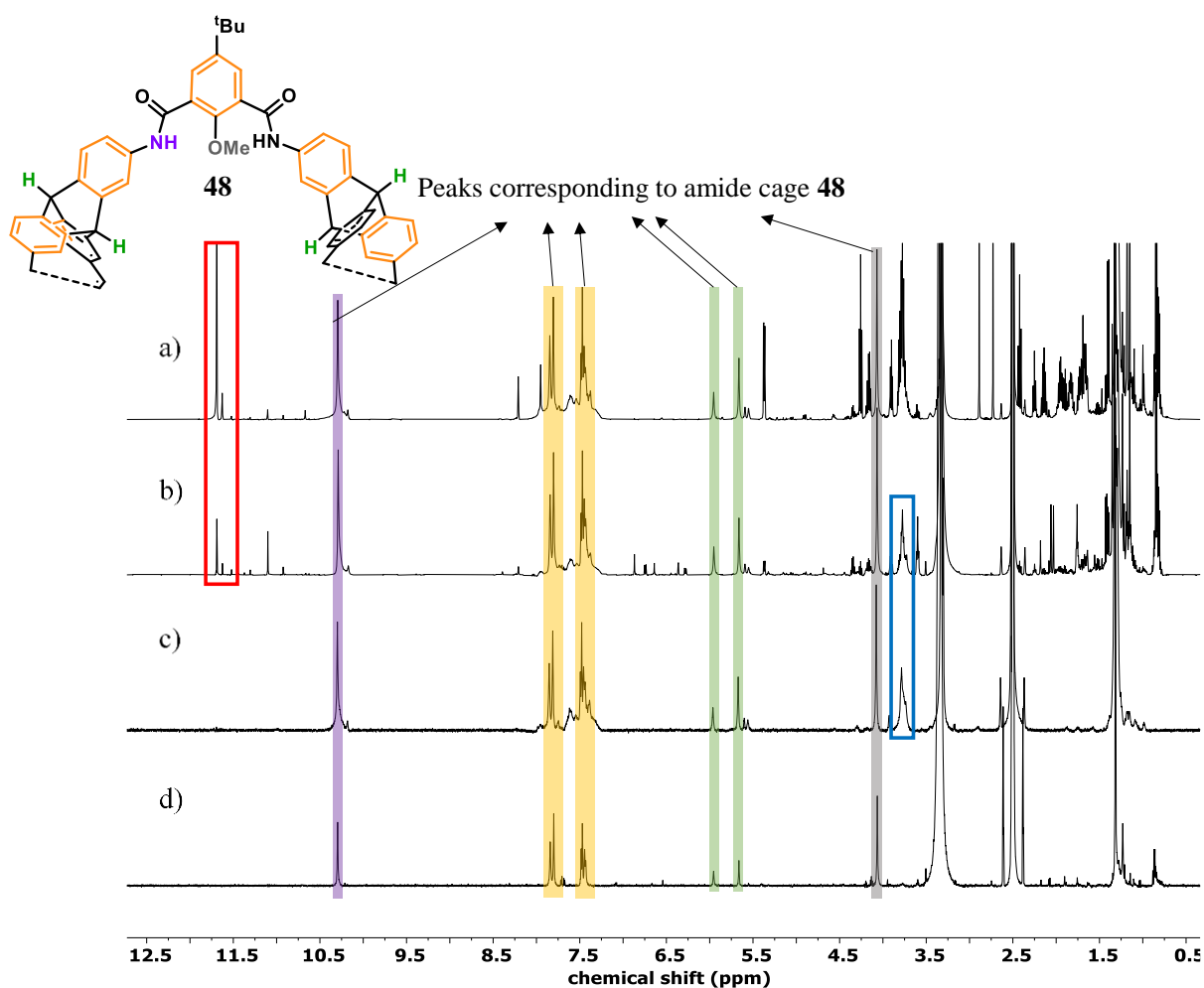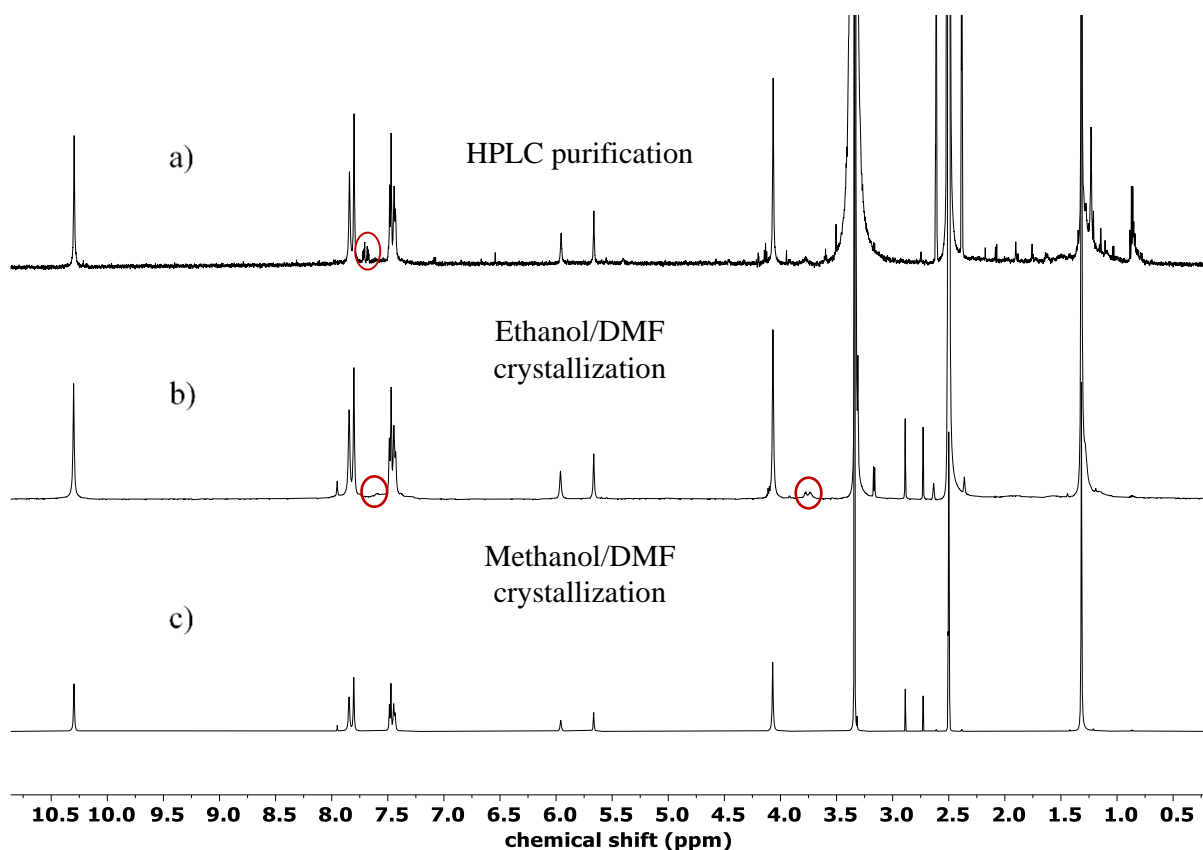
Figure 10. ^{1}H NMR spectra (DMSO-d$_6$, 500 MHz) comparison of the different washing steps of the crude material of amide cage **48**. a) crude material; b) washed with hexanes; c) washed with hexanes and MeOH; d) after HPLC purification. The red and blue boxes indicate some noticeable impurity peaks.

Isolation of the [4+6] amide cage (48)

The HPLC purification of the amide cage had a few limitations: 1) the yield of the reaction was only 11%; 2) the amide cage could only be obtained in very small quantities, due to HPLC as a means of purification; 3) the amide cage was still not pure enough to investigate material properties. Therefore, a different purification method was adopted to isolate the amide cage in its pure form.

The solubility of the crude mixture of the amide cage was investigated and the following was observed: 1) The crude mixture was soluble in polar aprotic solvents such as DMF, DMSO and THF. 2) It was partially soluble in acetonitrile and in hot methanol/ethanol. 3) It was completely insoluble in solvents like hexane, DCM, chloroform. Using this information, the amide cage was first suspended in ethanol, heated to 80°C under stirring and DMF was added dropwise until a clear solution was obtained. On gradually cooling this solution to room temperature, a

colourless precipitate was obtained which was filtered off and analysed (Spectrum b, Figure 11). To attain further purity of the amide cage, the same procedure was repeated using methanol instead of ethanol. In this attempt, colourless crystals of the amide cage were obtained on gradual cooling (Spectrum c, Figure 11). Hence, with this improved purification method, it was possible to obtain larger quantities of the [4+6] salicylbisamide cage **48** in a yield of 21%.

Figure 11. ^{1}H NMR spectra (DMSO-d$_6$, 500 MHz) comparison of the different purification methods to isolate the [4+6] amide cage **48**. a) amide cage obtained by HPLC purification; b) ethanol/DMF precipitation; c) methanol/DMF. Peaks corresponding to impurities are shown in red circles.

Characterization of the [4+6] amide cage (48)

The ^{1}H NMR is fairly simple with the characteristic peak of the amide protons resonating at $\delta =10.30$ ppm in DMSO-d$_6$ (as shown in Figure 12). The triptycene protons appear between $\delta = 7.43$ to 7.5 ppm and 7.85 ppm with the protons of the other aromatic ring at 7.81 ppm. The bridgehead protons are seen at 5.96 and 5.66 ppm followed by the methoxy peaks at 4.07 ppm. The assignment of individual peaks was done utilizing ^{1}H-^{1}H NOESY NMR, wherein a coupling between the bridgehead protons and the closest aromatic proton provided the major clue. The complete conversion of the imine bonds to amide bonds is also confirmed by FTIR spectroscopy wherein the imine band at $\bar{v} = 1625$ cm^{-1} completely disappears and instead the carbonyl stretching mode of the amide group appears at $\bar{v} = 1655$ cm^{-1}.
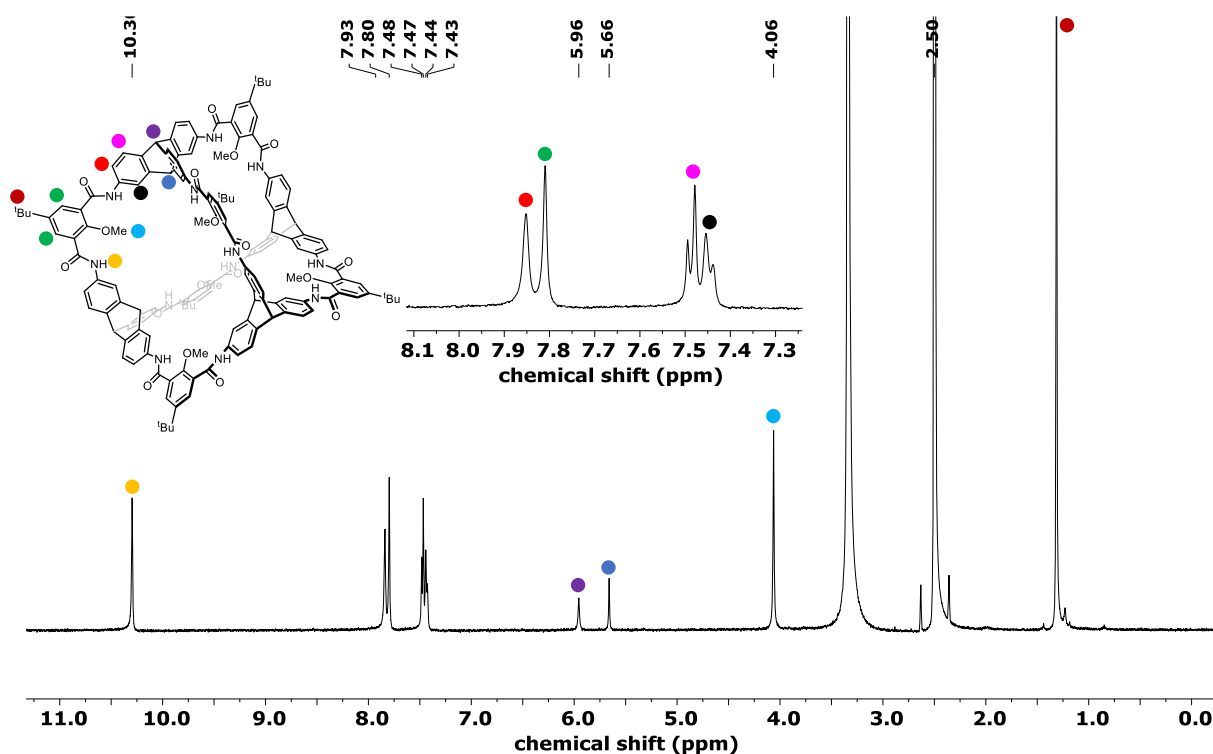
Figure 12. ^{1}H NMR spectrum (DMSO-d_6, 500 MHz) of the [4+6] amide cage **48**.

Final confirmation of the structure of the amide cage was obtained by single crystal X-ray diffraction (as shown in Figure 13). Amide cage **48** crystallizes in the monoclinic space group $P\overline{2}_1$ with four molecules in a unit cell. It is interesting to note that the inner triptycene bridgehead atoms form a regular tetrahedron, similar to the corresponding imine cage **47**, hence proving the retention of shape-persistence during the transformation of an imine cage to an amide cage. Lastly, the internal diameter of the cage cavity varies from 1 nm to 1.3nm as measured from the crystal structure of cage **48**. The packing of the cage molecules in the unit cell also exhibits clear accessible pore channels for gases. The gas adsorption investigations are discussed in a later section.

a)

b)

c)
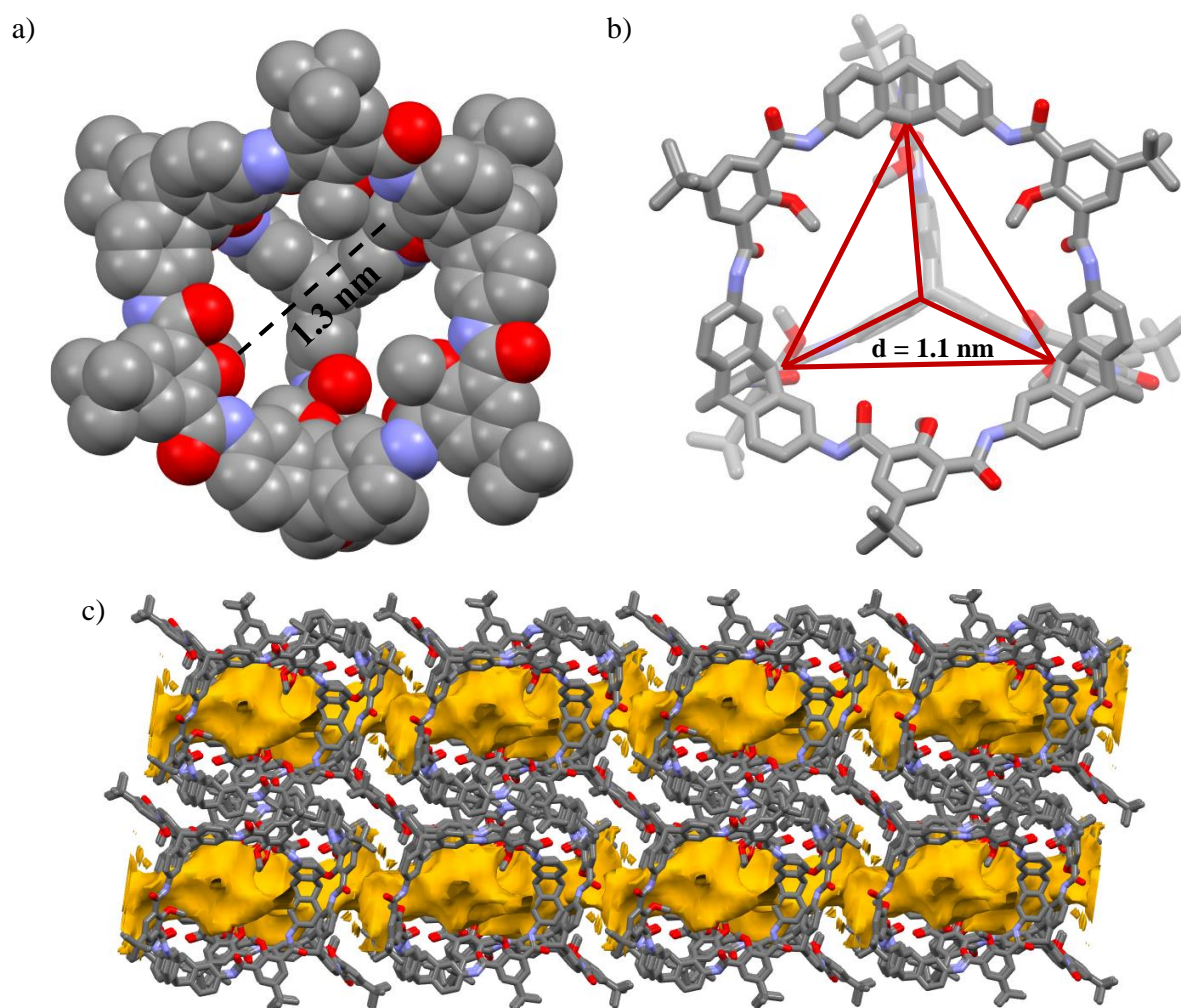
Figure 13. Single crystal structure of the [4+6] amide cage **48**: a) space filled model of the amide cage showing the size of the internal cavity; b) showing the inner bridgehead atoms form a regular tetrahedron, the hydrogen atoms are omitted for clarity; c) solvent accessible pores for a probe of 1.8 Å shown as a 2 x 2 x 2 unit cell. Red = oxygen, blue = nitrogen, grey = carbon.

1.2. Formation of the [4+6] salicylbisamide cage via an irreversible reaction

While several amide cages have been synthesized by an irreversible amide bond forming reaction, it is worth noticing that the formation of these structures required a certain simplicity in the geometry of the resulting cage/macrocycle molecule with regard to the precursors.[8, 56a, 61] However, this [4+6] amide cage has a very complex geometry (adamantoid structure) with a tetrahedral cavity, starting from a simple C_3 symmetric triptycene precursor. Utilizing the 'self-healing' property of the irreversible imine condensation reaction, it was possible to form such a cage structure, but it would be challenging to form such a complex molecule via an irreversible reaction. This reaction would require twelve particular amide bonds to form in a very specific fashion that led to the formation of such a cage molecule (as shown in Scheme

31), instead of several other possible 'mismatches' that could lead to alternative oligomeric and polymeric structures.

To realize this experiment, the appropriate acid chloride **58** was synthesized as shown in Scheme 30. The salicyl-dialdehyde **23** used to make the [4+6] salicylbisimine cage (cage **24**) was methylated via Williamson ether synthesis, followed by a Pinnick oxidation to obtain the dicarboxylic acid **57**. Compound **57** was treated with thionyl chloride to deliver the acid chloride **58**.
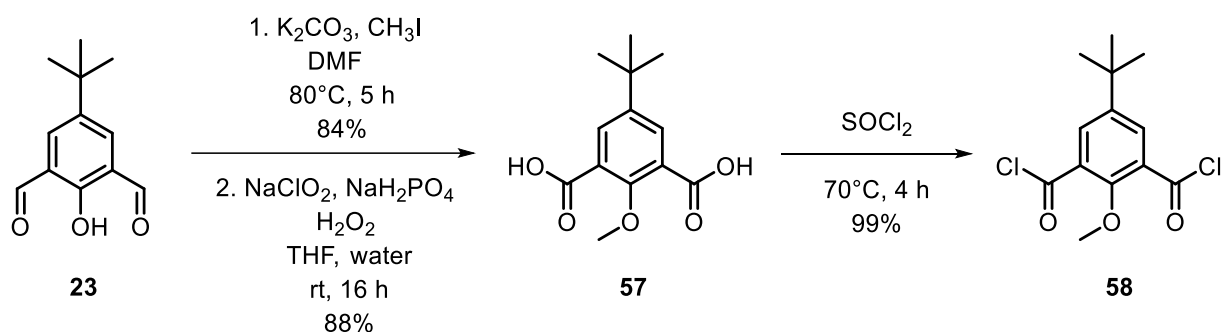
Scheme 30. Synthesis of acid chloride **58**.

A solution of acid chloride **58** with triamine **16** in dry DCM was reacted in the presence of triethylamine in water free conditions, under argon (as shown in Scheme 31). On quenching the reaction with water, a yellow solid was obtained. This solid was analysed by NMR, MALDI-MS and UPLC-MS.
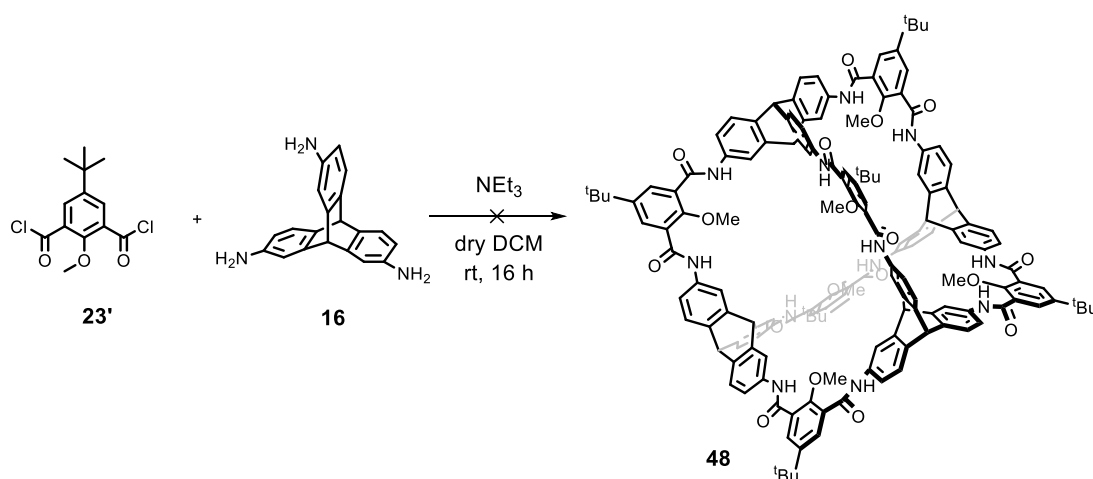
Scheme 31. Synthesis of amide cage **48** via an irreversible amide bond forming reaction.

Although the ^{1}H NMR shows all the characteristic peaks corresponding to the amide group, the triptycene bridgehead atoms and the methoxy group, it can be seen that all these peaks are slightly shifted (as shown in Figure 14). Moreover, the peaks corresponding to the triptycene

aromatic protons does not exhibit the same pattern as that of the amide cage **48**. This already suggests that the desired amide cage **48** is not formed, but instead fragments similar to cage molecule was present.
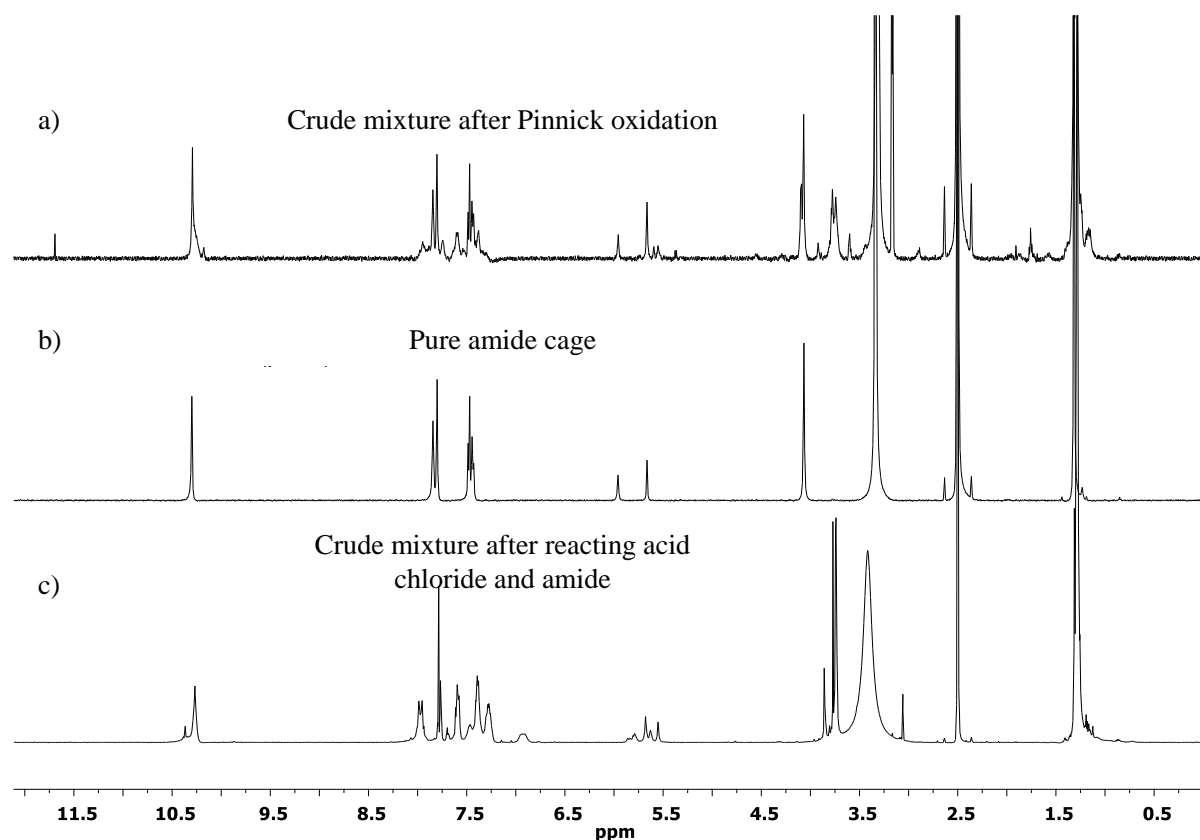

Figure 14. ^{1}H NMR (300 MHz, DMSO-d$_6$) comparison of: a) crude substance of the Pinnick reaction; b) pure amide cage; c) crude substance of the irreversible bond forming reaction.

Analysis by MALDI-MS showed peaks ranging from a mass corresponding to a [1+1] addition of the two precursors, all the way to a [9+10] species and maybe higher (as shown in Figure 15). Although the peaks cannot be assigned to the exact number of the *m/z* values, the approximate value suggests the formation of a probably species. This suggests the formation of a complex mixture of cyclic or linear species. Furthermore, a UPLC-MS analysis of this crude mixture not only showed that it was a complex mixture but also showed that the desired amide cage was not formed (as shown in Figure 16). The mass spectrum corresponding to the major peaks showed the [1+1], [1+2] and [1+3] species but species of higher mass could not be detected in the UPLC-MS.
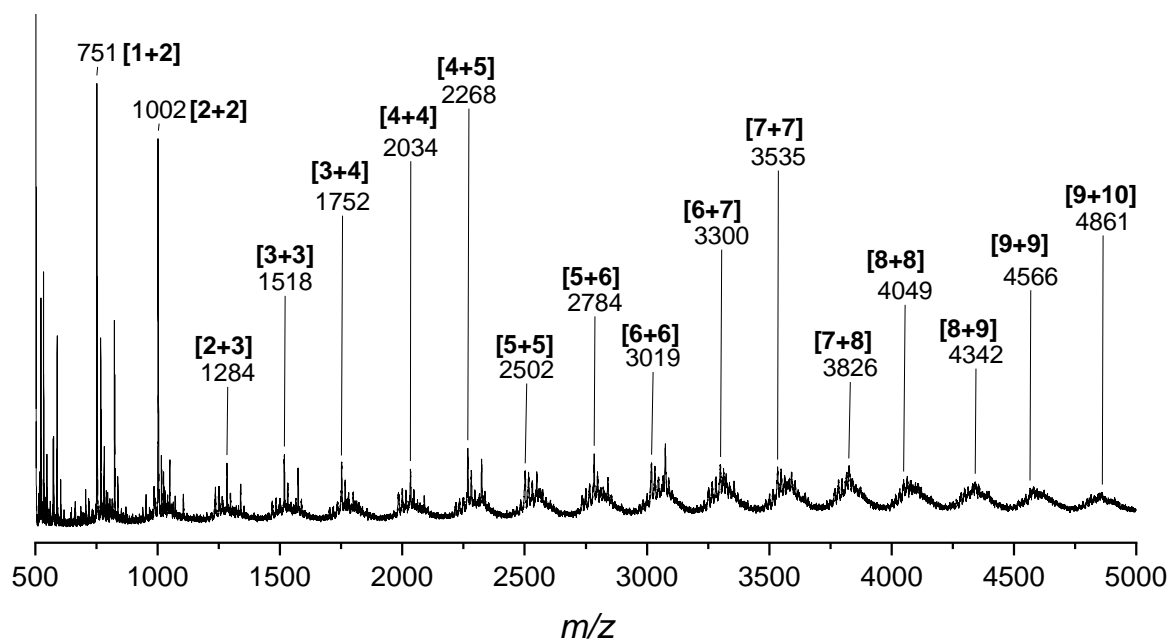
Figure 15. MALDI-MS (DCTB matrix, positive linear mode) of the crude mixture of the reaction shown in Scheme 31. The assignment of the *m/z* value are not accurate but denotes a probable species (linear or cyclic adduct) which has a molecule mass in that range.
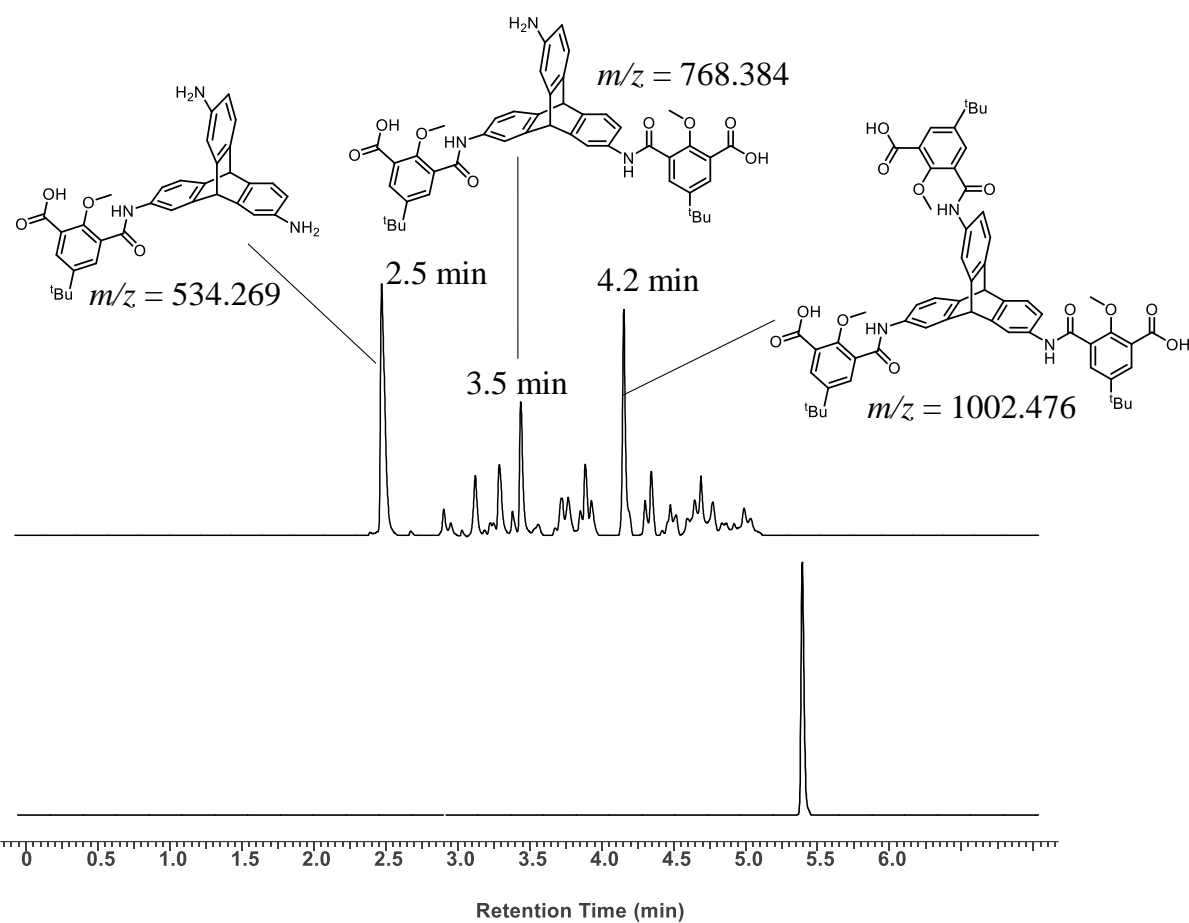

Figure 16. UPLC-MS analysis (C-18 reverse phase column, acetonitrile:water = 90:10, 0.6 mL/min flow rate, apci-MS) of: a) the crude substance of the irreversible bond forming reaction with the values of the apci mass spectrum peaks of the three major peaks; b) pure amide cage **48** as reference.

This shows the superiority of combining DCC with Pinnick oxidation to obtain large and complex amide-based cage molecules over the irreversible amide coupling reaction.

## 1.3. Post-functionalization of the [4+6] salicylbisamide cage

Imine bonds are highly susceptible to acids, bases and nucleophiles making it very challenging to post-functionalize imine cages. To highlight this deficiency, imine cage **47** was subjected to bromination and nitration reactions, the ^{1}H NMR of the resulting product shows cleavage of the imine bond to an aldehyde (peak at around 10.3 ppm) as shown below in Figure 17.
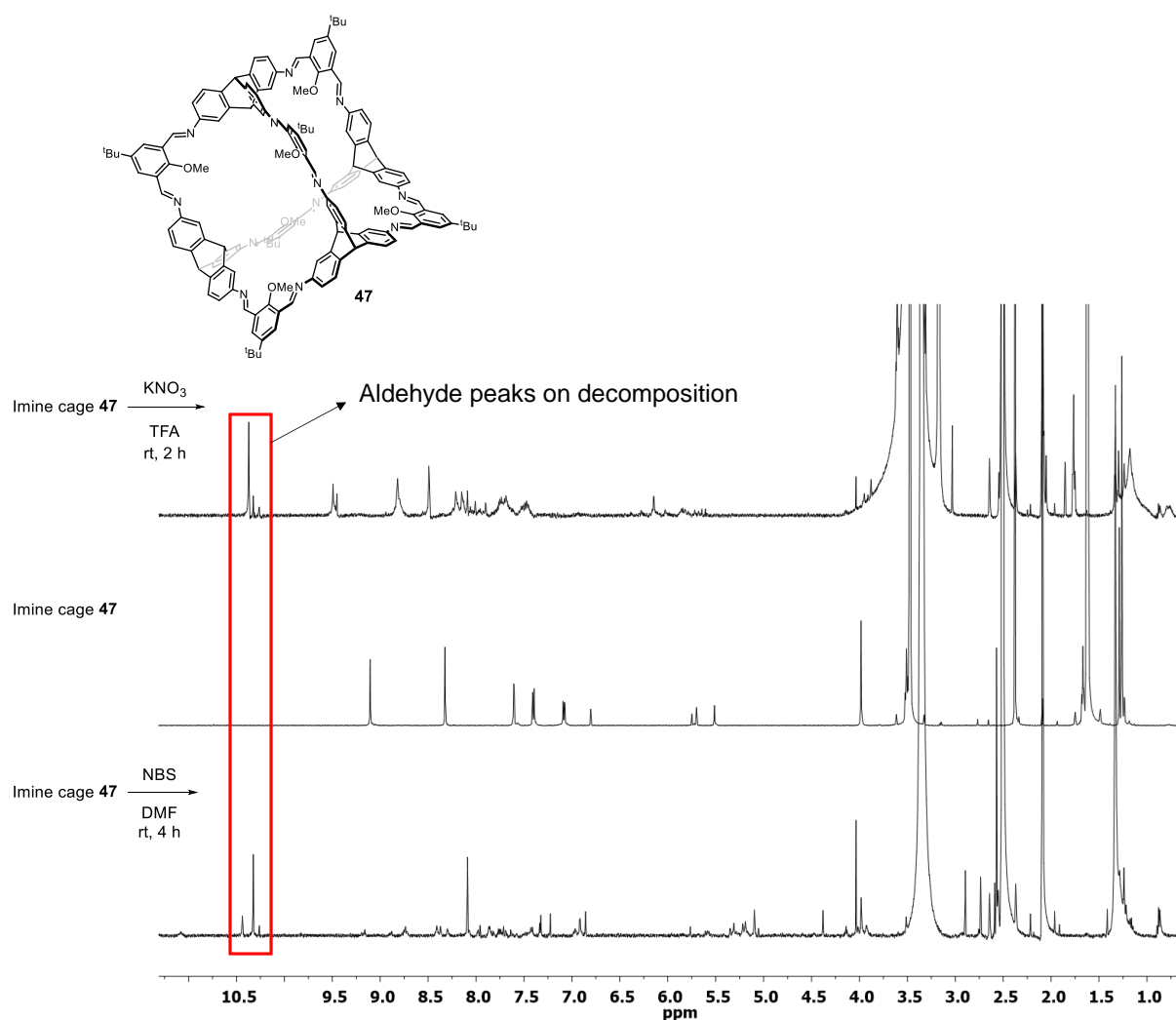
Figure 17. Reactions on the imine cage **47** showing decomposition of the imine cage.

In contrast to imines, amide bonds are chemically robust making post-functionalization possible. Figure 18 below shows the electronic properties of the different aromatic rings in amide cage **48** for conducting electrophilic aromatic substitution reactions. The aromatic ring in blue is deactivated to attack an electrophile due to the electron withdrawing nature of the carbonyl bonds but the triptycene rings in red are less deactivated for S_EAr reactions from the

41

(acyl protected) amino group on it. Nevertheless, the steric shielding offered by any substituent 'X' plays a major role in hindering S_EAr reactions on the aromatic ring marked in blue, and more so when 'X' is a bulky tert-butyl group (as it is in amide cage **48**), although the methoxy group has an activating effect for S_EAr reactions.
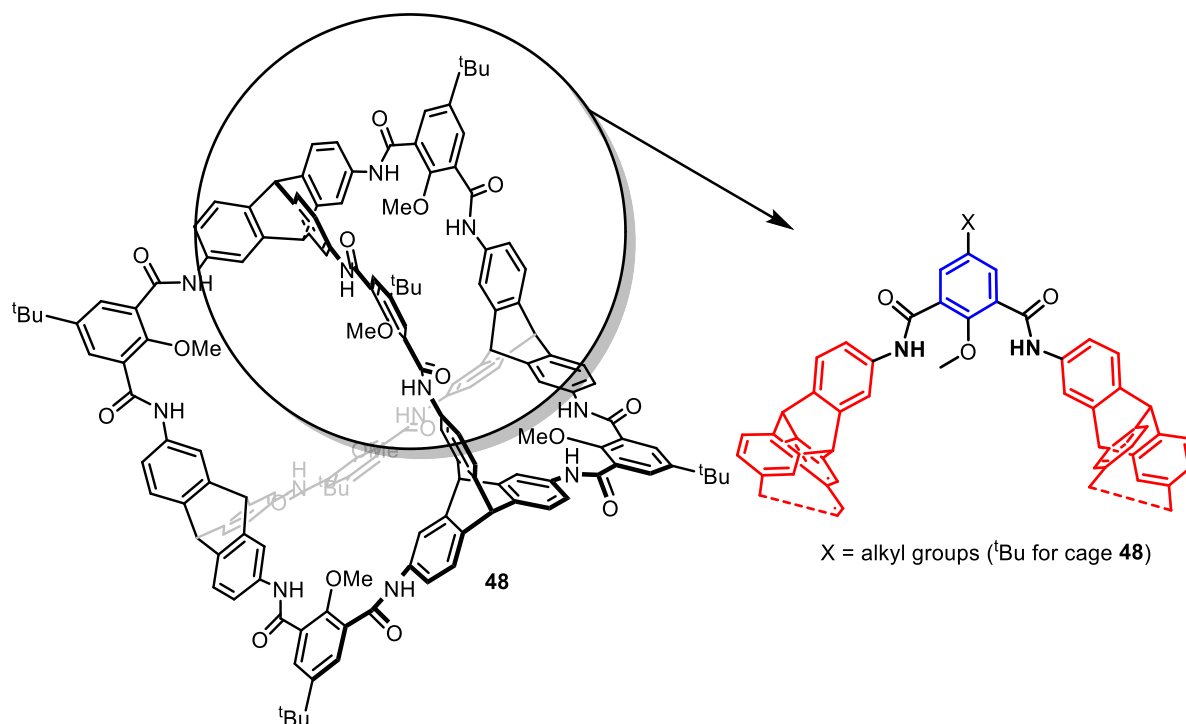
Figure 18. A unit of the [4+6] amide cage **48** showing the electronic properties of the aromatic rings. In blue: deactivated aromatic ring for S_EAr reactions; in red: less deactivated aromatic ring for S_EAr reactions.

1.3.1. Chemical stability of the [4+6] Salicylbisamide cage

Before conducting reactions on the amide cage, the chemical stability of the amide cage over a range of pH was investigated. While imines are known to undergo hydrolysis in acidic media (especially in mineral acids), these experiments emphasise on the chemical stability of amide bonds in harsh chemical environments. For this purpose, 5 mg of the amide cage compound **48** was stirred in different aqueous solutions of varying pH at room temperature for 16 hours. The solutions/suspensions were diluted with water, filtered, washed with water and dried under high vacuum. The amide cage was found to be stable in a pH range of -1 to 14.5. The results from Table 2 were followed by a comparison of the ^{1}H NMR spectra of all the resulting products after stirring in the aforementioned solutions of different pH. As seen in the NMR spectra (in Figure 19), the amide cage was seen to undergo a change only in concentrated sulphuric acid, whereas MALDI-TOF-MS analysis revealed sulphonation of the amide cage.

Table 2. Aqueous solutions of different pH in which the amide cage was stirred, remarks on any observable changes and the weight of sample after the experiment.

Solution	pH	Remarks	Wt. after test
Conc. H_2SO_4 (36 M)	-1.8	Changes observed [a)]	4.6 mg
4 M H_2SO_4	-0.9	No change	5.5 mg
2 M HCl	-0.3	No change	5.3 mg
Water	7	No change	5.5 mg
DMSO-d_6	-	No change	5 mg
3 M NaOH	14.5	No change	4.9 mg

a- The solution turned yellow while the rest were colourless. Also changes seen in ^{1}H NMR spectrum.
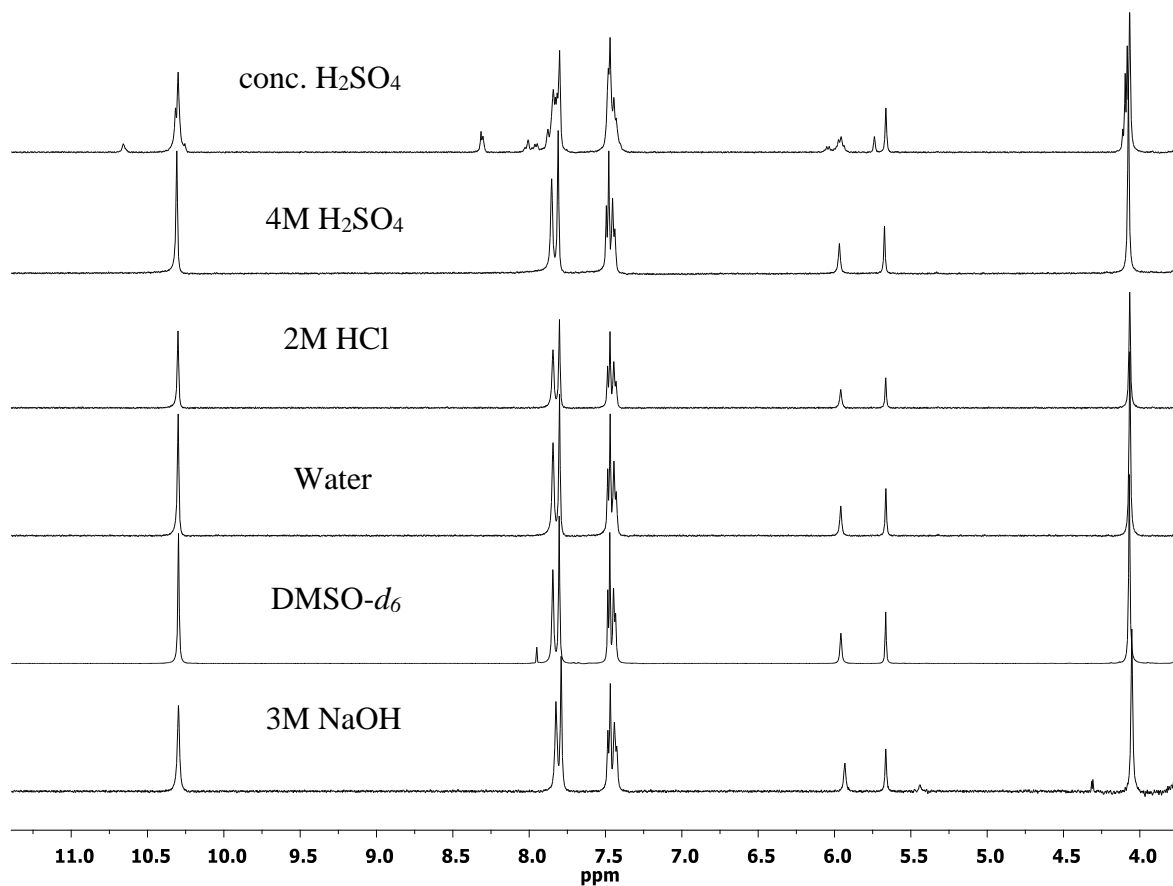
Figure 19. ^{1}H NMR spectra (500 MHz, DMSO-d$_6$) comparison of the chemical stability test of cage **48**.

1.3.2. Bromination followed by Suzuki coupling

Bromination of amide cage **48** was first attempted by a textbook method, by stirring the amide in pure bromine. The MALDI-MS of the resulting product showed peaks corresponding to

17,18,19 and 20-fold brominated species, but it was unclear the position at which the bromination could occur beyond the 12-fold reaction. Therefore, to brominate in a controlled manner, the milder electrophilic bromine source NBS method was utilized (as shown in Scheme 32).[123]
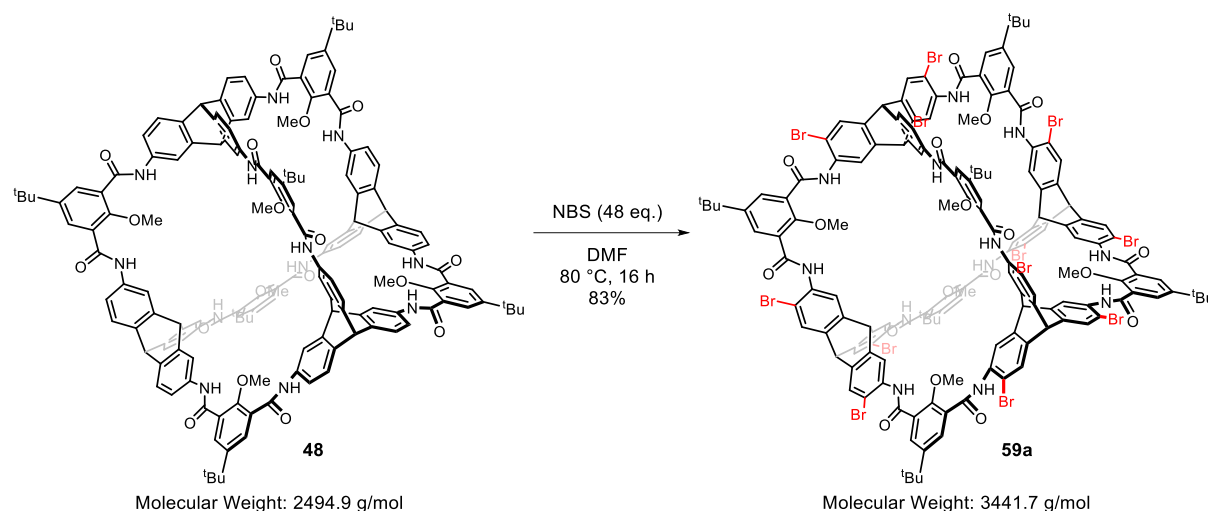
Scheme 32. Bromination of amide cage **48** using NBS-DMF to get brominated amide cage **59a**.

A brief screening experiment by varying the reaction temperature, the amount of NBS used and the concentration of the reaction mixture, revealed the right conditions to achieve a 12-fold bromination. Using 4 equivalents of NBS per reactive centre (12 reactive centres) and a temperature of 80 °C, the reaction reached completion to afford the brominated amide cage **59a** in a yield of 83%.

Formation of the brominated amide cage was detected by MALDI-MS, where a peak corresponding to **59a** was observed as the [M]$^+$ peak at m/z = 3438 (Calc. MW = 3441.7, Scheme 32). Further confirmation of the structure was realized by NMR spectra, with three singlets observed for the aromatic protons on the triptycene moiety (as seen in Figure 20). The peak corresponding to the amide protons shifted from δ = 10.30 ppm for the parent amide cage **48** to δ = 10.20 ppm for the brominated cage showing a change in the chemical environment around the amide group. The change in polarity of the amide bonds is relevant for adsorption of polar gases such as CO_2 (discussed in a later section).
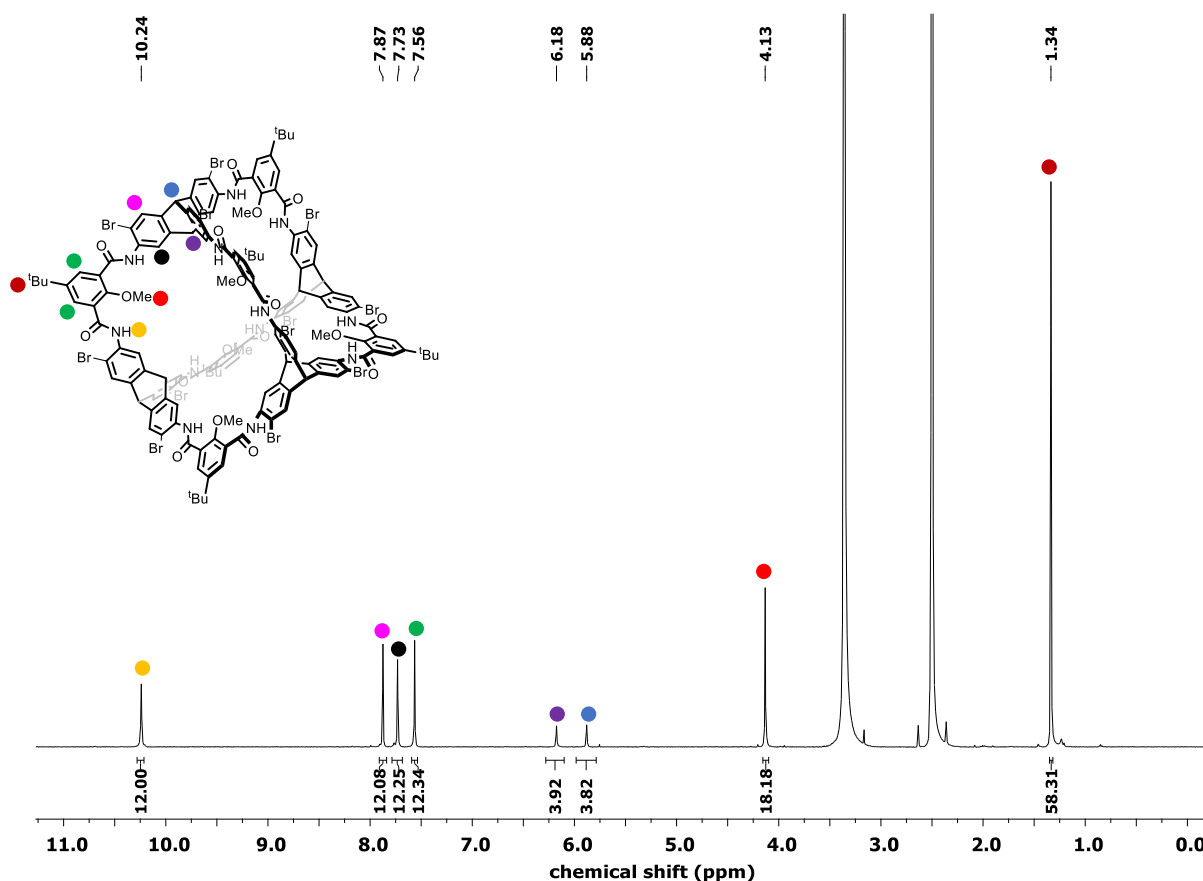
Figure 20. ^{1}H NMR spectrum (500 MHz, DMSO-d$_6$) of brominated amide cage **59a** with the assignment of the protons with the help of 2D NMR spectra.

The resulting product exhibits poor solubility in most solvents except in polar solvents such as DMF and DMSO (only under heating). It was also possible to grow crystals of cage **59a** by gradually cooling down a hot saturated solution in DMSO, however, a crystal structure proved impossible to resolve.

Following the bromination of the amide cage **48**, it was demonstrated that a subsequent Suzuki coupling reaction was possible. The Suzuki coupling was initially done with boronic acid A (Scheme 33) using Pd$_2$ (dba)$_3$ as a catalyst (4 mol%) and ^{t}Bu$_3$PHBF$_4$ as the active ligand (25 mol%) in THF to furnish the cage compound **59b** in a yield of 56%. A second analogue (cage **59c**) was also prepared by coupling boronic acid B, which can be readily functionalized by amide coupling. Although the yield of coupling reactions range between 40-56%, it accounts to around 94% per coupling (12-fold coupling). Saponification of the ester bonds in **59c** could be achieved with a 3M solution of NaOH, wherein an amide cage decorated with carboxylic acid groups at its exterior could be detected by a peak at $\delta = 12.9$ ppm (in the ^{1}H NMR spectrum). However, neither cage **59c** nor the following carboxylic acid containing cage compound was not isolated in large enough amounts for complete characterization.
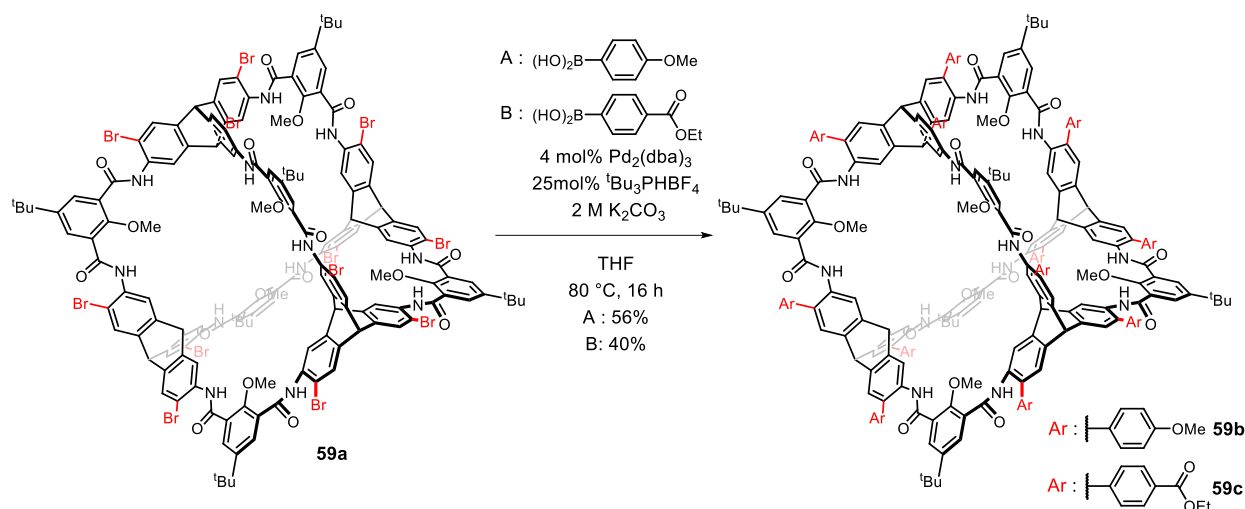
Scheme 33. Suzuki-Miyaura coupling with the brominated amide cage **59a**.

1.3.3. Nitration

Similar to bromination, the triptycene rings were also nitrated. Nitration was initially attempted with 66-68% conc. nitric acid which led to no change in the starting material. Although an undesired result, this further highlights the chemical stability of amide cage **48**. Stronger nitration condition of using fuming nitric acid or KNO_3 in TFA were utilized (as shown in Scheme 34). Although both furnish the 12-fold nitrated product, KNO_3 in TFA offers better reaction control as the nitrating reagents can be measured more effectively by weight, which is important as further nitration was observed as the by-product.
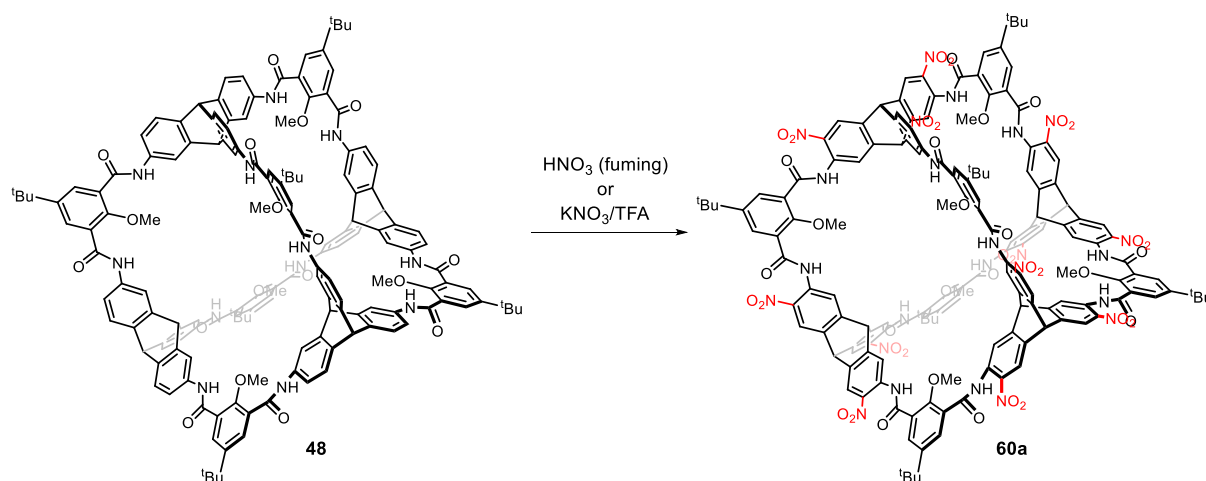
Scheme 34. Nitration of amide cage **48**.

In an effort to optimise this process the equivalency of KNO_3 was examined, principally at 36 eq and secondly in a very large excess. It became apparent from the ^{1}H NMR spectrum that an excess of KNO_3 led to over-nitration of the cage, from the chemical shift of the amide signal

(10.7 ppm to 11.0 ppm) (as shown in Figure 21). On comparing this to the ^{1}H NMR spectrum of the reaction conducted with 36 eq. of KNO$_3$, it was evident that although the over-nitration is suppressed at 36 eq. it is still present. Therefore, the amount of KNO$_3$ was reduced to 24 eq. and the reaction monitored over time by UPLC (as shown in Figure 22).
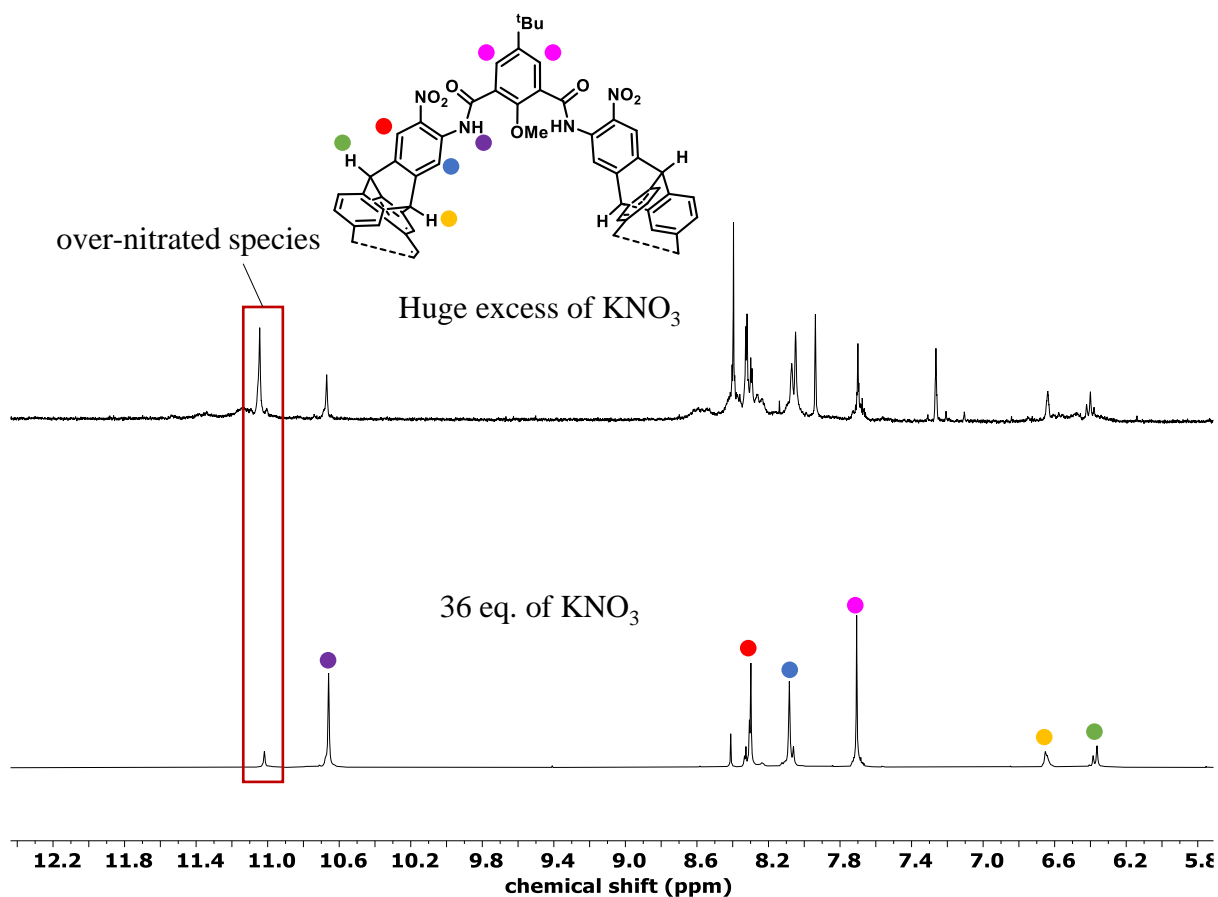

Figure 21. ^{1}H NMR (500 MHz, DMSO-d$_6$) comparison to determine if the extra peak at 11.1 ppm is from an over-nitrated species.

In Figure 22, the peak marked by a blue dashed line (at 5.65 min) corresponds to the 12-fold nitrated product and the peak at the right-end of the trace (marked by a red dashed line) at 5.75 min corresponds to the starting material, which were later confirmed with reference material. Moreover, the cluster of peaks between these two peaks increases as the starting material is consumed (0 to 20 min), then subsequently decrease when the product is formed (20 to 60 min), possibly correspond with unsymmetrically nitrated cage isomers en-route to the symmetrical 12-fold product. Later, new peaks appear at lower retention times (1 h to 5 h) marked by a green dashed line, which likely corresponds to over-nitrated species. These peaks increase in relative intensity on stirring the reaction mixture for 16 hours.

47
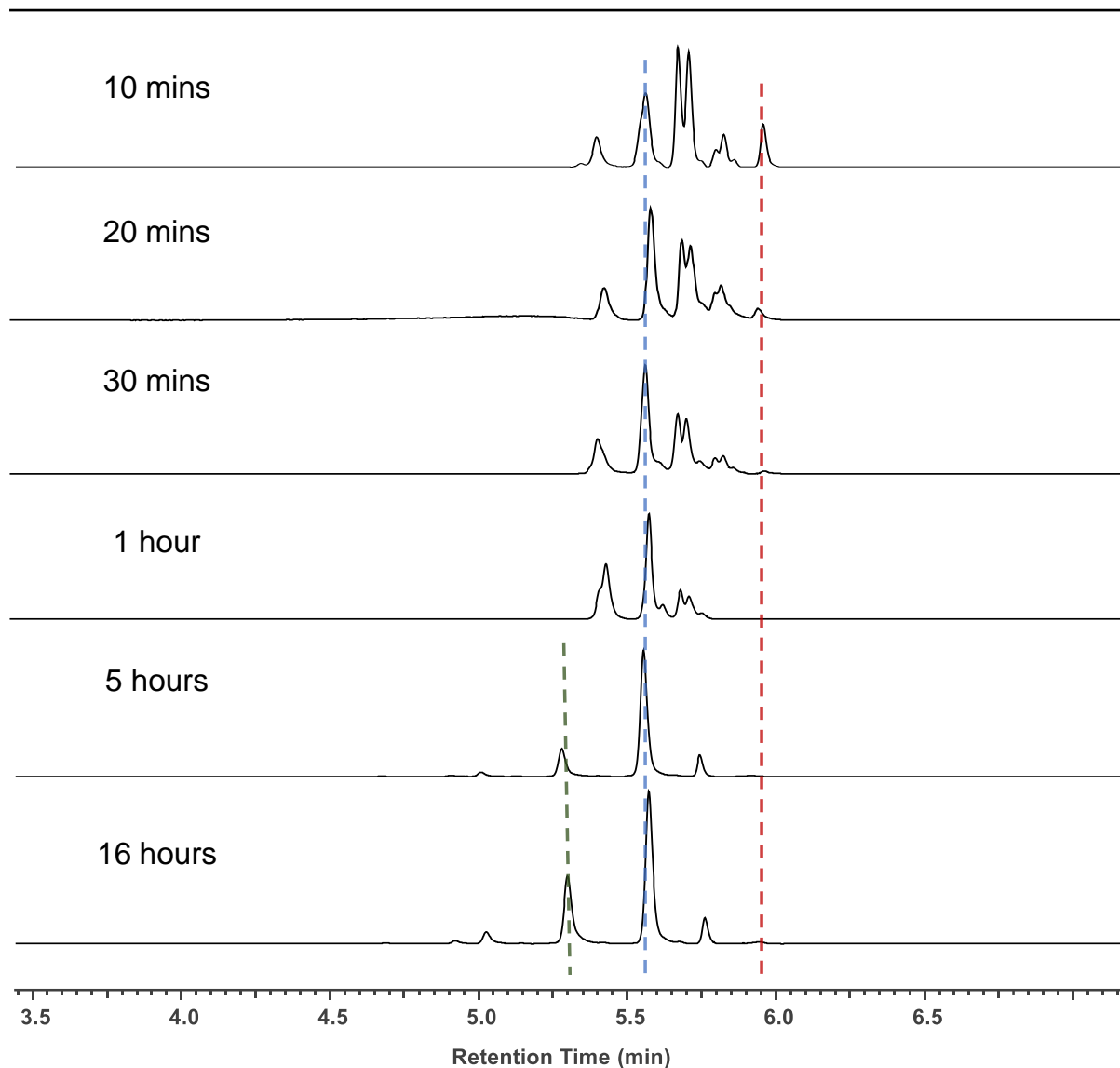
Figure 22. UPLC (C-18 column, MeCN:water gradient, 0.6 mL/min) traces monitoring the nitration reaction (as shown in Scheme 34) by time.

It was inferred from the reaction screening that the reaction was complete between 1-5 hours and further equivalents of KNO_3 only proceeded to deliver over-nitration. Therefore, a further decrease in KNO_3 equivalency (14 eq) and a shorter reaction time of 3 h was chosen as the optimised conditions, delivering cage **60a** with a yield of 84% (as shown in Scheme 35).
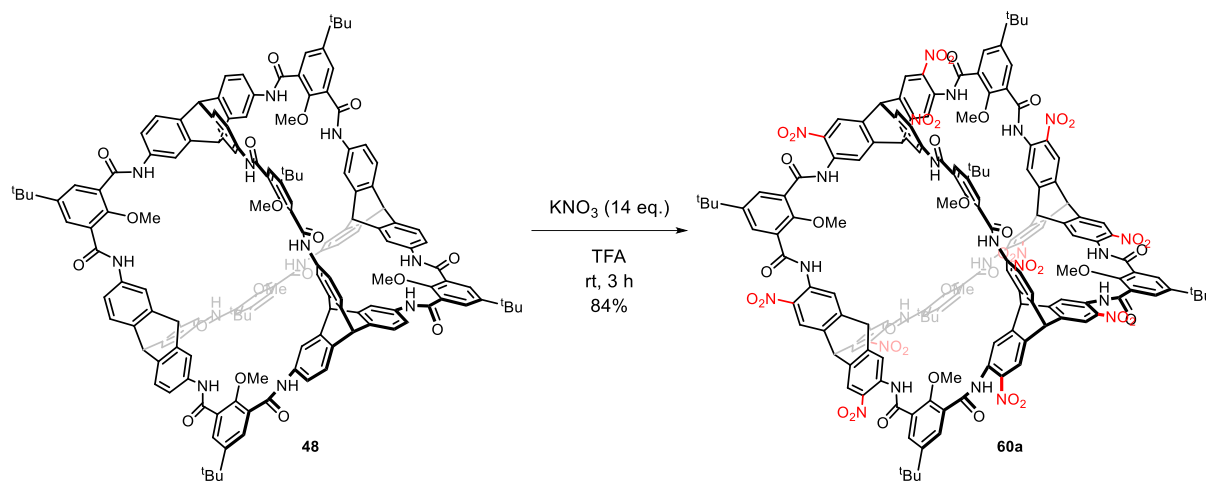
Scheme 35. Optimized reaction conditions to obtain the nitrated amide cage **60a**.

Following nitration, the selective nitro-reduction was attempted, anticipating that a subsequent in-situ, ring-closure would generate the desired benzimidazole structure **60b** (as shown in Scheme 36) as had been reported in similar structures.[124]
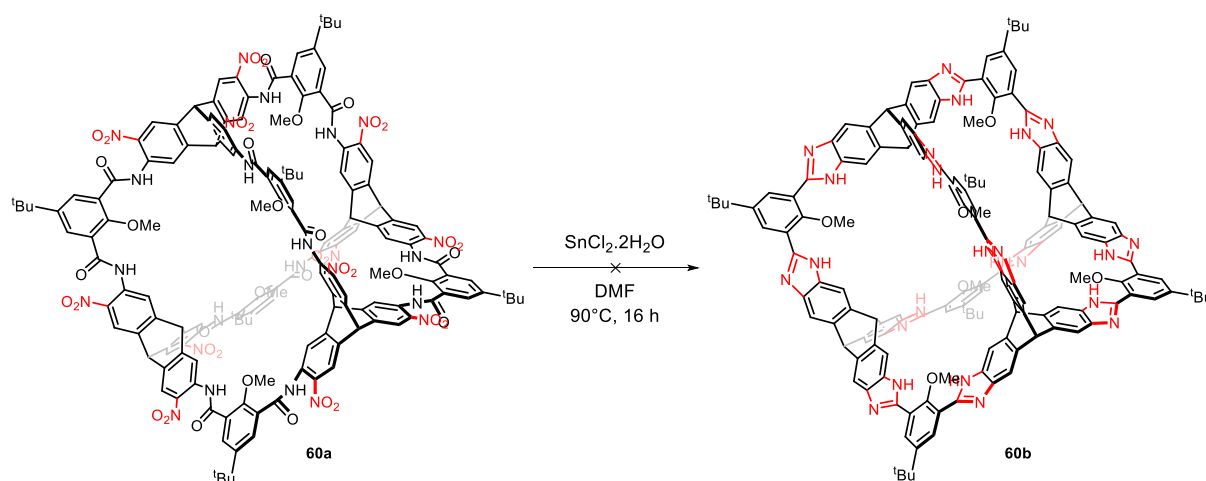
Scheme 36. Attempted synthesis of the benzimidazole-based cage **60b**.

However, under standard reduction conditions no product could be identified by MALDI-MS of the crude reaction mixture. Monitoring the reaction by ^{1}H NMR proved ineffective since partial reduction/ partial ring closure results in a highly unsymmetrical cage molecule. On attempting different reduction conditions, namely, $SnCl_2$ in HCl and Pd/C with hydrogen, neither the 12-fold amino substituted cage compound nor the benzimidazole-based cage compound could be detected. After attempts at isolating the resulting products by HPLC (C18 column, 10% H_2O in MeCN, 20 ml/min) followed by ^{1}H NMR analysis, no clear conclusions could be made whether the failure of this reaction was due to incomplete reduction of the nitro groups or due to the failure of the ring-closure step. Lastly, it could also be hypothesized that

the closure of the benzimidazole rings exerts a very strong bending strain on the structure of the cage compound, which could be a reason for the failure of this reaction.

1.3.4. Demethylation of the methoxy groups inside the cavity

As shown by Mastalerz and co-workers in 2013, post-modification of the interior of the cage molecule influences the gas sorption properties of the [4+6] salicylbisimine cages.[120] The methoxy groups inside the cavity of the [4+6] amide cage **48** were unprotected phenolic moieties. This would result in a cage molecule decorated with a hydrophobic exterior (with tert-butyl groups and aromatic rings on the edges) and a hydrophilic interior with 6 -OH groups and 12 amide groups (-NH and C=O groups in an alternate manner) pointing towards the cavity of the cage molecule. The deprotection was realized using AlCl$_3$ as a Lewis acid generating methyl chloride and an aluminium-phenol adduct as by-products. The desired phenol group was achieved by quenching the reaction with HCl, facilitating the protonation of the phenol-Al adduct (as shown in Scheme 37). However, incomplete protonation of the phenolic groups could result in the aluminium adducts as impurities.
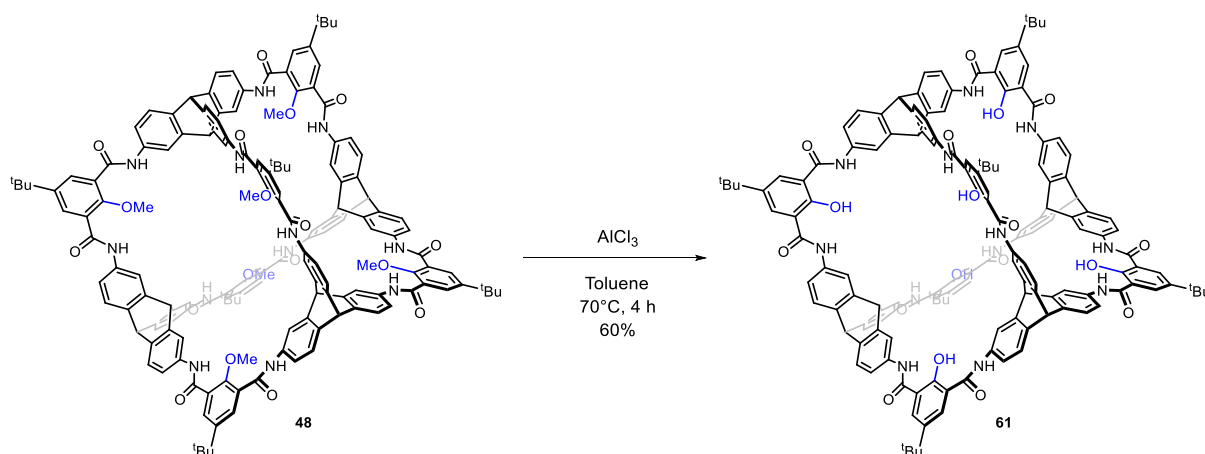
Scheme 37. Demethylation of the methoxy groups inside the cavity to obtain the [4+6] amide cage **61**.

Formation of cage **61** was confirmed by ^{1}H NMR with the absence of the methoxy peak at $\delta = 4.07$ ppm and the appearance of a peak at $\delta = 14.13$ ppm corresponding to the phenol hydrogen (as seen in Figure 23).
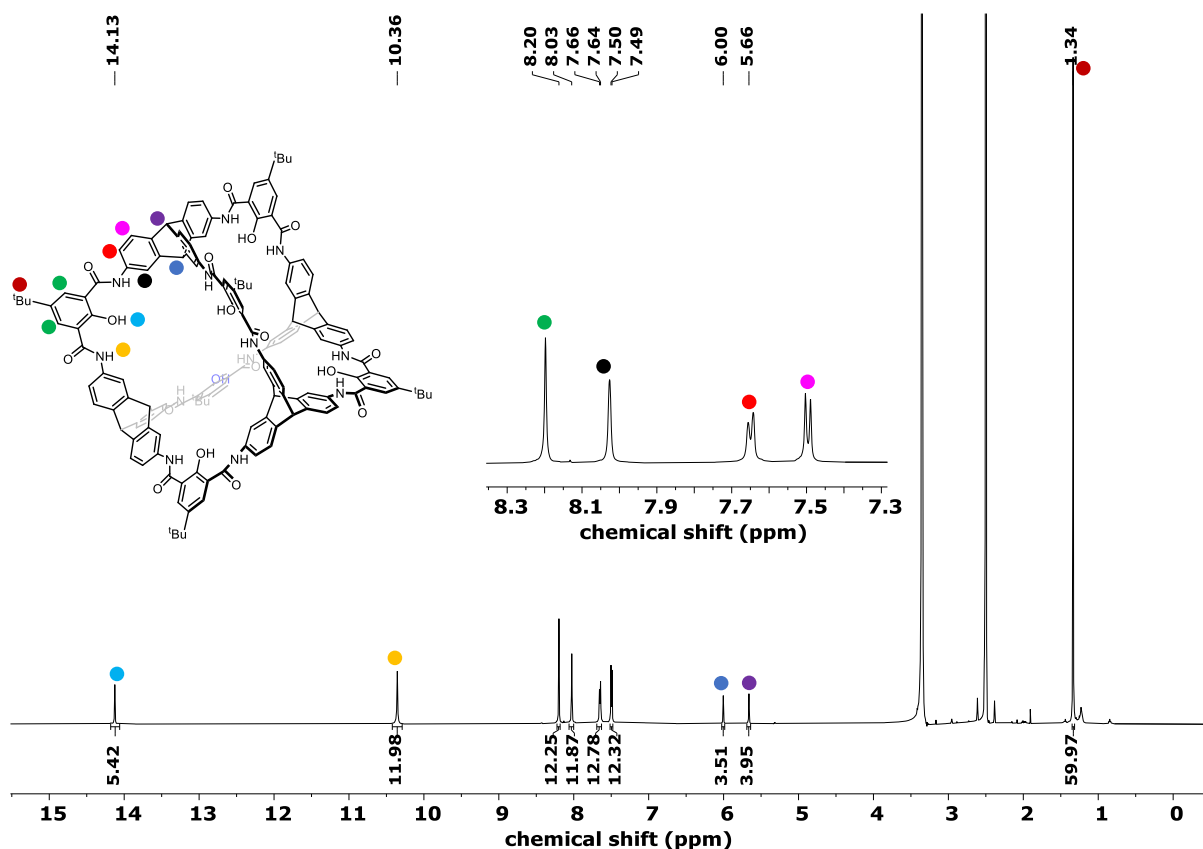
Figure 23. ^{1}H NMR spectrum (500 MHz, DMSO-d$_6$) of amide cage (-OH) **61** with the assignment of the protons with the help of 2D NMR spectra.

Cage **61** could be isolated in a yield of only 60% due to the harsh reaction conditions used. There was no indication of cleavage of tert-butyl groups (by MALDI-MS analysis) during this reaction, although using AlCl$_3$ to remove tert-butyl groups is a commonly used strategy (for example in calixarene chemistry).[125] The resulting product was observed to be brown in colour although small molecules with a similar structure was reported to be colourless.[126] The reason for the brown colour was unclear, although the presence of aluminium adduct impurity could be one of the possibilities but however, this could not be evidenced by MALDI-MS. Despite ^{1}H and ^{13}C NMR experiments exhibited no impurities, the crude product was passed through a Celite pad and an SEC column (using CHCl$_3$), albeit with the brown colouration persisting, and therefore being used for further studies without further purification. A noteworthy observation was that the demethylated amide cage **61** is soluble in non-polar solvents like chloroform and DCM while amide cage **48** was only soluble in highly polar solvents like DMF and DMSO. Final confirmation of cage **61** was achieved by growing crystals from a solution of the cage compound in THF and water (Figure 24).
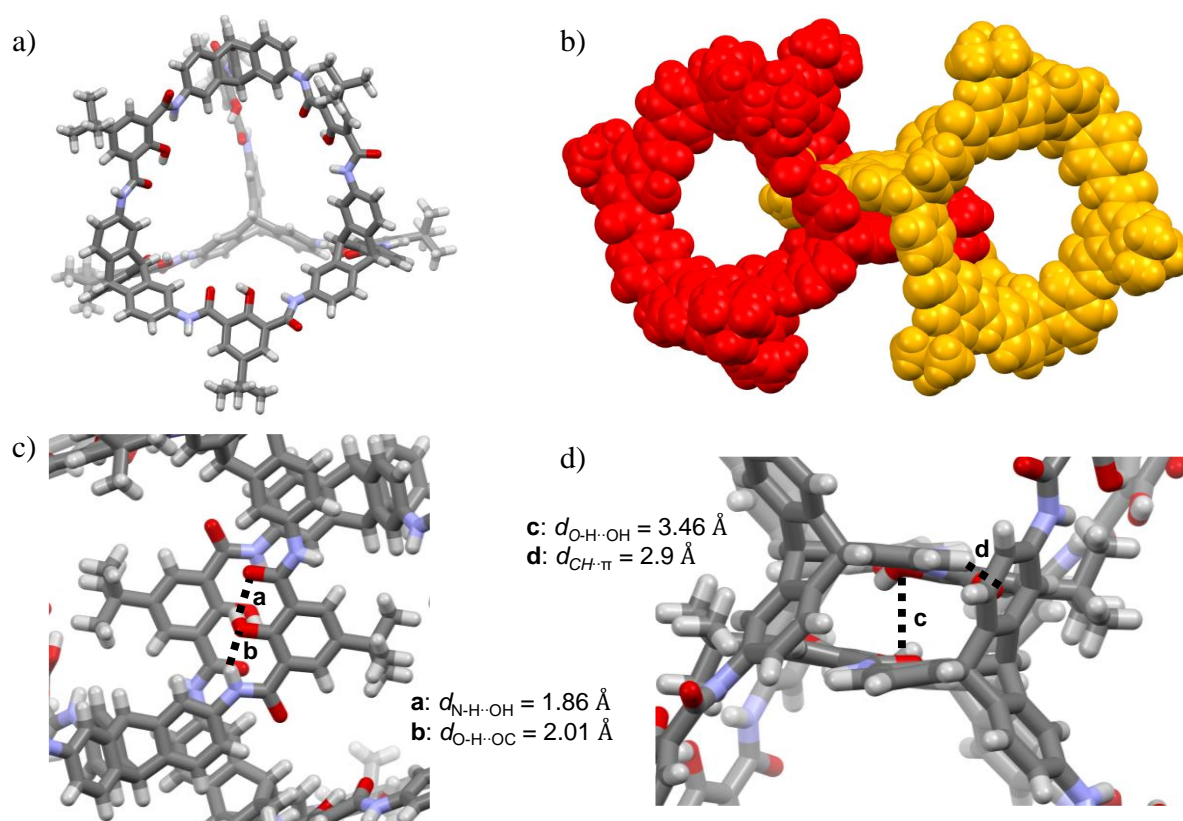
Figure 24. a) Single crystal structure of amide cage **61**; b) space-filled structure showing the packing of two molecules of amide cage **61** in a unit cell; c and d) zoomed image at the point of contact of two molecules of **61** in the unit cell showing only intra-molecular hydrogen bonding and CH-π interactions. Colours: carbon: gray; Nitrogen: blue; Oxygen: red; Hydrogen: white.

No inter-molecular hydrogen bonding is observed in the crystal packing (with a bond distance of 3.46 Å between the OH groups of the two salicylbisamide rings, Figure 24d) of cage **61** despite an overlap of the salicylbisamide rings of two molecules in the unit cell (as seen in Figure 24). Only intra-molecular hydrogen bonding between the amide groups and the neighbouring hydroxy group in a -N-H···O-H···O=C manner is observed with bond distances of 1.86 Å (N-H···O-H) and 2.01 Å (O-H···O=C). The triptycene rings are close enough to form CH-π interactions (2.9 Å) as shown in Figure 24d. Lastly, non-covalent dispersion interactions are noticed to be present between the tert-butyl groups and the aromatic rings of the triptycenes with distances ranging from 2 to 3 Å. Such dispersion interactions occurring with tert-butyl groups has been extensively studied by Schreiner et al.[127]

1.4. Gas sorption studies with the [4+6] Salicylbisamide cages

The gas sorption properties of four amide cages (**48**, **59a**, **60a** and **61**) with varying substituents were investigated (Figure 25). Refer to appendix section 5.0 for a theoretical background on the adsorption of gases by porous materials.
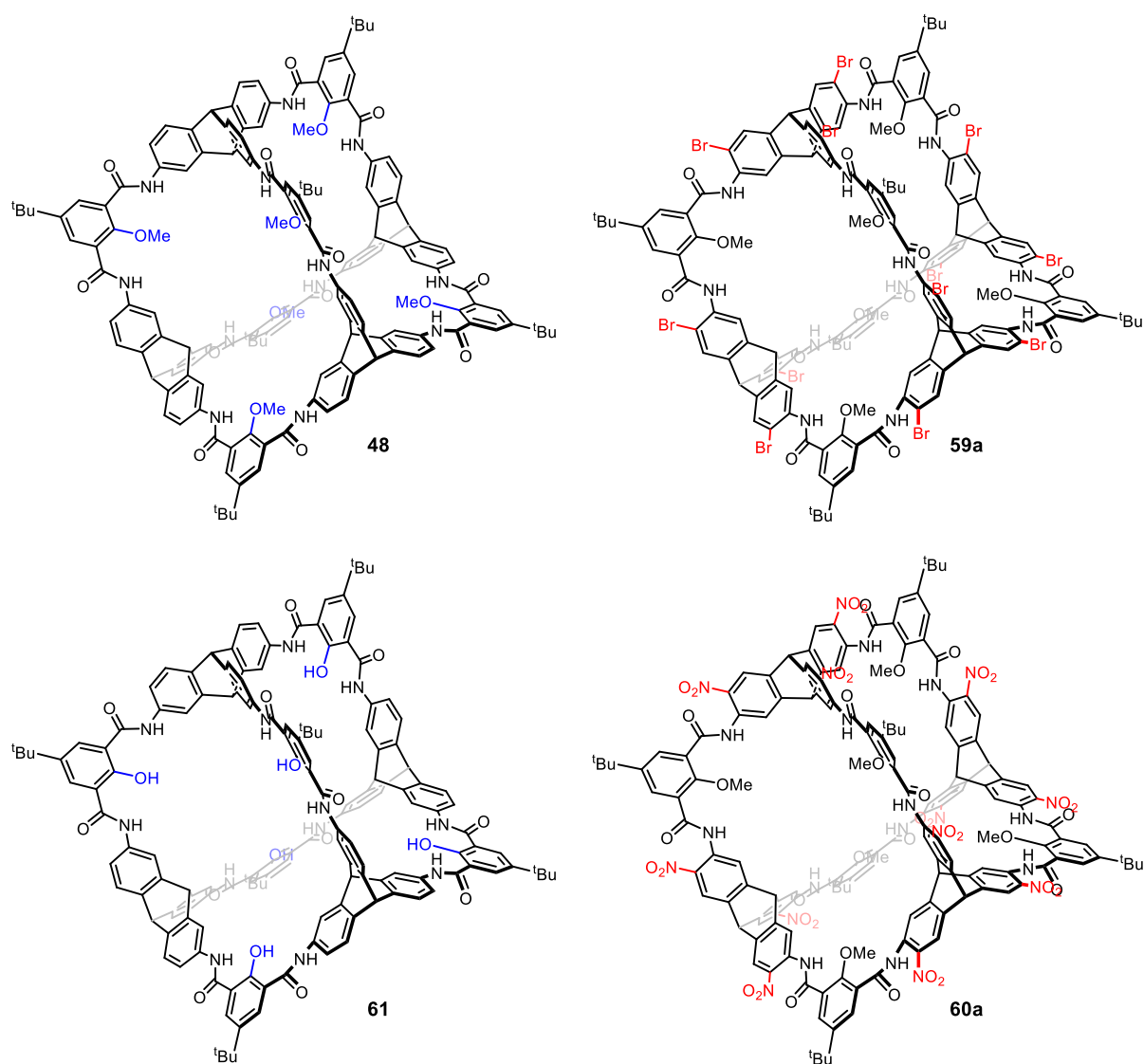
Figure 25. The four cage compounds that are investigated by gas sorption.

1.4.1. Nitrogen gas adsorption of the amide cages

Cage compounds have intrinsic porosity at the molecular level but the accessible pores for gases is mainly determined by the solid-state packing of the cage molecules. The [4+6] salicylbisimine cage **24** has the second highest specific surface area for imine cages recorded to date.[29b] The most obvious method to transform such an imine cage into a chemically robust structure is to reduce the imine bonds to amine bonds, which when realized exhibited a collapse of structure in solid-state and hence loss of porosity.[43b] However, transformation of imine bonds to amide bonds is not expected to have the same effect since amide bonds are not as flexible as amine bonds. This retention of shape-persistence plays a major role in both intrinsic and extrinsic porosity of the cage compounds since it provides porous channels for gases

through the internal cavity of the cage, as well as allowing a uniform crystal packing of cage molecules to form extrinsic pores.

To investigate the porosity of cage compounds **48**, **59a**, **60a** and **61**, the activated porous material was prepared by firstly triturating with DMF/MeOH and washing with diethyl ether, followed by pore activation under high vacuum at 150°C. Since X-ray powder diffraction analysis proved ambiguous in inferring the crystallinity of the cage compounds, these samples were studied under SEM (as shown in Figure 26). Amide cage (-OMe) **48** shows a mixture of crystalline and amorphous particles while the nitrated amide cage **60a** contains larger particles with well-defined edges suggesting a smooth homogeneous surface but the bulk appeared to have a more amorphous nature. Furthermore, TGA analysis of the four amide cages proved that there were no trapped solvent molecules and all amide cages also exhibited excellent thermal stability wherein no change was observed up to a temperature of 370°C.
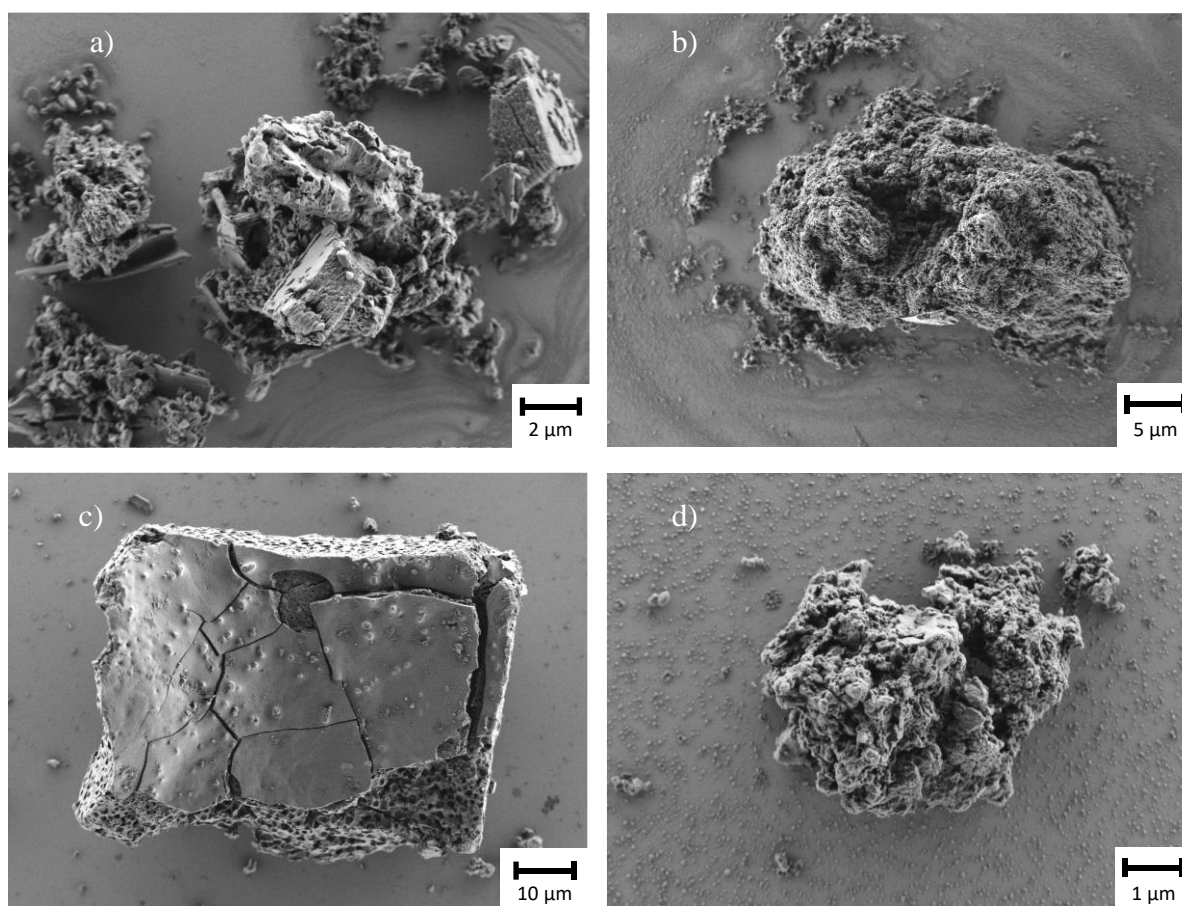
Figure 26. SEM micrographs of: a) amide cage (-OMe) **48**; b) brominated amide cage **59a**; c) nitrated amide cage **60a**; d) amide cage (-OH) **61**. Measured by Dr. Wen-Shan Zhang (BioQuant, Heidelberg University).

The nitrogen sorption isotherms at 77K for all amide cages follow a type I isotherm indicating a microporous material.[128] Table 3 summarizes the values of the specific surface area (S_A),

pore diameter and pore volume obtained for four amide cages in this study in comparison to the reported values of corresponding imine cage (-OH) **24** and imine cage (-OMe) **47** (Note: the gas sorption of imine cages **24** and **47** were reported for both amorphous and crystalline materials but only the values for the amorphous material is considered for comparison since none of the activated amide cage materials displayed perfectly crystalline character).

Table 3. The specific surface area, pore diameter and pore volume of the amide cages in comparison to the previously reported imine cages obtained from Nitrogen sorption at 77K.

Cage compound	S_A (BET) (in m^2/g)	Pore size distribution (in Å) [b]	Pore volume (in cm^3/g)
Amide cage (-OMe) **48**	275	15.2	0.17
Amide cage (-OH) **61**	398	14.5, 22.7	0.31
Brominated amide cage **59a**	102	23.5	0.12
Nitrated amide cage **60a**	288	15.0	0.16
Imine cage (-OH) **24** [a]	1377	5, 11 *	0.6
Imine cage (-OMe) **47** [a]	824	5.5, 7.8, 11.7 *	0.43

a – data reported for the amorphous material[29b, 120]; b - calculated by QSDFT, using the kernel: N_2 on carbon at 77 K (cylindrical pores, equilibrium model); The asterisk symbols denotes the pore size distribution calculated by NLDFT method.

The most recognizable observation from Table 3 is that the specific surface area of the amide cages calculated according to the BET model shows a significant decrease in value compared to the imine cages. The same observation was made by Yaghi et al. when imine-based COFs were converted to amide-based COFs via the Pinnick oxidation.[95] The pore sizes of all the amide cages are consistently larger compared to the imine cages **24** and **47**. It is safe to assume that a higher number of smaller pores provides a larger surface for adsorption of gases compared to lower number of bigger pores. However, it is noteworthy that the pore sizes of amide cages **48** and **60a** are predominantly in the range of the internal diameter of the cage cavity while the brominated cage **59a** only has pore sizes greater than 20 Å suggesting that gases are not able to access the internal pore of the cage. On the other hand, amide cage (-OH) **61** exhibits pores of 14.5 Å (size of the internal cavity) and also larger pores of around 23, 33

and 62 Å suggesting that the accessible pores for the gases is dominated by the external pores rather than by the internal cavity of the cage compound.

The amide cage (-OH) **61** has a higher surface area compared to amide cage (-OMe) **48**, which is the same trend observed with the imine cages before and after post-modification of the interior cavity. In conclusion, introduction of nitro groups on the triptycene rings barely changed the surface area of the amide cage (cage **60a** in Table 3) while the introduction of a bromo group (cage **59a**) at the same position seemed to significantly decrease the surface area of the amide cage. The nitrogen sorption isotherms and pore size distribution of the four amide cages are shown below in Figure 27.
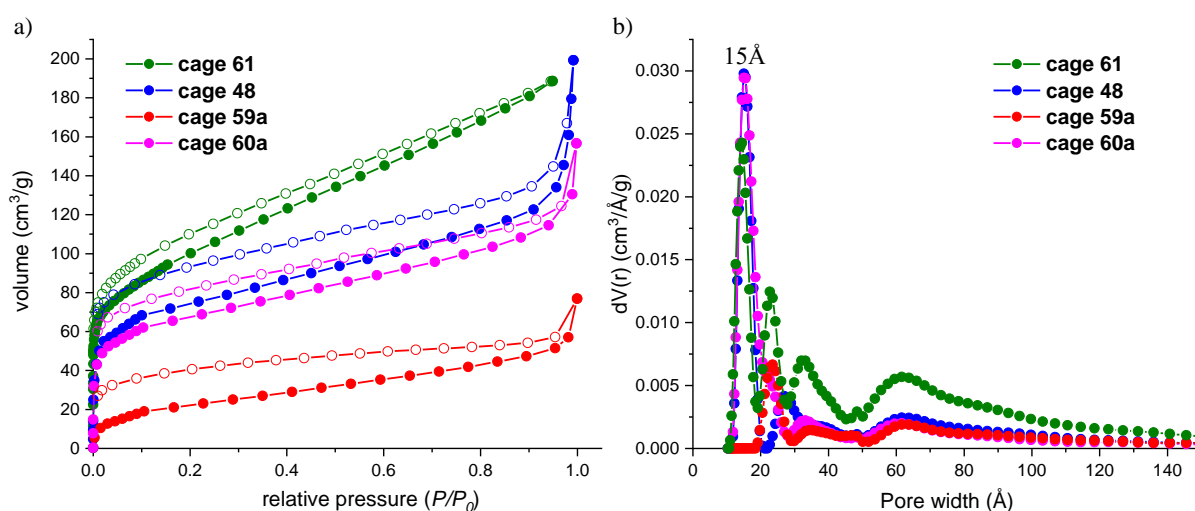
Figure 27. a) Nitrogen adsorption (in solid circles) and desorption (in hollow circles) isotherm; b) pore size distribution (QSDFT) plot. Blue circles correspond to amide cage (-OMe) **48**, green circles correspond to amide cage (-OH) **61**, red circles correspond to brominated amide cage **59a**, pink circles correspond to nitrated amide cage **60a**.

The significant reduction in specific surface area can either be attributed to the rotational degree of freedom or the fact that the crystallinity of the amide cages was partially lost while preparing the porous material, in particular, when the cage compound was triturated in DMF/MeOH. Therefore, crystals of the amide cage obtained from the crude material were treated directly with isopropanol, diethyl ether and n-hexane, and activated at room temperature under low pressure. The SEM images (in Figure 28a) of the resulting material now shows clear facets and smooth surfaces strongly indicating crystallinity which was obtained by the new activation method (in contrast Figure 26a only shows partial crystalline character of same cage compound treated by trituration). Pleasingly, the specific surface area increased to 370 m^2/g from 275 m^2/g (Table 3) with this method.
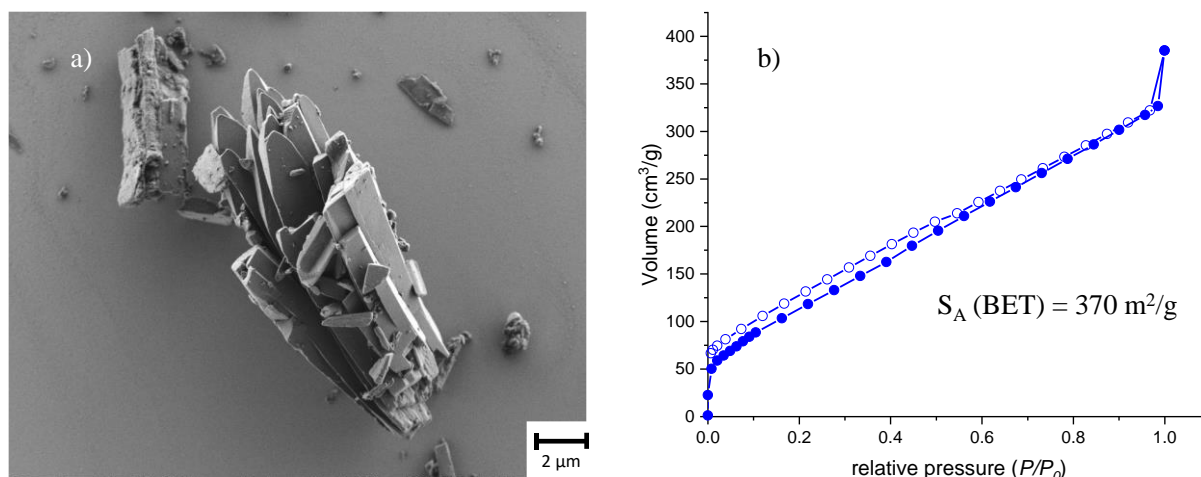
Figure 28. a) SEM image of the crystals of the amide cage (-OMe) **48** after the new activation method Measured by Dr. Wen-Shan Zhang (BioQuant, Heidelberg University); b) Nitrogen sorption isotherm at 77K with the crystals of the amide cage **48** as seen in the SEM image.

This follows the same trend as seen with the imine cage **24**, where the crystalline material was seen to have a much higher surface area compared to the amorphous material.

1.4.2. A comparative study of the uptake of CO_2 and CH_4

Structurally, the interior of cages **48**, **59a** and **60a** are very similar with the amide and -OMe groups orientated towards the cavity of the cage. However, there is a marked difference in electronic contribution from a NO_2, H or Br substituent which is evidenced by the shift of the CO stretching band in the IR spectrum. The brominated cage **59a** shows the peak at $\bar{v} = 1668$ cm^{-1}, the nitrated cage **60a** at $\bar{v} = 1678$ cm^{-1} while the parent amide cage **54** has the CO stretching band at $\bar{v} = 1655$ cm^{-1}. This is expected to affect the strength and polarity of the amide groups, which in turn could affect the adsorption of easily polarizable gases like CO_2. Furthermore, the amide cage (-OH) **61** has reduced steric influence and improved hydrogen bonding capability with an additional 6-hydroxy groups that may influence adsorption of polar gases.

On measuring the uptake of CO_2 and CH_4, it was found that all amide cage compounds adsorbed similar amounts of CO_2 and CH_4 at 273 K and 1 bar. The ratio (w/w) of CO_2 uptake to CH_4 uptake was around 10:1 for all the amide cages which was the same as that observed with the imine cage **24**.

Table 4. Henry selectivity and IAST selectivity of CO_2/CH_4 for the amide cages.

Compound	Henry selectivity CO_2/CH_4	CO_2/CH_4 (1:1) IAST-Selectivity at 0.1 bar	CO_2/CH_4 (1:1) IAST-Selectivity at 1 bar
Amide cage (-OMe) (**48**)	30	13	11
Brominated amide cage (**59a**)	38	12	10
Nitrated amide cage (**60a**)	28	13	11
Amide cage (-OH) (**61**)	17	8	7

The Henry selectivity of CO_2 over CH_4 for amide cage (-OMe) **48** was found to be 20.4 and the selectivity was seen to be slightly higher for the nitrated amide cage **60a** at 28.6 (Table 4). The amide cage (-OH) unfortunately did not show a higher selectivity for CO_2 over CH_4 in spite of the predicted improvement, and is in fact significantly lower at 14.4. This could be due to the self-complimentary arrangement of the amide bonds with the hydroxy group such that disruption to this by a CO_2 molecule is energetically disfavoured (see Figure 24c). The IAST selectivity assuming a hypothetical 1:1 mixture of CO_2 and CH_4 shows a similar trend as that of the Henry selectivity. Figure 29a shows that the IAST selectivity is higher at low pressures but shows a 10:1 selectivity at 1 bar pressure.
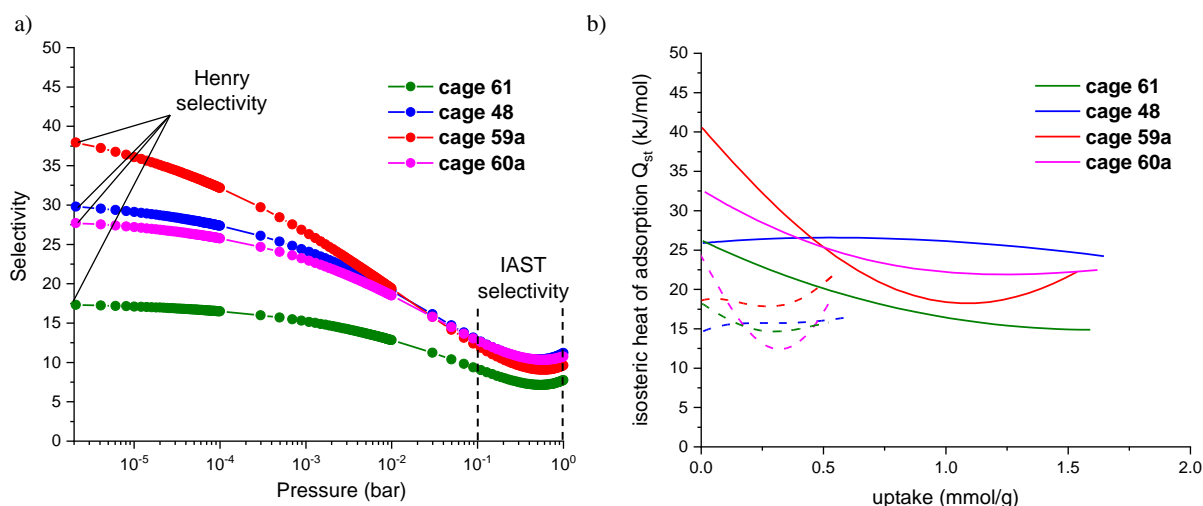
Figure 29. a) Pressure vs IAST-selectivity plot (CO_2, CH_4 1:1 mixture); b) Calculated heat of adsorption curves for CO_2 (solid lines) and CH_4 (dashed lines). Blue circles/line correspond to amide cage (-OMe) **48**, green circles/line correspond to amide cage (-OH) **61**, red circles/line correspond to brominated amide cage **59a**, orange circles/line correspond to nitrated amide cage **60a**.

Figure 29b shows the isosteric heats of adsorption curves for the four different amide cages. As expected, the heat of adsorption of CO_2 at a hypothetical zero loading of the gases is high

but gradually decreases with increasing uptake for amide cage (-OH) **61**, and nitrated amide cage **60a**, but the value remains almost the same for amide cage (-OMe) **48** with the uptake of CO_2. The curve seemed to vary quite erratically for the brominated cage **59a** due to a much lower R^2 value while fitting the CO_2 and CH_4 uptake isotherms with the virial equation (see section 5 in the appendix for more details).

Table 5 shows a comparative study of the isosteric heat of adsorption for the uptake of CO_2 and CH_4. Imine cage **24** with hydroxy groups inside the cavity of the cage was seen to have a very high $\Delta H_{ads} = 60$ kJ/mol at very low uptake volume but goes down to $\Delta H_{ads} = 25$ kJ/mol at higher uptake volumes.[120] Moreover, this imine cage **24** shows a larger difference in Q_{st} values between CO_2 and CH_4 which is highly beneficial for applications in selective uptake of CO_2. However, the same was not observed with the amide cage (-OH) **61**. Although the Q_{st} value is observed to decrease with increasing uptake of CO_2, the difference in Q_{st} values between CO_2 and CH_4 is not significant. This was unexpected since the conversion of imine bonds to amide bonds was expected to increase the polarity in the cavity of the cage, hence making it more selective for CO_2. Nevertheless, the nitrated amide cage **60a** shows an increase in Q_{st} value compared to the parent amide cage **48** at the hypothetical zero loading, which likely occurs from strong adsorbate-adsorbent interactions due to the dipole moment of the oxygen atoms (of the nitro group) and the quadrupole moment of CO_2. This observation is in agreement with a recent report where MOFs containing nitro groups showed a higher Q_{st} value compared to one without a nitro group.[129] However, the observation that amide cage (-OMe) **48** shows a higher difference in Q_{st} than the amide cage (OH) **61** could not be explained rationally, and therefore requires further investigation through repeated experiments.

Table 5. Table showing the value of the isosteric heat of adsorption of CO_2 and CH_4 with the amide cages.

Compound	Q_{st} (CO_2) at zero uptake (in kJ/mol)	Q_{st} (CH_4) at zero uptake (in kJ/mol)	Q_{st} (CO_2) at 0.5 mmol/g uptake (in kJ/mol)	Q_{st} (CH_4) at 0.5 mmol/g uptake (in kJ/mol)
Amide cage (-OMe) (**58**)	26	15	26	15
Nitrated amide cage (**63**)	33	24	23	19
Amide cage (-OH) (**65**)	26	18	20	16

1.5. Summary

The [4+6] salicylbisimine cage could be converted to a [4+6] salicylbisamide cage by a 12-fold Pinnick oxidation. This conversion was achieved in a yield of 21% (88% per imine bond). The purification of the amide cage **48** was optimized such that the cage compounds could be crystallized out of the crude mixture, therefore allowing the preparation of greater quantities of it. This allowed the post-functionalization of the amide cage by nitration, bromination and Suzuki coupling reactions which is the first in the field of organic cage compounds.
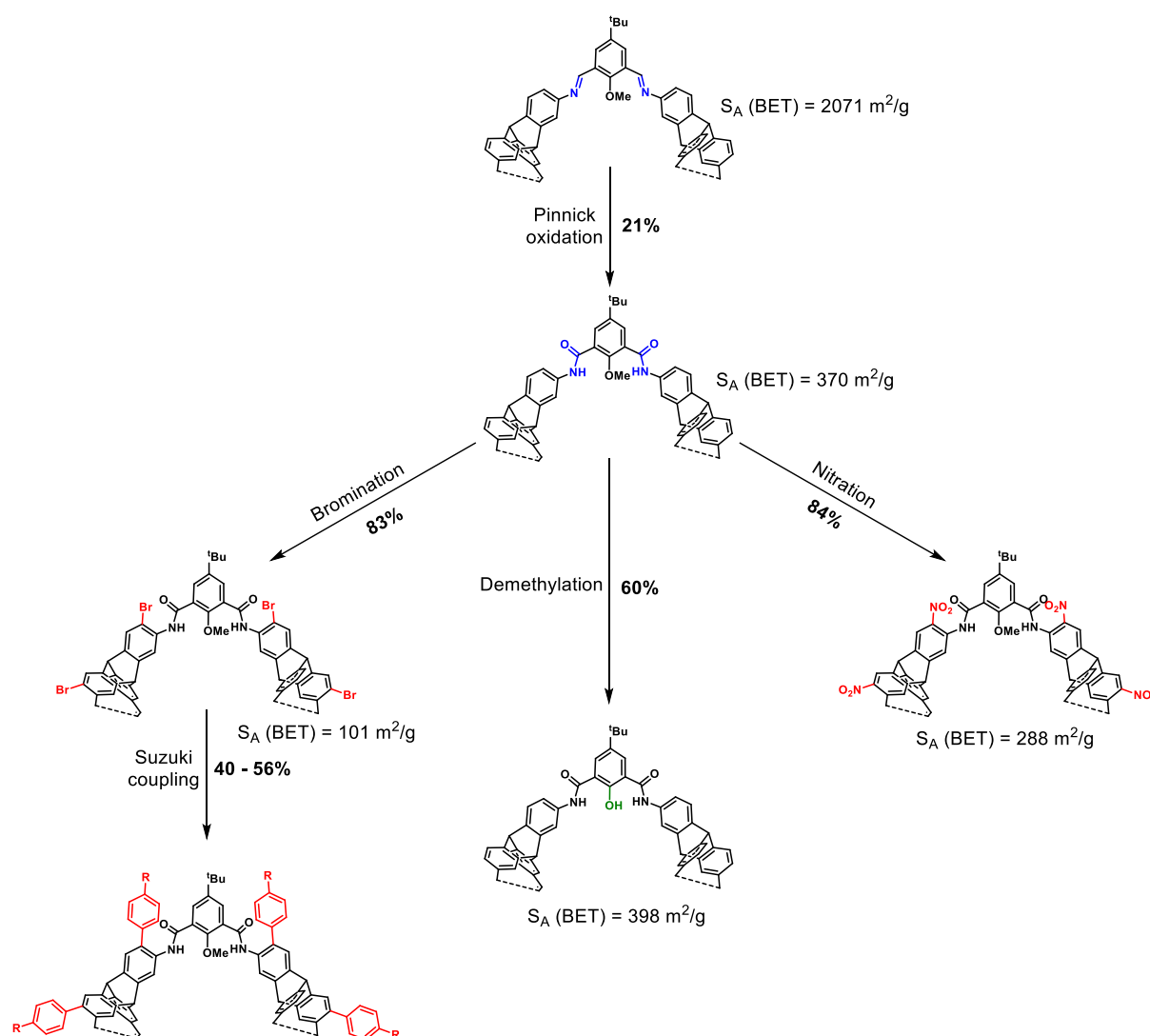
Scheme 38. Synthesis of the [4+6] amide cage followed by post-functionalization. All cage molecules are represented as partial structures, displaying the chemical transformations, yields and their respective specific surface areas.

It was found that the transformation of imine bonds to amide bonds via the Pinnick oxidation retained the shape-persistence of the cage compound, however leading to a decrease in the surface area for gas adsorption. Post-functionalization of the amide cage gave an opportunity

to make the first investigation of the influence of polar substituents on the gas sorption properties. Although there were small changes observed in the S_A (BET), there was no specific trend observed for the selective adsorption of CO_2 by any of the amide cages.

2. Scope and limitation of obtaining amide cages via the Pinnick oxidation

The use of Pinnick oxidation presents a superior method in comparison to direct amide bond forming reactions to access larger amide cages (as discussed in previous sections). However, the previous section presents just one example of applying this method, and hence requires a deeper investigation into its scope and limitations. Hence, this section consists of the preparation of a series of [2+3] imine cages made from easily accessible precursors, a brief study of their hydrolytic stability, followed by Pinnick oxidation on the series of imine cages.

2.1. Synthesis of a series of imine cage compounds

A small series of triamines and dialdehydes were targeted based upon those known to react and deliver [2+3] imine cages. Firstly, based upon the parent 1,3,5-tribenzylamine, three structures were targeted that would allow the influence of changes to the electronic structure of the core aryl ring to be examined (Triamines **A-C**) (as shown in Figure 30). Moreover, the structurally divergent tris(2-aminoethyl)amine (TREN) was tested to examine the reactivity of non-benzylic imines (Triamine **D**).
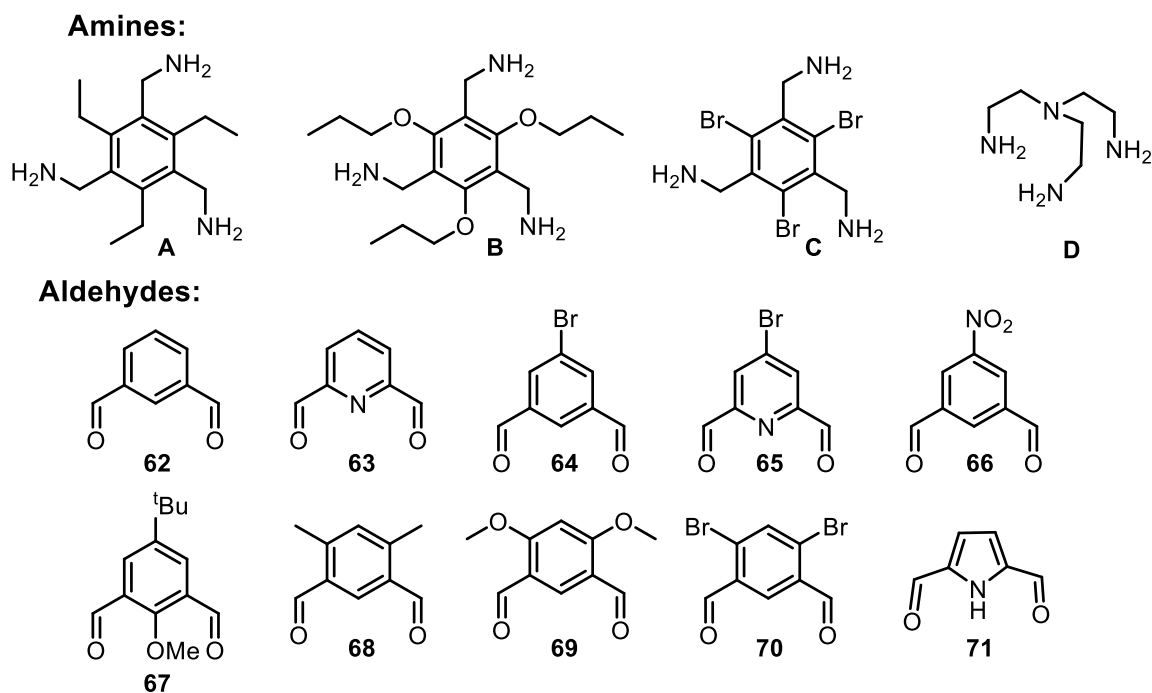
Figure 30. Chart of the different triamines **A-D** and dialdehydes **62-71** used to prepared a series of imine cages.

Secondly, a wide array of dialdehydes were prepared, with the aim of examining the electronic requirements of the position undergoing oxidation and the added effect on the solubility of the resulting imine cage (aldehydes **62-67**) (Figure 30). Secondary to this influence, the steric impact of substituents *ortho* to the reacting imine could also be examined (Aldehydes **68**-**70**).
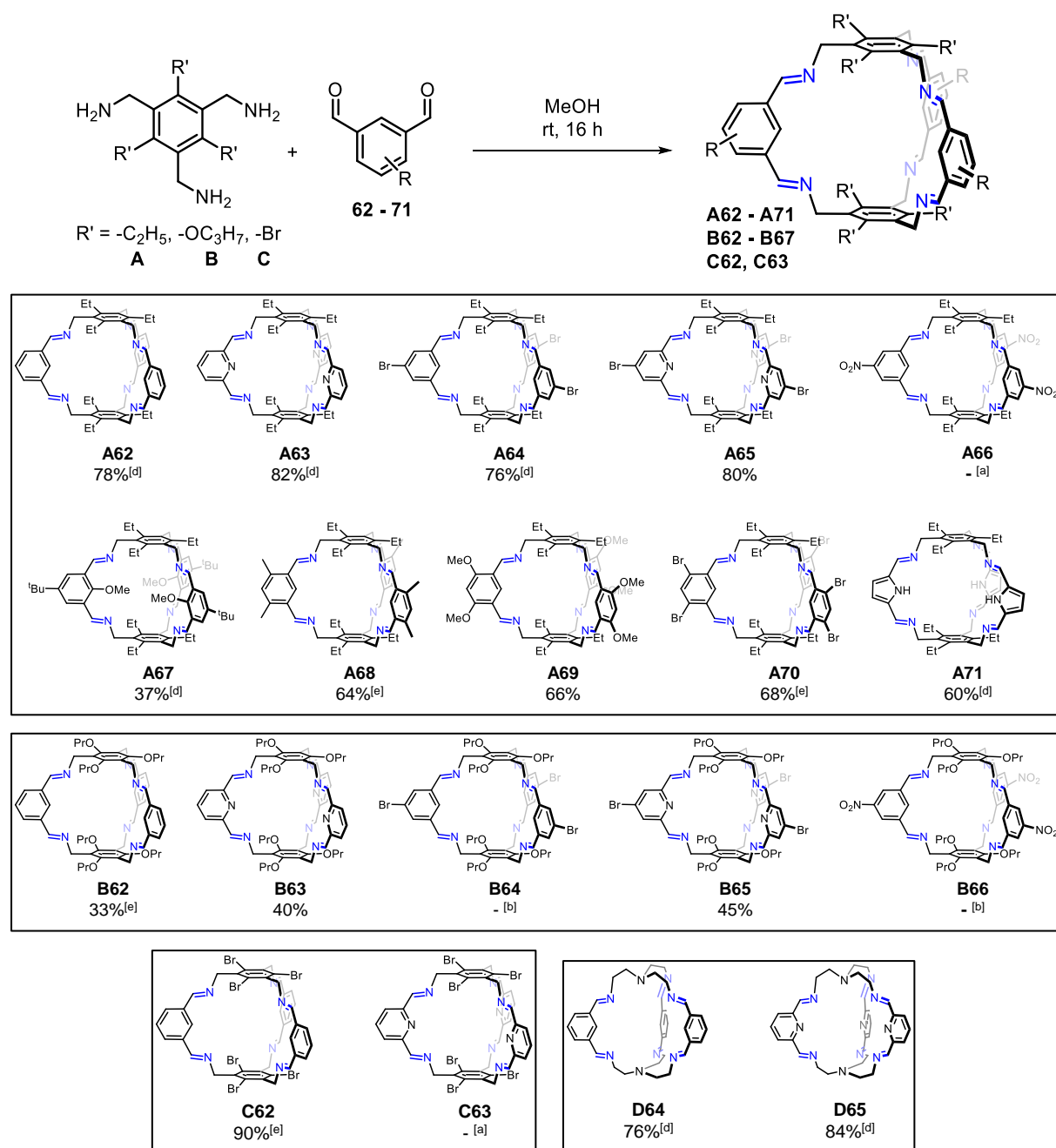
(a) imine cage was insoluble in most commonly used solvents, detected only by MALDI-MS; (b) imine cage was not stable enough for complete characterization (evidenced only by detection of imine cage by MALDI-MS and no clear peaks observed by ^{1}H NMR); (c) imine cage did not precipitate from the reaction mixture, hence required a different work-up; (d) literature known; (e) procedure obtained from colleagues (Tobias Schick, Jochen Lauer or Zishuo Zhou, Mastalerz group, Heidelberg University).

Scheme 39. Synthesis of a series of [2+3] imine cages.

The preparation of the imine cages required for this investigation was carried out using conditions as previously reported (Scheme 39). In particular, the reaction in which a nitro group was present upon the dialdehyde resulted in poor solubility, only being identified by MALDI-MS and therefore hindered their use in further oxidation experiments. Similarly, imine cages derived from triamine **C** also showed poor solubility rendering their use in further oxidation experiments futile.

Furthermore, a marked difference in isolated yield was noted between cages formed from triamine **A** and triamine **B**, the reason for which shall be discussed in the next section. A second general trend was noted in which dialdehydes substituted *meta-* delivered increased yields (>75%) over those substituted *ortho-* (<70%), perhaps highlighting a change in the equilibrium position of the imine formation due to steric encumbrance surrounding the aldehyde.

2.2. Hydrolytic stability of the [2+3] imine cages

Prior to commencing the investigation of the Pinnick oxidation it was considered prudent to first examine the stability of the imine cages. This is of particular importance because the Pinnick oxidation is carried out under mildly acidic, aqueous conditions, that would typically be associated with imine hydrolysis. The difference in stability between substituted imine cages was first noted in the workup in which some cages underwent a colour change or formed insoluble solids, likely due to decomposition. To further examine their stability under conditions relevant to the Pinnick oxidation, imine cages **A62**, **A63** and **B63** were chosen and submitted to various conditions and analysed by ^{1}H NMR.

^{1}H NMR of the imine cages **A62, A63** and **B63** was first recorded in THF-d_8, then in THF-d_8: $D_2O = 10:1$, and finally by addition of 1 eq. of CD_3COOD, in that order. This was done because Pinnick oxidation would be conducted in a THF/water mixture in an acidic environment. As seen in Figure 31, imine cage **A62** is stable in a THF/water mixture but addition of the acetic acid leads to the appearance of a peak at $\delta = 10.2$ ppm (possibly due to formation of an aldehyde), indicating hydrolysis of the imine bonds.
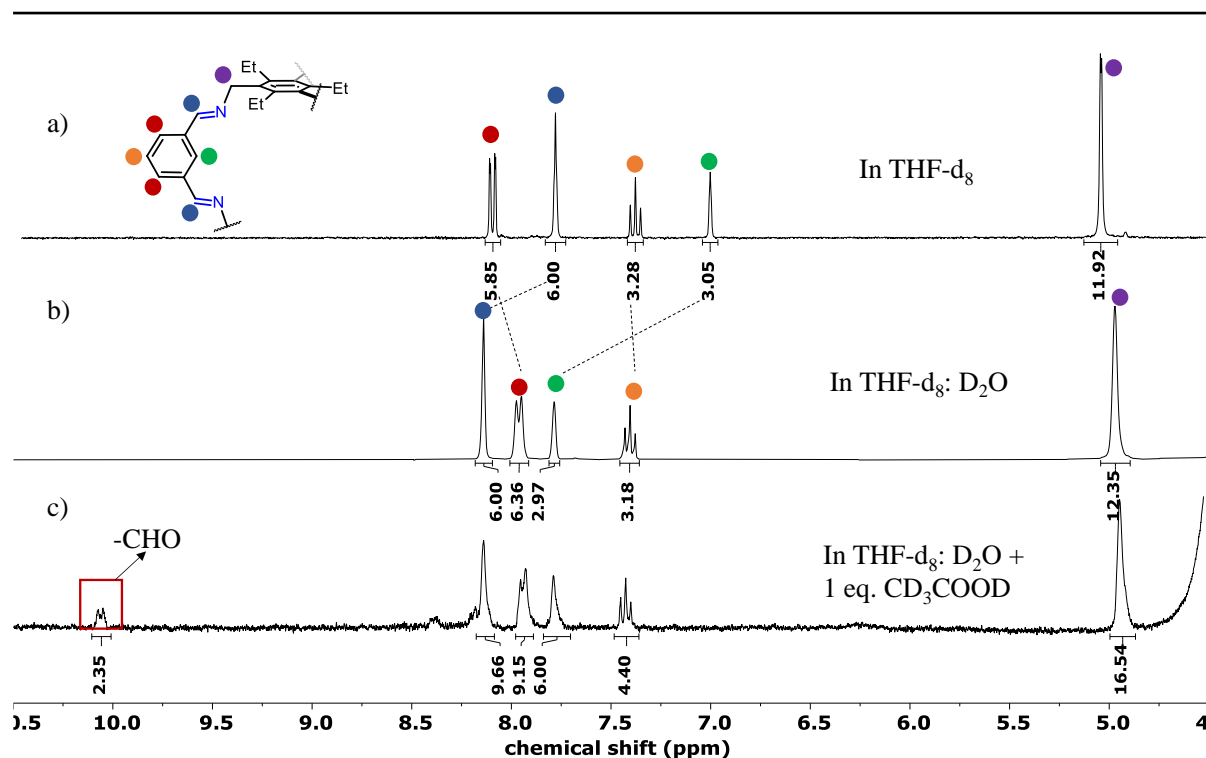
Figure 31. a) ^{1}H NMR (300 MHz) of imine cage **A62** in THF-d$_8$; b) in THD-d$_8$:D$_2$O = 10:1; c) in in THD-d$_8$:D$_2$O = 10:1 with 1 eq. of CD$_3$COOD. The assignments of the peaks are done by colour coding the specific protons in the partial chemical structure with the corresponding peaks. The red box in 'c' indicates the appearance of the aldehyde peak.

As seen in Figure 31, the peak corresponding to the imine protons (marked by blue circles) shift from 7.83 ppm to 8.13 ppm in the presence of water. This suggests a possible hydrogen bonding between the imine nitrogen atoms (as acceptors) and a water molecule (as shown in Figure 32). Similarly, the peak corresponding to the aromatic C-H proton pointing into the cavity of the cage compound (marked by green circles) shifts from 7.05 ppm to 7.78 ppm. The close proximity of the water molecule to the aromatic C-H proton inside the cavity of the cage molecule could possibly result in a weak hydrogen bond with the water's oxygen as the acceptor and the aromatic C-H as the donor, [130] explaining the downfield shift of the peak corresponding to this proton. Moreover, the doublet corresponding to the aromatic C-H protons outside the cavity of the cage molecule (marked by red) is seen to be upfield shifted, probably due to a reduced mesomeric effect of the imine groups. Further investigation could reveal vital information on the interaction of imine cages with water molecules (and consequently hydrolysis).
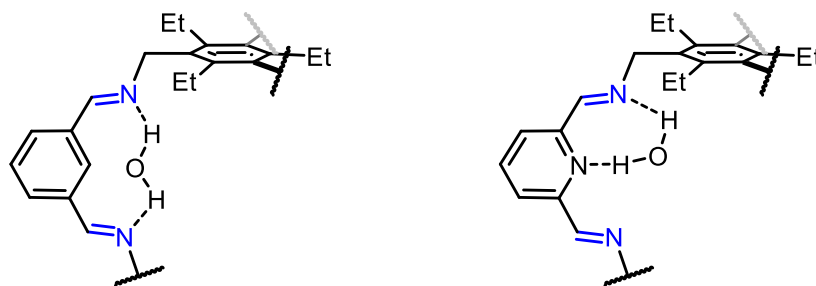
Figure 32. Possible mechanism of water approaching the imine bonds in **A62** and **A63** by entering the cage cavity, evidenced by ^{1}H NMR studies.

The same observation was made with imine cage **A63** where the imine protons shifted downfield from 7.86 ppm to 7.94 ppm (as seen in Figure 33), but the shift of imine peaks is much smaller compared to imine cage **A62**. Moreover, the triplet corresponding to the proton on the C-4 position (labelled by orange circles) is slightly shifted, which was not observed in the case of imine cage **A62.** This can be explained by the fact that the nitrogen atom of the pyridine ring, which is pointing into the cavity of the cage molecule, is in competition with the imine nitrogen atoms to act as a hydrogen bond donor to the water molecule. Again, appearance of the aldehyde peak at δ = 10.1 ppm is only observed after adding the acetic acid.
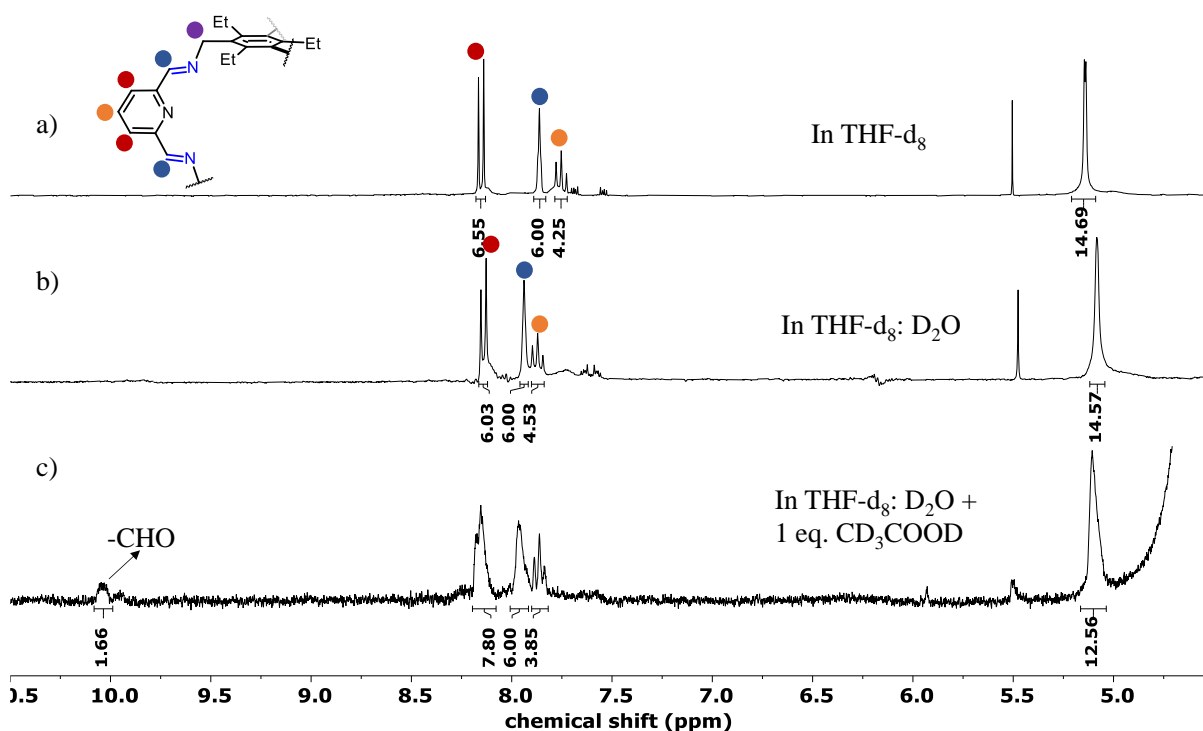
Figure 33. a) ^{1}H NMR (300 MHz) of imine cage **A63** in THF-d$_8$; b) in THD-d$_8$: D$_2$O = 10 : 1; c) in in THD-d8 : D$_2$O = 10 : 1 with 1 eq. of CD$_3$COOD. The assignments of the peaks are done by colour coding the specific protons in the partial chemical structure with the corresponding peaks.

In comparison to the previous two imine cages, imine cage **B63** (derived from triamine precursor **B**) was expected to exhibit lower stability due to the observations during its synthesis.

Indeed, it was observed that this imine cage hydrolysed just by addition of water (as shown in Figure 34). In fact, the hydrolysis was almost complete just with the addition of water since the relative intensity of the aldehyde peak only slightly increased on addition of acetic acid. Although it is clearly evident that replacing ethyl groups with propoxy groups results in a deterioration of hydrolytic stability, the rationale behind this observation cannot be established purely based on the electronic effects (of O-alkyl vs -alkyl groups) due to the alternating arrangement of these moieties on the aromatic ring.
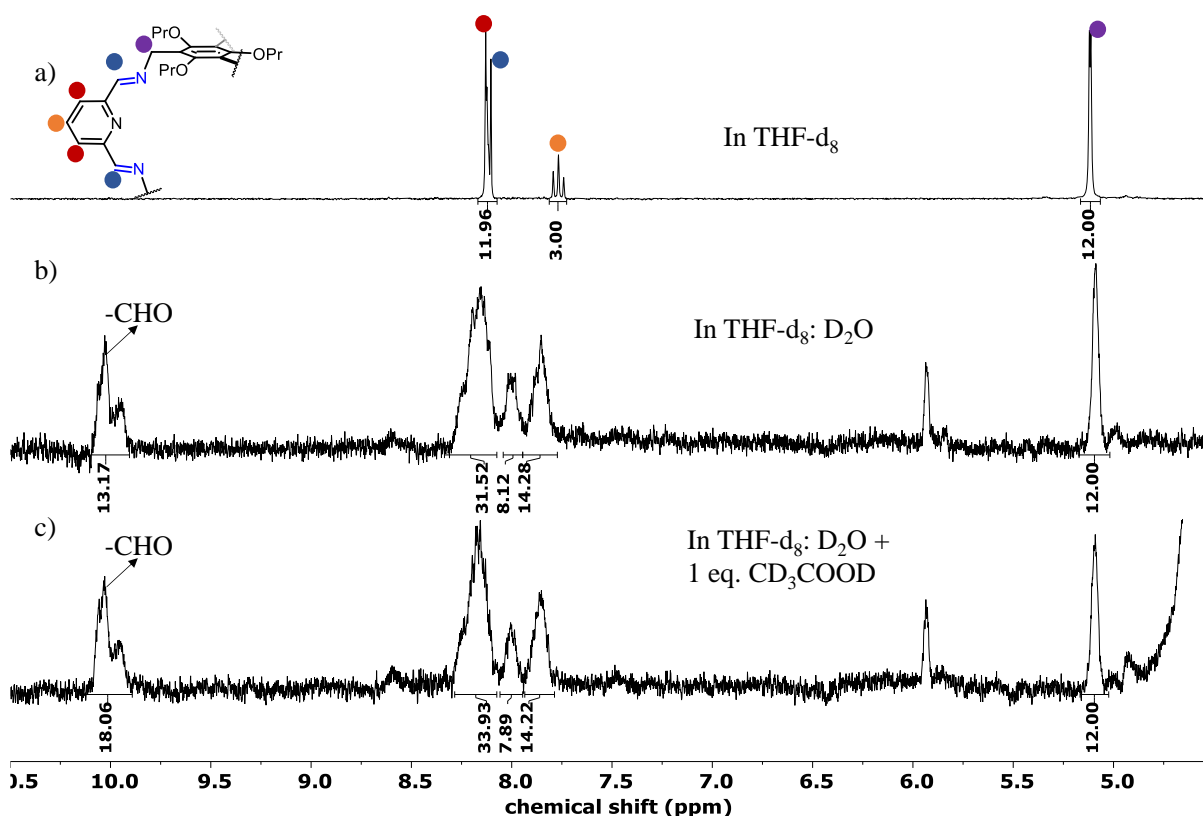
Figure 34. a) ^{1}H NMR (HMz) of imine cage **B63** in THF-d$_8$; b) in THD-d$_8$: D$_2$O = 10 : 1; c) in in THD-d8 : D$_2$O = 10 : 1 with 1 eq. of CD$_3$COOD. The assignments of the peaks are done by colour coding the specific protons in the partial chemical structure with the corresponding peaks.

These series of NMR experiments resulted in two important conclusions: 1. The imine cages derived from triamine **B** are clearly less stable than those derived from trimaine **A**; 2. Addition of the acid medium must be done as the last step in the reaction set-up, since this should favour the oxidation of imine bonds over hydrolysis in the presence of an excess of NaClO$_2$.

2.3. Conversion of the [2+3] imine cages to [2+3] amide cages via the Pinnick oxidation

The series of imine cages with varying substituents (EDG and EWG), solubilities, steric parameters and stabilities were subjected to the Pinnick oxidation. But firstly, imine cage **A62**

was chosen as a model system to optimize the reaction conditions for the Pinnick oxidation. On successfully isolating some of the amide cages, the yield of these reactions was determined via UPLC assay (see experimental section 1.4 for the general procedure), also acting as a standardized method to compare and discuss the yields.

2.3.1. Optimization of the Pinnick oxidation procedure

Three components of the Pinnick oxidation were varied (as shown in Scheme 40): 1) The scavenger: which prevents unwanted side reactions of the highly reactive HOCl, that is formed during the reaction; 2) Jencks et al. investigated the mechanism of hydrolysis of Schiff bases derived from aliphatic amines.[131] They report that in a pH range between 5-9 the rate of hydrolysis is in general higher and further depends on the electronic effects of the substituents on the aromatic ring. On the other hand, at a pH range below 4, the rate of hydrolysis decreases for all Schiff bases and is independent of the electronic effect of the substituents. Therefore, the acid medium (as hence the pH of the reaction mixture): which forms the active species, $HClO_2$ from $NaClO_2$; 3) The reaction solvent: which influences the solubility and stability of the imine cage. While the time parameter was not varied, varying the temperature seemed challenging since drastic cooling would lead to solubility problems (and also freezing of water) whereas heating the reaction was assumed to be unsafe due to the evolution of chlorine dioxide gas during the reaction.[132] Although the reaction would be complete within a couple of minutes, the reaction mixture was still left to stir for 16 hours to make sure all side-products end up in their most oxidized state.
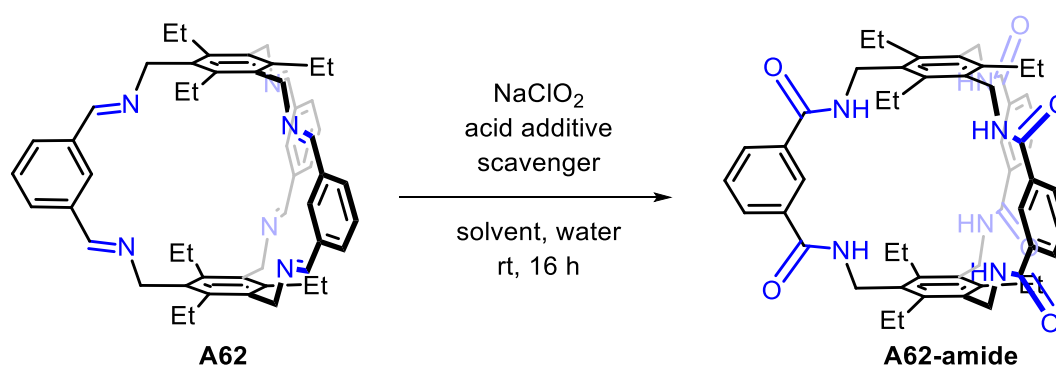
Scheme 40. Pinnick oxidation on the model system **A62** to optimize the reaction conditions.

Firstly, two different scavengers were chosen, 2-methyl-2-butene (the one used for the [4+6] cages as described in the previous chapter), and hydrogen peroxide. Both scavengers delivered the desired amide cage in nearly the same yield (26% with 2-methyl-2-butene and 28% with H_2O_2), but 2-methyl-2-butene produced a crude substance which exhibited a ^1H NMR spectrum

with a lot of impurities in the aliphatic region (likely due to further reaction of the halohydrin by-product), rendering the work-up process tedious. On the other hand, the crude substance obtained by using H_2O_2 as the scavenger exhibited an almost clean NMR spectrum (see Figure 35). It can be seen that there was a lot of aliphatic impurities present in spectrum 'a' which could not be washed away completely with non-polar solvents like hexane or pentane. Due to a difference in solubility compared to the [4+6] triptycene-based cages, the [2+3] amide cage proved to be more challenging to achieve purity, making H_2O_2 as the preferred scavenger.
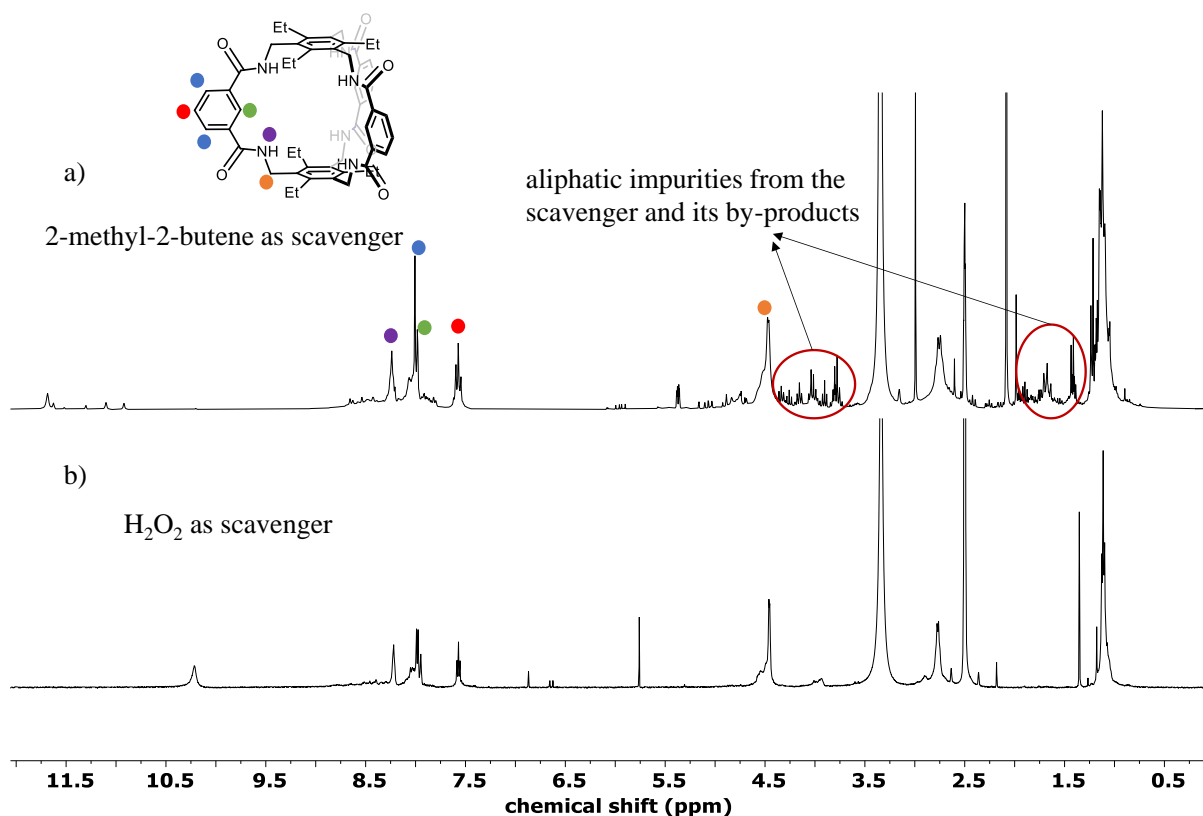
Figure 35. ^{1}H NMR (300 MHz, DMSO-d_6) comparison of the crude material of the Pinnick oxidation using different scavengers: a) using 2-methyl-2-butene as scavenger; b) using H_2O_2 as scavenger.

Using H_2O_2 as the scavenger, three different acid media were tested, NaH_2PO_4 (which was previously used for the 4+6 cage), 1 M acetic acid solution in water and an acetate buffer (NaOAc/AcOH) adjusted to pH = 3.8. The underlying thought process behind choosing the acidic media was that the competing hydrolysis of the imine bonds, must occur slower than the Pinnick oxidation. Although it was impossible to completely exclude imine hydrolysis (without excluding water from the reaction), the domination of the hydrolysis would lead to a reduced yield. It was found that a NaH_2PO_4 solution (pH = 6-7) was not optimal for the Pinnick oxidation on the [2+3] imine cages derived from aliphatic amines delivering a yield of 25% in comparison to acetic acid (as the acid medium) with 48% (see Figure 36a and b for UPLC assay). In contrast, using acetic acid/H_2O_2 for the Pinnick oxidation on triptycene-based [4+6]

salicylbisimine cage **47** (from section 1.1.3) resulted in complete failure of the reaction. Hence, it can be inferred that for imine cage compounds derived from aromatic amines (e.g., triptycene-based salicylbisimine cage), the Pinnick oxidation must be conducted in a pH range of 6-7 (offered by a 1M NaH_2PO_4 solution), and for imine cages derived from aliphatic amines the Pinnick oxidation works better when conducted at a pH 2-4. The reason for the importance of pH could be attributed to the rate of hydrolysis of the imine bonds in comparison to the Pinnick oxidation. Lastly, it is worth mentioning that the use of stronger acids such as TFA and HCl as 1 M solutions (pH < 2) led to complete hydrolysis of the imine cage, wherein isophthalic acid was isolated in significant quantities. Furthermore, on discovering that the pH of the reaction mixture plays a big role on the outcome of the Pinnick oxidation, an acetate buffer solution was prepared with AcOH/NaOAc at a pH of 3.8, delivering a slightly greater yield of 54% as determined by UPLC-MS analysis (Figure 36d). However, with the improvement being so small, it was decided that the originally used acetic acid would be utilised in further experiments.

Finally, the Pinnick oxidation was attempted in two different solvents: THF and DCM. The imine cage was insoluble in solvents such as alcohols, hydrocarbon solvents, highly polar solvents like acetonitrile, DMF and DMSO. THF being miscible with water was expected to be a better solvent for the Pinnick oxidation compared to DCM. Indeed, this hypothesis proved correct as the UPLC-MS traces of the crude reaction exhibited many new by-products as can be observed in the comparison of traces b (THF) and c (DCM), Figure 36. Further details on the UPLC traces (with peak integrations) can be found in Figure 191, appendix section 6.1.

The optimisation allowed the generation of conditions for the Pinnick oxidation of [2+3] imine cages to amide cages as shown in Scheme 41, using similar amounts of reagents (per imine bond) as with the [4+6] cages.
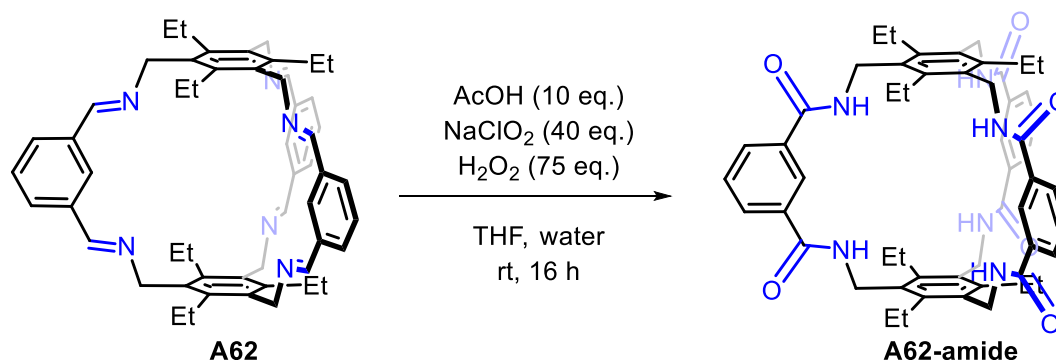
Scheme 41. Optimized synthesis used to transform the [2+3] imine cages to [2+3] amide cages.
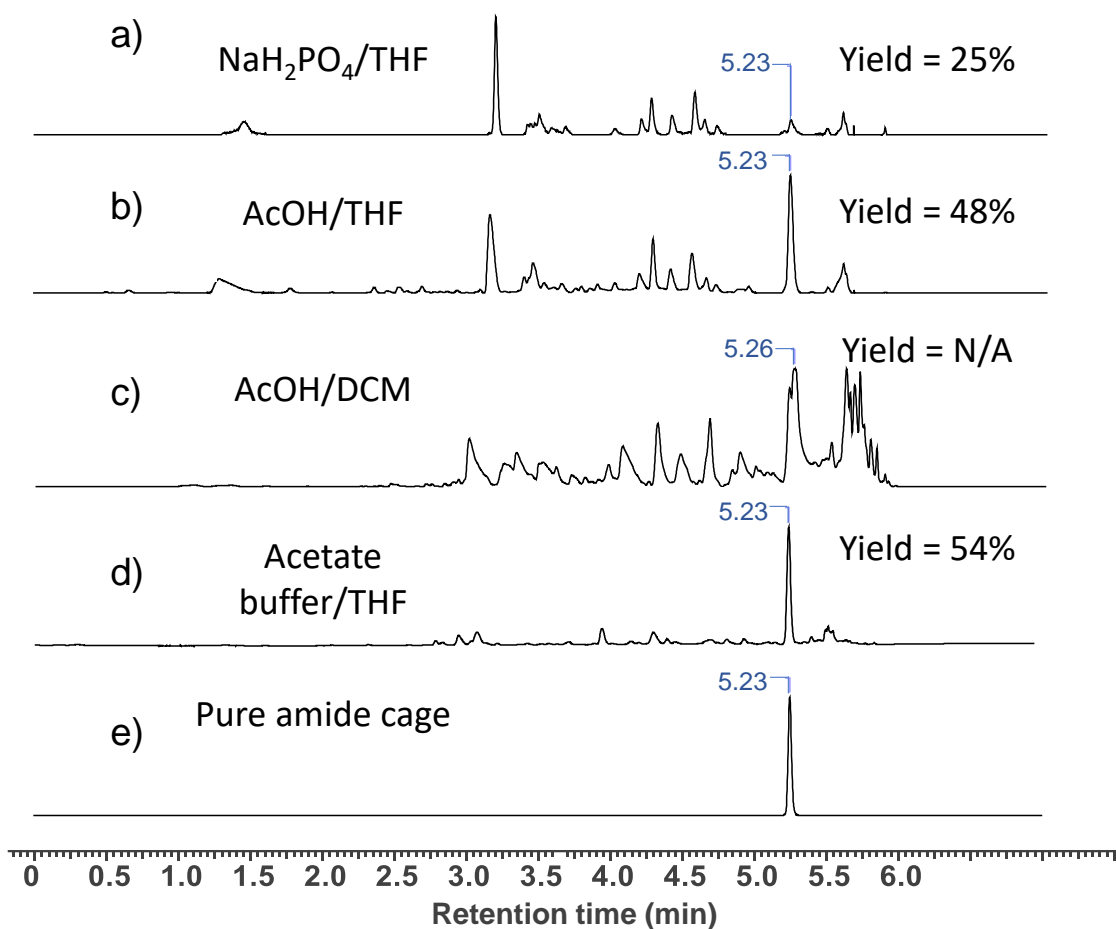
Figure 36. UPLC traces (C-8 column, acetonitrile/water) of the crude mixture of the Pinnick oxidation: a) using NaH$_2$PO$_4$ as the acid medium; b) using acetic acid as the acid medium; c) Using DCM as the reaction solvent; d) Using the acetate buffer conditions; e) Pure amide cage **A62-amide** as the reference. Anthracene was used as the internal standard to estimate the yields (see Figure 191 in appendix section 6.1)

2.3.2. Synthesis and purification of the [2+3] amide cage compounds

With conditions optimised upon model cage **A62** and analysis carried out by UPLC-MS, the purification of the cage was first targeted from the crude reaction mixture, before moving onto more complex cage structures. Initial investigations attempted to use preparative HPLC to facilitate purification, however, this proved to be inefficient to carry out on a large scale as only small quantities (< 20 mg) could be purified at a time. Therefore, a more scalable trituration from MeOH/H$_2$O was used to remove inorganic residues, before a recrystallisation from hot MeOH/Et$_2$O delivered the pure amide cage in a yield of 28% (Figure 37).
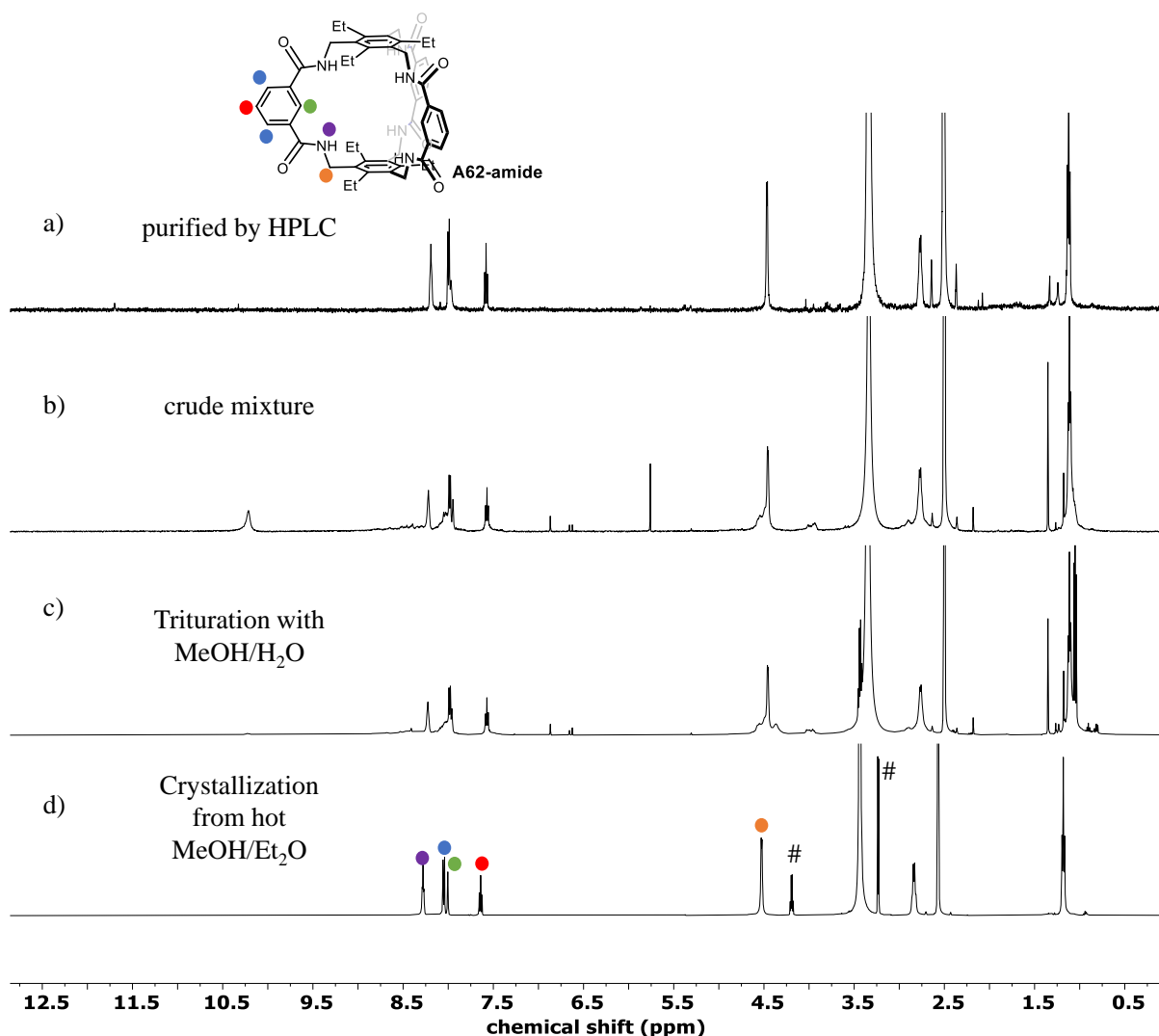
Figure 37. ^{1}H NMR (300 MHz, DMSO-d$_6$) comparison of the different purification steps of the amide cage **A62-amide**. a) After HPLC purification; b) crude substance after the Pinnick oxidation; c) crude substance after MeOH/H$_2$O trituration; d) Pure amide cage after crystallization. # - peaks of residual methanol after crystallization.

Having ascertained the isolation of pure cage **A62-amide**, the reaction was carried out with **A63**, containing a pyridyl unit in the dialdehyde. Pleasingly the cage with a pyridine moiety delivered a much better yield of 42% following recrystallisation from hot MeOH (Figure 38). This was an important finding as having a pyridyl unit facing the inside of the cage could be used as a metal binding site, or hydrogen bond acceptor. Importantly, this reaction could be scaled up (to 1 g of the imine cage), albeit resulting in lower yields with increasing scales (~15% with 1 g).

71

A62 - A71

A62-amide
28%[a]

A63-amide
42%[a]

A64-amide
15%[b]

A65-amide
N/A[c]

A66-amide
N/A[c]

A67-amide
35%[d]

A68-amide
0%[e]

A69-amide
0%[e]

A70-amide
1%[b]

A71-amide
0%[e]

(a) Purified by recrystalisation; (b) Purified by reverse-phase HPLC; (c) Product identified by MALDI-MS, but too insoluble for purification; (d) Purified by rGPC; (e) no product detected.
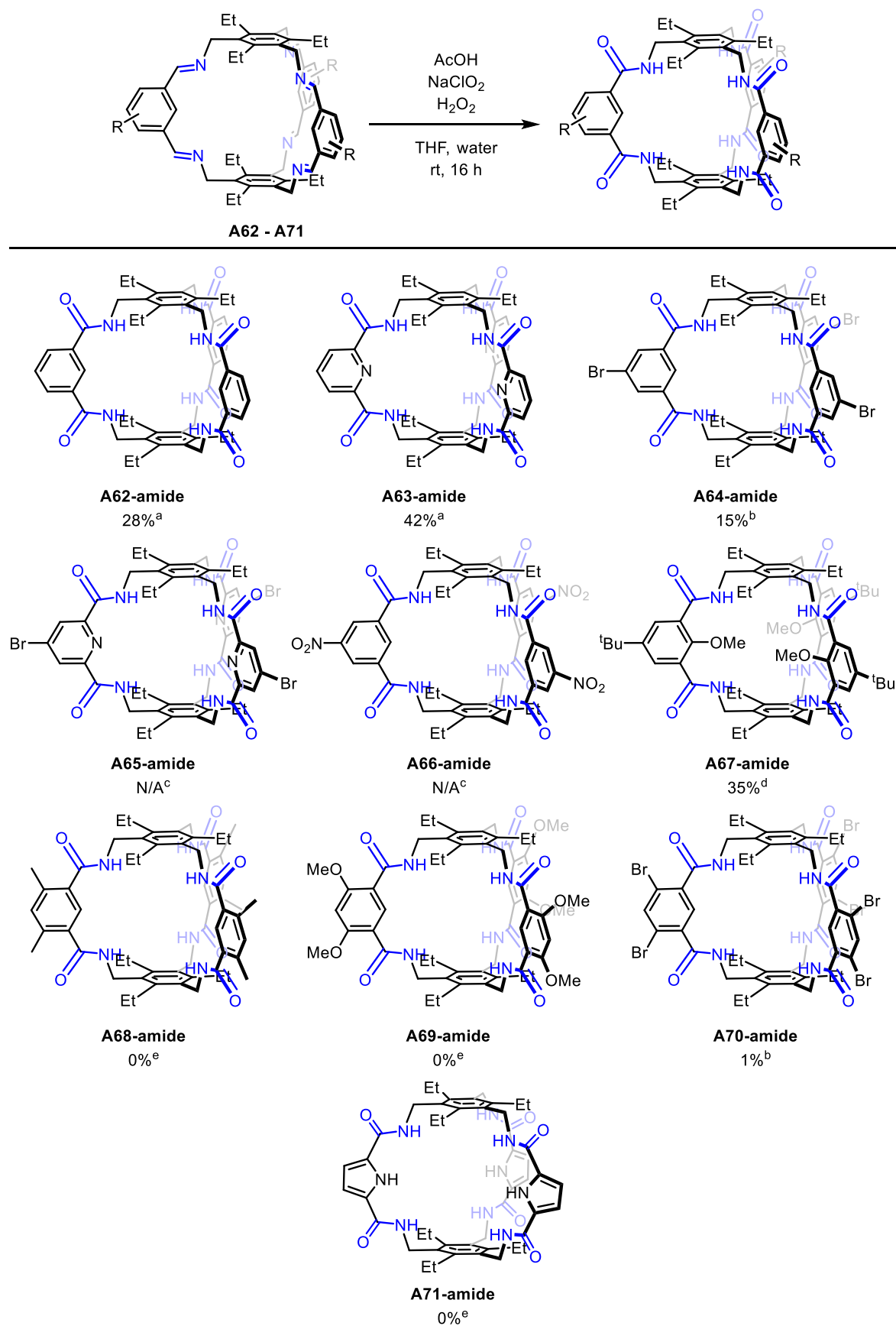
Figure 38. Substrate scope of the Pinnick oxidation for conversion of [2+3] imine cages to amide cages.

To allow further derivatisation of the cage exterior, bromide containing imine cage **A64** (Figure 38) was subjected to the general reaction conditions and showed a good initial reactivity. However, the introduction of the bromide significantly changed the solubility of the cage, and any attempt at recrystallisation failed. However, the change in polarity allowed the purification of the cage by preparative HPLC, albeit in a reduced yield of 15%, likely arising from the large quantities of insoluble solid that was discarded by filtration from the crude mixture of the Pinnick oxidation. Moreover, **A64-amide** exhibited poor solubility in most solvents except DMF and DMSO (i.e., poor solubility in the HPLC mobile phases, MeCN and water), which was probably another reason for the low isolated yield. Unfortunately, the observed decrease in solubility of cage **A64-amide** was further exemplified in cages **A65-amide** and **A66-amide**, containing a pyridyl-4-bromide and nitro unit, respectively. Both cages could be identified from the reaction mixture in MALDI-MS (see Figure 156 and Figure 157 in appendix section 2.1) but were of such low solubility that they could not be isolated and characterised. Pleasingly, by introducing solubilising groups onto the dialdehyde in cage **A67-amide**, in the form of tert-butyl groups, exhibited high reactivity and offered good solubility. The solubility was improved so significantly that typical organic solvents like DCM and chloroform dissolved the cage effectively. This allowed the cage to be isolated by GPC, in a good yield of 35%. This example further exemplifies the tolerance of the reaction to substitution at the position between the two imine groups inside the cavity of the cage.

To further examine the tolerance of the Pinnick reaction to substitution of the dialdehyde, imine cages **A68**, **A69** and **A70** were subjected to the reaction. However, only very low reactivity was identified in the case of **A71** delivering amide cage **A71-amide** with a mere yield of 1%. These cases display a new limitation of the Pinnick oxidation that arises only on applying it to cage compounds. As discussed in the introduction section 2.2, the Pinnick oxidation has a good functional group tolerance and the presence of bulky groups next to the aldehyde/imine generally does not hinder the reaction.[102, 113] However, due to the three-dimensional structure of cage compounds, the approach of the $HClO_2$ species to the imine bonds is highly restricted, and the corresponding hydrolysis occurs preferentially. It is so far unclear whether the Pinnick oxidation with imines takes place via a nucleophilic attack of the $^-ClO_2$ or a concerted mechanism (as previously described in introduction section 2.2), but a nucleophile-mediated mechanism may require a specific trajectory for the approach of the nucleophile (similar to the Bürgi-Dunitz trajectory)[133] which could be hindered in cage compounds. Interestingly, the steric parameter (according to the Taft equation)[134] is nearly the same for methyl groups and

bromide groups, but however, the reaction was observed to form the amide product with only with the latter (Figure 39).
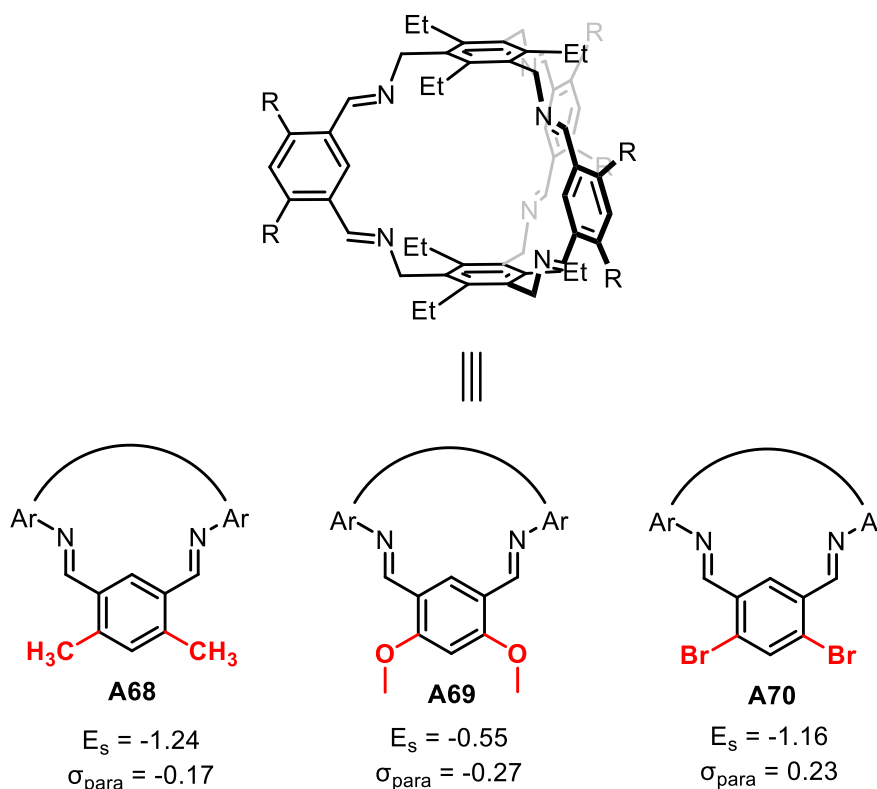
Figure 39. Comparison of the steric (E_s) and Hammet parameters (σ_{para})[135] of the substituents in imine cages **A68**, **A69** and **A70**.

Finally, the oxidation of electron rich pyrrole base dialdehyde cage **A71** was attempted, as was expected based upon previous reports this reaction proved ineffective. Indeed, only hydrolysis products could be identified. Reinforcing that the Pinnick oxidation must proceed significantly faster than hydrolysis for a productive process.

Pinnick oxidation on imine cages derived from triamine B and C

Next, to examine the influence of the amine moiety on the Pinnick oxidation the substitution pattern of the aryl triamine was modified. In the first instance an alkoxy chain was added to improve the solubility of the product amide cage. However, based upon stability test with **B63** (see above) the oxidation was expected to be problematic as the hydrolysis was recognised to occur very quickly in aqueous conditions. Despite this, the cage with a pyridyl dialdehyde **B63-amide** was found to be successfully produced from the reaction in a 19% yield, but failed in the case of cage **B62** (Scheme 42). To further test the influence of change in the aryl triamine, a tribromo-substituted imine cage was utilised (**C62**) in the oxidation. However, as had previously been observed in cages that contained bromide substituents the solubility was very

low in the reaction mixture and only unreacted starting material could be identified after the reaction.
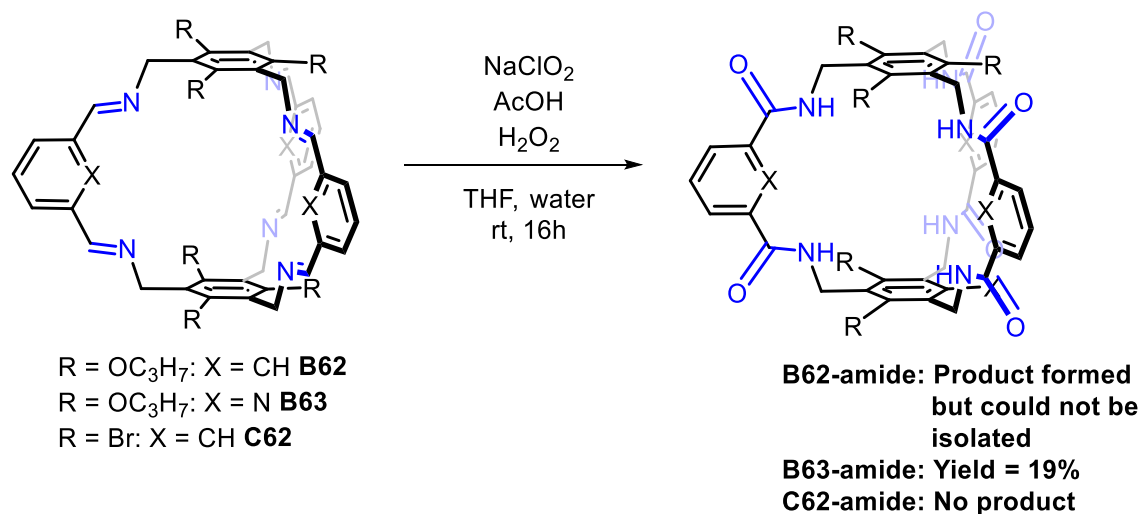
Scheme 42. Pinnick oxidation on the imine cages obtained from propoxy-trimiane **B**.

Lastly, another imine cage **B65** with a bromine atom at the 4-position of the pyridine ring (was subjected to the Pinnick oxidation. The enhanced solubility of the cages (derived from triamine **B**) made it possible to purify this imine cage by HPLC, which was not possible with a similar amide cage **A65-amide** due to poor solubility (Scheme 43).
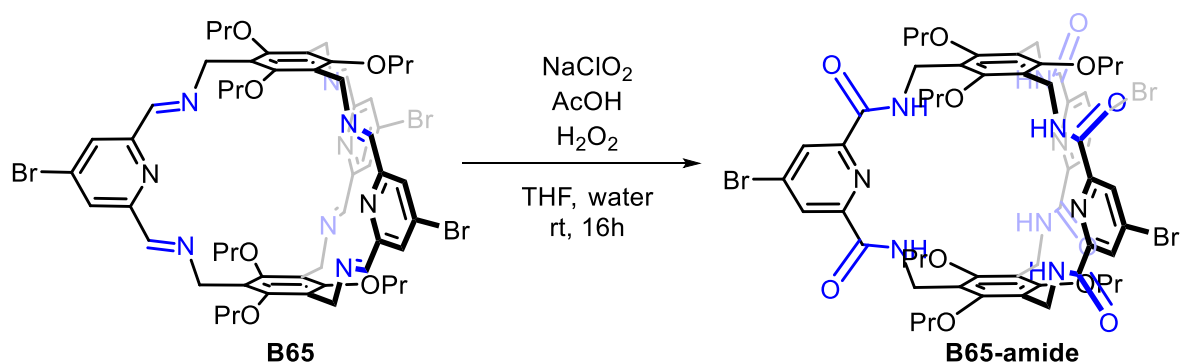
Scheme 43. Pinnick oxidation on imine cage **B65** to deliver amide cage **B65-amide**.

Formation of amide cage **B65-amide** was indicated by MALDI-TOF-MS (Figure 151 in the appendix section) but could only be isolated in a substandard purity (Figure 40). With very little promise for the [2+3] cage compounds derived from triamine **B,** it was assessed unnecessary to put in further efforts to purify this cage compound.
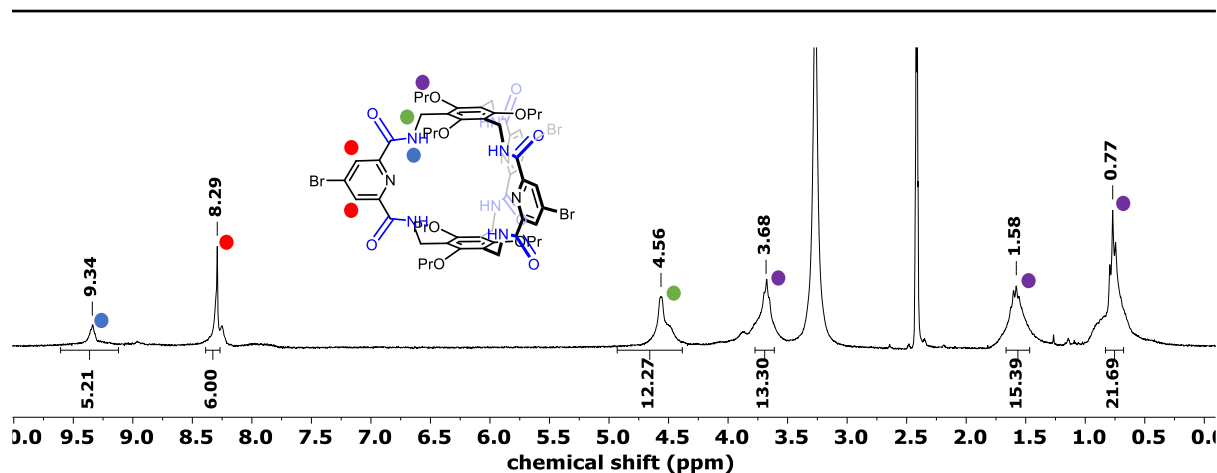
Figure 40. ^{1}H NMR (300 MHz, DMSO-d[6]) of the amide cage **B65-amide** showing expected peaks, albeit in substandard purity.

TREN-based cage compounds

Finally, recognising the potential of TREN-based cages for anion binding applications,[65] the oxidation of imine cages **D62** and **D63** was attempted (Scheme 44). Having a tertiary-amine present in the structure however is believed to be detrimental, as protonation under the reaction conditions can occur leading to insoluble or unreactive species. In the first instance with isopthalaldehyde derived cage **D62**, no product amide cage was observed and only isophthalic acid was identified after the reaction, indicating a rapid hydrolysis of the imine cage and oxidation of the formed aldehyde. The second structure bearing a pyridyl moiety provided more promising results with the cage being soluble in water and identified by ^{1}H NMR (Figure 41). However, successful oxidation to cage **D63-amide** could not be detected by MALDI-MS or ESI-MS probably due to multiple protonation occurring under acidic conditions of the Pinnick oxidation. Lastly, the oxidation of imine cage **D63** could neither be effectively reproduced nor could the resulting product be isolated pure (due to its solubility in water), and hence requires further experiments by using reaction conditions that avoid imine hydrolysis.
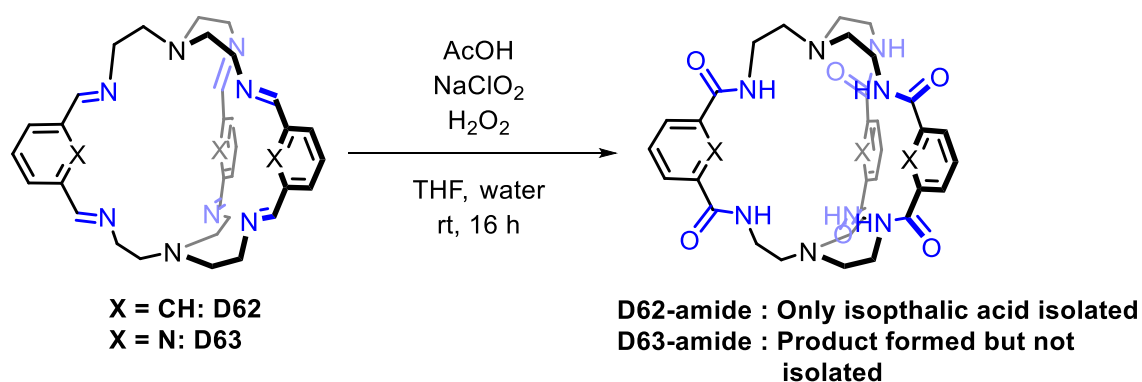
Scheme 44. Pinnick oxidation on the TREN-based imine cages.
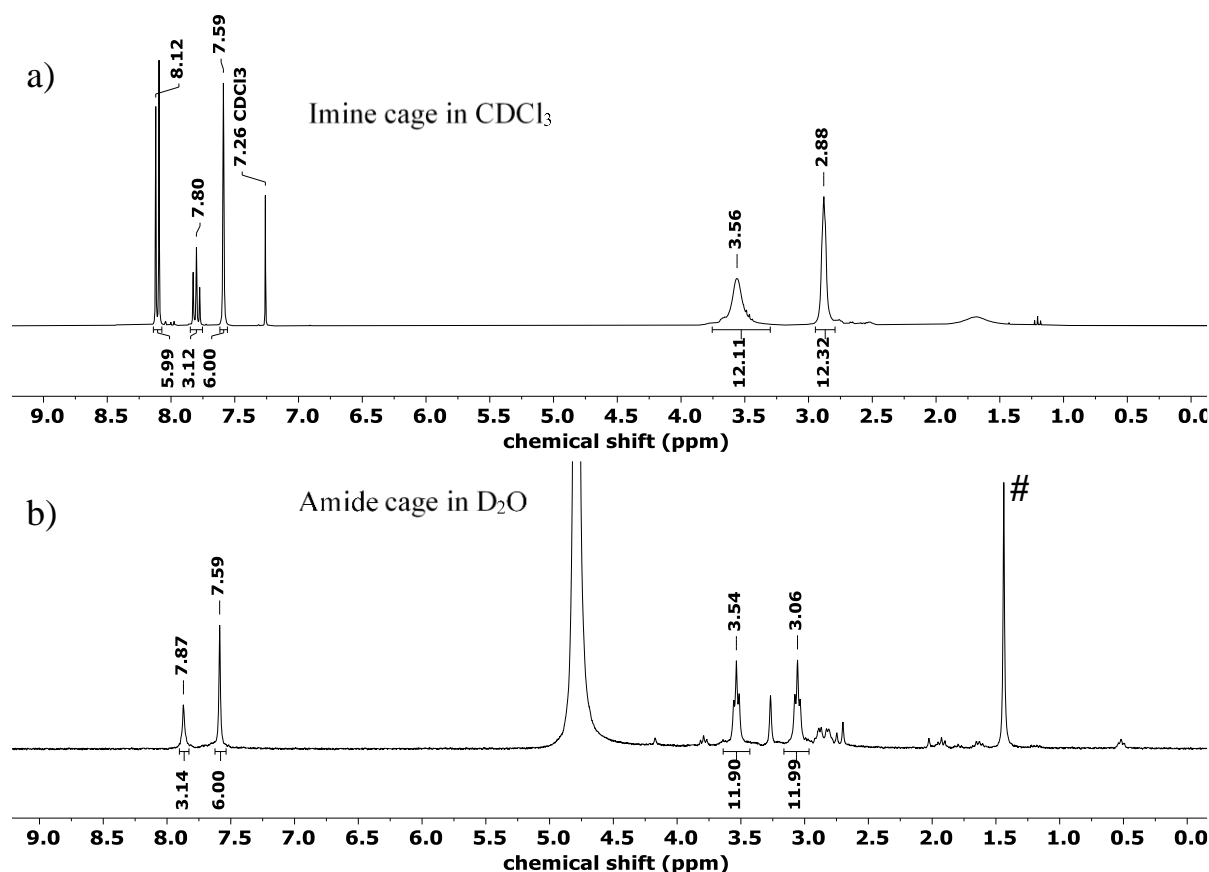
Figure 41. [superscript: 1]H NMR (300 MHz) of: a) The imine cage **D63**; b) amide cage **D63-amide. # -** speculated to correspond to free TREN.

2.3.3. UPLC assay: A standardized method to compare the yields of the Pinnick oxidation

On successfully isolating 5 different amide cages, it was important to address a crucial point; The yield of the reaction prior to work up, this meant identifying a quantitative method for the analysis of the crude reaction mixture.

A UPLC assay (C8 column, acetonitrile/water mixtures as eluents) was performed using anthracene as an internal standard. The response factor of each of the amide cages was determined and subsequently, the yield of each reaction could be calculated. A detailed description of the UPLC assay can be found in appendix section 6. Table 6 shows a comparison of the isolated yields and the yield determined by UPLC assay each of the amide cages.

Table 6. Comparison of the isolated yield and the yield determined by UPLC assay for the Pinnick oxidation.

Ar-group of amide cage (compound label)	Isolated Yield	Yield from UPLC assay	Yield with acetate buffer, pH = 3.8[a]
A62-amide	28%	48%	54%
A63-amide	42%	67%	74%
A64-amide	15%	23%	48%
A67-amide	35%	57%	43%
A70-amide	1%	9%	_[b]
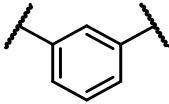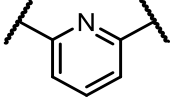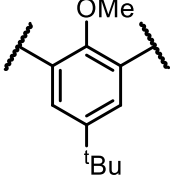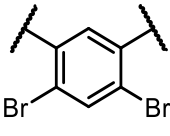
a- determined by UPLC assay (see appendix section 6).

b- Could not be determined due to unreliable data.

Firstly, it is interesting to note that the exact same trend is observed with the UPLC assay in comparison to isolated yields, which verifies the authenticity of the UPLC assay method (as seen in Table 6). With amide cage **A62-amide** and **A63-amide**, it can be seen that crystallization as a purification method leads to a greater loss of substance. Comparison of these two yields (48% for **A62-amide** and 67% for **A63-amide**) suggests that the pyridine ring results in a better conversion of the imine cage to the amide cage. Amide cage **A64-amide** shows a very poor yield even according to the UPLC assay (23%), which is probably because large quantities of insoluble solid had to be discarded by filtration from the crude mixture of the Pinnick oxidation (as mentioned previously). Alternatively, using a highly soluble imine cage **A67** formed the amide cage **A67-amide** in a yield estimated to be 57% (determined by UPLC assay).

Lastly, the yield for amide cage **A70-amide**, containing two bromine atoms adjacent to the amide groups, was estimated to be a mere 9% (as shown in Table 6) (The steric effect of such 4,6-disubstituted isophthalaldehydes was discussed previously). However, in contrast to imine cages **A68** and **A69** (containing methyl and methoxy groups adjacent to the imine groups respectively), imine cage **A70** did lead to the formation of amide cage **A70-amide**, albeit in a very low yield**.** This maybe be explained by the fact that electron rich systems are known to form chlorination products due to the highly reactive HOCl species formed during the reaction.[102]

The yield for generating these amide cages could be improved by using an acetate buffer (at pH of 3.8) as the acid medium, although the exact reason for the increase in yield could not be determined. The yield of every reaction increases for every Pinnick oxidation but not proportionately in every case. A much higher increase in seen for amide cage **A64-amide** (48% from 23%), compared to amide cages **A62-amide** (54% from 48%) and **A63-amide** (74% from 67%). It was mentioned previously that imine cage **A64** poorly exhibited solubility in THF, hence resulting in a low yield for the Pinnick oxidation. It could be hypothesized that the stable pH offered by an acetate buffer could influence the rate of hydrolysis.

Moreover, the larger amount of acetate ions in the reaction mixture (due to the acetate buffer) could possibly drive the formation of the amide cage by a template effect. The high affinity for acetate ions by amide cage **A63-amide** has already been prove by Anslyn et al.,[61] where such a C_3 symmetric amide cage binds to acetate ions due to the specific arrangement of the amide -NH bonds, and the pyridine nitrogen played no role in anion binding. Hence, such a phenomenon could be expected for all the above amide cage compounds, which could be the driving force for the formation of the amide cages. Another observation that reinforces the templet effect hypothesis is the yield of amide cage **A67-amide**. Cage **A67-amide** containing methoxy groups that are pointing towards the cavity of the cage, was obtained in a lower yield (43%) with the acetate buffer than with acetic acid (57%) as the acid medium. A reduced binding to acetate ions due to the steric crowding of methoxy groups, could suppress the template effect of the acetate ions. Lastly, the yield of amide cage **A70-amide** using the acetate buffer could not be determined by UPLC assay since it was not possible to get reliable data.

2.4. [2+3] amide cages via an irreversible amide-bond forming reaction

It has been proven that large amide cages with complex geometry cannot be synthesized by simple amide bond forming reactions (section 1.2), but however, amide cage **A63-amide** was

synthesized by Anslyn et al. in a surprisingly (for amide cages obtained by direct amide bond forming reaction) high yield of 40% (as shown in Scheme 45). It was suggested that the pre-organisation of the precursors, and the hydrogen bonding between the pyridine N atoms and the amide H atoms is a driving force for the formation of the cage structure.[61] It is worth mentioning that this procedure/yield could not be reproduced after multiple attempts. More importantly, it could be shown that an analogous amide cage **A62-amide**, where hydrogen bonding is not present to drive the formation of the cage, could not be synthesized in a similar manner.
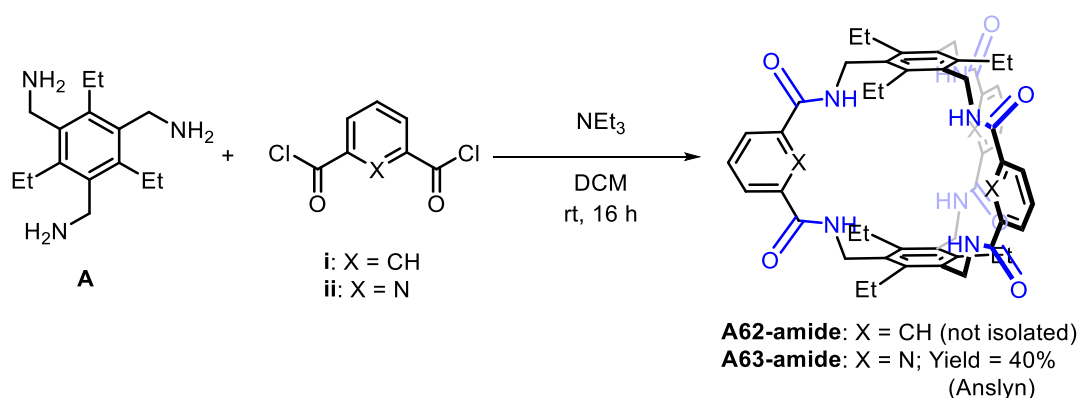
Scheme 45. Synthesis of [2+3] amide cages **A62-amide** and **A63-amide** via an irreversible amide bond forming reaction.

Formation of amide cage **A62-amide** was monitored by UPLC-MS, where the peak corresponding to **A62-amide** had a peak area (integration) lesser than 1% (as shown in Figure 42). Such small amounts of the amide cage could not be isolated by preparative HPLC, hence showing the superiority of the method of preparing amide cages utilizing DCC followed by Pinnick oxidation.
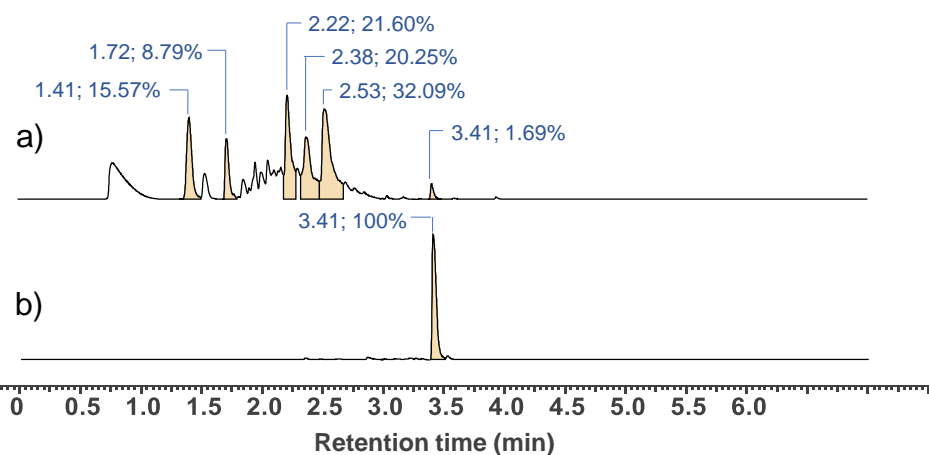
Figure 42. UPLC traces (C-18 column 1.7 μm ethylene bridged BEH particles, eluent: acetonitrile/water gradient) of the reaction to obtain amide cage **A62-amide** (as shown in Scheme 45): a) The irreversible amide bond forming reaction; b) Pure amide cage **A62-amide** as the reference.

On establishing the advantages of generating amide cages via the Pinnick oxidation, a more complex cage molecule with a greater number of amide bonds, was attempted to be synthesized starting from a similar tripodal 1,3,5-benzyltriamine precursor.

2.5. The [4+4] truncated tetrahedron cage compounds

In 2018, Mastalerz and co-workers reported the synthesis of a kinetically controlled [4+4] truncated tetrahedron imine cage.[39] Such truncated tetrahedron imine cages were shown to encapsulate different size anions depending on the dimensions of the cage windows, and also biologically active molecules like acetylcholine.[136] Later in 2020, Schmidt et al, synthesized a fluorinated [4+4] truncated tetrahedron imine cage with one of the highest uptakes of CO_2 (19 wt. %) for porous organic cages.[137] With the growing development in the area of truncated tetrahedral cages the preparation of a [4+4] amide cage was targeted.

From the triamine **A** used to prepare the series of [2+3] imine cages (as described in section 2.1), a [4+4] imine cage **A72** was synthesized according to literature procedure.[39] The imine cage was then subjected to the Pinnick oxidation conditions to convert it into an amide cage **A72-amide** (as shown in Scheme 46).
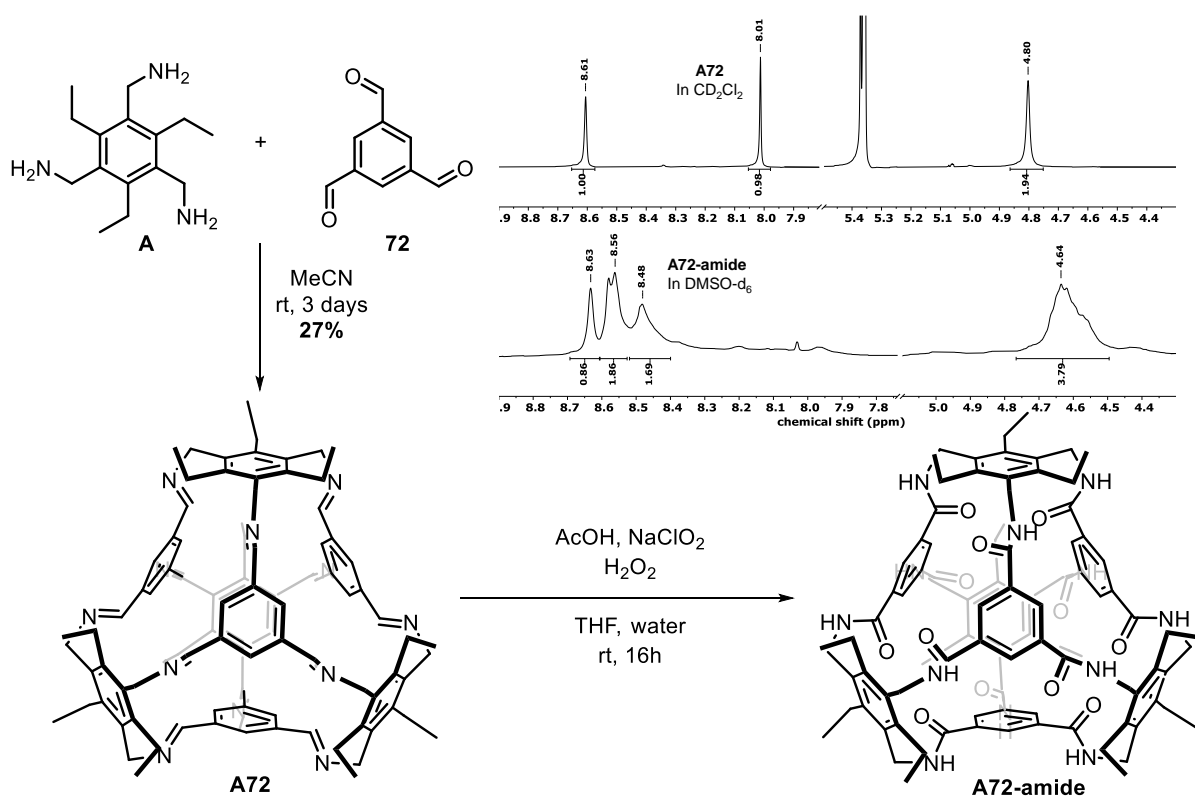
Scheme 46. Synthesis of the [4+4] truncated tetrahedron imine cage **A72** from the triamine precursor **A,** followed by the Pinnick oxidation. Top right: ^{1}H NMR comparison of the imine cage (pure) and the impure amide cage.

Unfortunately, the amide cage **A72-amide** was insoluble in most solvents except hot DMSO, and trituration (or washing) steps was not adequate to fully purify the amide cage, hence making isolation unfeasible. Nevertheless, formation of the amide cage was detected by MALDI-MS exhibiting a signal at m/z = 1644.866 corresponding to the $[M+Na]^+$ peak. To circumvent the solubility problem, [4+4] imine cage **B73** was synthesized with a new set of precursors containing larger hydrophobic units, thus enhancing solubility in organic solvents. Imine cage **B73** was prepared according to a procedure borrowed from a colleague, *Jochen Lauer (Mastalerz group)*.[138] Imine cage **B73** was subsequently treated under the Pinnick oxidation conditions to obtain the amide cage (**B73-amide**) in a yield of 52% over two steps, using acetate buffer (pH = 3.8) as the acid medium (as shown in Scheme 47).
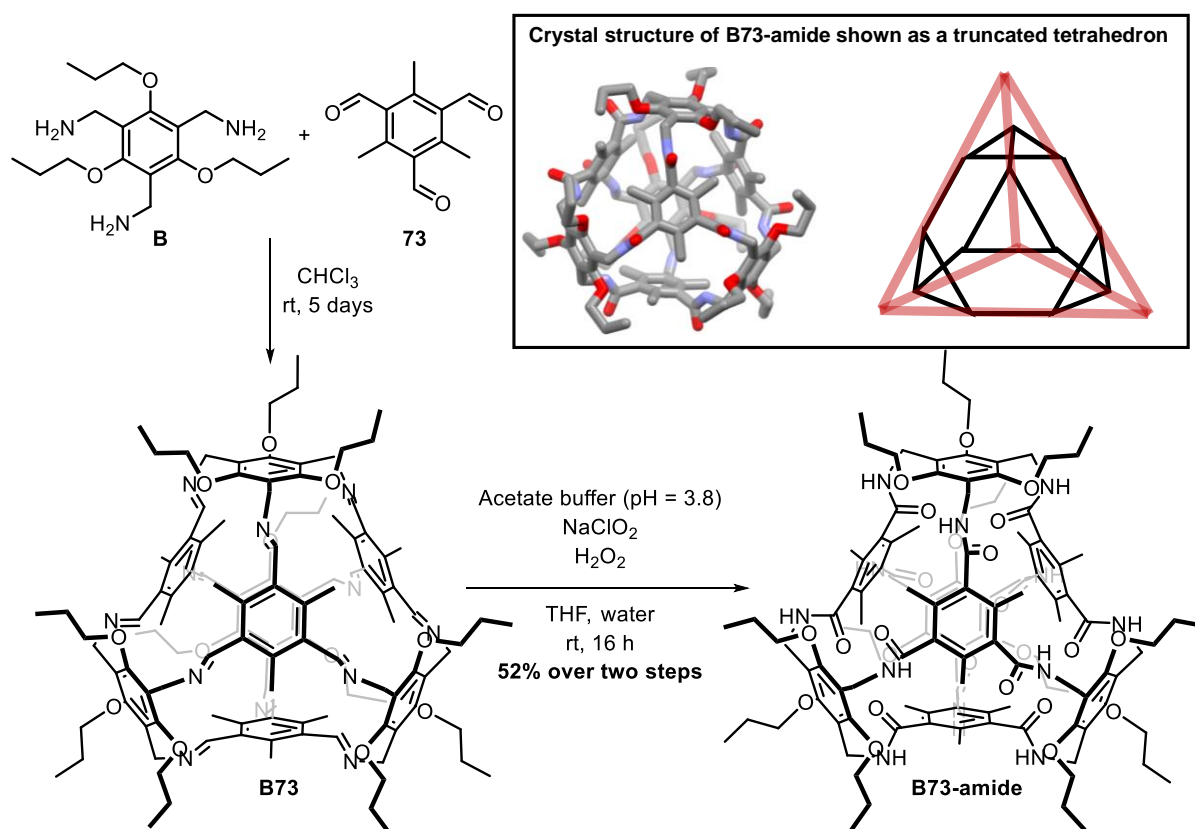
Scheme 47. Synthesis of the [4+4] truncated tetrahedron imine cage **B73** from the triamine precursor **B**, followed by the Pinnick oxidation. Top right: Amide cage **B73-amide** represented as a truncated tetrahedron.

The absence of any hydrogen atoms on the aromatic rings and broad peaks in the aliphatic region rendered the ^{1}H NMR (of amide cage **B73-amide**) ineffective but however, ^{13}C NMR exhibited the exact number of peaks as expected. MALDI-MS spectra exhibited signals corresponding to a $[M+Na]^+$ and $[M+K]^+$ species confirming the formation of amide cage **B73-amide** (see Figure 152 in appendix). Interestingly, the MALDI-TOF-MS contains peaks that correspond to an encapsulated solvent molecule $[M+DCM]^+$ at m/z = 2235.429, due to a

significantly closed nature of the surface of the cage molecule. The elemental analysis provided further evidence for the encapsulation of solvent molecules, although the cage compound was treated at 180 °C for 16 hours under high vacuum. Finally, crystals of amide cage **B73-amide** could be grown from a hot solution in DMSO, providing final confirmation of the [4+4] amide cage (as shown in Figure 43).
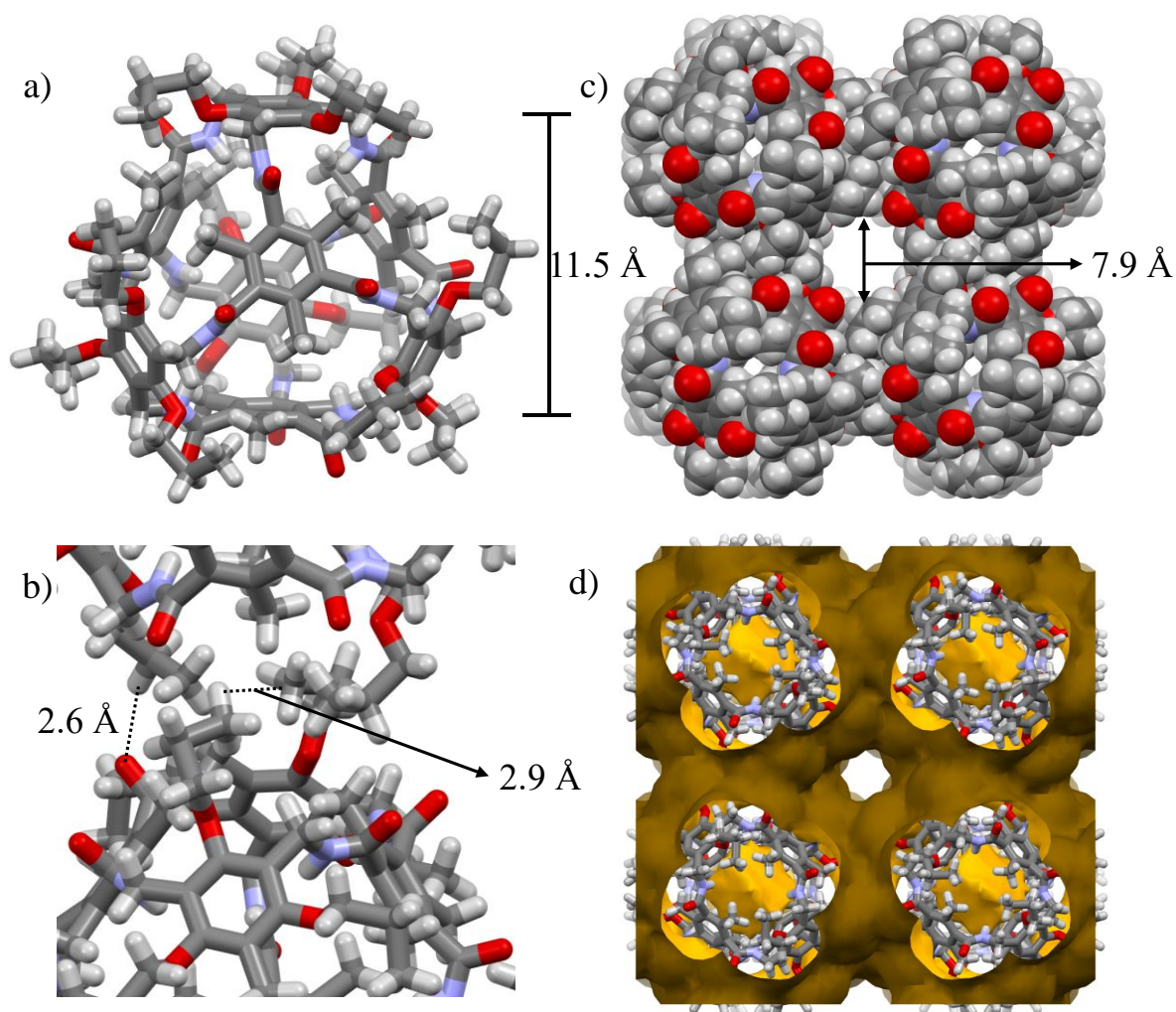
Figure 43. SCXRD structure of the [4+4] amide cage **B73-amide**: a) Single molecule of the amide cage with the size showing the size of the cavity; b) non-covalent interactions at the point of contact; c) Cubic crystal packing of 8 molecules of the amide cage in a unit cell; d) Solvent accessible surface area with a probe radius of 1.2 Å. Colours: carbon: gray; Nitrogen: blue; Oxygen: red; Hydrogen: white.

The amide cage crystallizes in a cubic space group $F\bar{4}3c$ with 8 molecules in a unit cell (as shown in Figure 43). All amide -NH bonds can be seen pointing towards the cavity of the cage, with varying size of windows due to flexible propoxy-chains. The molecules of the unit cell are held together by multiple dispersion interactions between the propyl chains at the point of contact. The solvent accessible surface area exhibits clear channels (of two types) for the flow

of gases but however, activation by solvent exchange (with isopropanol and hexane) and subsequent gas sorption analysis showed a surface area (BET) of a mere 8 m^2/g.

2.6. Summary and Outlook

A series of [2+3] imine cage compounds were synthesized and converted to their respective amide variants via the Pinnick oxidation. In the process, some limitations were established for this method in addition to the existing (published) limitations of the Pinnick oxidation:

1. The hydrolytic stability of the imine cage is key to the successful progress of the oxidation. Further investigation on the hydrolytic stability of imine cages would offer a deeper insight into the applicability of this method.

2. Solubility of the imine cage in organic solvents (that are miscible with water) is critical for an efficient process. Poor solubility of amide cages was a problem encountered very often, and hence requires the use of building block containing better solubilizing group for further studies.

3. Sterically bulky substituents adjacent to the imine bonds significantly hinder the Pinnick oxidation, which has not been encountered with small molecules.

Nevertheless, conversion of imine cages derived from aliphatic amines to their respective amide cages has been demonstrated in addition to the same being carried out with aromatic imines (as discussed in the previous section). An excellent functional group tolerance of the Pinnick oxidation has been reaffirmed showing the versatility of this method to obtain chemically robust amide cages.

Synthesis and purification of five [2+3] amide cage compounds with a C_3-symmetry have been carried out, containing the important isophthalamide and a 2,6-pyridine dicarboxamide motifs, which are used as pincer ligands for metal complexes.[139] These amide cages are rich in chemistry for post-functionalization on the exterior (as discussed in the next section) as well as functionality on the interior by formation of metal complexes. Moreover, amide cage **A64-amide** already contains a bromine atom which can be subjected to coupling reactions to attach functional moieties. Although, amide cages exhibiting enhanced solubility (**B63-amide** and **B65-amide**) could be formed, they could neither be isolated in good yields nor with good purity. Therefore, the pursuit to synthesize amide cages in good yields which also exhibit good solubility in organic solvents is still ongoing.

Furthermore, the synthesis of a novel [4+4] amide cage with a truncated tetrahedron geometry has been achieved in a good yield of 52%. This amide cage presents very small windows which could possibly be advantageous for encapsulation of guest molecules.

3. Post-functionalization of [2+3] amide cages

Amide cage **A63-amide** was chosen to be the best candidate to post-functionalize since it could be prepared most efficiently and on a large scale. Moreover the 2,6-pyridine-dicarboxamide motif has been shown to be more effective for anion recognition compared to an isophthalamide motif.[82] Although the synthesis of [2+3] amide cages with bromine atoms at the periphery could be achieved (cage **A64-amide**), the isolation of such a highly insoluble cage compounds proved inefficient. Therefore, post-functionalization strategies were attempted to introduce moieties which allow for applications in supramolecular chemistry and the construction of hierarchical structures like cage-based polymers or frameworks. This could be realized using a simple strategy as shown below in Figure 44.

Amide cage compound
(tripodal)

spacer
(linker)

Covalent organic framework
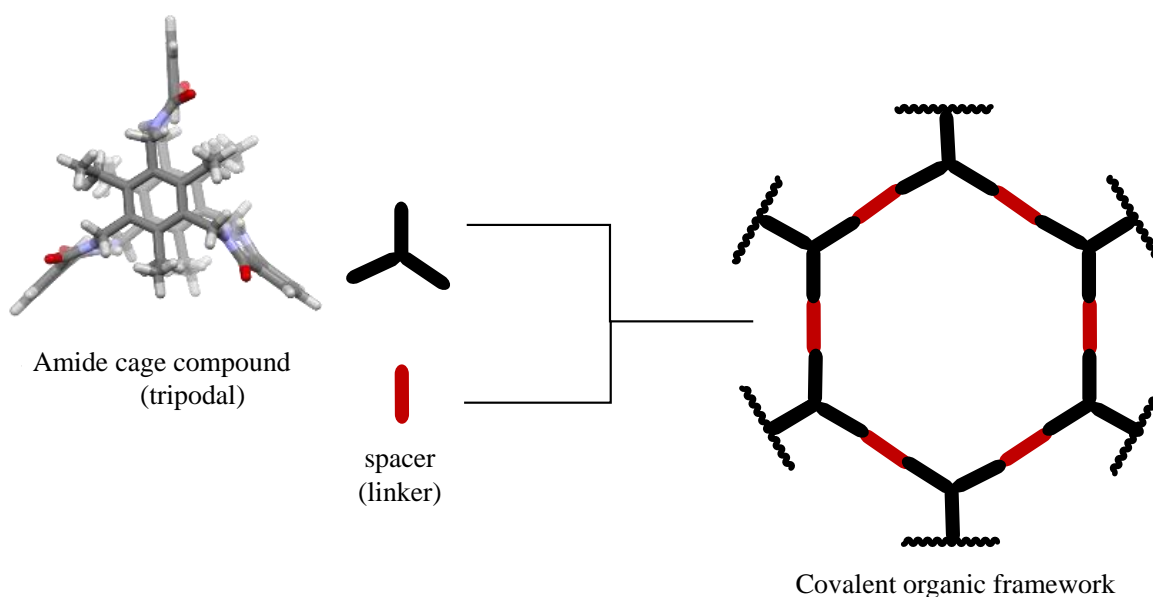
Figure 44. Construction of hexagonal units of a framework using a C_3-symmetric cage molecule and a linear building block as a spacer.

3.1. Electrophilic aromatic substitutions

The [4+6] triptycene-based amide cage **48** could be post-functionalized by utilizing the chemically active centres for S_EAr reactions. However, between the two aromatic rings in amide cage **A63-amide**, the pyridine ring in combination with the amide groups renders the aromatic system deactivated for S_EAr reactions, while the other aromatic ring contains no free positions for S_EAr reactions. Therefore, when amide cage **A63-amide** was subjected to

85

bromination or nitration, the 2,6-pyridine dicarboxamide ring could not be functionalized. Moreover, upon applying the same reaction conditions to amide cage **A62-amide**, containing an isophthalamide moiety, similar observations were made. It is noteworthy that partial nitration reactions could be detected, indicated by a large number of peaks in the ^{1}H NMR (explained by an asymmetric cage molecule due to partial nitration). But such a partially nitrated amide cage could not be isolated by HPLC or identified by mass spectroscopy. Therefore, further efforts to post-functionalize cage **A63-amide** required an alternate strategy.

3.2. C-H borylation

It was clearly evident that utilization of the aromatic π-system as a nucleophile was not effective. Therefore, a C-H borylation reaction of the amide cages was attempted. Amide cage **A63-amide** was subjected to an Iridium catalysed C-H borylation, as reported by Hartwig and Ishiyama.[140] Since this reaction proceeds under steric control, the borylation was expected to occur in the 4-position of the pyridine ring. Moreover, the acidity of the C-H hydrogen at this position would further facilitate the C-H insertion (as shown in Scheme 48).
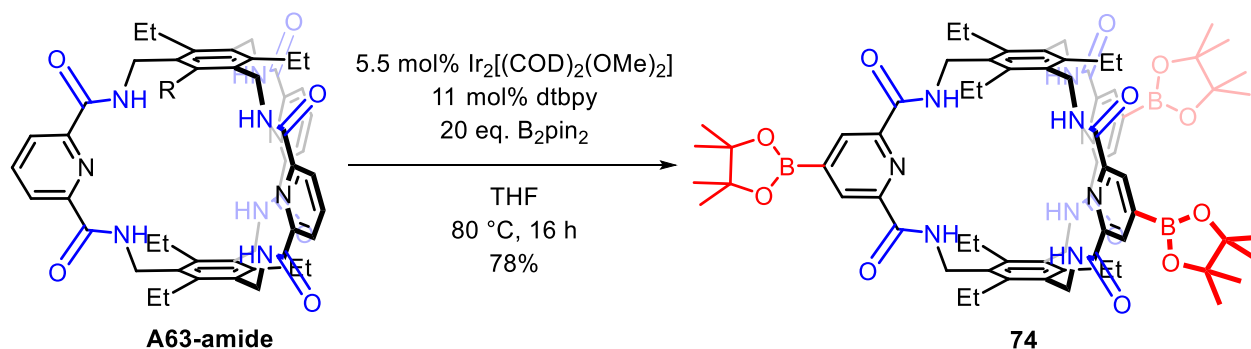
Scheme 48. Ir-catalysed C-H borylation of the [2+3] amide cage **A63-amide**.

The reaction was first attempted with 3 mol% of the Ir-catalyst and 10 equivalents of B$_2$pin$_2$. ^{1}H NMR analysis of the crude mixture indicted a mixture of fully and partially borylated cage compound. By GPC analysis, three distinct peaks were observed (Figure 45), the largest of which belongs to the 3-fold borylated product (**74**), the second largest to the 2-fold-borylated product (characterization in Figure 46), and the third likely to a one-fold borylated product (the amount obtained was not adequate for characterization). Therefore, the amount of Ir-catalyst was increased to 5.5 mol% (and hence the ligand, dtbpy to 11 mol%) and B$_2$pin$_2$ to 20 equivalents to drive the reaction to completion. Finally, GPC purification to remove residual impurities of the reagents, afforded the 3-fold borylated amide cage **74** in a yield of 78%.

Formation of the 3-fold borylated amide cage **74** was confirmed by ^{1}H NMR, ^{13}C NMR, 2D NMR and elemental analysis and final confirmation of cage **74** was achieved by post-synthetic modifications, as described in the following section.
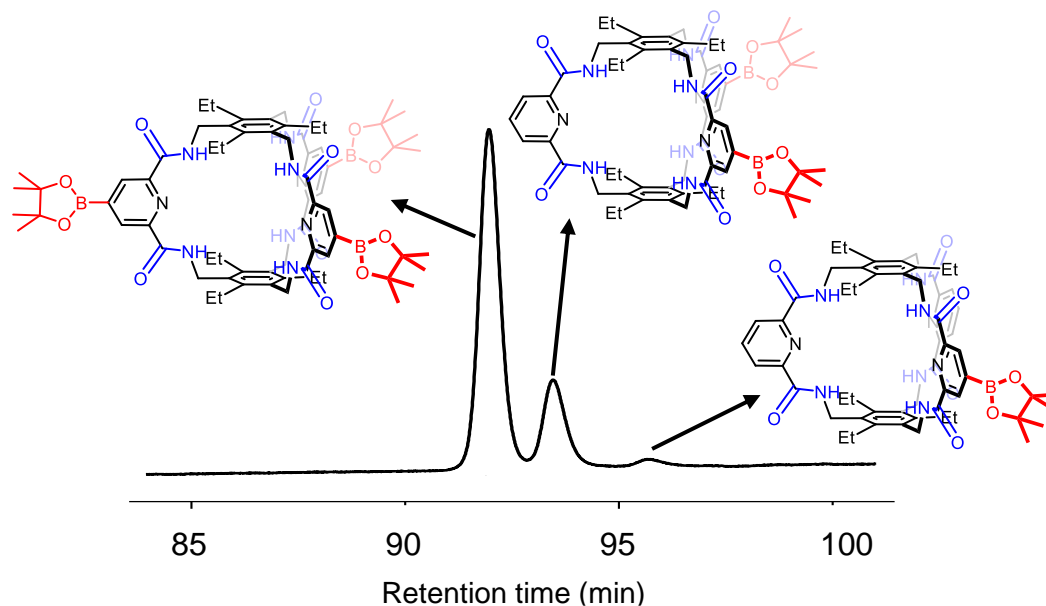
Figure 45. rGPC traces (CHCl$_3$, 254 nm) of the borylation of amide cage **A63-amide** generating a mixture of borylation products. The trace shows the peaks separated after the third cycle (~30-35 min per cycle).
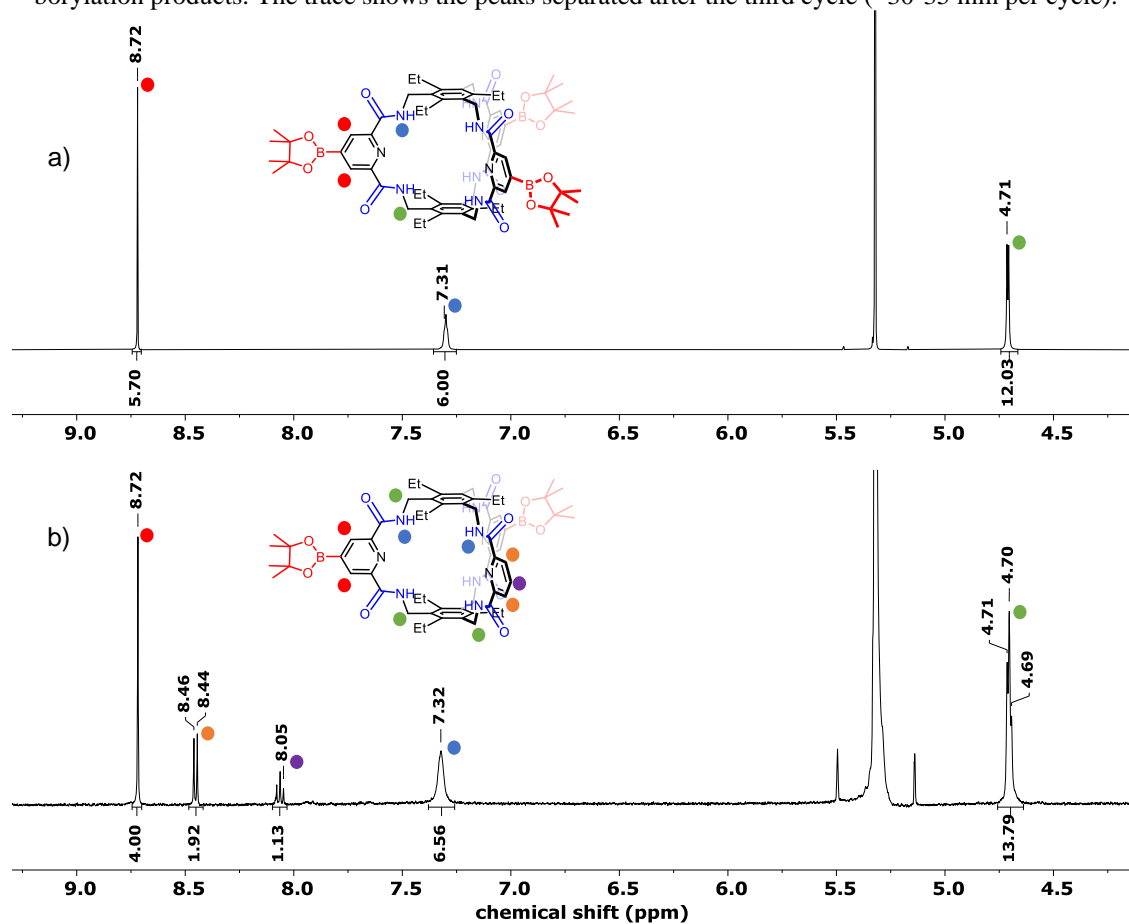
Figure 46. ^{1}H NMR spectrum (600 MHz, CD$_2$Cl$_2$) comparison of the 3-fold borylated amide cage **74** (top) and the 2-fold borylated amide cage (bottom) with assignment of the peaks in coloured circles.

^{1}H NMR of **74** is rather simple exhibiting a singlet for the amide -NH protons at $\delta = 7.31$ ppm and a singlet (at $\delta = 8.73$ ppm) for the aromatic protons on the 3,5-posotions of the pyridine ring (as shown in Figure 46a). The peak corresponding to the methyl groups on the pinacol residue resonate as a singlet at $\delta = 1.37$ ppm. In comparison, the 2-fold borylated exhibits a triplet at $\delta = 7.99$ ppm and a doublet at $\delta = 8.37$ ppm corresponding to the protons on the pyridine ring which is not borylated (Figure 46b). Moreover, the integrals corresponding to the amide peak and the methylene group next to the amide group have a slightly increased value due to the asymmetric nature of the cage compound.

3.3. Post-synthetic modification of the borylated amide cage

The rich chemistry associated with aromatic boryl-species opened up many avenues for diversification at the periphery of amide cage **A63-amide**. Of particular interest were derivatives that could have application as novel building blocks in the construction of supramolecular polymers or frameworks.

The boronic acid pinacol esters (in cage **74**) were deprotected according to a literature procedure with sodium periodate to afford the free boronic acids (cage **75**) in yields of 90% as shown in Scheme 49.[141]
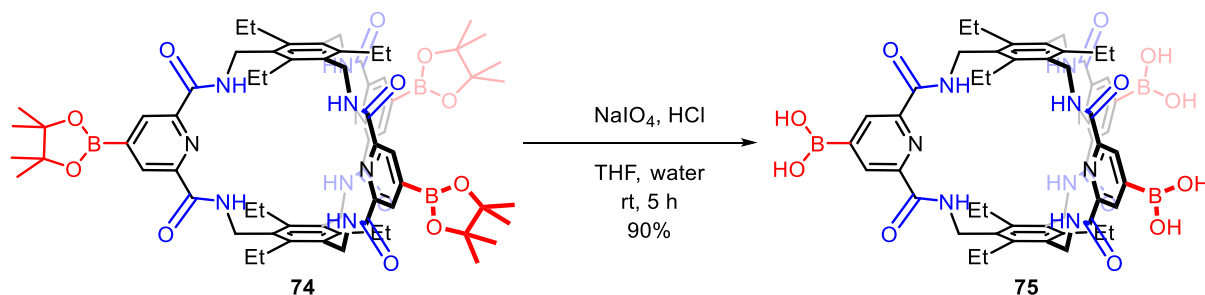
Scheme 49. Deprotection of the boronic acid pinacol esters in cage **74** to give the boronic acid-based cage **75.**

The resulting colourless solid of cage compound **75** with a C_3 symmetry was highly insoluble in most organic solvents (except DMF and DMSO), hinting towards the formation of boroxine-based higher-order structures (as shown in Scheme 50). A powder X-ray diffraction analysis exhibited sharp distinct peaks at low-angles of 4° and 7° (as shown in Figure 47a). Activation of the porous material was realized by solvent exchange in THF and diethyl ether followed by drying under high vacuum at 100 °C. It is worth noting that heating the boronic acid at high temperatures may also facilitate boroxine formation. On measuring the N_2 sorption at 77K, a BET surface area of 260 m^2/g was achieved. Additionally, QSDFT estimated pore sizes of 34 Å, 46 Å and 64 Å (as shown in Figure 47b) suggested a possible formation of large pores from

a three-dimensional arrangement of the cage molecules in a boroxine-based framework. Formation of a cage-based COF directly on deprotection of the boronic ester presents a very promising direction for the progress of this field. However, further experiments to fully characterize and study the applications of such a cage-based framework is yet to be done.

100 °C, 16 h

35 Å

COF (Simulated structure)

Structure of one pore
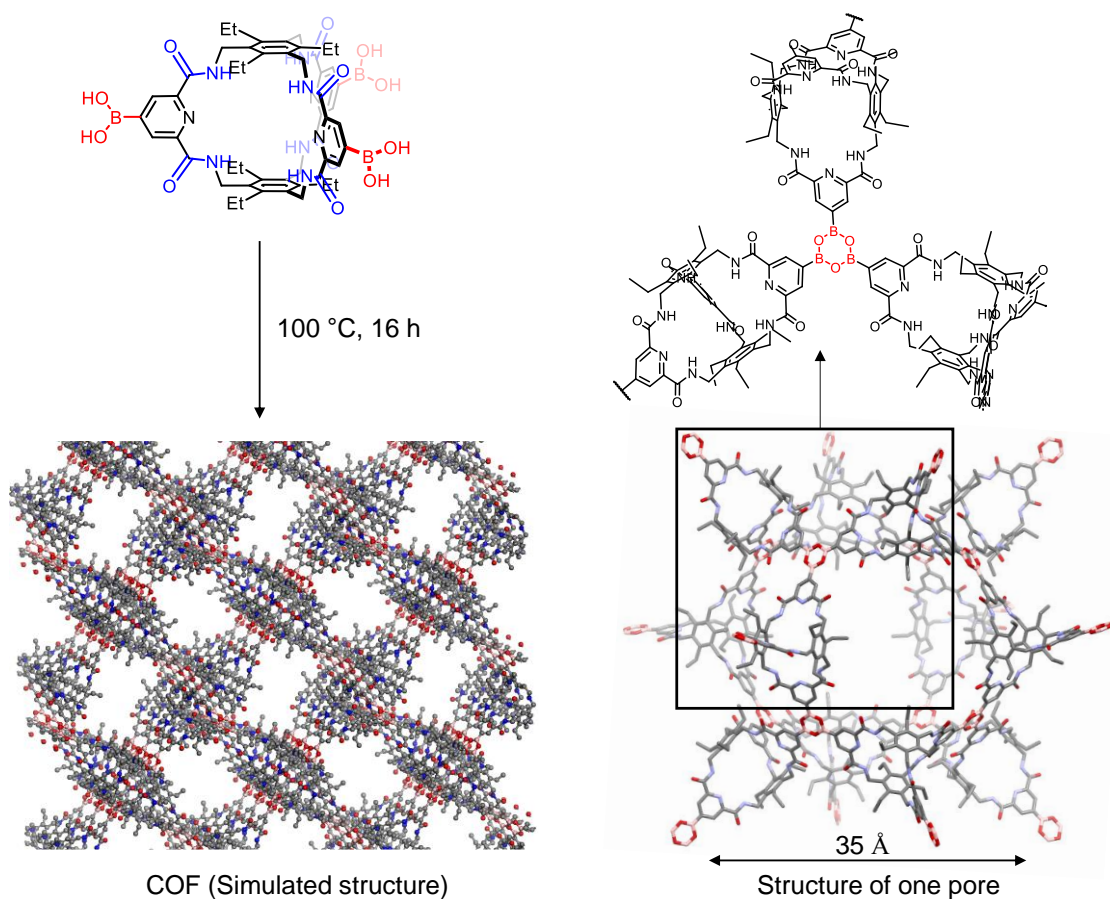
Scheme 50. Attempted formation of a 3D boroxine COF. Structure of a single pore was optimized by MM2 force field calculations and the COF structure was optimized using *Materials Studio* using srs-c topology.
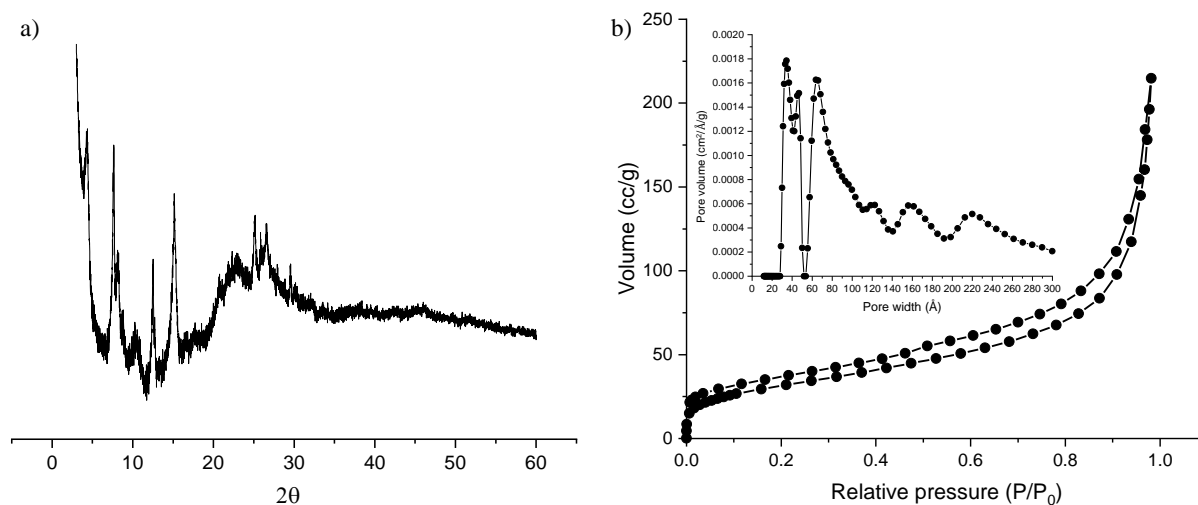
Figure 47. a) PXRD pattern of the pure boronic acid-based amide cage **75**; b) Nitrogen sorption isotherm for cage **79** at 77K (Inset : QSDFT pore size distribution).

Despite the poor solubility of cage **75** in most solvents, it was reacted with hexahydroxytriphenylene (HHTP) at 120°C in a 4:1 mixture of dioxane and mesitylene, to produce a three-dimensional COF structure. But it was found that the resulting solid exhibited the exact same PXRD pattern as that of the starting material, and moreover, it was soluble in DMSO-d_6 allowing a ^{1}H NMR spectra to be recorded, revealing peaks corresponding to both cage **75** and HHTP as separate species. Moreover, FT-IR analysis further showed no distinct peaks expected for a boronic ester moiety.[142]

The boronic acid pinacol ester could either be oxidized to a phenol or subjected to a nucleophilic substitution reaction to introduce hydrogen bond donor/acceptor moieties at the periphery of the cage molecule (as shown in Scheme 51). Oxidation of the pinacol esters was achieved by a procedure from Watson and co-workers to obtain the phenolic derivative, amide cage **76**, in a yield of 82%.[143] The reaction worked seamlessly producing no impurities but the extraction of cage **76** into an organic layer is likely to be the cause for the loss of a small amount of the substance. Cage **76** exhibited a surface area of 129 m^2/g and an enhanced solubility in polar solvents (compared to the parent amide cage **A63-amide**). Subsequent esterification reactions could deliver amide cages with interesting properties (e.g., PEG-chains for water solubility or acrylic groups for printing applications), making cage **76** a potential candidate for future applications in supramolecular chemistry.
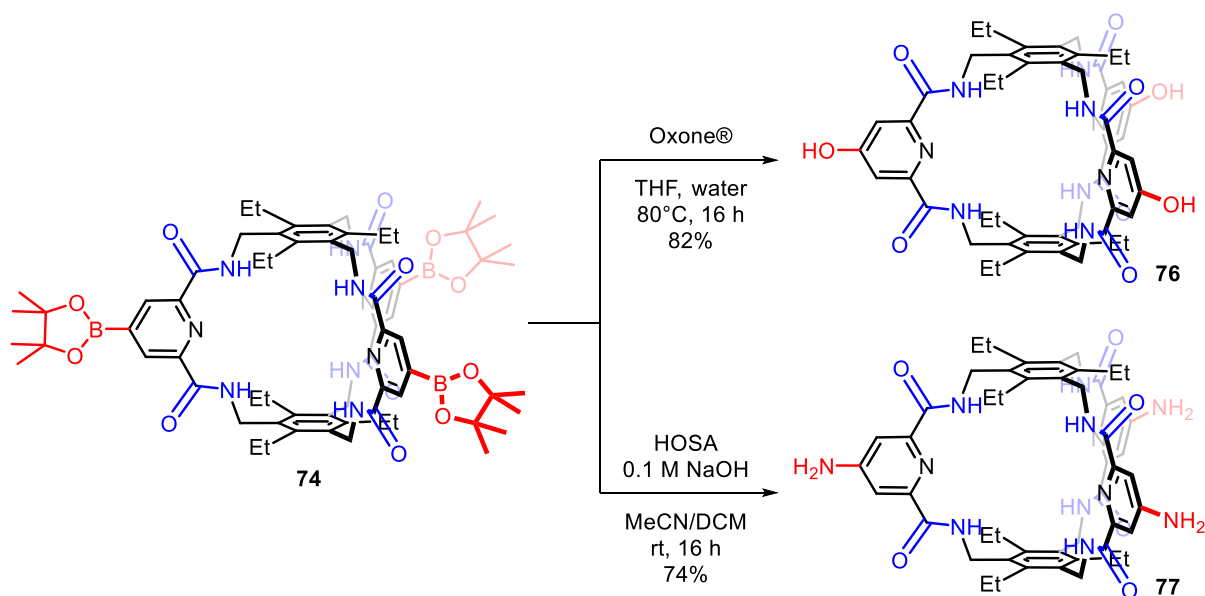
Scheme 51. Conversion of cage **74** to cage compounds **76** and **77**, containing hydrogen bond acceptor/donor moeities at the periphery.

Access to the aniline derivative of the amide cage **77** was realized via a literature procedure from McCubbin and co-workers, with a good yield of 74% (Scheme 51).[144] This cage

compound was observed to be unstable in air, since it showed the emergence of unexplained peaks in the ^{1}H NMR after being store at room temperature (without an inert atmosphere) for 24 hours. Hence, it was necessary to store **77** at 0°C under an inert atmosphere.

The hydrogen bonding ability of the phenolic or aniline moieties could be utilized to form supramolecular self-assembled structures. Formation of such self-assemblies was indeed detected while attempting to construct cage-based COFs via imine condensation using cage **77**. Reaction of cage **77** with terephthalaldehyde under acid catalysis (as shown in Scheme 52) was expected to furnish an imine-based framework but however, the starting material was unchanged, confirmed by FT-IR and ^{1}H NMR.
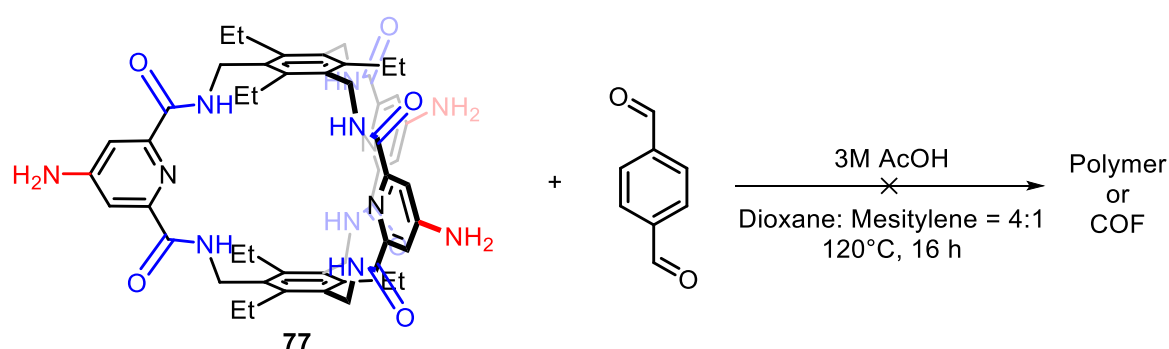
Scheme 52. Attempted synthesis of hierarchical structures using cage **77**.

Interestingly, on investigating the gas sorption properties of the amide cage **77** before and after being subjected to the imine condensation reaction, the surface area drastically rose from 110 m^2/g (before the condensation reaction) to 500 m^2/g (after the reaction). As expected, the pore size distribution suggested a greater number of smaller pores (mode = 16.6 Å) for the latter in comparison to the former (mode = 21.2 Å) (as shown in Figure 48). This observation could be explained by an effective removal of trapped water molecules from the cage cavity or by an interesting (but unlikely) formation of a hydrogen-bond driven inter-molecular assembly between the -NH$_2$ groups (of the aniline) and the C=O groups (of the amide) pointing towards the exterior of the cage.
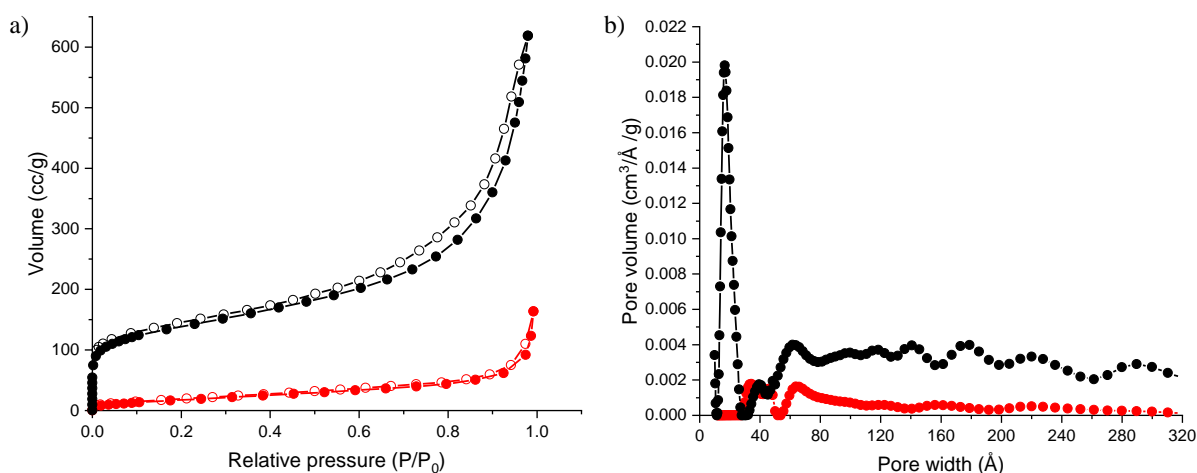
Figure 48. Gas sorption analysis of the aniline-based amide cage **77**. a) N_2 sorption isotherms; b) QSDFT pore size distribution curves. Red: Cage **77** before subjecting it to the imine condensation conditions (Dioxane/Mesitylene = 4:1, 120°C, 16 h); black: after subjecting it to the imine condensation reaction.

Lastly, Suzuki-Miyaura coupling reaction was employed to decorate the exterior of the [2+3] amide cage with anthracene units and aldehyde units. However, both reactions offered moderate yields of 42% and 32% respectively (as shown in Scheme 53).
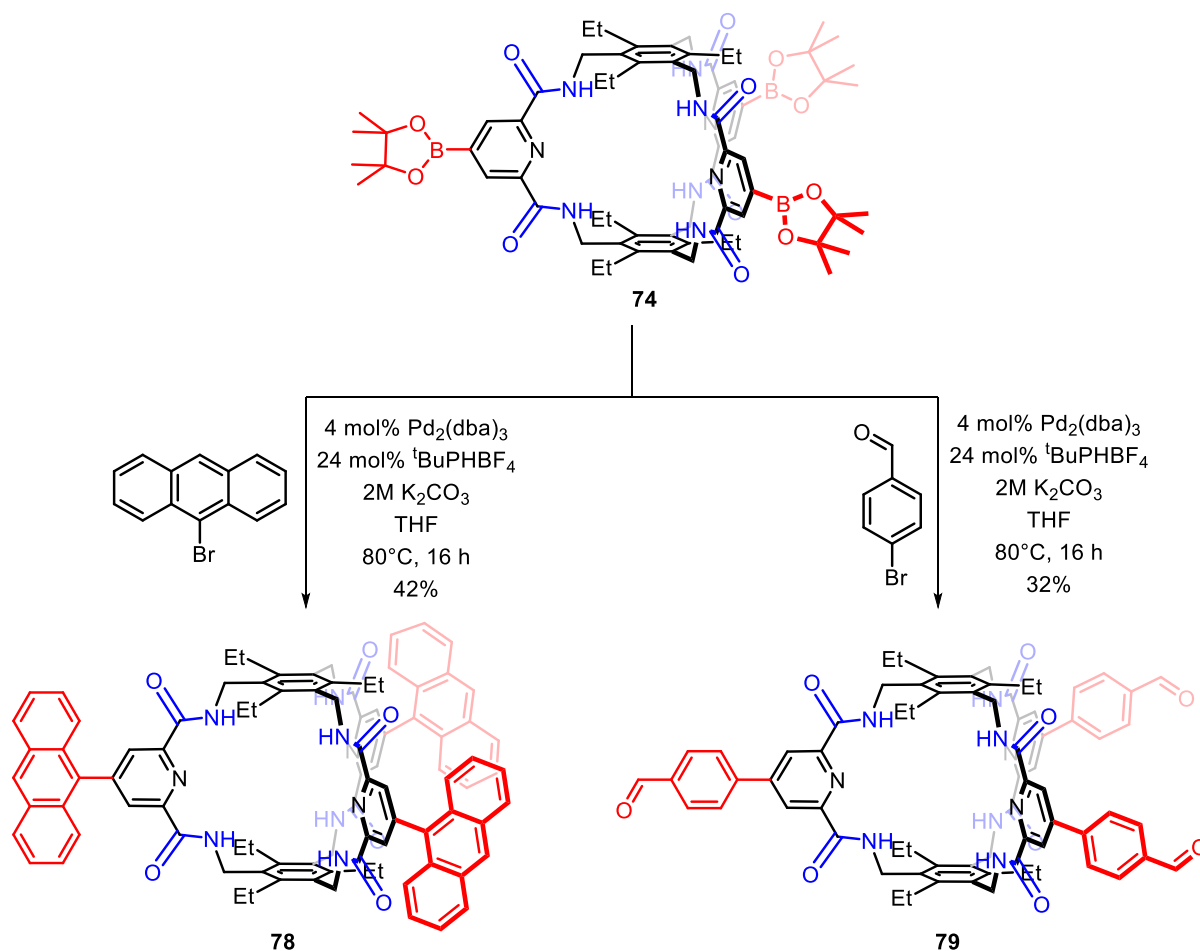
Scheme 53. Suzuki coupling reactions with cage **74** to attach anthracene moieties **78** and to introduce aldehyde groups **79** at the periphery.

Since the early reports of photodimerization of anthracene,[145] several researchers have used this concept to prepare polymers and frameworks as functional materials.[146] The face-on-face π-stacking of the anthracene is crucial to synthesize such materials. The use of functional cage molecules as a monomeric unit in such polymerizations has not yet been investigated. After successful isolation of cage **78** by HPLC (normal phase, 5% IPA in DCM), crystals were grown by vapour diffusion of diethyl ether into a solution of **78** in DCM.

A favourable π-stacking of the anthracene units was expected before conducting a photopolymerization reaction but unfortunately, the crystal structure couldn't be resolved well enough to indicate favourable π-stacking interactions. Instead, dispersion and dipole-dipole interactions dominate (as seen in Figure 49). An extensive screening of different crystallization conditions is necessary to find the best medium to force the desired stacking mode.
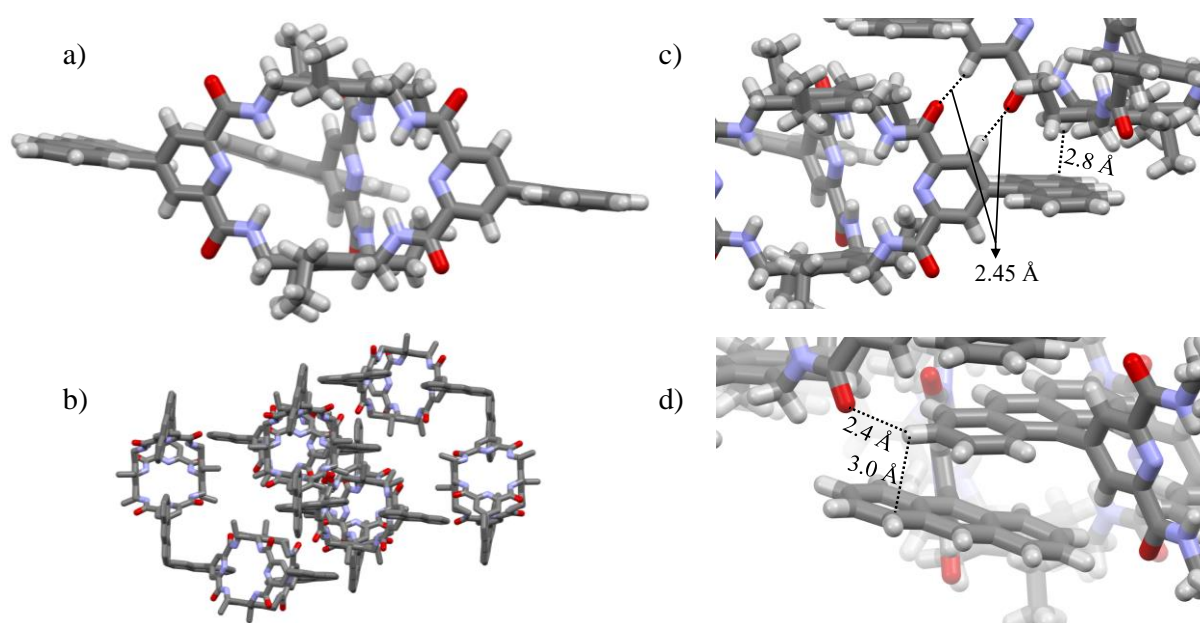
Figure 49. SCXRD structure of the anthracene decorated amide cage **78**. a) A single molecule of cage **78**; b) Packing of cage **78** with 8 molecules in a unit cell; c) intermolecular dipole-dipole and dispersion interactions; d) anthracene units of two molecules not packing in a face-on-face manner. Colours: carbon: gray; Nitrogen: blue; Oxygen: red; Hydrogen: white.

Finally, cage compound **79** was used to construct cage-based COF structures. In contrast to the boronic acid-decorated cage **75** which was highly insoluble in most solvents, cage **79** exhibited good solubility in most solvents. In comparison to reported cage-based COFs that have a non-functional monomeric cage unit,[147] cage **79** offers a functional unit which is shown not only to be shape-persistent, but also capable of selectively binding certain anions.[61] Therefore, the

synthesis of a three-dimensional COF was attempted by reacting cage **79** with p-phenylenediamine (as shown in Scheme 54).
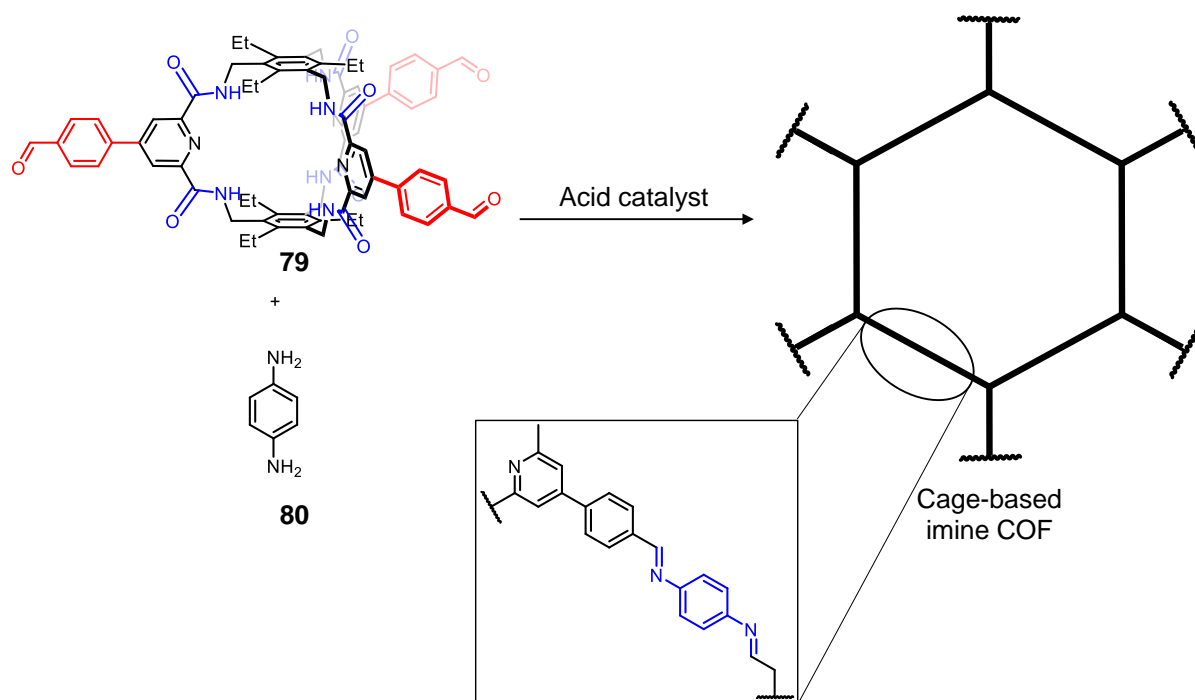
Scheme 54. Synthesis of cage-based COF via imine condensation using cage **79**.

Firstly, the imine condensation was optimized by varying the ratio of dioxane and mesitylene, and the concentration of the acid (acetic acid). The complete consumption of all the aldehyde groups to form imine groups was monitored by FT-IR spectroscopy, wherein, the peak corresponding to the aldehyde at $\bar{\nu} = 1705$ cm^{-1} had completely disappeared at the optimized reaction conditions (as shown in Figure 50).

No further characterization of the COF could be achieved since it was not generated in large enough quantities, primarily due to a lack of access to the precursor amide cage **79** in larger scales. However, the envisioned amide cage-based COF (Scheme 54) is a prospective direction to continue this research.
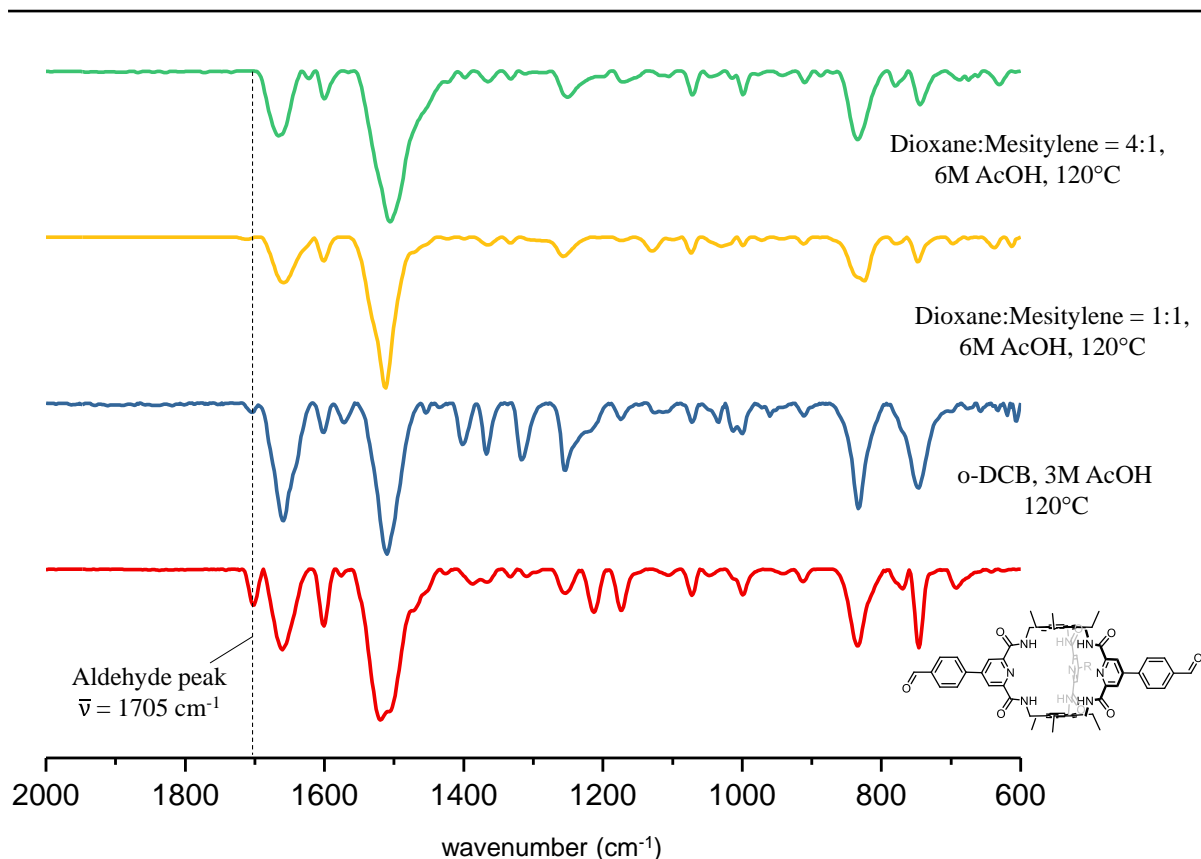
Figure 50. Monitoring the consumption of the aldehyde building block during the imine condensation, monitored by FT-IR (ATR) spectroscopy.

3.4. Summary and Outlook

To summarize, a three-fold C-H activated borylation of a cage compound (cage **74**) was achieved which is the first till date. While doing so, unsymmetric cage compounds could be isolated (two-fold borylated amide cage) which is being pursued in the Mastalerz group for applications in 3D printing. The 'Bpin' group at the exterior of the cage molecule could be converted into other functional groups which provides functionality to these [2+3] amide cages.

Functional groups containing hydrogen bond acceptor/donor (-NH$_2$ or -OH groups in cages **77** and **76** respectively) were introduced and also an anthracene group (cage **78**) which is capable of forming π-π interactions. Furthermore, the introduction of boronic acid (cage **75**) and aldehyde groups (cage **79**) on the periphery of the cage molecule provides an opportunity to further conduct DCC mediated construction of hierarchical structures (frameworks or polymers). However, the poor solubility and an inefficient synthetic route for the preparation of cages **75** and **79** respectively, renders this direction unsuitable.

Possible solutions to these problems can be realized by preparing an analogue of cage **75** with enhanced solubility (as shown in Scheme 55a) and by choosing an alternative synthetic route to obtain cage **79** (as shown in Scheme 55b).
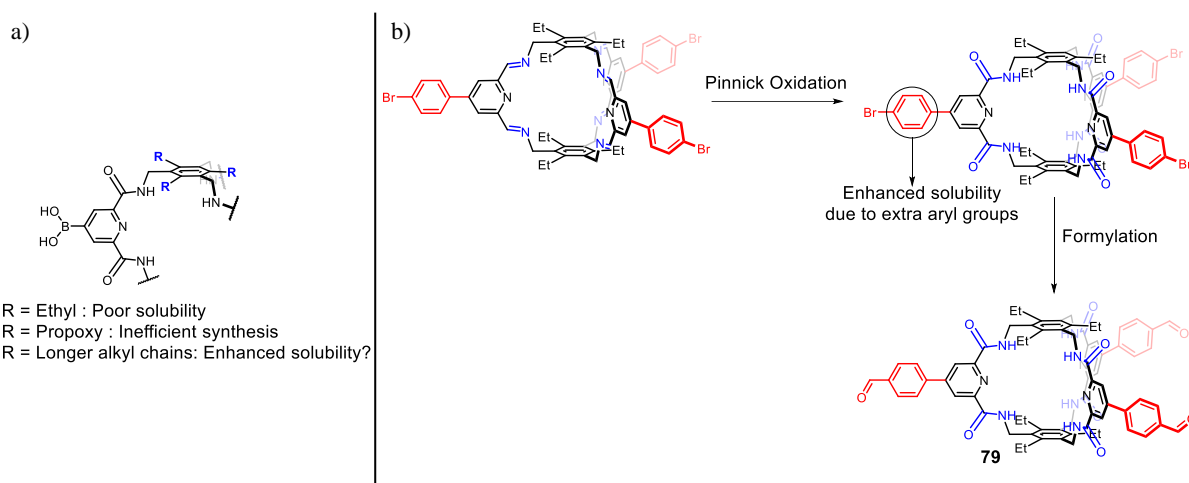
Scheme 55. a) Partial structure of an amide cage containing boronic acid group at its periphery, showing the effect of 'R' groups; b) Alternate synthetic route to obtain amide cage **79**.

In addition to functionality at the exterior of the cage molecule, it would be highly interesting to also introduce functionality at the interior cavity. This could be achieved by forming metal complexes utilizing the pincer-type ligands (with the pyridine N atom and the amide -NH groups acting as complexing centres) present in cage **A63-amide**. Preliminary attempts towards forming metal complexes at the interior cavity either led to unexplainable results (see crystal structure in appendix section 4.6) or could not be realized within the time constraints of this thesis, however, remains a promising direction for this project.

IV. Summary and Outlook

This thesis covers the synthesis and characterization of a series of new amide cage compounds, half of which were obtained directly from the Pinnick oxidation and the other half via post-synthetic modifications. A novel approach to prepare a large variety of amide cages has been established, making it possible to access amide cages that were previously unfeasible. The synthesis of these amide cages provided an opportunity to study their chemical properties such as solubility, thermal and chemical stability, and crystal packing in solid state. Furthermore, the enhanced chemical robustness enabled post-functionalization of the amide cages resulting in functional cage compounds for prospective utilization in construction of hierarchical structures (e.g., COFs and supramolecular self-assembled structures).

The Pinnick oxidation is known to have very few limitations and a high functional group tolerance delivering excellent yields. However, the applicability of this reaction on imine cage compounds depends strongly on the stability and solubility of the starting imine cage. Additionally, one novel limitation was observed based on structural preferences – the presence of bulky substituents adjected to the imine groups possibly hinders the approach of the oxidant, resulting in failure of the reaction.

Nonetheless, the Pinnick oxidation was carried out on imine cages derived from aliphatic amines as well as aromatic amines, delivering novel amide cages of different geometry and sizes that could not be accessed effectively by conventional amide coupling reactions (as shown in Figure 51).
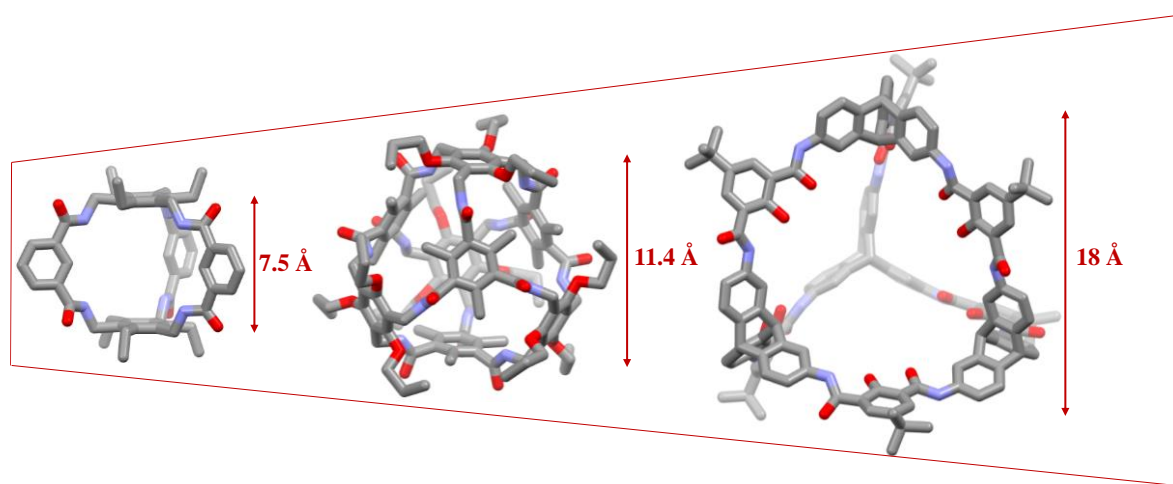
Figure 51. SCXRD structures of amide cages from the left: **A62'**, **A73'** and **48** shown in an ascending order of the size of their internal cavities.

By choosing appropriate precursors, the library of amide cages could be extended to include more geometries and larger cage molecules, which is currently being pursued in the Mastalerz group. Utilization of such a vast array of amide cages for anion recognition may finally offer a better understanding of the geometrical requirement (and hence the spatial arrangement of hydrogen bond donors) of receptors for effective binding.[148] It is worth mentioning that the recognition of a chloride anion by receptor **A63-amide** (as reported by Anslyn et al.)[61] was reproduced with a change in solvent (in THF compared to MeCN/DCM in literature) and indeed a binding was observed by ^{1}H NMR titration experiment, with an association constant of $K_a = 178$ M^{-1} (see Figure 137 in appendix section 1.3 for further details).

Perhaps, the greatest advantage of this method is a combination of its versatility and the chemical robustness of the end products, which can prove to be a vital tool in delivering a combinatorial library of cage structures that can be isolated by chromatographic methods (ongoing project in the Mastalerz group). While imine cages are often not stable enough to withstand the chemical environment of the stationary phase and mobile phase of chromatographic separation, amide cages exhibit excellent chemical stability. Moreover, amide bonds are not in dynamic equilibrium in solution, hence eliminating the risk of decomposition during isolation.

V. Experimental Section

1. General Remarks

All reactions were carried out under ambient conditions unless otherwise noted. For the exclusion of moisture and/or air, the reactions were carried out under a constant argon atmosphere using common Schlenk techniques.

Column Chromatography: Flash column chromatography was performed using silica gel with particle sizes of 0.063-0.200 mm (Sigma-Aldrich Chemie GmbH) or 0.040-0.063 mm (Macherey-Nagel & Co. KG, Düren) using petroleum ether, ethyl acetate, dichloromethane, or their mixtures as eluents. For determination of the right eluent, thin layer chromatography was performed in a way that the fraction with the highest R_f value was $R_f < 0.4$ and this mixture was then used for the corresponding column chromatography.

Thin Layer Chromatography (TLC): For thin layer chromatography fluorescent labelled silica coated aluminium plates (60 F254, Merck) were used and examined using UV-light irradiation with $\lambda_{ex} = 254$ and 366 nm.

High Performance Liquid Chromatography (HPLC): HPLC was performed on an Agilent Technologies 1200 chromatograph equipped with a Macherey-Nagel C8 RP/5P column using MeCN/H_2O gradients.

Recycling High Performance Liquid Chromatography (rHPLC): Preparative HPLC was performed on a Shimadzu LC-20AP recycling System using a normal phase column (SiO$_2$, 250 mm × 21 mm) and reverse phase column (Nucleodur C8 column, 250 mm × 21 mm) from Macharey-Nagel with a flow-rate of 0.1-150 mL/min and a pressure maximum of 300 bar. Detection of the sample were realized by an SPD-M20A photo diode array with a wavelength range of 190-800 nm.

Recycling Gel Permeation chromatography (rGPC): rGPC was performed with a Shimadzu DGU-20A3R degassing unit, LC-20AD pump unit, CTO-20AC column oven, CBM-20A communication bus module, SPD-M20A diode array detector, FRC10A fraction collector, FCV-20AH2 valve unit, a PSS SDV (20 × 50 mm) precolumn and three SDV 100 Å (20 × 300 mm) columns connected in series.

Ultra-Performance Liquid Chromatography – Mass Spectrometry (**UPLC-MS**): Ultra-Performance Liquid Chromatography was performed on a Waters UPLC-SQD2 machine

connected to a single quadrupole mass spectrometer with an APCI (Atmospheric Pressure Chemical Ionization) source. A 1.7 µm ethylene bridged- BEH-C8 column, 2.1×50 mm with a gradient of water/acetonitrile and a flow of 0.6 mL/min was used.

Nuclear Magnetic Resonance Spectroscopy (NMR): NMR spectra (^{1}H, 2D coupling experiments) were recorded in CDCl$_3$, CD$_2$Cl$_2$, DMSO-d_6, CD$_3$OD or THF-d_8 using a Bruker DRX 300 (^{1}H: 300 MHz; ^{13}C: 75 MHz), Bruker Avance III 300 (^{1}H: 300 MHz; ^{13}C: 75 MHz), Bruker Avance III 400 (^{1}H: 400 MHz; ^{13}C: 101 MHz), Bruker Avance III 500 (^{1}H: 500 MHz; ^{13}C: 126 MHz) or Bruker Avance III 600 (^{1}H: 600 MHz; ^{13}C: 151 MHz) spectrometer at 298 K, unless otherwise mentioned. Chemical shifts are reported in parts per million (ppm) relative to the traces of CHCl$_3$ ($\delta_H = 7.26$ ppm, $\delta_C = 77.2$ ppm), CD$_2$Cl$_2$ ($\delta_H = 5.32$ ppm, $\delta_C = 53.8$ ppm), DMSO-d_6 ($\delta_H = 2.50$ ppm, $\delta_C = 39.5$ ppm) or THF-d_8 ($\delta_H = 3.58$, 1.72 ppm, $\delta_C = 67.2$, 25.3 ppm) in the corresponding fully deuterated solvent.[149]

Melting Points (M.p.): Melting points (not corrected) were determined in open glass capillaries using a Büchi Melting Point B-540 apparatus.

Mass Spectrometry (MS): High resolution mass spectrometry experiments were carried out on a Fourier Transform Ion Cyclotron Resonance (FT-ICR) mass spectrometer ApexQe hybrid 9.4 T (Bruker Daltonik GmbH, Bremen, Germany) equipped with a 9.4 T superconducting magnet and interfaced to an Apollo II MTP Dual ESI/MALDI source for DART, ESI and MALDI experiments. MALDI-TOF MS experiments were carried out on a Bruker AutoFlex Speed time-of-flight with DCTB (*trans*-2-[3-(4-*tert*-butylphenyl)-2-methyl-2-propenylidene]malo-nonitrile) as matrix. Electrospray ionization (ESI) mass spectra were recorded on a Finnigan LCQ quadrupole ion trap. Molecule fragments were given as a mass-to-charge proportion (*m/z*).

Infrared (IR) Spectroscopy: IR spectra were recorded on a Fourier transform spectrophotometer (Bruker Lumos) equipped with a Zn/Se or Ge ATR crystal. The positions of the peaks are reported in wavenumbers (cm^{-1}) and their signal intensity is described with vs (very strong), s (strong), m (medium), w (weak), br (broad).

Elemental Analysis (EA): Elemental analysis was performed by the microanalytical Laboratory of the University of Heidelberg using an Elementar Vario EL machine.

Thermal Gravimetric Analysis (TGA): Thermal gravimetric analyses were measured on a Mettler-Toledo TGA/DSC1 instrument with a TGA/DSC-Sensor 1100 equipped with a MX1

balance (Mettler-Toledo) and a GC100 gas control box for nitrogen supply. TGA samples were measured in 70 HL Al_2O_3 crucibles. All measurements were carried out under a flow of nitrogen or air (10-20 mL/min) as mentioned for the corresponding measurement.

Powder X-ray Diffractometry (PXRD): X-ray powder diffraction data in Figure 47 was collected using a SmartLab X-ray diffractometer from Rigaku equipped with a HyPix-3000 detector. All measurements were carried out with special glass capillaries (0.6 mm diameter) in Debye-Scherrer geometry using monochromatic Cu Kα_1 radiation ($\lambda = 1.54059$ Å). 1D scan was performed on all samples with the capillaries rotated at a speed of 60 rpm. Background data for baseline correction was recorded with an empty capillary under identical measurement conditions. The measurement was performed by Dr. Sven Elbert (OCI, Heidelberg University).

X-ray Crystal Structure Analysis: Crystal structure analysis was accomplished on a Quazar Bruker APEX I ($\lambda_{MoK\alpha} = 0.71073$ Å), Bruker APEX II ($\lambda_{MoK\alpha} = 0.71073$ Å) or a Stoe Stadivari ($\lambda_{CuK\alpha} = 1.54186$ Å) diffractometer. Intensities were corrected for Lorentz and polarization effects; an empirical absorption correction was applied using SADABS based on the Laue symmetry of the reciprocal space.[150] The structures were solved by intrinsic phasing or by direct methods with dual-space recycling and refined by full-matrix least squares methods based on F2 against all unique reflections.[151] All non-hydrogen atoms were given anisotropic displacement parameters. Hydrogen atoms were input at calculated positions and refined with a riding model. When found necessary, disordered groups and/or solvent molecules were subjected to suitable geometry and *adp* restraints and/or constraints.

Scanning Electron Microscopy (SEM): Electron micrographs in Figure 26 and Figure 28 were acquired using an Ultra 55 field emission scanning electron microscope (Carl Zeiss Microscopy, Germany). Imaging was performed with a working distance of 3.0 mm and a landing energy of 1.2 keV and an aperture of 10 μm. The secondary electron images were recorded by a SE2-detector and the backscattered electron images recorded by an EsB-detector. The powder sample was suspended in isopropanol or cyclohexane, treated with ultrasound and drop-casted onto a silicon wafer substrate pre-cleaned in air-plasma. Silicon wafer: single side polished p-type (100), pursued from Si-Mat, Germany. Electron micrographs of figures 65, 66 and 98 were acquired using a Crossbeam 540 field emission scanning electron microscope (Carl Zeiss Microscopy, Germany). Imaging was performed with a working distance of 3.0 mm and a landing energy between 1.0 keV and 3.0 keV. The secondary electron images were recorded by an Inlens-detector and the backscattered electron images recorded by an

EsB-detector. The powder sample was suspended in isopropanol, treated with ultrasound and drop-casted onto a silicon wafer substrate pre-cleaned in air-plasma. Silicon wafer: single side polished p-type (100), from Si-Mat, Germany. The measurements were performed by Dr. Wen-Shan Zhang (BioQuant, Heidelberg University).

1.1. Solvents

The solvents were used from stock without further purification or drying unless otherwise noted

Acetone	Honeywell ≥ 99.5%
Acetone-d_6	Deutero 99%
Acetonitrile	Sigma-Aldrich ≥ 99.9%
Acetonitrile-d_3	Deutero 99.8%
Chlorobenzene	Sigma-Aldrich 99.8%
o-Dichlorobenzene	Sigma-Aldrich 99%
1,2-Dichloroethane	Honeywell 99%
Chloroform-d	Sigma-Aldrich 99.8%
4,6-Dibromoisophthalaldehyde	From Tobias Schick (AK Mastalerz)
Dichloromethane	VWR Chemicals stab. with 0.2% ethanol
Diethyl ether	Sigma-Aldrich ≥ 99.5%
Diethylene glycol diethyl ether	Acros Organics > 98%
Dimethoxyethane	Sigma-Aldrich > 99.5%
4,6-Dimethylisophthalaldehyde	From Tobias Schick (AK Mastalerz)
N,N-Dimethylformamide	Sigma-Aldrich ≥ 99.8%
1,4-Dioxane	VWR Prolabo ≥ 99.9%
DMSO-d6	Sigma-Aldrich 99.9%
Ethanol abs.	VWR Chemicals > 99.9%
Ethyl acetate	Honeywell ≥ 99.5%
n-Heptane	Acros Organics ≥ 99%
n-hexane	VWR Chemicals 98%
Mesitylene	Sigma-Aldrich 99%
Methanol	Sigma-Aldrich ≥ 99.8%
2-Methyl-tetrahydrofuran	Sigma-Aldrich > 99% inhibitor free
Nitrobenzene	Merck ≥ 99%
n-Pentane	Sigma-Aldrich 98%
Petroleum ether (40-60 °C)	Honeywell puriss.

Propionitrile	Sigma-Aldrich 99%
Pyridine	Grüssing 99.5%
Pyridine-d$_5$	Deutero 99.5%
Tetrahydrofuran	Sigma-Aldrich ≥ 99.9% stab. with 250 ppm BHT
Toluene	Sigma-Aldrich ≥ 99.7%
2,4,6-Trimethylbenzene-1,3,5-tricarbaldehyde	From Jochen Lauer (AK Mastalerz)
Water	deionized

1.2. Chemicals and Reagents

Acetic acid (Glacial)	Sigma-Aldrich, 100%
Aluminium chloride	abcr, 99%
Anthracene	Sigma-Aldrich, 97%
Anthracene (certified reference material)	Sigma-Aldrich, TraceCert®
Anthranilic acid	Merck, 99%
Bis-(pinacolato)-diboron	Carbolution, 99%
Bromine	Sigma-Aldrich reagent grade
9-Bromoanthracene	Acros Organics, 96%
4-Bromobenzaldehyde	Acros Organics, 99%
N-Bromosuccinimide	Sigma-Aldrich, 99% or Carbolution 98%
n-Butyllithium solution 2.5M in hexanes	Sigma-Aldrich
Celite® 545	VWR Chemicals
Chelidamic acid	Sigma-Aldrich
Di-μ-chlorobis[(1,2,5,6-η)-1,5-cyclooctadiene]diiridium	Sigma-Aldrich, 97%
4,4′-Di-tert-butyl-2,2′-dipyridyl	Sigma-Aldrich, 98%
1,3-Dimethoxybenzene	Sigma-Aldrich
Hydrazine monohydrate	Merck, 98%
Hydrochloric acid (conc.)	Sigma-Aldrich, 36%
Hydrogen peroxide	Sigma-Aldrich, 34.5-36.5%
Hydroxylamine-O-sulfonic acid	Sigma-Aldrich, 99.999%
Iron powder	Merck puriss
Iso-amyl nitrite	TCI, >95%
Isophthalaldehyde	TCI, 98%

Magnesium sulphate	Sigma-Aldrich, 98%
Maleic anhydride	Sigma-Aldrich, 99%
2-Methyl-2-butene	Sigma-Aldrich, 95%
Methyl iodide	Acros Organics, 99%
Molecular sieve (4Å)	Carl Roth
Nitric acid (conc.)	Sigma-Aldrich, 64-66%
Nitric acid (fuming)	Merck, 100%
Oxone® monopersulphate compound	Sigma-Aldrich
Palladium on act. Charcoal (5% Pd)	Degussa
Paraformaldehyde	VWR chemicals, pellets
Phosphoryl chloride	Merck, synthesis grade
Phosphorous pentabromide	Acros Organics, 95%
Potassium carbonate	Grüssing, 99%
Potassium nitrate	Grüssing, 99%
2,6-Pyridinedicarbonyl dichloride	abcr, 97%
Pyridine-2,6-dicarboxaldehyde	Sigma-Aldrich, 97%
Selenium dioxide	Sigma-Aldrich, 98%
Sodium acetate	Grüssing, 99%
Sodium azide	Acros Organics, 99%
Sodium borohydride	Sigma-Aldrich, 99%
Sodium bromide	Grüssing, 99.5%
Sodium chloride	Sigma Aldrich, 99%
Sodium chlorite	Sigma Aldrich, 80%
Sodium dihydrogen phosphate monohydrate	AppliChem, 99.5%
Sodium hydroxide	Merck, 99%
Sodium periodate	Sigma-Aldrich, 99.8%
Sulfuric acid (conc)	Sigma-Aldrich, 95-97%
4-*tert*-Butyl-2,6-diformylphenol	Sigma-Aldrich, 96%
Thionyl chloride	Acros Organics, 99.7%
Tris(dibenzylideneacetone)bispalladium(0)	Carbolution, 98%
1,3,5-Triethylbenzene	Sigma-Aldrich, 97%
Triethylamine	Sigma-Aldrich, 99.5%
Triphenylphosphine	Sigma-Aldrich 95%
Tri-*tert*-butylphosphonium tetrafluoroborate	abcr, 99%

1.3. Gas Sorption Measurements

The surface areas and porosities were characterized by nitrogen adsorption and desorption analysis at 77.35 K with an autosorb computer-controlled surface analyser (AUTOSORB-iQ2, Quantachrome). The activation methods are listed in chapter IV4 p. 197. The Brunauer-Emmett-Teller (BET) surface areas were calculated assuming a cross sectional area of 0.162 nm^2 for the nitrogen molecules in the pressure range $P/P_0 = 0.01$-0.1. Rouquerol plots were created to assure the pressure range used for the BET equations, here only the relative pressure values with a positive slope in the Rouquerol plot were taken into account. The quenched solid-density functional theory (QSDFT model) and isotherm data were used to calculate the pore size distribution. Measurements of N_2, H_2, CH_4, and CO_2 at 273 K were carried out using a simple Dewar vacuum flask with a ice/water mixture. A temperature of 263 K was applied by using a frozen mixture of water/EtOH (80:20, v/v) and for measurements between 298 K and 363 K a Lauda C6 CS thermostat was used, which was equipped with a Fryka KT 12-52 cryostat for the measurements at 298 K and 313 K. The temperatures were frequently monitored by a VWR TD 131 digital thermometer.

1.4. UPLC assay

General procedure: To a suspension of the imine cage (1 eq.) in THF was added 30% solution of hydrogen peroxide (75 eq.), $NaClO_2$ (40 eq.) in that order and stirred vigorously. While stirring vigorously, 1M acetic acid (10 eq.) in water was added dropwise. The reaction was left to stir for 16 hours. The reaction mixture was evaporated under reduced pressure to remove THF. The resulting suspension was diluted with water (50 mL) and the precipitate was filtered. The precipitate was washed thoroughly with water (5×40 mL) and dried under high vacuum.

The crude mixture was dissolved in a solvent and a known amount of the internal standard (anthracene) was added. This mixture was passed through the UPLC-MS. Using the area of the peak of anthracene, area of the peak of the cage compound and the response factor, the amount of cage compound in the crude mixture was calculated, and subsequently the yield of the reaction as shown below:

$$\text{Amount of cage compound in the crude mixture}$$
$$= \frac{(\text{Conc. of Int. Std})(\text{Area of peak corr. to amide cage})(\textbf{Response factor})}{\text{Area of peak corr. to Int. Std}}$$

$$\text{Yield} = \frac{\text{Amount of cage compound in the crude mixture (in mmol)}}{\text{Amount of starting material (in mmol)}} \times 100$$

Calculation of response factor: A known amount of the pure cage compound was dissolved in a solvent, denoted by vial 1. Anthracene was dissolved in the same solvent, denoted by vial 2. Three solutions were made with a linear concentration gradient of the two solutions. A graph was plotted with ratio of the concentration of internal standard to the concentration of cage compound (C_{is}/C_s) on the X-axis and area of the peak of internal standard to the cage compound on the Y-axis. The slope of this linear curve gives the response factor.

2. Synthetic procedures

2.1. Compounds of Chapter III, Section 1.

Synthesis of N-(p-tolyl)benzamide (50')
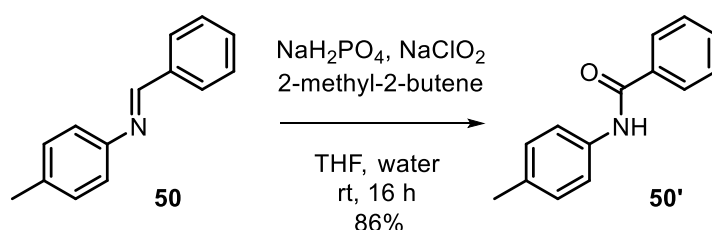
To a solution of **50** (500 mg, 2.5 mmol, 1 eq.) in 20 mL THF, 2-methyl-2-butene (5.3 mL, 250 mmol, 20 eq.), NaClO$_2$ (1.1 g, 12.5 mmol, 5 eq.) was added and stirred vigorously. While stirring, 2 mL of a 2 M aqueous solution of NaH$_2$PO$_4$ (450 mg, 3.85 mmol, 1.5 eq.) was added dropwise. The solution turned from yellow to orange in 10 minutes. The reaction mixture was left to stir for another 4 hours. Upon completion (monitored by TLC), the reaction mixture was concentrated by evaporating the THF, diluted with water and then extracted with ethyl acetate (3 × 25 mL). The organic layer was washed with brine, dried over MgSO$_4$ and concentrated. Purification by silica gel column chromatography (PE: acetone = 7:3) gave the amide **50'** as an orange-brown solid (454 mg, 2.15 mmol, 86%). Analytical data was in agreement with the literature.[152]

^{1}H NMR (300 MHz, CDCl$_3$) δ 7.88-7.86 (d, 2 H, Ar-*H*), 7.76 (bs, 1H, -CO-N*H*), 7.58-7.46 (m, 5H, Ar-*H*), 7.19-7.17 (d, 2H, Ar-*H*), 2.35 (s, 3H, -CH$_3$).

Melting point = 157 °C (Lit.: 156-157 °C)

Synthesis of 3,5-di-tert-butyl-N-(3,4-dimethylphenyl)-2-methoxybenzamid (52')
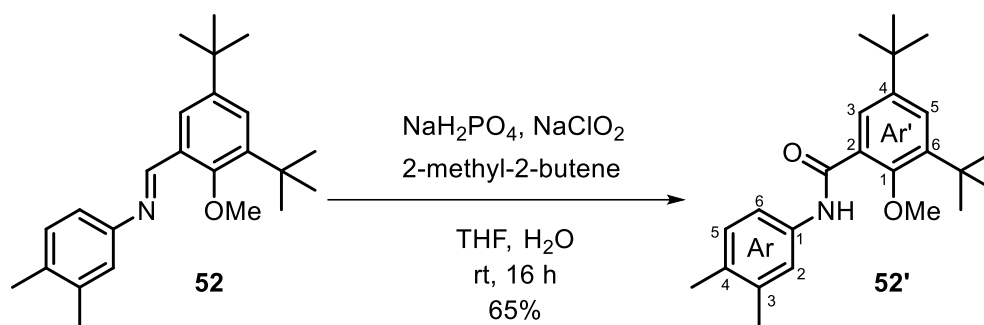
To a solution of **52** (100 mg, 0.28 mmol, 1 eq.) in 4 mL THF, 2-methyl-2-butene (3.1 mL, 28 mmol, 20 eq.), $NaClO_2$ (128 g, 0.42 mmol, 5 eq.) was added and stirred vigorously. While stirring, 0.4 mL of a 2 M aqueous solution of NaH_2PO_4 (53 mg, 0.45 mmol, 1.5 eq.) was added dropwise. The reaction mixture was left to stir for 16 hours. Upon completion (monitored by TLC), the reaction mixture was concentrated by evaporating the THF, diluted with water and then extracted with ethyl acetate (3×10 mL). The organic layer was washed with brine, dried over $MgSO_4$ and concentrated. Purification by silica gel column chromatography (PE: acetone = 7:3) gave the amide **52'** as a colourless solid (67 mg, 0.18 mmol, 65%).

^{1}H NMR (400 MHz, CDCl3) δ = 8.71 ppm (s, 1H, -N*H*CO-), 7.80 (d, J = 2.6 Hz, 1H, Ar'-*H*-3), 7.51 (m, 1H, Ar'-5), 7.49 (d, J = 2.6 Hz, 1H, Ar-*H*-6), 7.41 (dd, J = 8.1 Hz, 2.4 Hz, 1H, Ar-*H*-2), 7.13 (d, J = 8.1 Hz, 1H, Ar-*H*-5), 3.81 (s, 3H, -OC*H₃*), 2.29 (s, 3H, Ar-C*H₃*), 2.25 (s, 3H, Ar-C*H₃*), 1.44 (s, 9H, -C(C*H₃*)₃), 1.33 (s, 9H, -C(C*H₃*)₃).

^{13}C NMR (101 MHz, CDCl₃) δ = 165.3 ppm (-NH*C*O-), 155.2 (Ar'-*C*-1), 146.6 (Ar'-*C*-6), 142.3 (Ar'-*C*-4), 135.9 (Ar-*C*-4), 133.9 (Ar-*C*-1), 129.6 (Ar-*C*-3,5), 128.3 (Ar'-*C*-2), 127.5 (Ar'-*C*-5), 126.5 (Ar'-*C*-3), 119.9 (Ar-*C*-2,6), 62.9 (-O*C*H₃), 35.5 (-*C*(CH₃)₃), 34.7 (-*C*(CH₃)₃), 31.4 (-C(*C*H₃)₃), 30.4 (-C(*C*H₃)₃), 20.9 (Ar-*C*H₃), 18.4 (Ar-*C*H₃).

IR (neat, ATR) $\tilde{v}$ = 3274 cm^{-1} (w), 2954 (s), 2941 (s), 2858 (m), 1730 (m), 1649 (s), 1597 (s), 1516 (vs), 1467 (s), 1359 (m), 1327 (s), 1118 (s), 1008 (s), 817 (vs), 705 (s).

EI-MS: m/z = 367.2495 [M]$^+$ (Calculated for $C_{24}H_{33}NO_2$: m/z = 367.2511).

Melting point = 173 °C - 176 °C

Elemental analysis: Calculated for $C_{24}H_{33}NO_2$: C 78.43, H 9.05 N 3.81; found: C 78.11, H 8.84, N 3.70.

Synthesis of 2,7,14-trinitrotriptycene (55a)
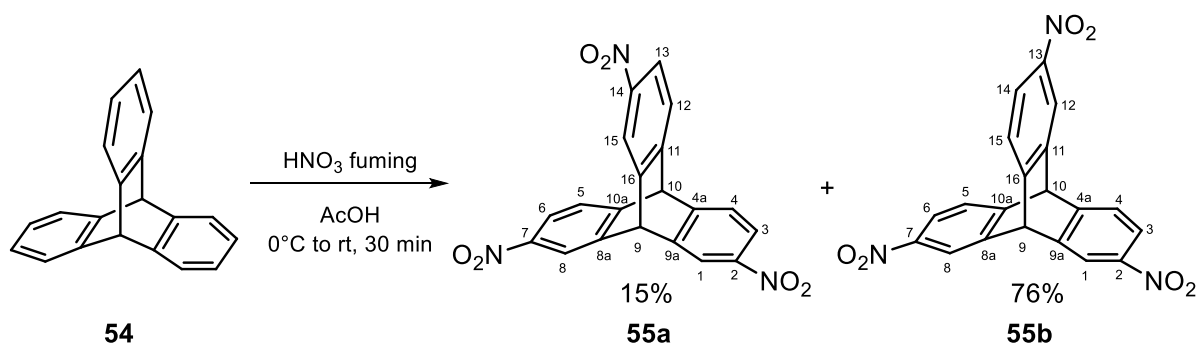
Triptycene **53** (40 g, 157 mmol, 1.0 eq.) was suspended in acetic acid (300 mL) and the mixture was cooled to 0 °C. Fuming nitric acid (150 mL) was added over 5 mins at 0 °C and the reaction mixture was stirred for 10 min. It was allowed to warm to room temperature and stirred for a further 1 hour. The dark red solution was poured onto water (2 L) and the white precipitate was stirred for 30 min. The solid was filtered and washed with water (1 L), dissolved in DCM (400 mL), extracted with water (3 × 300 mL) and dried over $MgSO_4$. The solvent was removed under reduced pressure and the crude yellow solid was purified via flash column chromatography, PE/EE (1/4, v/v to 1/2, v/v) to afford 2,7,13-trinitrotriptycene **55b** (46.5 g, 119.3 mmol, 76%) as a pale-yellow foam and 2,7,14-trinitrotriptycene **55a** (9.1 g, 23.5 mmol, 15%) of as colourless crystals. Analytical data was in agreement with the literature.[153]

55a:

¹H NMR (300 MHz, DMSO-d_6): δ = 8.39 ppm (d, J = 2.2 Hz, 3H, Ar-1,8,13-*H*), 8.04 (dd, J = 8.2, 2.3 Hz, 3H, Ar-3,6,15-*H*), 7.83 (d, J = 8.2 Hz, 3H, Ar-4,5,16-*H*), 6.44 (s, 1H, bridgehead-9-*H*), 6.39 (s, 1H, bridgehead-10-*H*).

Melting point = 345 °C (Lit.: >300 °C)

55b:

¹H NMR (300 MHz, CDCl₃): δ = 8.34 ppm (m, 3H,), 8.05 (m, 3H), 7.62 (m, 3H), 5.84 (s, 1H, bridgehead-9-*H*), 5.80 (s, 1H, bridgehead-10-*H*).

Melting point = 178 °C (Lit.: 178-180 °C)

Synthesis of 2,7,14-triaminotriptycene (56)
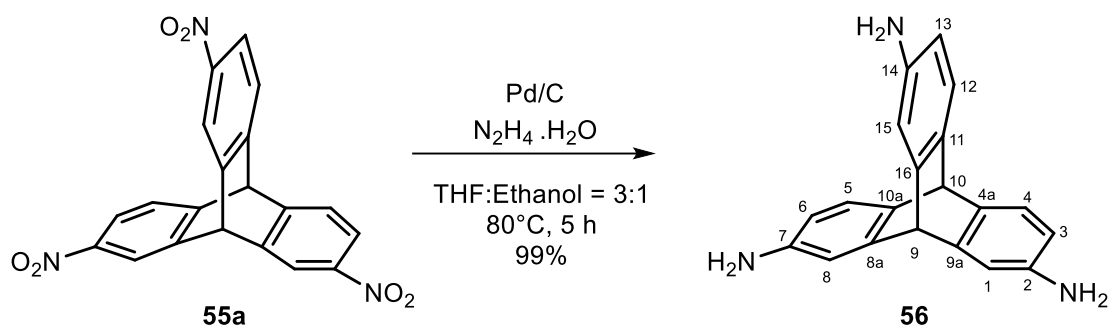
2,7,14-Trinitrotriptycene **55a** (1 g, 2.6 mmol, 1.0 eq.) and Pd/C (5%, 120 mg) were suspended in THF (30 mL) and EtOH (10 mL), heated to reflux, and stirred under an argon atmosphere. Hydrazinium hydroxide (1.5 mL, 31.2 mmol, 12.0 eq.) was added over 5 min and the reaction mixture was further refluxed for 2 hours. The reaction mixture was cooled to room temperature and the Pd/C was filtered and washed with THF. The solvents were evaporated under reduced pressure and the crude was passed through a silica gel column with an eluent mixture of DCM:MeOH = 9.5:0.5 to afford **56** (778 mg, 0.942 mmol, 99%) as a colourless solid. Spectral data was in agreement with the literature.[153]

^{1}H NMR (300 MHz, DMSO-d_6): δ = 6.86 ppm (d, J = 7.7 Hz, 3H, 4,5,12-*H*), 6.62 (d, J = 2.1 Hz, 3H, 1,8,15-*H*), 7.84 (dd, J = 2.2 Hz, 3H, 3,6,13-*H*), 4.88 (s, 2H, 9,10-*H*), 4.73 (bs, 6H, -N*H*$_2$).

Melting point = 281 °C (Lit.: 279-283 °C)

Synthesis of the [4+6] salicylbisimine cage (-OH) (24)
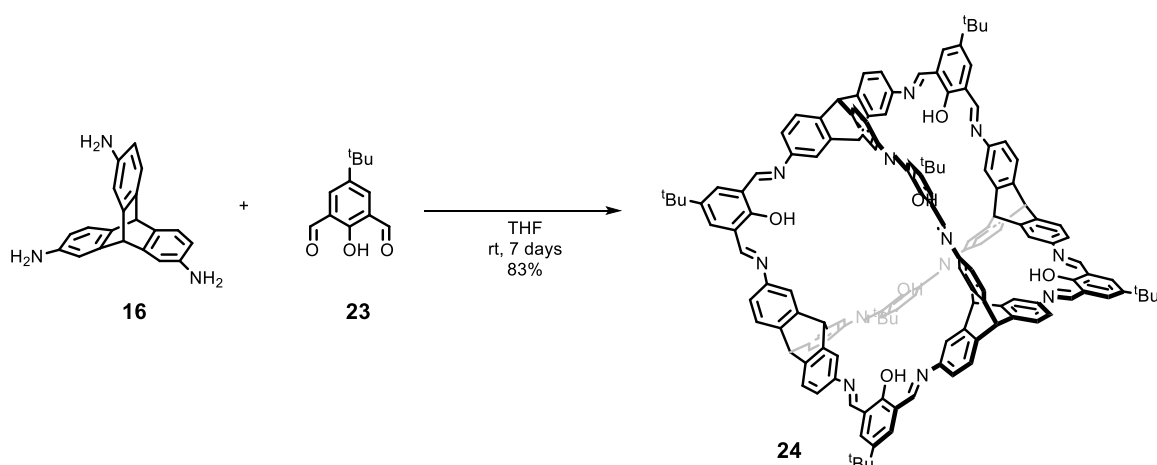
2,7,14-Triaminotriptycene **16** (100 mg, 0.33 mmol, 4.0 eq.) and 5-(*tert*-butyl)-2-hydroxyiso-phthalaldehyde **23** (103 mg, 0.5 mmol, 6.0 eq.) were dissolved in abs. THF (14 mL) under argon atmosphere and stirred for seven days at room temperature. The reaction mixture was

109

sonicated every day to remove the solids adhered to the sides of the flask. The orange precipitate was filtered over a glass frit (pore 4), washed with Et$_3$N/THF$_{abs.}$ solution (40 μL Et$_3$N in 4 mL THF$_{abs}$), dried under high vacuum (10^{-2} bar) to afford 154 mg (0.07 mmol, 83%) of cage compound **24** as a yellow solid. Analytical data was in agreement with the literature.[154]

¹H NMR (500 MHz, 360 K, DMSO-*d₆*): δ = 13.77 ppm (s, 6H, - O*H*), 9.17 (s, 12H, -C*H*=N), 8.04 (s, 12H, salicyl-Ar-*H*), 7.77 (d, 12H, *J* = 1.7 Hz, triptycene-Ar- 1,8,15-*H*), 7.59 (d, 12H, *J* = 7.5 Hz, triptycene-Ar-4,5,12-*H*), 7.28 (d, 12H, *J* = 7.1 Hz, triptycene-Ar-3,6,13-*H*), 6.02 (s, 4H, triptycene bridgehead-9-*H*), 5.78 (s, 4H, triptycene bridgehead-10-*H*), 1.33 (s, 54H, - C(C*H₃*)₃).

MALDI-TOF-MS (dithranol matrix): *m/z* 2218.605 (Calculated for C$_{152}$H$_{128}$N$_{12}$O$_6$: *m/z* = 2218.011).

Melting point: >400 °C.

Synthesis of the [4+6] salicylbisimine cage (-OMe) (47)
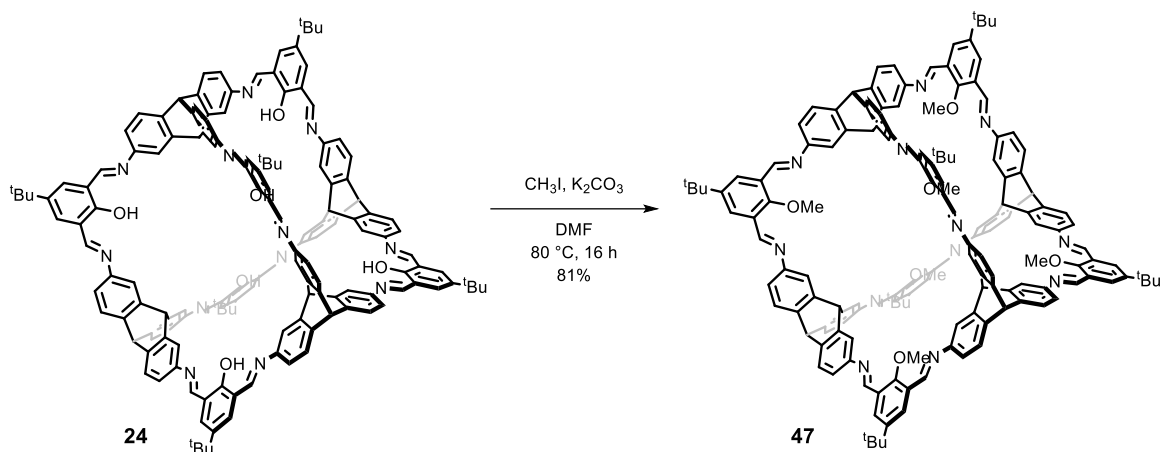
Cage **24** (100 mg, 0.045 mmol, 1.0 eq.) and K$_2$CO$_3$, (250 mg, 1.8 mmol, 40 eq.) were suspended in dry DMF (15 mL) under argon atmosphere. The reaction mixture was stirred for 10 min and MeI (63 μL, 0.9 mmol, 20 eq.) was added and the reaction mixture was stirred for 16 hours at 80 °C. The reaction mixture was cooled to room temperature, and the precipitate filtered over a glass frit (pore 4). The residue was washed with DMF (3 × 5 mL), MeOH (5 mL) and *n*-pentane (excess). Afterwards, the yellow solid was dissolved in abs. THF, filtered through a 25 mm syringe filter (0.45 μm PTFE) and concentrated under high vacuum (10^{-2} bar) to afford cage compound **47** (84 mg, 0.036 mmol, 81%) as a bright yellow solid. Analytical data was in agreement with the literature.[120]

¹H NMR (500 MHz, THF-d_8): δ = 9.21 ppm (s, 12H, -CH=N-), 8.43 (s, 12H, salicyl-Ar-H), 7.70 (d, 12H, J = 2.0 Hz, triptycene-Ar-1,8,15-H), 7.50 (d, 12H, J = 7.8 Hz, triptycene-Ar-4,5,12-H), 7.19 (dd, 12H, J = 2.0 Hz, triptycene-Ar-3,6,13-H), 5.83 (m, 4H, triptycene bridgehead-9-H), 5.61 (m, 4H, triptycene bridgehead- 10-H), 4.09 (s, 18H, -OCH₃) 1.33 (s, 54H, -C(CH_3)₃).

MALDI-TOF-MS (DCTB matrix): m/z = 2302.254 (Calculated for $C_{158}H_{140}N_{12}O_6$: m/z = 2302.105)

Melting point: >400 °C.

Synthesis of the [4+6] amide cage (-OMe) (48)
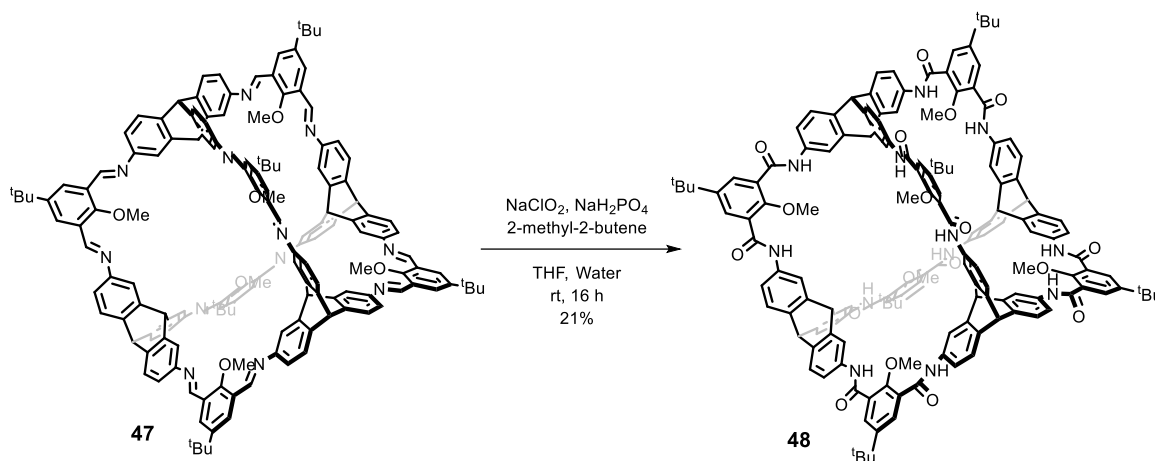
Cage **47** (250 mg, 0.108 mmol, 1eq.) was dissolved in THF (50 mL) and 2-methyl-2-butene (1.1 mL, 10.8 mmol, 100 eq.) was added, followed by sodium chlorite (586 mg, 6.48 mmol, 60 eq.). An aqueous solution of NaH_2PO_4 (1 M, 233 mg, 1.94 mmol, 18 eq.) was added dropwise over 3 minutes and the reaction mixture was stirred for 16 hours at room temperature. The reaction mixture was then washed with brine (30 mL), dried over $MgSO_4$ and concentrated to get a highly viscous orange liquid. After stirring with petroleum ether (20 mL) for 30 minutes, a yellow precipitate was formed, which was filtered and washed with methanol. The crude product was then suspended in methanol (20 mL), heated to reflux and DMF was added dropwise until a clear solution was obtained. On cooling gradually to room temperature, crystals were formed which were filtered, washed with methanol and dried under high vacuum (10^{-2} bar) at 150 °C to obtain the cage compound **48** as a colourless solid (55 mg, 0.022 mmol, 21%).

111

¹H NMR (500 MHz, DMSO-d_6): δ = 10.30 ppm (s, 12 H, -CO-NH-), 7.84 (s, 12 H, triptycene-Ar-1,8,13-H), 7.80 (s, 12 H, salicyl-Ar-H), 7.49-7.43 (m, 24 H, triptycene-Ar-4,5,16-H), 7.43 (s, 12 H, triptycene- Ar-3,6,15-H), 5.96 (s, 4H, triptycene bridgehead-9-H), 5.66 (s, 4H, triptycene bridgehead-10-H), 4.07 (s, 18H, -OCH₃, 1.32 (s, 54H, -C(CH₃)₃).

¹³C NMR (150 MHz, DMSO-d_6) δ = 164.9 ppm (-CO-NH-), 154.5 (salicyl-Ar-C-OMe), 146.1 (salicyl-Ar-C), 142.4 (triptycenyl-Ar-C), 135.8 (triptycenyl-Ar-C), 129.9 (salicyl-Ar-C), 129.1 (salicyl-Ar-C), 124.1 (triptycenyl-Ar-C), 118.8 (triptycenyl-Ar-C), 63.2 (-OCH₃), 53.1 (triptycene bridgehead-9-C), 51.9 (triptycene bridgehead-10-C), 35.0 (C-(CH₃)₃), 31.6 (C-(CH₃)₃).

IR (neat, ATR) $\tilde{v}$ = 3342 cm⁻¹ (b), 2964 (m), 1655 (s), 1599 (m), 1537 (s), 1474 (s), 1423 (m), 1355 (m), 1304 (w), 1263 (m), 1200 (w), 1107 (m), 1030 (w), 999 (m), 856 (w), 812 (w), 779 (w), 663 (m).

MALDI-TOF-MS (DCTB matrix): m/z = 2495.116 (Calculated for C₁₅₈H₁₄₀N₁₂O₁₈: m/z = 2495.05)

Elemental analysis: Calculated for C₁₅₈H₁₄₀N₁₂O₁₈·12 H₂O: C 69.08, H 6.16 N 6.12; found: C 68.99, H 6.06, N 5.99.

Melting point: Decomposes above 350 °C

Synthesis of the [4+6] brominated amide cage (59a)
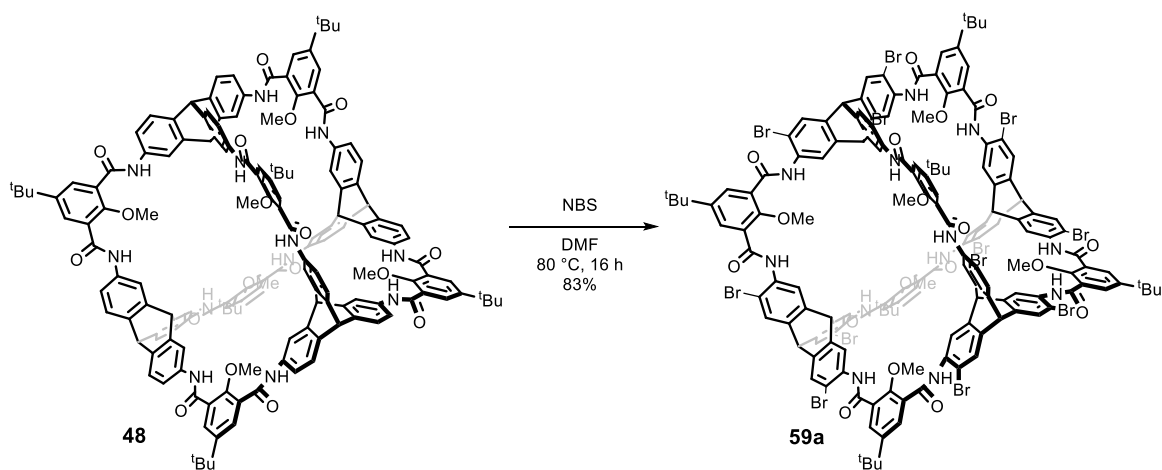
To a solution of the amide cage **48** (50 mg, 0.02 mmol, 1 eq.) in DMF (15 mL), N-bromosuccinimide (178 mg, 1 mmol, 50 eq.) was added and stirred at 80 °C for 16 hours. The orange solution was diluted with water and cooled to 0 °C. The obtained yellow precipitate

was filtered, washed with water (2 × 20 mL), methanol (2 × 20 mL) and dried under high vacuum (10^{-2} bar) at room temperature. The pale orange solid was suspended in DMSO (7 mL) and heated to 120 °C to give a saturated solution. On gradual cooling, crystals of the cage compound were formed, which were filtered, washed with methanol (50 mL) and dried under high vacuum (10^{-2} bar) at 100 °C. The cage compound **50a** was obtained as a colourless solid (56 mg, 0.016 mmol, 83%).

^{1}H NMR (500 MHz, DMSO-d_6): δ = 10.24 ppm (s, 12 H, -CO-NH-), 7.87 (s, 12 H, triptycene-Ar-1,8,13-H), 7.73 (s, 12 H, triptycene-Ar-4,5,16-H), 7.56 (s, 12 H, salicyl-Ar-H), 6.18 (s, 4H, triptycene bridgehead-9-H), 5.88 (s, 4H, triptycene bridgehead-10-H), 4.13 (s, 18H, -OCH_3), 1.34 (s, 54H, -C(CH_3)$_3$).

^{13}C NMR (150 MHz, DMSO-d_6) δ = 166.5 ppm (-CO-NH-), 153.1 (salicyl-Ar-C-OMe), 145.8 (Salicyl-Ar-C), 145.3 (triptycenyl-Ar-C), 145.1 (triptycenyl-Ar-C), 133.9 (triptycenyl-Ar-C), 131.4 (salicyl-Ar-C), 128.7 (triptycenyl-Ar-C), 127.2 (salicyl-Ar-C), 125.9 (triptycenyl-Ar-C), 118.1 (triptycenyl-Ar-C), 63.4 (-OCH$_3$), 51.2 (triptycene bridgehead-9,10-C), 50.9 (triptycene bridgehead-9,10-C), 34.8 (C-(CH$_3$)$_3$), 31.8 (C-(CH$_3$)$_3$).

IR (neat, ATR) $\tilde{v}$ = 3354 cm^{-1} (b), 2964 (m), 2876 (w), 2357 (w), 1668 (s), 1583 (m), 1510 (s), 1475 (s), 1402 (m), 1364 (m), 1310 (w), 1271 (s), 1200 (w), 1111 (m), 1030 (w), 991 (m), 897 (m), 816 (w), 795 (w), 768 (w), 681 (s), 629 (s).

MALDI-TOF-MS (DCTB matrix): m/z = 3440.268 (Calculated for C$_{158}$H$_{128}$Br$_{12}$N$_{12}$O$_{18}$: m/z = 3440.958)

Elemental analysis: Calculated for C$_{158}$H$_{128}$Br$_{12}$N$_{12}$O$_{18}$·19 H$_2$O: C 49.91, H 4.45 N 4.42; found: C 49.90, H 4.52, N 4.31.

Melting point: Decomposes above 350 °C

Synthesis of the [4+6] nitrated amide cage (60a)
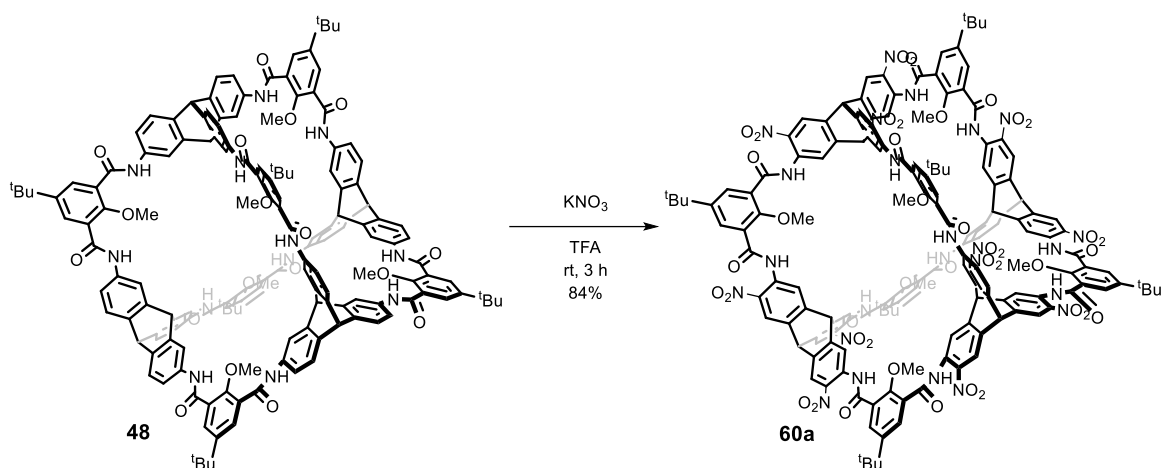
To a solution of amide cage **48** (40 mg, 0.016 mmol, 1 eq.) in TFA (18 mL) was added KNO_3 (22 mg, 0.224 mmol, 14 eq.). The reaction mixture was stirred at room temperature for 3 hours to obtain a yellow clear solution. After diluting with water (50 mL) and neutralizing to pH 7, a yellow precipitate was formed, which was filtered and, washed with water (20 mL) and methanol (20 mL). The bright yellow solid was dissolved in DMSO (8 mL) and methanol (8 mL) was layered on the DMSO. After 18 hours, yellow crystals were formed of the cage compound which were filtered, washed with methanol (4 × 15 mL) and dried under high vacuum (10^{-2} bar) at 100 °C. The cage compound **60a** was obtained as a yellow solid (41 mg, 0.013 mmol, 84%).

^{1}H NMR (500 MHz, DMSO-d_6): δ = 10.64 ppm (s, 12 H, -CO-NH-), 8.31 (s, 12 H, triptycene-Ar-1,8,13-H), 8.10 (s, 12 H, triptycene-Ar-4,5,16-H), 7.72 (s, 12 H, salicyl-Ar-H), 6.66 (s, 4H, triptycene bridgehead-9-H), 6.37 (s, 4H, triptycene bridgehead-10-H), 4.16 (s, 18H, -OCH$_3$), 1.36 (s, 54H, -C(CH_3)$_3$).

^{13}C NMR (100 MHz, DMSO-d_6) δ = 165.2 ppm (-CO-NH-), 154.0 (salicyl-Ar-C-OMe), 148.5 (triptycenyl-Ar-C), 146.05 (Salicyl-Ar-C), 142.1 (triptycenyl-Ar-C), 141.4 (salicyl-Ar-C), 129.7 (triptycenyl-Ar-C), 129.3 (triptycenyl-Ar-C), 128.6 (salicyl-Ar-C), 124.7 (triptycenyl-Ar-C), 121.6 (triptycenyl-Ar-C), 63.4 (-OCH$_3$), 51.3 (triptycene bridgehead-9-C), 50.0 (triptycene bridgehead-10-C), 34.7 (C-(CH$_3$)$_3$), 31.4 (C-(CH$_3$)$_3$).

IR (neat, ATR) $\tilde{v}$ = 3377 cm^{-1} (b), 2978 (m), 1678 (s), 1624 (m), 1589 (m), 1529 (m), 1477 (s), 1339 (s), 1265 (s), 1196 (m), 997 (m), 912 (m), 845 (m), 750 (w), 700 (w).

MALDI-TOF-MS (DCTB matrix): *m/z* = 3000.635, 3016.882, 3032.910 (Calculated C$_{158}$H$_{140}$N$_{24}$O$_{42}$: *m/z* = 3032.940)

Elemental analysis: Calculated for C$_{158}$H$_{140}$N$_{24}$O$_{42}$·44 H$_2$O: C 49.58, H 5.69 N 8.78; found: C 49.64, H 5.48, N 8.66.

Melting point: Decomposes above 350 °C.

Synthesis of the [4+6] amide cage (-OH) (61)
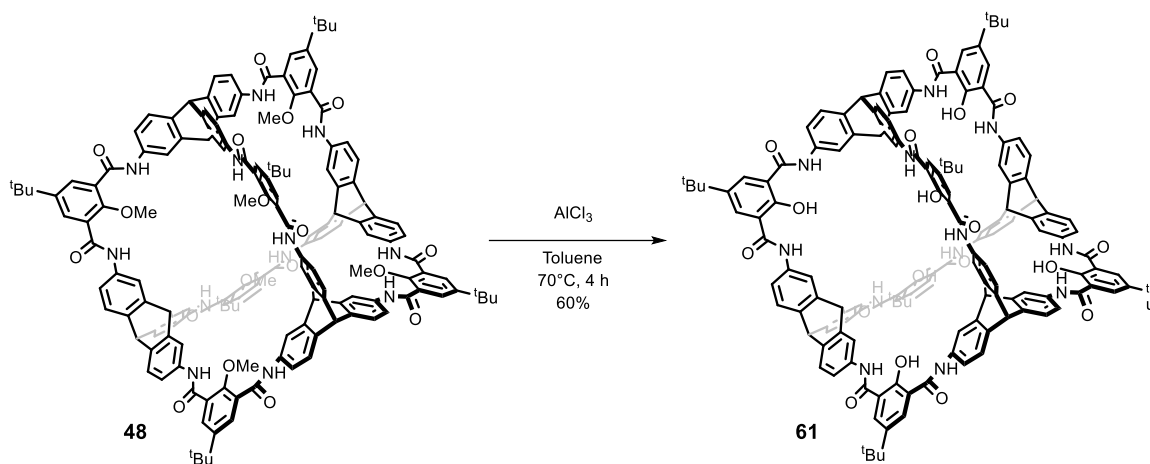
Amide cage **48** (40 mg, 0.016 mmol, 1 eq.) was suspended in dry toluene (20 mL) and aluminium chloride (210 mg, 1.6 mmol, 100 eq.) was added under argon. The reaction mixture was stirred at 70 °C for 4 h. The dark brown reaction mixture was quenched with 2 M HCl (10 mL) and extracted with ethyl acetate (2 × 30 mL). The combined organic layer was washed with 2 M HCl (2 × 30 mL), water (3 × 50 mL) and brine (40 mL). The organic phase was dried over anhydrous MgSO$_4$ and concentrated to a sticky dark red solid. The crude solid was washed with methanol (20 mL) and petroleum ether (5 × 20 mL). The resulting solid was dried under high vacuum (10^{-2} bar) to obtain demethylated cage **61** as a brown powder (23 mg, 0.009 mmol, 60%).

^{1}H NMR (500 MHz, DMSO-*d$_6$*): δ = 14.13 ppm (s, 6H, Ar-O*H*), 10.36 (s, 12 H, -CO-N*H*-), 8.21 (s, 12 H, salicyl-Ar-*H*), 8.03 (s, 12 H, triptycene-Ar- 1,8,13-*H*), 7.68-7.65 (d, 12 H, triptycene-Ar-4,5,16-*H*), 7.52-7.50 (d, 12 H, triptycene-Ar-3,6,15-*H*), 6.02 (s, 4H, bridgehead-9-*H*), 5.67 (s, 4H, bridgehead-10-*H*), 1.34 (s, 54H, -C(C*H$_3$*)$_3$).

^{13}C NMR (100 MHz, DMSO-*d$_6$*): δ = 166.1 ppm (-*C*O-NH-), 157.4 (salicyl-Ar-*C*-OH), 146.2 (triptycenyl-Ar-*C*), 142.0 (salicyl-Ar-*C*), 141.5 (salicyl-Ar-*C*), 135.5 (salicyl-Ar-*C*) 131.2

(salicyl-Ar-*C*), 123.9 (triptycenyl-Ar-*C*), 118.6 (triptycenyl-Ar-*C*), 117.8 (triptycene-Ar-*C*), 116.8 (triptycenyl-Ar-*C*), 53.0 (triptycene bridgehead-9-*C*), 51.6 (triptycene bridgehead-10-*C*), 34.7 (*C*-(CH$_3$)$_3$), 31.5 ((C-(*C*H$_3$)$_3$).

IR (neat, ATR) $\tilde{v}$ = 3624 cm^{-1} (b), 3356 (b), 2957 (m), 2351 (w), 1657 (s), 1599 (s), 1533 (s), 1475 (s), 1427 (m), 1369 (s), 1342 (s), 1269 (s), 1182 (s), 1113 (m), 1024 (w), 949 (w), 893 (w), 856 (w), 795 (m), 725 (w), 654 (m).

MALDI-TOF-MS (DCTB matrix): *m/z* = 2408.9492 (Calculated for C$_{152}$H$_{128}$N$_{12}$O$_{18}$: *m/z* = 2408.9470)

Melting point: Decomposes above 350 °C.

Synthesis of the Suzuki Coupling Products (59b)
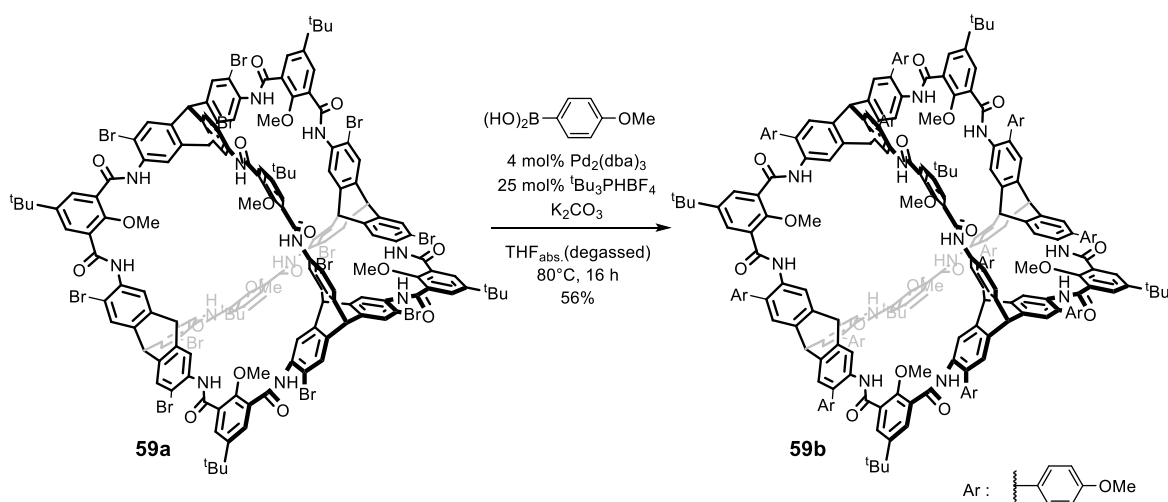
Cage compound **59a** (30 mg, 8.71 µmol, 1 eq.) and 4-methoxyphenylboronic acid (132 mg, 0.87 mmol, 100 eq.) were flushed with argon. To this, degassed THF$_{abs}$ (2mL) and a degassed aqueous solution of 2 M K$_2$CO$_3$ (0.17 mL, 0.35 mmol, 40 eq.) were added. Pd$_2$(dba)$_3$ (0.32 mg, 0.35 µmol) and ^{t}Bu$_3$PHBF$_4$ (0.63 mg, 2.17 µmol) were added under argon. The reaction mixture was stirred at 80 °C under argon atmosphere for 16 hours. On cooling to room temperature, the reaction mixture was diluted with water (5 mL), extracted with ethyl acetate (3 × 5 mL) and the organic phase was washed with water (2 × 5 mL) and brine (3 mL). The organic phase was dried over anhydrous MgSO$_4$ and then concentrated to an orange solid. The crude material was first purified by column chromatography with eluent mixture DCM:MeOH = 100:0 to 90:10 to remove one impurity at R_f = 0.55 (in DCM). The desired compound eluted

after adding methanol, which was concentrated to give an orange solid. This was further purified by preparative GPC (CHCl₃, 40 °C, 38 mbar) to obtain the product **59b** as a colourless solid (18 mg, 4.8 µmol, 56%).

¹H NMR (500 MHz, DMSO-d_6): δ = 9.82 ppm (s, 12 H, -CO-NH-), 7.65 (s, 12 H, triptycene-Ar-1,8,13-H), 7.51 (s, 12 H, triptycene-Ar-4,5,16-H), 7.38-7.36 (d, J = 8.3 Hz 24 H, Ar-H), 7.03-7.02 (d, J = 8.5 Hz 24 H, Ar-H), 6.85 (s, 12H, salicyl-Ar-H), 6.23 (s, 4H, bridgehead-9-H), 5.88 (s, 4H, bridgehead-10-H), 4.16 (s, 18 H), 3.79 (s, 36 H), 1.14 (s, 54H, -C(CH_3)₃).

¹³C NMR (150 MHz, DMSO-d_6): δ = 166.9 ppm (-CO-NH-), 159.2 (Ar-C-OMe), 152.4 (salicyl-Ar-C-OMe), 145.2 (triptycenyl-Ar-C), 145.0 (salicyl-Ar-C), 144.9 (salicyl-Ar-C), 136.3 (triptycenyl-Ar-C), 132.2 (triptycenyl-Ar-C), 131.8 (Ar-C), 130.9 (Ar-C), 126.2 (salicyl-Ar-C), 126.0 (triptycenyl-Ar-C), 125.2 (triptycenyl-Ar-C), 114.2 (Ar-C), 63.3 (salicyl-OCH₃), 55.8 (Ar-OCH₃), 52.1 (triptycene bridgehead-9-C), 51.3 (triptycene bridgehead-10-C), 34.7 (C-(CH₃)₃), 31.7 ((C-(CH₃)₃).

IR (neat, ATR) $\tilde{v}$ = 3443 cm⁻¹ (b), 2964 (m), 2365 (w), 2259 (w), 2131 (w), 1661 (s), 1610 (m), 1585 (m), 1514 (s), 1468 (s), 1425 (m), 1366 (m), 1292 (m), 1246 (s), 1178 (s), 1113 (w), 1024 (s), 1005 (s), 897 (w), 835 (s), 787 (w), 762 (m), 690 (w).

MALDI-TOF-MS (DCTB matrix): m/z = 3766.899 (Calculated for C₂₄₂H₂₁₂N₁₂O₃₀: m/z = 3766.551).

Melting point: Decomposes above 350 °C.

117
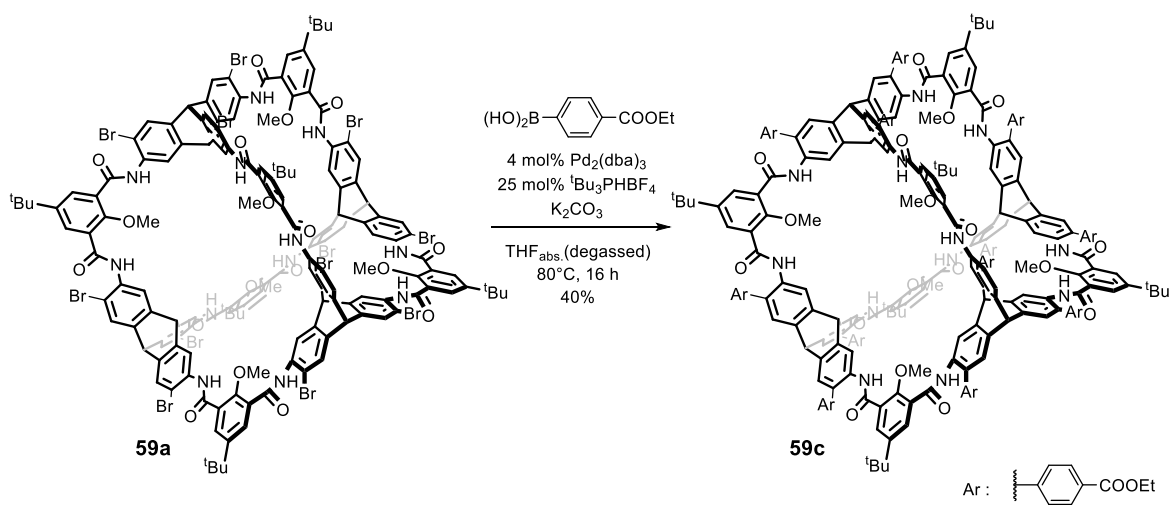
Cage compound **59a** (15 mg, 4.36 µmol, 1 eq.) and 4-ethoxycarbonylphenylboronic acid (169 mg, 0.87 mmol, 100 eq.) were flushed with argon. To this, degassed THF_{abs} (2mL) and a degassed aqueous solution of 2 M K_2CO_3 (0.17 mL, 0.35 mmol, 40 eq.) were added. $Pd_2(dba)_3$ (0.32 mg, 0.35 µmol) and $^tBu_3PHBF_4$ (0.63 mg, 2.17 µmol) were added under argon. The reaction mixture was stirred at 80 °C under argon atmosphere for 16 hours. On cooling to room temperature, the reaction mixture was diluted with water (5 mL), extracted with ethyl acetate (3 × 5 mL) and the organic phase was washed with water (2 × 5 mL) and brine (3 mL). The organic phase was dried over anhydrous $MgSO_4$ and then concentrated to give an orange solid. The crude material was first purified by column chromatography with eluent mixture DCM:MeOH = 100:0 to 90:10. The desired compound eluted after adding methanol, which was concentrated to get an orange solid. This was further purified by preparative GPC ($CHCl_3$, 40 °C, 38 mbar) to obtain the product **59c** as a colourless solid (7 mg, 1.7 µmol, 40%).

^{1}H NMR (500 MHz, DMSO-d_6): δ = 9.93 ppm (s, 12H, -CO-N*H*-), 8.03 (d, J = 7.9 Hz, 24H, Ar-*H*), 7.73 (s, 12H, triptycene-Ar- 1,8,13-*H*), 7.63 (s, 12H, triptycene-Ar-4,5,16-*H*), 7.57 (d, J = 8.0 Hz, 24H, Ar-*H*), 6.66 (s, 12H, salicyl-Ar-*H*), 4.34 (q, J = 6.8 Hz, 24H, -C*H*$_2$CH$_3$), 4.16 (s, 18H, -OC*H*$_3$), 1.33 (t, J = 7.0 Hz, 36H, -CH$_2$C*H*$_3$), 1.04 (s, 54H, -C(C*H*$_3$)$_3$).

MALDI-TOF-MS (DCTB matrix): m/z = 4274.289 (Calculated for $C_{266}H_{236}N_{12}O_{42}$: m/z = 4269.670).

Synthesis of 5-(tert-butyl)-2-methoxyisophthalaldehyde
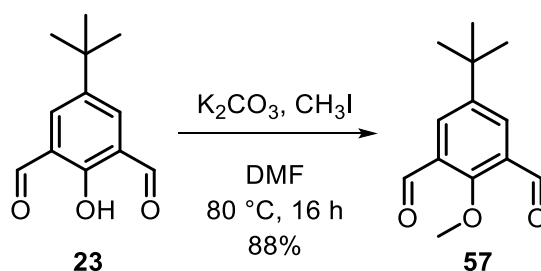
To a suspension of **23** (6 g, 28 mmol, 1 eq.) in DMF (150 mL) was added potassium carbonate (23 g, 168 mmol, 6 eq.) and methyl iodide (10.4 mL, 168 mmol, 6 eq.). The orange suspension was left to stir at 70 °C for 16 h. The reaction mixture was then diluted with water (200 mL) and extracted with DCM (3 × 200 mL). The organic phase was washed with water (6 × 200 mL), brine (200 mL) and dried over anhydrous $MgSO_4$. After concentrating under reduced pressure, to **57** (5.4 g, 24.64 mmol, 88%) was obtained as a pale yellow solid. Analytical data was in agreement with literature.[40]

118

¹H-NMR (300 MHz, CDCl₃): δ = 10.44 (s, 2H, -CHO), 8.16 (s, 2H, Ar-H), 4.08 (s, 3H, -OMe), 1.38 (s, 9H, C(CH_3)$_3$).

Melting point: 84°C (Lit.: 82-84 °C)

Synthesis of 5-(*tert*-Butyl)-2-methoxyisophthalic acid
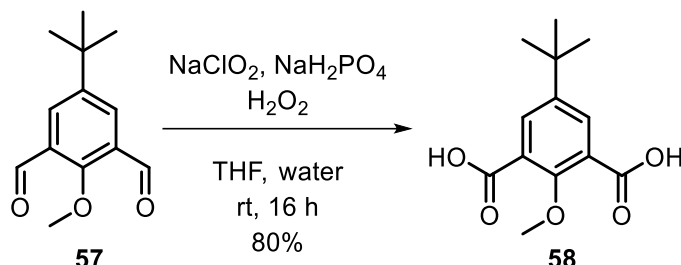
To a solution of **57** (3 g, 13.6 mmol, 1 eq.) in 180 mL THF was added H₂O₂ (45 mL of a 30% w/w solution in water, 408 mmol, 30 eq.) and NaH₂PO₄ (4.9 g, 40.8 mmol, 3 eq.). While stirring vigorously, sodium chlorite (12 g, 136 mmol, 10 eq.) was added and it was left to stir at room temperature for 16 h. The reaction mixture was concentrated by removing the THF, followed by diluting with water (200 mL) and extracting with ethyl acetate (3 × 150 mL). The organic phase was washed with 2 M NaHCO₃ solution (2 ×100 mL), water (2 × 150 mL) and then with brine (150 mL). The organic phase was dried over MgSO₄ and concentrated to obtain a colourless solid **58** (2.75 g, 10.9 mmol, 80%). Analytical data was in agreement with literature.[155]

¹H-NMR (300 MHz, DMSO-d_6): δ = 13.04 (bs, 2H, -COOH), 7.79 (s, 2H Ar-H), 3.78 (s, 3H, -OMe), 1.29 (s, 9H, C(CH_3)$_3$).

Melting point: 180 °C (Lit.: 178-180 °C)

Synthesis of 5-(*tert*-Butyl)-2-methoxyisophthaloyl dichloride
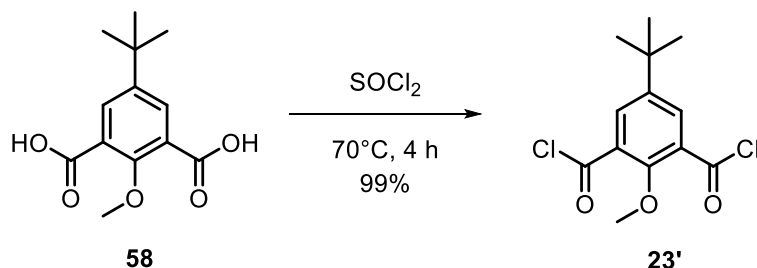
To a flask containing **58** (500 mg, 1.98 mmol, 1 eq.) thionyl chloride (60 mL) was added and stirred under a constant argon flow at 70 °C for 4 hours. The flask was then connected to a vacuum distillation apparatus and the thionyl chloride was distilled off at 60 °C at a pressure of 450 mbar. The product **23'** was obtained as a yellow oil (570 mg, 1.97 mmol, 99%).

¹H-NMR (500 MHz, DMSO-d_6): δ = 8.20 (s, 2H, Ar-*H*), 3.93 (s, 3H, -OC*H₃*), 1.39 (s, 9H, -C(C*H₃*)₃.

¹³C NMR (100 MHz, DMSO-d_6): δ = 164.34 (-*C*OCl), 156.72 (Ar-*C*-OMe), 147.54 (Ar-*C*-C(CH₃)₃), 135.19 (Ar-*C*), 129.40 (Ar-*C*-COCl), 64.23 (-O*C*H₃), 34.88 (*C*-(CH₃)₃), 31.03 ((C-(*C*H₃)₃).

2.2. Compounds of Chapter III, Section 2

2.2.1. Synthesis of triamines

Synthesis of (2,4,6-triethylbenzene-1,3,5-triyl)trimethanamine (A)
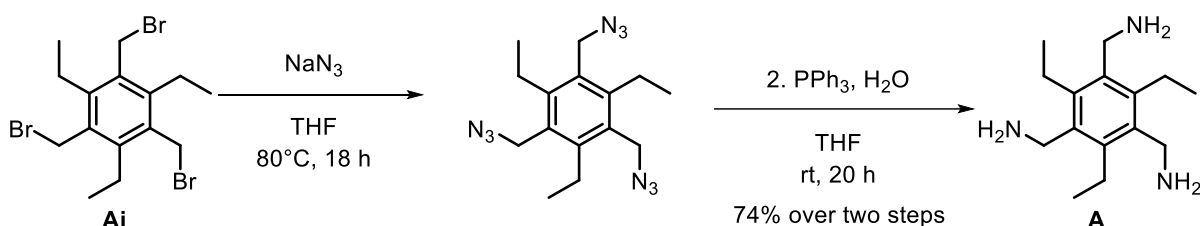
To a solution of **Ai** (3 g, 6.8 mmol, 1eq.) in 80 mL THF was added sodium azide (1.75 g, 27 mmol, 6 eq.) and left to stir overnight at 80 °C. The reaction was cooled to room temperature, triphenylphosphine (3.2 g, 36 mmol, 6 eq.) and water (1 mL, 55 mmol, 14 eq.) was added and stirred overnight at room temperature. The solvent was then evaporated and 6 M HCL was added to the residue. The aqueous solution was washed with diethylether (2 × 30 mL) and then neutralized with NaOH. After extracting into DCM (6 × 50 mL) and washing with brine, the organic layer was dried over MgSO₄. On evaporation of the solvent under reduced pressure, a yellow solid **A** (1.25 g, 5.03 mmol, 74 %) was obtained. The analytical data was in agreement with literature.[156]

¹HNMR (300 MHz, CDCl₃) δ = 3.88 ppm (s, Hz 6H, -C=N-C*H₂*-), 2.83 (q, *J* = 7.5, 6H, -C*H₂*CH₃), 1.34 (s, 6H, -NH₂), 1.24 (t, *J* = 7.5, 9H, -CH₂C*H₃*).

Melting point: 138°C (Lit.: 138 °C)[157]

Synthesis of (2,4,6-tribromobenzene-1,3,5-triyl)trimethanamine (C)
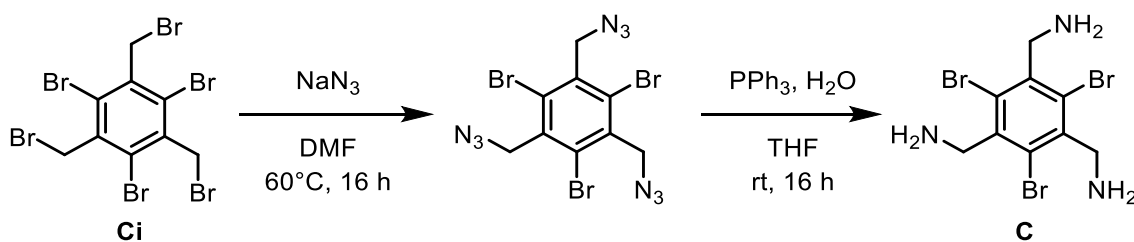
To a flask containing 1,3,5-tribromo-2,4,6-tris(bromomethyl)benzene **Ci** (3 g, 5 mmol, 1 eq.) in DMF (30 mL) was added sodium azide (1.6 g, 25 mmol, 5 eq.) and stirred at 70 °C for 16 hours. The reaction mixture was diluted with 1 M NH$_4$Cl solution (60 mL) and the aqueous layer was extracted with DCM (3 × 50 mL). The combined organic phase was washed with water (3 × 50 mL) and brine (50 mL). The organic phase was dried over MgSO$_4$ and concentrated to give a colourless solid. The solid was dissolved in THF (30 mL) and water (3 mL), and triphenylphosphine (6.5 g, 25 mmol, 5 eq.) was added. The reaction was stirred at room temperature for 16 hours. The reaction mixture was concentrated (to remove THF) and 2M HCl (30 mL) was added. The aqueous layer was extracted with diethyl ether (5 × 70 mL) and then neutralized to basic pH with a 3 M NaOH solution. The aqueous layer was extracted with DCM (3 × 70 mL). The combined organic phase was washed with water (3 × 70 mL) and brine (50 mL). The organic phase was dried over MgSO$_4$ and concentrated to yield **C** (1.2 g, 3 mmol, 60%) as a yellow solid. The analytical data was in agreement with literature.[158]

^{1}HNMR (300 MHz, CDCl$_3$) δ = 4.21 ppm (s, Hz 6H, -C=N-CH_2-), 1.50 (s, 6H, -NH$_2$).

Melting point: 198°C (Lit.: 198 °C)

2.2.2. Synthesis of aldehydes

Synthesis of diethyl 4-bromopyridine-2,6-dicarboxylate (65b)
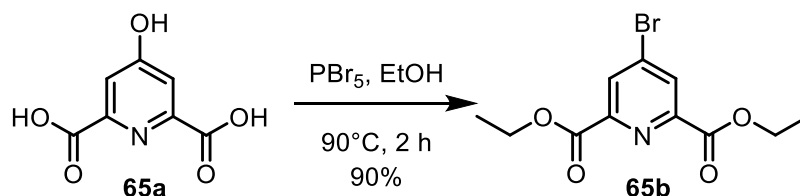
Chelidamic acid **65a** (1 g, 5.5 mmol, 1 eq.) was mixed with PBr$_5$ (12 g, 27.5 mmol, 5 eq.) and heated to 90 °C. The reaction was stirred at 90 °C for 2 hours. On cooling, chloroform (30 mL) was added and the reaction mixture was filtered. The filtrate was cooled to 0 °C, ethanol (50 mL) was added and stirred for 10 minutes. On warming to room temperature, the solvents were removed under reduced pressure. The crude was diluted with water (50 mL) and extracted with diethyl ether (3 × 50 mL). The combined organic phase was washed with 1 M NaOH solution (3 × 50 mL), water (3 × 50 mL) and brine (50 mL). The organic phase was dried over MgSO$_4$ and concentrated to yield diethyl 4-bromopyridine-2,6-dicarboxylate **65b** (1.5 g, 4.95 mmol, 90%) as a colourless solid. Analytical data was in agreement with literature.[159]

^{1}H NMR (300 MHz, CDCl$_3$) δ = 8.35 ppm (s, 2H, pyridine-*H*), 4.45 (q, 4H, -C*H$_2$*CH$_3$), 1.35 (t, 6H, -CH$_2$C*H$_3$*).

Melting point: 95 °C (Lit.: 95-96 °C)

Synthesis of (4-bromopyridine-2,6-diyl)dimethanol (65c)
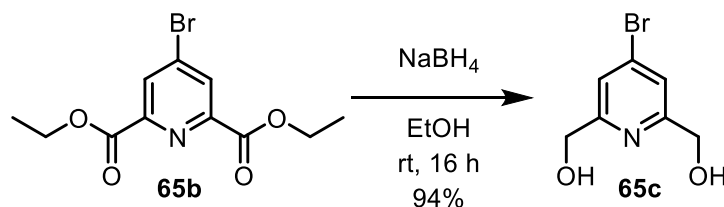
Diethyl-4-bromopyridine-2,6-dicarboxylate **65b** (1.4 g, 4.7 mmol, 1 eq.) was suspended in ethanol (20 mL) and sodium borohydrate (1.7 g, 47 mmol, 10 eq.) was added in portions at 0 °C. The reaction mixture was warmed to room temperature and refluxed for 16 hours. The solvent was removed under reduced pressure and saturated NaHCO$_3$ (50 mL) was added. The aqueous layer was extracted with ethyl acetate (3 × 50 mL). The combined organic phase was washed with water (3 × 50 mL) and brine (50 mL). The organic phase was dried over MgSO$_4$ and concentrated to yield **65c** (840 mg, 3.85 mmol, 82%) as a colourless solid. Analytical data was in agreement with literature.[160]

^{1}H NMR (300 MHz, DMSO-d$_6$) δ = 7.51 ppm (s, 2H, pyridine-*H*), 5.53 (t, 2H, -O*H*), 4.52 (d, 4H, -C*H$_2$*OH).

Melting point: 160 °C (Lit.: 162-164 °C)

Synthesis of 4-Bromopyridine-2,6-dicarbaldehyde (65)
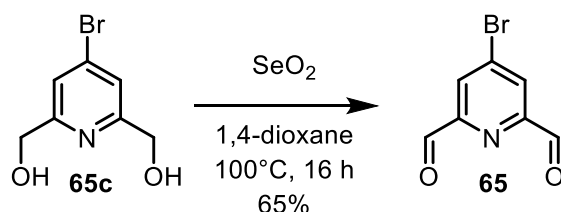
(4-bromopyridine-2,6-diyl)dimethanol **65c** (800 mg, 3.65 mmol, 1 eq.) and selenium dioxide (800 mg, 7.3 mmol, 2 eq.) were suspended in 1,4 dioxane (40 mL). The reaction was stirred at 100 °C for 16 hours. The reaction mixture was filtered to remove the black solids. The filtrate was concentrated and the crude was passed through a silica gel column with DCM to yield **65** (440 mg, 65%) as an orange solid. Analytical data was in agreement with literature.[161]

^{1}H NMR (300 MHz, CDCl$_3$) δ = 10.11 (s, 2H, -C*H*O), 8.29 (s, 2H, pyridine-*H*).

Melting point: Decomposed above 150 °C

Synthesis of 1,5-dibromo-2,4-dimethoxybenzene (69b)
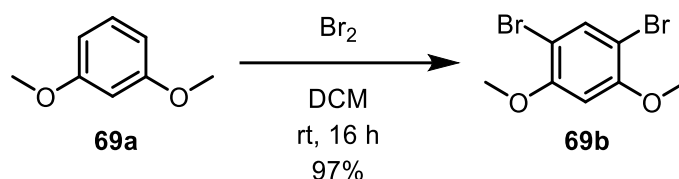
1,3-Dimethoxybenzene **69a** (10 g, 73 mmol, 1 eq.) was dissolved in DCM (70 mL), cooled to 0 °C and bromine (9 mL, 176 mmol, 2.4 eq.) was added. It was warmed to room temperature and stirred for 16 hours. On completion, the reaction mixture was washed with water (3 × 50 mL), 1 M NaOH solution (3 × 50 mL) and brine (50 mL). The organic phase was dried over MgSO$_4$ and concentrated to yield 1,5-dibromo-2,4-dimethoxybenzene **69b** (21 g, 71 mmol, 97%) as a beige solid. Analytical data was in agreement with literature.[162]

^{1}H NMR (300 MHz, CDCl$_3$) δ = 7.66 ppm (s, 1H, Ar-6-*H*) 6.49 (s, 1H, Ar-3-*H*), 3.90 (s, 6H, -OC*H$_3$*).

Melting point: 141 °C (Lit.: 142 °C)

Synthesis of 4,6-dimethoxyisophthalaldehyde (69)
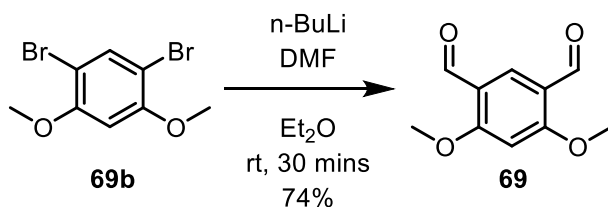
To a flame dried flask was added 1,5-dibromo-2,4-dimethoxybenzene **69b** (8g, 33.5 mmol, 1 eq.) and evacuated under vacuum and flushed with argon. The flask was charged with dry diethyl ether (60 mL) to dissolve the starting material. The reaction was cooled to 0 °C and *n*-butyllithium (2.5M in hexane) (32 mL, 85 mmol, 2.5 eq.) was added under a constant argon flow. The cooling bath was removed and stirred for 5 minutes. Dimethylformamide (18 mL, 235 mmol, 7 eq.) was added and stirred at room temperature for 2 minutes. 1 M HCl (40 mL) was added to the reaction mixture and the product precipitated as a colourless solid. The precipitate was filtered, washed with water (3 × 50 mL) and dried under high vacuum to yield **69** (4.8 g, 24.7 mmol, 74%) as a colourless solid. Analytical data was in agreement with literature.[163]

¹H NMR (300 MHz, CDCl₃) δ = 10.26 ppm (s, 2H, -C*H*O), 8.34 (s, 1H, Ar-5-*H*) 6.44 (s, 1H, Ar-2-*H*), 4.01 (s, 6H, -OC*H₃*)

Melting point: 215 °C (Lit.: 215-217 °C)

Synthesis of Ethyl (E)-2-cyano-3-(1H-pyrrol-2-yl)acrylate (71b)

71a Toluene **71b**
reflux (Dean-Stark trap 150°C)
4 h, 83%
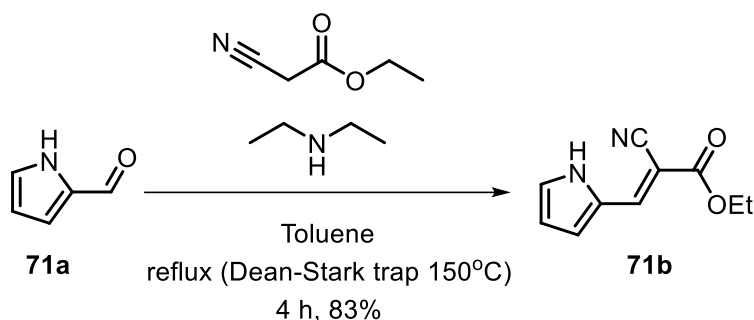
To a flask containing toluene (30 mL), pyrrol-2-carbaldehyde **71a** (2 g, 21 mmol, 1 eq.), diethylamine (0.21 mL, 2.1 mmol, 0.1 eq.) and 2-cyanoethylacetate (3.3 mL, 31.5 mmol, 1.5 eq.) were added and the flask was connected to a Dean-Stark trap. The reaction mixture was stirred at 150 °C for 5 hours and left to cool for 16 hours during which crystals had formed. The crystals were filtered, washed with diethyl ether and dried under high vacuum to get the pure product as brown crystals **71b** (3.3 g, 83%). Analytical data was in agreement with the literature.[164]

¹H-NMR: (300 MHz, DMSO-*d₆*) δ = 12.06 (bs, 1H, pyrrol-N*H*) 8.16 (s, 1H, -C=C*H*-), 7.43 (d, *J* = 4.2 Hz, 2H, pyrrol-C*H*), 6.49 (m, *J* = 4.2 Hz, 1H, pyrrol-C*H*), 4.29-4.22 (q, *J* = 7.1 Hz, 2H, -C*H₂*CH₃) 1.30-1.25 (t, *J* = 14.2 Hz, 3H, -CH₂C*H₃*).

Melting point: 137-139 °C (Lit.: 135-138 °C)[165]

Synthesis of Ethyl (E)-2-cyano-3-(5-formyl-1H-pyrrol-2-yl)acrylate

71b POCl₃, DMF **71c**
1,2-Dichloroethane
0°C to rt, 16 h
46%
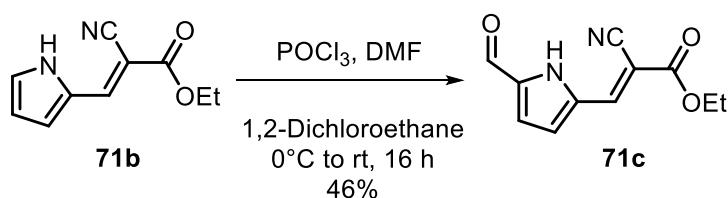
Phosphoryl chloride (0.55 mL, 6.3 mmol, 1.2 eq.) was added to dry DCE (10 mL) and cooled to 0°C. To this, DMF (0.44 mL, 6.3 mmol, 1.2 eq.) was added at 0 °C while stirring and left to stir for 15 minutes. Compound **71b** (1 g, 5.3 mmol, 1 eq.) was added to the reaction mixture under a slight flow of argon, warmed to room temperature and stirred for 16 hours. The reaction

mixture was diluted with water (20 mL) and extracted with ethyl acetate (4 × 30 mL). The organic layer was washed with brine and dried over MgSO$_4$. After concentrating, the crude product was passed through a silica gel column, eluting with a solvent mixture of DCM:MeOH = 9:1. The pure product **71c** (526 mg, 46%) was obtained as a pink solid. Analytical data was in agreement with the literature.[164]

^{1}H NMR (300 MHz, CDCl$_3$) δ = 10.22 (bs, 1H, pyrrol-N*H*), 9.89 (s, 1H, -C*H*O), 8.06 (s, 1H, -C=C*H*-), 7.78 (dd, 1H, pyrrol-C*H*), 7.34 (q, 1H, pyrrol-C*H*), 4.40-4.33 (q, 2H, -C*H$_2$*CH$_3$), 1.41-1.36 (t, 3H, -CH$_2$C*H$_3$*).

Synthesis of 1H-Pyrrole-2,5-dicarbaldehyde
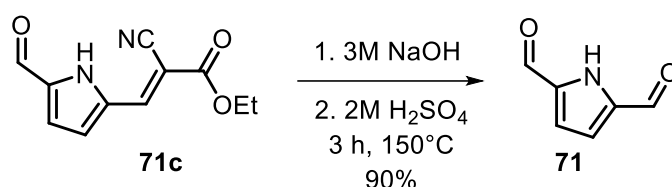
A solution of compound **71c** (180 mg, 0.82 mmol, 1 eq.) in 50 ml of 3 M NaOH solution was stirred under reflux for 3 hours. The reaction mixture was then neutralized to pH = 4 using 2 M H$_2$SO$_4$. A black precipitate was formed which was filtered off and the filtrate was extracted with ethyl acetate (3 x 50 mL). The organic layer was then washed with brine, dried over MgSO$_4$ and concentrated to obtain a black solid. This was then passed through a silica gel column with a solvent mixture of DCM:MeOH = 7:3 to obtain the pure product as an orange solid **71** (98 mg, 90%). Analytical data was in agreement with the literature.[164]

^{1}H NMR (300 MHz, DMSO-*d$_6$*) δ = 13.16 ppm (bs, 1H, pyrrol-N*H*), 9.76 (s, 2H, -C*H*O), 7.06 (d, *J* = 2.2 Hz, 2H, pyrrol-C*H*).

Melting point: 124 °C (Lit.: 124 °C)[166]

2.2.3. Synthesis of [2+3] imine cages

General procedure for synthesis of [2+3] imine cages (GP)

To a solution of the triamine precursor dissolved in methanol was added a solution of the aldehyde in methanol, dropwise over 30 minutes. The reaction was stirred at room temperature for 16 hours. The precipitate was collected by filtration, washed with methanol (3 × 30 mL) and dried under vacuum (10 mbar, 40 °C) to give the cage compound.

Synthesis of imine cage A62
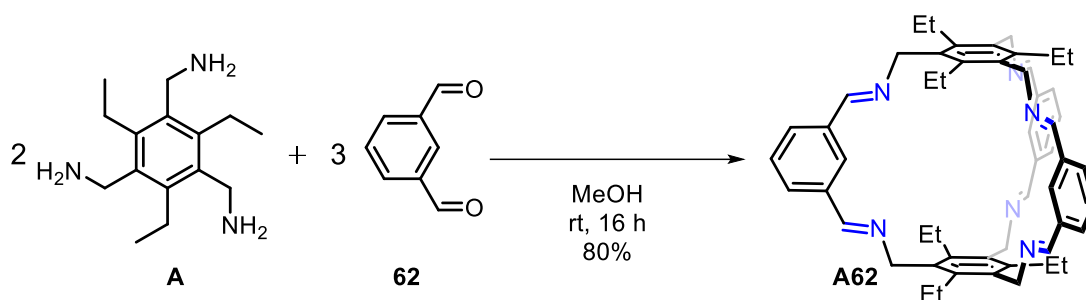
According to GP, isophthalaldehyde **62** (242 mg, 1.8 mmol, 1.5 eq.) in 40 mL MeOH, triamine **A** (300 mg, 1.2 mmol, 1 eq.) in 40 mL MeOH. Imine cage **A62** (753 mg, 80%) was obtained as a colourless solid. Analytical data was in agreement with the literature.[167]

¹HNMR (300 MHz, CDCl₃) δ = 8.17-8.15 ppm (d, 6H), 7.76 (s, 6H), 7.52-7.47 (t, 3H), 6.99 (s, 3H), 5.09 (s, 12 H), 2.35-2.27 (q, 12H), 1.25-1.20 (t, 18H).

MALDI-TOF-MS: m/z = 793.459 [M+H]⁺ (Calculated for $C_{54}H_{61}N_6$: m/z = 793.496).

Melting point: Decomposes at 280 °C

Synthesis of imine cage A63
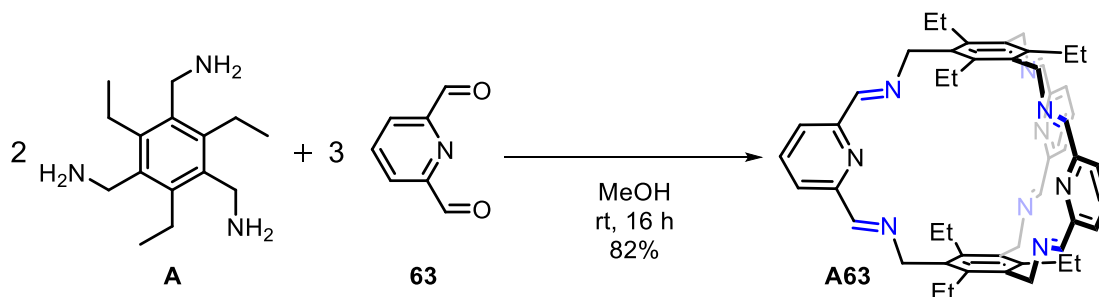
According to GP, pyridine-2,6-dicarbaldehyde **63** (243 mg, 1.8 mmol, 1.5 eq.) in 50 mL MeOH, triamine **A** (300 mg, 1.2 mmol, 1 eq.) in 50 mL MeOH. Imine cage **A63** (780 mg, 82%) obtained as an off-white solid. Analytical data was in agreement with the literature.[168]

¹HNMR (300 MHz, CDCl₃) δ = 8.17-8.14 ppm (d, 6H), 7.94 (s, 6H), 7.78-7.73 (t, 3H), 5.14 (s, 12 H), 2.34-2.26 (q, 12H), 1.27-1.22 (t, 18H).

MALDI-TOF-MS: m/z = 796.474 [M+H]⁺ (Calculated for $C_{51}H_{58}N_9$: m/z = 796.482) 818.458 [M+Na]⁺, 834.435 [M+K]⁺.

Melting point: Decomposes at 290 °C

Synthesis of imine cage A64
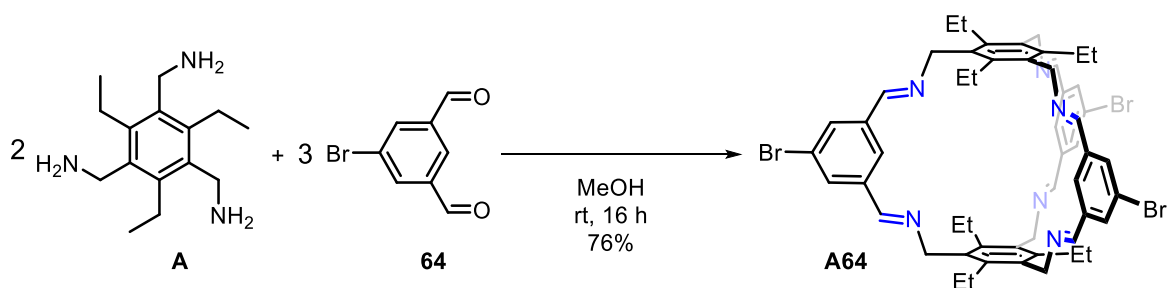
According to GP, 5-bromoisophthalaldehyde **64** (770 mmg, 3.6 mmol, 1.5 eq.) in 80 mL MeOH, triamine **A** (600 mg, 2.4 mmol, 1 eq.) in 80 mL MeOH. Imine cage **A64** (964 mg, 0.93 mmol, 78%) was obtained as a colourless solid. Analytical data was in agreement with the literature.[169]

1H NMR (301 MHz, CDCl$_3$) δ = 8.30 ppm (s, 6 H, -CON*H*), 7.63 (s, 6H, Ar-*H*), 6.82 (s, 3 H, Ar-*H*), 5.09 (d, 12 H, Ar-C*H$_2$*-C=N-, 2.29- 2.22 (q, 12 H, -C*H$_2$*-CH$_3$, 1.24-1.19 (t, 18 H, -CH$_2$-C*H$_3$*).

MALDI-TOF-MS: m/z = 1028.570 (Calculated for C$_{54}$H$_{57}$N$_6$Br$_3$: m/z = 1028.217).

Melting point: Decomposes at 300 °C.

Synthesis of imine cage A65
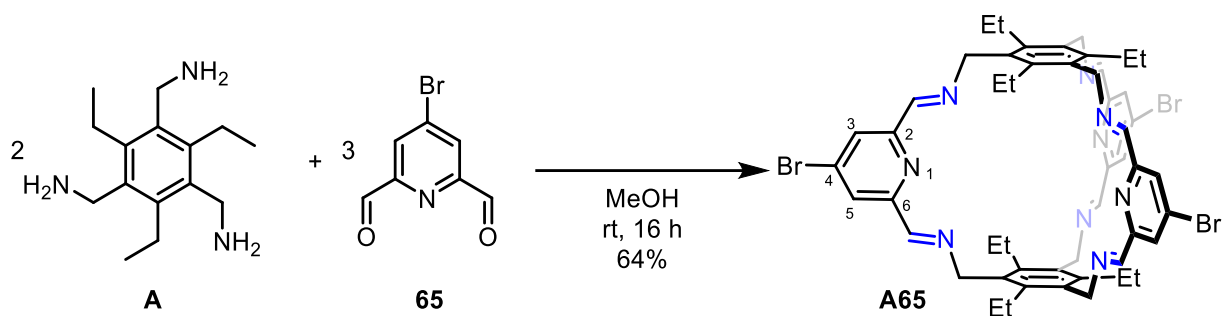
According to GP, to a solution 4-bromopyridine-2,6-dicarbaldehyde **65** (400 mg, 1.9 mmol, 3 eq.) in 20 mL MeOH, was added a solution of triamine **A** (310 mg, 1.25 mmol, 1 eq.) in 20 mL MeOH, dropwise over 30 minutes. The reaction was stirred at room temperature for 16 hours. The precipitate was collected by filtration, washed with methanol (3 × 30 mL) and dried under vacuum (10 mbar, 40°C) to give the imine cage **A65** (410 mg, 0.39 mmol, 64%) as an off-white solid.

1H NMR (400 MHz, CDCl$_3$): δ = 8.71 ppm (s, 6H, -*H*C=N-), 8.41 (s, 3H, Ar-*C*-5), 6.39 (s, 3H, Ar-*C*-2), 4.80 (s, 12 H, -CH$_2$-N=C), 2.72 (q, 12H, -CH$_2$), 1.20 (t, 18H, -CH$_3$).

^{13}C NMR (150 MHz, CDCl$_3$) δ = 158.6 ppm (-HC=N-), 156.0 (pyridine-C-2,6), 144.6 (Ar-C), 134.1 (pyridine-C-Br), 131.1 (Ar-C), 125.2 (pyridine-C-3,5), 54.6 (-HC=N-CH$_2$), 24.1 (-CH$_2$-CH$_3$), 16.3 (-CH$_2$-CH$_3$).

IR (neat, ATR) $\tilde{v}$ = 2964 cm^{-1} (m), 2875 (w), 2360 (w), 1645 (m), 1560 (vs), 1452 (w), 1342 (s), 1263 (w) , 1188 (w), 1043 (m), 977 (s), 873 (w), 713 (s), 667 (s), 653 (m).

MALDI-MS (HR-MS): *m/z* = 1054.1926 (Calculated for C$_{51}$H$_{54}$N$_9$Br$_3$.Na: *m/z* = 1054.1930)

Melting point: Decomposes above 260 °C

Elemental analysis: Calculated for C$_{52}$H$_{58}$Br$_3$N$_9$·1 CH$_3$OH: C 58.66 H 5.49 N 11.84, found: C 58.36 H 5.45 N 11.61.

Synthesis of imine cage A66
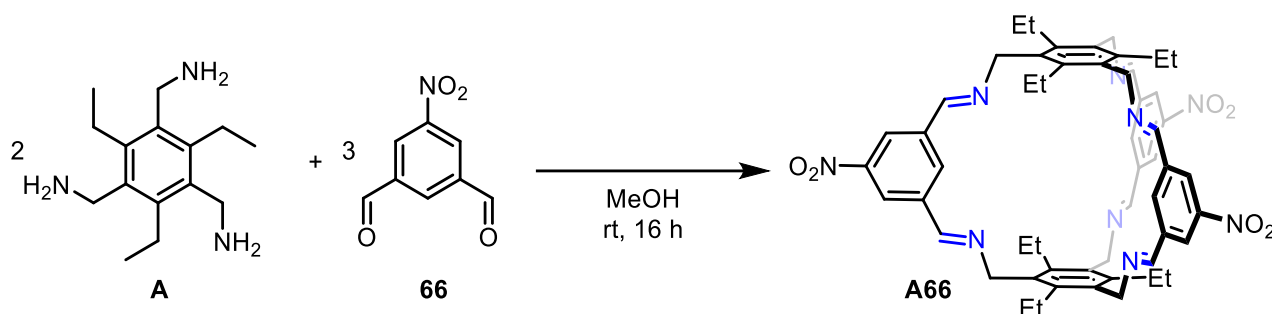
According to GP, 5-nitroisophthalaldehyde **66** (323 mmg, 1.8 mmol, 3 eq.) in 50 mL MeOH, triamine **A** (300 mg, 1.2 mmol, 2 eq.) in 50 mL MeOH. An insoluble colourless solid was obtained and the presence of imine cage **A66** in the crude mixture was confirmed by MALDI-MS and used for further reaction without any purification.

MALDI-MS: *m/z* = 927.451 (Calculated for C$_{54}$H$_{57}$N$_9$O$_6$ *m/z* = 927.4432), 832.414.

Melting point: Decomposes at 280 °C

Synthesis of imine cage A67

128
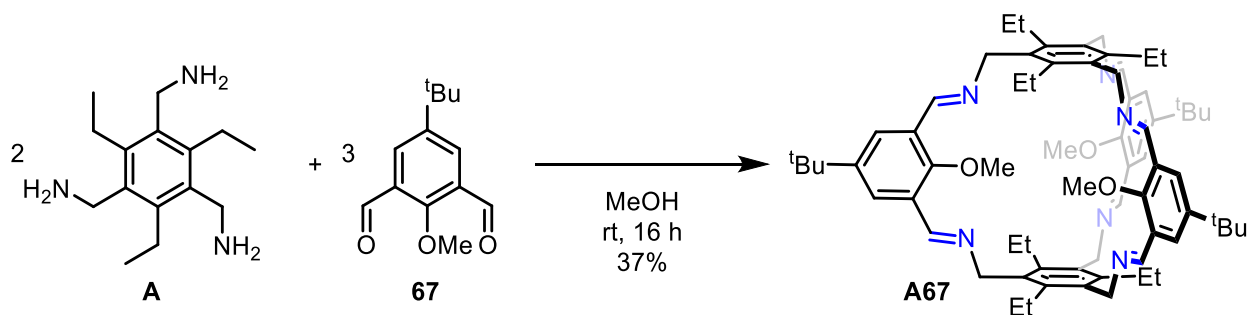
5-(*tert*-Butyl)-2-methoxyisophthalaldehyde **67** (100 mg, 0.45 mmol, 3 eq.) in 20 mL MeOH, triamine **A** (75 mg, 0.3, 2 eq.) in 20 mL MeOH. After the solid was washed with methanol, it was suspended in n-hexane, sonicated and then filtered. The filtrate was concentrated to obtain the imine cage **A67** (58 mg, 0.055 mmol, 37%) as a colourless solid. Analytical data was in agreement with literature.[47]

¹H NMR (400 MHz, CDCl₃): δ = 8.17 (s, 6H, HC=N), 8.05 (s, 6H, Ar'-3/5-H), 5.11 (s, 12H, Ar-CH₂), 3.03 (s, 9H, OCH₃), 2.36 (q, J=7.5 Hz, 12 H, Ar-CH₂CH₃), 1.36 (s, 27H, *t*-butyl), 1.26 (t, J = 7.6 Hz, 18H, Ar-CH₂CH₃).

MALDI-TOF-MS: m/z = 1051.881 [M+H]⁺ (Calculated for C₆₉H₉₀N₆O₃: m/z = 1051.711).

Melting point: Decomposes at 290 °C

Synthesis of imine cage A69
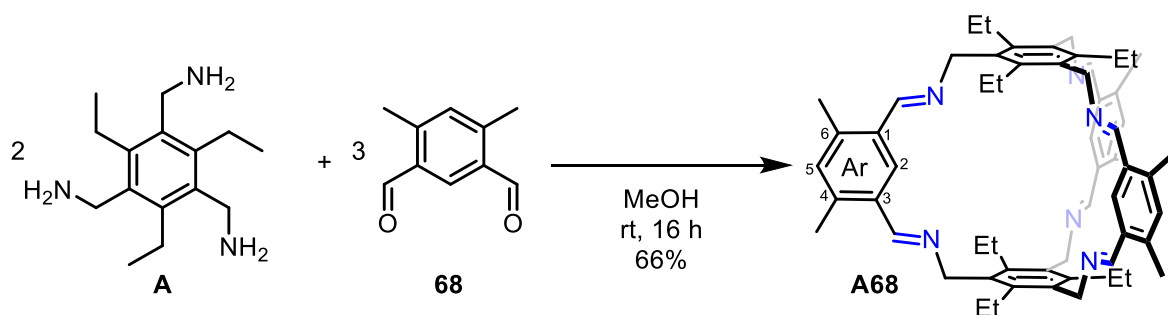
According to GP, 4,6-dimethylisophthalaldehyde **68** (200 mg, 1.23 mmol, 1.5 eq.) in 30 mL MeOH, triamine **A** (205 mg, 0.82 mmol, 1 eq.) in 30 mL MeOH. Imine cage **A68** (237 mg, 0.27 mmol, 66%) was obtained as a colourless solid. The procedure was adopted from the PhD thesis of *Tobias Schick (AK Mastalerz)* and the spectral data was in agreement.[170]

¹H NMR (300 MHz, CDCl₃): δ = 8.63 (s, 6H, -*H*C=N-), 8.26 (s, 3H, Ar-*H*-5), 6.96 (s, 3H, Ar-*H*-2), 4.89 (s, 12 H, -C*H₂*-N=C), 2.72 (q, 12H, -C*H₂*CH₃), 1.22 (t, 18H, -CH₂C*H₃*).

MALDI-TOF-MS: m/z = 877.665 [M+H]⁺ (Calculated for C₆₀H₇₂N₆: m/z = 877.585).

Melting point: Decomposes at 280 °C

Synthesis of imine cage A69
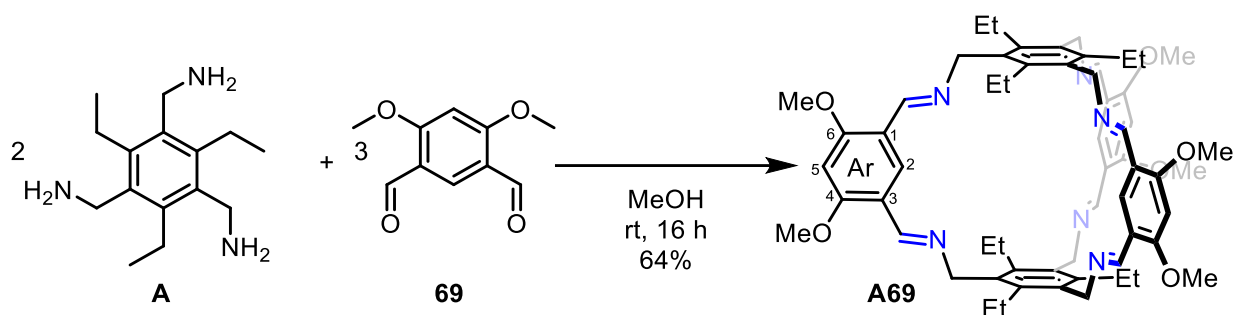
According to GP, to a solution of 4,6-dimethoxyisophthalaldehyde **69** (250 mg, 1.29 mmol, 3 eq.) in 30 mL MeOH, was added a solution of triamine **A** (214 mg, 0.86 mmol, 2 eq.) in 30 mL MeOH dropwise over 30 minutes. The reaction was stirred at room temperature for 16 hours. The precipitate was collected by filtration, washed with methanol (3 × 30 mL) and dried under vacuum (10 mbar, 40 °C) to give the imine cage **A69** (268 mg, 0.28 mmol, 64%) as a colourless solid.

¹H NMR (400 MHz, CDCl$_3$): δ = 8.71 (s, 6H, -*H*C=N-), 8.41 (s, 3H, Ar-*H*-5), 6.39 (s, 3H, Ar-*H*-2), 4.80 (s, 12 H, -C*H*$_2$-N=C), 2.72 (q, 12H, -C*H*$_2$CH$_3$), 1.20 (t, 18H, -CH$_2$C*H*$_3$).

¹³C NMR (100 MHz, CDCl$_3$) δ = 161.3 (Ar-*C*-4,6), 156.4 (-H*C*=N-), 143.43 (Ar'-*C*), 133.38 (Ar-*C*-1,3), 129.95 (Ar'-*C*), 118.69 (Ar-*C*-5), 94.10 (Ar-*C*-2), 59.30 (O-*C*H$_3$), 55.76 (-HC=N-*C*H$_2$), 22.26 (-*C*H$_2$-CH$_3$), 15.29 (-CH$_2$-*C*H$_3$).

IR (neat, ATR) $\tilde{v}$ = 2974 cm^{-1} (m), 1661 (vs), 1519 (s), 1435 (s), 1383 (vs), 1278 (s) , 1141 (vs), 966 (m), 850 (s), 750 (s), 694 (s).

MALDI-TOF-MS: *m/z* = 973.554 (Calculated for C$_{60}$H$_{72}$N$_6$O$_6$.H: *m/z* = 973.559)

Melting point: Decomposes above 240 °C.

Elemental analysis: Calculated for C$_{60}$H$_{72}$N$_6$O$_6$·2 CH$_3$OH: C 71.79 H 7.77 N 8.10, found: C 71.80 H 7.50 N 8.19.

Synthesis of imine cage A70
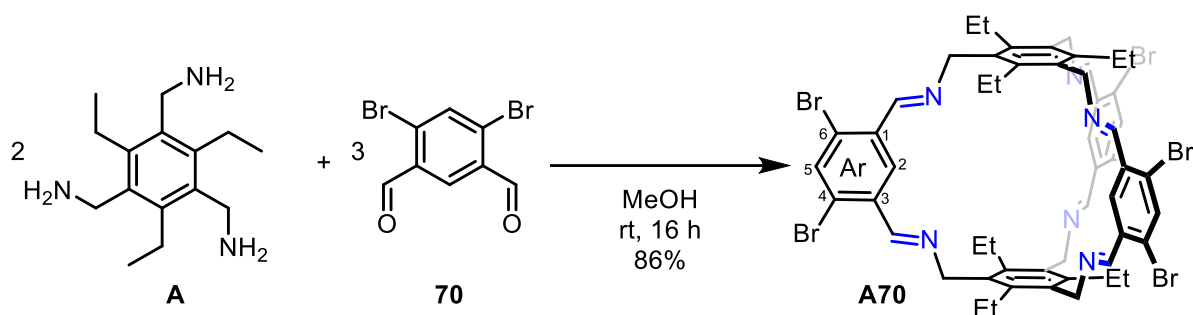
According to GP, 4,6-bromoisophthalaldehyde **70** (150 mg, 0.51 mmol, 1.5 eq.) in 20 mL MeOH, triamine **A** (85 mg, 0.34 mmol, 1 eq.) in 30 mL MeOH. Imine cage **A70** (187 mg, 0.15 mmol, 86%) was obtained as a colourless solid. The procedure was adopted from the Bachelor thesis of *Ron Bellemann (AK Mastalerz)* and the spectral data was in agreement.[170]

¹H NMR (300 MHz, CDCl₃): δ = 8.87 (s, 6H, -*H*C=N-), 8.28 (s, 3H, Ar-*H*-5), 7.91 (s, 3H, Ar-*H*-2), 4.80 (s, 12 H, -C*H₂*-N=C), 2.72 (q, 12H, -C*H₂*CH₃), 1.20 (t, 18H, -CH₂C*H₃*).

MALDI-TOF-MS: *m/z* = 1200.254 (Calculated for C₅₄H₅₄N₆Br₅: *m/z* = 1200.052)

Melting point: Decomposes at 270 °C

Synthesis of imine cage A71
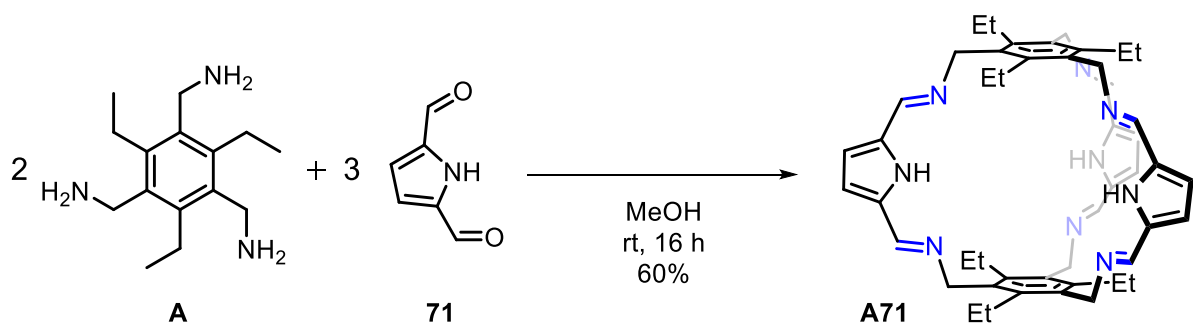
According to GP, pyrrol-2,5-dicarboxaldehyde **71** (200 mg, 1.62 mmol, 1.5 eq.) in 30 mL MeOH, triamine **A** (270 mg, 1.08 mmol, 1 eq.) in 30 mL MeOH. Imine cage **A71** (247 mg, 0.32 mmol, 60%) was obtained as a colourless solid. Analytical data was in agreement with the literature.[45a]

¹H NMR (300 MHz, CDCl₃): δ = 7.87 (s, 6H, -*H*C=N-), 6.62 (s, 6H, pyrrol-*H*-5), 7.91 (s, 3H, Ar-*H*-2), 4.81 (s, 12 H, -C*H₂*-N=C), 3.19 (bs, 3H + H₂O, pyrrol-N*H*), 2.47 (q, 12H, -C*H₂*CH₃), 1.19 (t, 18H, -CH₂C*H₃*).

MALDI-TOF-MS: *m/z* = 760.422 (Calculated for C₄₈H₅₇N₉: *m/z* = 760.477)

Melting point: Decomposes at 270 °C

Synthesis of imine cage B63
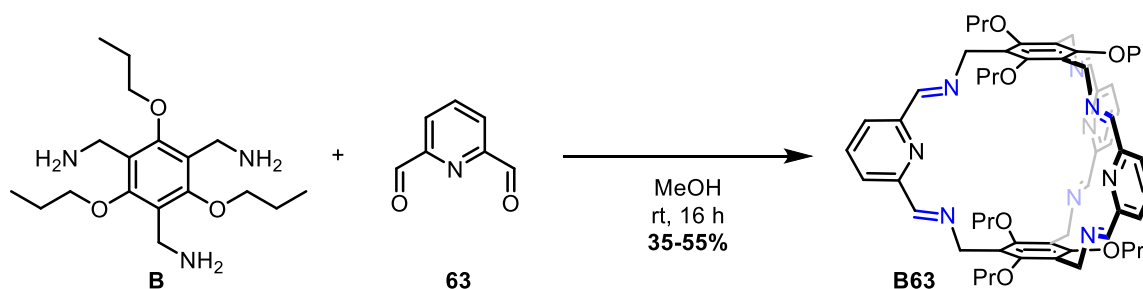
To a solution pyridine-2,6-dicarbaldehyde **63** (400 mg, 1.9 mmol, 3 eq.) in 20 mL MeOH, was added a solution of triamine **B** (310 mg, 1.25 mmol, 1 eq.) in 20 mL MeOH dropwise over 30 minutes and stirred at room temperature for 16 hours. The precipitate was collected by filtration, washed with methanol (3 × 30 mL) followed by suspending the residue in DCM (20 mL) and filtration (3 times). The combined filtrate was concentrated under reduced pressure (10 mbar, 40 °C) to afford the imine cage **B63** (410 mg, 0.39 mmol, 64%) as an off-white solid.

^{1}H NMR (600 MHz, CD$_2$Cl$_2$): δ = 8.15 (t, 6H, -N=CH), 8.10 (d, 6H, pyridine-3,5-H), 7.77 (t, 3H, pyridine-4-H), 5.10 (d, 12H, -CONH-CH_2-), 3.61 (t, 12H, -O-CH$_2$C$_2$H$_5$), 1.57 (m, 12H, -O-CH$_2$CH_2CH$_3$), 0.81 (t, 12H, -O-C$_2$H$_4$CH_3).

^{13}C NMR (150 MHz, CD$_2$Cl$_2$): δ = 159.7 (-HC=N-), 159.7 (Ar'-C-OPr), 155.0 (Ar'-C-CH$_2$NHCO-), 137.2 (Ar-C-4), 121.9 (Ar-C-3,5), 120.4 (Ar-C-2,6), 76.6 (-O-CH$_2$C$_2$H$_5$), 51.2 (-C=N-CH$_2$), 23.67 (-O-CH$_2$$CH_2CH_3$), 10.27 (-O-CH$_2CH_2$$CH_3$).

IR (neat, ATR) $\tilde{v}$ = 2966 cm^{-1} (w), 2924 (w), 1641 (w), 1583 (s), 1435 (m), 1229 (m), 1101 (vs), 989 (s), 806 (m).

MALDI-TOF-MS: m/z = 976.488 [M+H]$^+$ (Calculated for C$_{57}$H$_{69}$N$_9$O$_6$.H: m/z = 976.545), 998.460 [M+Na]$^+$, 1014.461 [M+K]$^+$.

Melting point: Decomposes above 150 °C.

Synthesis of imine cage B65
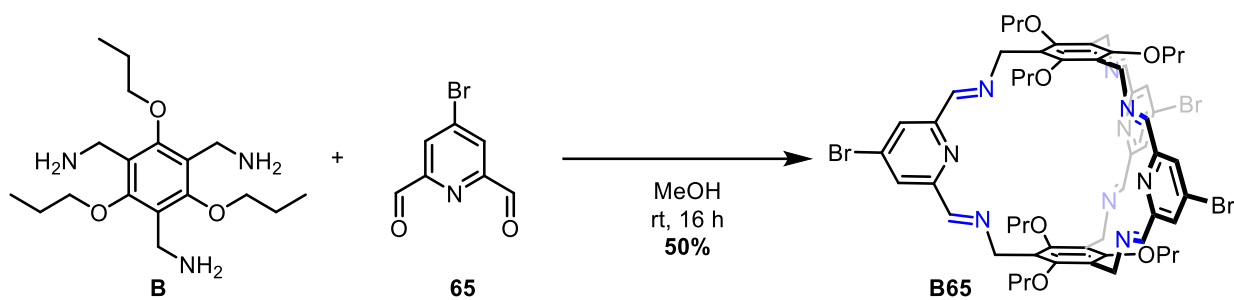
To a solution of 4-bromopyridine-2,6-dicarbaldehyde **65** (200 mg, 0.93 mmol, 3 eq.) in 20 mL MeOH, was added a solution of triamine **B** (211.4 mg, 0.622 mmol, 1 eq.) in 20 mL MeOH dropwise over 30 minutes and stirred at room temperature for 16 hours. The precipitate was collected by filtration, washed with methanol (3 × 30 mL) followed by suspending the residue in DCM (20 mL) and filtration (3 times). The combined filtrate was concentrated under reduced pressure (10 mbar, 40 °C) to afford the imine cage **B65** (376 mg, 0.31 mmol, 50%) as an off-white solid.

^{1}H NMR (600 MHz, CDCl$_3$): δ = 8.25 (t, 6H, -N=C*H*), 8.02 (d, 6H, pyridine-3,5-*H*), 5.11 (d, 12H, -CONH-C*H$_2$*-), 3.62 (t, 12H, -O-CH$_2$C$_2$H$_5$), 1.63 (m, 12H, -O-CH$_2$C*H$_2$*CH$_3$), 0.87 (t, 12H, -O-C$_2$H$_4$C*H$_3$*).

^{13}C NMR (150 MHz, CDCl$_3$): δ = 159.4 (-H*C*=N-), 158.5 (Ar'-*C*-OPr), 155.8 (Ar'-*C*-CH$_2$NHCO-), 133.9 (Ar-*C*-4), 124.7 (Ar-*C*-3,5), 119.8 (Ar-*C*-2,6), 76.4 (-O-*C*H$_2$C$_2$H$_5$), 50.8 (-C=N-*C*H$_2$), 23.4 (-O-CH$_2$*C*H$_2$CH$_3$), 10.2 (-O-CH$_2$CH$_2$*C*H$_3$).

IR (neat, ATR) $\tilde{v}$ = 2962 cm^{-1} (w), 2929 (w), 2877 (w), 2360 (vw), 1647 (w), 1573 (w), 1433 (m), 1344 (m), 1245 (m), 1103 (vs), 948 (s), 754 (m), 690 (m).

MALDI-TOF-MS: m/z = 1232.166 [M+Na]$^+$ (Calculated for C$_{54}$H$_{66}$N$_9$O$_6$Br$_3$.Na: m/z = 1232.258)

Melting point: decomposes above 140°C

Elemental analysis: Calculated for C$_{57}$H$_{66}$Br$_3$N$_9$O$_6$· 1 CH$_3$OH: C 55.96 H 5.67 N 10.13, found: C 55.85 H 5.63 N 10.24.

Synthesis of imine cage D62
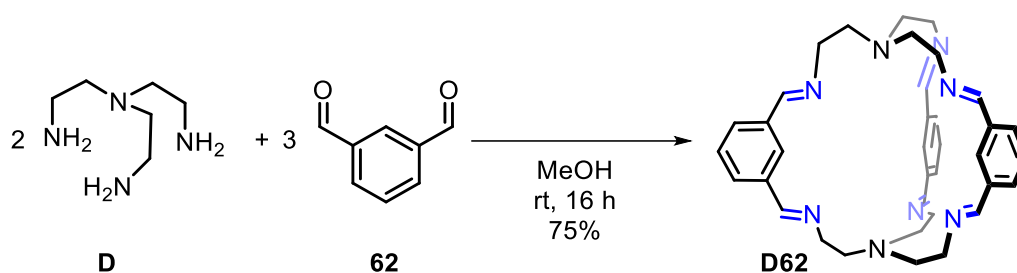
According to GP, triamine **D** (300 mg, 2.05 mmol, 1 eq.) in 50 mL MeOH, isophthalaldehyde **62** (412 mg, 3.08 mmol, 1.5 eq.) in 30 mL MeOH. Imine cage **D62** (481 mg, 0.82 mmol, 80%) was obtained as a colourless solid. Analytical data was in agreement with the literature.[171]

¹H NMR (300 MHz, CDCl₃): δ = 8.20 (dd, J = 7.7, 1.6 Hz, 6H, -Ar-*H*-4,6), 7.59 (s, 6H, -*H*C=N-), 7.53 (t, J = 7.7 Hz, 3H, Ar-*H*-5), 5.34 (s, 3H, Ar-*H*-2), 3.53 (d, J = 134.4 Hz, 12H, TREN-C*H₂*), 2.87 (d, J = 80.7 Hz, 12H, TREN-C*H₂*).

MALDI-TOF-MS: m/z = 586.362 (Calculated for $C_{36}H_{42}N_8$: m/z = 586.353).

Melting point: Decomposes at 240 °C

Synthesis of imine cage D63
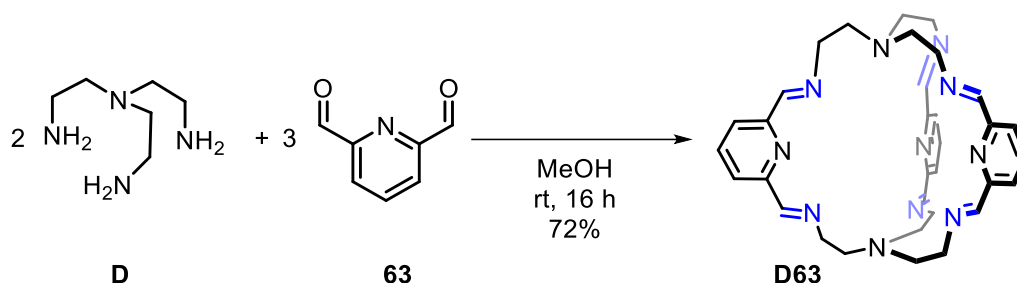
According to GP, triamine **D** (300 mg, 2.05 mmol, 1 eq.) in 50 mL MeOH, pyridine-2,6-dicarboxaldehyde **63** (412 mg, 3.08 mmol, 1.5 eq.) in 30 mL MeOH. After removal of MeOH, diethyl ether (40 mL) was added followed by filtration to obtained imine cage **D63** (435 mg, 0.74 mmol, 72%) as a yellow solid. Analytical data was in agreement with the literature.[172]

¹H NMR (300 MHz, CDCl₃): δ = 8.12 (d, J = 7.7, 1.6 Hz, 6H, -Ar-*H*-4,6), 7.80 (t, J = 7.7 Hz, 3H, Ar-*H*-5), 7.59 (s, 6H, -*H*C=N-), 3.56 (bs, 12H, TREN-C*H₂*), 2.88 (bs, 12H, TREN-C*H₂*).

MALDI-TOF-MS: m/z = 590.355 (Calculated for $C_{33}H_{39}N_{11}$: m/z = 589.347).

Melting point: Decomposes at 250 °C

2.2.4. Synthesis of [4+4] imine cages

Synthesis of imine cage A72
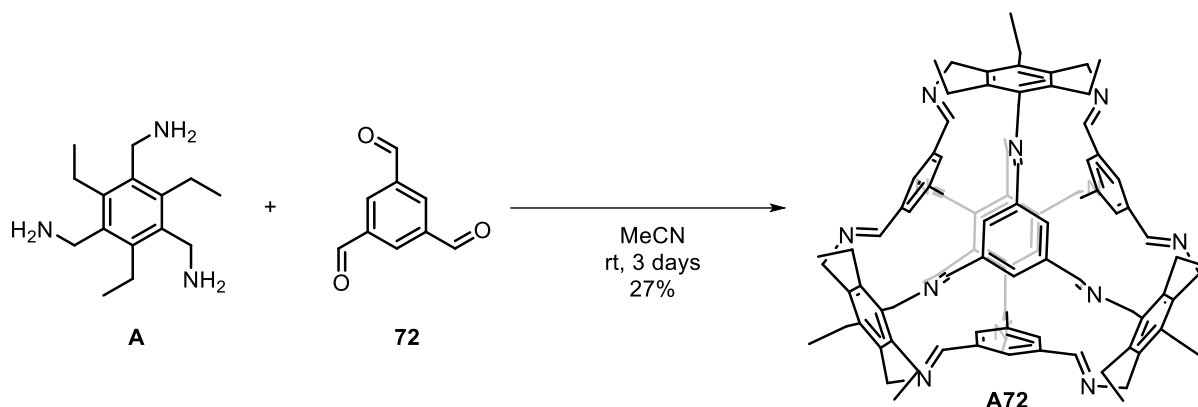
To a solution of 1,3,5-triformylbenzene **72** (120 mg, 740 µmol, 4 eq.) in MeCN (15 mL) was 2,4,6-triethylbenzene-1,3,5-trimethanamine **A** (185 mg, 740 µmol, 4 eq.) in MeCN (22 mL), dropwise over 3 hours. The suspension was stirred for 3 days and the precipitate was filtered and washed with MeCN (20 mL). The solid residue washed with DCM (200 mL) and the filtrate was concentrated give **A72** (70 mg, 50 µmol, 27%) as a colourless solid. Analytical data was in agreement with the literature.[39]

¹H NMR (600 MHz, CDCl₃)**:** δ = 8.56 ppm (s, 12H, -C*H*N-), 7.97 (s, 12H, Ar-*H*), 4.76 (s, 24H, -C*H₂*N=C-), 3.18 (q, *J* = 7.5 Hz, 24H, -C*H₂*CH₃), 1.28 (t, *J* = 7.4 Hz, 36H, -CH₂C*H₃*).

MALDI-TOF-MS: *m/z* = 1429.897 (Calculated for $C_{96}H_{108}N_{12}$: *m/z* = 1429.885)

Melting point: Decomposes at 220 °C.

Synthesis of imine cage B73

ExperimeEEExperimental Section
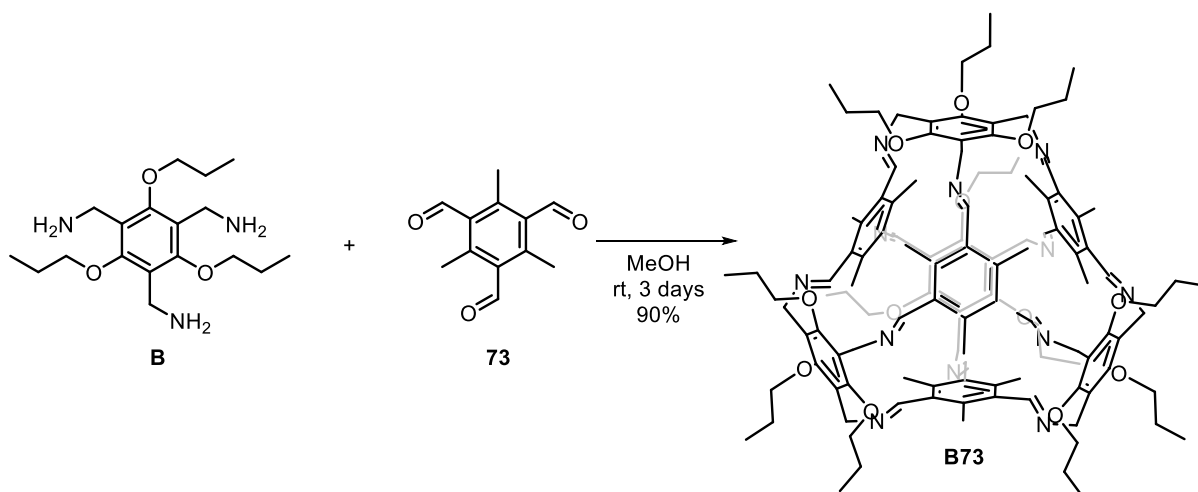
The amine (2,4,6-tripropoxybenzene-1,3,5-triyl)trimethanamine **B** (300 mg, 0.88 mmol, 4 eq.) and 2,4,6-trimethylbenzene-1,3,5-tricarbaldehyde **73** (180 mg, 0.88 mmol, 4 eq.) were dissolved in methanol (24 mL), and stirred at room temperature for 3 days. The solution was filtered and washed with acetonitrile (60 mL). The residue was extracted with chloroform (90 mL) and the solvent was removed under reduced pressure to give **B73** (390 mg, 0.2 mmol, 90 %) as a colourless solid. The procedure was borrowed and reproduced exactly as performed by a colleague, *Jochen Lauer (Mastalerz group)* and the spectral data was in agreement.[138]

^{1}H NMR (600 MHz, CDCl$_3$)**:** δ = 7.70 ppm (s, 12H, Ar-*H*C=N-), 4.85 (s, 24H, -C*H$_2$*N=C-), 3.91-3.86 (t, 24H, -OC*H$_2$*CH$_2$CH$_3$), 1.94 (s, 36H, Ar-C*H$_3$*), 1.85-1.76 (m, 24H, -OCH$_2$C*H$_2$*CH$_3$), 1.06 (t, 36H, -OCH$_2$CH$_2$C*H$_3$*).

MALDI-TOF-MS: *m/z* = 1957.876 (Calculated for C$_{120}$H$_{156}$N$_{12}$O$_{12}$: *m/z* = 1958.200)

Melting point: Decomposes at 240 °C

2.2.4. Transformation of [2+3] Imine Cages to [2+3] Amide Cages

Synthesis of cage A62-amide

A62 → **A62-amide**
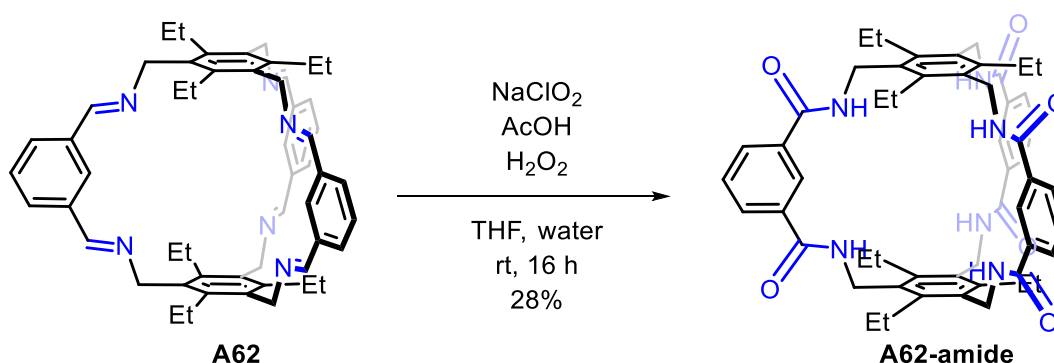
To a solution of the imine cage **A62** (250 mg, 0.31 mmol, 1 eq.) in THF (20 mL) was added 35% w/w solution of hydrogen peroxide (2.4 mL, 23.6 mmol, 75 eq.), and NaClO$_2$ (1.1 g, 12.6 mmol, 40 eq.) in that order and stirred vigorously. While stirring, acetic acid (1 M, 0.31 mL, 3.1 mmol, 10 eq.) was added dropwise over 10 minutes. The suspension turned into a clear solution in 10 minutes and the reaction mixture was left to stir for another 16 hours. The reaction mixture was evaporated to reduce the amount of THF to minimum. The resulting suspension was diluted with water (50 mL) and, the precipitate was filtered and washed thoroughly with water (5 × 40 ml). The crude mixture was suspended in Et$_2$O (10 mL), heated to reflux and methanol was added dropwise until a clear solution was obtained. On gradual cooling, crystals of the cage compound were obtained after 2 days. The crystals were filtered,

136

washed with Et$_2$O and dried under high vacuum to obtain the product **A62-amide** as a colourless solid (77 mg, 0.09 mmol, 28%).

^{1}H NMR (600 MHz, DMSO-d_6) δ = 8.19-8.16 ppm (t, 6H, -CO-N*H*-), 8.00-7.97 (dd, 6H, Ar-*H*), 7.93 (s, 3H, Ar-*H*), 7.59-7.55 (t, 3H, Ar-*H*), 4.47-4-46 (d, 12H, -C*H$_2$*-NHCO-), 2.81-2.75 (q, 12 H, -C*H$_2$*-CH$_3$), 1.14-1.10 (t, 18 H, -CH$_2$-C*H$_3$*).

^{13}C NMR (150 MHz, DMSO-d_6): δ = 167.2 (Ar-*C*-CO-NH-), 145.1 (Ar'-*C*-C$_2$H$_5$), 135.3 (Ar-*C*-1,3), 132.5 (Ar'-*C*-CH$_2$-NHCO-), 131.3 (Ar-*C*-4,6), 129.3 (Ar-*C*-5), 125.70 (Ar-*C*-2), 37.73 (-*C*H$_2$-NH-), 22.83 (-*C*H$_2$-CH$_3$), 16.32 (-CH$_2$-*C*H$_3$).

IR (neat, ATR) $\tilde{v}$ = 3393 cm^{-1} (b), 2973 (m), 1634 (s), 1636 (s), 1528 (s), 1373 (m), 1273 (m), 1160 (w), 1081 (w), 828 (w), 732 (m), 674(w).

MALDI-MS (HR-MS): *m/z* = 889.4657 (Calculated for C$_{54}$H$_{61}$N$_6$O$_6$: *m/z* = 889.4653) [M+H]$^+$, 911.4587 [M+Na]$^+$, 927.4217 [M+K]$^+$.

Melting point: >350°C (decomposed).

Elemental analysis: Calculated for C$_{54}$H$_{60}$N$_6$O$_6$·4 H$_2$O·2 CH$_3$OH: C 65.60 H 7.47 N 8.20, found: C 65.31 H 7.21 N 8.50.

SCXRD: See appendix section 4.2

Synthesis of cage A63-amide
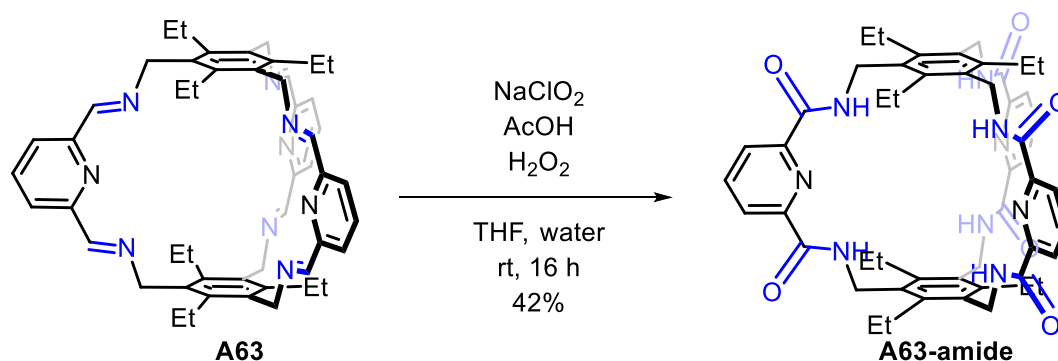
To a suspension of the imine cage **A63** (250 mg, 0.31 mmol, 1 eq.) in 20 mL THF was added 35% w/w solution of hydrogen peroxide (10 M, 2.4 mL, 23.6 mmol, 75 eq.), and NaClO$_2$ (1.1 g, 12.6 mmol, 40 eq.) in that order and stirred vigorously. While stirring, acetic acid (0.28 mL, 5 mmol, 10 eq.) dissolved in 1.3 mL water was added dropwise. The reaction mixture was left to stir for another 16 hours during which the solution turned clear. The reaction mixture was evaporated to remove the THF. The resulting suspension was diluted with water (50 mL) and

the precipitate was filtered. The precipitate was washed thoroughly with water (5×40 ml) and then with Et$_2$O (3×30 mL). The crude product was then suspended in methanol (20 mL) and then heated to 80 °C. Methanol was added until a clear solution was obtained and then cooled gradually to room temperature. The cage compound **A63-amide** (77 mg, 0.09 mmol, 28%) was obtained as colourless crystals which was filtered, washed with diethyl ether and dried under high vacuum. The mother liquor was concentrated to form a saturated solution and left aside to deliver more crystals of amide cage (39 mg, 0.04 mmol, 14%).

¹H NMR (300 MHz, DMSO-d_6) δ = 8.74-8.72 (t, 6H, -CO-N*H*-), 8.24-8.22 (m, 6H, Ar-*H*), 8.17-8.13 (m, 3H, Ar-*H*), 4.59 (d, 12H, -C*H*$_2$-NHCO-), 2.71-2.66 (q, 12 H, -C*H*$_2$-CH$_3$), 1.13-1.09 (t, 18 H, -CH$_2$-C*H*$_3$).

¹³C NMR (100 MHz, DMSO-d_6): δ = 164.3 (Ar-*C*O-NH-), 150.1 (Ar-*C*-2,6), 145. (Ar'-*C*-C$_2$H$_5$), 139.5 (Ar-*C*-4), 132.5 (Ar'-*C*-CH$_2$-NHCO-), 125.7 (Ar-*C*-3,5), 37.7 (-*C*H$_2$-NH-), 22.8 (-*C*H$_2$-CH$_3$), 16.3 (-CH$_2$-*C*H$_3$).

IR (neat, ATR) $\tilde{v}$ = 3429 cm^{-1} (m), 2963 (m), 1666 (s), 1500 (s), 1435 (m), 1371 (w), 1155 (m), 1072 (m), 998 (m), 848 (m), 755 (s), 647 (m).

MALDI-MS (HR-MS): m/z = 892.4510 (Calculated for C$_{54}$H$_{61}$N$_6$O$_6$: m/z = 892.4465) [M+H]$^+$, 914.4322 [M+Na]$^+$, 930.4053 [M+K]$^+$.

Melting point: >350°C (decomposed).

Elemental analysis: Calculated for C$_{54}$H$_{60}$N$_6$O$_6$·6 H$_2$O: C 61.25 H 6.95 N 12.60, found: C 61.83 H 6.06 N 12.85.

SCXRD: See appendix section 4.3

Synthesis of cage A64-amide

A64   NaClO₂   AcOH   H₂O₂   THF, water   rt, 16 h   15%   **A64-amide**
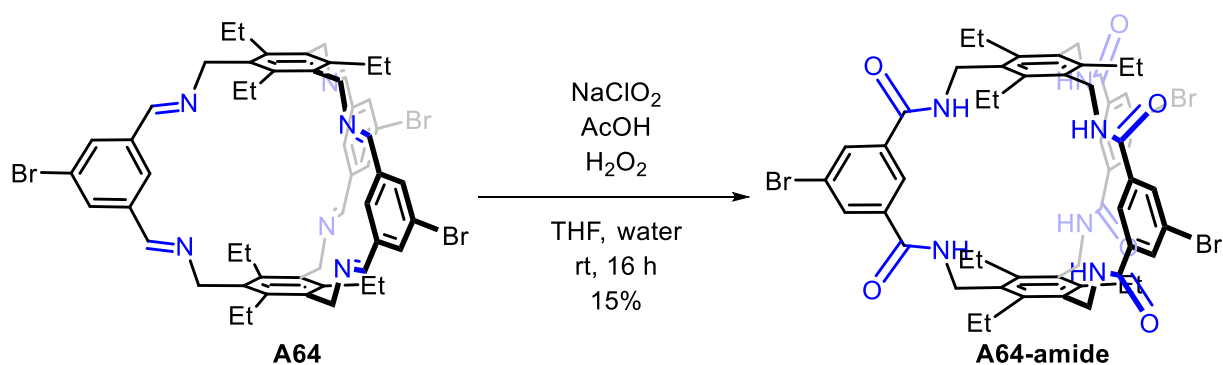
To a suspension of the imine cage **A64** (200 mg, 0.19 mmol, 1 eq.) in 20 mL THF was added 35% w/w solution of hydrogen peroxide (10 M, 1.5 mL, 14.56 mmol, 75 eq.), and NaClO$_2$ (702 mg, 7.76 mmol, 40 eq.) in that order and stirred vigorously. While stirring, acetic acid (1 M solution, 1.94 mL, 1.94 mmol, 10 eq.) was added dropwise over 10 minutes. The reaction mixture remained turbid throughout the reaction. The reaction mixture was evaporated to reduce the amount of THF. The resulting suspension was diluted with water (50 mL) and the precipitate was filtered. The precipitate was washed thoroughly with water (5 × 40 ml) and then with methanol (5 × 30 mL) to obtain a colourless solid. The solid was suspended in DMF (10 mL), heated to 80 °C and filtered (3 times). The combined filtrate was concentrated to obtain the crude mixture as a dark yellow solid. It was dissolved in DMF (10 mL) and passed through reverse phase HPLC (1 mL injections, C-8 column, MeCN: H$_2$O = 60:40 to 90:10, 20 mL/min). The desired product **A64-amide** was obtained as a colourless solid (32 mg, 0.03 mmol, 15%).

¹H NMR (300 MHz, CDCl$_3$) δ = 8.48 ppm (t, 6 H, -CON*H*), 8.13 (s, 6H, Ar-*H*), 7.98 (s, 3 H, Ar-*H*), 4.44 (d, 12 H, -C*H$_2$*-NHCO-), 2.85 (q, 12 H, -C*H$_2$*-CH$_3$, 1.10 (t, 18 H, -CH$_2$-C*H$_3$*).

¹³C NMR (100 MHz, DMSO-*d₆*): δ = 165.3 (Ar-*C*O-NH-), 144.8 (Ar'-*C*-C$_2$H$_5$), 137.3 (Ar-*C*-1,3), 133.1 (Ar'-*C*-CH$_2$-NHCO-), 132.2 (Ar-*C*-4,6), 125.70 (Ar-*C*-5), 122.1 (Ar-*C*-2), 38.3 (-*C*H$_2$-NH-), 22.6 (-*C*H$_2$-CH$_3$), 16.6 (-CH$_2$-*C*H$_3$).

IR (neat, ATR): $\tilde{v}$ = 3310 cm^{-1} (b), 2972 (m), 1641 (s), 1528 (s), 1367 (m), 1296 (s), 1049 (m), 895 (m), 719 (s).

MALDI-TOF-MS: m/z = 1144.948 (Calculated for C$_{54}$H$_{57}$N$_6$O$_6$Br$_3$.Na: m/z = 1145.179) [M+Na]$^+$, 1160.906 [M+K]$^+$.

Melting point: >340°C (decomposed).

Synthesis of cage A67-amide
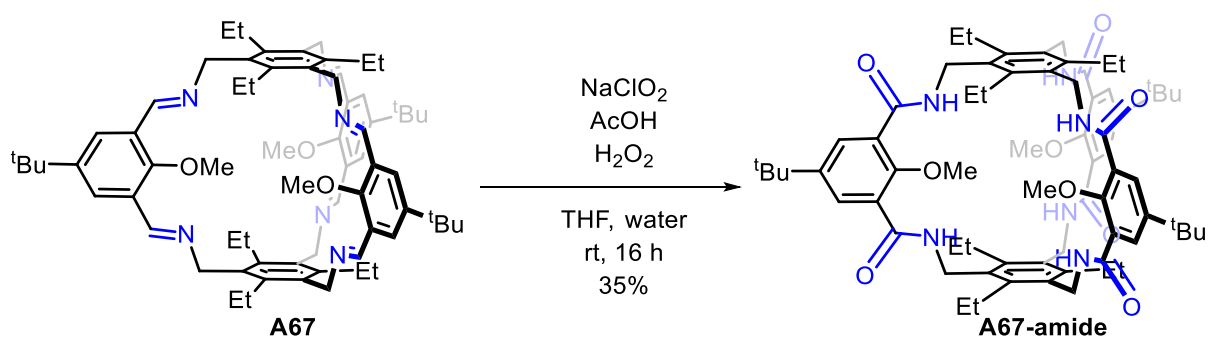
To a solution of the imine cage **A67** (100 mg, 0.095 mmol, 1 eq.) in 10 mL THF was added 35% w/w solution of hydrogen peroxide (10 M, 0.71 mL, 7.1 mmol, 75 eq.), and $NaClO_2$ (345 mg, 3.8 mmol, 40 eq.) in that order and stirred vigorously. While stirring, acetic acid (1M, 0.95 mL, 0.95 mmol, 10 eq.) was added dropwise over 10 minutes. The reaction was left to stir at room temperature for 16 hours. Ethyl acetate (10 mL) and brine (10 mL) was added to the reaction mixture. The organic and aqueous layers were separated. The organic phase was dried over $MgSO_4$ and concentrated to get a yellow solid. The crude mixture was dissolved in DCM and passed through a GPC (DCM, 5 ml/min, 30°C) where two major fractions were obtained. The first fraction was concentrated to obtain the amide cage **A67-amide** as a pale-yellow solid (38 mg, 0.033 mmol, 35%).

^{1}H NMR (600 MHz, CD_2Cl_2) δ = 8.20 ppm (s, 6H, Ar-H), 7.07 (t, 6H, -CO-NH-), 4.61 (d, 12H, -CH_2-NHCO-), 3.68 (s, 9H, -OCH_3), 2.67-2.64 (q, 12 H, -CH_2-CH$_3$), 1.36 (s, 27H, -C(CH_3)$_3$) 1.27 (t, 18 H, -CH$_2$-CH_3).

^{13}C NMR (150 MHz, CD_2Cl_2) δ = 164.8 ppm (Ar-CO-NH-), 153.8 (Ar-C-OCH$_3$), 148.9 (Ar-C-^{t}Bu), 145.0 (Ar'-C-C$_2$H$_5$), 132.4 (Ar-C-4,6), 132.1 (Ar-C-CH$_2$-NHCO), 126.8 (Ar-C-1,3), 63.7 (-OCH$_3$), 38.8 (-CH$_2$-NHCO), 35.0 (-C-(CH$_3$)$_3$), 31.2 (-C-(CH$_3$)$_3$), 23.3 (-CH$_2$-CH$_3$), 16.3 (-CH$_2$-CH$_3$).

IR (neat, ATR): $\tilde{v}$ = 3406 cm^{-1} (b), 2963 (m), 1645 (s), 1516 (s), 1366 (m), 1256 (s), 1111 (m), 988 (s), 812 (2), 673 (w).

APCI-MS: m/z = 1147.687 [M+H]$^+$ (Calculated for $C_{69}H_{91}N_6O_9$.H: m/z = 1147.685), 1164.695 [M+H$_2$O]$^+$.

Melting point: >300°C (decomposed).

Synthesis of cage A70-amide

To a suspension of the imine cage **A70** (100 mg, 0.079 mmol, 1 eq.) in 10 mL THF was added 35% w/w solution of hydrogen peroxide (10 M, 0.6 mL, 5.9 mmol, 75 eq.), $NaClO_2$ (286 mg, 3.16 mmol, 40 eq.) in that order and stirred vigorously. While stirring, acetic acid (1 M, 0.8 mL, 0.79 mmol, 10 eq.) was added dropwise over 10 minutes. The suspension turned into a clear solution in 10 minutes and the reaction mixture was left to stir for another 16 hours. The reaction mixture was evaporated to reduce the amount of THF to a minimum. The resulting suspension was diluted with water (50 mL) and the precipitate was filtered, washed thoroughly with water (5 × 40 ml) and dried in air. It was dissolved in DMF (5 mL) and passed through reverse phase HPLC (1 mL injections, C-8 column, MeCN: H_2O = 60:40 to 90:10, 20 mL/min). The desired product **A70-amide** was obtained as a colourless solid (1 mg, 1%).

¹H NMR (600 MHz, DMSO-d_6) δ = 8.37 ppm (t, 6 H, -CONH), 8.05 (s, 6H, Ar-H), 7.08 (s, 3 H, Ar-H), 4.43 (d, 12 H, -CH_2-NHCO-), 2.85 (q, 12 H, -CH_2-CH₃), 1.12 (t, 18 H, -CH₂-CH_3).

¹³C NMR (500 MHz, DMSO-d_6): δ = 166.4 (Ar-CO-NH-), 144.7 (Ar'-C-C₂H₅), 137.4 (Ar-C-1,3), 137.3 (Ar'-C-CH₂-NHCO-), 132.7 (Ar-C-4,6), 128.5 (Ar-C-5), 121.6 (Ar-C-2), 38.3 (-CH₂-NH-), 22.6 (-CH₂-CH₃), 16.6 (-CH₂-CH₃).

MALDI-TOF-MS: m/z = 1378.718 [M+Na]⁺ (Calculated for $C_{54}H_{54}N_6O_6Br_6$.Na: m/z = 1378.910)

Melting point: >330°C (decomposed).

To a solution of the imine cage **B63** (200 mg, 0.2 mmol, 1 eq.) in 20 mL THF was added 35% w/w solution of hydrogen peroxide (10 M, 1.5 mL, 15 mmol, 75 eq.), and $NaClO_2$ (720 mg, 8 mmol, 40 eq.) in that order and stirred vigorously. While stirring, acetic acid (1M, 2 mL, 2 mmol, 10 eq.) was added dropwise over 10 minutes. The reaction was left to stir at room temperature for 16 hours. Ethyl acetate (10 mL) and brine (10 mL) was added to the reaction mixture. The organic and aqueous layers were separated and the organic phase was dried over $MgSO_4$ to afford a colourless solid on removal of solvents. This solid was first dissolved in MeOH (10 mL) and precipitated by adding water (20 mL) dropwise. The solid was filtered and washed with water. The solid was again dissolved in methanol (5 mL) and diethyl ether (10 mL) was added dropwise. The precipitate was filtered and washed with diethyl ether. The solid was dissolved in MeOH and purified by rHPLC (C8 column, 10% water in MeCN, 20 mL/min) to obtain the amide cage compound **B63-amide** as a colourless solid (41 mg, 0.038 mmol, 19%).

^{1}H NMR (600 MHz, CDCl$_3$) δ = 9.18 ppm (t, 6 H, -CON*H*), 8.27 (s, 6H, Ar-*H*), 8.15 (s, 3 H, Ar-*H*), 4.62 (d, 12 H, -C*H$_2$*-NHCO-), 3.72 (s, 12H, Ar-O-C*H$_2$*C$_2$H$_5$), 1.61 (m, 12 H, -O-CH$_2$-C*H$_2$*-CH$_3$, 0.81 (t, 18 H, -O-C$_2$H$_4$-C*H$_3$*).

^{13}C NMR (150 MHz, DMSO-*d$_6$*): δ = 163.8 (Ar-*C*O-NH-), 158.8 (Ar'-*C*-OC$_3$H$_7$), 149.8 (Ar-*C*-2,6), 140.1 (Ar-*C*-4), 125.70 (Ar-*C*-3,5), 121.9 (Ar'-*C*-CH$_2$-NHCO-), 38.3 (-*C*H$_2$-NH-), 22.6 (-*C*H$_2$-CH$_3$), 16.6 (-CH$_2$-*C*H$_3$).

IR (neat, ATR): $\tilde{v}$ = 3271 cm^{-1} (b), 2966 (m), 1659 (s), 1524 (s), 1443 (m), 1383 (m), 1109 (vs), 895 (w), 752 (m).

MALDI-TOF-MS: m/z = 1094.393 (Calculated for C$_{57}$H$_{69}$N$_9$O$_{12}$.Na: m/z = 1094.496) [M+Na]$^+$.

Melting point: >280°C (decomposed).

Synthesis of cage B73-amide
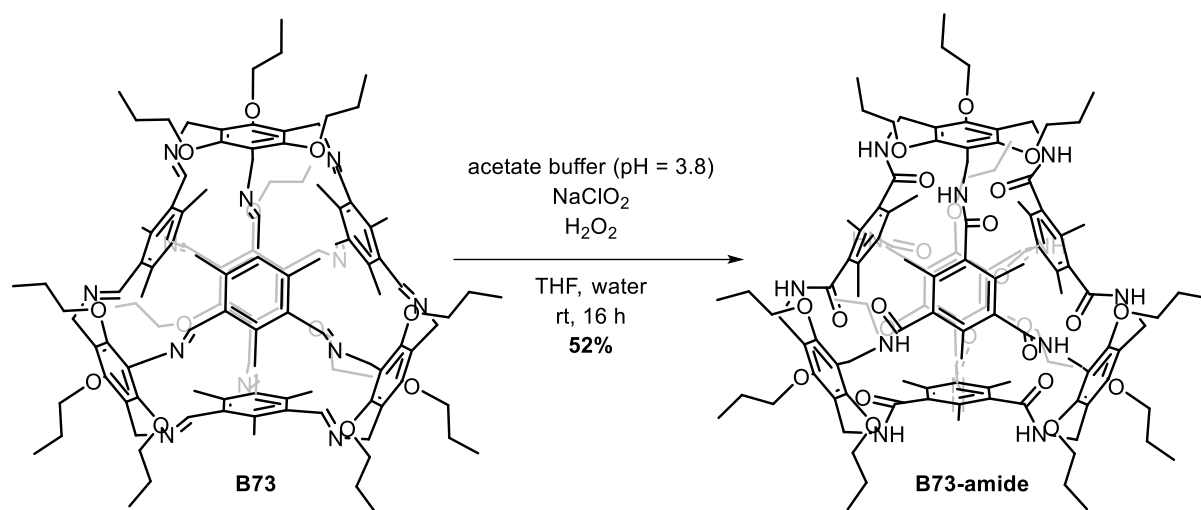
To a solution of imine cage **B73** (100 mg, 0.05 mmol, 1 eq.) in 10 mL THF was added 35% w/w solution of hydrogen peroxide (0.5 mL, 5 mmol, 100 eq.), and NaClO$_2$ (277 mg, 3 mmol, 60 eq.) in that order and stirred vigorously. While stirring, acetic acid (1 M, 0.92 mL, 0.92 mmol, 18 eq.) was added dropwise over 5 minutes. The suspension turned into a clear solution in 10 minutes and the reaction mixture was left to stir for another 16 hours. The reaction mixture was evaporated to reduce the amount of THF to minimum. The resulting suspension was diluted with water (50 mL) and the precipitate was filtered. The colourless solid was stirred in DCM (50 mL) for 16 hours at room temperature. The suspension was filtered, washed with DCM (3 × 30 mL) and the solid was dried under vacuum to obtain the amide cage **B73-amide** as a colourless solid (56 mg, 0.026 mmol, 52%).

^{1}H NMR (500 MHz, DMSO-d_6) δ = 8.20 ppm (m, 6H, Ar-*H*), 7.07 (s, 6H, -CO-N*H*-), 4.61 (d, 12H, -C*H*$_2$-NHCO-), 3.68 (s, 9H, -OC*H*$_3$), 2.67-2.64 (q, 12 H, -C*H*$_2$-CH$_3$), 1.36 (s, 27H, -C(C*H*$_3$)$_3$) 1.27 (t, 18 H, -CH$_2$-C*H*$_3$).

^{13}C NMR (150 MHz, CD$_2$Cl$_2$) δ = 164.8 ppm (Ar'-*C*O-NH-), 153.8 (Ar'-*C*), 148.9 (Ar'-*C*-^{t}Bu), 145.0 (Ar-*C*-C$_2$H$_5$), 132.4 (Ar'-*C*), 132.1 (Ar-*C*-CH$_2$-NHCO), 126.8 (Ar'-*C*), 63.7 (-O*C*H$_3$), 38.8 (-*C*H$_2$-NHCO), 35.0 (-*C*-(CH$_3$)$_3$), 31.2 (-C-(*C*H$_3$)$_3$), 23.3 (-*C*H$_2$-CH$_3$), 16.3 (-CH$_2$-*C*H$_3$).

MALDI-TOF-MS: *m/z* = 2172.369 (Calculated for C$_{120}$H$_{156}$N$_{12}$O$_{24}$.Na: *m/z* = 2172.125) [M+Na]$^+$, 2188.342 [M+K]$^+$, 2203.716 [M+Na+K+CH$_3$]$^+$, 2235.429 [M+CH$_2$Cl$_2$]$^+$, 2256.386 [M+ CH$_2$Cl$_2$+Na]$^+$.

IR (neat, ATR): $\tilde{v}$ = 3252 cm^{-1} (b), 2966 (m), 2928 (m) 1639 (s), 1531 (s), 1445 (m), 1254 (m), 1111 (s), 951 (m).

Elemental analysis: Calculated for $C_{54}H_{60}N_6O_6 \cdot 4 \, CH_2Cl_2 \cdot 8 \, H_2O$: C 56.53 H 6.89 N 6.38, found: C 56.69 H 7.07 N 6.39.

Melting point: >350°C (decomposed).

SCXRD: See appendix section 4.4

2.3. Compounds of chapter III, Section 3

Synthesis of amide cage 74
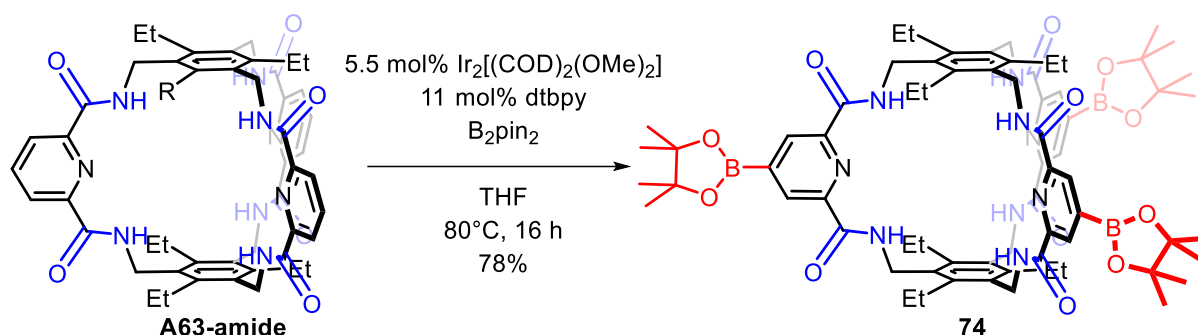
In a screw capped vial (V1) **A63-amide** (200 mg, 0.22 mol, 1 eq.) and bis(pinacolato)diboron (1.14 g, 4.5 mmol, 20 eq.) were weighed in, taken into a glove box and dissolved in THF (4 mL). In the glove box, Ir$_2$[(COD)$_2$(OMe)$_2$] (8 mg, 0.01 mmol, 0.055 eq.) and *4,4'-ditertbutyl-2,2'-bipyridyl* (7 mg, 0.02 mmol, 0.11 eq.) were dissolved in THF (0.4 mL) with a small portion of B$_2$pin$_2$ in another screw capped vial (V2). This solution was stirred for 5 minutes until it turned reddish-brown and then transferred into the first vial V1. It was capped tightly and stirred at 80 °C for 16 hours. The reaction mixture was concentrated, and the crude product was precipitated with petroleum ether (20 mL), filtered and washed with petroleum ether (3 × 20 mL). The cage compound was dissolved in DCM (10 mL) and passed through a celite pad. On concentrating, the product **74** was obtained as an off-white solid. (222 mg, 0.17 mmol, 1 eq.).

^{1}H NMR (600 MHz, CD$_2$Cl$_2$) δ = 8.72 (s, 6H, pyridine ring-C*H*), 7.30 (bs, 6H, -CO-N*H*-), 4.71 (d, 12H, -C*H$_2$*-NHCO-), 2.69 (q, 12 H, -C*H$_2$*-CH$_3$), 1.37 (s, 36H, Bpin-C*H$_3$*), 1.21 (t, 18H, -CH$_2$-C*H$_3$*).

¹³C NMR (150 MHz, CD$_2$Cl$_2$): δ = 164.0 ppm (Ar'-CO-NH-), 148.5 (pyridine-C-2,6), 146.1 (Ar'-C), 131.5 (Ar'-C), 131.1 (pyridine-C-3,5), 85.3 (-B-O-C-(CH$_3$)$_2$), 38.7 (-CH$_2$-NH-), 24.9 (-B-O-C-(CH$_3$)$_2$)-23.6 (-CH$_2$-CH$_3$), 16.0 (-CH$_2$-CH$_3$).

IR (neat, ATR) $\tilde{v}$ = 3305 cm^{-1} (b), 2968 (w), 1645 (vs), 1527 (vs), 1411 (s), 1375 (s), 1278 (s), 1060 (s), 999(m), 937 (m), 748 (m), 655 (s).

Elemental analysis: Calculated for C$_{69}$H$_{90}$B$_3$N$_9$O$_{12}$·7 H$_2$O: C 59.36 H 7.51 N 9.03, found: C 59.00 H 7.38 N 9.03.

Melting point: Decomposes above 270°C.

Synthesis of amide cage 75

74 → NaIO$_4$, HCl / THF, water / rt, 5 h / 90% → **75**
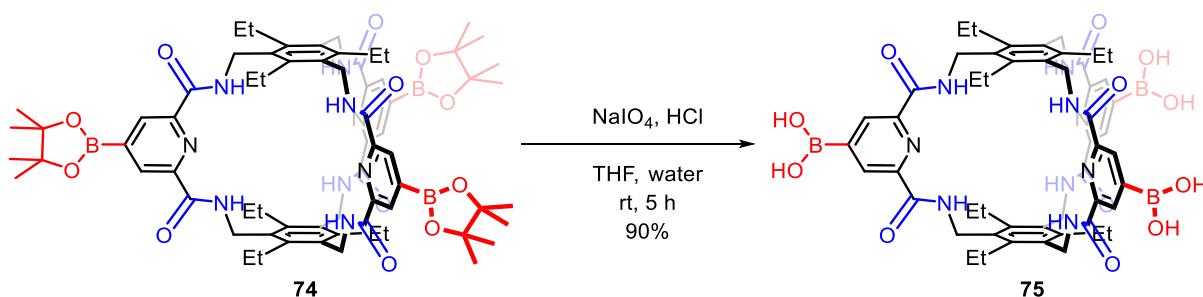
To a solution of the cage compound in **74** (100 mg, 0.08 mmol, 1 eq.) in THF (4 mL) was added a solution of NaIO$_4$ (170 mg, 0.8 mmol, 1 eq.) in water (1 mL) under vigorous stirring. After adding, the reaction mixture was warmed to room temperature while stirring vigorously. The reaction was stirred at room temperature for 3 hours and 1 M HCl (4 mL) was added at 0°C. The reaction was warmed to room temperature and stirred for 2 hours. The precipitate was filtered, washed with water (3 × 10 mL) and methanol (2 × 10 mL). The residue was dried under vacuum to obtain the product **75** as a colourless solid (74 mg, 0.072 mmol, 90%).

¹H NMR (600 MHz, DMSO-d_6) δ = 8.70 ppm (bs, 6H, -CO-NH- and -B-OH), 8.57 (s, 6H, pyridine-H), 4.69 (d, 12H, -CH_2-NHCO-), 2.74 (q, 12 H, -CH_2-CH$_3$), 1.1 (t, 18H, CH$_2$-CH_3).

¹³C NMR (150 MHz, DMSO-d_6): δ = 164.6 ppm (Ar'-CO-NH-), 149.2 (Ar'-C), 146.3 (pyridine-C-2,6), 131.5 (Ar'-C), 131.1 (pyridine-C-3,5), 85.3 (-B-O-C-(CH$_3$)$_2$), 38.7 (-CH$_2$-NH-), 24.9 (-B-O-C-(CH$_3$)$_2$)-23.6 (-CH$_2$-CH$_3$), 16.0 (-CH$_2$-CH$_3$).

IR (KBr pellet,) $\tilde{v}$ = 2970 cm^{-1} (w), 1651 (vs), 1531 (vs), 1412 (m), 1379 (m), 1286 (m), 1059 (m), 752 (m), 663 (s).

Elemental analysis: Calculated for $C_{51}H_{60}B_3N_9O_{12} \cdot 11\ H_2O$: C 50.14 H 6.77 N 10.32, found: C 50.36 H 6.35 N 9.86.

Melting point: Decomposes above 330 °C.

Synthesis of amide cage 76
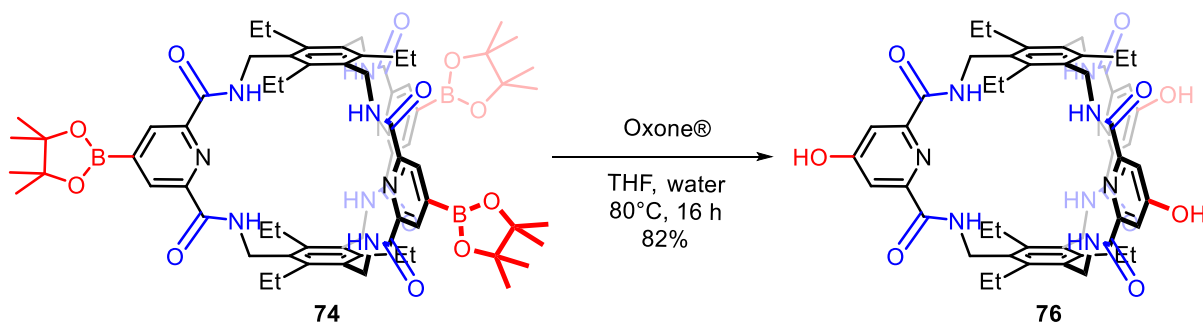
To a solution of the cage compound **74** (100 mg, 0.08 mmol, 1 eq.) in THF (4 mL) was added a slurry of Oxone® (245 mg, 0.8 mmol, 10 eq.) in THF (2 mL) and water (3 mL). The reaction mixture was stirred at 80 °C for 16 h. On cooling, ethyl acetate (2 mL) was added for better separation of the organic and aqueous phases. The aqueous phase was extracted with a 2:1 mixture of THF:ethyl acetate (2 × 10 mL). The combined organic phase was washed with brine (10 mL), dried over $MgSO_4$ and concentrated. The cage compound **76** was obtained as a yellow solid (60 mg, 0.064 mmol, 82%).

¹H NMR (500 MHz, DMSO-d_6) δ = 11.39 ppm (bs, 3H, -OH), 8.61 (bs, 6H, -CO-N*H*-), 7.54 (s, 6H, pyridine ring-C*H*), 4.53 (d, 12H, -C*H*$_2$-NHCO-), 2.65 (q, 12 H, -C*H*$_2$-CH$_3$), 1.07 (t, 18H, -CH$_2$-C*H*$_3$).

¹³C NMR (100 MHz, DMSO-d_6): δ = 166.81 (pyridine-*C*-OH), 164.36 (Ar'-*C*O-NH-), 152.17 (pyridine-*C*-2,6), 145.18 (Ar-*C*), 132.60 (Ar-*C*), 113.09 (pyridine-*C*-3,5), 38.02 (-*C*H$_2$-NH-), 23.10 (-*C*H$_2$-CH$_3$), 16.59 (-CH$_2$-*C*H$_3$).

IR (neat, ATR) $\tilde{v}$ = 3420 cm^{-1} (w), 2970 (w), 2924 (w), 1659 (vs), 1609 (s), 1512 (vs), 1335 (m), 1246 (m), 1128 (w), 1057 (w), 995 (w), 887 (w), 752 (m).

MALDI-MS (HR-MS): m/z = 938.4207 [M-H]$^-$ (Calculated for $C_{54}H_{59}N_6O_6$: m/z = 938.4201)

Elemental analysis: Calculated for $C_{51}H_{57}N_9O_9 \cdot 5\ H_2O$: C 59.46 H 6.56 N 12.24, found: C 59.64 H 6.44 N 11.93.

Melting point: Decomposes above 300 °C.

Synthesis of amide cage 77
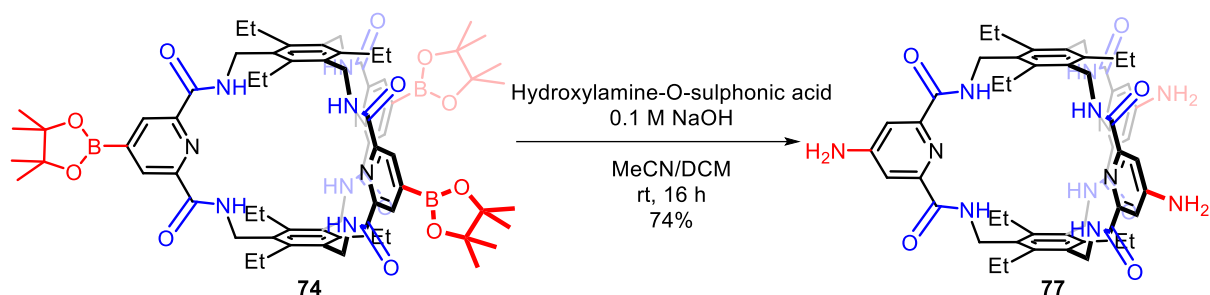
To a solution of cage compound **74** (50 mg, 0.04 mmol, 1 eq.) in MeCN (2 mL) and DCM (2 mL), hydroxylamine-o-sulfonic acid (45 mg, 0.4 mmol, 10 eq.) was added. While stirring vigorously at room temperature, 0.2 M NaOH solution (2 mL, 10 eq.) was added dropwise over 2 mins. The reaction mixture was left to stir at rt for 16 hours. On completion, the reaction mixture was concentrated to remove the organic solvents and then diluted with water (5 mL). A yellow precipitate was formed, which was filtered, washed with water (3×10 mL) and dried under vacuum to obtain a pale-yellow solid **77** (28 mg, 0.03 mmol, 74%).

^{1}H NMR (300 MHz, DMSO-d_6) δ = 8.72 ppm (t, 6H, -CO-N*H*-), 8.58 (s, 6H, pyridine ring-C*H*), 4.59 (d, 12H, -C*H*$_2$-NHCO-), 2.68 (q, 12 H, -C*H*$_2$-CH$_3$), 1.10 (t, 18 H, -CH$_2$-C*H*$_3$).

^{13}C NMR (100 MHz, DMSO-d_6): δ =164.6 (Ar'-*C*O-NH-), 158.2 (pyridine-*C*-NH$_2$), 149.2 (pyridine-*C*-2,6), 145.0 (Ar-*C*), 132.5 (Ar-*C*), 113.3 (pyridine-*C*-3,5), 37.7 (-*C*H$_2$-NH-), 22.8 (-*C*H$_2$-CH$_3$), 16.3 (-CH$_2$-*C*H$_3$).

IR (neat, ATR) $\tilde{v}$ = 3496 cm^{-1} (vs) , 2974 (w), 1647 (vs), 1526 (vs), 1412 (m), 1377 (s), 1283 (m), 1055 (s), 997 (w), 939 (w), 746 (w), 656 (m).

MALDI-TOF-MS: *m/z* = 959.466 [M+Na]$^+$(Calculated for C$_{51}$H$_{60}$N$_{12}$O$_6$.Na: *m/z* = 959.466)

Elemental analysis: Calculated for C$_{51}$H$_{57}$N$_9$O$_9$·4 H$_2$O·3 CH$_2$Cl$_2$: C 53.99 H 6.16 N 14.26, found: C 53.67 H 6.24 N 10.79.

Melting point: Decomposes above 220 °C.

Synthesis of amide cage 78
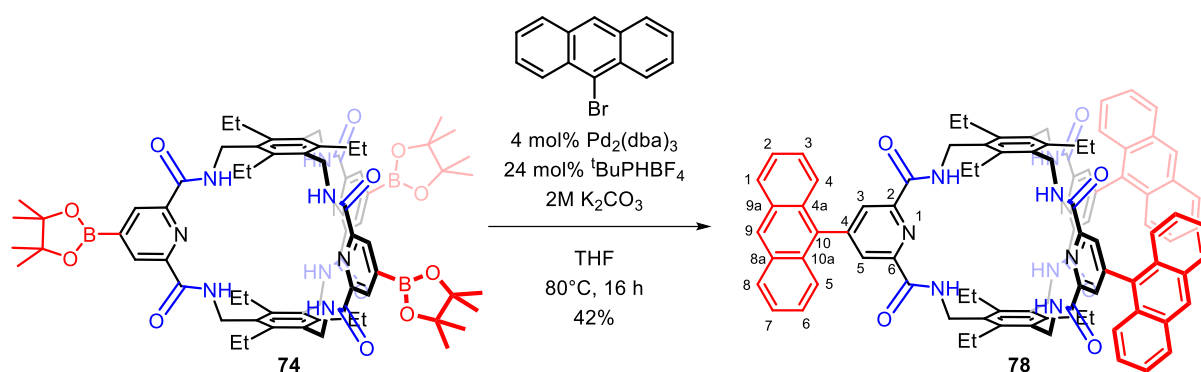
A solution of cage compound **74** (100 mg, 0.08 mmol, 1 eq.) and 9-bromoanthracene (205 mg, 0.8 mmol, 10 eq.) in THF$_{abs}$ (3mL) was flushed with argon for 10 minutes. To this, 2 M K$_2$CO$_3$ solution (1.5 mL) was added followed by Pd$_2$(dba)$_3$ (3 mg, 3.2 µmol, 0.04 eq.) and ^{t}Bu$_3$PHBF$_4$ (5.6 mg, 0.02 mmol, 0.24 eq.). The reaction mixture was stirred under argon at 80 °C for 16 hours. On completion, the reaction mixture was concentrated to remove the solvent and diethyl ether was added and stirred for 30 minutes. The orange precipitate was filtered and washed with diethyl ether (3 × 10 mL). The crude mixture was dissolved in DCM and passed through a normal phase HPLC (5% iso-propanol in DCM, 10 mL/min). The product **78** was obtained as a bright yellow solid (47 mg, 0.03 mmol, 42%).

^{1}H NMR (500 MHz, CDCl$_3$) δ = 8.68 ppm (s, 6H, pyridine ring-C*H*), 8.61 (s, 3H, anthracene-10-C*H*), 8.12 (d, 6H, anthracene-*H*-4,5), 7.55-7.51 (m, 12H, -CO-N*H*- and anthracene-*H*-1,8), 7.49-7.46 (m, 6H, anthracene-*H*-3,6) 7.42-7.39 (m, 6H, anthracene-*H*-2,7), 4.82 (d, 12H, -C*H$_2$*-NHCO-), 2.83 (q, 12 H, -C*H$_2$*-CH$_3$), 1.34 (t, 18 H, -CH$_2$-C*H$_3$*).

^{13}C NMR (100 MHz, CDCl$_3$) δ = 164.2 ppm (pyridine-*C*O-NH-), 151.1 (pyridine-*C*-4), 149.4 (pyridine-*C*-1,6), 146.4 (CH$_3$-CH$_2$-Ar-*C*), 131.9 (anthracene-*C*-8a, 9a), 131.2 (-NH-CH$_2$-Ar-*C*), 129.4 (anthracene-*C*-4a, 10a), 129.3 (pyridine-*C*-3,5), 128.8 (anthracene-*C*-4,5), 128.5 (anthracene-*C*-9), 126.5 (anthracene-*C*-2,7), 125.5 (anthracene-*C*-3,6), 125.4 (anthracene-*C*-1,8), 38.9 (-*C*H$_2$-NH-), 23.7 (-*C*H$_2$-CH$_3$).

IR (neat, ATR) $\tilde{v}$ = 3425 cm^{-1} (w), 2970 (w), 1670 (vs), 1605 (w), 1512 (vs), 1312 (w), 1248 (w), 1057 (w), 889 (w), 793 (w), 735 (s), 629 (w).

MALDI-MS (HR-MS): *m/z* = 1442.6211 (Calculated for C$_{54}$H$_{60}$N$_6$O$_6$.Na: *m/z* = 1442.6208)

Elemental analysis: Calculated for C$_{93}$H$_{81}$N$_9$O$_6$·5 H$_2$O: C 73.94 H 6.07 N 8.34, found: C 73.61 H 5.90 N 8.12.

Melting point: Decomposes above 270 °C.

SCXRD: See appendix section 4.5.

Synthesis of amide cage 79
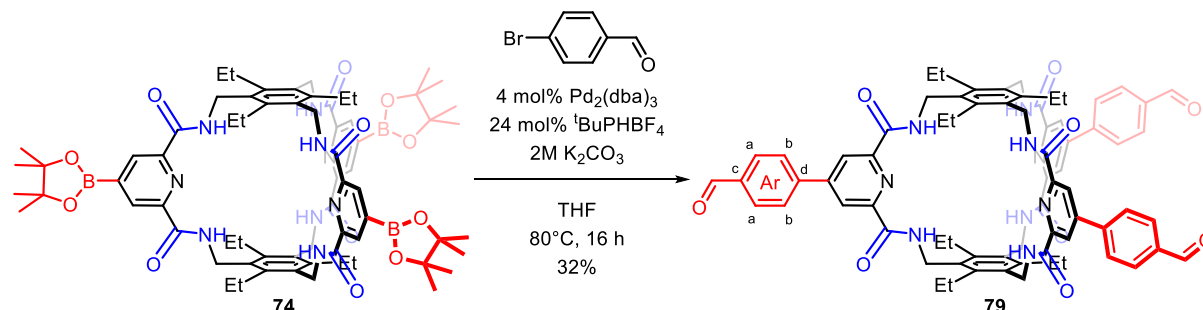
A solution of cage compound **74** (100 mg, 0.08 mmol, 1 eq.) and *p*-bromobenzaldehyde (148 mg, 0.8 mmol, 10 eq.) in THF$_{abs}$ (3mL) was flushed with argon for 10 minutes. To this, 2 M K$_2$CO$_3$ solution (degassed) (1.5 mL) was added followed by Pd$_2$(dba)$_3$ (3 mg, 3.2 µmol, 0.04 eq.) and ^{t}Bu$_3$PHBF$_4$ (5.6 mg, 0.02 mmol, 0.24 eq.). The reaction mixture was stirred under argon at 80 °C for 48 hours. On completion, the reaction mixture was concentrated to remove THF. The crude mixture was dissolved in DCM, washed with water (3 × 15 mL), brine (15 mL) and dried over MgSO$_4$. Diethyl ether (20 mL) was added to the resulting solid and stirred for 30 minutes. The orange precipitate was filtered and washed with diethyl ether (3 × 10 mL). The product was obtained as a pale-yellow solid **79** (31 mg, 0.026 mmol, 32%).

^{1}H NMR (500 MHz, CD$_2$Cl$_2$) δ = 10.15 ppm (s, 3H, -CHO), 8.77 (s, 6H, pyridine ring-C*H*), 8.06-8.01 (q, 12H, Ar'-*H*), 7.61 (d, 6H, -CO-N*H*-), 4.76 (d, 12H, -C*H$_2$*-NHCO-), 2.77 (q, 12 H, -C*H$_2$*-CH$_3$), 1.26 (t, 18 H, -CH$_2$-C*H$_3$*).

^{13}C NMR (100 MHz, CD$_2$Cl$_2$) δ = 191.6 (-*C*HO), 163.5 (pyridine-*C*O-NH-), 150.5 (pyridine-*C*), 149.6 (pyridine-*C*), 145.8 (CH$_3$-CH$_2$-Ar-*C*), 142.3 (Ar'-*C*-d), 137.1 (Ar'-*C*-c), 131.1 (-NH-CH$_2$-Ar-*C*), 130.3 (Ar'-*C*-a), 128.0 (Ar'-*C*-b), 123.6 (pyridine ring-*C*H) 37.73 (-*C*H$_2$-NH-), 22.83 (-*C*H$_2$-CH$_3$), 16.32 (-CH$_2$-*C*H$_3$).

IR (neat, ATR) $\tilde{v}$ = 3404 cm^{-1} (b), 2972 (w), 1697 (s), 1661 (vs), 1603 (s), 1522 (vs), 1331 (w), 1256 (w), 1215 (w), 1177 (w), 1070 (w), 999 (w), 837 (m), 748 (s), 694 (m).

MALDI-MS (HR-MS): *m/z* = 1226.5124 (Calculated for C$_{54}$H$_{60}$N$_6$O$_6$.Na: *m/z* = 1226.5116)

Melting point: Decomposes above 300°C.

VI. References

[1]   P. Muller, *Pure Appl. Chem.* **1994**, *66*, 1077-1184.

[2]   a) H. Hopf, *Classics in hydrocarbon chemistry*, Wiley-VCH, **2000**; b) G. Maier, S. Pfriem, U. Schäfer, R. Matusch, *Angew. Chem. Int. Ed. Engl.* **1978**, *17*, 520-521; c) L. A. Paquette, R. J. Ternansky, D. W. Balogh, G. Kentgen, *J. Am. Chem. Soc.* **1983**, *105*, 5446-5450; d) P. E. Eaton, T. W. Cole, *J. Am. Chem. Soc.* **1964**, *86*, 3157-3158.

[3]   a) R. W. Saalfrank, A. Stark, K. Peters, H. G. von Schnering, *Angew. Chem. Int. Ed. Engl.* **1988**, *27*, 851-853; b) M. Tominaga, K. Suzuki, M. Kawano, T. Kusukawa, T. Ozeki, S. Sakamoto, K. Yamaguchi, M. Fujita, *Angew. Chem. Int. Ed.* **2004**, *43*, 5621-5625; c) R. Chakrabarty, P. S. Mukherjee, P. J. Stang, *Chem. Rev.* **2011**, *111*, 6810-6918.

[4]   G. Zhang, M. Mastalerz, *Chem. Soc. Rev.* **2014**, *43*, 1934-1947.

[5]   C. J. Pedersen, *J. Am. Chem. Soc.* **1967**, *89*, 7017-7036.

[6]   B. Dietrich, J. Lehn, J. Sauvage, *Tetrahedron Lett.* **1969**, *10*, 2885-2888.

[7]   a) D. J. Cram, S. Karbach, Y. H. Kim, L. Baczynskyj, G. W. Kallemeyn, *J. Am. Chem. Soc.* **1985**, *107*, 2575-2576; b) R. Warmuth, J. Yoon, *Acc. Chem. Res.* **2001**, *34*, 95-105; c) M. E. Tanner, C. B. Knobler, D. J. Cram, *J. Am. Chem. Soc.* **1990**, *112*, 1659-1660.

[8]   C. Seel, F. Vögtle, *Angew. Chem. Int. Ed. Engl.* **1992**, *31*, 528-549.

[9]   Z. Wu, S. Lee, J. S. Moore, *J. Am. Chem. Soc.* **1992**, *114*, 8730-8732.

[10]   C. Bucher, R. S. Zimmerman, V. Lynch, J. L. Sessler, *J. Am. Chem. Soc.* **2001**, *123*, 9716-9717.

[11]   W. Kiggen, F. Vögtle, *Angew. Chem. Int. Ed. Engl.* **1984**, *23*, 714-715.

[12]   T. J. McMurry, S. J. Rodgers, K. N. Raymond, *J. Am. Chem. Soc.* **1987**, *109*, 3451-3453.

[13]   J. Jazwinski, J.-M. Lehn, D. Lilienbaum, R. Ziessel, J. Guilhem, C. Pascard, *J. Chem. Soc., Chem. Commun.* **1987**, 1691-1694.

[14]   M. L. Quan, D. J. Cram, *J. Am. Chem. Soc.* **1991**, *113*, 2754-2755.

[15]   J. M. Lehn, *Chem. Eur. J.* **1999**, *5*, 2455-2463.

[16]   X. Liu, R. Warmuth, *J. Am. Chem. Soc.* **2006**, *128*, 14120-14127.

[17]   a) N. Cao, Y. Wang, X. Zheng, T. Jiao, H. Li, *Org. Lett.* **2018**, *20*, 7447-7450; b) S. J. Rowan, S. J. Cantrill, G. R. Cousins, J. K. Sanders, J. F. Stoddart, *Angew. Chem. Int. Ed.* **2002**, *41*, 898-952.

[18]   a) X. Liu, Y. Liu, R. Warmuth, *Supramol. Chem.* **2008**, *20*, 41-50; b) M. Kołodziejski, A. R. Stefankiewicz, J.-M. Lehn, *Chem. Sci.* **2019**, *10*, 1836-1843.

[19]   a) C. Bravin, C. A. Hunter, *Chem. Sci.* **2020**, *11*, 9122-9125; b) A. Galán, E. C. Escudero-Adán, P. Ballester, *Chem. Sci.* **2017**, *8*, 7746-7750.

[20]   a) A. P. Cote, A. I. Benin, N. W. Ockwig, M. O'Keeffe, A. J. Matzger, O. M. Yaghi, *Science* **2005**, *310*, 1166-1170; b) S. S.-Y. Chui, S. M.-F. Lo, J. P. Charmant, A. G.

Orpen, I. D. Williams, *Science* **1999**, *283*, 1148-1150; c) H. Li, M. Eddaoudi, M. O'Keeffe, O. M. Yaghi, *Nature* **1999**, *402*, 276-279.

[21] a) P. S. Mukherjee, K. Acharyya, *Angew. Chem. Int. Ed.* **2019**; b) M. Mastalerz, *Angew. Chem. Int. Ed.* **2010**, *49*, 5042-5053; c) M. E. Briggs, A. I. Cooper, *Chem. Mater.* **2017**, *29*, 149-157.

[22] a) N. Fujita, S. Shinkai, T. D. James, *Chem.: Asian J.* **2008**, *3*, 1076-1091; b) F. Beuerle, B. Gole, *Angew. Chem. Int. Ed.* **2018**, *57*, 4850-4878.

[23] C. Zhang, Q. Wang, H. Long, W. Zhang, *J. Am. Chem. Soc.* **2011**, *133*, 20995-21001.

[24] Y. C. Horng, T. L. Lin, C. Y. Tu, T. J. Sung, C. C. Hsieh, C. H. Hu, H. M. Lee, T. S. Kuo, *Eur. J. Org. Chem.* **2009**, *2009*, 1511-1514.

[25] S. Ro, S. J. Rowan, A. R. Pease, D. J. Cram, J. F. Stoddart, *Org. Lett.* **2000**, *2*, 2411-2414.

[26] P. Mateus, R. Delgado, P. Brandao, S. Carvalho, V. Felix, *Org. Biomol. Chem.* **2009**, *7*, 4661-4673.

[27] X. Liu, Y. Liu, G. Li, R. Warmuth, *Angew. Chem.* **2006**, *118*, 915-918.

[28] A. P. Davis, R. S. Wareham, *Angew. Chem. Int. Ed.* **1998**, *37*, 2270-2273.

[29] a) T. Tozawa, J. T. Jones, S. I. Swamy, S. Jiang, D. J. Adams, S. Shakespeare, R. Clowes, D. Bradshaw, T. Hasell, S. Y. Chong, *Nat. Mater.* **2009**, *8*, 973-978; b) M. W. Schneider, I. M. Oppel, H. Ott, L. G. Lechner, H. J. S. Hauswald, R. Stoll, M. Mastalerz, *Chem. Eur. J.* **2012**, *18*, 836-847.

[30] S. M. Elbert, F. Rominger, M. Mastalerz, *Chem. Eur. J.* **2014**, *20*, 16707-16720.

[31] P. Skowronek, B. Warżajtis, U. Rychlewska, J. Gawroński, *Chem. Commun.* **2013**, *49*, 2524-2526.

[32] J. D. Evans, K. E. Jelfs, G. M. Day, C. J. Doonan, *Chem. Soc. Rev.* **2017**, *46*, 3286-3301.

[33] a) T. H. Schick, F. Rominger, M. Mastalerz, *J. Org. Chem.* **2020**, *85*, 13757-13771; b) K. Acharyya, P. S. Mukherjee, *Chem. Commun.* **2015**, *51*, 4241-4244.

[34] P. Skowronek, J. Gawronski, *Org. Lett.* **2008**, *10*, 4755-4758.

[35] B. D. Egleston, M. C. Brand, F. Greenwell, M. E. Briggs, S. L. James, A. I. Cooper, D. E. Crawford, R. L. Greenaway, *Chem. Sci.* **2020**.

[36] T. Hasell, M. Miklitz, A. Stephenson, M. A. Little, S. Y. Chong, R. Clowes, L. Chen, D. Holden, G. A. Tribello, K. E. Jelfs, *J. Am. Chem. Soc.* **2016**, *138*, 1653-1659.

[37] A. Kewley, A. Stephenson, L. Chen, M. E. Briggs, T. Hasell, A. I. Cooper, *Chem. Mater.* **2015**, *27*, 3207-3210.

[38] S. Hong, M. R. Rohman, J. Jia, Y. Kim, D. Moon, Y. Kim, Y. H. Ko, E. Lee, K. Kim, *Angew. Chem. Int. Ed.* **2015**, *54*, 13241-13244.

[39] J. C. Lauer, W.-S. Zhang, F. Rominger, R. R. Schröder, M. Mastalerz, *Chem. Eur. J.* **2018**, *24*, 1816-1820.

[40] M. Mastalerz, *Chem. Commun.* **2008**, *0*, 4756-4756.

[41] M. W. Schneider, I. M. Oppel, M. Mastalerz, *Chem. Eur. J.* **2012**, *18*, 4156-4160.

[42] M. W. Schneider, H.-J. S. Hauswald, R. Stoll, M. Mastalerz, *Chem. Commun.* **2012**, *48*, 9861-9863.

[43] a) K. Su, W. Wang, S. Du, C. Ji, M. Zhou, D. Yuan, *J. Am. Chem. Soc.* **2020**, *142*, 18060-18072; b) M. Mastalerz, M. W. Schneider, I. M. Oppel, O. Presly, *Angew. Chem. Int. Ed.* **2011**, *50*, 1046-1051.

[44] M. Brutschy, M. W. Schneider, M. Mastalerz, S. R. Waldvogel, *Chem. Commun.* **2013**, *49*, 8398-8400.

[45] a) O. Francesconi, A. Ienco, G. Moneti, C. Nativi, S. Roelens, *Angew. Chem.* **2006**, *118*, 6845-6848; b) M. Arunachalam, I. Ravikumar, P. Ghosh, *J. Org. Chem.* **2008**, *73*, 9144-9147; c) P. Mateus, R. Delgado, P. Brandão, V. t. Félix, *J. Org. Chem.* **2009**, *74*, 8638-8646.

[46] J. L. Culshaw, G. Cheng, M. Schmidtmann, T. Hasell, M. Liu, D. J. Adams, A. I. Cooper, *J. Am. Chem. Soc.* **2013**, *135*, 10007-10010.

[47] T. H. G. Schick, J. C. Lauer, F. Rominger, M. Mastalerz, *Angew. Chem. Int. Ed.* **2019**, *58*, 1768-1773.

[48] M. Liu, M. A. Little, K. E. Jelfs, J. T. A. Jones, M. Schmidtmann, S. Y. Chong, T. Hasell, A. I. Cooper, *J. Am. Chem. Soc.* **2014**, *136*, 7583-7586.

[49] X.-Y. Hu, W.-S. Zhang, F. Rominger, I. Wacker, R. R. Schröder, M. Mastalerz, *Chem. Commun.* **2017**, *53*, 8616-8619.

[50] P.-E. Alexandre, W.-S. Zhang, F. Rominger, S. M. Elbert, R. R. Schröder, M. Mastalerz, *Angew. Chem. Int. Ed.* **2020**, *59*, 19675-19679.

[51] S. D. Roughley, A. M. Jordan, *J. Med. Chem.* **2011**, *54*, 3451-3479.

[52] a) Y.-R. Luo, *Comprehensive handbook of chemical bond energies*, CRC press, **2007**; b) I. I. Marochkin, O. V. Dorofeeva, *Comput. Theor. Chem.* **2012**, *991*, 182-191.

[53] a) T. B. Nguyen, J. Sorres, M. Q. Tran, L. Ermolenko, A. Al-Mourabit, *Org. Lett.* **2012**, *14*, 3202-3205; b) L. Becerra-Figueroa, A. Ojeda-Porras, D. Gamba-Sánchez, *J. Org. Chem.* **2014**, *79*, 4544-4552; c) M. Zhang, S. Imm, S. Bähn, L. Neubert, H. Neumann, M. Beller, *Angew. Chem. Int. Ed.* **2012**, *51*, 3905-3909.

[54] N. A. Stephenson, J. Zhu, S. H. Gellman, S. S. Stahl, *J. Am. Chem. Soc.* **2009**, *131*, 10003-10008.

[55] a) R. J. Williams, A. M. Smith, R. Collins, N. Hodson, A. K. Das, R. V. Ulijn, *Nat. Nanotechnol.* **2009**, *4*, 19-24; b) J. W. Sadownik, R. V. Ulijn, *Curr. Opin. Biotechnol.* **2010**, *21*, 401-411; c) Y. Ruff, V. Garavini, N. Giuseppone, *J. Am. Chem. Soc.* **2014**, *136*, 6333-6339.

[56] a) S. Grammenudi, F. Vögtle, *Angew. Chem. Int. Ed. Engl.* **1986**, *25*, 1122-1125; b) P. Belser, L. De Cola, A. von Zelewsky, *J. Chem. Soc., Chem. Commun.* **1988**, 1057-1058.

[57] S. Grammenudi, M. Franke, F. Vögtle, E. Steckhan, *J. Inclusion Phenom. Mol. Recognit. Chem.* **1987**, *5*, 695-707.

[58] a) Y. Murakami, J.-I. Kikuchi, H. Tenma, *J. Chem. Soc., Chem. Commun.* **1985**, 753-755; b) F. Ebmeyer, F. Vögtle, *Angew. Chem. Int. Ed. Engl.* **1989**, *28*, 79-81; c) A. Wallon, J. Peter-Katalinića, U. Werner, W. M. Müller, F. Vögtle, *Chem. Ber.* **1990**, *123*, 375-379; d) F. Ebmeyer, F. Vögtle, *Chem. Ber.* **1989**, *122*, 1725-1727.

[59] H. Masu, K. Katagiri, T. Kato, H. Kagechika, M. Tominaga, I. Azumaya, *J. Org. Chem.* **2008**, *73*, 5143-5146.

[60] H.-J. Choi, D. Bühring, M. L. C. Quan, C. B. Knobler, D. J. Cram, *J. Chem. Soc., Chem. Commun.* **1992**, 1733-1735.

[61] A. P. Bisson, V. M. Lynch, M.-K. C. Monahan, E. V. Anslyn, *Angew. Chem. Int. Ed. Engl.* **1997**, *36*, 2340-2342.

[62] G. Lecollinet, A. P. Dominey, T. Velasco, A. P. Davis, *Angew. Chem.* **2002**, *114*, 4267-4270.

[63] B. A. Arndtsen, H. Erguven, E. Keyzer, *Chem. Eur. J.* **2020**.

[64] A. P. Davis, *Chem. Soc. Rev.* **2020**, *49*, 2531-2545.

[65] S. O. Kang, J. M. Llinares, D. Powell, D. VanderVelde, K. Bowman-James, *J. Am. Chem. Soc.* **2003**, *125*, 10152-10153.

[66] M. Chen, S. Chen, W. Chen, B. E. Lucier, Y. Zhang, A. Zheng, Y. Huang, *Chem. Mater.* **2018**, *30*, 3613-3617.

[67] N. H. Evans, *Eur. J. Org. Chem.* **2019**, *2019*, 3320-3343.

[68] a) R. T. Shannon, C. T. Prewitt, *Acta. Cryst. B* **1969**, *25*, 925-946; b) R. D. Shannon, *Acta. Cryst. A* **1976**, *32*, 751-767.

[69] P. D. Beer, P. A. Gale, *Angew. Chem. Int. Ed.* **2001**, *40*, 486-516.

[70] M. Müller, M. Albrecht, J. Sackmann, A. Hoffmann, F. Dierkes, A. Valkonen, K. Rissanen, *Dalton Trans.* **2010**, *39*, 11329-11334.

[71] Y. Liu, W. Zhao, C.-H. Chen, A. H. Flood, *Science* **2019**, *365*, 159-161.

[72] C. J. Massena, A. M. S. Riel, G. F. Neuhaus, D. A. Decato, O. B. Berryman, *Chem. Commun.* **2015**, *51*, 1417-1420.

[73] M. J. Chmielewski, J. Jurczak, *Chem. Eur. J.* **2005**, *11*, 6080-6094.

[74] F. Moreau, I. Da Silva, N. H. Al Smail, T. L. Easun, M. Savage, H. G. Godfrey, S. F. Parker, P. Manuel, S. Yang, M. Schröder, *Nat. Commun.* **2017**, *8*, 1-9.

[75] K. Choi, A. D. Hamilton, *Coord. Chem. Rev.* **2003**, *240*, 101-110.

[76] A. Bisson, E. Anslyn, *J. Chem. Soc., Perkin Trans. 2* **1999**, 1111-1114.

[77] S. Kubik, R. Goddard, R. Kirchner, D. Nolting, J. Seidel, *Angew. Chem. Int. Ed.* **2001**, *40*, 2648-2651.

[78] S. J. Brooks, S. E. García-Garrido, M. E. Light, P. A. Cole, P. A. Gale, *Chem. Eur. J.* **2007**, *13*, 3320-3329.

[79] J. L. Sessler, E. Katayev, G. D. Pantos, P. Scherbakov, M. D. Reshetova, V. N. Khrustalev, V. M. Lynch, Y. A. Ustynyuk, *J. Am. Chem. Soc.* **2005**, *127*, 11442-11446.

[80] S. O. Kang, V. W. Day, K. Bowman-James, *J. Org. Chem.* **2010**, *75*, 277-283.

[81] M. J. Chmielewski, J. Jurczak, *Chem. Eur. J.* **2006**, *12*, 7652-7667.

[82] M. A. Hossain, S. O. Kang, J. M. Llinares, D. Powell, K. Bowman-James, *lnorg. Chem.* **2003**, *42*, 5043-5045.

[83] B. Meunier, *Metal-oxo and metal-peroxo species in catalytic oxidations, Vol. 97*, Springer, **2003**.

[84] N. Lopez, D. J. Graham, R. McGuire, G. E. Alliger, Y. Shao-Horn, C. C. Cummins, D. G. Nocera, *Science* **2012**, *335*, 450-453.

[85] J. H. Oh, J. H. Kim, D. S. Kim, H. J. Han, V. M. Lynch, J. L. Sessler, S. K. Kim, *Org. Lett.* **2019**, *21*, 4336-4339.

[86] a) C. A. Hunter, *J. Am. Chem. Soc.* **1992**, *114*, 5303-5311; b) F. Vögtle, S. Meier, R. Hoss, *Angew. Chem. Int. Ed. Engl.* **1992**, *31*, 1619-1622.

[87] A. G. Johnston, D. A. Leigh, R. J. Pritchard, M. D. Deegan, *Angew. Chem. Int. Ed. Engl.* **1995**, *34*, 1209-1212.

[88] A. G. Johnston, D. A. Leigh, A. Murphy, J. P. Smart, M. D. Deegan, *J. Am. Chem. Soc.* **1996**, *118*, 10662-10663.

[89] a) A. Altieri, G. Bottari, F. Dehez, D. A. Leigh, J. K. Wong, F. Zerbetto, *Angew. Chem.* **2003**, *115*, 2398-2402; b) E. M. Pérez, D. T. Dryden, D. A. Leigh, G. Teobaldi, F. Zerbetto, *J. Am. Chem. Soc.* **2004**, *126*, 12210-12211.

[90] K. L. Hudson, G. J. Bartlett, R. C. Diehl, J. Agirre, T. Gallagher, L. L. Kiessling, D. N. Woolfson, *J. Am. Chem. Soc.* **2015**, *137*, 15152-15160.

[91] T. J. Mooibroek, J. M. Casas-Solvas, R. L. Harniman, C. M. Renney, T. S. Carter, M. P. Crump, A. P. Davis, *Nature chemistry* **2016**, *8*, 69-74.

[92] P. Ríos, T. J. Mooibroek, T. S. Carter, C. Williams, M. R. Wilson, M. P. Crump, A. P. Davis, *Chem. Sci.* **2017**, *8*, 4056-4061.

[93] T. Hasell, A. I. Cooper, *Nat. Rev. Mater.* **2016**, *1*, 1-14.

[94] a) W. G. Jin, W. Chen, P. H. Xu, X. W. Lin, X. C. Huang, G. H. Chen, F. Lu, X. M. Chen, *Chem. Eur. J.* **2017**, *23*, 13058-13066; b) R. Ullah, M. Atilhan, B. Anaya, S. Al-Muhtaseb, S. Aparicio, H. Patel, D. Thirion, C. T. Yavuz, *ACS Appl. Mater. Interfaces* **2016**, *8*, 20772-20785.

[95] P. J. Waller, S. J. Lyle, T. M. Osborn Popp, C. S. Diercks, J. A. Reimer, O. M. Yaghi, *J. Am. Chem. Soc.* **2016**, *138*, 15519-15522.

[96] J. Larsen, K. A. Jørgensen, D. Christensen, *J. Chem. Soc., Perkin Trans. 1* **1991**, 1187-1190.

[97] a) Y. Tamaru, Y. Yamada, Z.-i. Yoshida, *Synthesis* **1983**, *1983*, 474-476; b) T. Naota, S. I. Murahashi, *Synlett* **1991**, *1991*, 693-694; c) A. Tillack, I. Rudloff, M. Beller, *Eur. J. Org. Chem.* **2001**, *2001*, 523-528; d) W.-J. Yoo, C.-J. Li, *J. Am. Chem. Soc.* **2006**, *128*, 13064-13065.

[98] G. I. An, M. Kim, J. Y. Kim, H. Rhee, *Tetrahedron Lett.* **2003**, *44*, 2183-2186.

[99] J. Gao, G. W. Wang, *J. Org. Chem.* **2008**, *73*, 2955-2958.

[100] B. O. Lindgren, T. Nilsson, *Acta Chem. Scand.* **1973**, *27*, 888-890.

[101] B. S. Bal, W. E. Childers Jr, H. W. Pinnick, *Tetrahedron* **1981**, *37*, 2091-2096.

[102] E. Dalcanale, F. Montanari, *J. Org. Chem.* **1986**, *51*, 567-569.

[103] M. A. Mohamed, K. i. Yamada, K. Tomioka, *Tetrahedron Lett.* **2009**, *50*, 3436-3438.

[104] a) M. Ball, M. J. Gaunt, D. F. Hook, A. S. Jessiman, S. Kawahara, P. Orsini, A. Scolaro, A. C. Talbot, H. R. Tanner, S. Yamanoi, *Angew. Chem.* **2005**, *117*, 5569-5574; b) T. Magauer, H. J. Martin, J. Mulzer, *Angew. Chem. Int. Ed.* **2009**, *48*, 6032-6036; c) K.

Nicolaou, Q. Kang, S. Y. Ng, D. Y.-K. Chen, *J. Am. Chem. Soc.* **2010**, *132*, 8219-8222; d) N. S. Sheikh, C. J. Bataille, T. J. Luker, R. C. Brown, *Org. Lett.* **2010**, *12*, 2468-2471.

[105]   I. A. Pearl, J. S. Barton, *J. Am. Chem. Soc.* **1952**, *74*, 1357-1357.

[106]   R. Husband, C. Logan, C. Purves, *Can. J. Chem.* **1955**, *33*, 68-81.

[107]   a) K. Sarkanen, K. Kakehi, R. Murphy, H. White, *Tappi* **1962**, *45*, 24-28; b) K. Sarkanen, *Pure Appl. Chem.* **1962**, *5*, 219-232.

[108]   T. Ishikawa, M. Sumimoto, T. Kondo, *Japan Tappi J.* **1969**, *23*, 117-124.

[109]   a) G. A. Kraus, M. J. Taschner, *J. Org. Chem.* **1980**, *45*, 1175-1176; b) G. A. Kraus, B. Roth, *J. Org. Chem.* **1980**, *45*, 4825-4830.

[110]   B. S. Bal, W. E. Childers, H. W. Pinnick, *Tetrahedron* **1981**, *37*, 2091-2096.

[111]   J. M. Zenner, R. C. Larock, *J. Org. Chem.* **1999**, *64*, 7312-7322.

[112]   K. Kuramochi, S. Nagata, H. Itaya, K.-i. Takao, S. Kobayashi, *Tetrahedron Lett.* **1999**, *40*, 7371-7374.

[113]   A. Raach, O. Reiser, *J. Prakt. Chem.* **2000**, *342*, 605-608.

[114]   F. E. Ziegler, Y. Wang, *J. Org. Chem.* **1998**, *63*, 7920-7930.

[115]   O. Dirat, C. Kouklovsky, Y. Langlois, *J. Org. Chem.* **1998**, *63*, 6634-6642.

[116]   A. A. Hussein, A. A. Al-Hadedi, A. J. Mahrath, G. A. Moustafa, F. A. Almalki, A. Alqahtani, S. Shityakov, M. E. Algazally, *R. Soc. Open Sci.* **2020**, *7*, 191568.

[117]   K. S. Goh, C.-H. Tan, *RSC Adv.* **2012**, *2*, 5536-5538.

[118]   X. Han, J. Huang, C. Yuan, Y. Liu, Y. Cui, *J. Am. Chem. Soc.* **2018**, *140*, 892-895.

[119]   S. M. Elbert, **2018,** Doctoral dissertation, Universität Heidelberg, Heidelberg.

[120]   M. W. Schneider, I. M. Oppel, A. Griffin, M. Mastalerz, *Angew. Chem. Int. Ed.* **2013**, *52*, 3611-3615.

[121]   a) L. Friedman, F. M. Logullo, *J. Org. Chem.* **1969**, *34*, 3089-3092; b) L. Friedman, F. M. Logullo, *J. Am. Chem. Soc.* **1963**, *85*, 1549-1549.

[122]   C. Zhang, C. F. Chen, in *J. Org. Chem., Vol. 71*, **2006**, pp. 6626-6629.

[123]   R. H. Mitchell, Y. H. Lai, R. V. Williams, *J. Org. Chem.* **1979**, *44*, 4733-4735.

[124]   E. H. Menke, D. Leibold, V. Lami, Y. J. Hofstetter, M. Mastalerz, Y. Vaynzof, *Org. Electron.* **2017**, *47*, 211-219.

[125]   C. D. Gutsche, J. A. Levine, *J. Am. Chem. Soc.* **1982**, *104*, 2652-2653.

[126]   S. Samanta, S. Das, P. K. Samanta, S. Dutta, P. Biswas, *RSC Adv.* **2013**, *3*, 19455-19466.

[127]   a) J. P. Wagner, P. R. Schreiner, *Angew. Chem. Int. Ed.* **2015**, *54*, 12274-12296; b) S. Rösel, C. Balestrieri, P. R. Schreiner, *Chem. Sci.* **2017**, *8*, 405-410.

[128]   M. Thommes, K. Kaneko, A. V. Neimark, J. P. Olivier, F. Rodriguez-Reinoso, J. Rouquerol, K. S. Sing, *Pure Appl. Chem.* **2015**, *87*, 1051-1069.

[129]   D. K. Maity, A. Halder, B. Bhattacharya, A. Das, D. Ghoshal, *Cryst. Growth Des.* **2016**, *16*, 1162-1167.

[130] a) M. Marques, A. Amorim da Costa, P. J. Ribeiro-Claro, *J. Phys. Chem. A* **2001**, *105*, 5292-5297; b) A. V. Afonin, I. A. Ushakov, A. V. Vashchenko, D. E. Simonenko, A. V. Ivanov, A. M. Vasil'tsov, A. b. I. Mikhaleva, B. A. Trofimov, *Magn. Reson. Chem.* **2009**, *47*, 105-112; c) B. Ośmiałowski, E. Kolehmainen, A. Valkonen, M. Kowalska, S. Ikonen, *Struct. Chem.* **2013**, *24*, 2203-2209.

[131] E. H. Cordes, W. P. Jencks, *J. Am. Chem. Soc.* **1963**, *85*, 2843-2848.

[132] B. R. Deshwal, H. K. Lee, *J. Ind. Eng. Chem.* **2005**, *11*, 125-136.

[133] J. Dunitz, J. Lehn, G. Wipff, *Tetrahedron* **1974**, *30*, 1563-1572.

[134] a) T. Sotomatsu, T. Fujita, *Quant. Struct.-Act. Relat.* **1990**, *9*, 295-301; b) R. W. Taft Jr, *J. Am. Chem. Soc.* **1953**, *75*, 4538-4539.

[135] a) D. H. McDaniel, H. C. Brown, *J. Org. Chem.* **1958**, *23*, 420-427; b) C. Hansch, A. Leo, R. Taft, *Chem. Rev.* **1991**, *91*, 165-195.

[136] J. C. Lauer, Z. Pang, P. Janßen, F. Rominger, T. Kirschbaum, M. Elstner, M. Mastalerz, *ChemistryOpen* **2020**, *9*, 183-190.

[137] T. Kunde, E. Nieland, H. V. Schröder, C. A. Schalley, B. M. Schmidt, *Chem. Commun.* **2020**, *56*, 4761-4764.

[138] J. C. Lauer, Doctoral dissertation, **currently ongoing**, Heidelberg University (Heidelberg).

[139] D. Morales-Morales, *Pincer Compounds: Chemistry and Applications*, Elsevier, **2018**.

[140] T. Ishiyama, J. Takagi, K. Ishida, N. Miyaura, N. R. Anastasi, J. F. Hartwig, *J. Am. Chem. Soc.* **2002**, *124*, 390-391.

[141] J. M. Murphy, C. C. Tzschucke, J. F. Hartwig, *Org. Lett.* **2007**, *9*, 757-760.

[142] D. H. Hong, B. J. Knight, V. J. Catalano, L. J. Murray, *Dalton Trans.* **2019**.

[143] J. J. Molloy, T. A. Clohessy, C. Irving, N. A. Anderson, G. C. Lloyd-Jones, A. J. Watson, *Chem. Sci.* **2017**, *8*, 1551-1559.

[144] S. Voth, J. W. Hollett, J. A. McCubbin, *J. Org. Chem.* **2015**, *80*, 2545-2553.

[145] a) G. W. Breton, X. Vang, *J. Chem. Educ.* **1998**, *75*, 81; b) F. D. Greene, S. L. Misrock, J. R. Wolfe Jr, *J. Am. Chem. Soc.* **1955**, *77*, 3852-3855.

[146] a) R. Bhola, P. Payamyar, D. J. Murray, B. Kumar, A. J. Teator, M. U. Schmidt, S. M. Hammer, A. Saha, J. Sakamoto, A. D. Schlüter, *J. Am. Chem. Soc.* **2013**, *135*, 14134-14141; b) N. Huang, X. Ding, J. Kim, H. Ihee, D. Jiang, *Angew. Chem. Int. Ed.* **2015**, *54*, 8704-8707.

[147] a) J.-X. Ma, J. Li, Y.-F. Chen, R. Ning, Y.-F. Ao, J.-M. Liu, J. Sun, D.-X. Wang, Q.-Q. Wang, *J. Am. Chem. Soc.* **2019**, *141*, 3843-3848; b) Q. Zhu, X. Wang, R. Clowes, P. Cui, L. Chen, M. A. Little, A. I. Cooper, *J. Am. Chem. Soc.* **2020**, *142*, 16842-16848.

[148] X. Wu, A. M. Gilchrist, P. A. Gale, *Chem* **2020**.

[149] G. R. Fulmer, A. J. Miller, N. H. Sherden, H. E. Gottlieb, A. Nudelman, B. M. Stoltz, J. E. Bercaw, K. I. Goldberg, *Organometallics* **2010**, *29*, 2176-2179.

[150] G. Sheldrick, *Bruker AXC Inc., Madison, WI* **2014**.

[151] G. M. Sheldrick, *Acta Crystallogr. Sect. A: Found. Crystallogr.* **2008**, *64*, 112-122.

[152] L. Zhang, S. Su, H. Wu, S. Wang, *Tetrahedron* **2009**, *65*, 10022-10024.

[153] C. Zhang, C.-F. Chen, *J. Org. Chem.* **2006**, *71*, 6626-6629.

[154] M. Mastalerz, *Chem. Commun.* **2008**, *0*, 4756.

[155] C. J. Fahrni, A. Pfaltz, *Helv. Chim. Acta* **1998**, *81*, 491-506.

[156] Q. P. B. Nguyen, T. N. Le, T. H. Kim, *Bull. Korean Chem. Soc* **2009**, *30*, 1743.

[157] K. J. Wallace, R. Hanes, E. Anslyn, J. Morey, K. V. Kilway, J. Siegel, *Synthesis* **2005**, *2005*, 2080-2083.

[158] G. Hennrich, W. M. David, Y. J. Bomble, E. V. Anslyn, J. S. Brodbelt, J. F. Stanton, *Supramol. Chem.* **2004**, *16*, 521-528.

[159] H. Takalo, J. Kankare, *Acta Chem. Scand. B* **1987**, *41*, 219-221.

[160] H. Takalo, P. Pasanen, J. Kankare, K. Undheim, G. Wittman, L. Gera, M. Bartók, I. Pelczer, G. Dombi, *Acta Chem. Scand.* **1988**, *42b*, 373-377.

[161] P. V. Ivchenko, I. E. Nifant'ev, I. V. Buslov, *Tetrahedron Lett.* **2013**, *54*, 217-219.

[162] A. Schultz, X. Li, C. N. Moorefield, C. Wesdemiotis, G. R. Newkome, *Eur. J. Inorg. Chem.* **2013**, *2013*, 2492-2497.

[163] K. Grudzień, M. Malinska, M. Barbasiewicz, *Organometallics* **2012**, *31*, 3636-3646.

[164] G. M. Peters, J. B. Winegrad, M. R. Gau, G. H. Imler, B. Xu, S. Ren, B. B. Wayland, M. J. Zdilla, *lnorg. Chem.* **2017**, *56*, 3377-3385.

[165] K. Olsson, P. Pernemalm, *Acta. Chem. Scand. Ser. B.* **1979**, *33*, 125-132.

[166] J. Bergman, L. Renström, B. Sjöberg, *Tetrahedron* **1980**, *36*, 2505-2511.

[167] N. De Rycke, J. Marrot, F. Couty, O. R. P. David, *Tetrahedron Lett.* **2010**, *51*, 6521-6525.

[168] P. Mateus, R. Delgado, P. Brandão, V. Félix, *J. Org. Chem.* **2009**, *74*, 8638-8646.

[169] R. L. Greenaway, V. Santolini, M. J. Bennison, B. M. Alston, C. J. Pugh, M. A. Little, M. Miklitz, E. G. B. Eden-Rump, R. Clowes, A. Shakil, H. J. Cuthbertson, H. Armstrong, M. E. Briggs, K. E. Jelfs, A. I. Cooper, *Nat. Commun.* **2018**, *9*.

[170] T. H. G. Schick, **2018**, Doctoral dissertation, Universität Heidelberg, Heidelberg.

[171] W. Schilf, B. Kamieński, B. Kołodziej, E. Grech, Z. Rozwadowski, T. Dziembowska, *J. Mol. Struct.* **2002**, *615*, 141-146.

[172] D. J. Marrs, V. McKee, J. Nelson, Q. Lu, C. J. Harding, *Inorg. Chim. Acta* **1993**, *211*, 195-202.

[173] A. S. Bhat, S. M. Elbert, W.-S. Zhang, F. Rominger, M. Dieckmann, R. R. Schröder, M. Mastalerz, *Angew. Chem. Int. Ed.* **2019**, *58*, 8819-8823.

[174] P. Atkins, J. De Paula, *Atkins' Physical chemistry*, Oxford university press Oxford, **2006**.

[175] K. Sing, D. Everett, R. Haul, L. Moscou, L. Pierotti, J. Rouquerol, T. Siemieniewska, *Pure Appl. Chem* **1985**, *57*, 603-619.

[176] a) J. Rouquerol, F. Rouquerol, P. Llewellyn, G. Maurin, K. S. Sing, *Adsorption by powders and porous solids: principles, methodology and applications*, Academic press, **2013**; b) S. Lowell, J. E. Shields, M. A. Thomas, M. Thommes, *Characterization of porous solids and powders: surface area, pore size and density, Vol. 16*, Springer

Science & Business Media, **2012**; c) S. Brunauer, P. H. Emmett, E. Teller, *J. Am. Chem. Soc.* **1938**, *60*, 309-319.

[177]   J. Rouquerol, P. Llewellyn, F. Rouquerol, *Stud. Surf. Sci. Catal* **2007**, *160*, 1016.

[178]   J. Landers, G. Y. Gor, A. V. Neimark, *Colloids Surf. Physicochem. Eng. Aspects* **2013**, *437*, 3-32.

[179]   M. Thommes, K. A. Cychosz, *Adsor* **2014**, *20*, 233-250.

[180]   O. Talu, *Adv. Colloid Interface Sci.* **1998**, *76*, 227-269.

[181]   A. L. Myers, J. M. Prausnitz, *AIChE. J.* **1965**, *11*, 121-127.

[182]   a) B. Zheng, J. Bai, J. Duan, L. Wojtas, M. J. Zaworotko, *J. Am. Chem. Soc.* **2011**, *133*, 748-751; b) B. Chen, X. Zhao, A. Putkham, K. Hong, E. B. Lobkovsky, E. J. Hurtado, A. J. Fletcher, K. M. Thomas, *J. Am. Chem. Soc.* **2008**, *130*, 6411-6423; c) J. L. Rowsell, O. M. Yaghi, *J. Am. Chem. Soc.* **2006**, *128*, 1304-1315.

VII. Appendix

The following section contains NMR, MS and IR spectra, and crystal structures of compounds discussed in this thesis but are previously unpublished. The spectral data of compounds **48**, **59a**, **59b**, **60a, 61**, TGA analysis, PXRD analysis, SEM images, the gas sorption isotherms, and the crystal structure of **48** can be found in literature (also uploaded on the CCDC database: CCDC 1898128).[173] Note the following comments:

1. The crystal structure of compound **61** was not published and is hence found in section 4.1 of the appendix.
2. Crystal structure of **A63-amide** was produced in collaboration with B.Sc. Chantal Barwig obtained during the "Forschungspraktikum" work supervised by me.

1. NMR spectra

1.1. Pure compounds
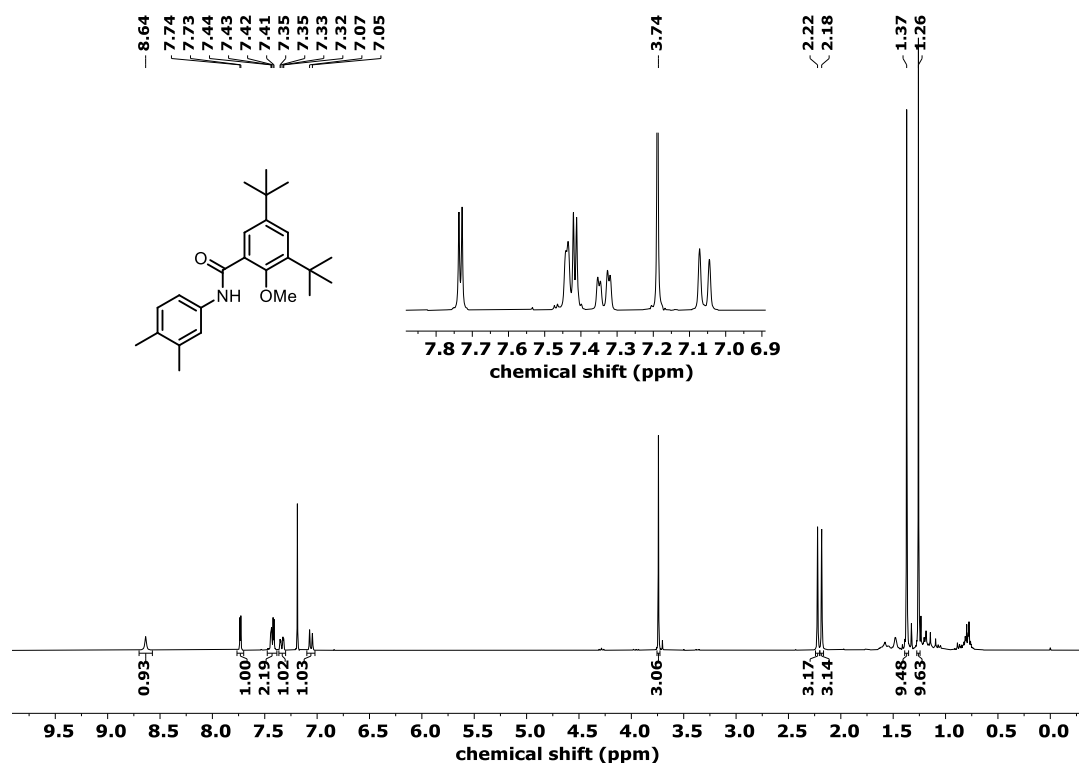
Figure 52. ^{1}H NMR (400 MHz, CDCl$_3$) spectrum of **52'**.
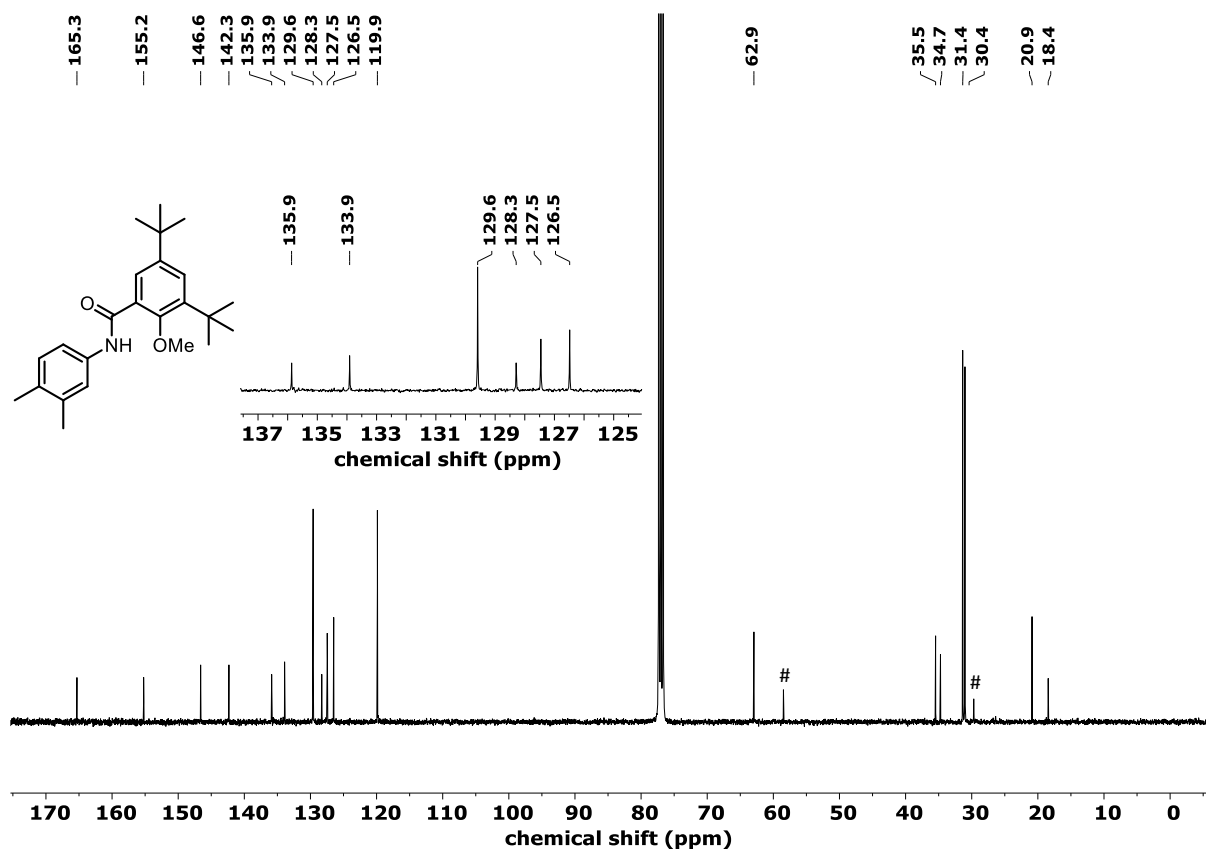
Figure 53. ^{13}C NMR (100 MHz, CDCl$_3$) spectrum of **52'**. # - unexplained impurity peaks.
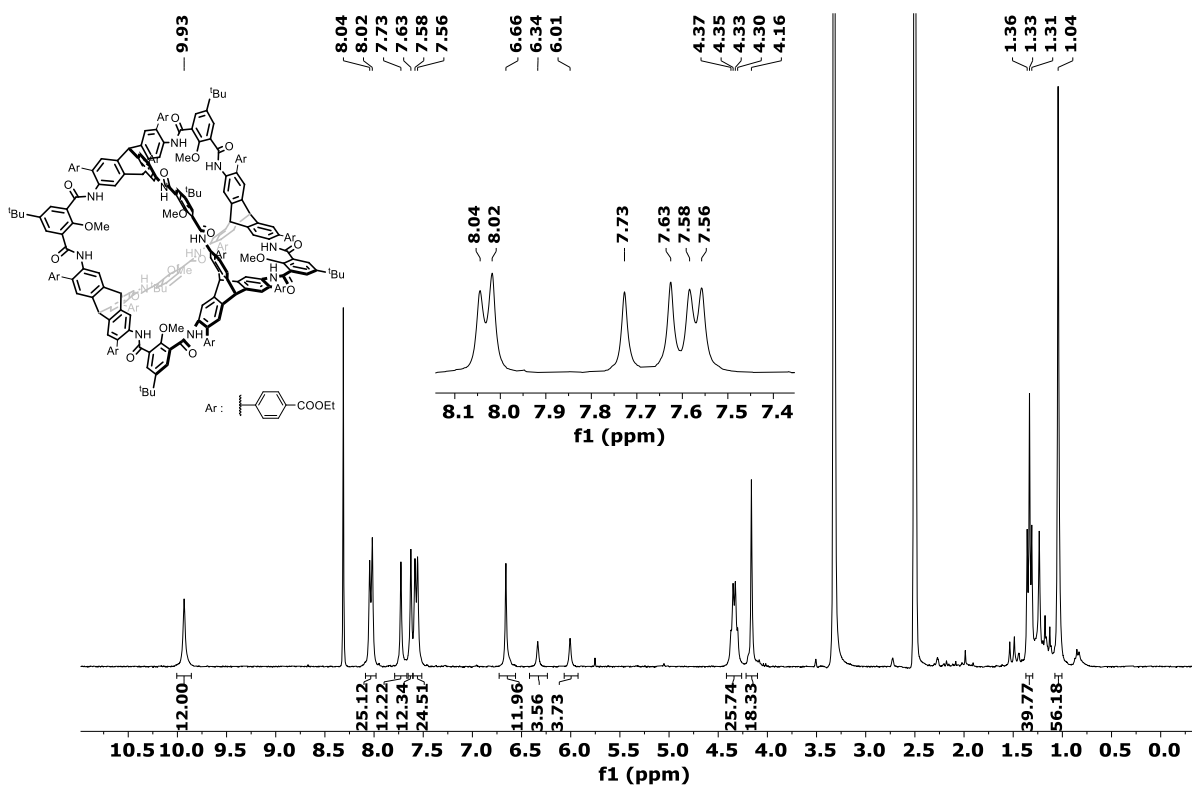
Figure 54. ^{1}H NMR (500 MHz, DMSO-d$_6$) spectrum of amide cage **59c**.

160
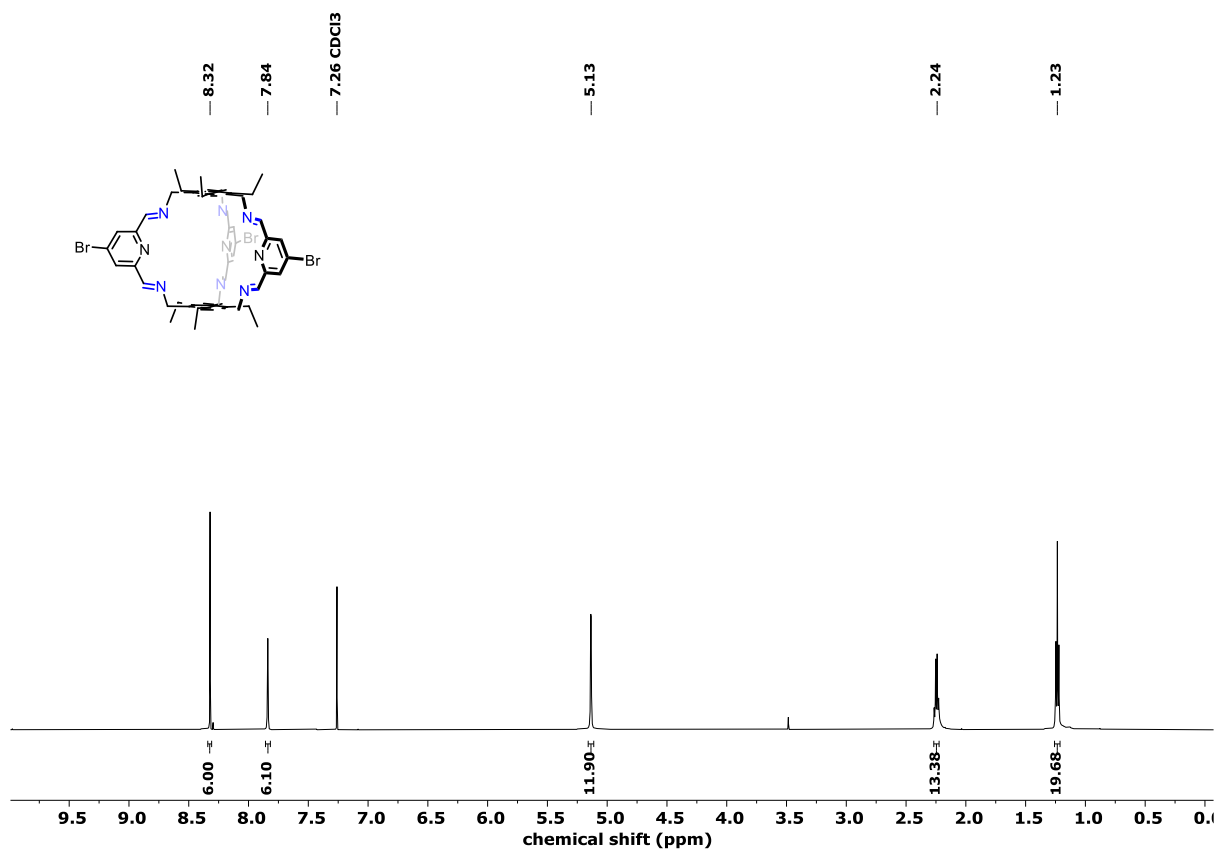
Figure 55. ^{1}H NMR (600 MHz, CDCl$_3$) spectrum of imine cage **A65**.
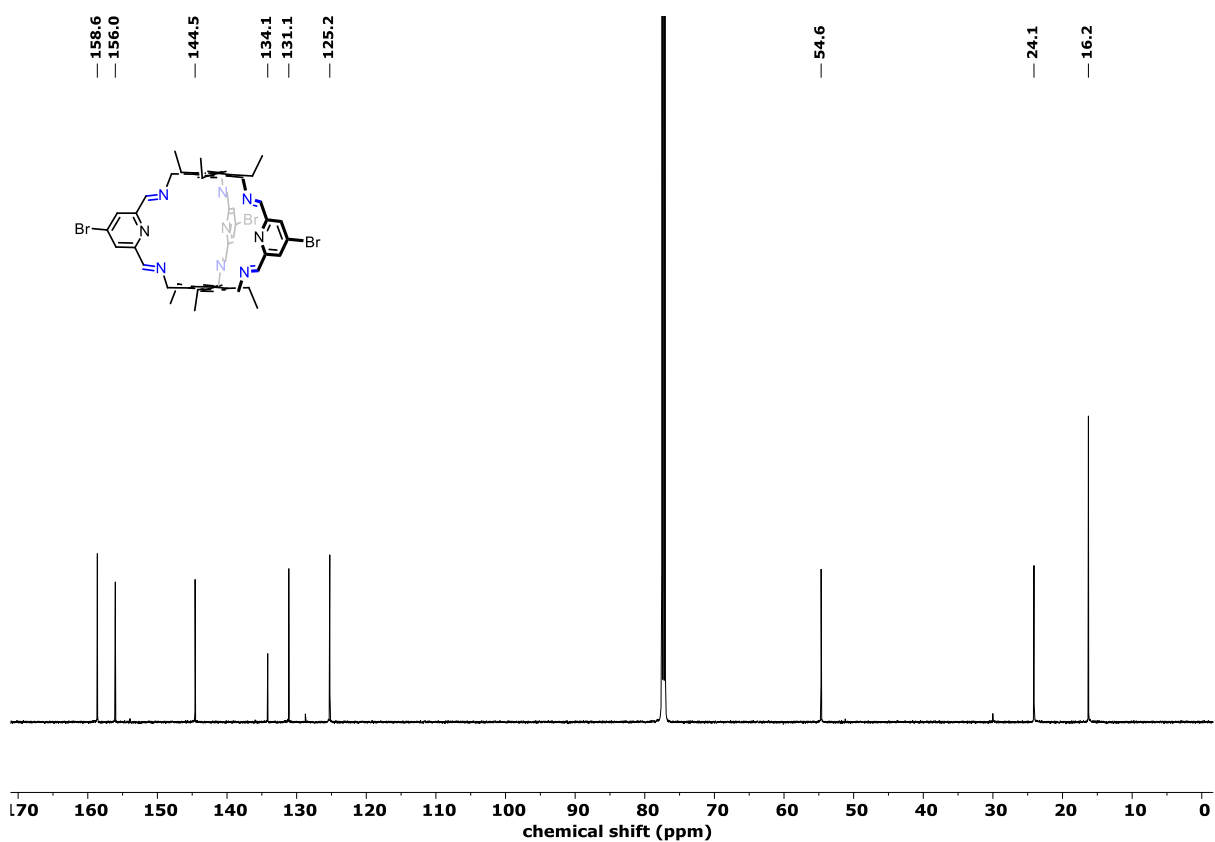
Figure 56. ^{13}C NMR (100 MHz, CDCl$_3$) spectrum of imine cage **A65**.
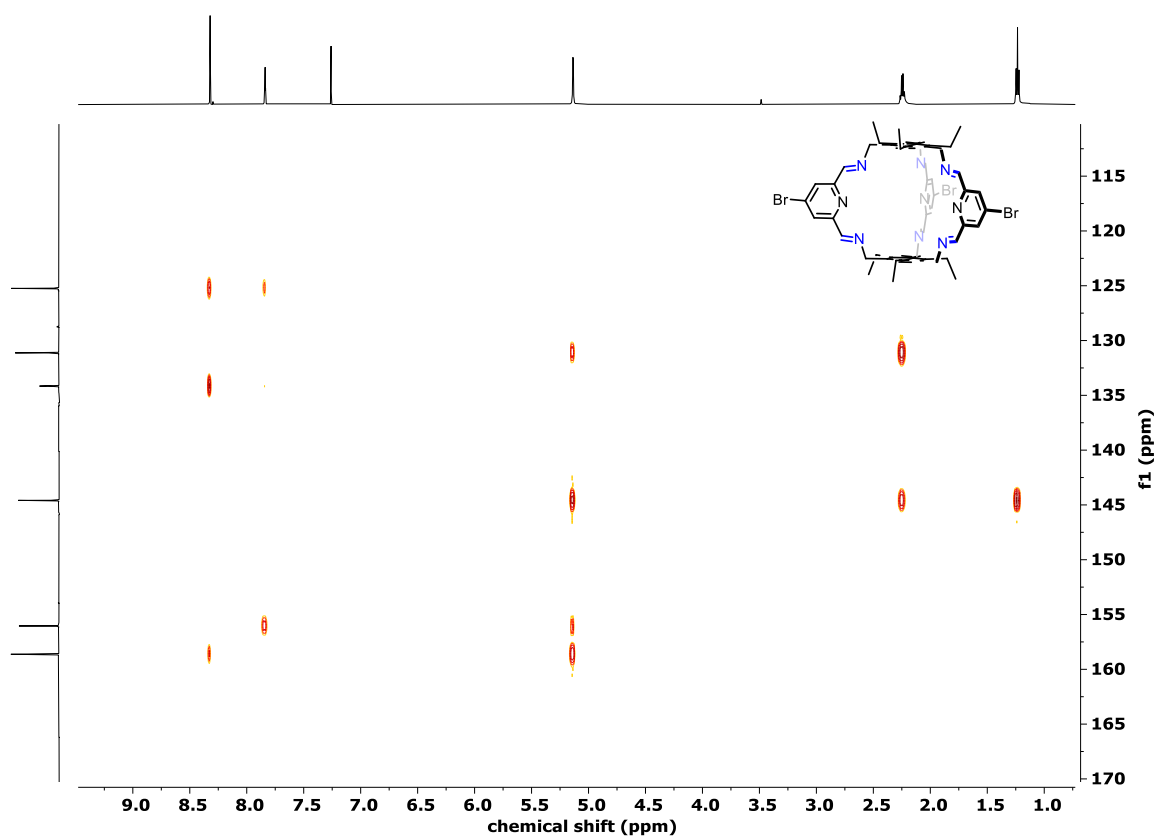
Figure 57. ^{1}H-^{13}C (600 MHz, 100 MHz) HMBC NMR spectrum of imine cage **A65**.
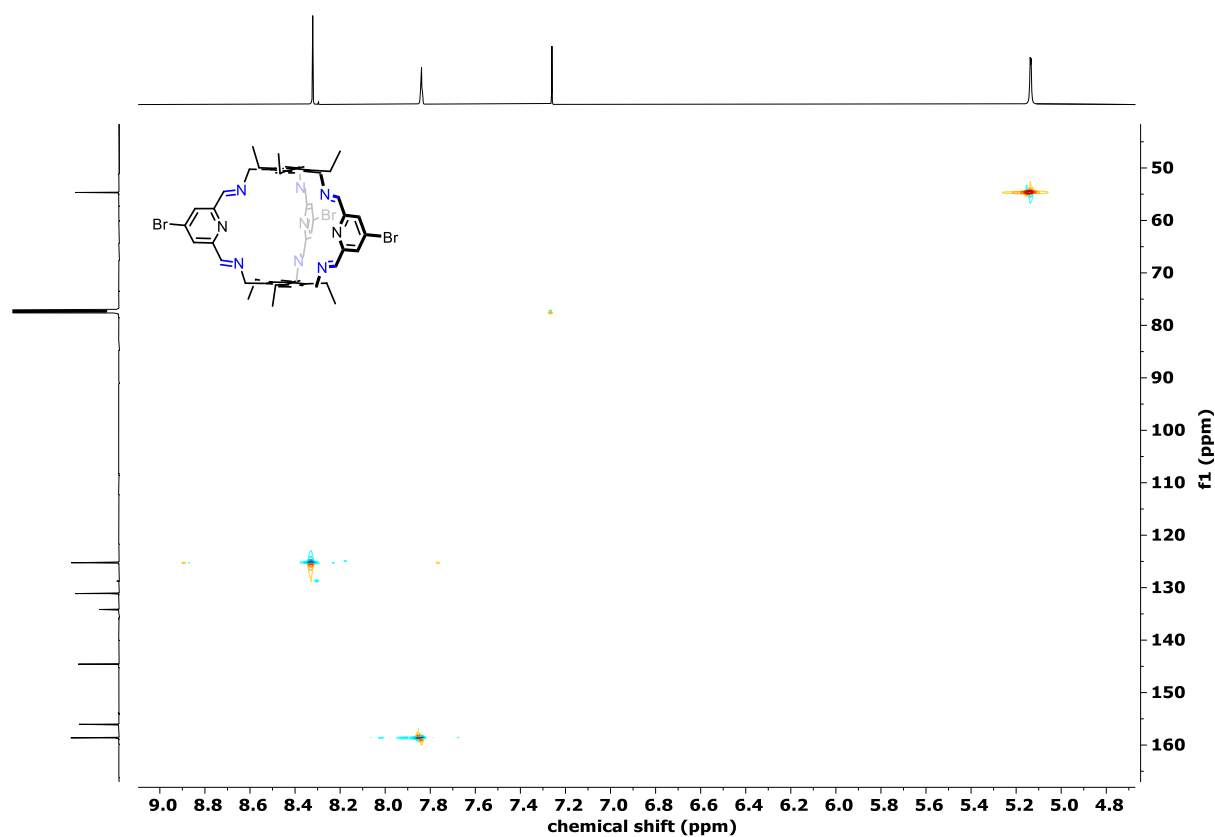
Figure 58. ^{1}H-^{13}C (600 MHz, 100 MHz) HSQC NMR spectrum of imine cage **A65**.
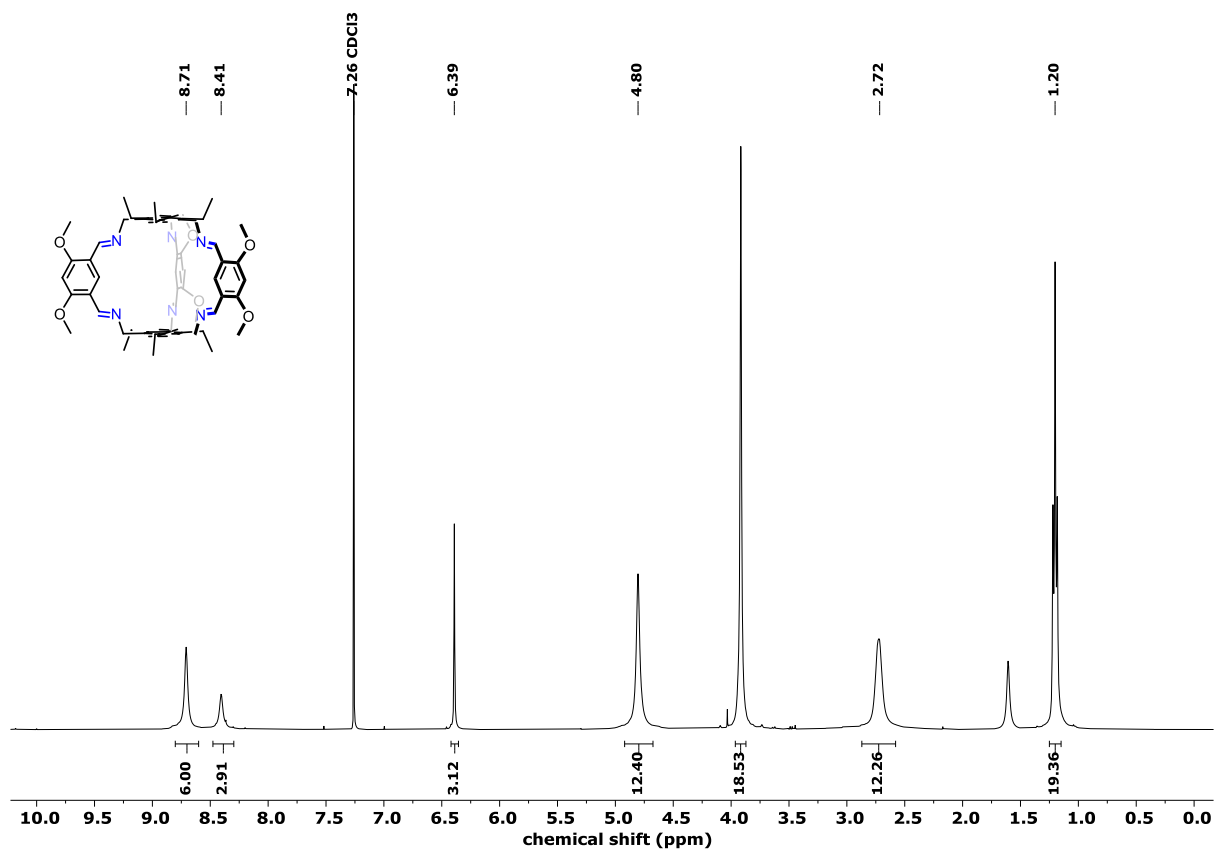
Figure 59. ^{1}H NMR (600 MHz, CDCl$_3$) spectrum of imine cage **A67**.
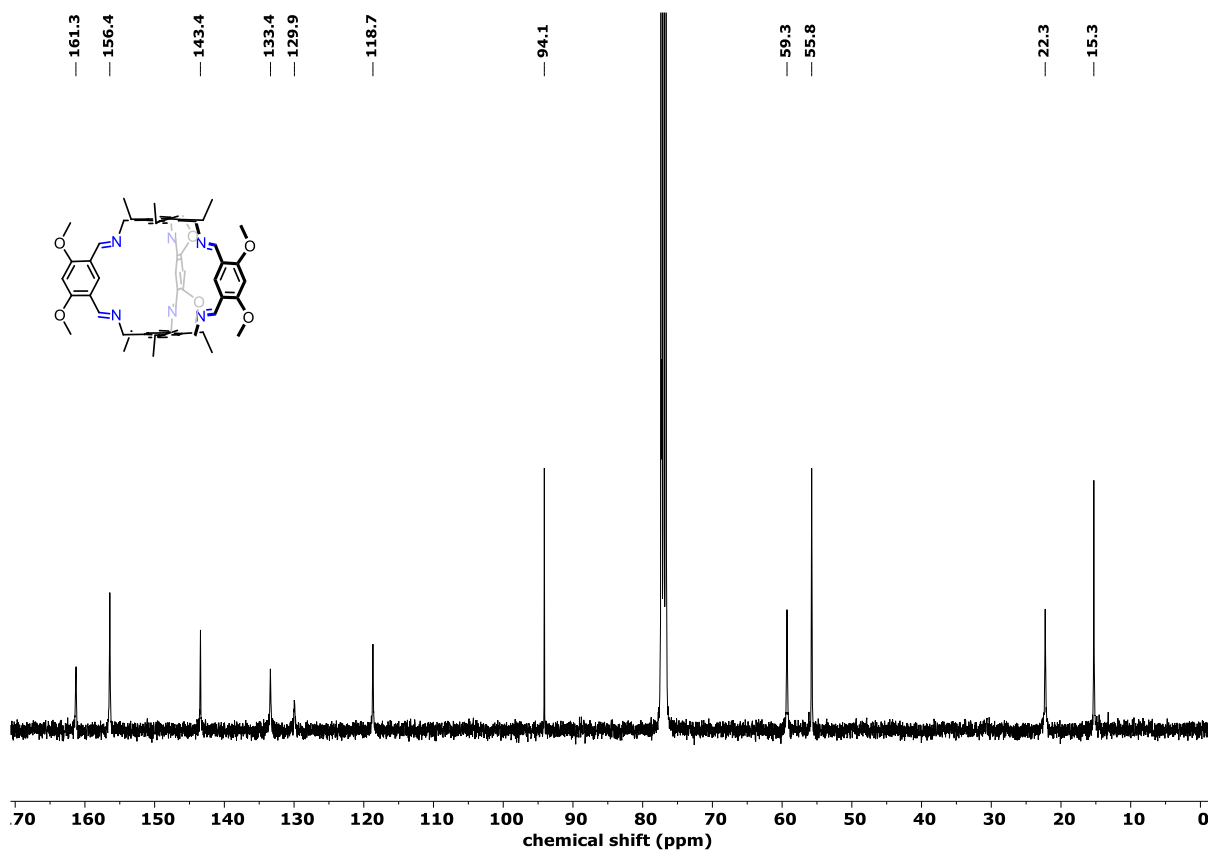
Figure 60. ^{13}C NMR (100 MHz, CDCl$_3$) spectrum of imine cage **A68**.
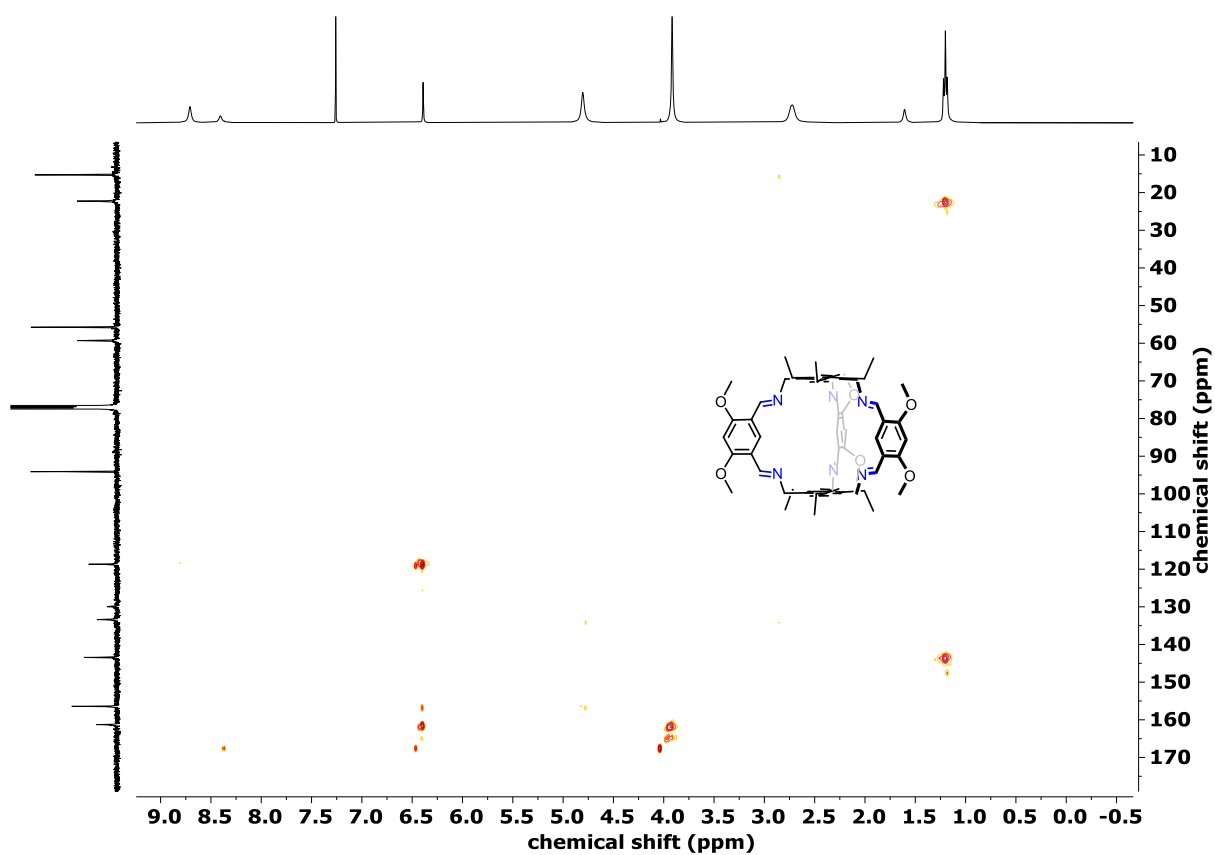
Figure 61. ^{1}H-^{13}C (600 MHz, 100 MHz) HMBC NMR spectrum of imine cage **A68**.
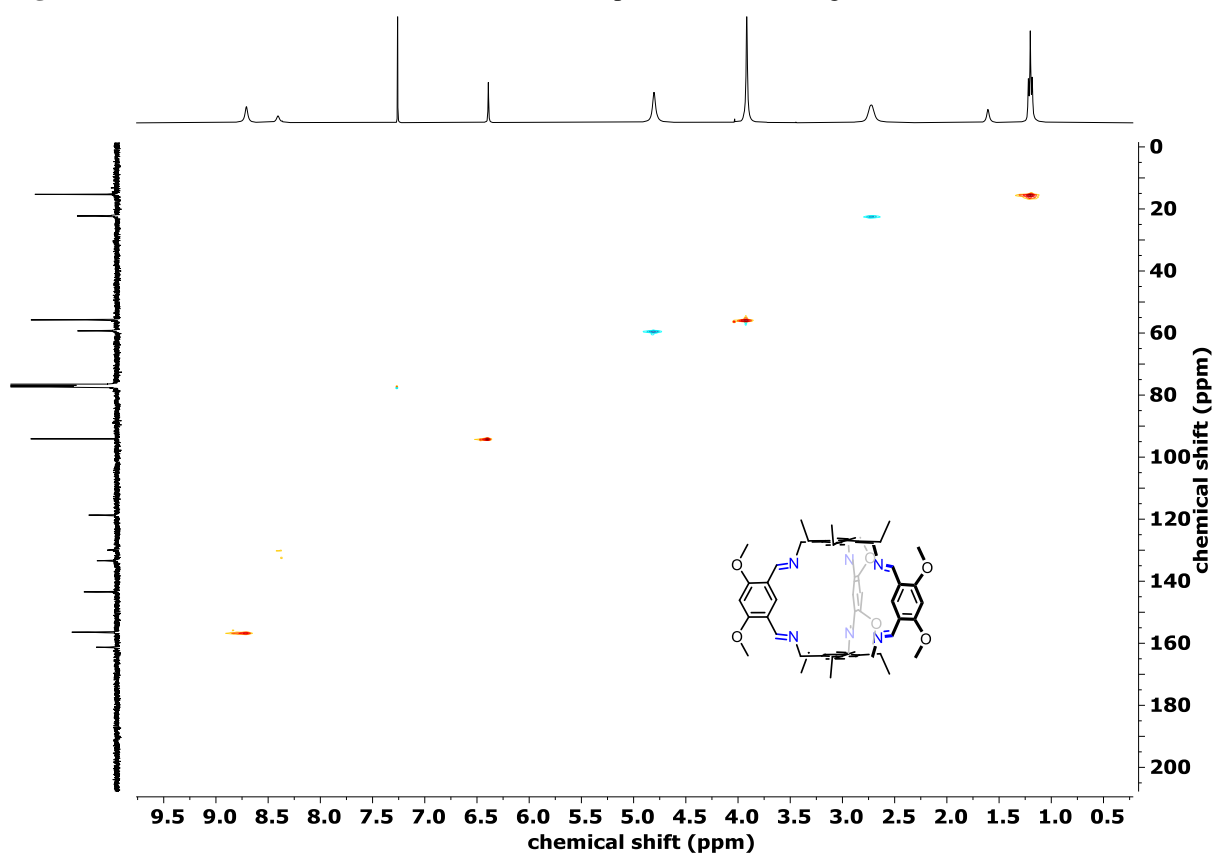
Figure 62. ^{1}H-^{13}C (600 MHz, 100 MHz) HSQC NMR spectrum of imine cage **A65**
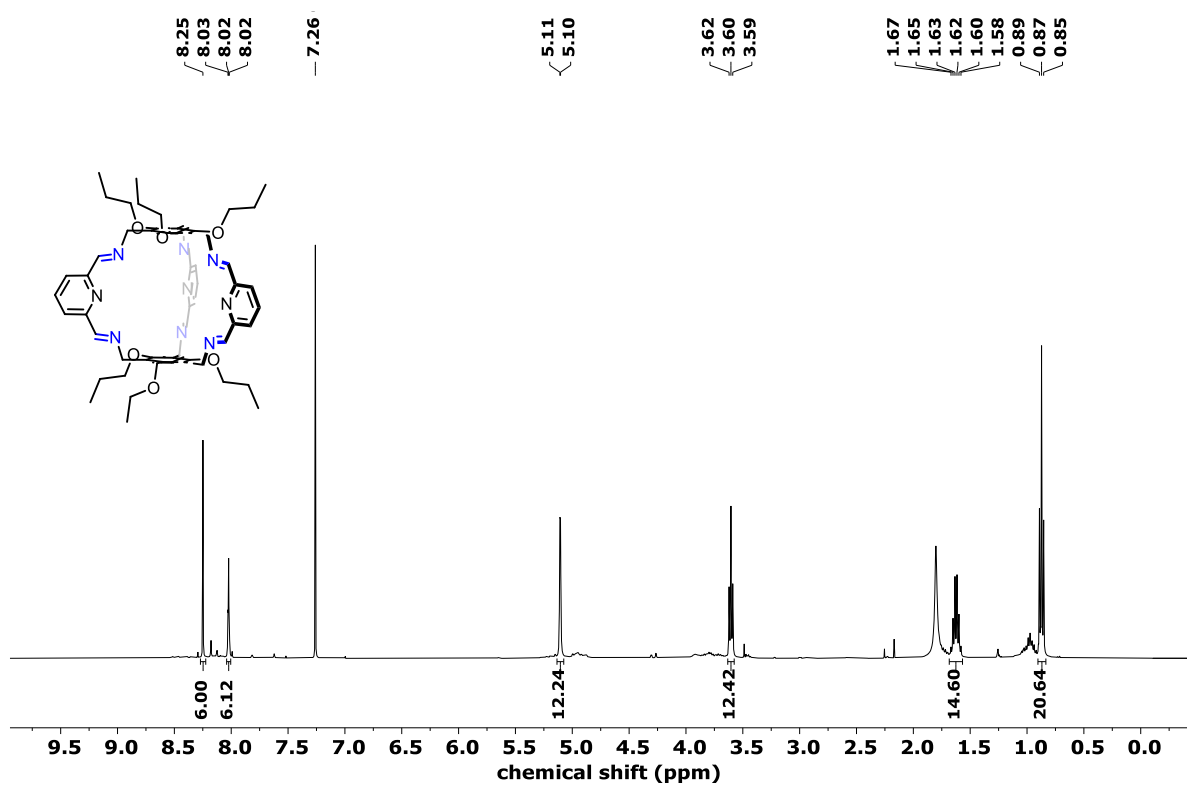
Figure 63. ^{1}H NMR (600 MHz, CDCl$_3$) spectrum of imine cage **B63**.
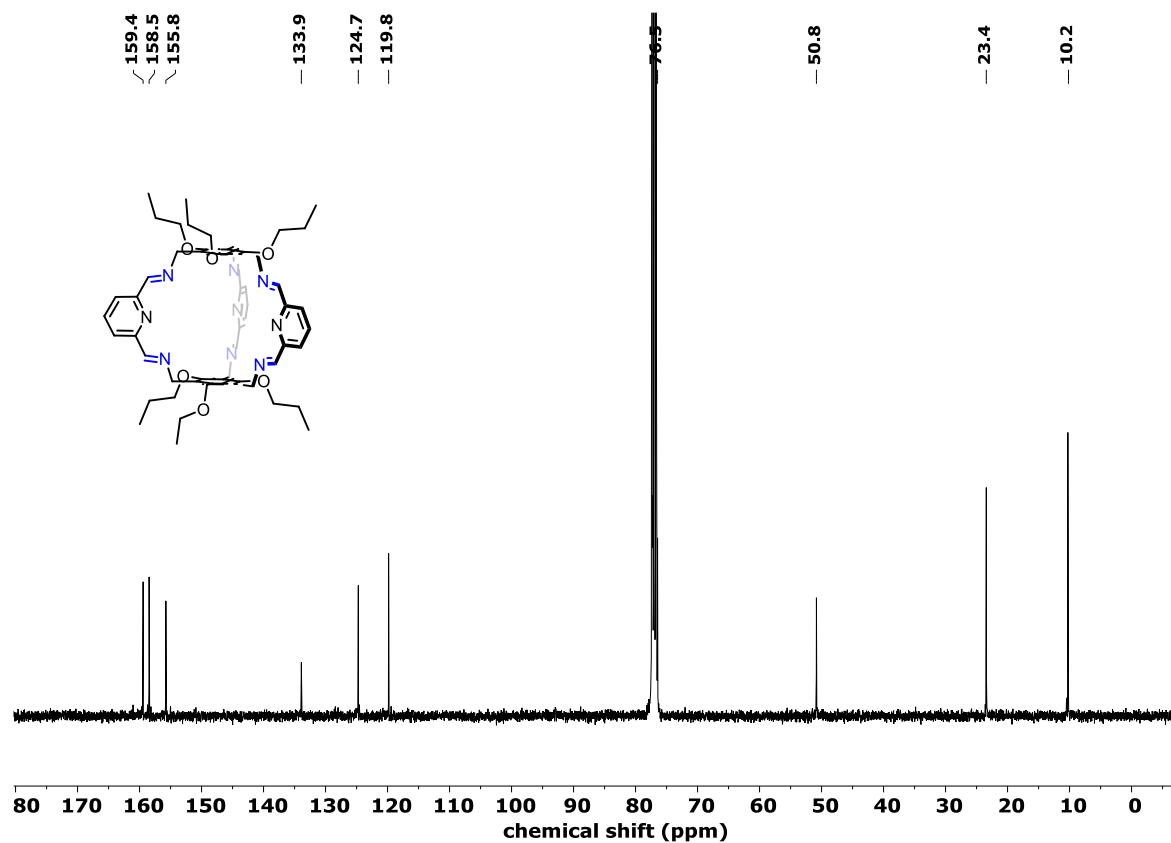
Figure 64. ^{13}C NMR (100 MHz, CDCl$_3$) spectrum of imine cage **B63**.
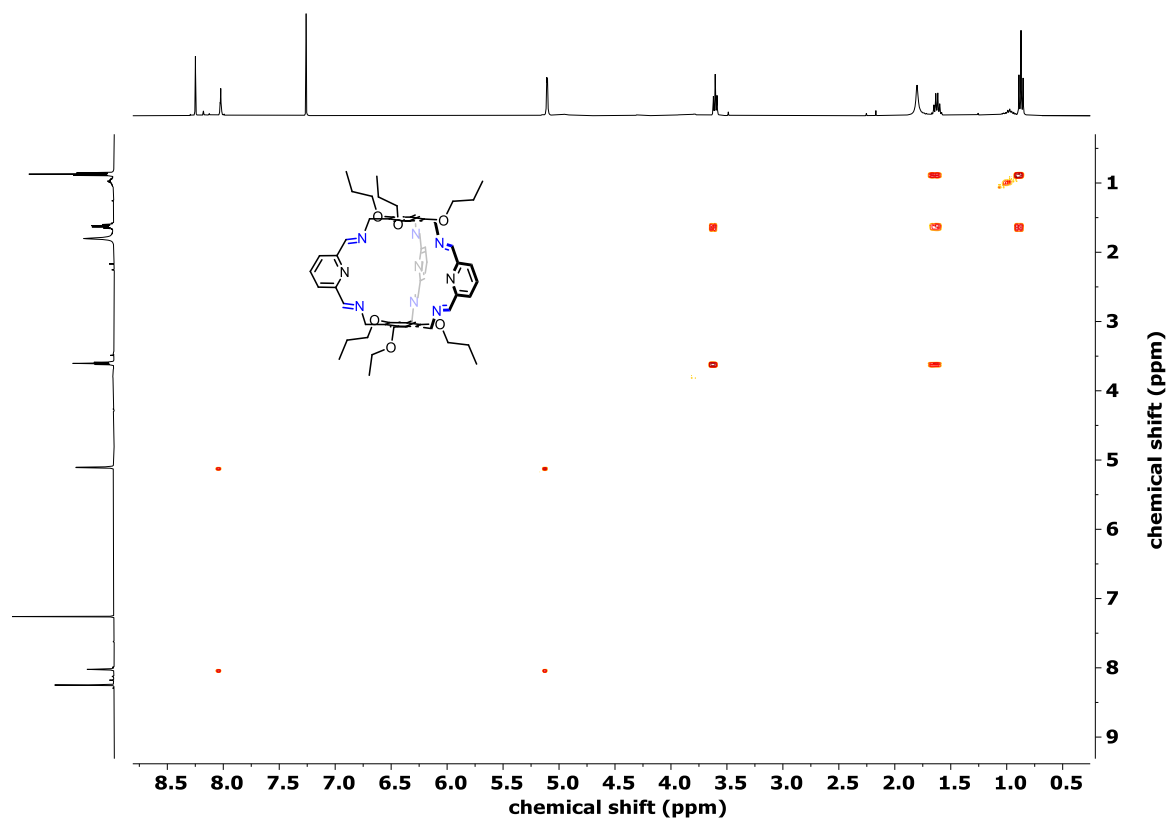
Figure 65. ^{1}H-^{1}H (600 MHz, 600 MHz) COSY NMR spectrum of imine cage **B63**.
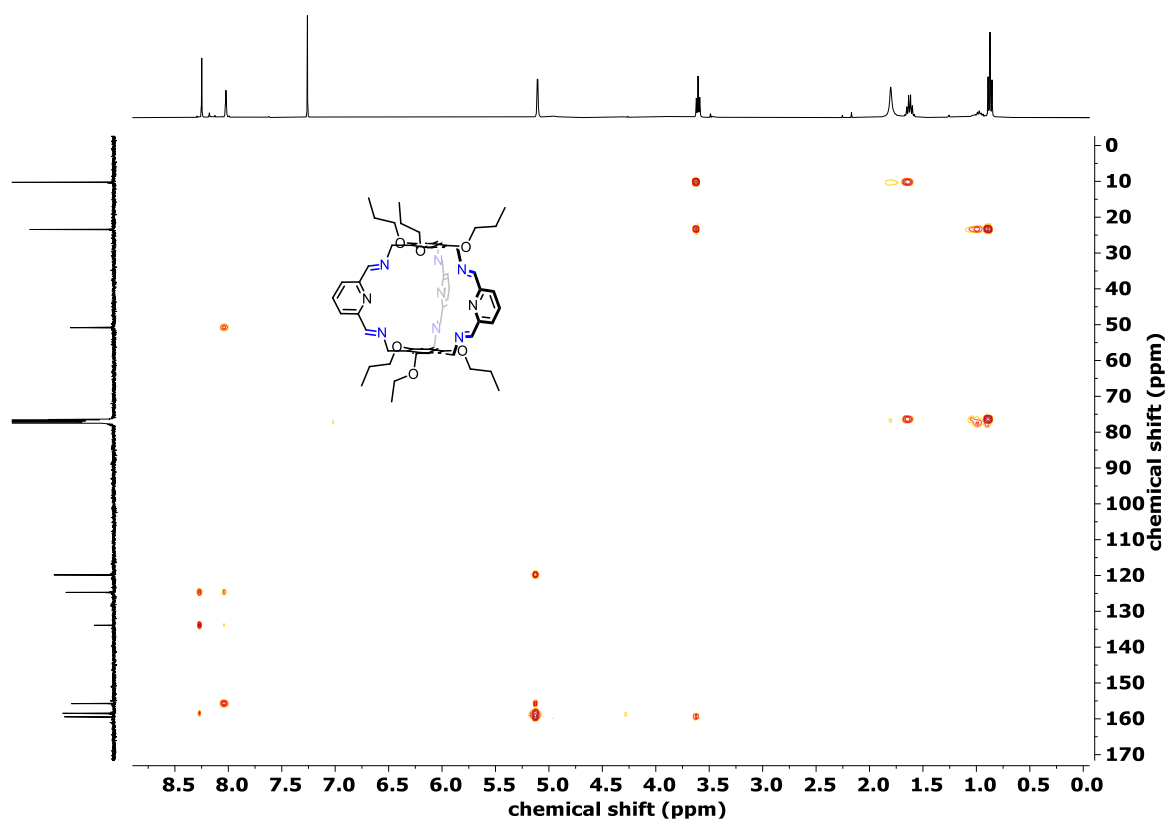
Figure 66. ^{1}H-^{13}C (600 MHz, 100 MHz) HMBC NMR spectrum of imine cage **B63**.

Figure 67. ^{1}H-^{13}C (600 MHz, 100 MHz) HSQC NMR spectrum of imine cage **B63**.

Figure 68. ^{1}H NMR (600 MHz, CDCl$_3$) spectrum of imine cage **B65**.
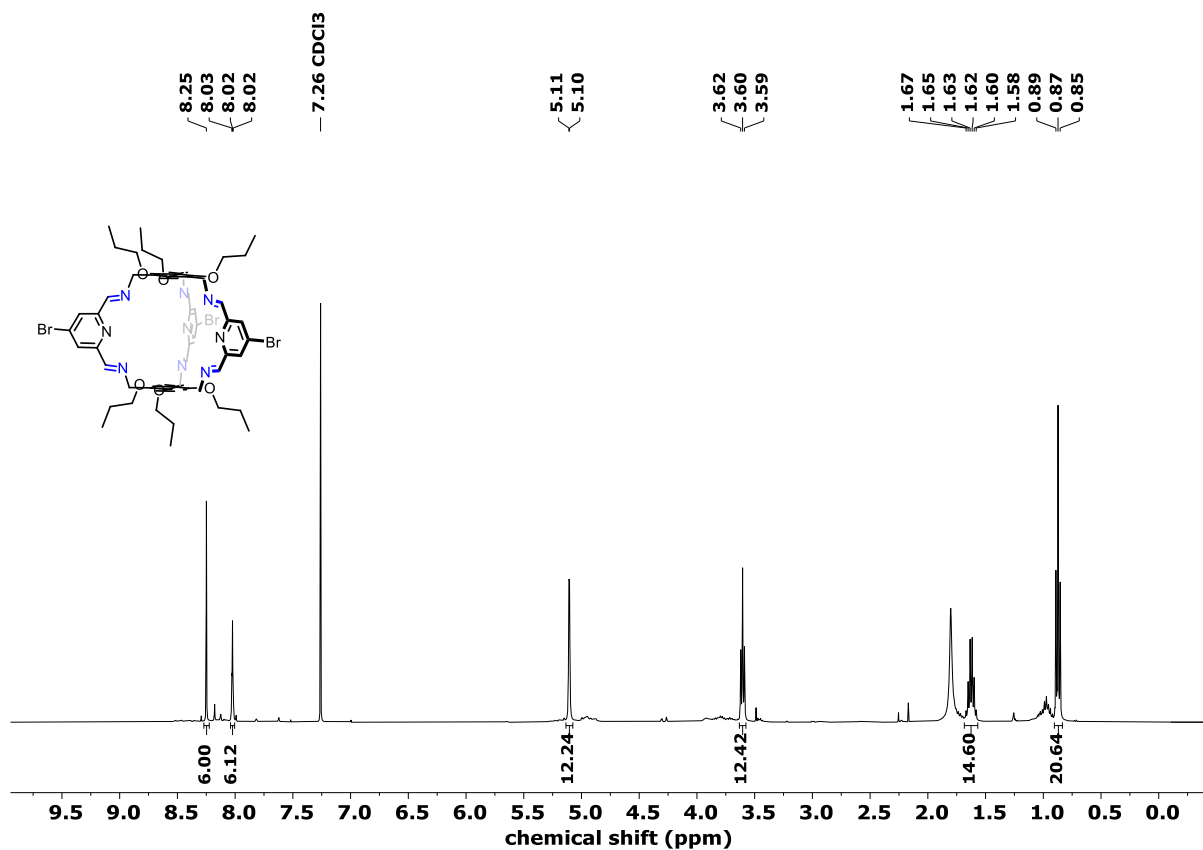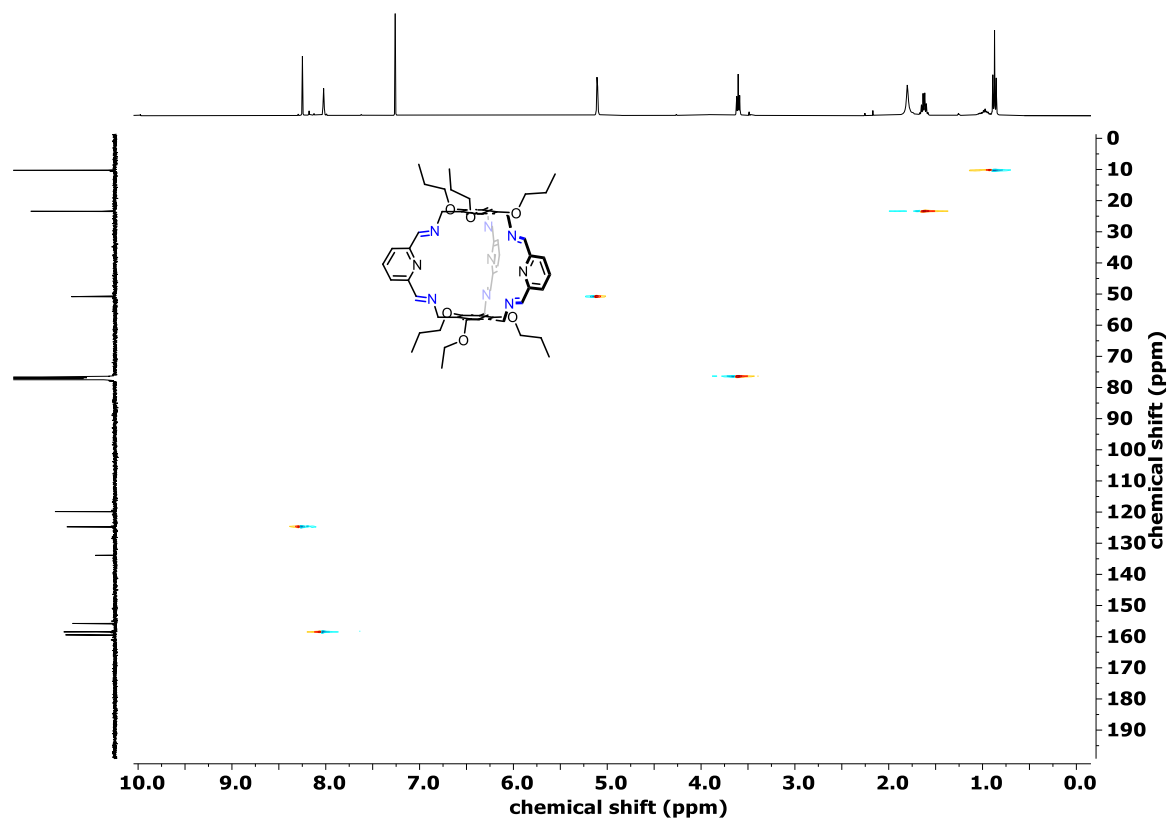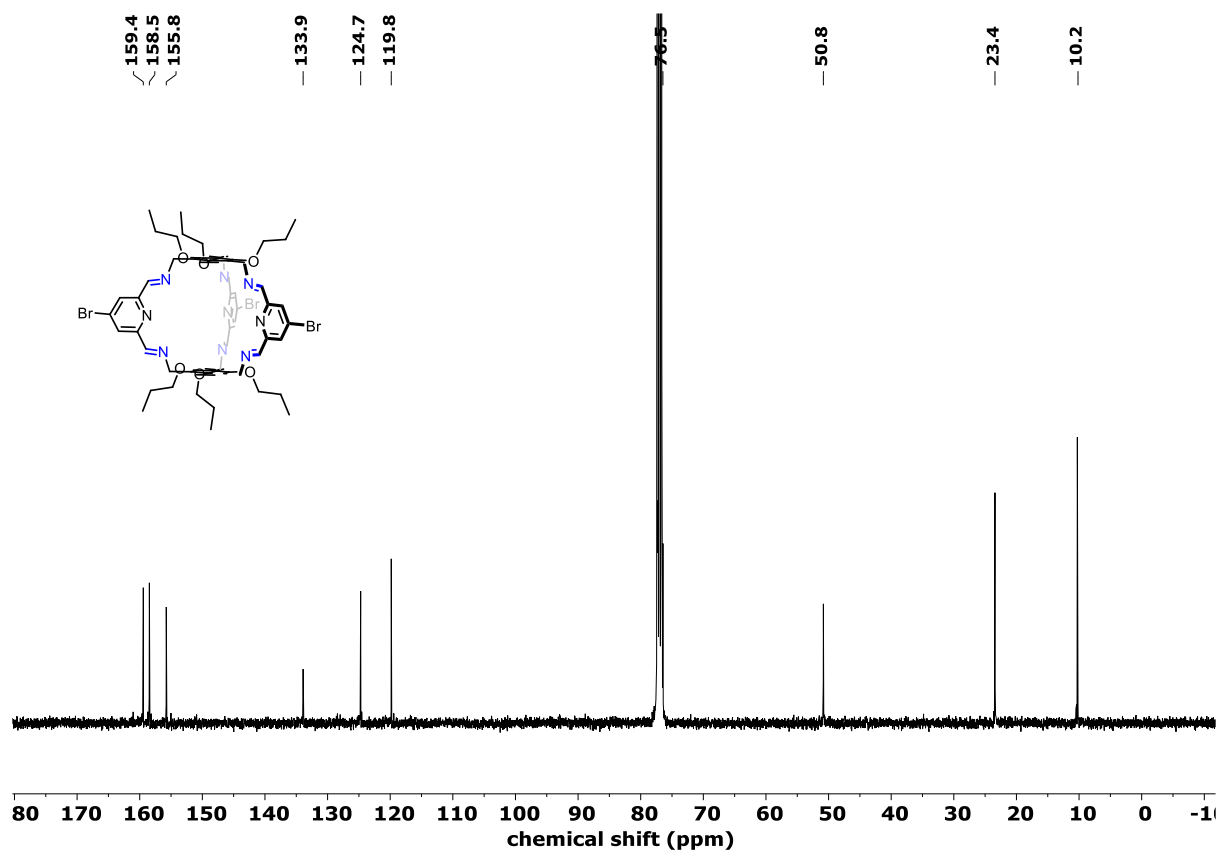
Figure 69. ^{13}C NMR (100 MHz, CDCl$_3$) spectrum of imine cage **B65**.
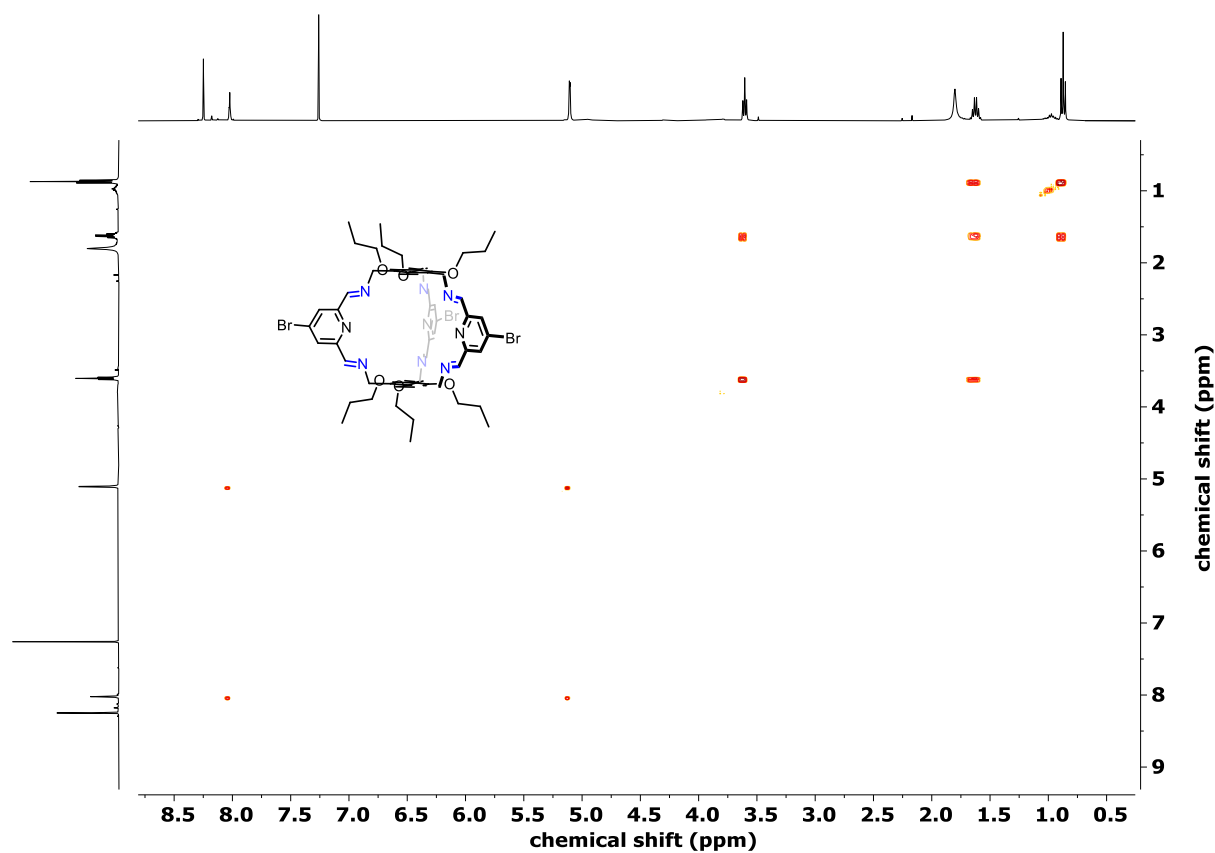
Figure 70. ^{1}H-^{1}H (600 MHz, 600 MHz) COSY NMR spectrum of imine cage **B65**.
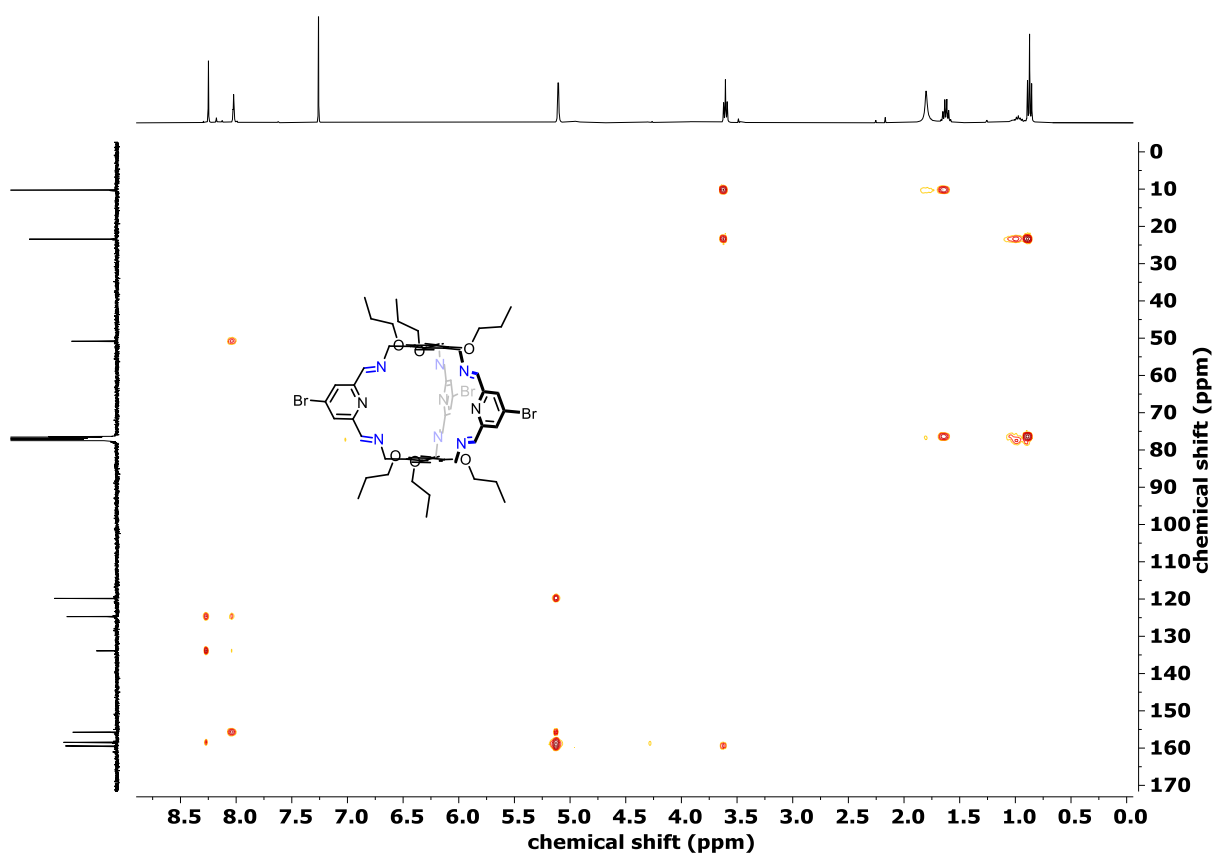
Figure 71. ^{1}H-^{13}C (600 MHz, 100 MHz) HMBC NMR spectrum of imine cage **B65**.
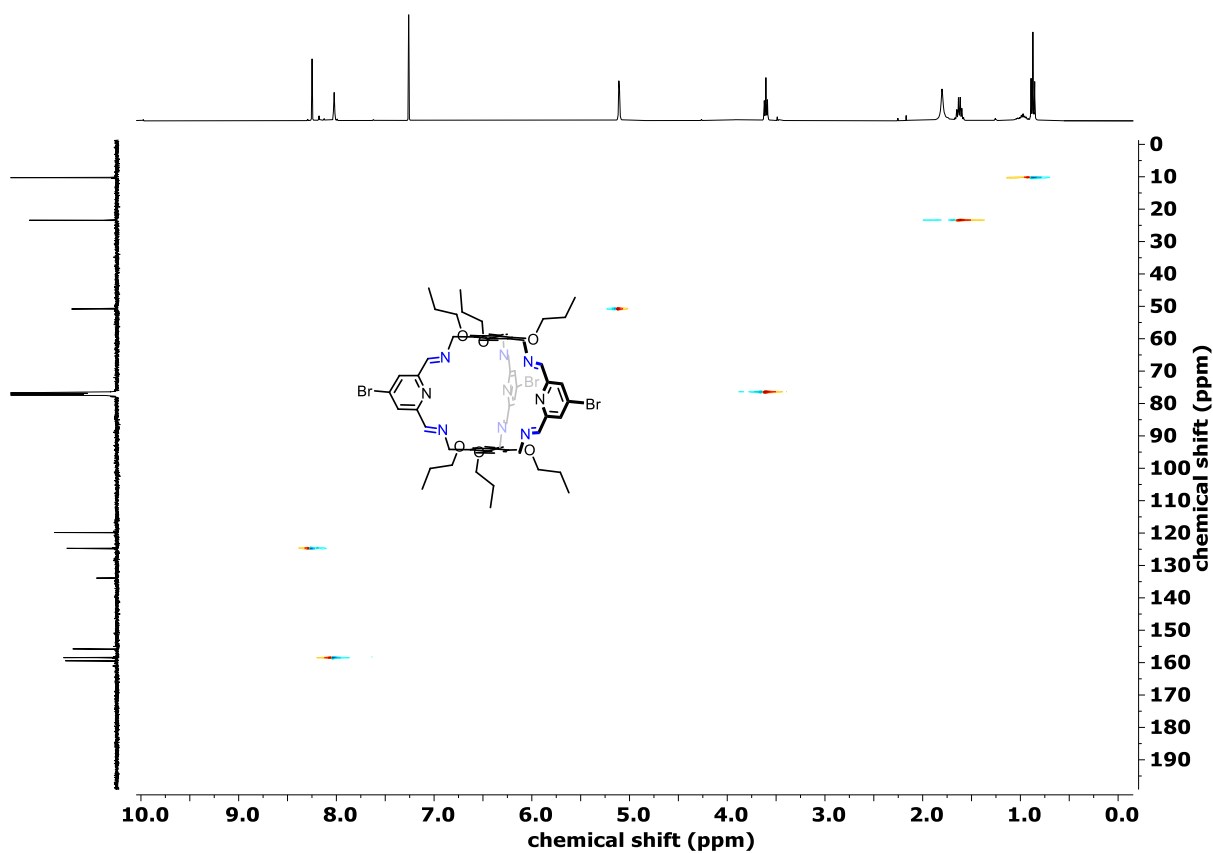
Figure 72. ^{1}H-^{13}C (600 MHz, 100 MHz) HSQC NMR spectrum of imine cage **B65**.

Figure 73. ^1H NMR (600 MHz, DMSO-d_6) spectrum of amide cage **A62-amide**.

Figure 74. ^{13}C NMR (100 MHz, DMSO-d_6) spectrum of amide cage **A62-amide**.
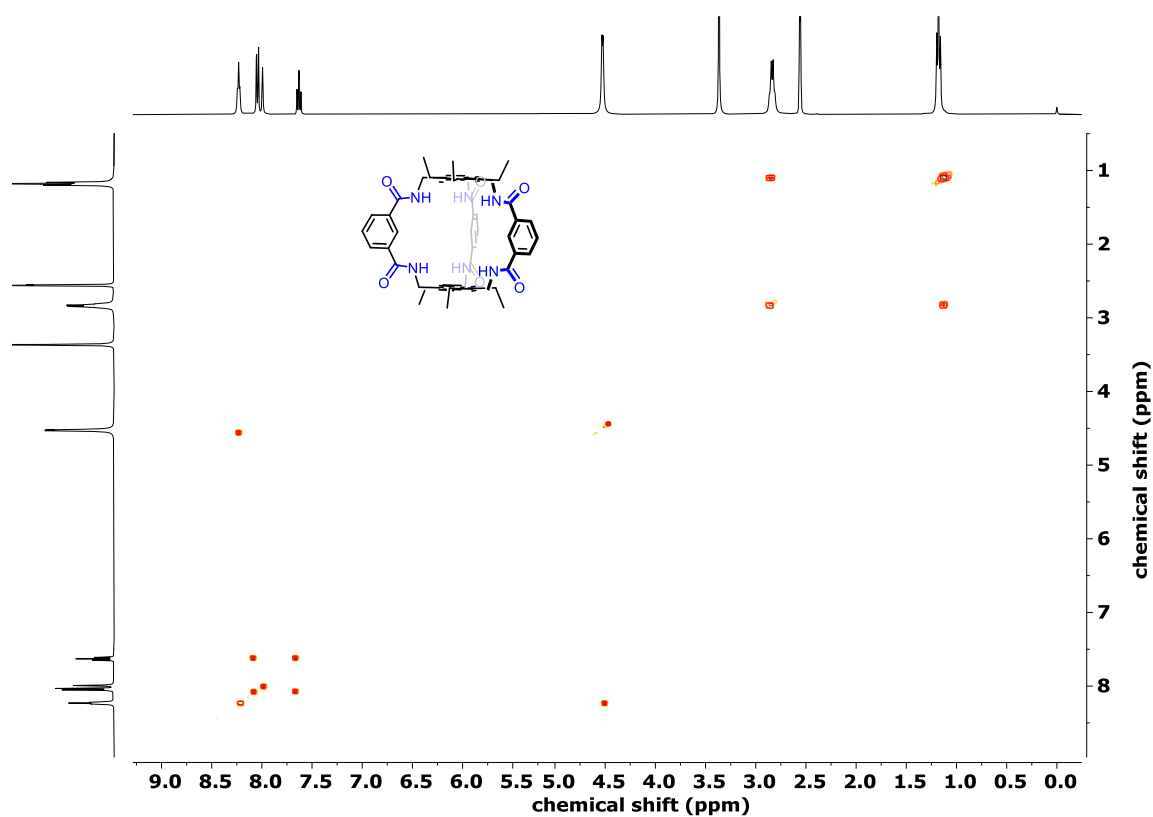
Figure 75. ^{1}H-^{1}H (600 MHz, 600 MHz) COSY NMR spectrum of amide cage **A62-amide**.
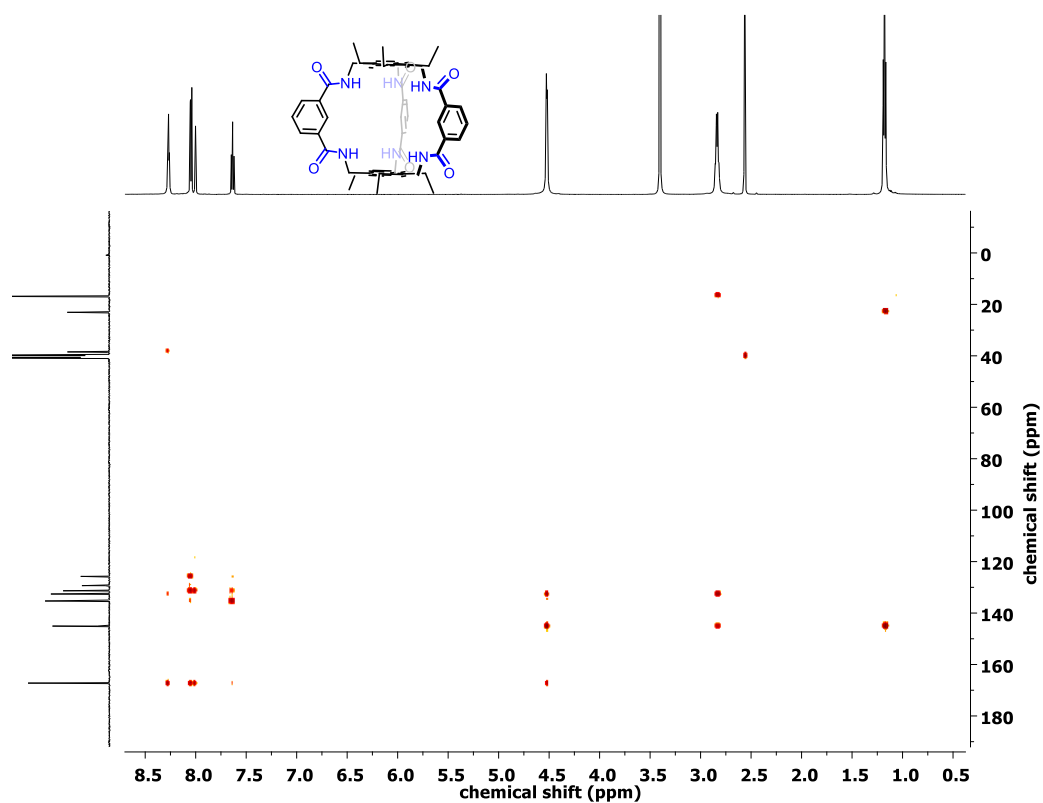
Figure 76. ^{1}H-^{13}C (600 MHz, 100 MHz) HMBC NMR spectrum of amide cage **A62-amide**.
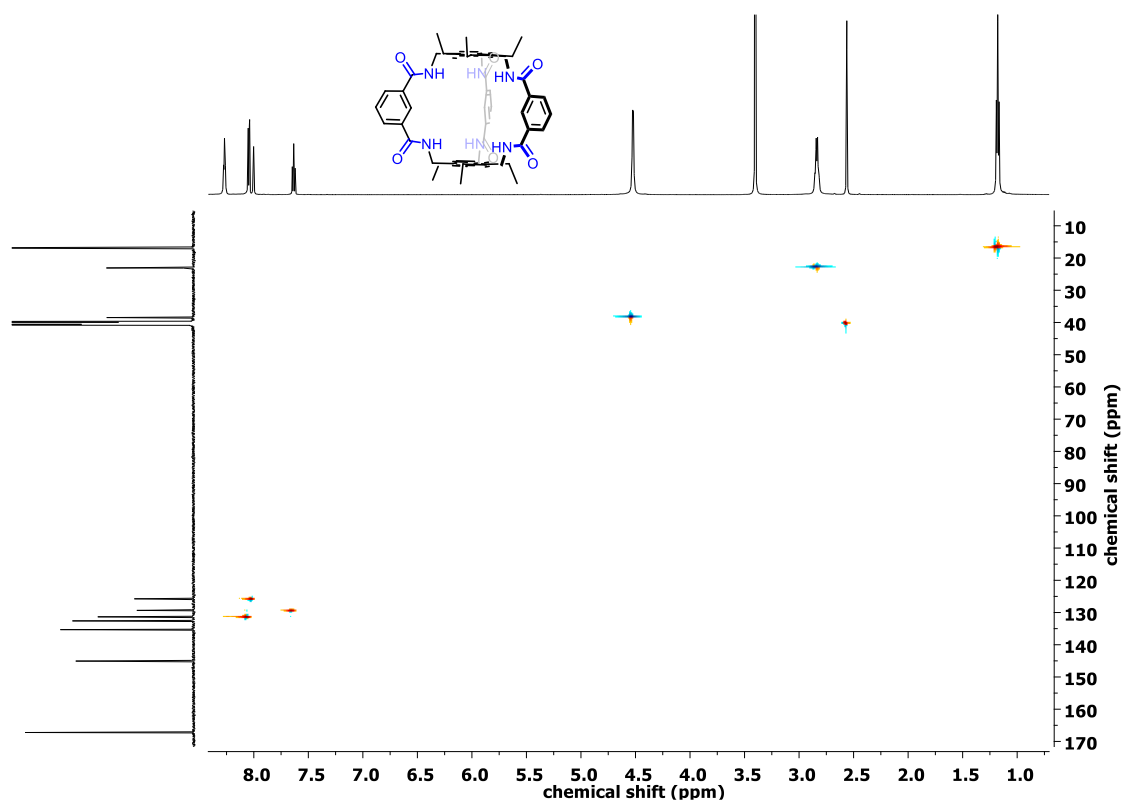
Figure 77. ¹H-¹³C (600 MHz, 100 MHz) HSQC NMR spectrum of amide cage **A62-amide**.
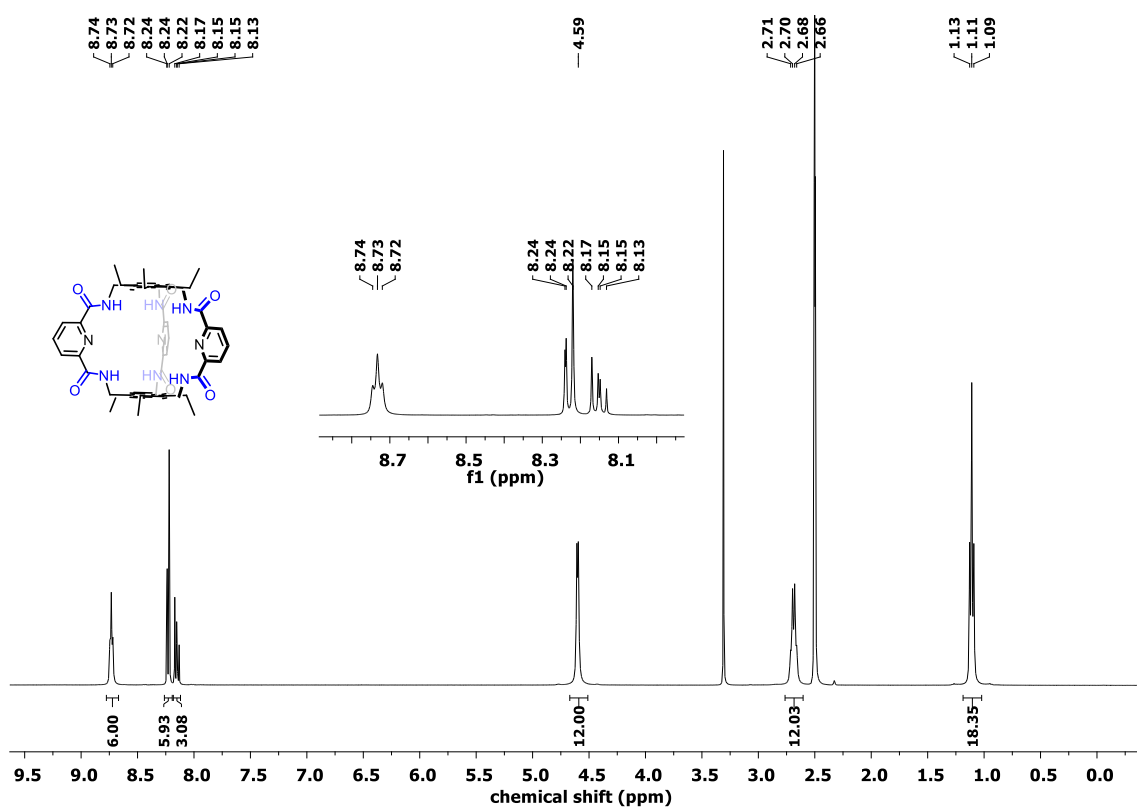
Figure 78. ¹H NMR (400 MHz, DMSO-d₆) spectrum of amide cage **A63-amide**.
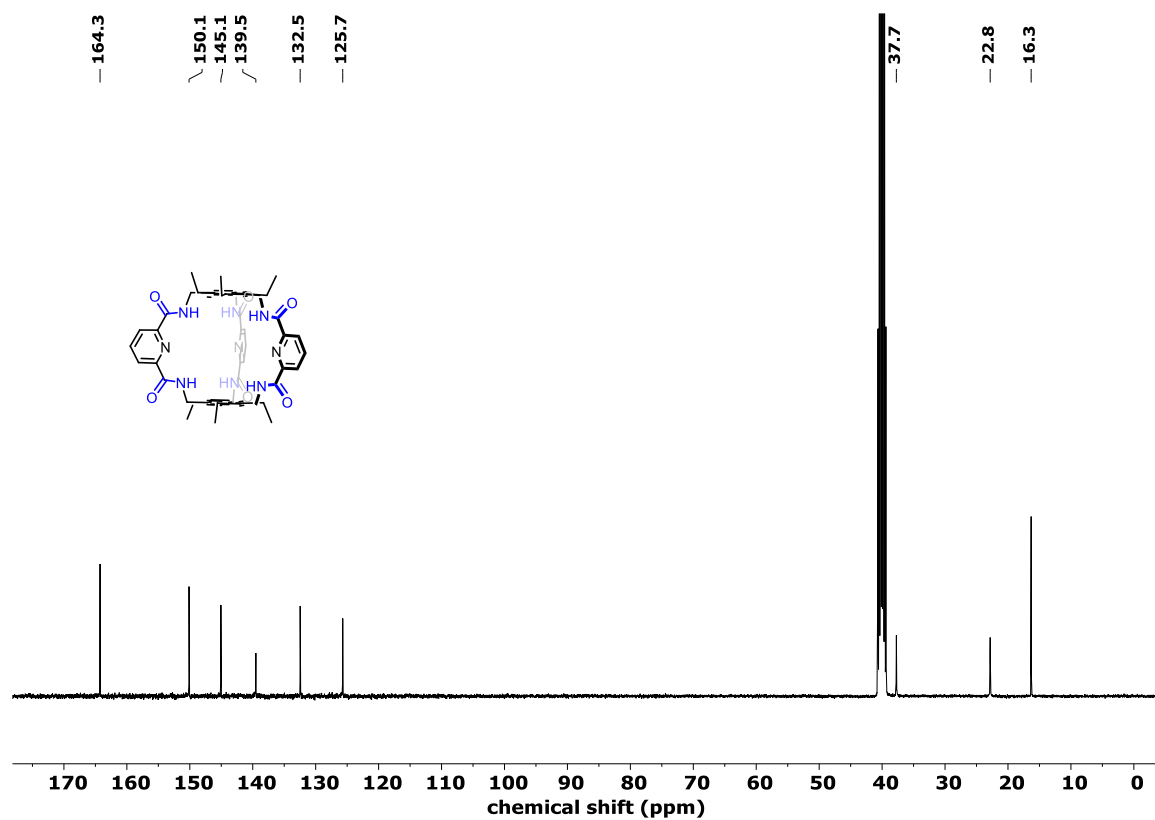
Figure 79. ^{13}C NMR (100 MHz, DMSO-d$_6$) spectrum of amide cage **A63-amide**.
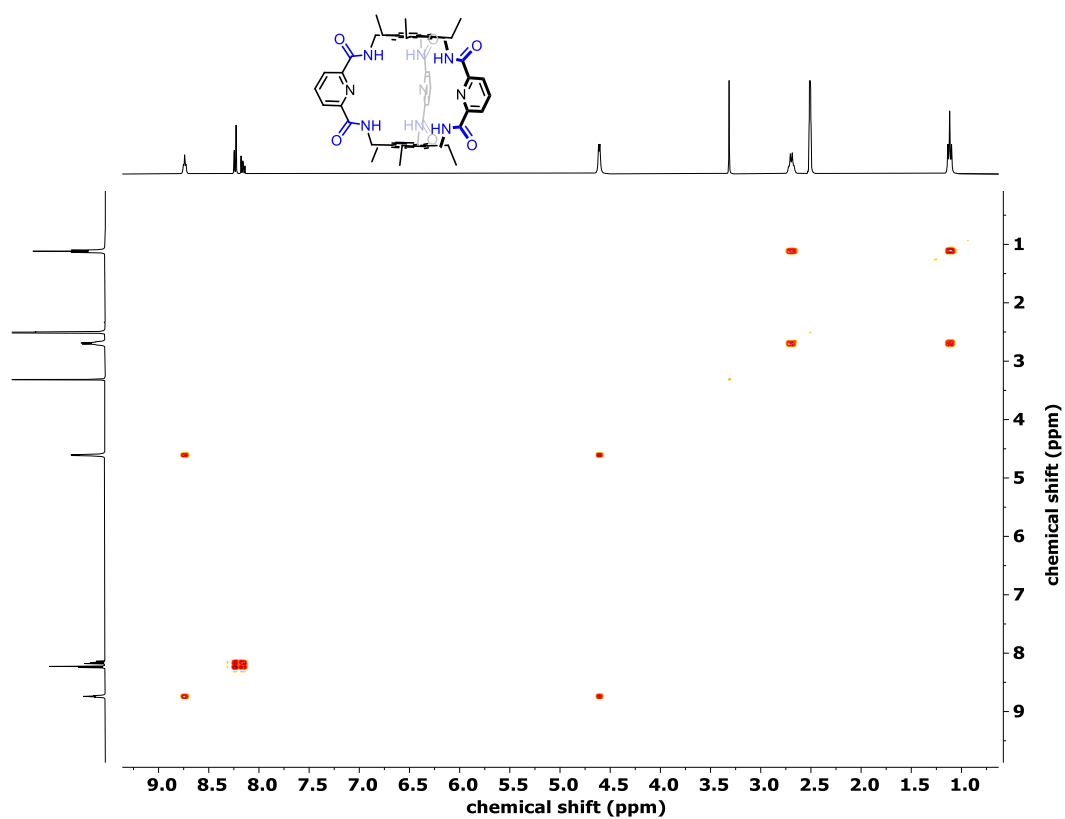
Figure 80. ^{1}H-^{1}H (400 MHz, 400 MHz) COSY NMR spectra of amide cage **A63-amide**.
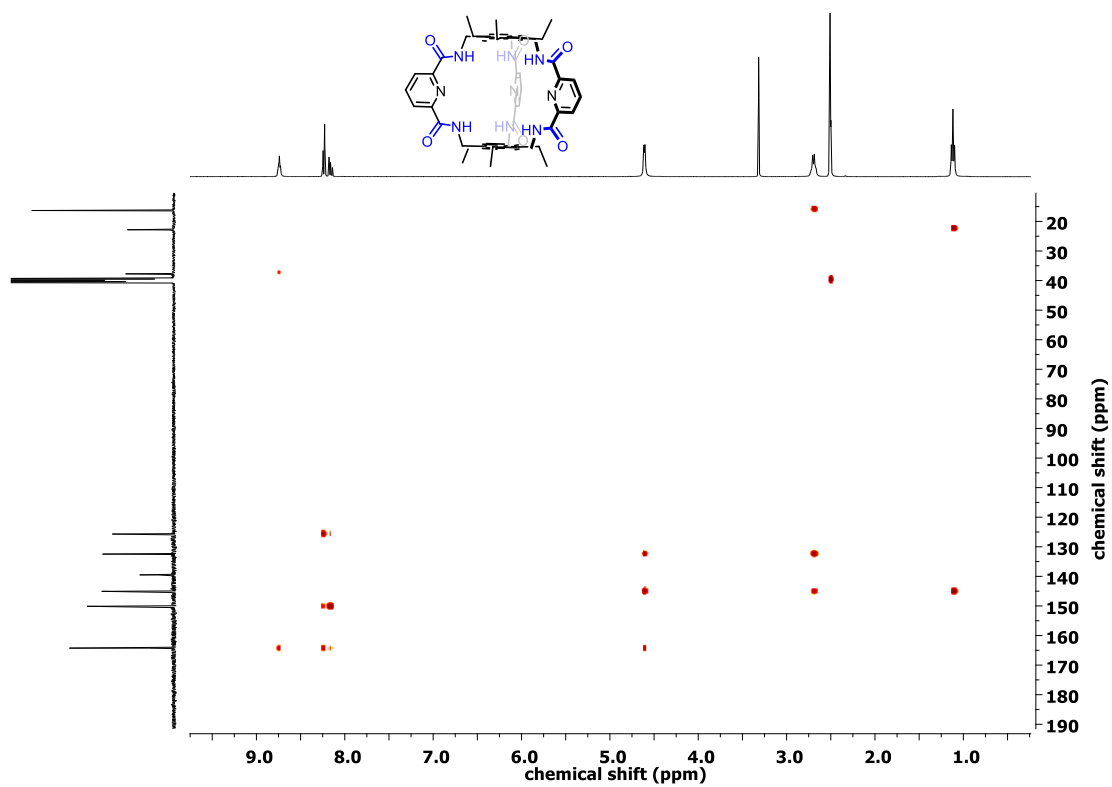
Figure 81. ^{1}H-^{13}C (400 MHz, 100 MHz) HMBC NMR spectrum of amide cage **A63-amide**.
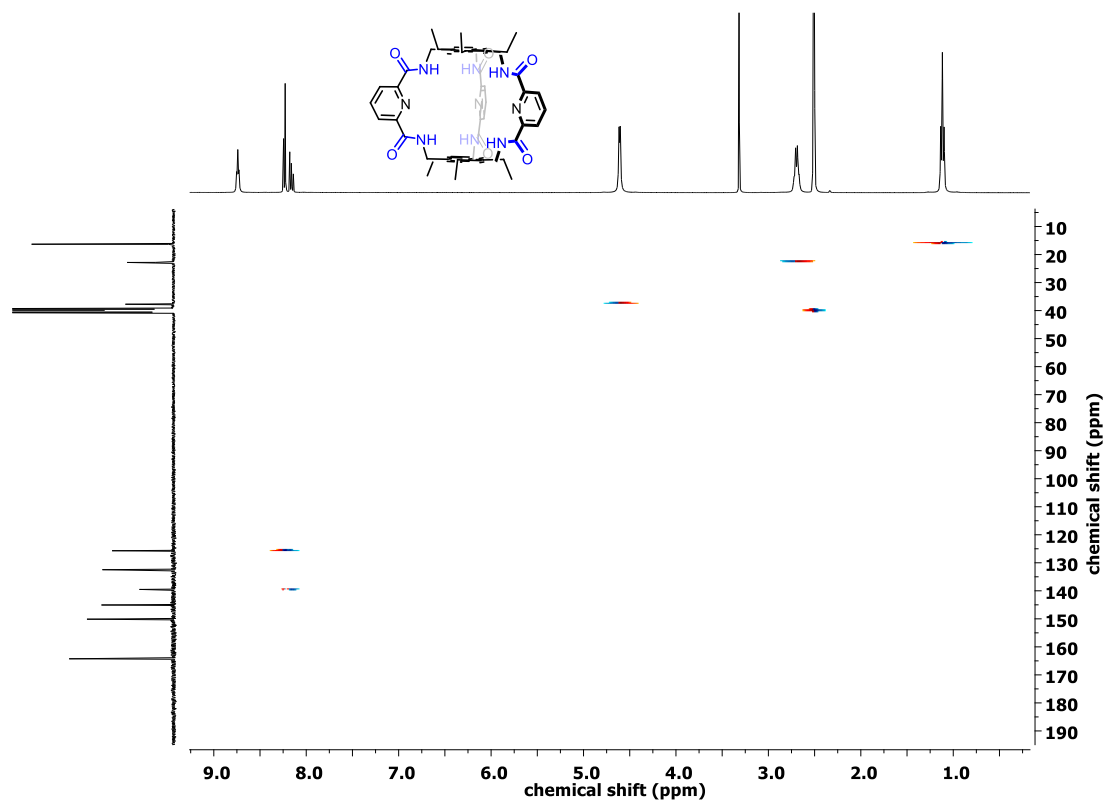
Figure 82. ^{1}H-^{13}C (400 MHz, 100 MHz) HSQC NMR spectrum of amide cage **A63-amide**.
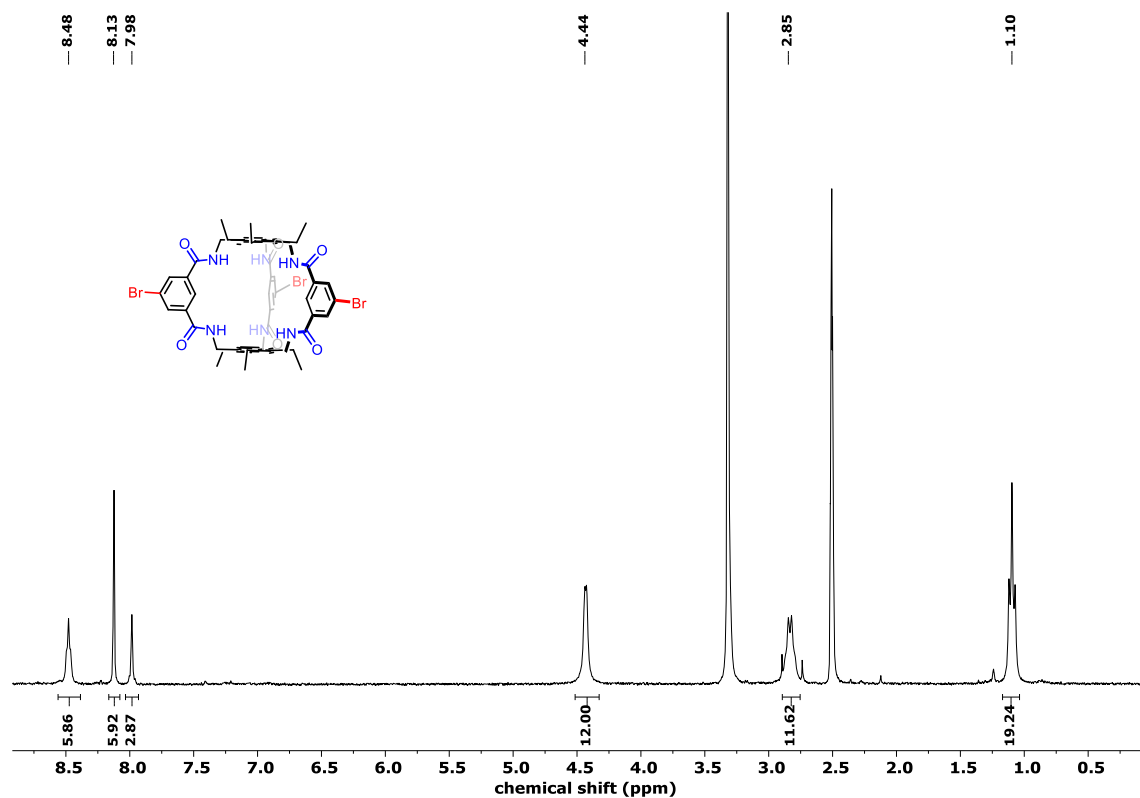
Figure 83. ^{1}H NMR (400 MHz, DMSO-d$_6$) spectrum of amide cage **A64-amide**.
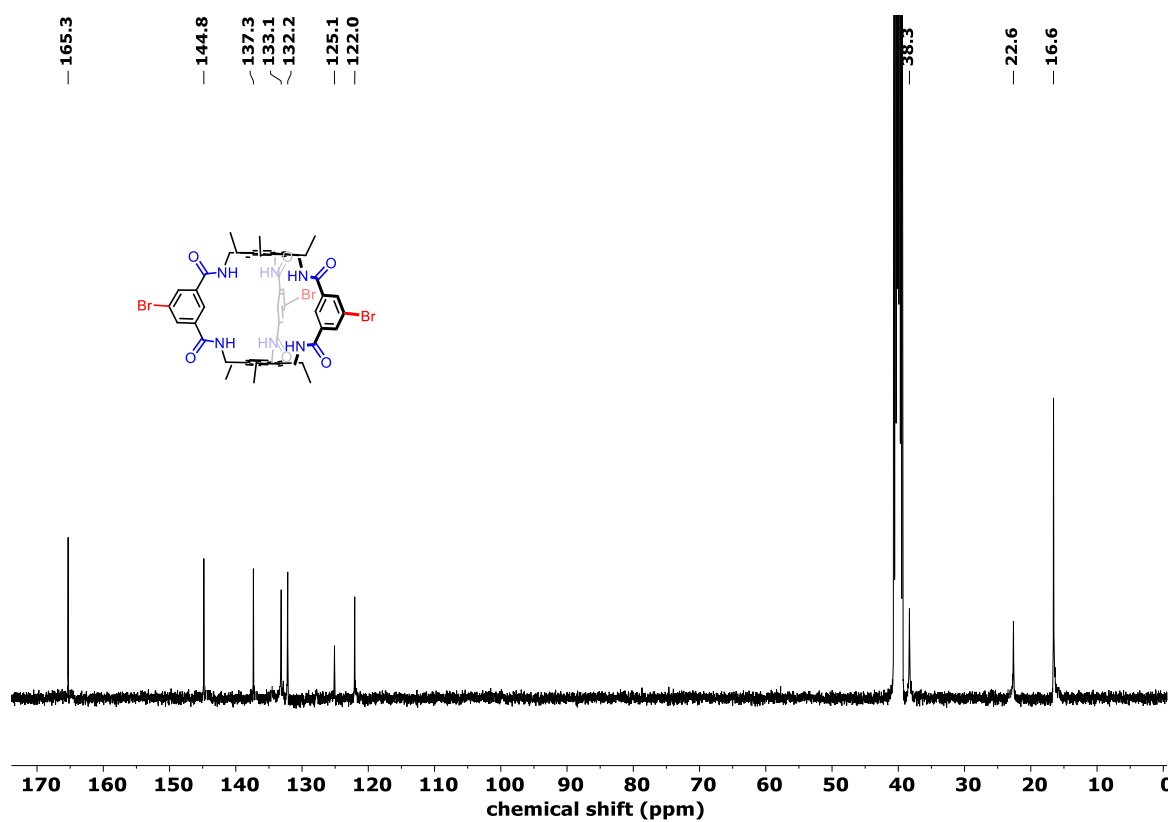
Figure 84. ^{13}C NMR (100 MHz, DMSO-d$_6$) spectrum of amide cage **A64-amide**.
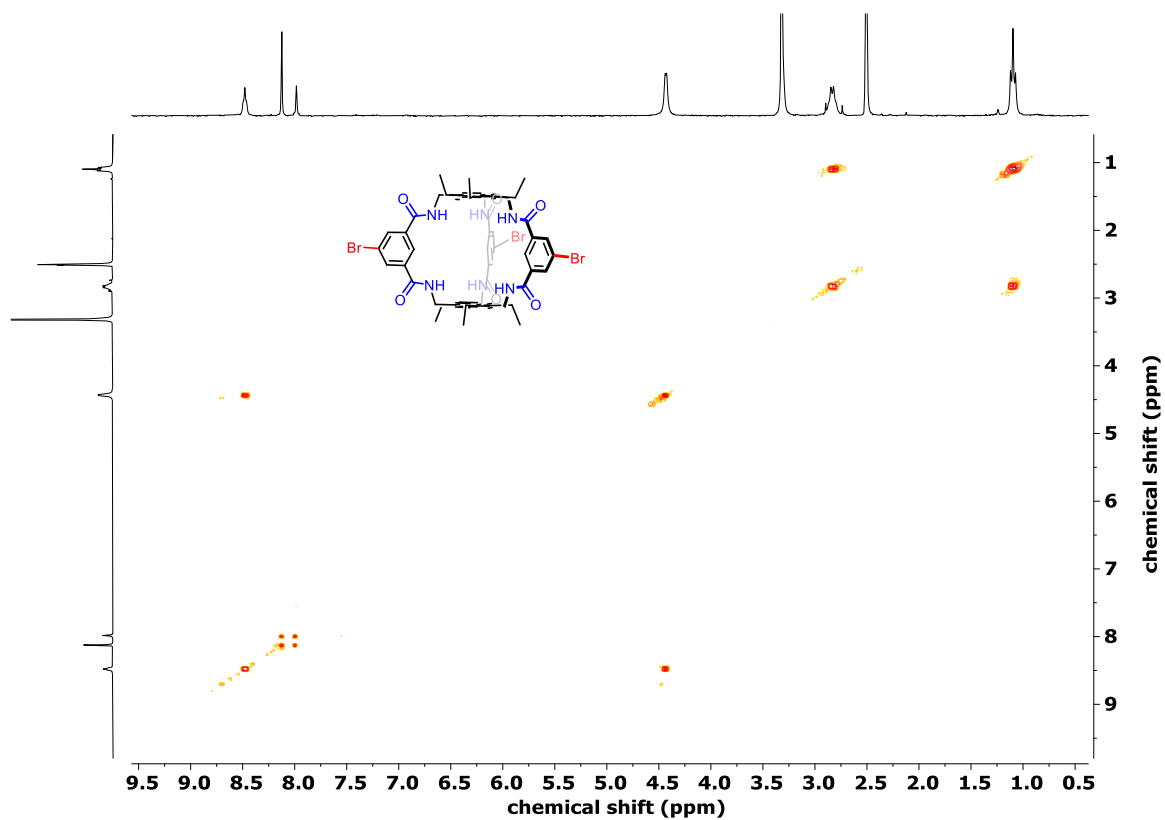
Figure 85. ¹H-¹H (400 MHz, 100 MHz) COSY NMR spectrum of amide cage **A64-amide**.
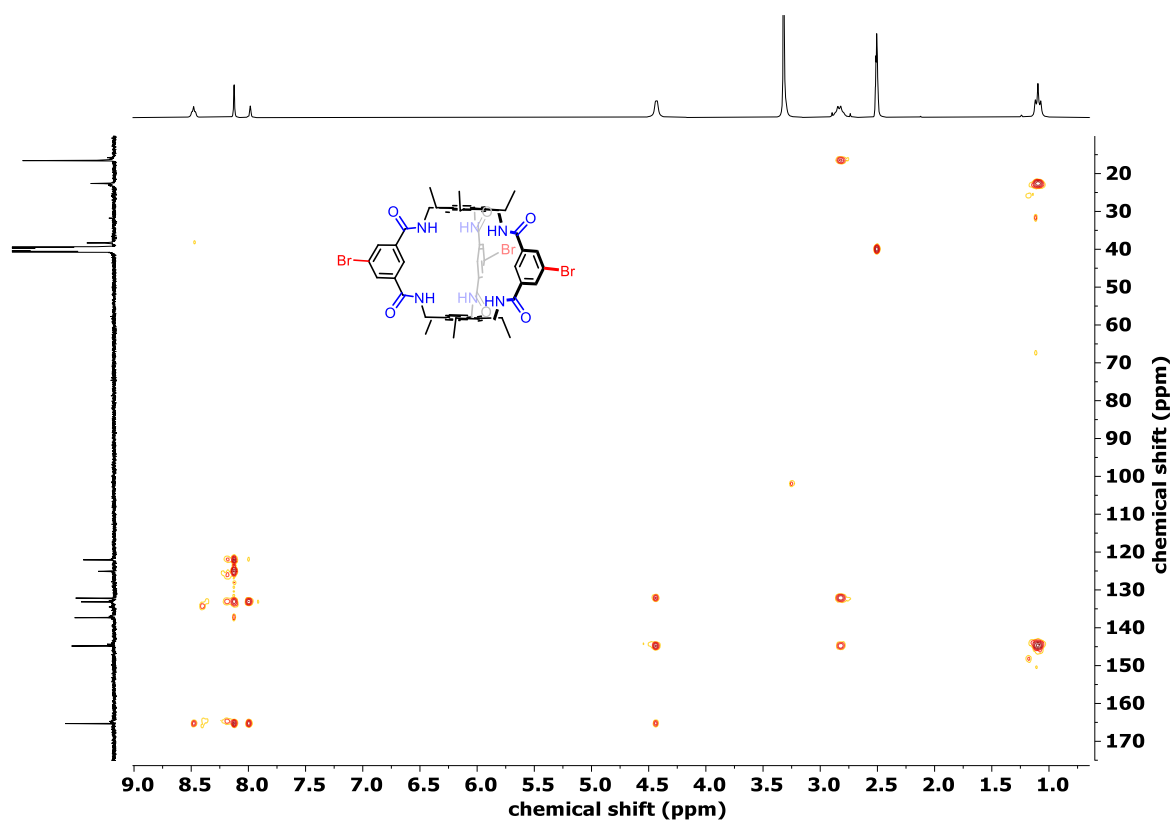
Figure 86. ¹H-¹³C (400 MHz, 100 MHz) HMBC NMR spectrum of amide cage **A64-amide**.
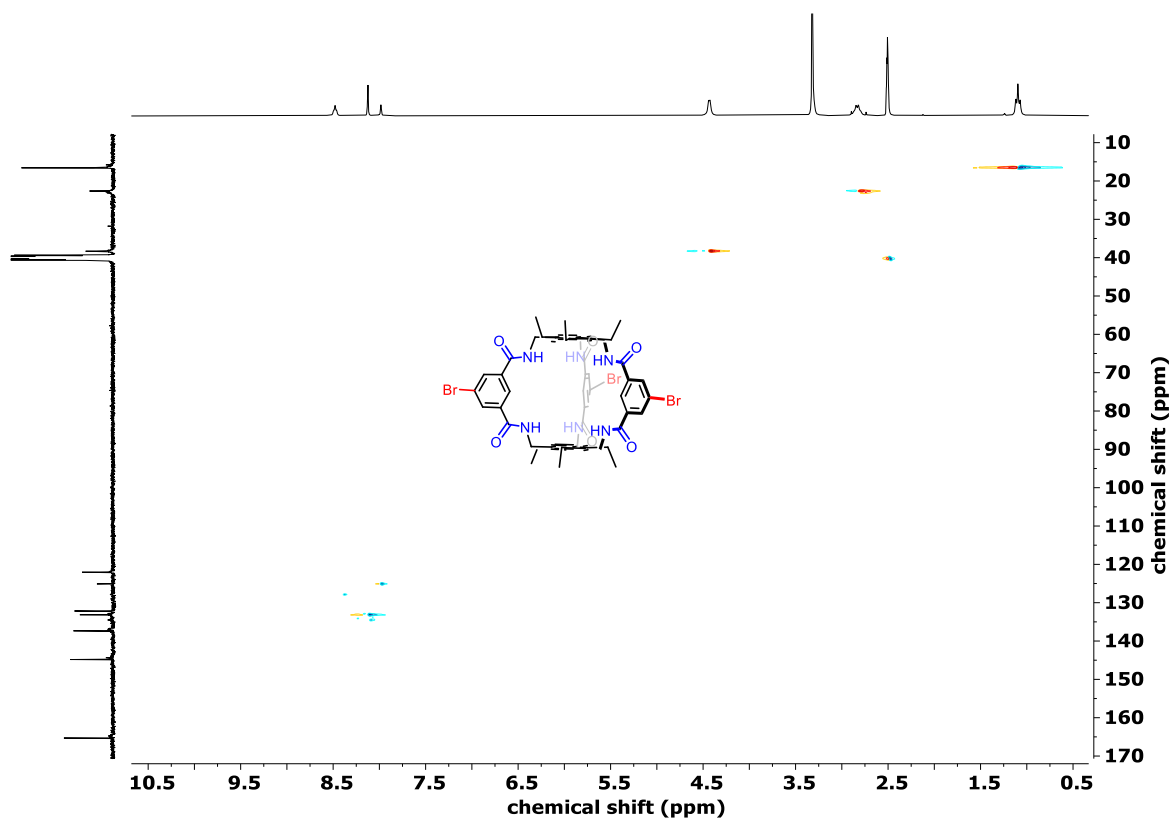
Figure 87. ^{1}H-^{13}C (400 MHz, 100 MHz) HSQC NMR spectrum of amide cage **A64-amide**.
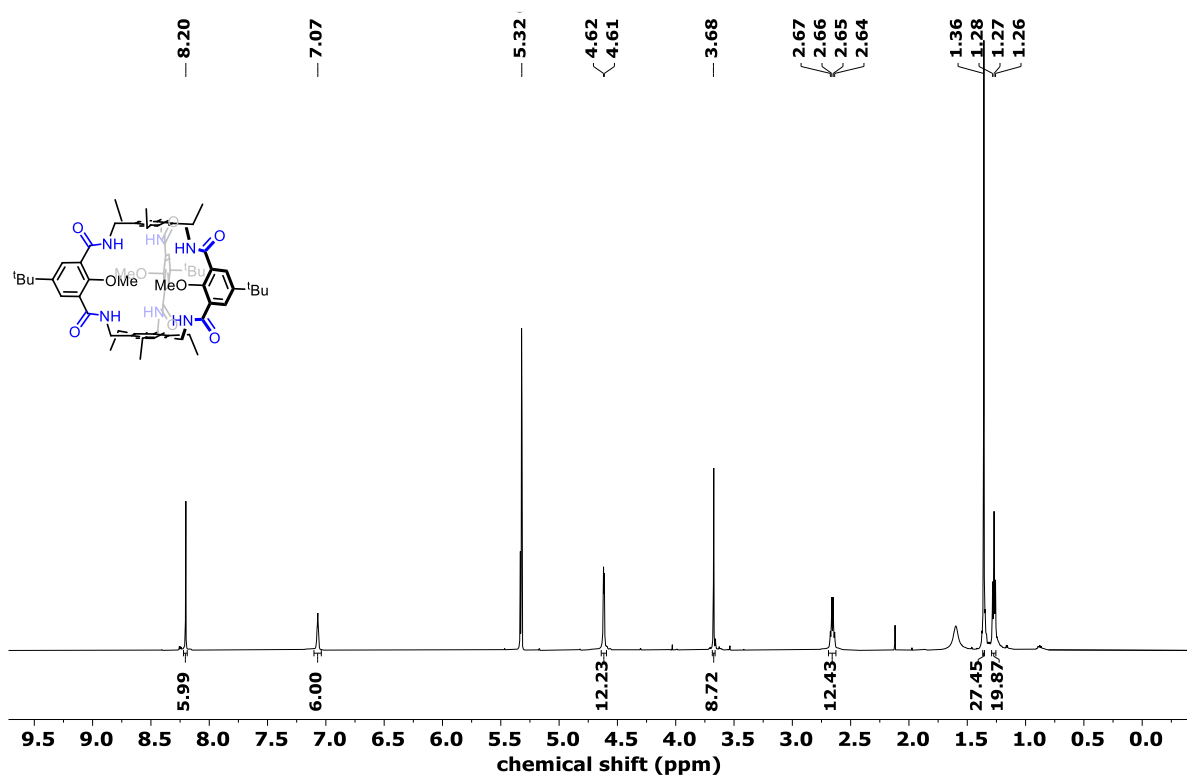
Figure 88. ^{1}H NMR (500 MHz, CD$_2$Cl$_2$) spectrum of amide cage **A67-amide**.
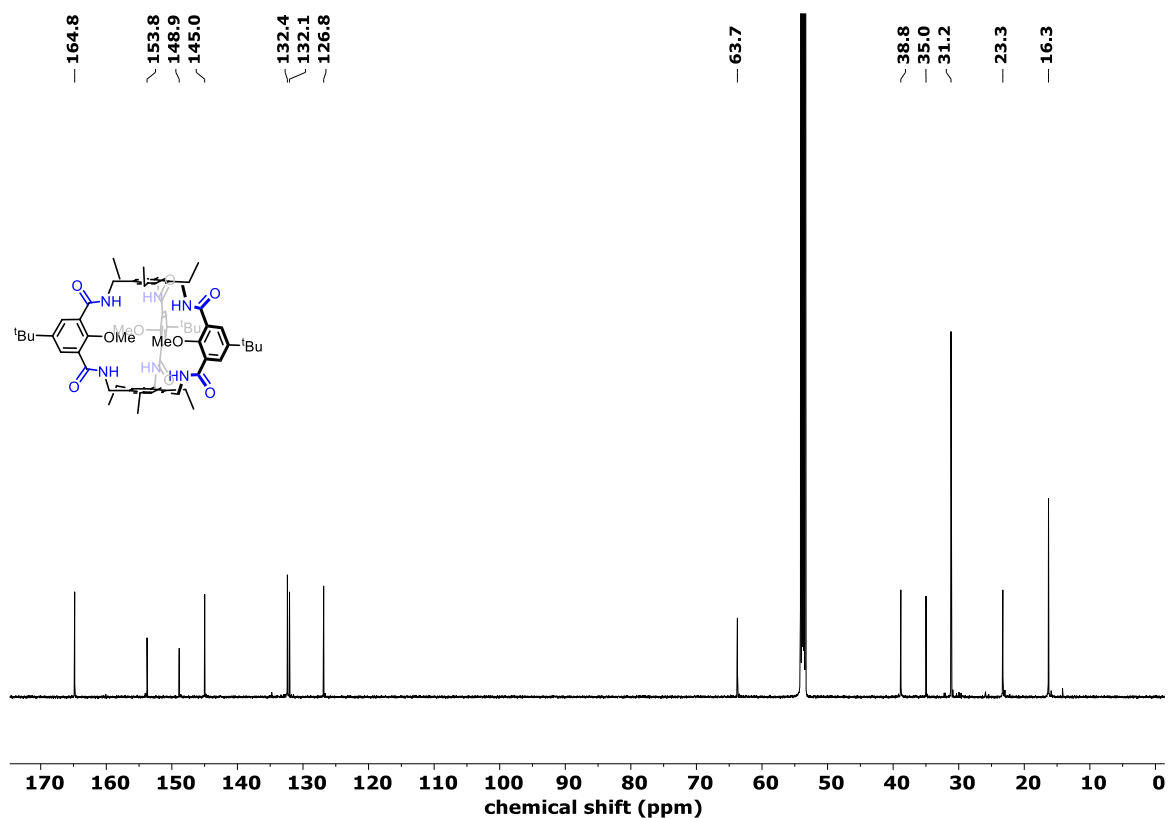
Figure 89. ^{13}C NMR (100MHz, CD$_2$Cl$_2$) spectrum of amide cage **A67-amide**.
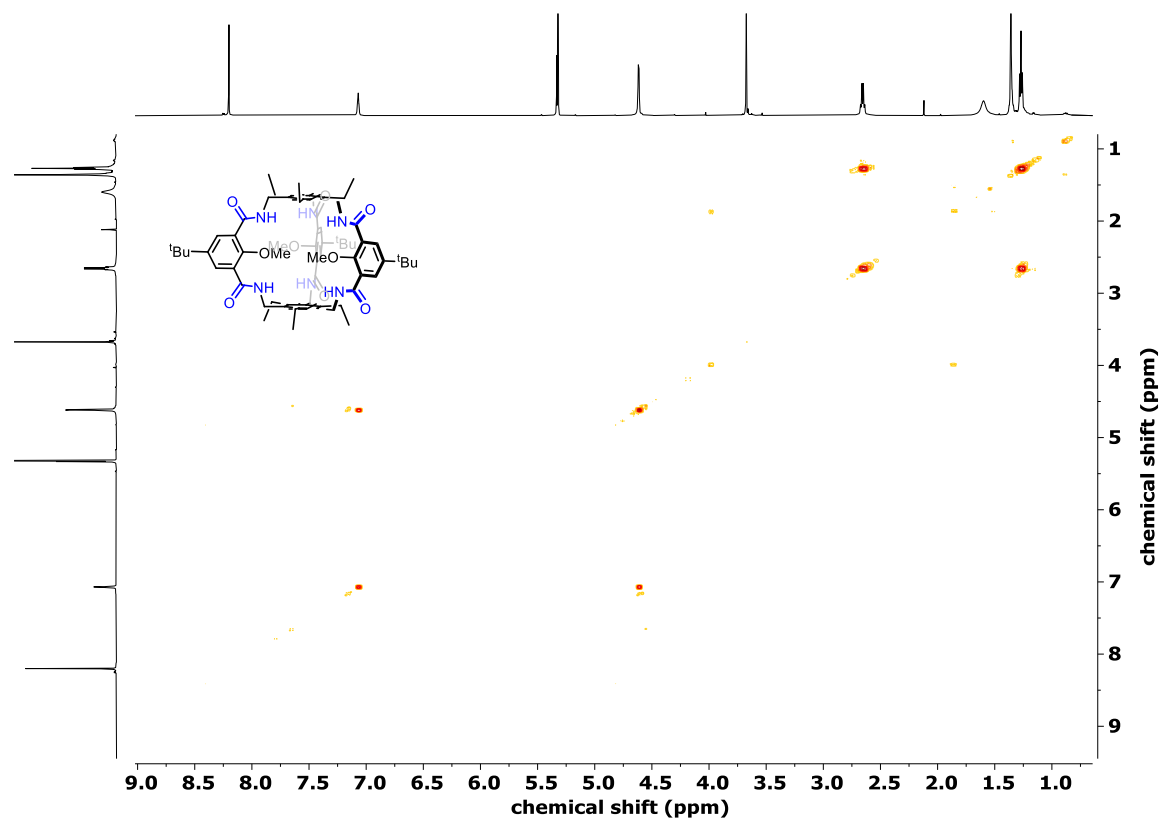
Figure 90. ^{1}H-^{1}H (500 MHz, 500 MHz) COSY NMR spectrum of amide cage **A67-amide**.
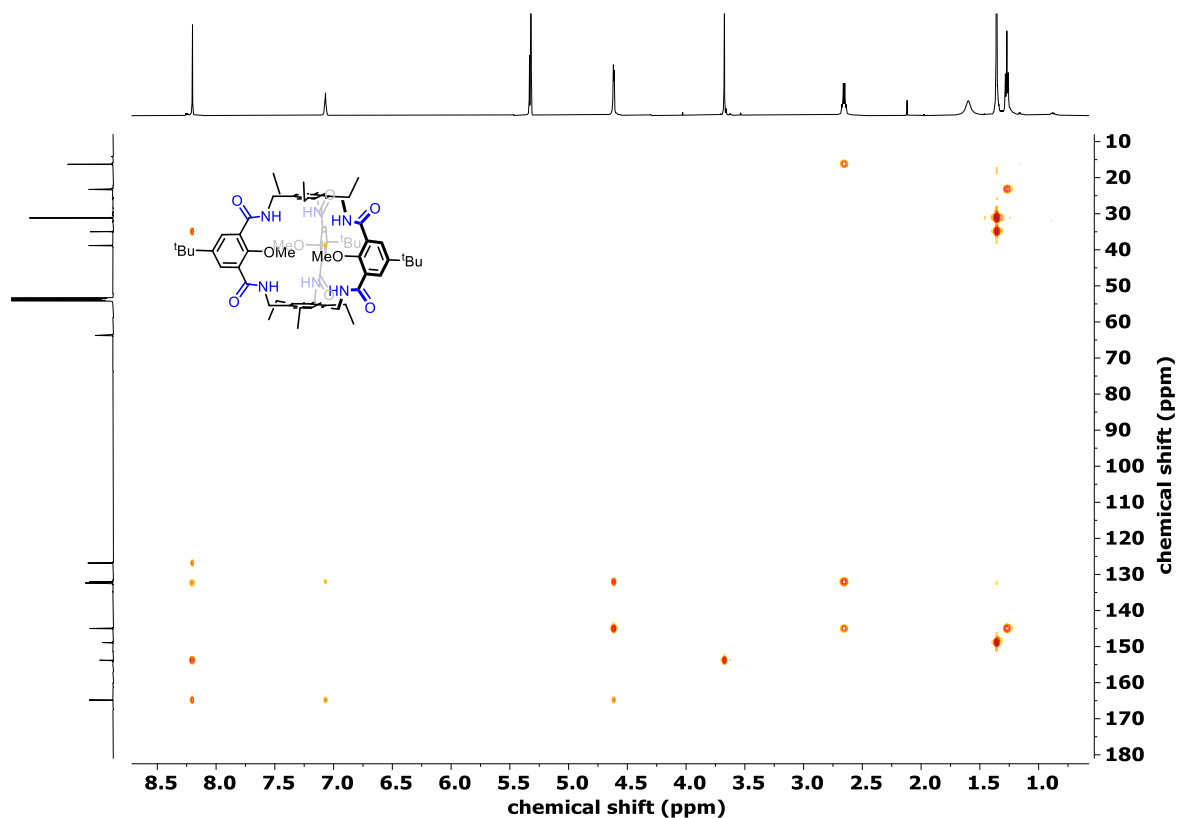
Figure 91. ^{1}H-^{13}C (500 MHz, 100 MHz) HMBC NMR spectrum of amide cage **A67-amide**.
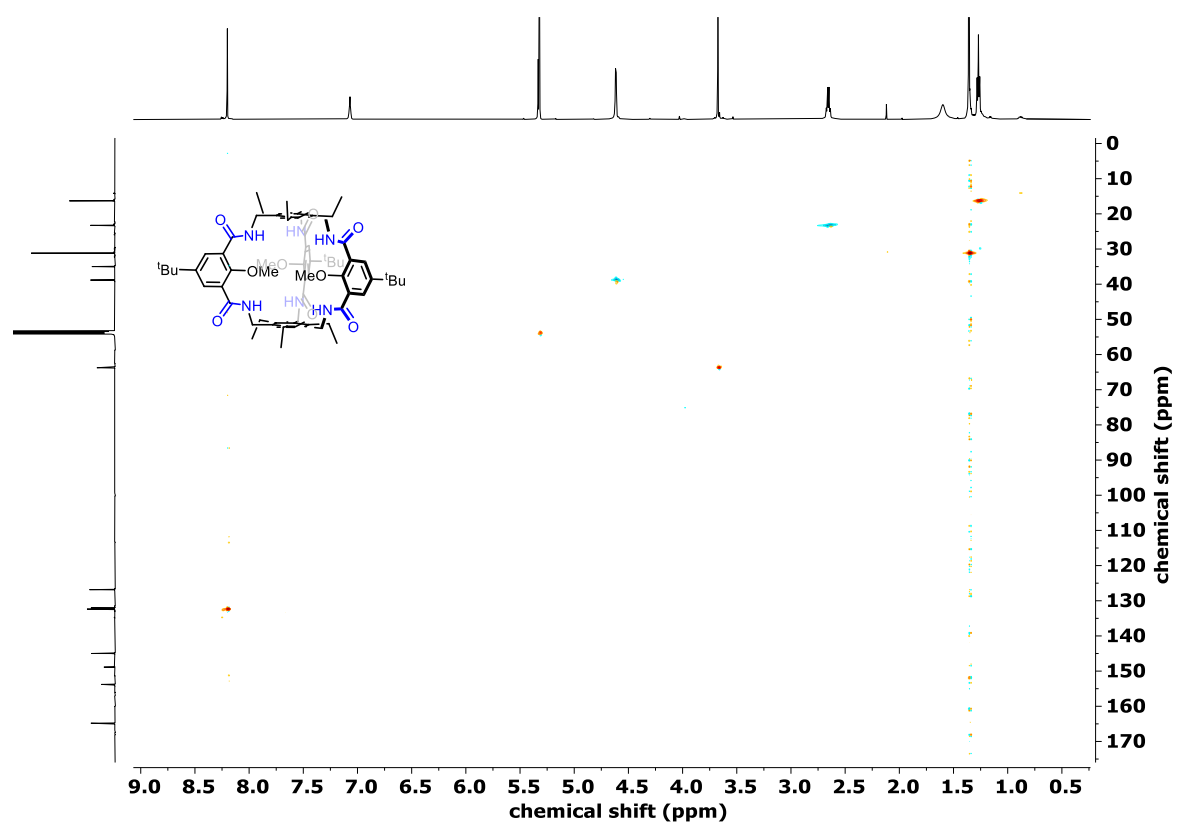
Figure 92. ^{1}H-^{13}C (500 MHz, 100 MHz) HSQC NMR spectrum of amide cage **A67-amide**.
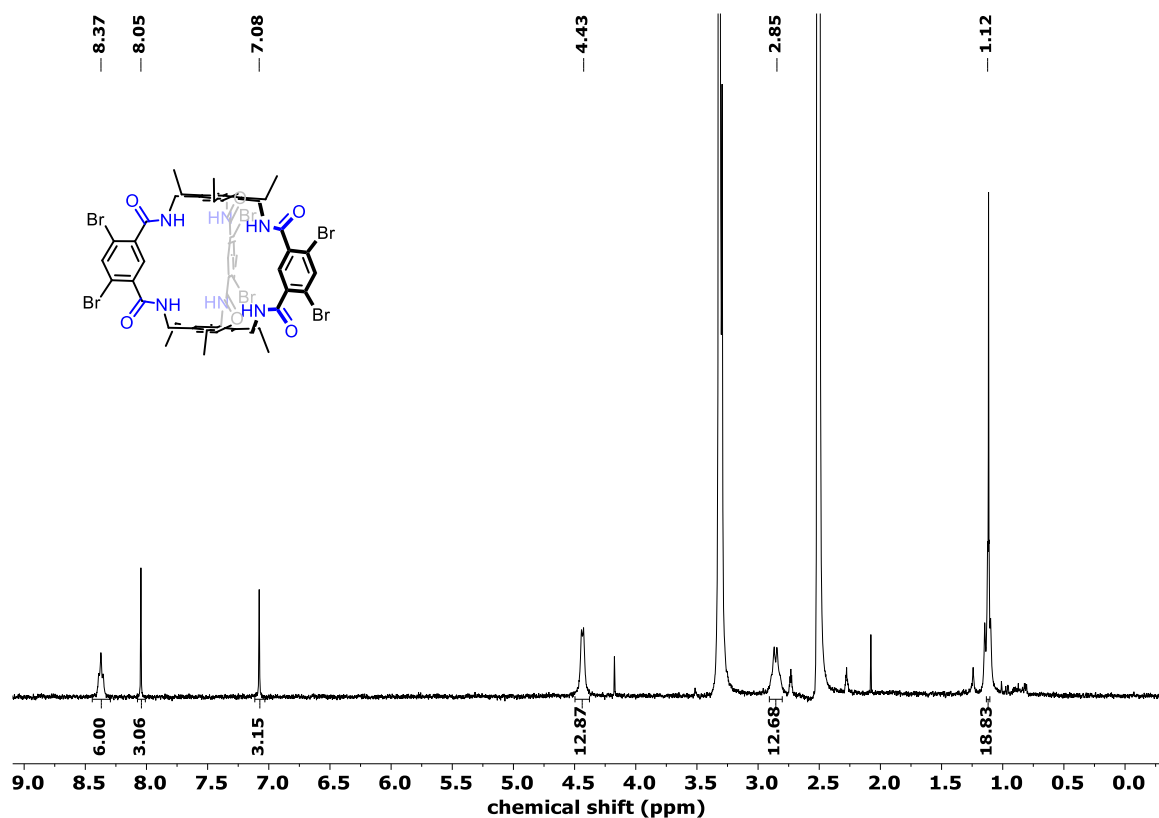
Figure 93. ^{1}H NMR (300 MHz, DMSO-d$_6$) spectrum of amide cage **A70-amide**.
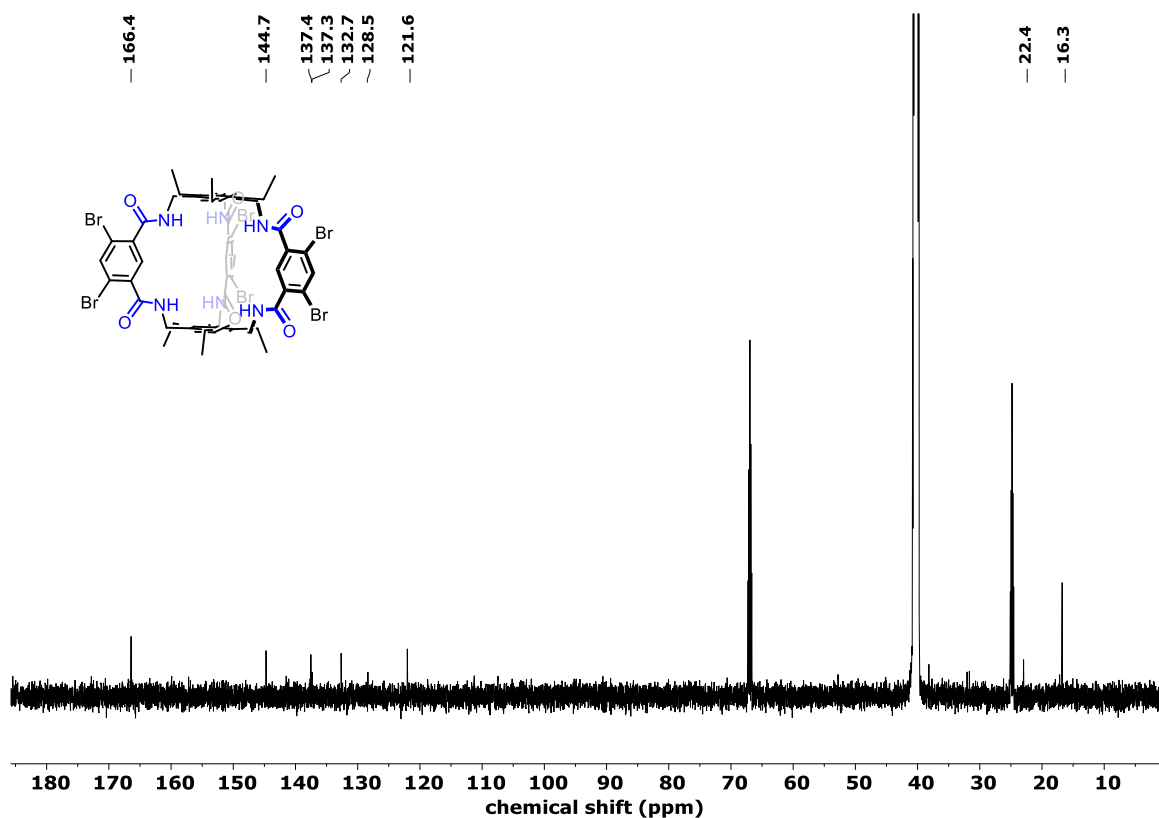
Figure 94. ^{13}C NMR (75 MHz, DMSO-d$_6$) spectrum of amide cage **A70-amide**.
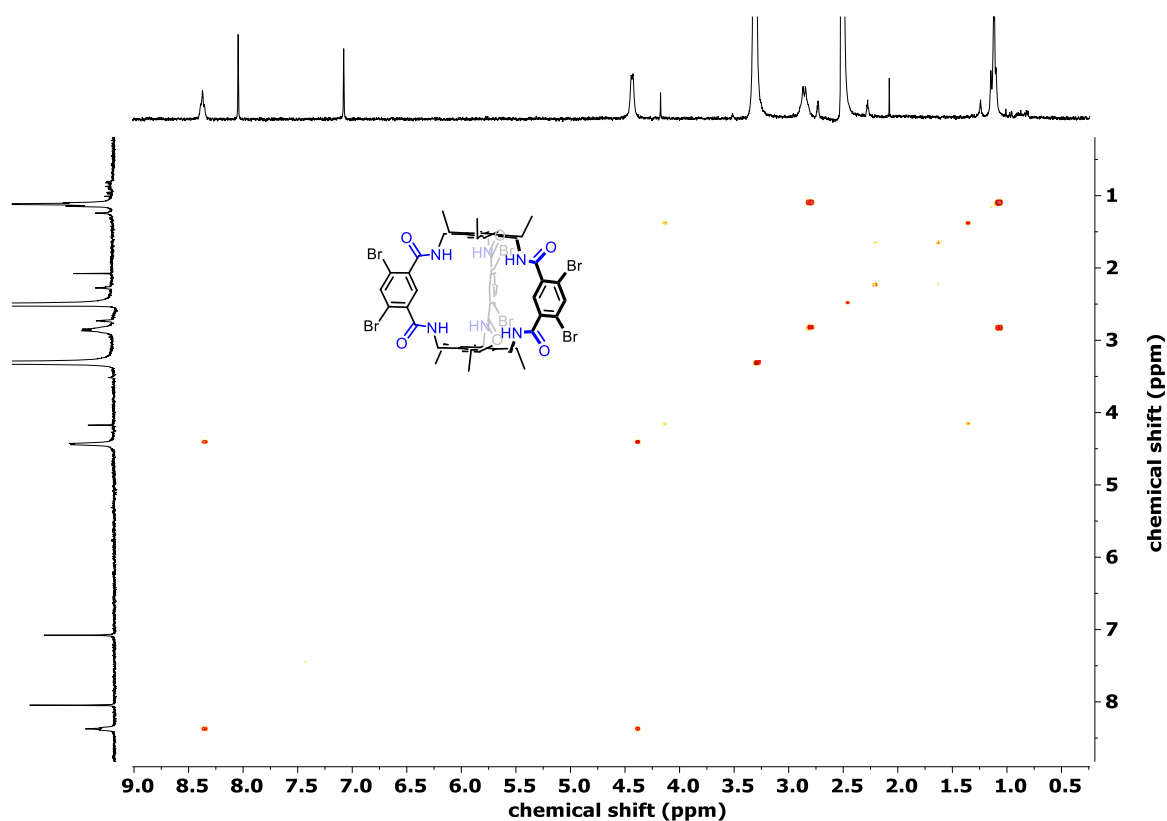
Figure 95. ^{1}H-^{1}H (300 MHz, 75 MHz) COSY NMR spectrum of amide cage **A70-amide**.
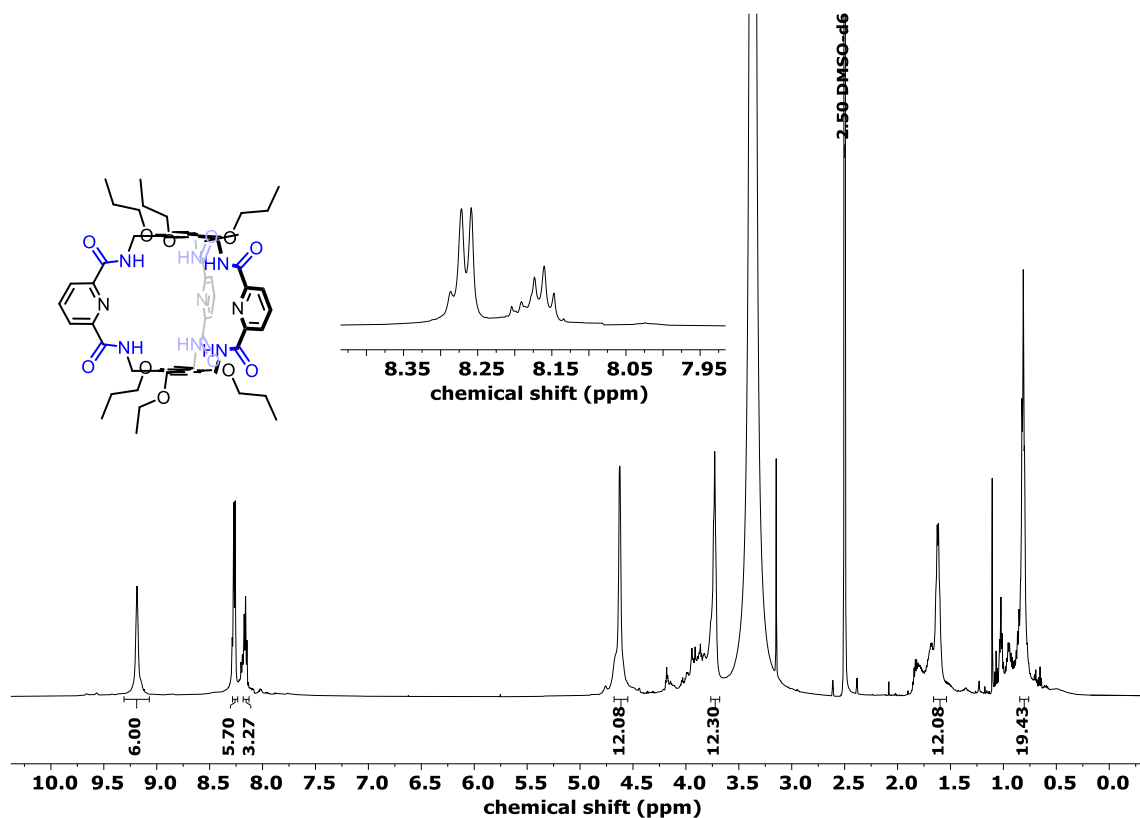
Figure 96. ^{1}H NMR (600 MHz, DMSO-d$_6$) spectrum of amide cage **B63-amide**.
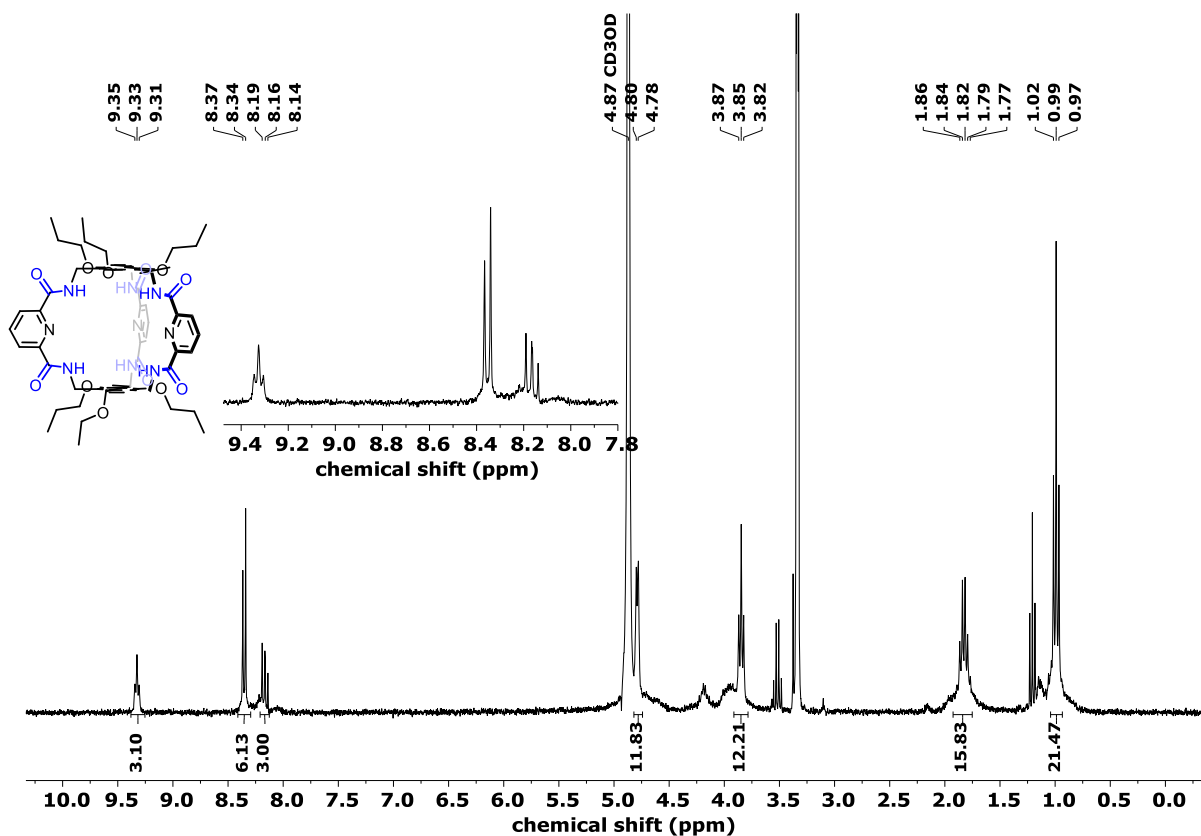
Figure 97. ^{1}H NMR (600 MHz, methanol-d$_4$) spectrum of amide cage **B63-amide**.
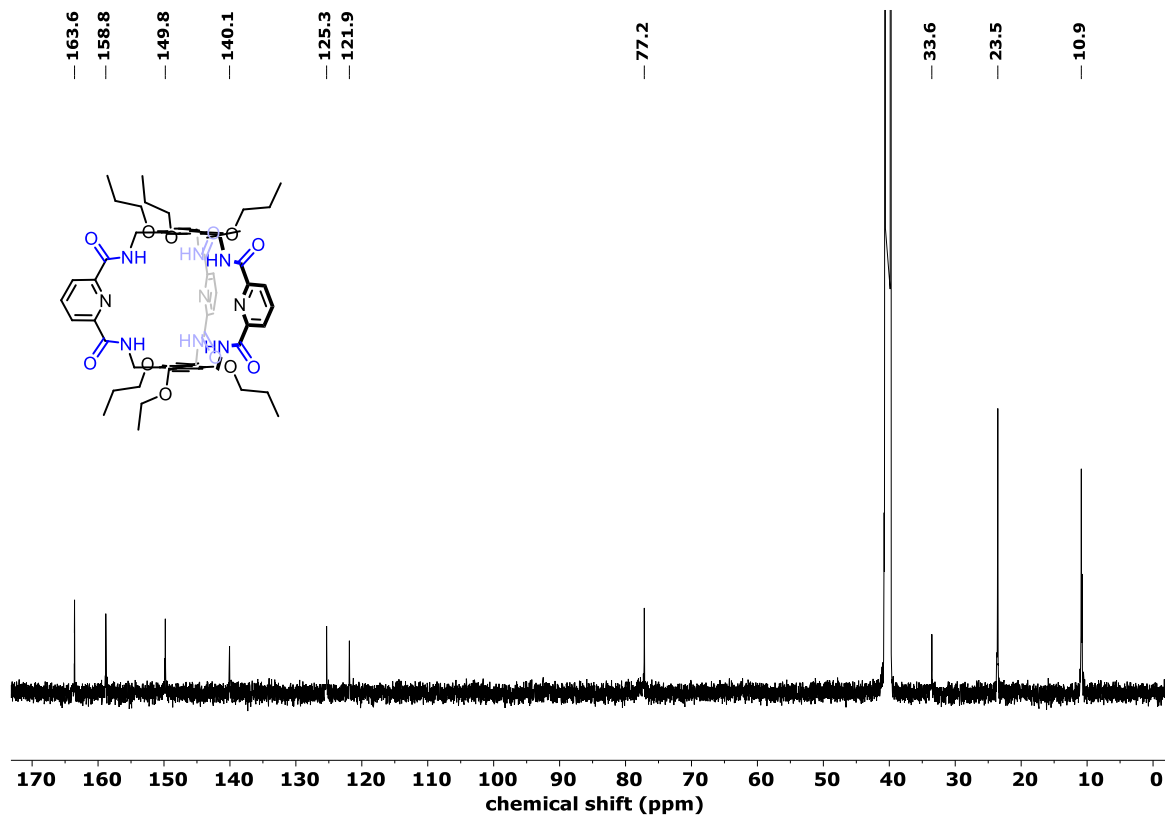
Figure 98. ^{13}C NMR (100 MHz, DMSO-d$_6$) spectrum of amide cage **B63-amide**.
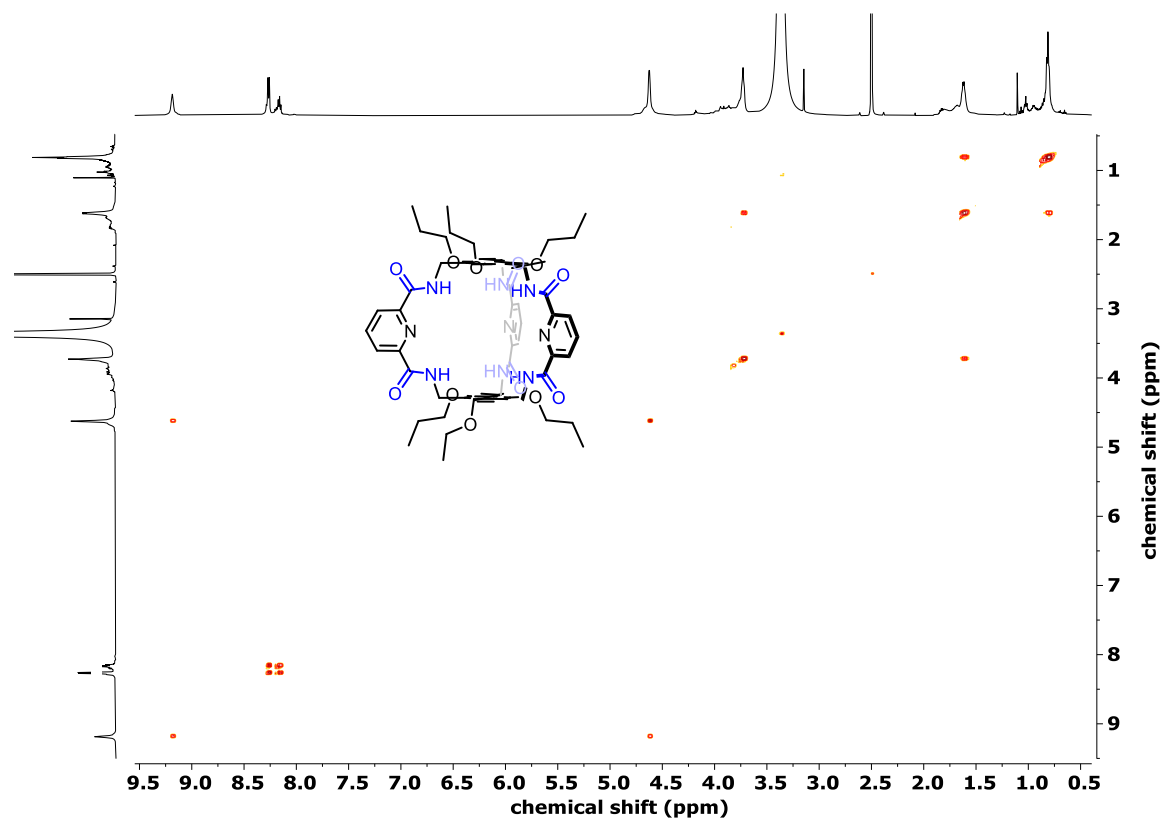
Figure 99. ^{1}H-^{1}H (600 MHz, 600 MHz) COSY NMR spectrum of amide cage **B63-amide**.
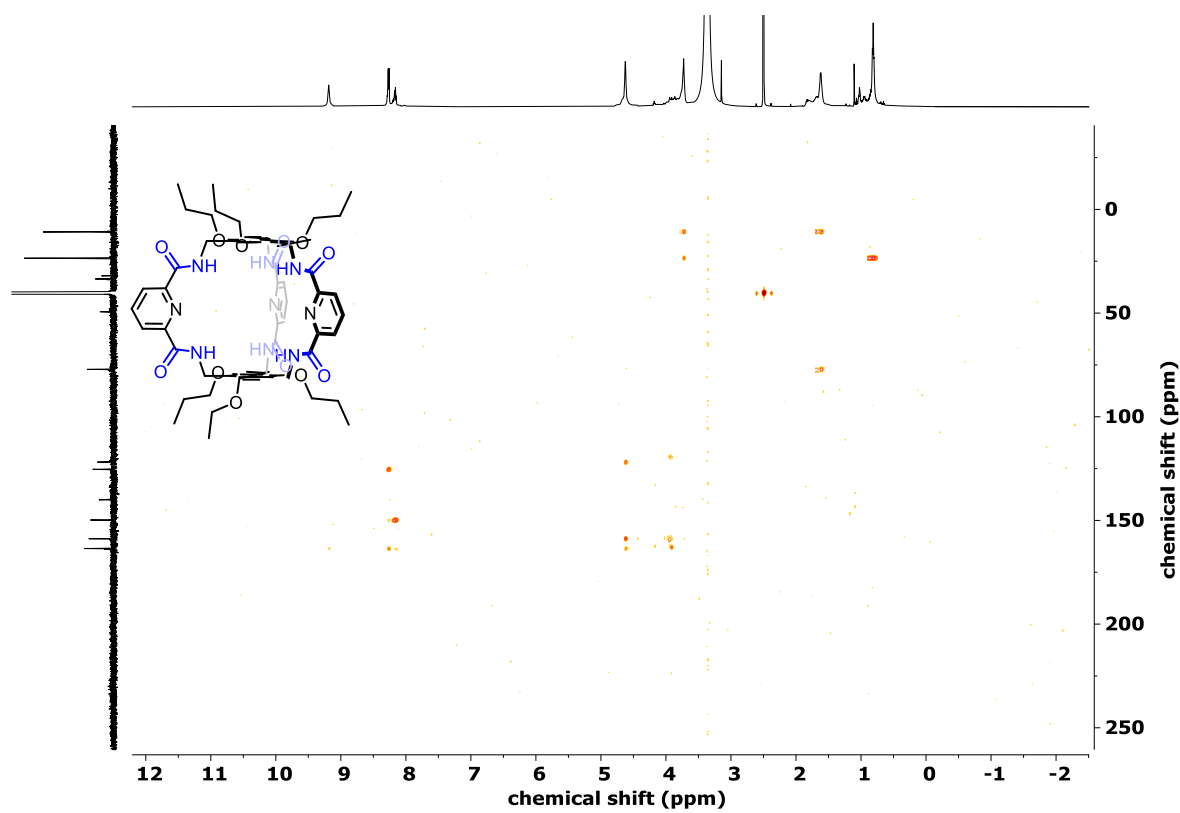
Figure 100. ^{1}H-^{13}C HMBC (600 MHz, 100 MHz) NMR spectrum of amide cage **B63-amide**.
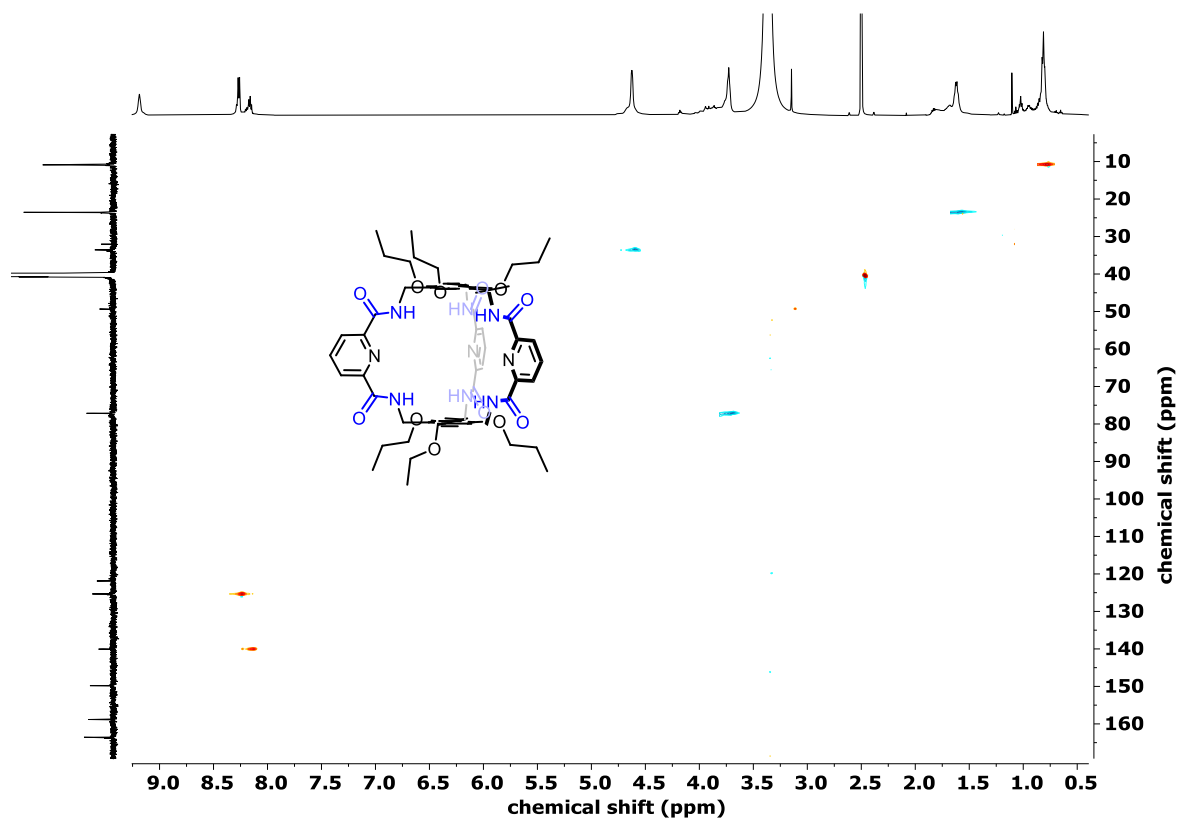
Figure 101. ^{1}H-^{13}C (600 MHz, 100 MHz) HSQC NMR spectrum of amide cage **B63-amide**.
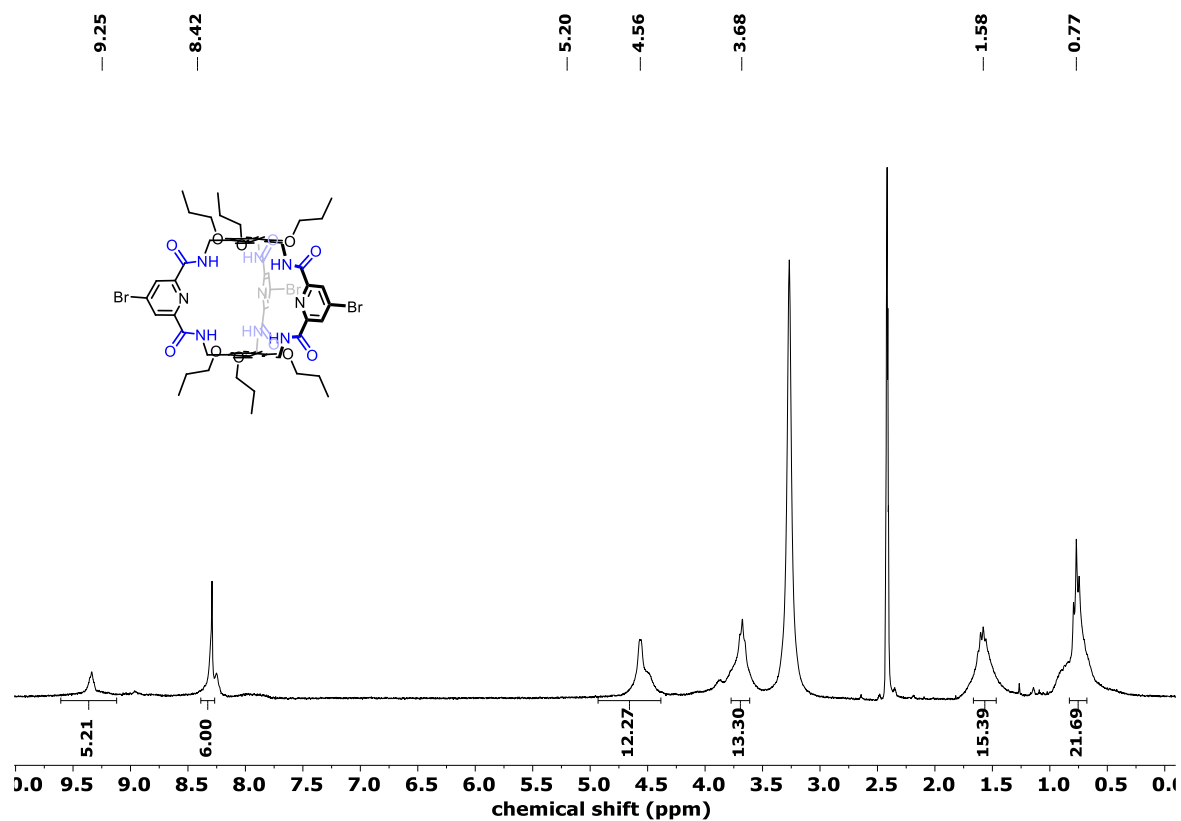
Figure 102. ^{1}H NMR (600 MHz, DMSO-d$_6$) spectrum of amide cage **B65-amide**.
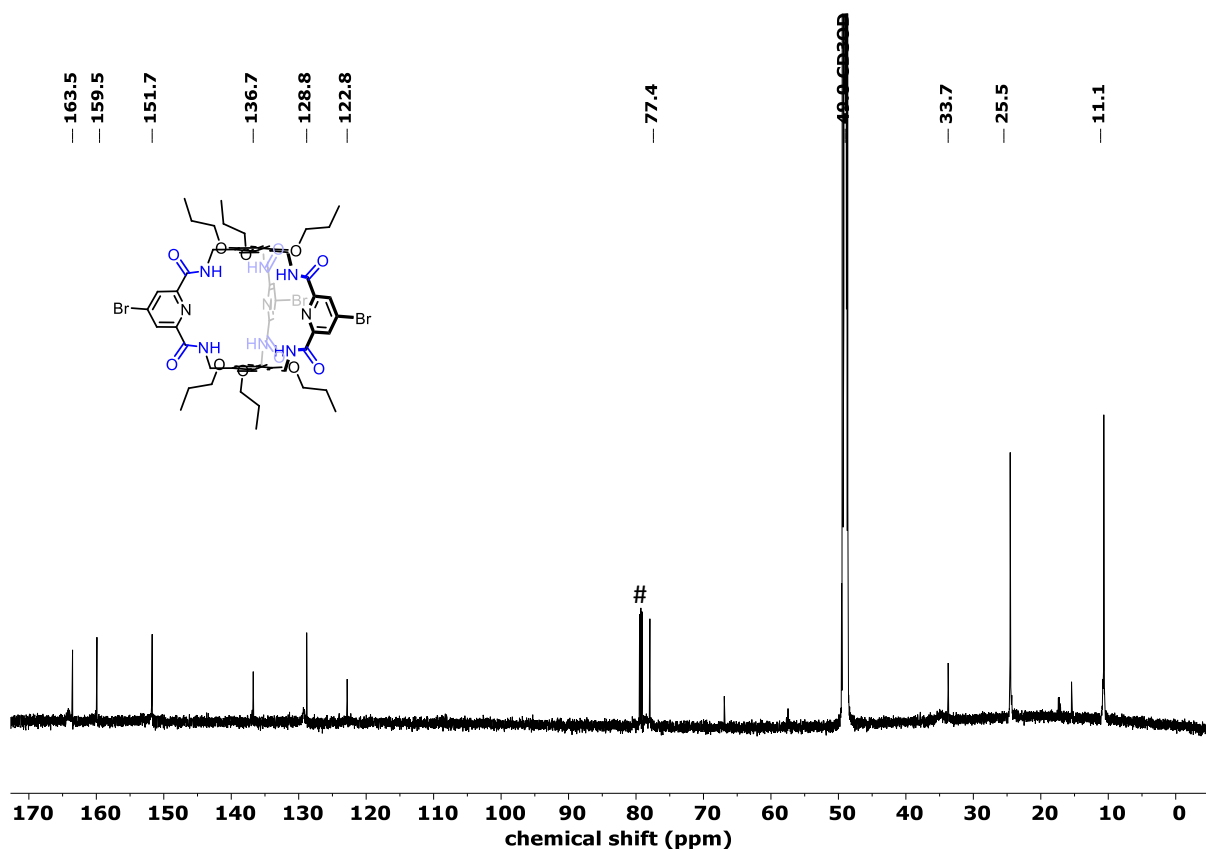
Figure 103. ^{1}H NMR (150 MHz, CD$_3$OD) spectrum of amide cage **B65-amide**. #- denotes residual chloroform.
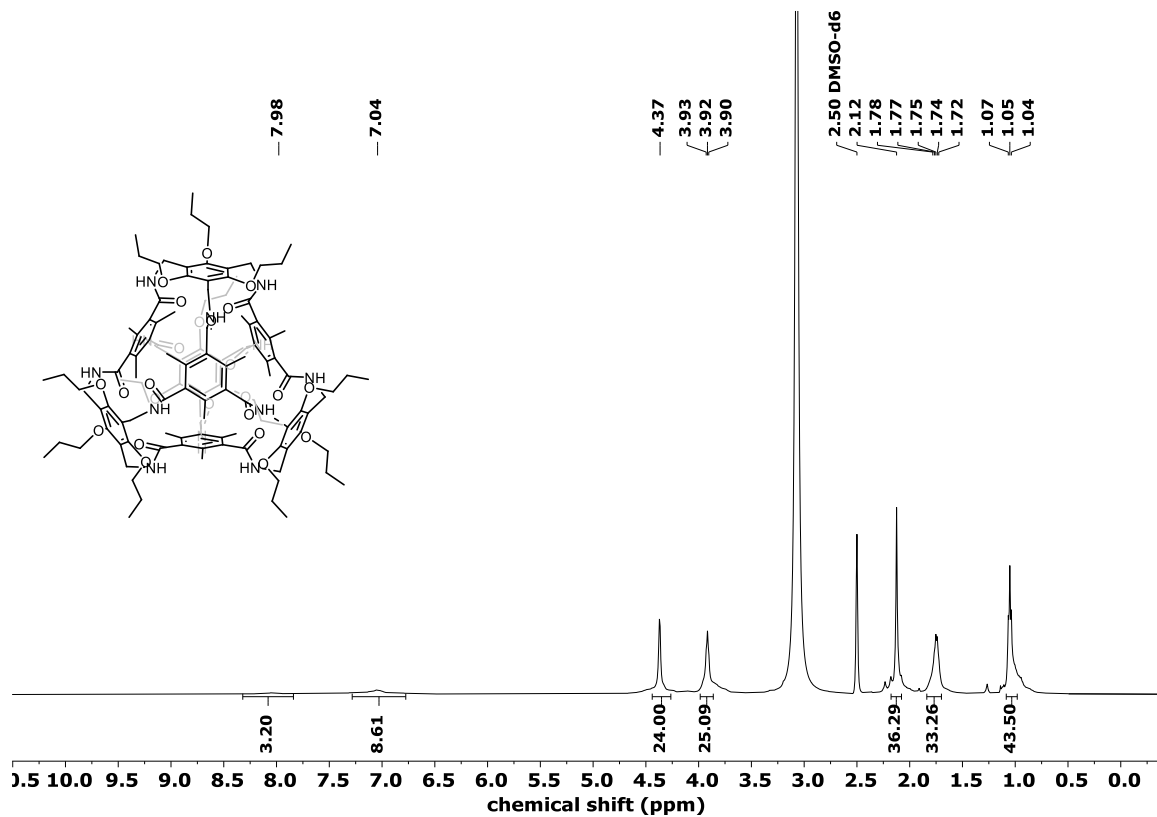
Figure 104. ^{1}H NMR (600 MHz, DMSO-d$_6$) spectrum of amide cage **B73-amide**.

185
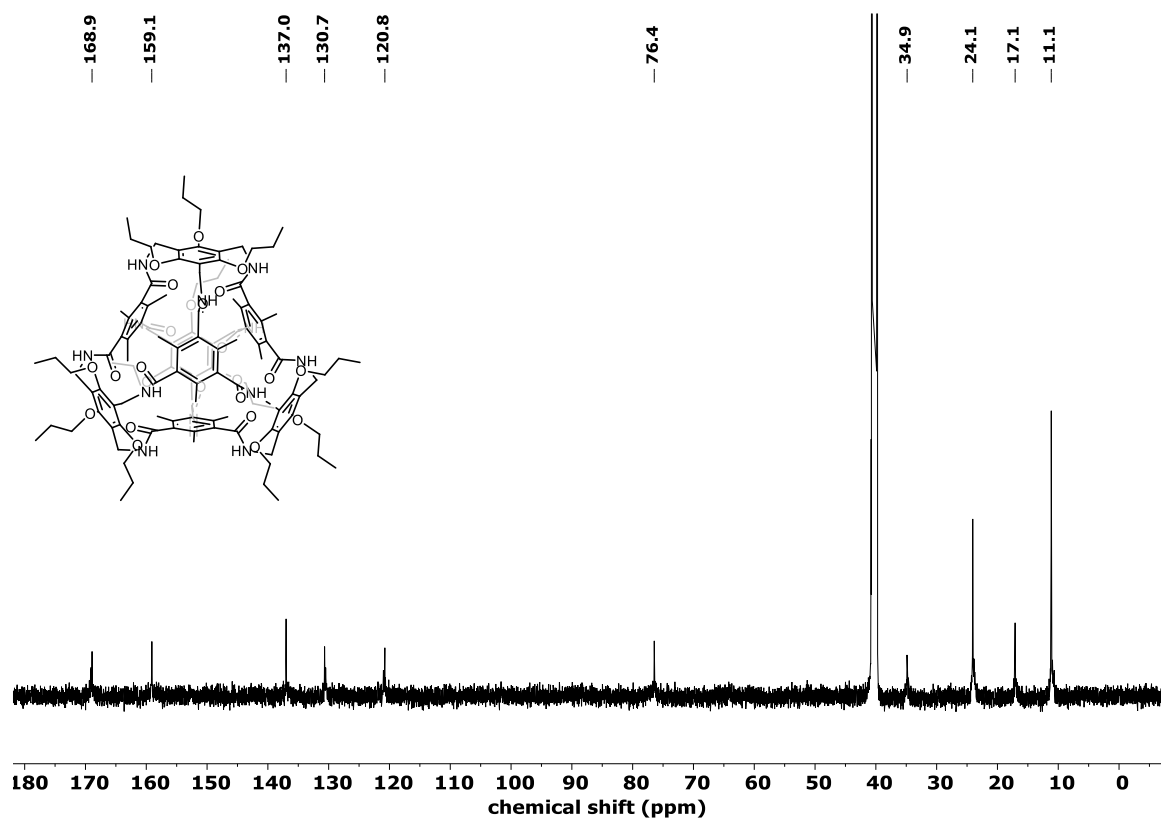
Figure 105. ^{13}C NMR (100 MHz, DMSO-d_6) spectrum of amide cage **B73-amide**.
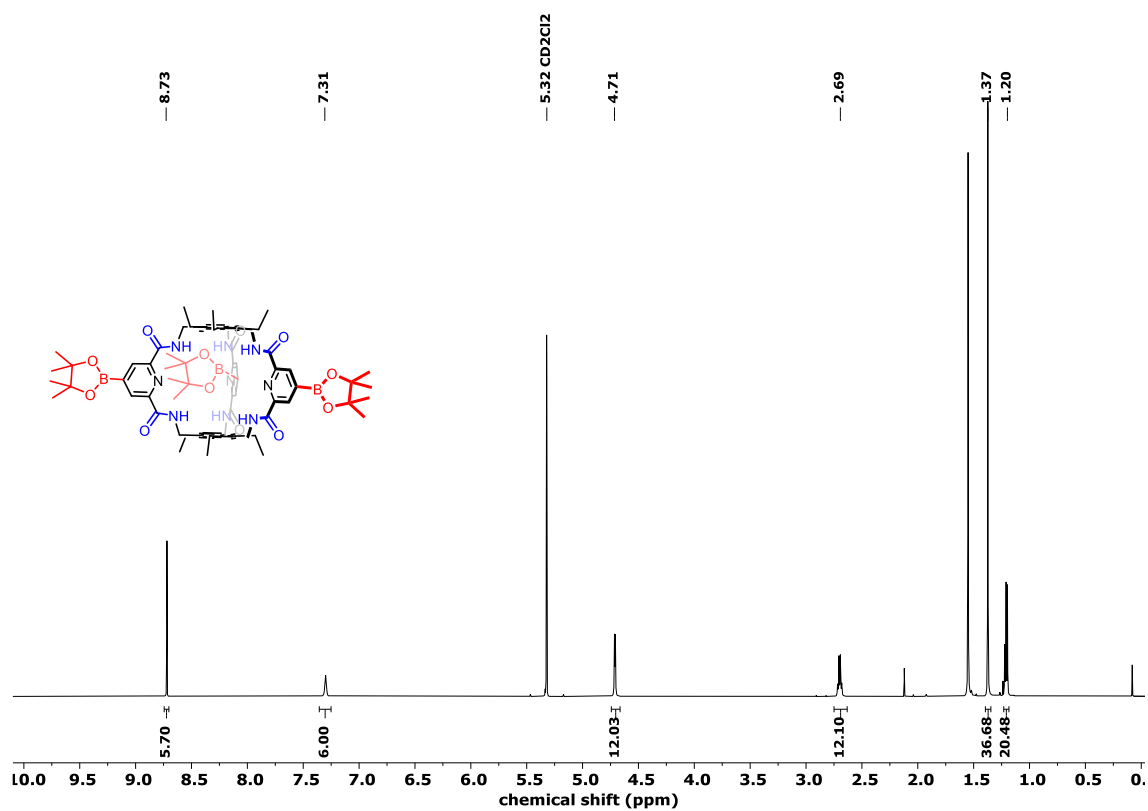
Figure 106. ^{1}H NMR (600 MHz, CD$_2$Cl$_2$) spectrum of amide cage **74**.
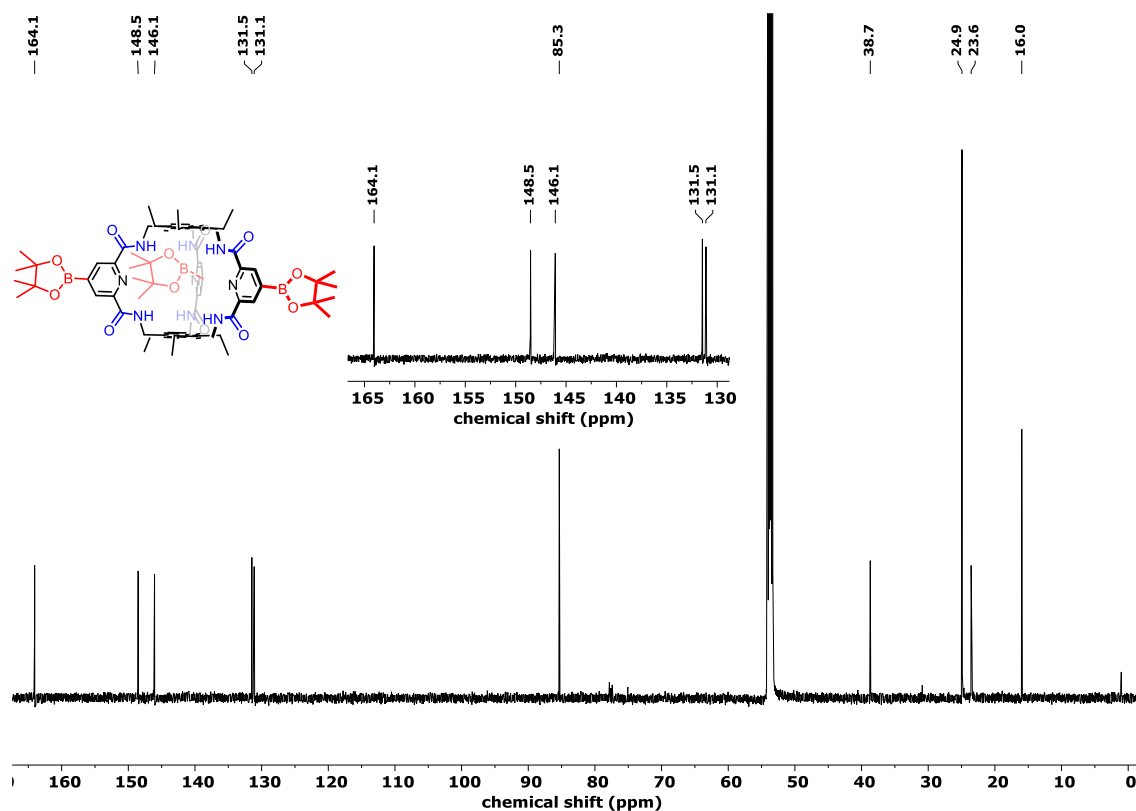
Figure 107. ^{13}C NMR (100 MHz, CD$_2$Cl$_2$) spectrum of amide cage **74**.
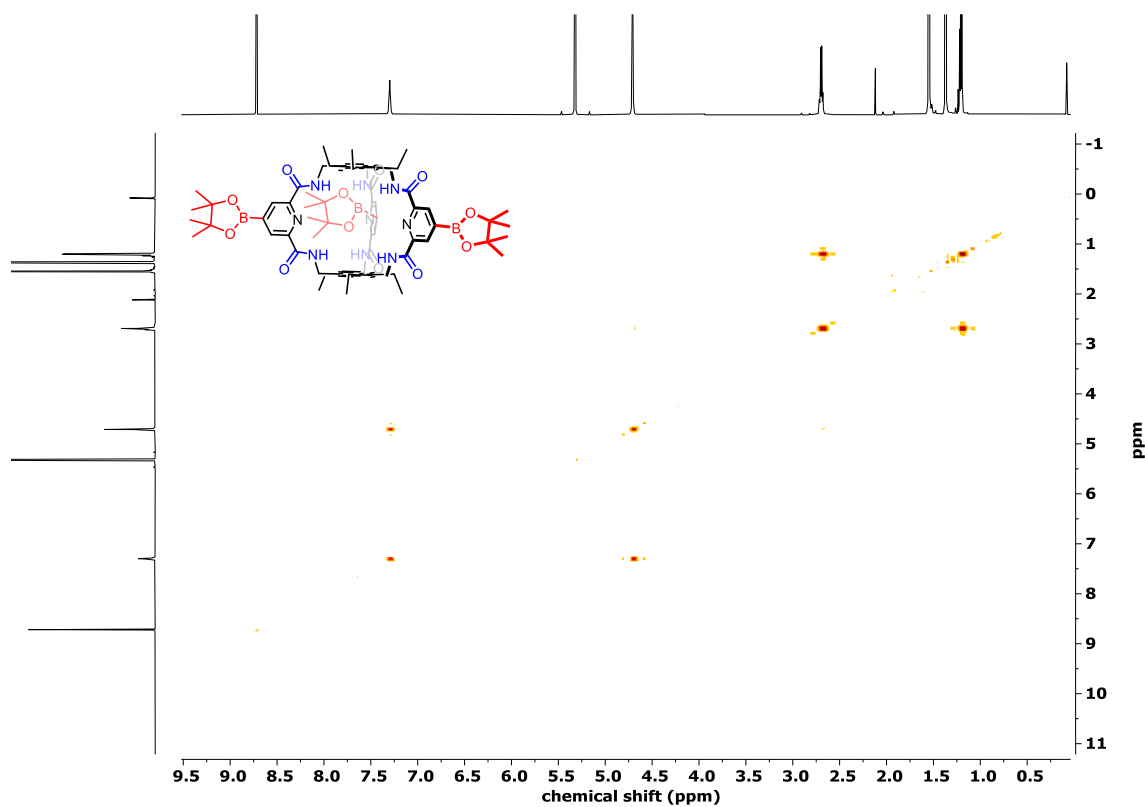
Figure 108. ^{1}H-^{1}H (600 MHz, 600 MHz) COSY NMR spectra of amide cage **74**.
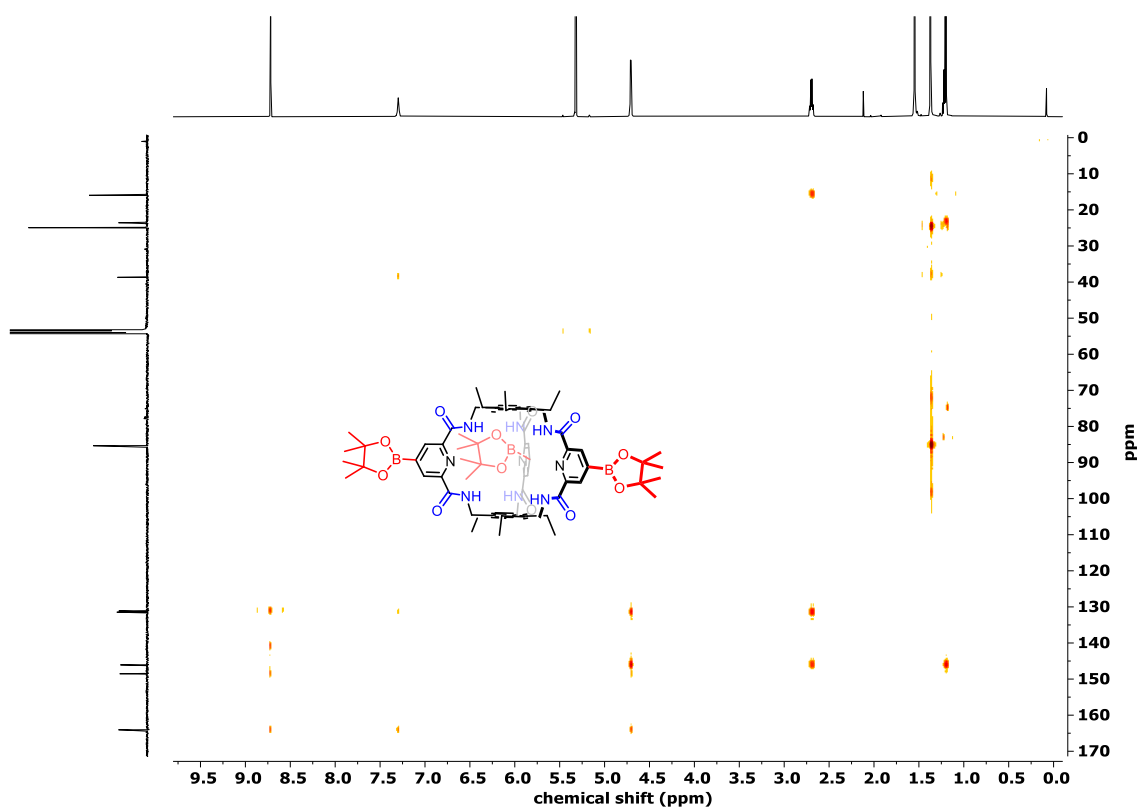
Figure 109. ^{1}H-^{13}C (600 MHz, 100 MHz) HMBC NMR spectrum of amide cage **74**.
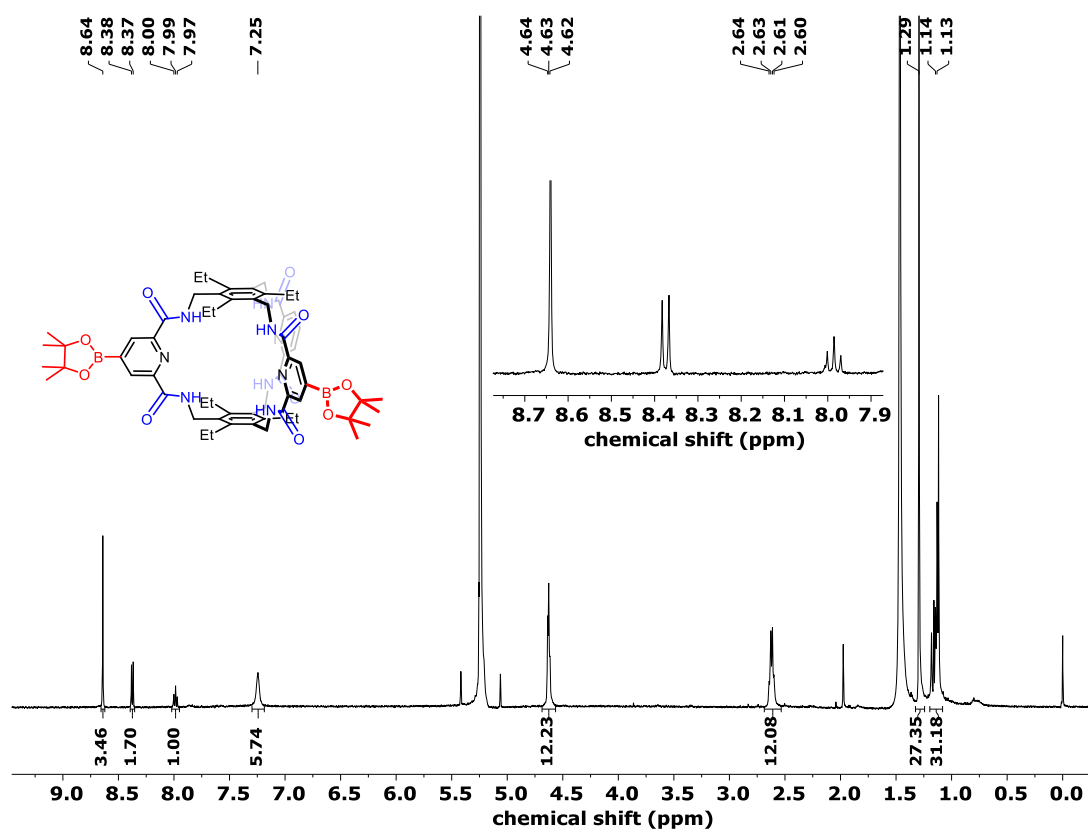
Figure 110. ^{1}H NMR (500 MHz, CD$_2$Cl$_2$) spectrum of the two-fold borylated amide cage **74a**.
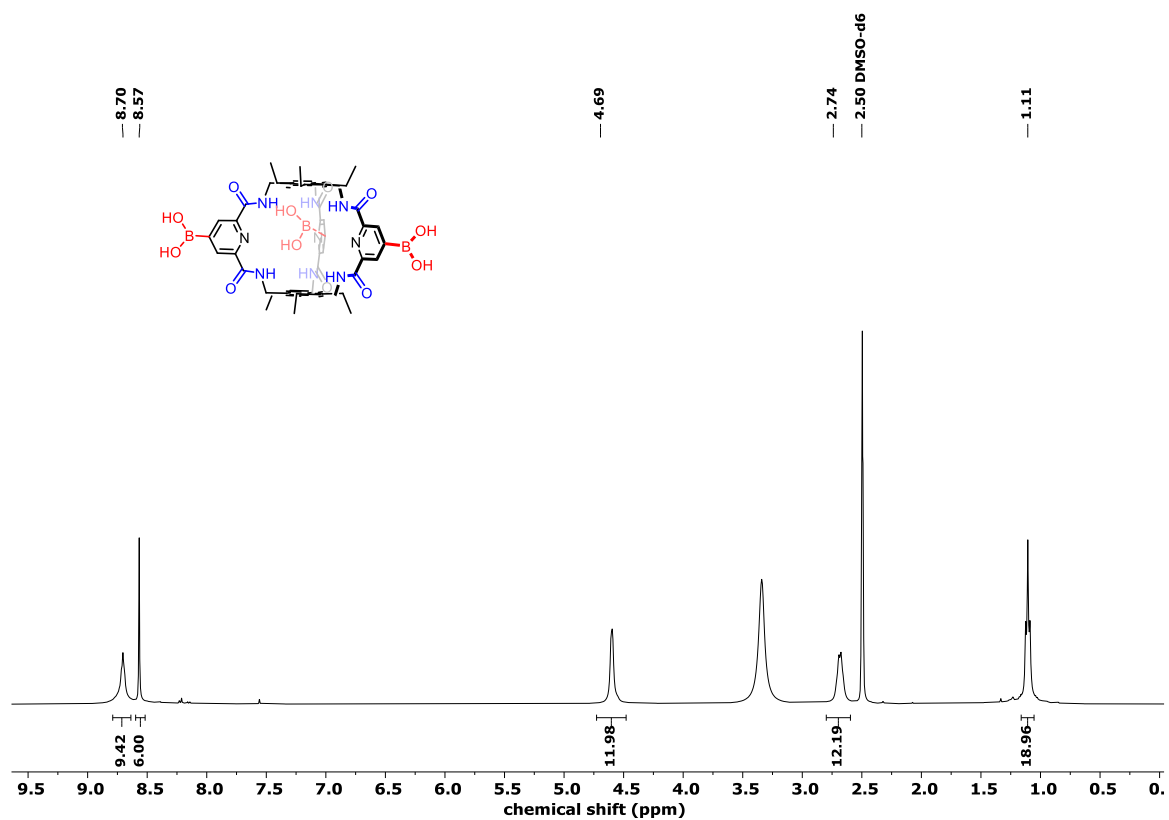
Figure 111. ^{1}H NMR (400 MHz, DMSO-d$_6$) spectrum of amide cage **75**.
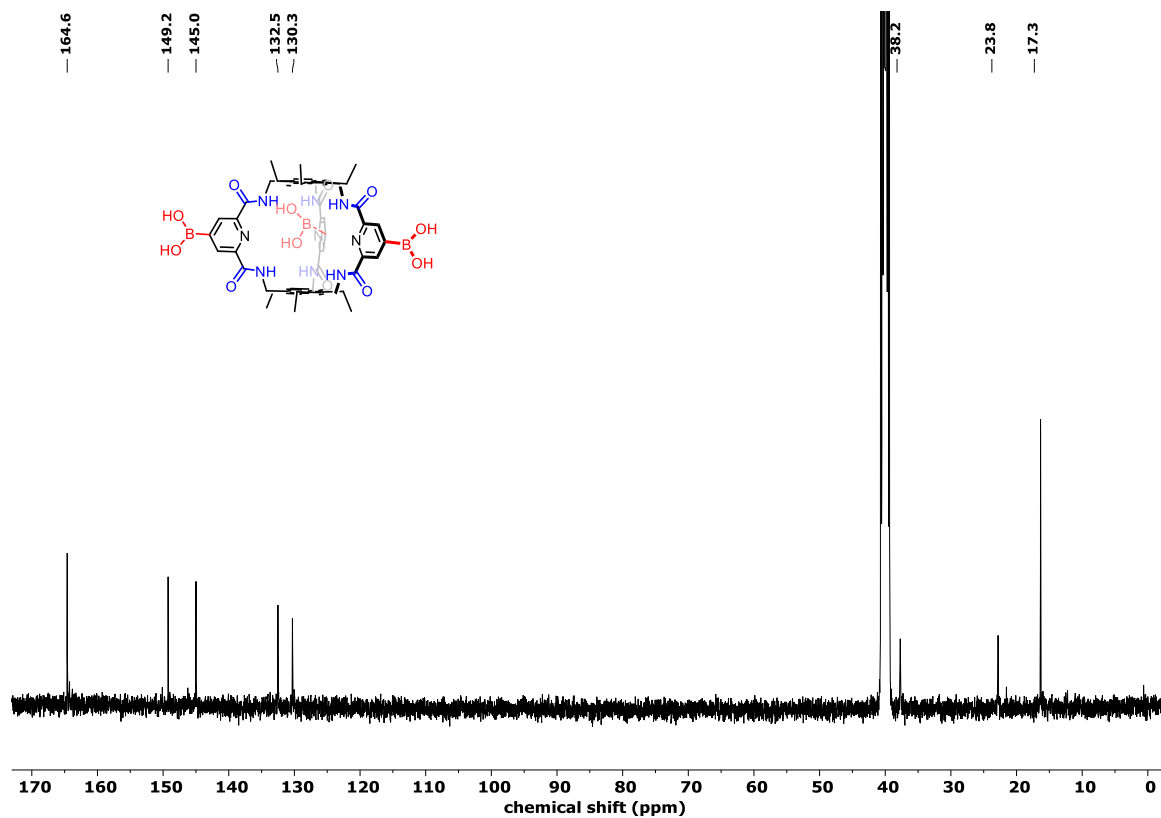
Figure 112. ^{13}C NMR (100 MHz, DMSO-d$_6$) spectrum of amide cage **75**.
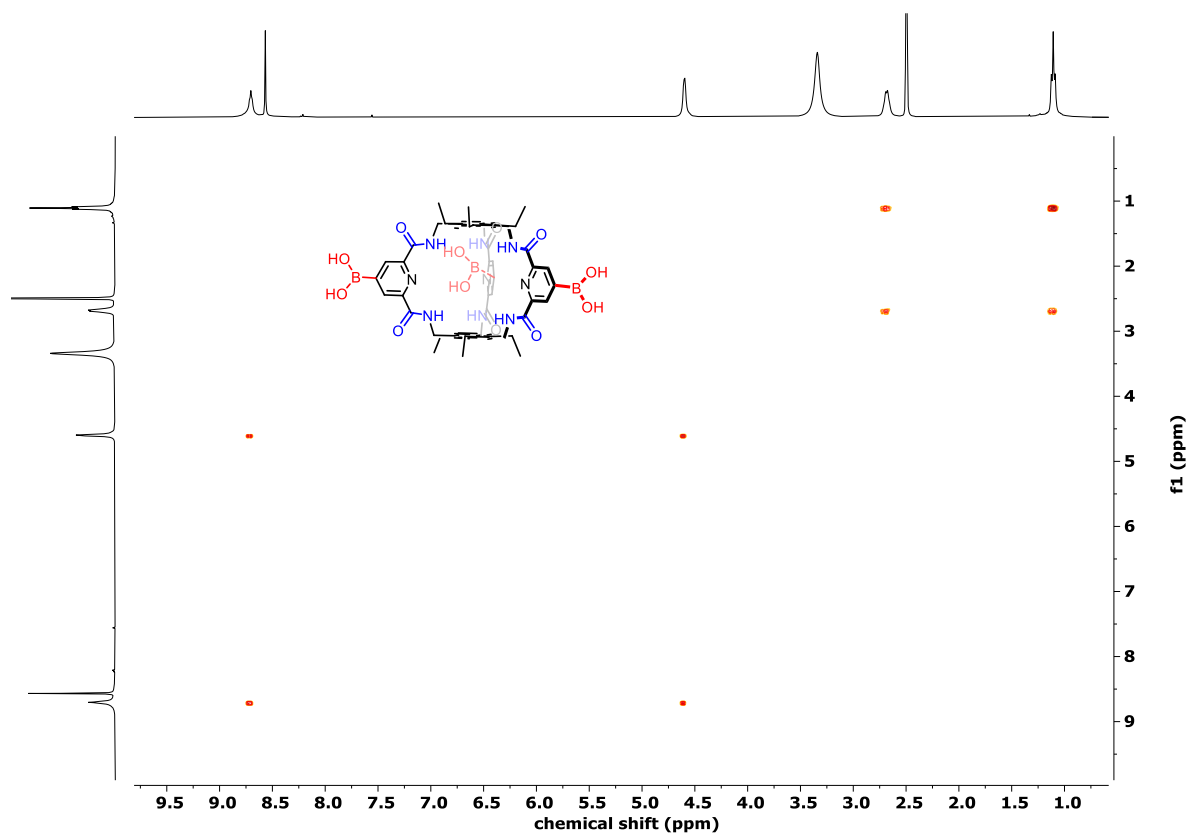
Figure 113. ^{1}H-^{1}H (400 MHz, 100 MHz) COSY NMR spectrum of amide cage **75**.
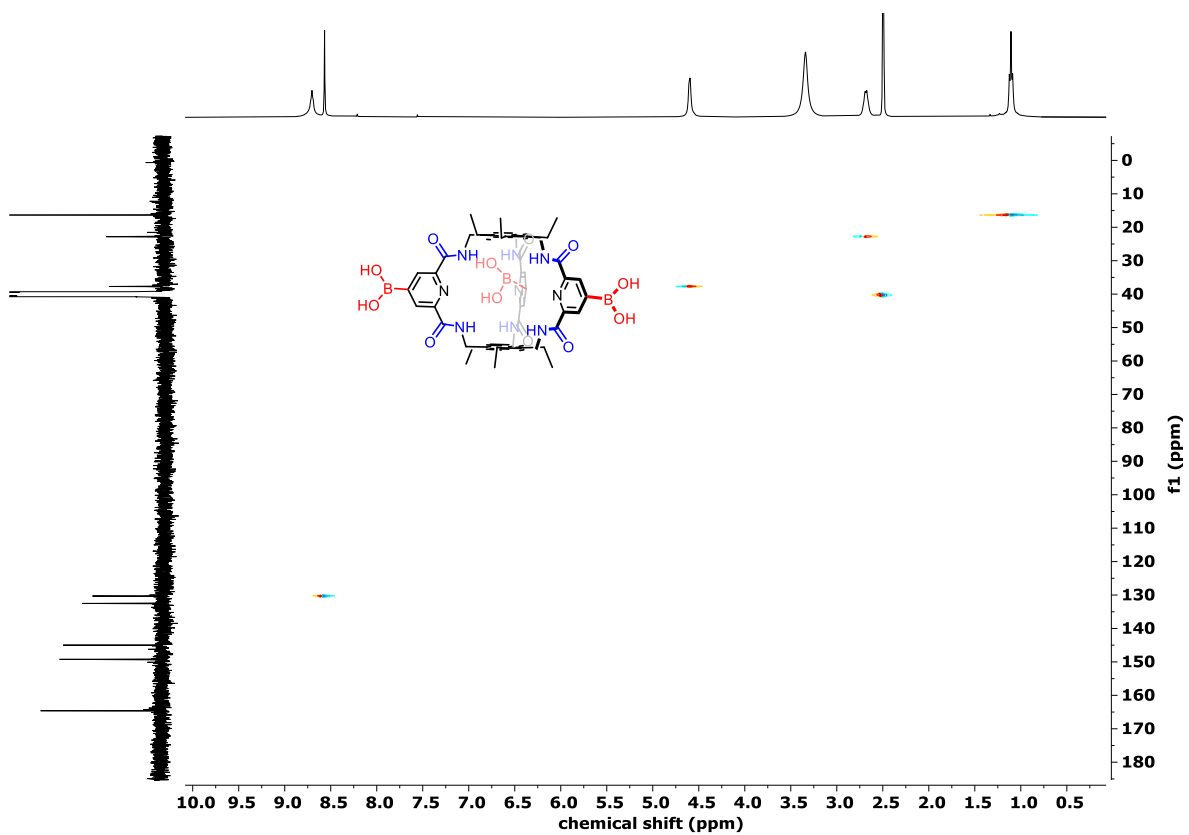
Figure 114. ^{1}H-^{13}C (600 MHz, 100 MHz) HSQC NMR spectrum of amide cage **75**.
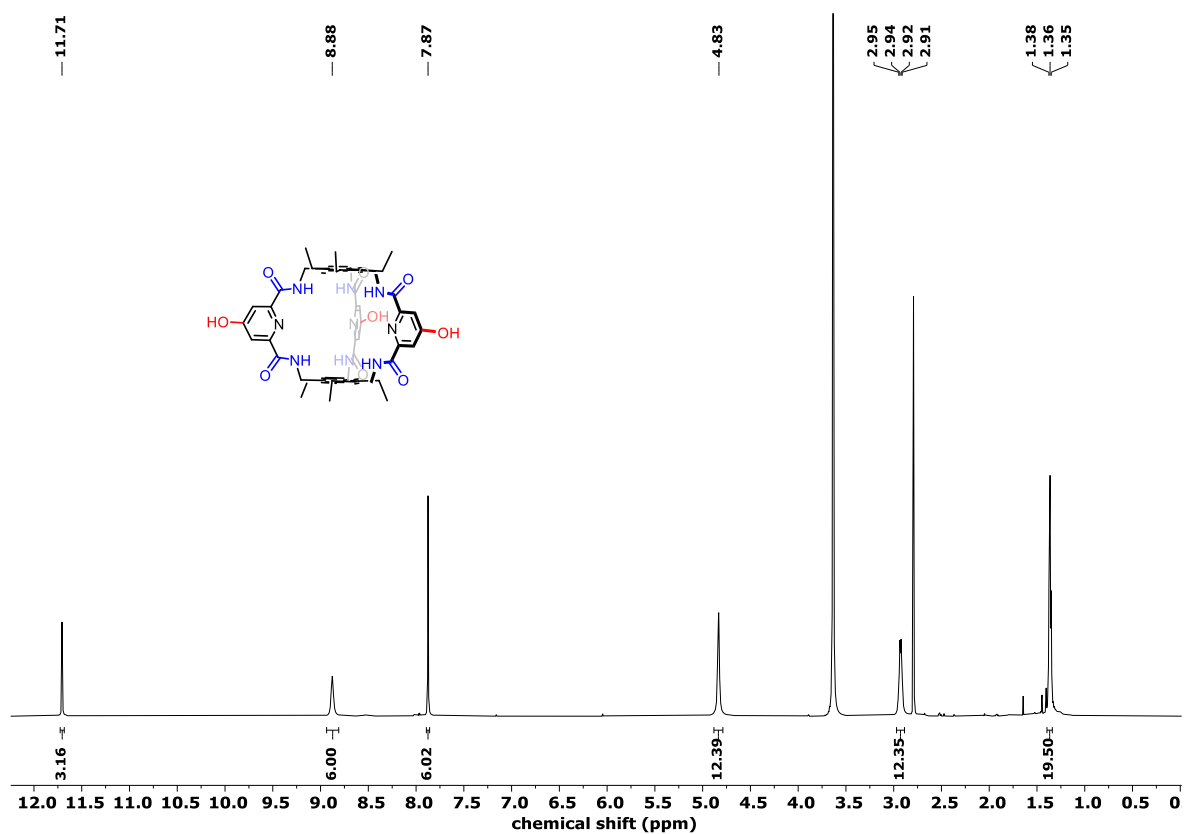
Figure 115. ^{1}H NMR (600 MHz, DMSO-d$_6$) spectrum of amide cage **76**.
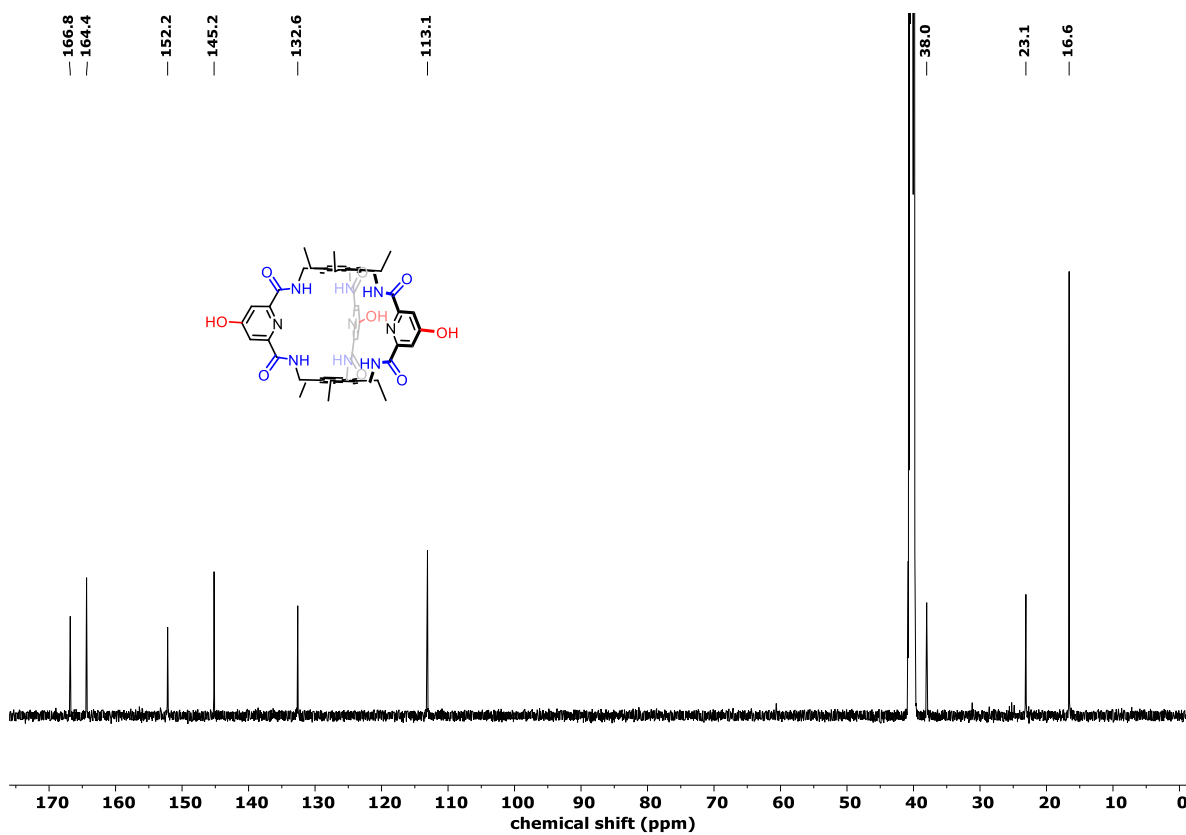
Figure 116. ^{13}C NMR (100 MHz, DMSO-d$_6$) spectrum of amide cage **76**.
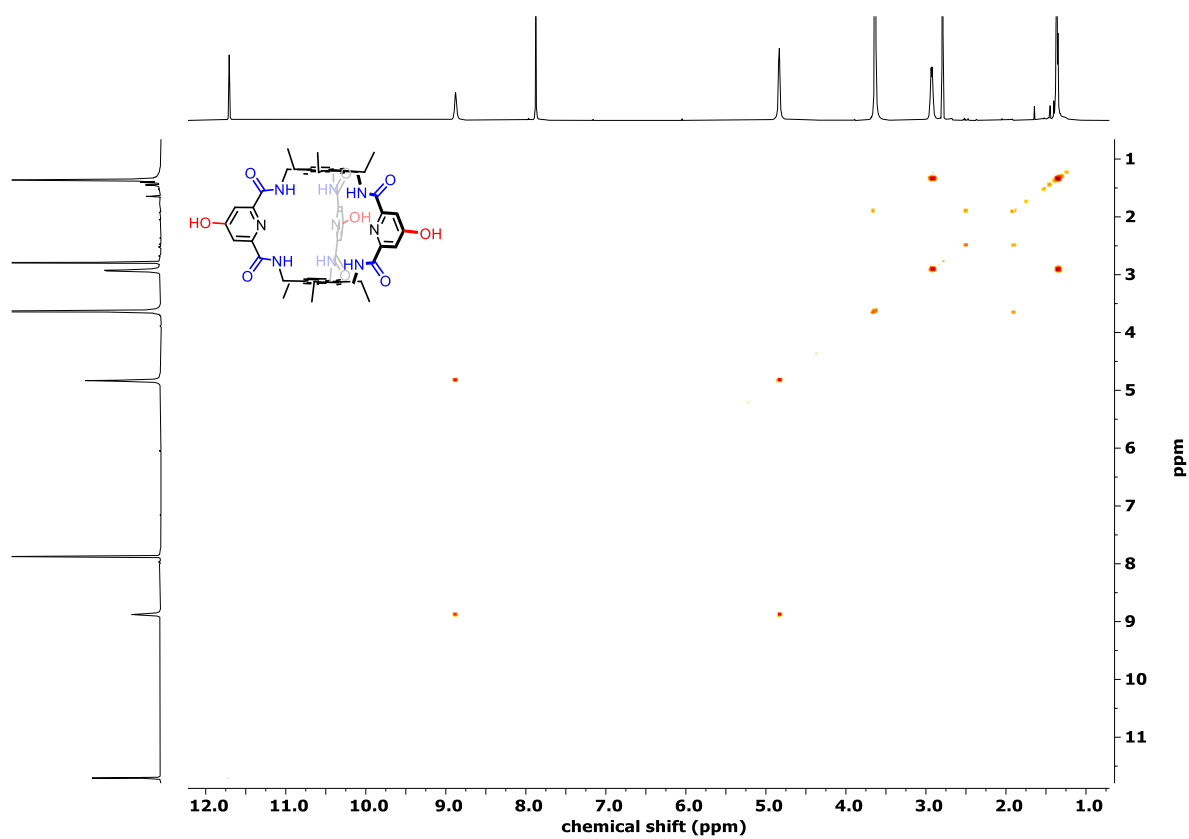
Figure 117. ^{1}H-^{1}H COSY (600 MHz, 600 MHz) NMR spectrum of amide cage **76**.
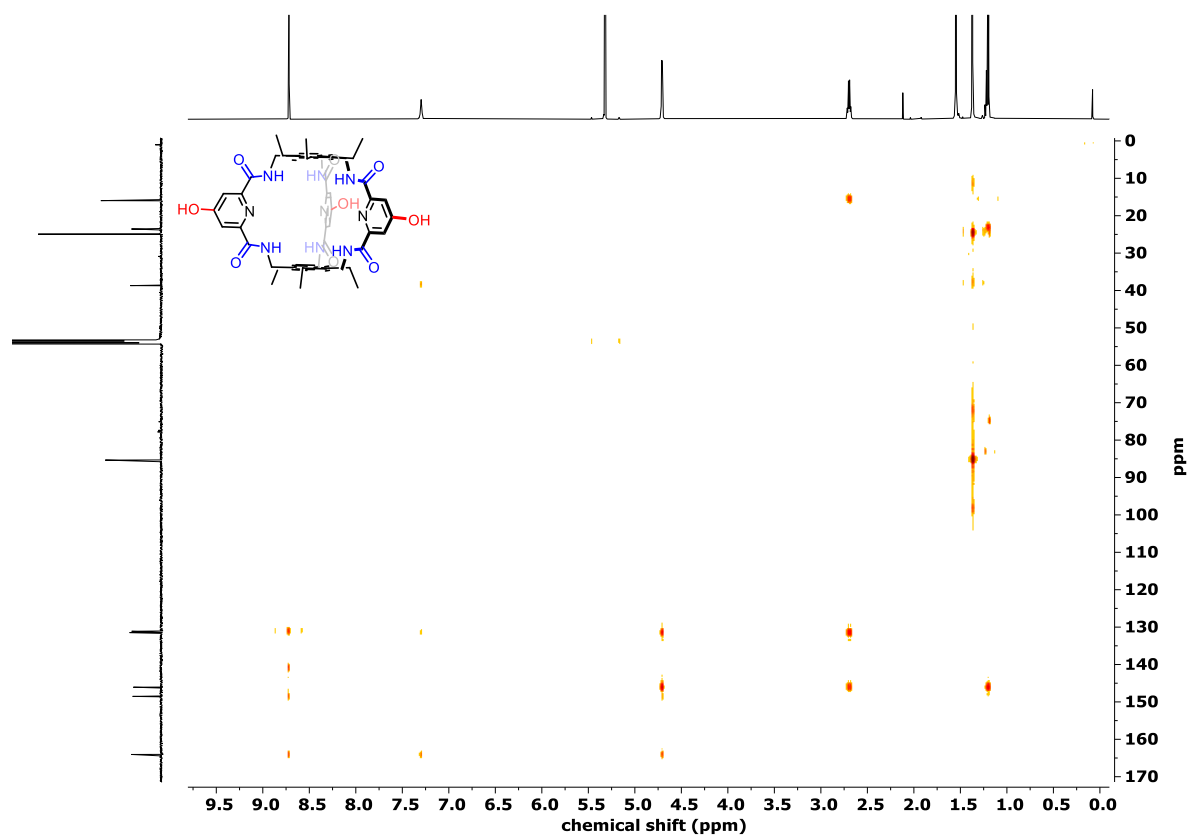
Figure 118. ^{1}H-^{13}C (600 MHz, 100 MHz) HMBC NMR spectrum of amide cage **76**.
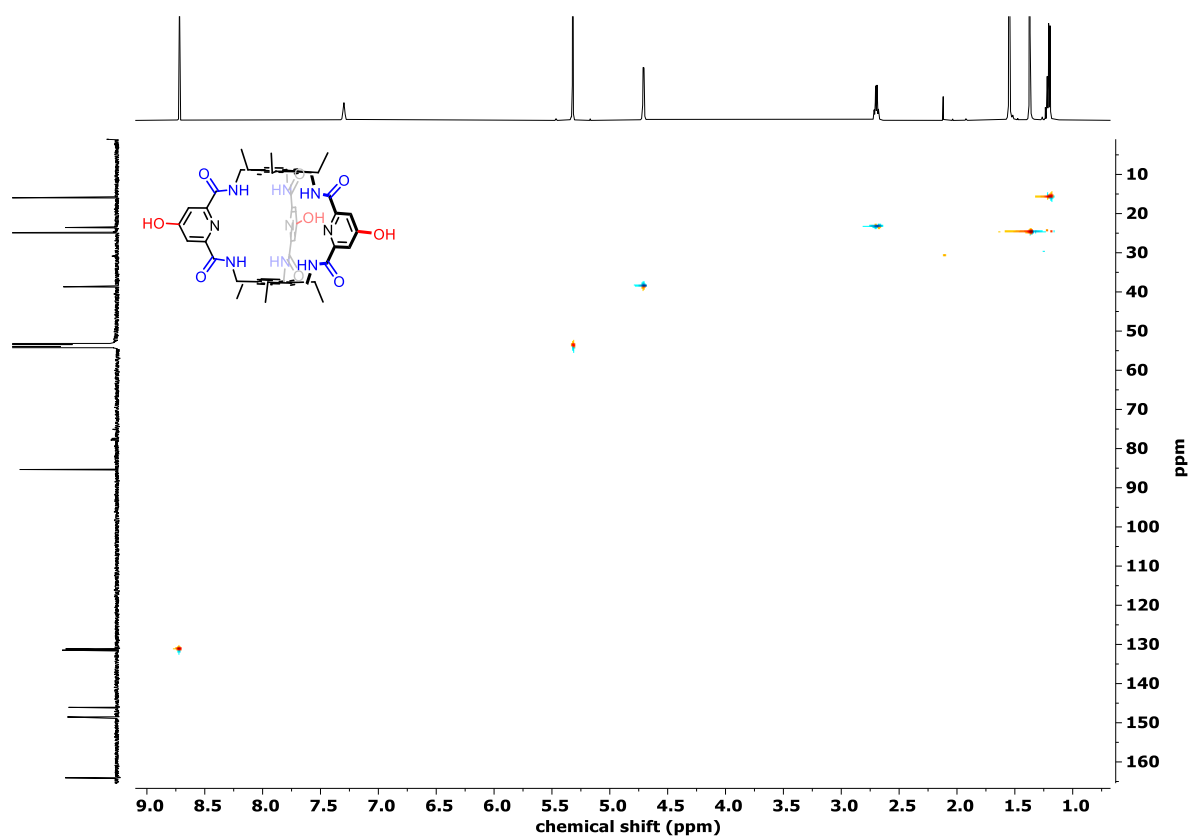
Figure 119. ^{1}H-^{13}C (600 MHz, 100 MHz) HSQC NMR spectrum of amide cage **76**.
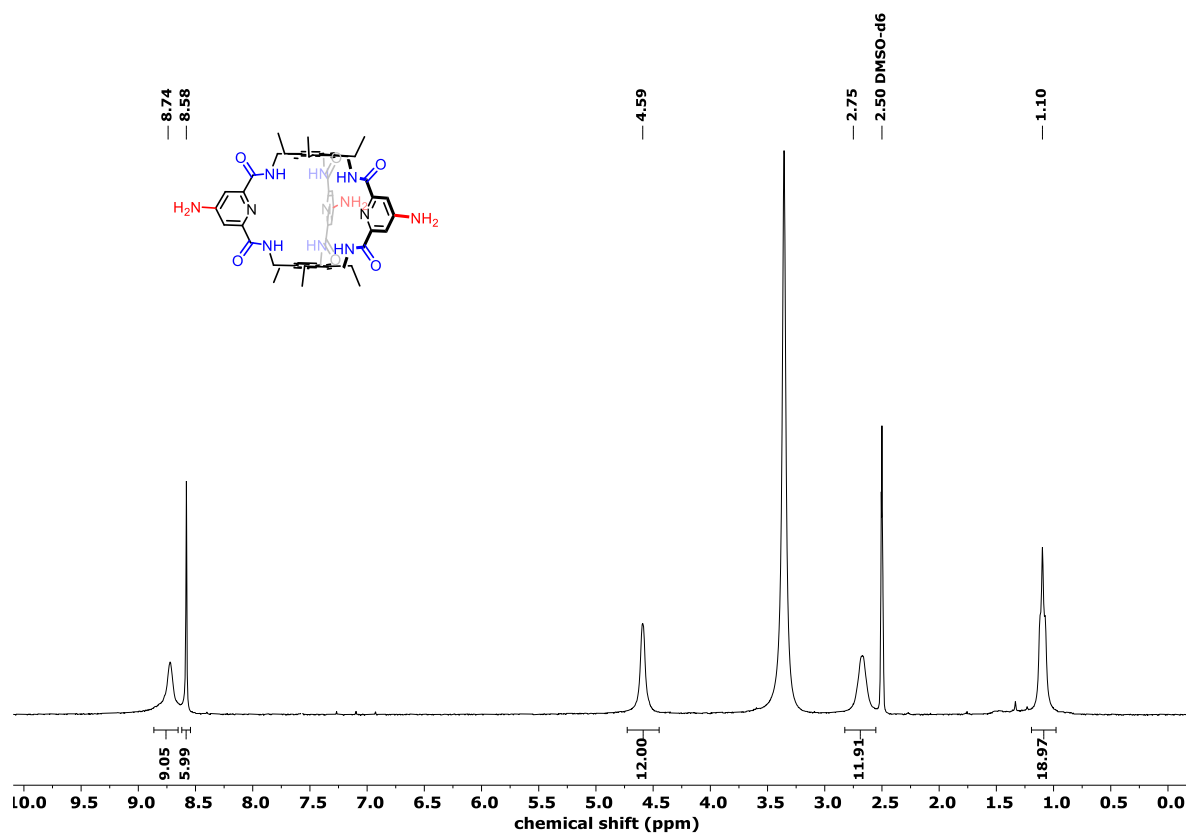
Figure 120. ^{1}H NMR (600 MHz, DMSO-d$_6$) spectrum of amide cage **77**.
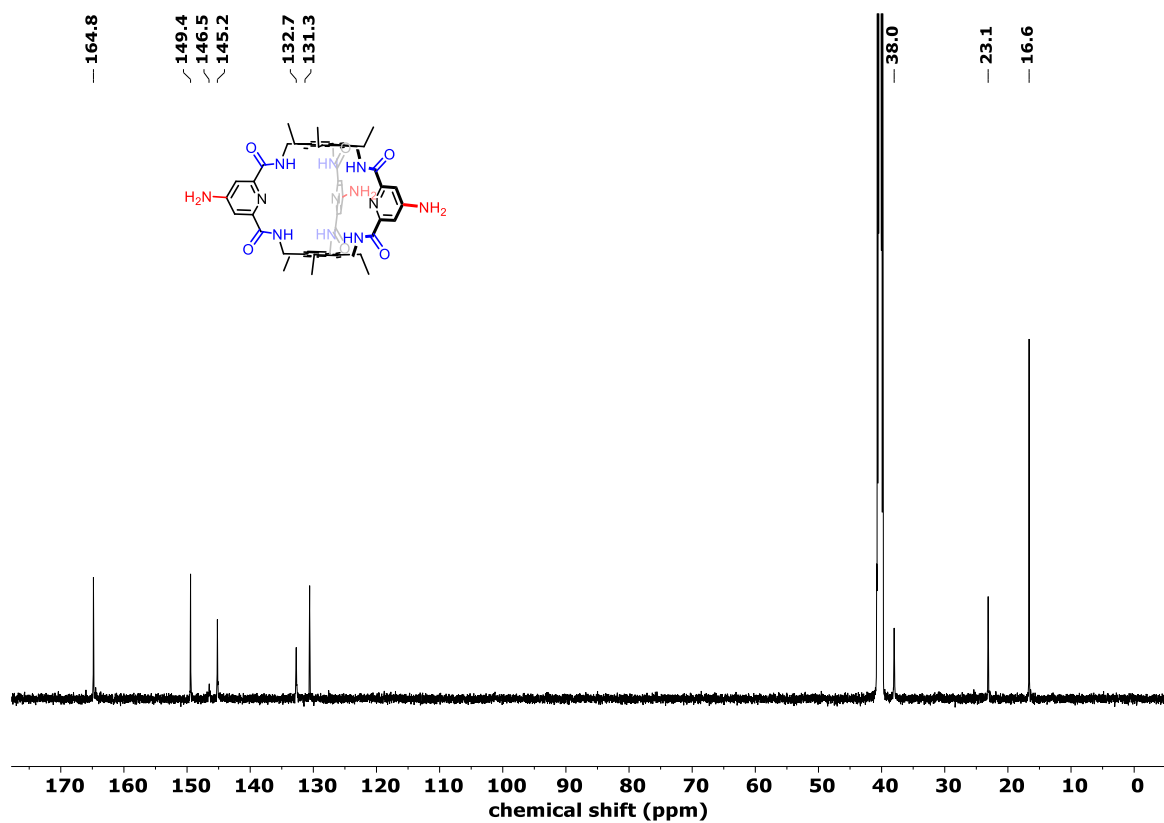
Figure 121. ^{13}C NMR (100 MHz, DMSO-d_6) spectrum of amide cage **77**.
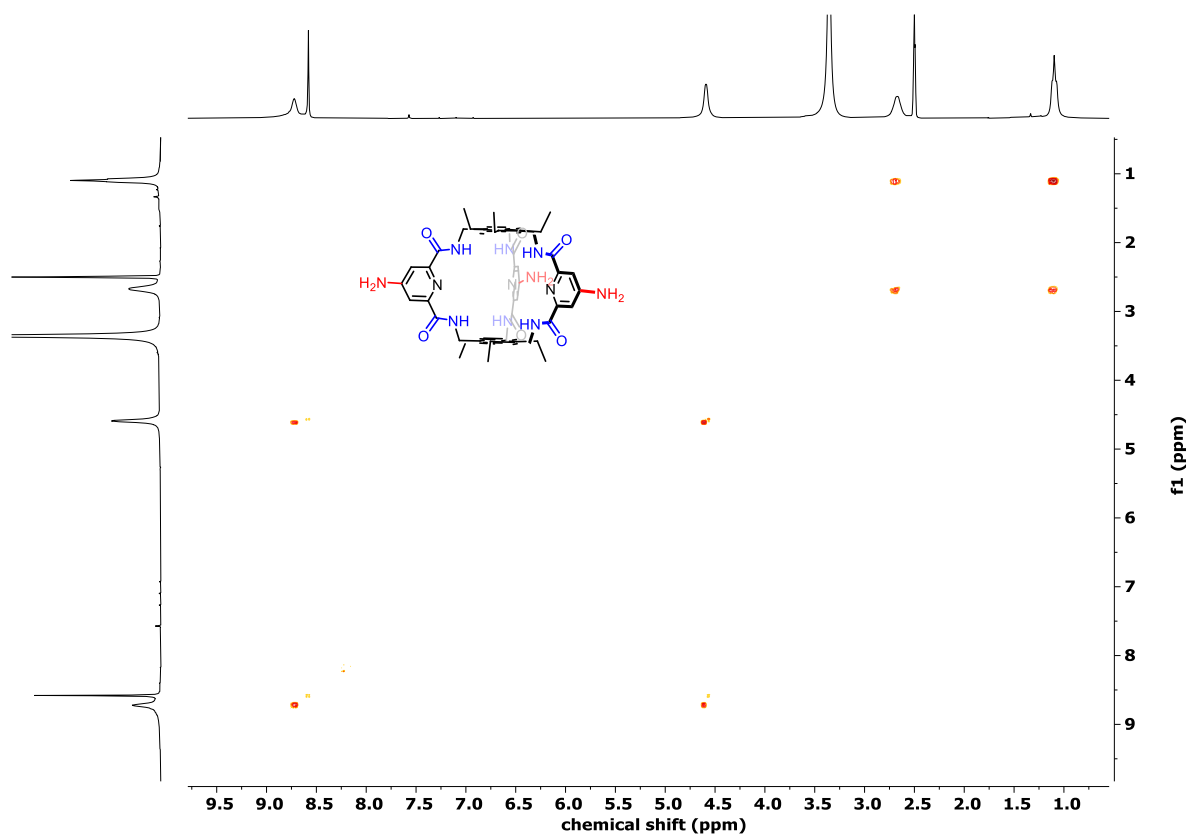
Figure 122. ^1H-^1H (600 MHz, 600 MHz) COSY NMR spectrum of amide cage **77**.
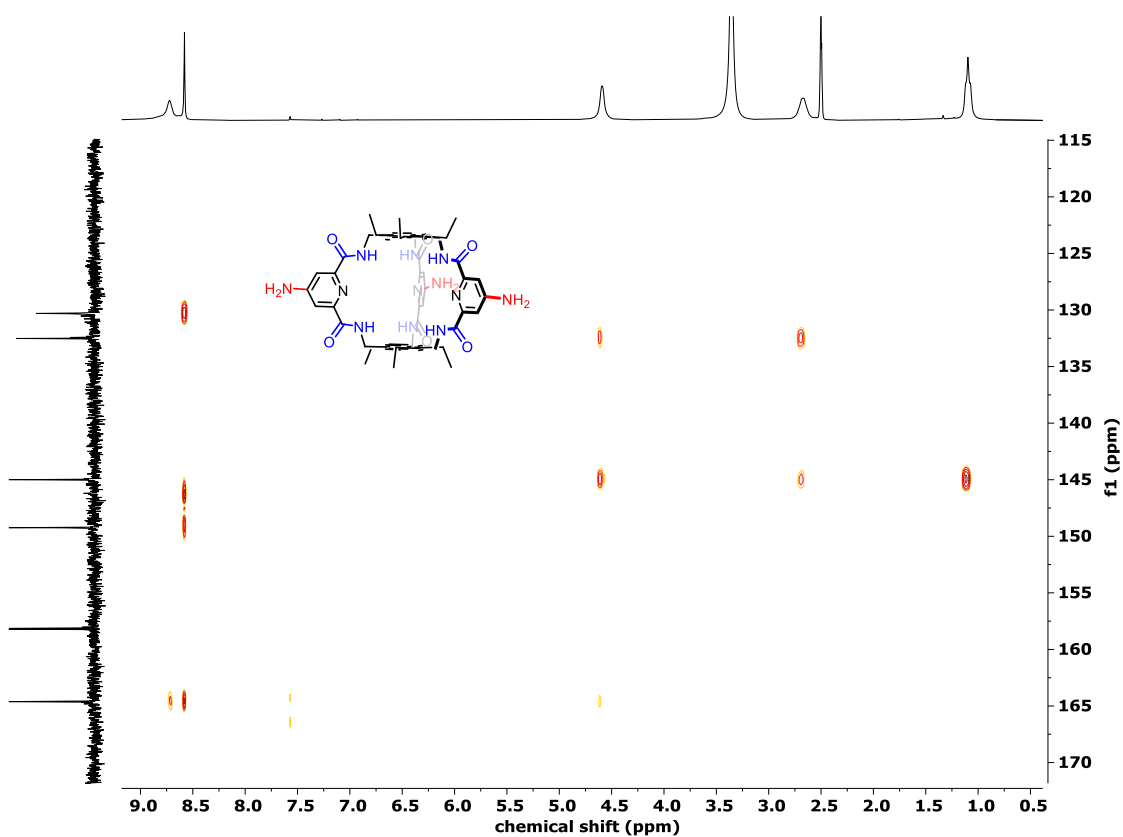
Figure 123. ^{1}H-^{13}C (600 MHz, 100 MHz) HMBC NMR spectrum of amide cage **77**.
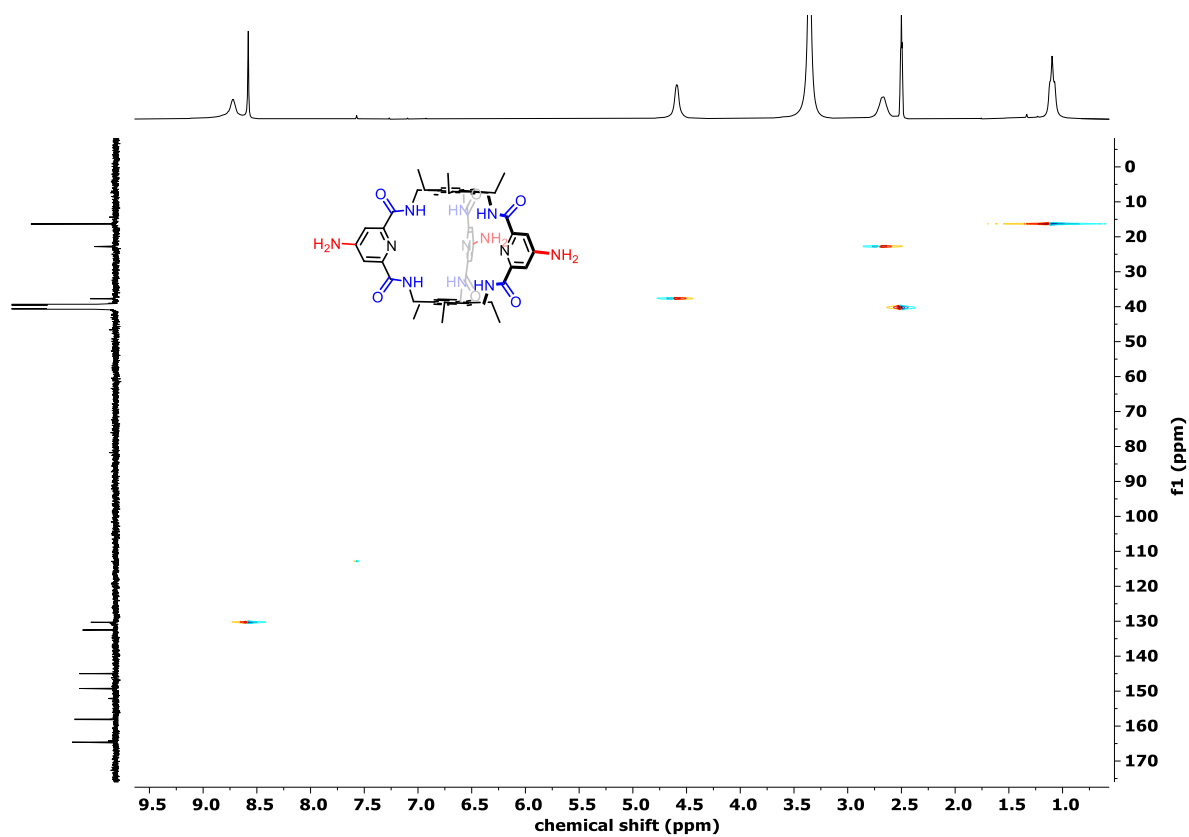
Figure 124. ^{1}H-^{13}C (600 MHz, 100 MHz) HSQC NMR spectrum of amide cage **77**.
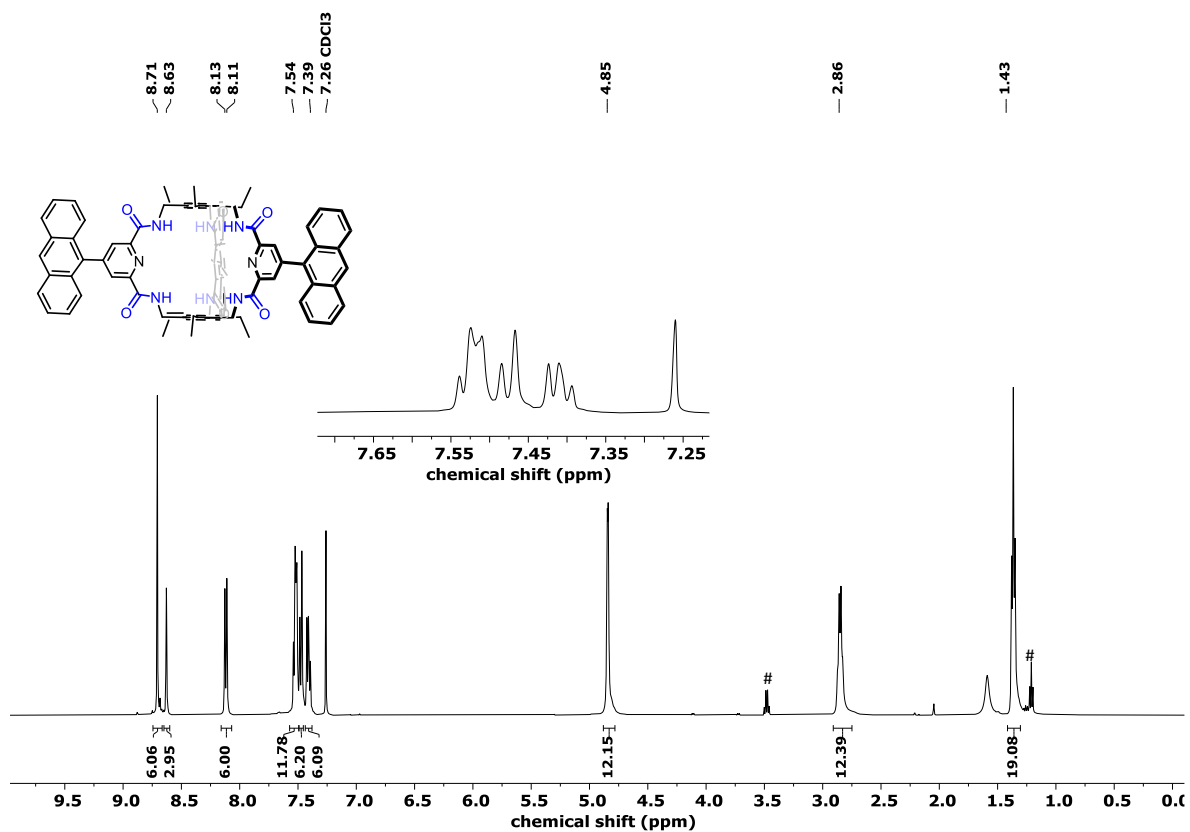
Figure 125. ^{1}H NMR (500 MHz, CDCl$_3$) spectrum of amide cage **78**. # - residual diethyl ether.
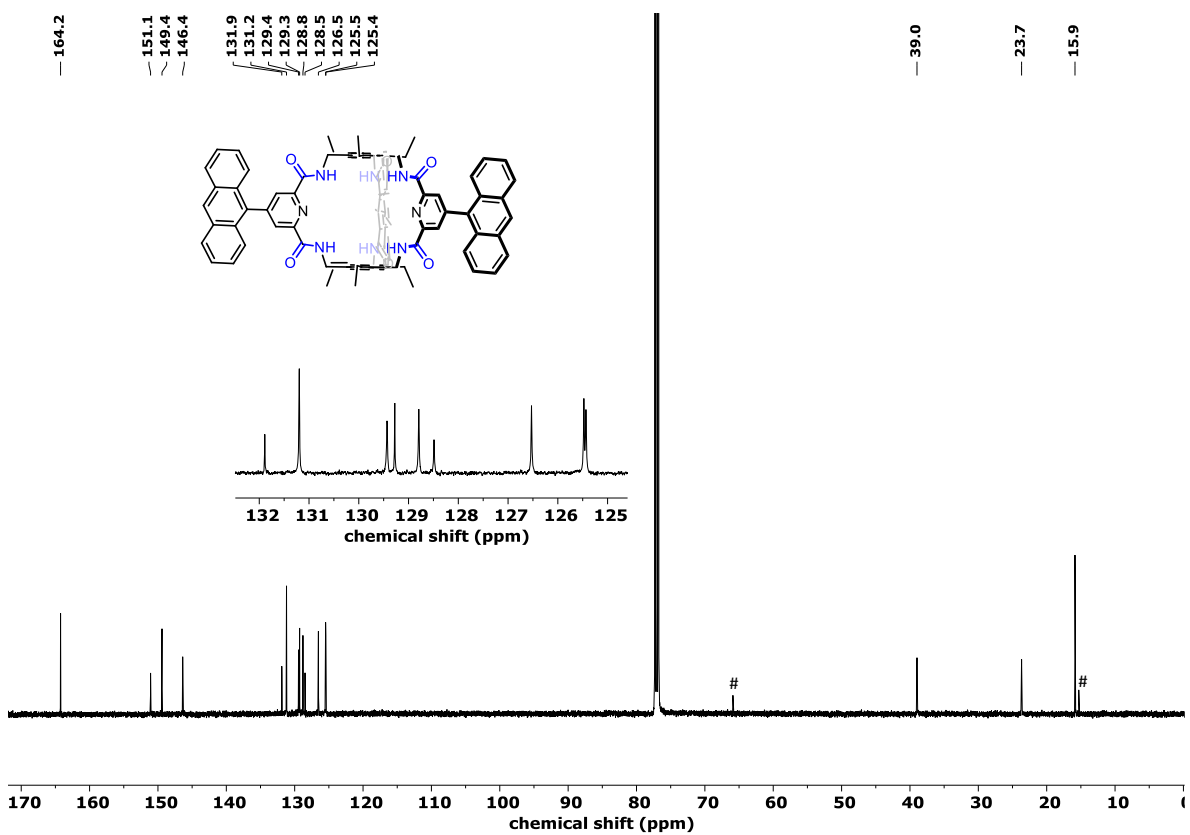
Figure 126. ^{13}C NMR (100 MHz, DMSO-d$_6$) spectrum of amide cage **78**. # - residual diethyl ether.
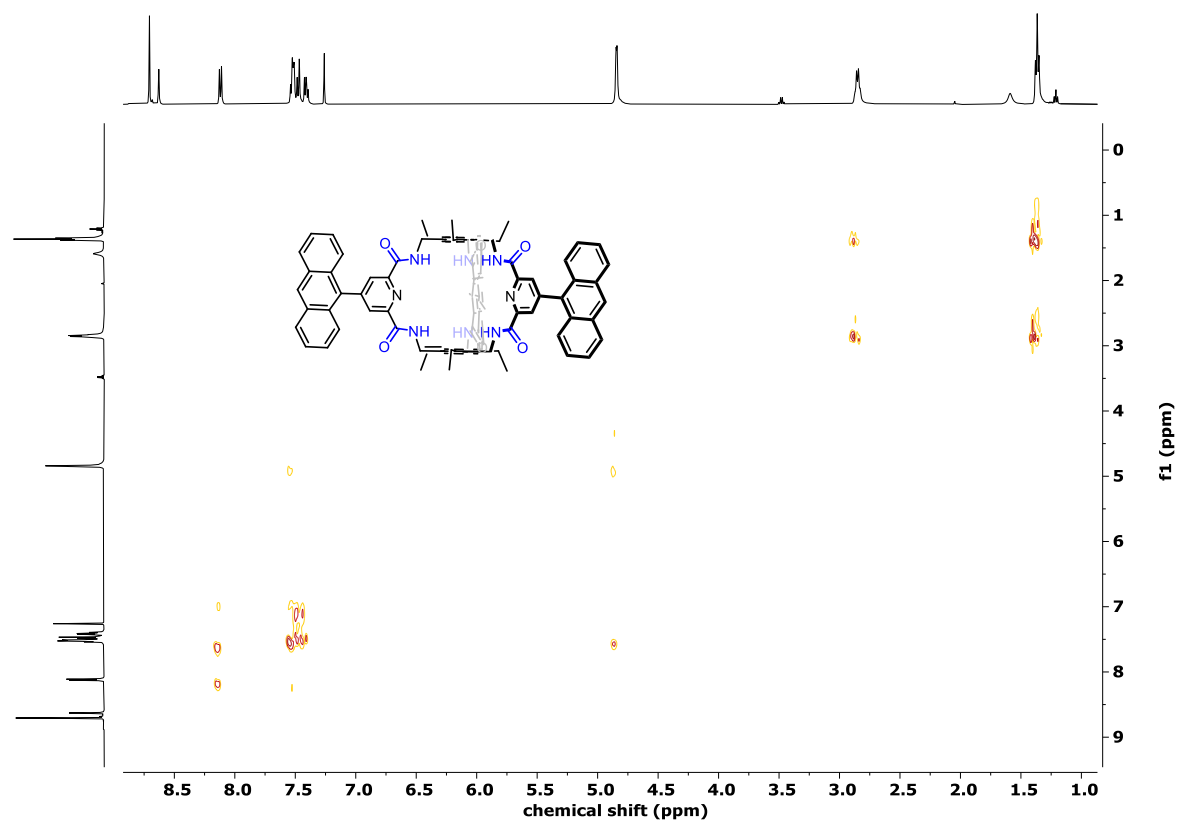
Figure 127. ^{1}H-^{1}H (500 MHz, 500 MHz) COSY NMR spectrum of amide cage **78**.
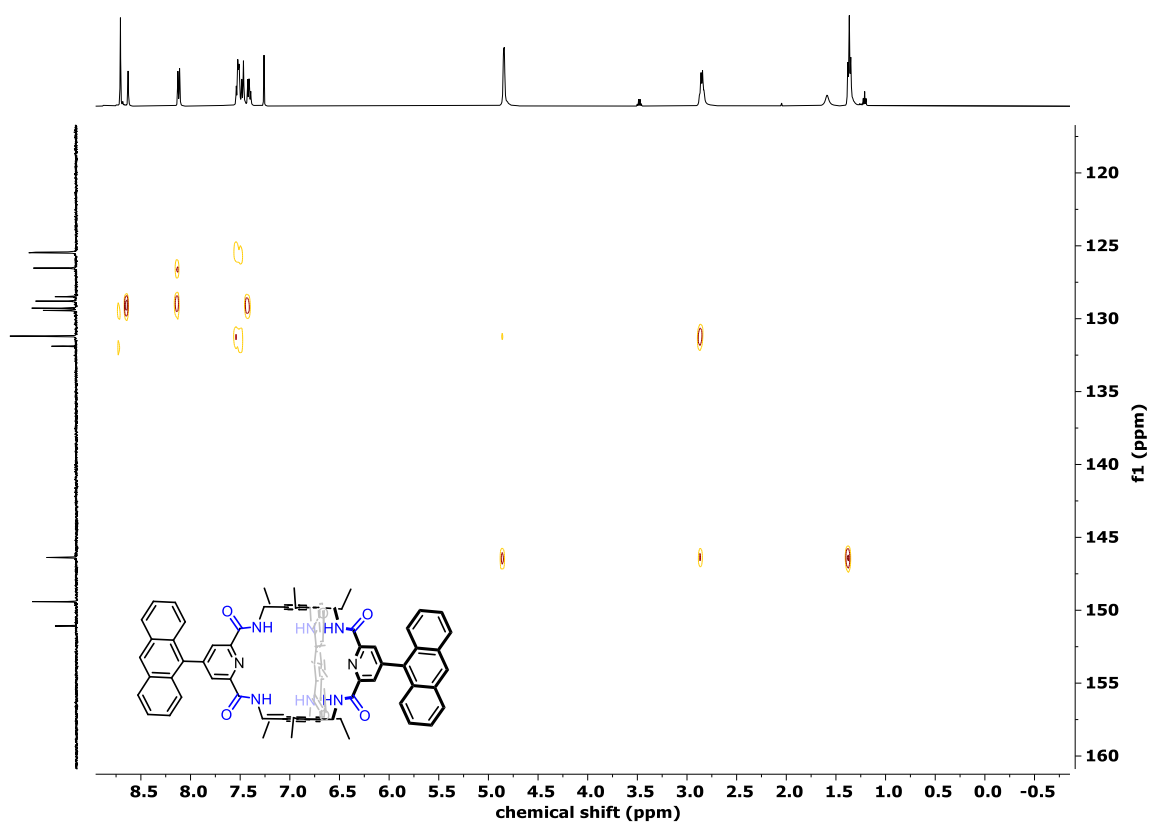
Figure 128. ^{1}H-^{13}C (500 MHz, 100 MHz) HMBC NMR spectrum of amide cage **78**.
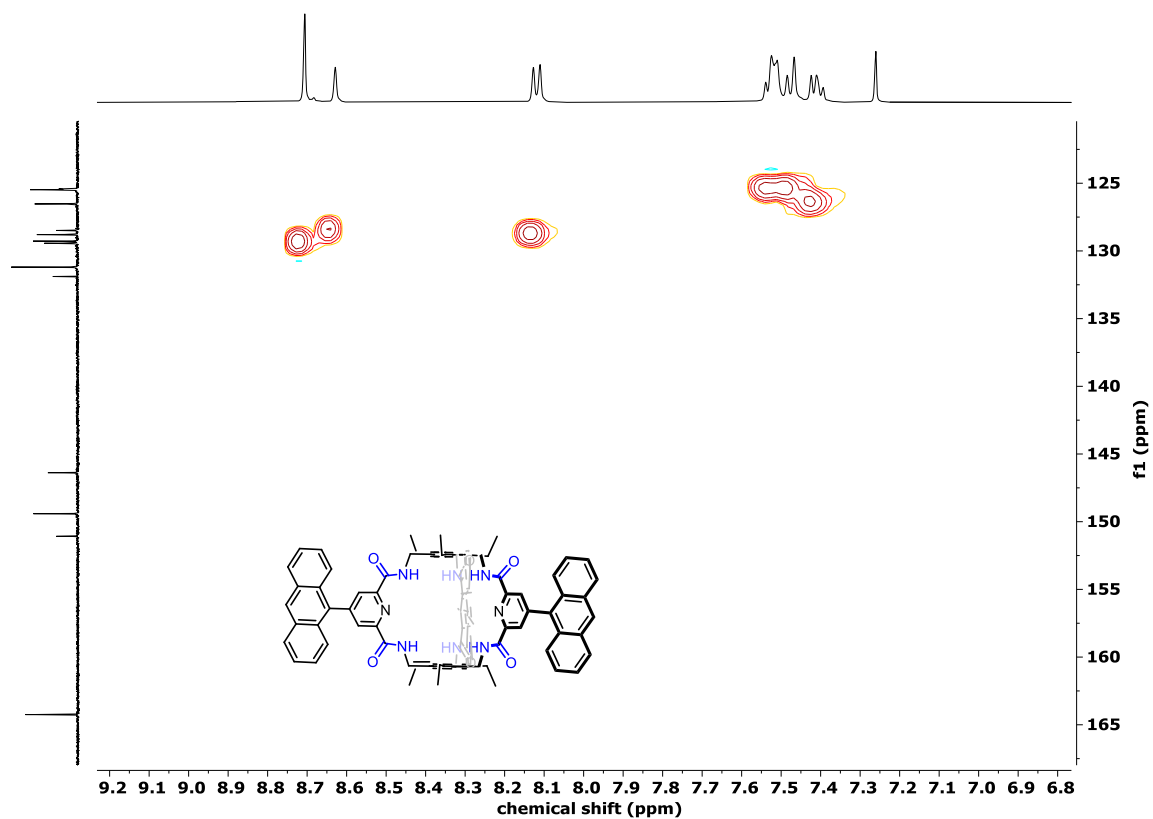
Figure 129. ^{1}H-^{13}C (500 MHz, 100 MHz) HSQC NMR spectrum of amide cage **78**.
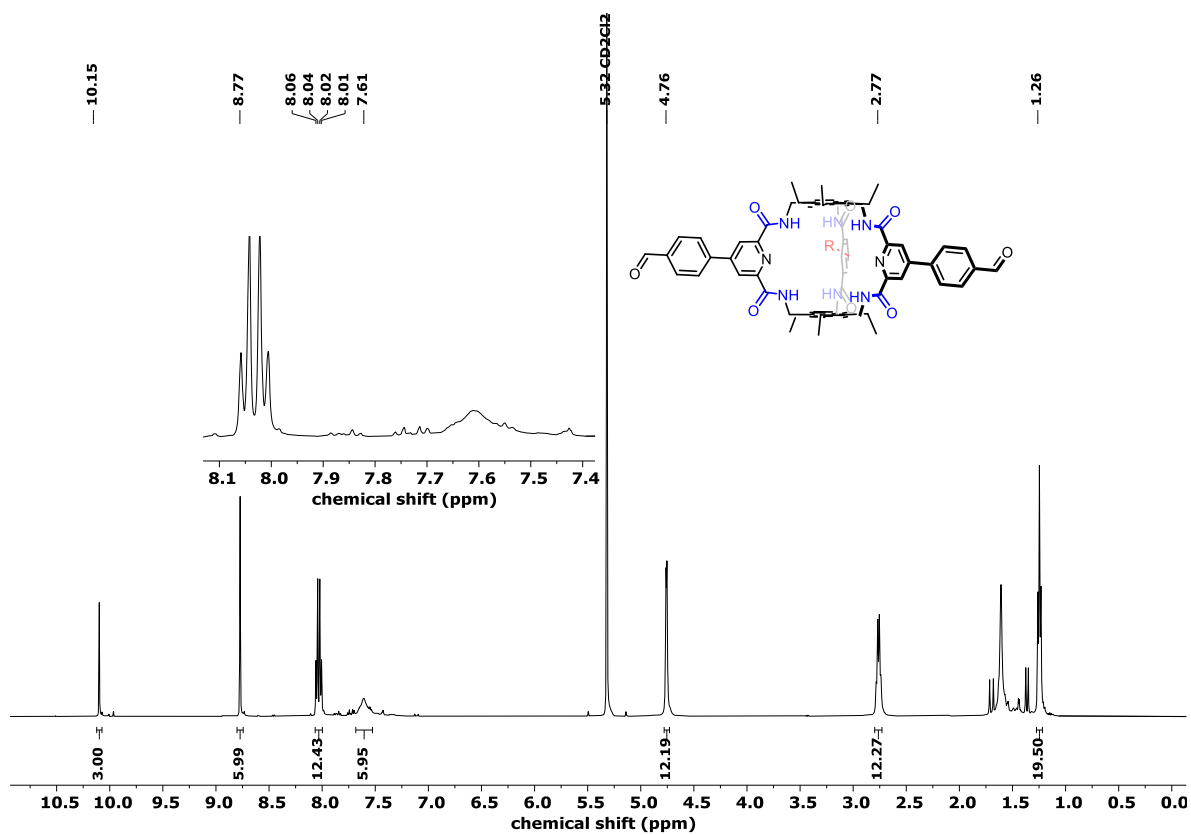
Figure 130. ^{1}H NMR (500 MHz, CD$_2$Cl$_2$) spectrum of amide cage **79**.
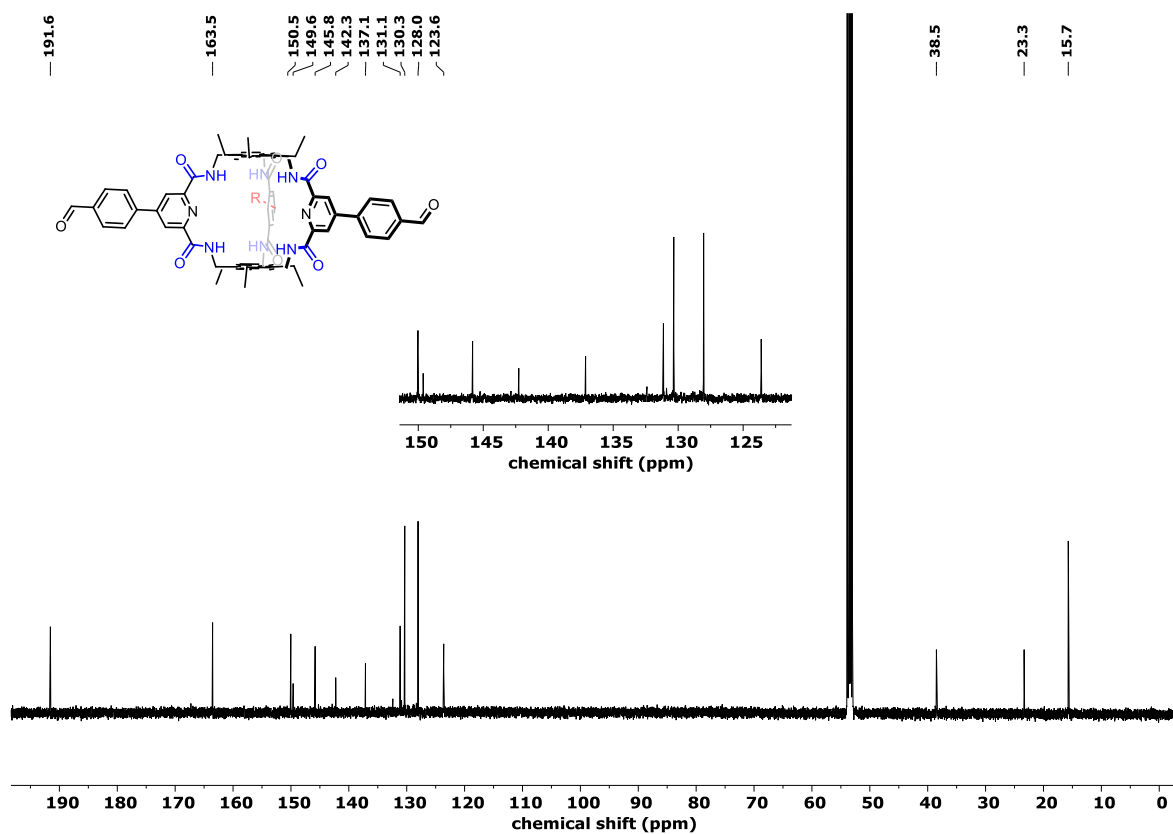
Figure 131. ^{13}C NMR (100 MHz, DMSO-d$_6$) spectrum of amide cage **79**.
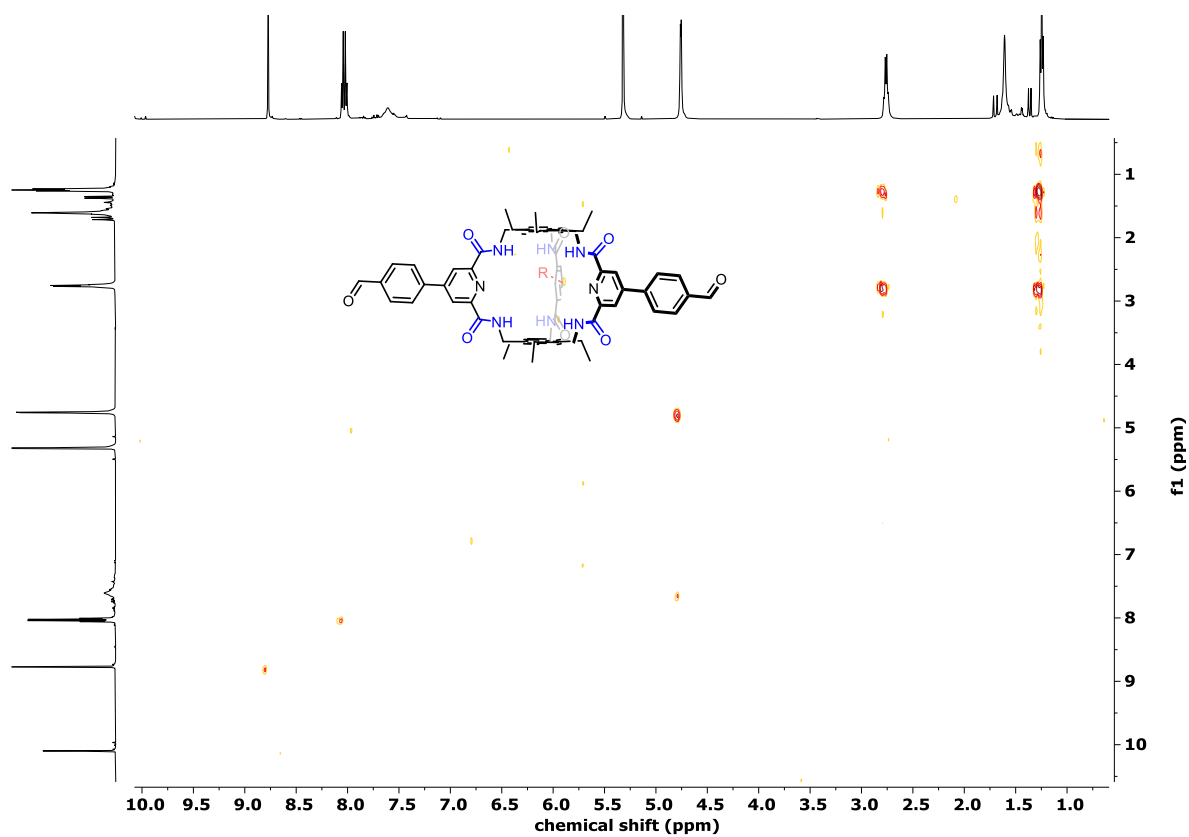
Figure 132. ^{1}H-^{1}H (500 MHz, 500 MHz) COSY NMR spectrum of amide cage **79**.
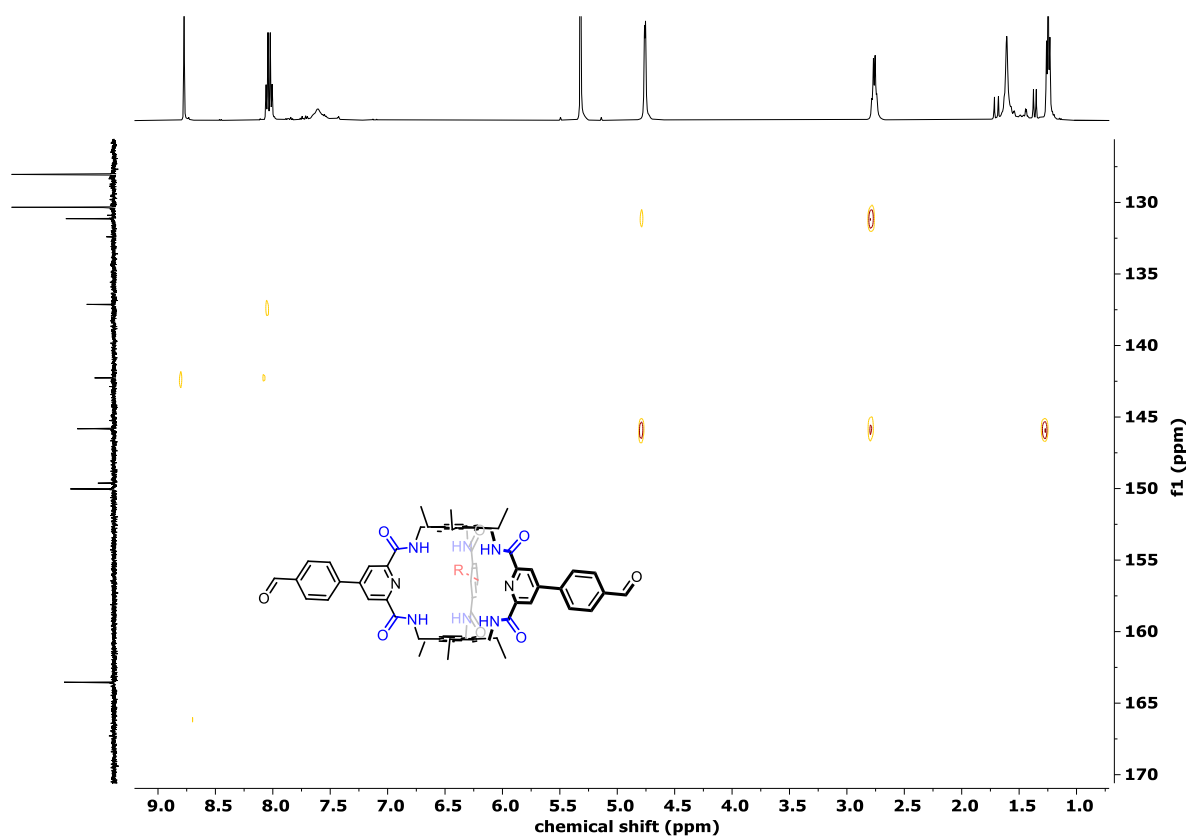
Figure 133. ^{1}H-^{13}C (500 MHz, 100 MHz) HMBC NMR spectrum of amide cage **79**.
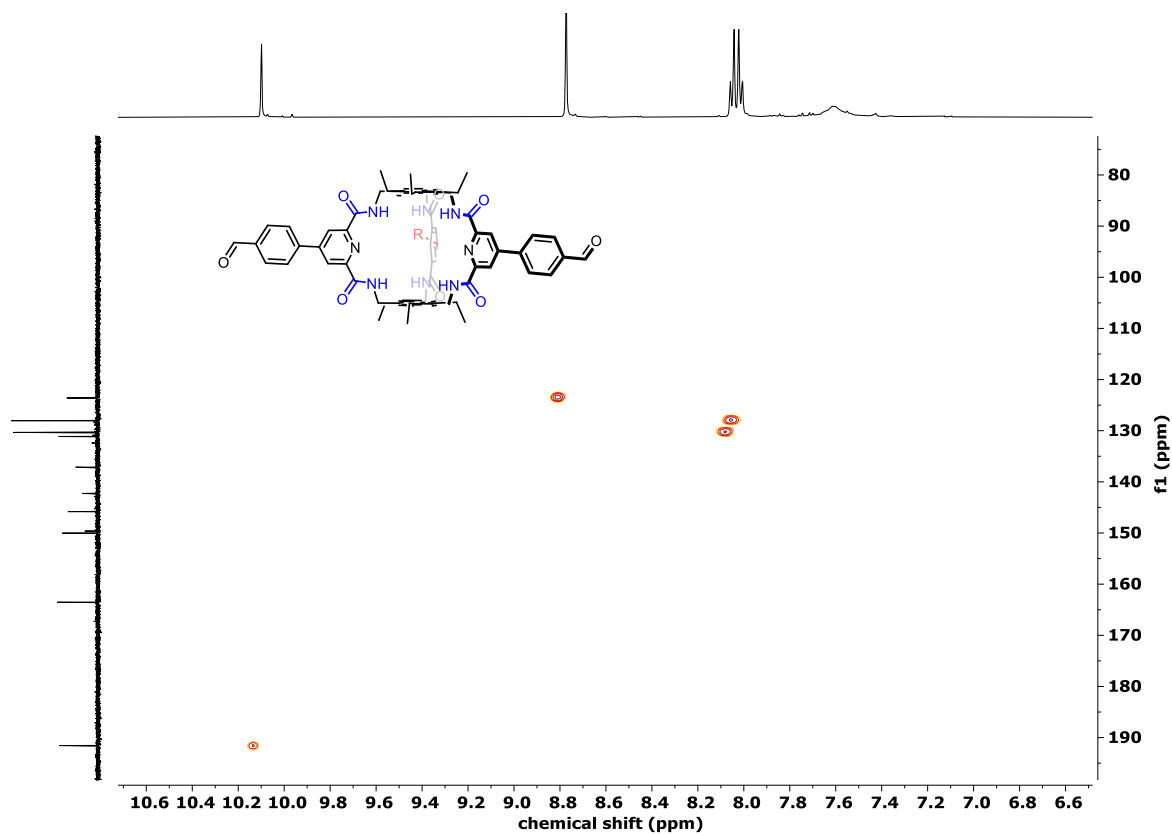
Figure 134. ^{1}H-^{13}C (500 MHz, 100 MHz) HSQC NMR spectrum of amide cage **79**.

1.2. Crude NMR comparison
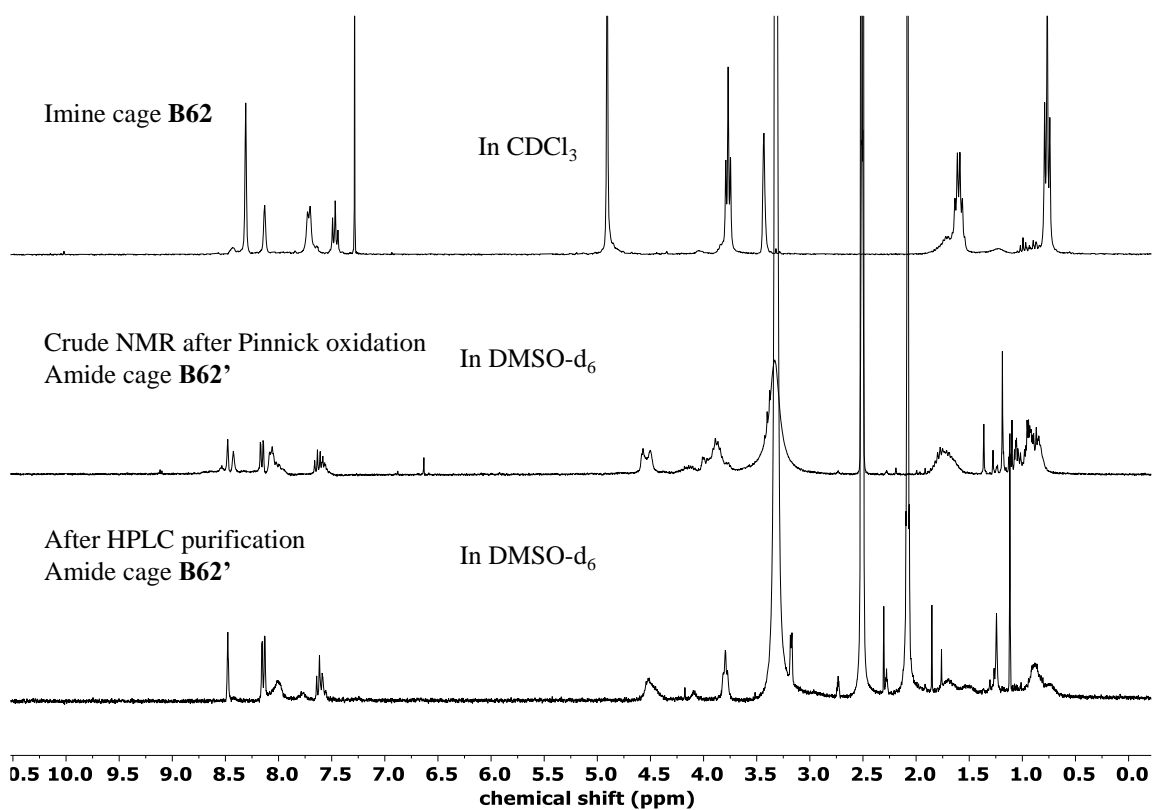
Figure 135. ^{1}H NMR (300 MHz) comparison of imine cage **B62**, and after subjecting it to the Pinnick oxidation followed by HPLC purification (amide cage **B62-amide**).
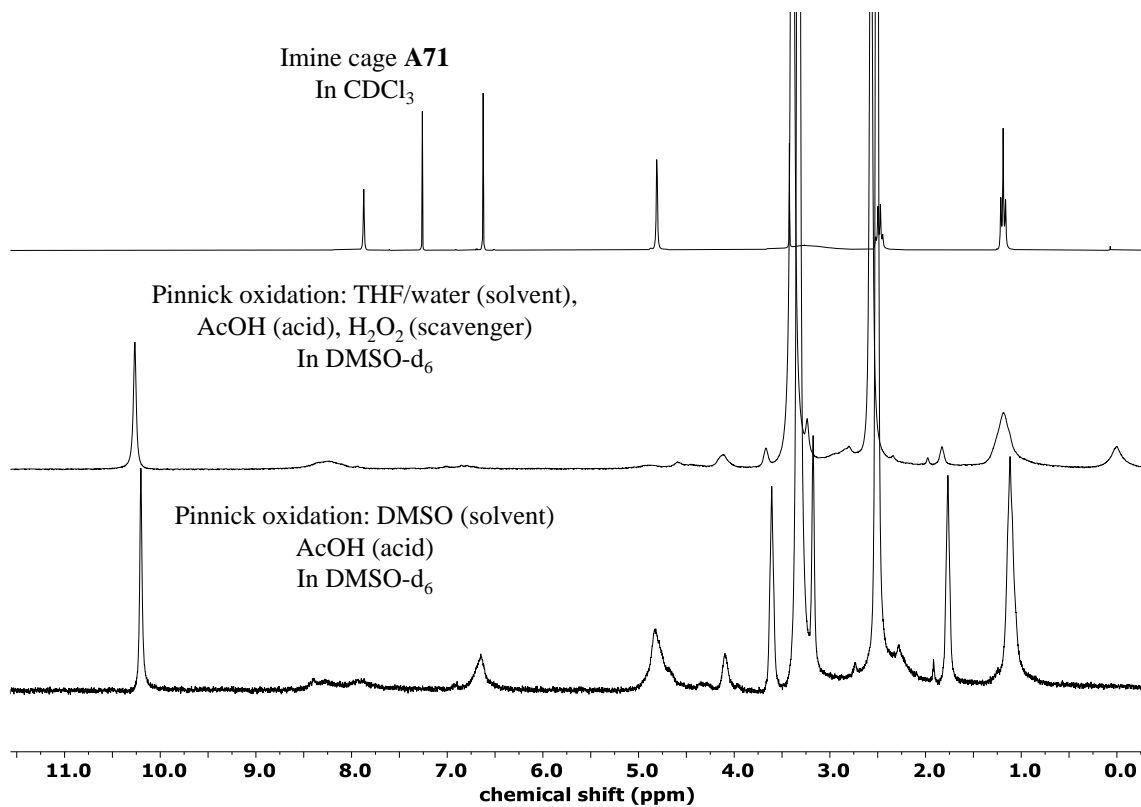
Figure 136. ^{1}H NMR (500 MHz) comparison of imine cage **A71** (top), and after subjecting it to the Pinnick oxidation with H₂O₂ as scavenger (middle) and DMSO as scavenger (and also as solvent).

1.3. NMR titration for chloride anion recognition
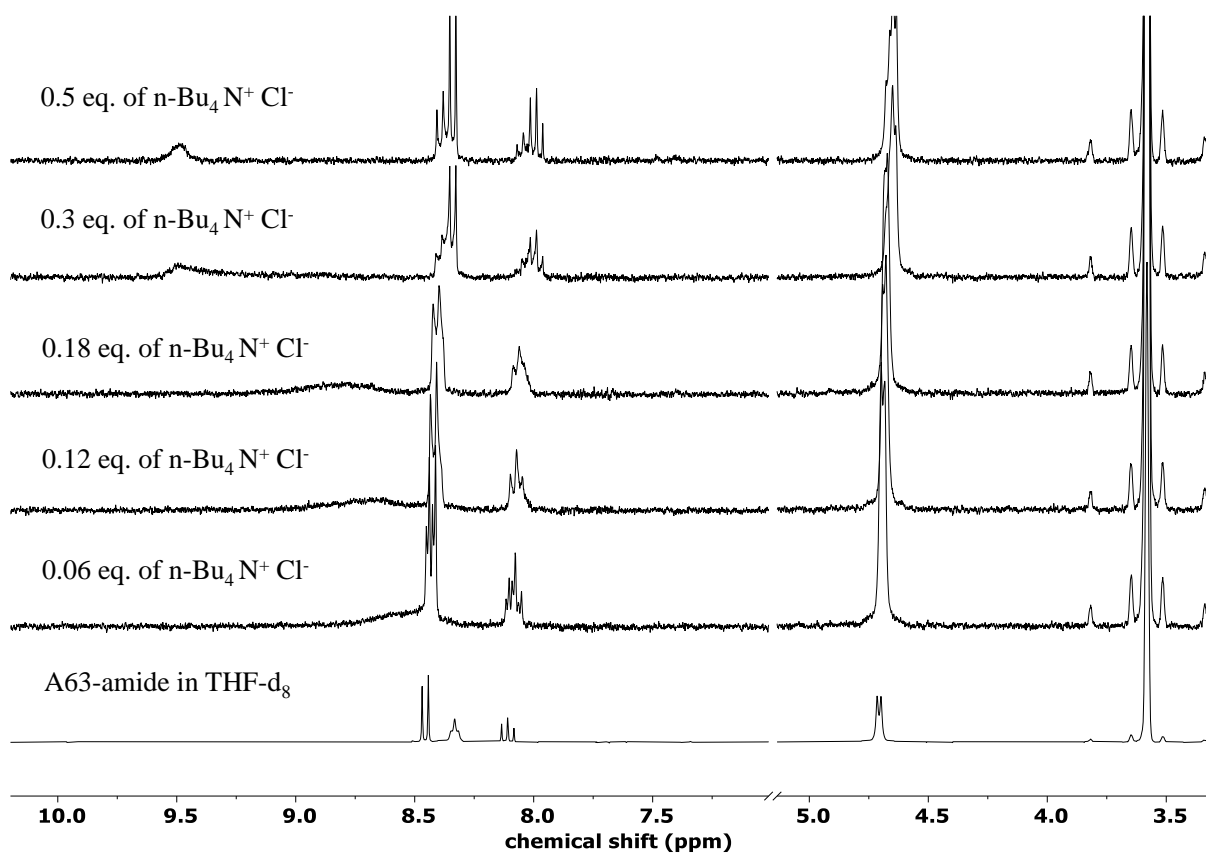
Figure 137. Partial ^{1}H NMR (300 MHz, THF-d$_8$) spectra of amide cage **A63-amide** in the presence of n-Bu$_4$N$^+$ Cl$^-$ in THF-d$_8$.

2. Mass spectra
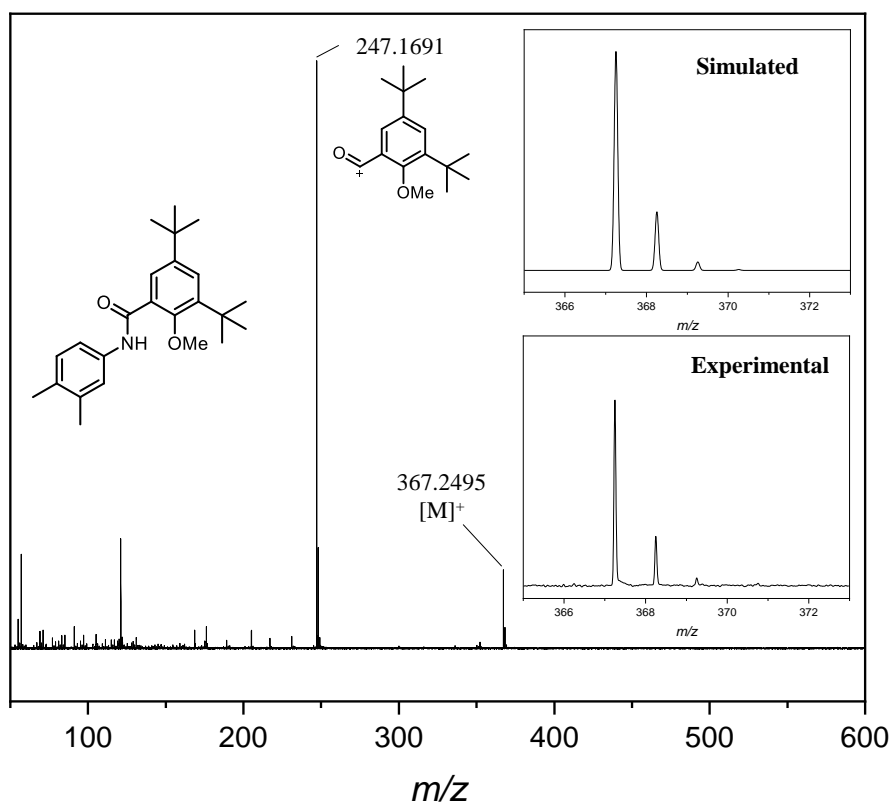
Figure 138. EI-MS (positive mode) spectrum of model compound **52'**.
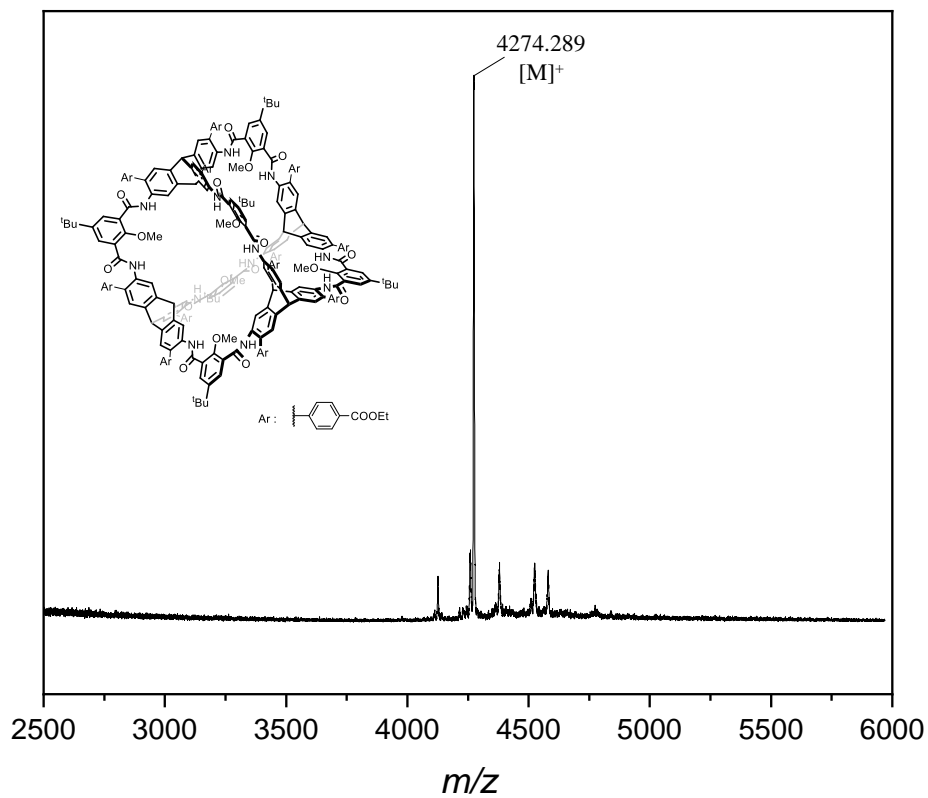
Figure 139. MALDI-TOF-MS (DCTB matrix, positive mode) spectrum of amide cage **59c**.
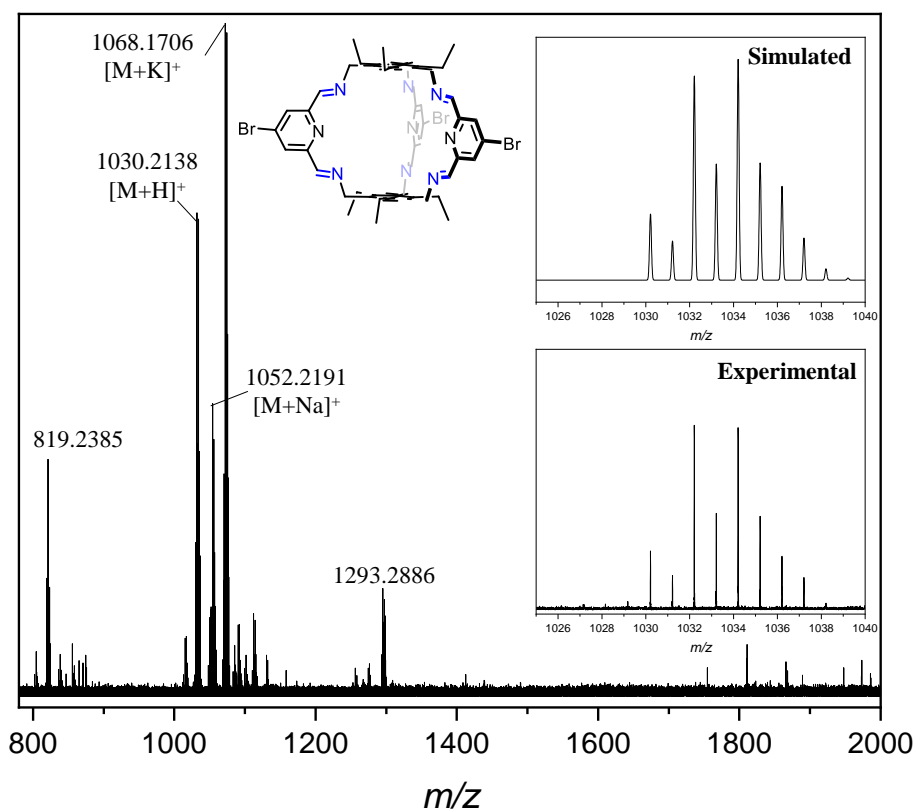
Figure 140. MALDI-MS (HR-MS, DCTB matrix, positive mode) spectrum of imine cage **A65**.
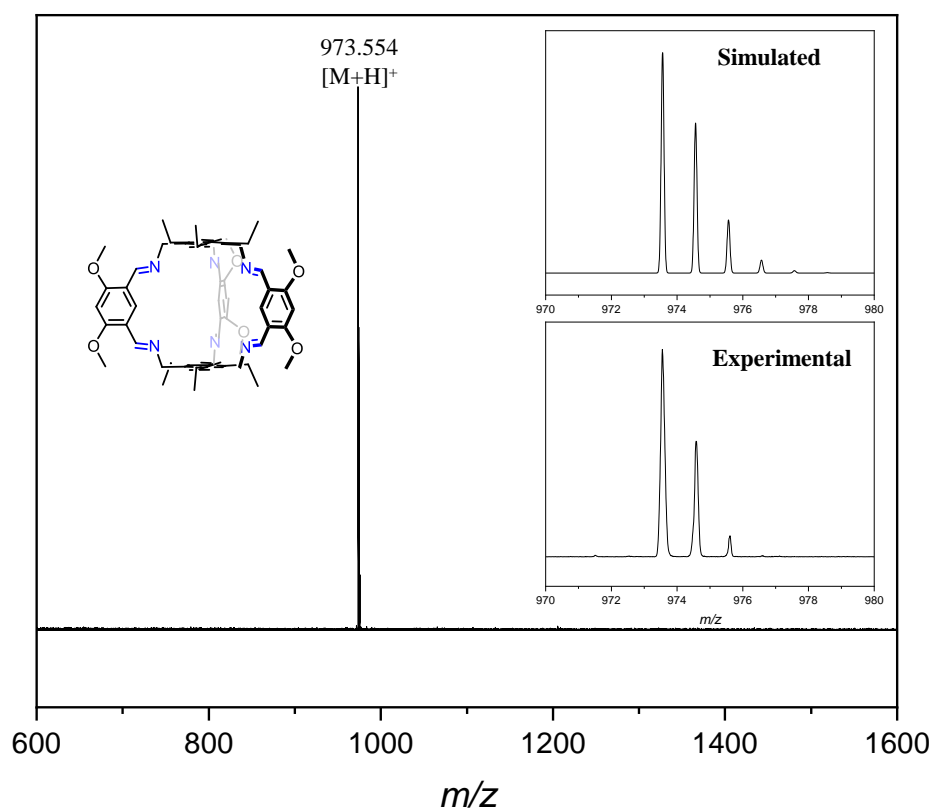
Figure 141. MALDI-TOF-MS (DCTB matrix, positive mode) spectrum of imine cage **A68**.
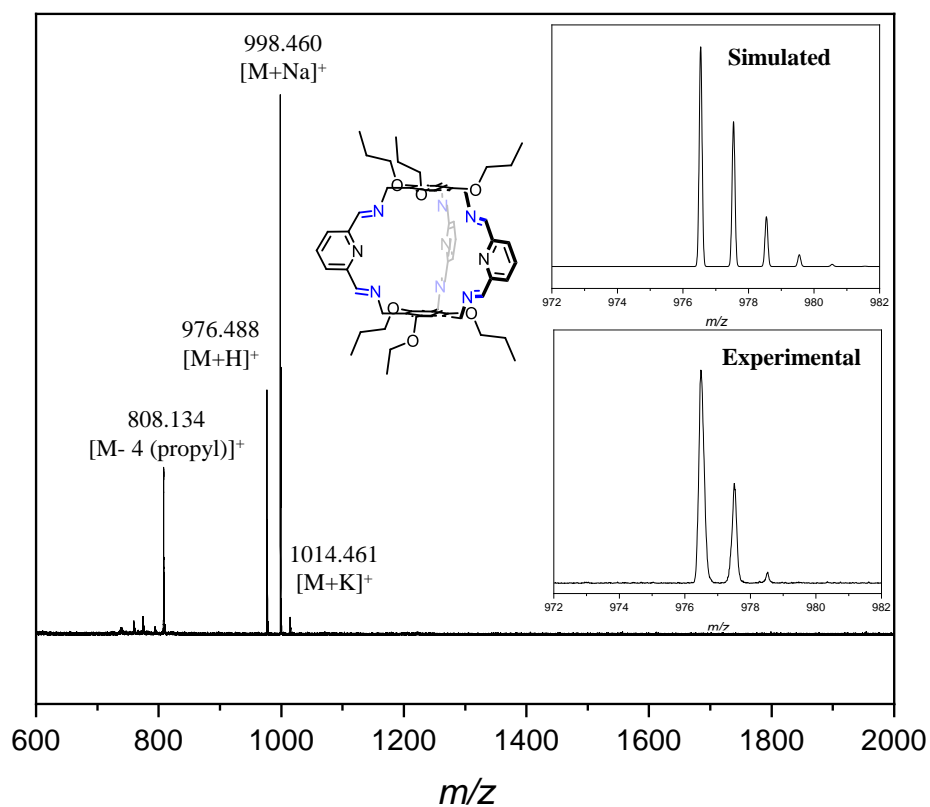
Figure 142. MALDI-TOF-MS (DCTB matrix, positive mode) spectrum of imine cage **B63**.
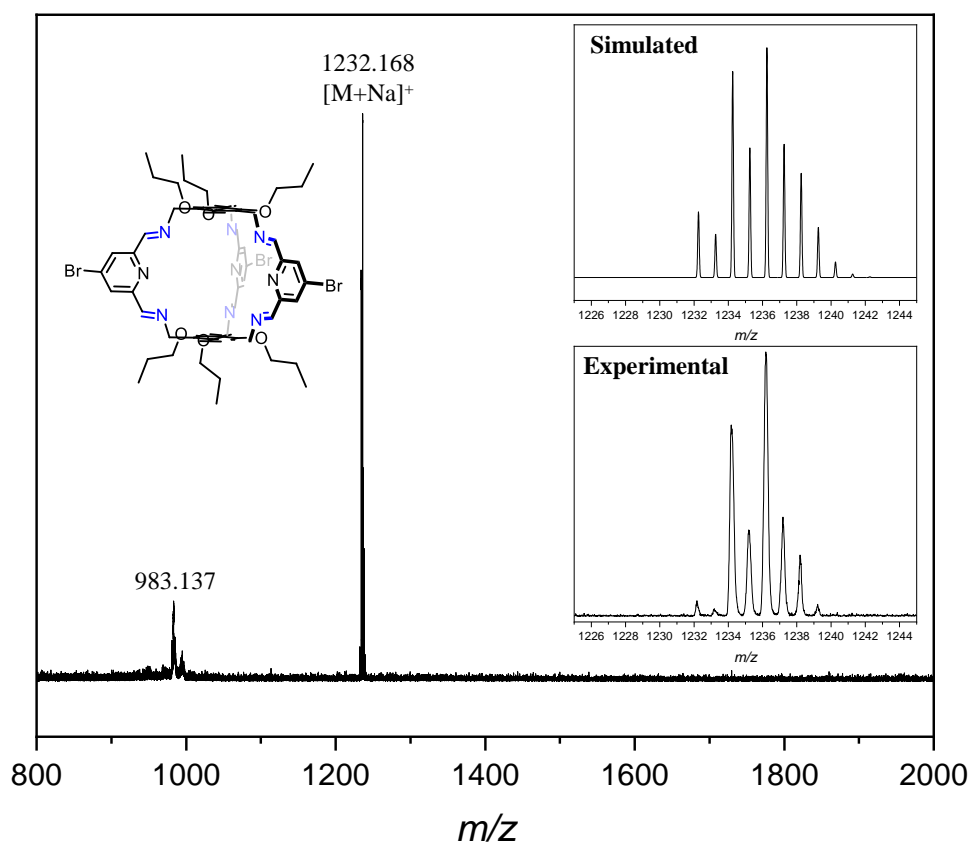
Figure 143. MALDI-TOF-MS (DCTB matrix, positive mode) spectrum of imine cage **B65**.
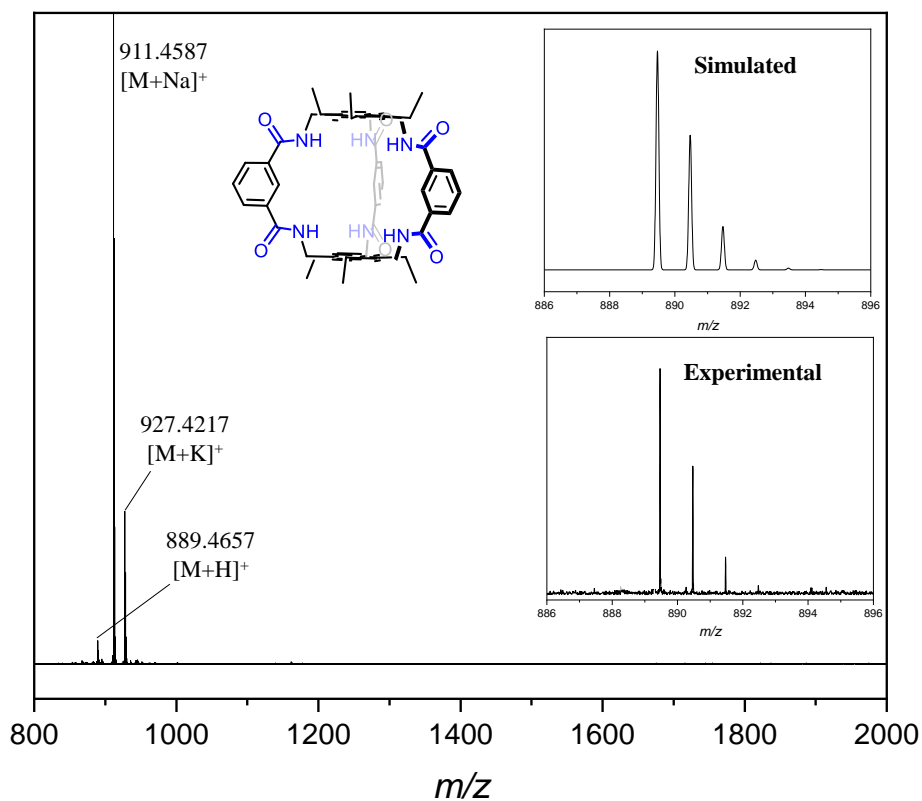
Figure 144. MALDI-MS (HR-MS, DCTB matrix, positive mode) spectrum of amide cage **A62-amide.**
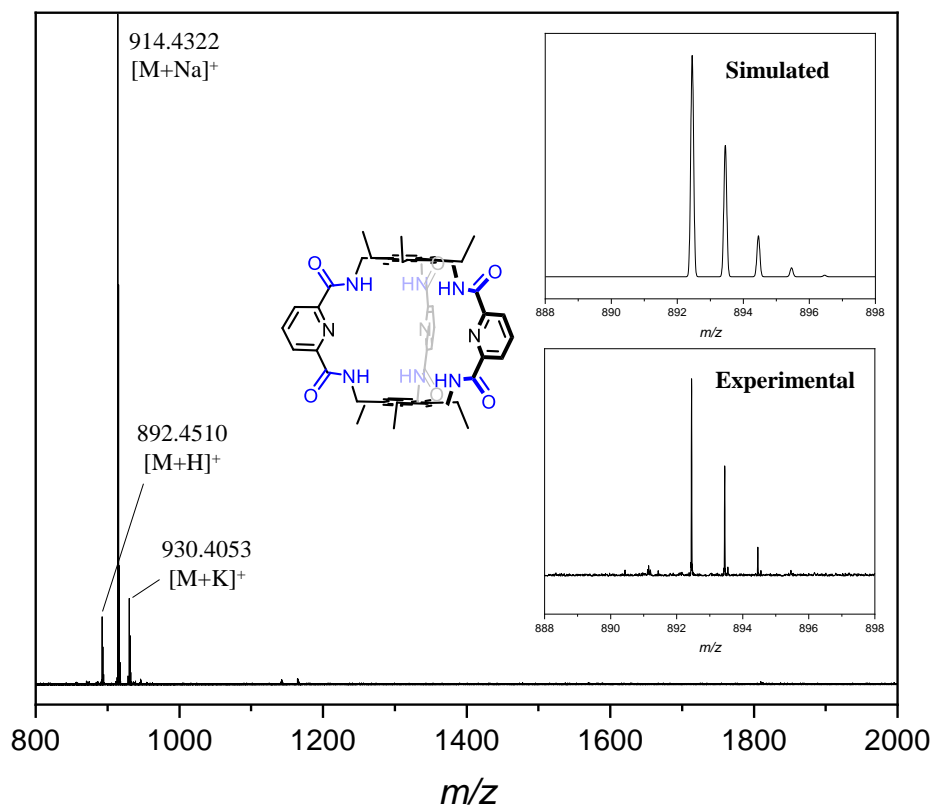
Figure 145. MALDI-MS (HR-MS, DCTB matrix, positive mode) spectrum of amide cage **A63-amide**.
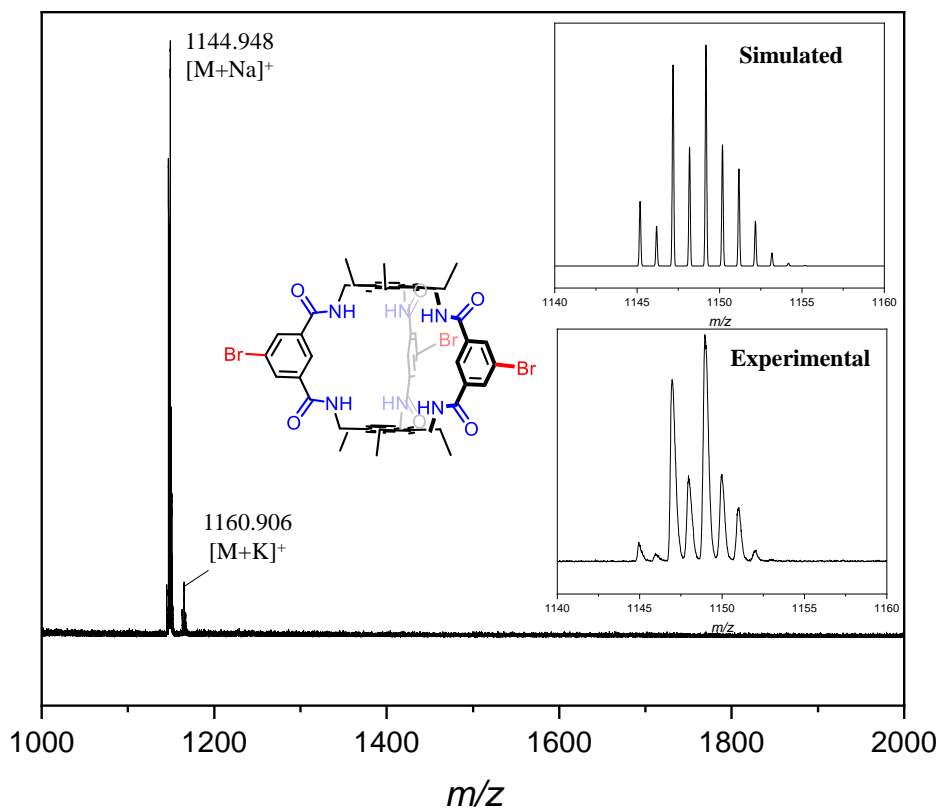
Figure 146. MALDI-TOF-MS (DCTB matrix, positive mode) spectrum of amide cage **A64-amide**.
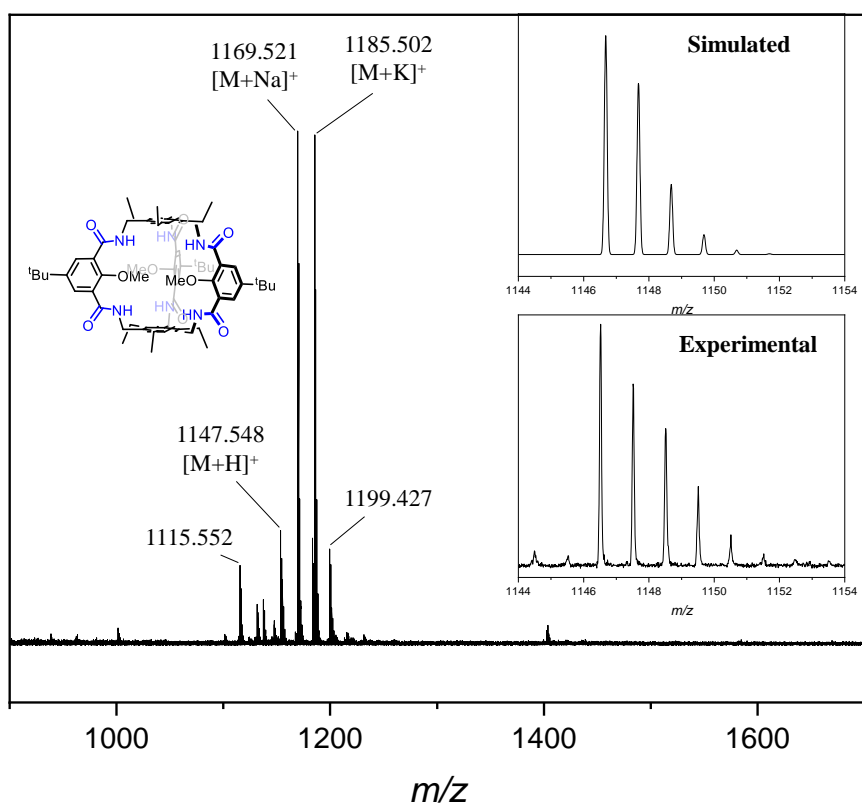
Figure 147. MALDI-TOF-MS (DCTB matrix, positive mode) spectrum of amide cage **A67-amide**.
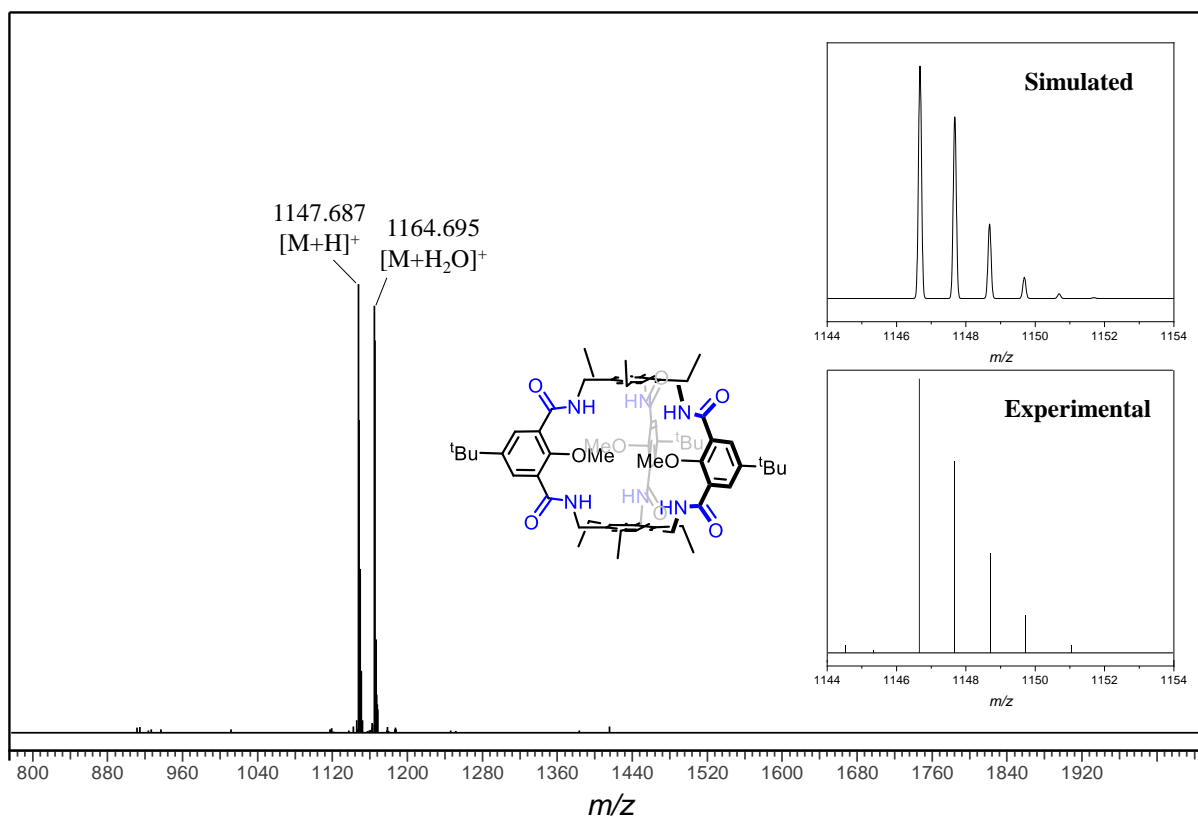
Figure 148. APCI-MS (positive mode) spectrum of amide cage **A67-amide**.
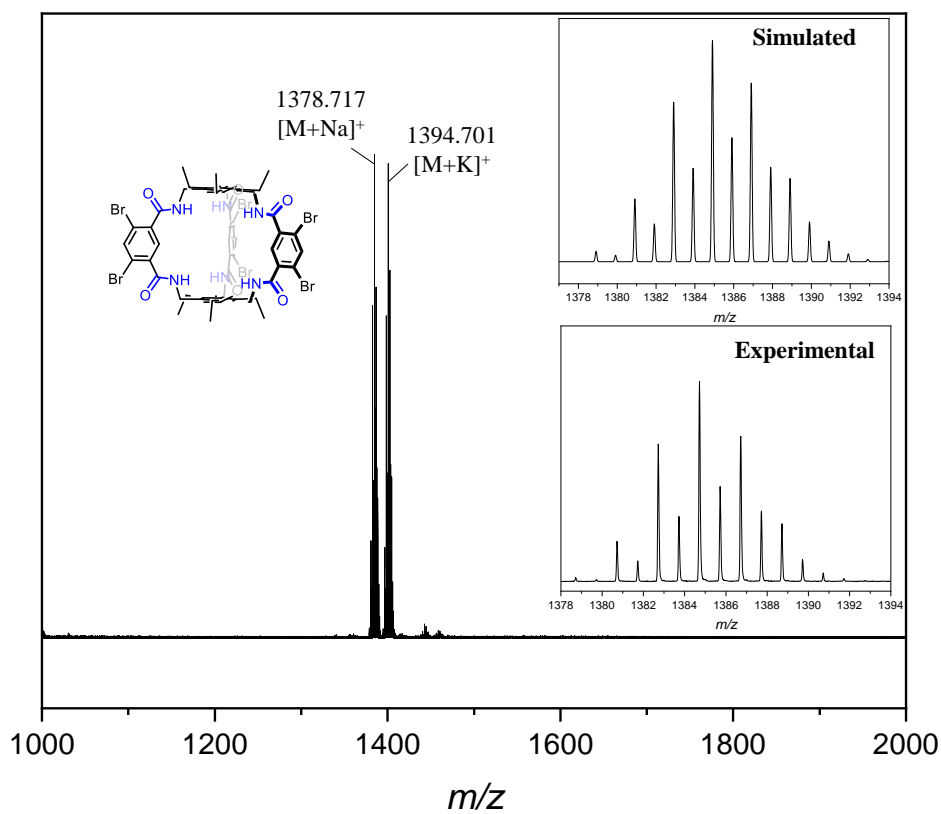
Figure 149. MALDI-TOF-MS (DCTB matrix, positive mode) spectrum of amide cage **A70-amide**.
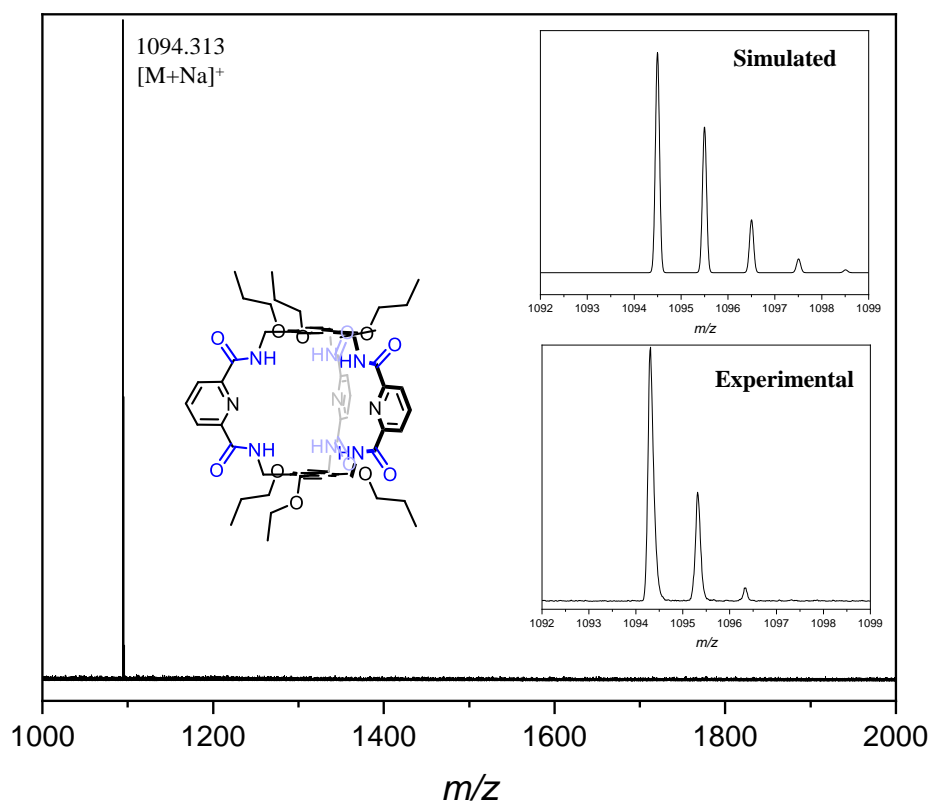
Figure 150. MALDI-TOF-MS (DCTB matrix, positive mode) spectrum of amide cage **B63-amide**.
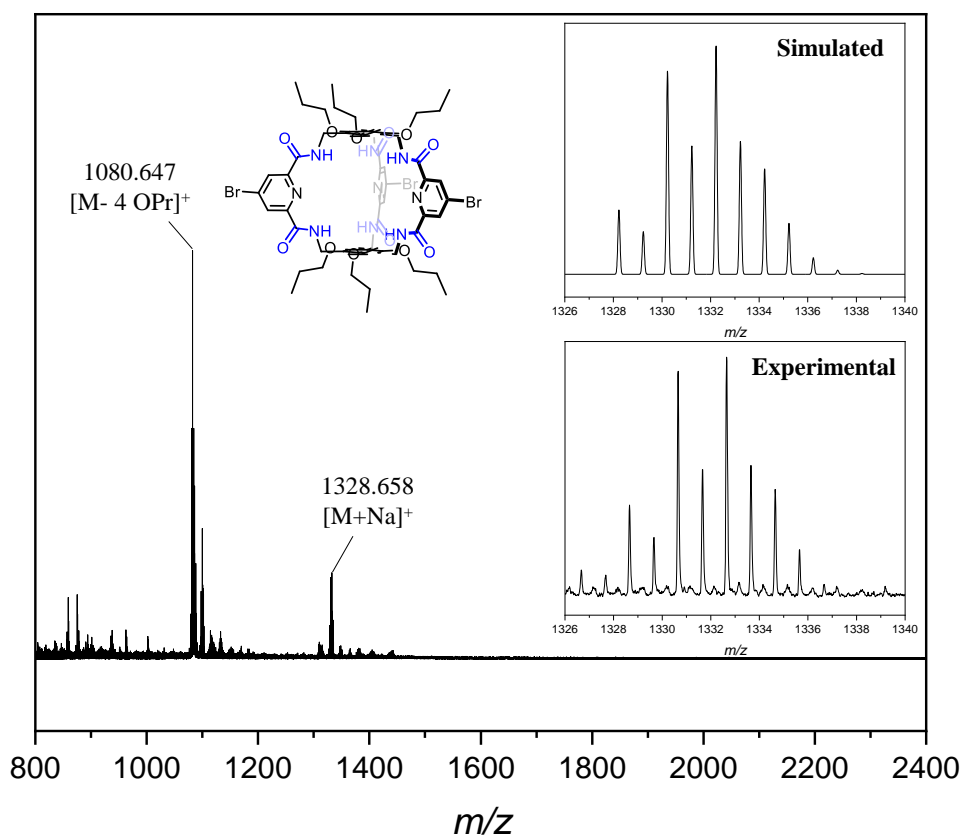
Figure 151. MALDI-TOF-MS (DCTB matrix, positive mode) spectrum of amide cage **B65'**.
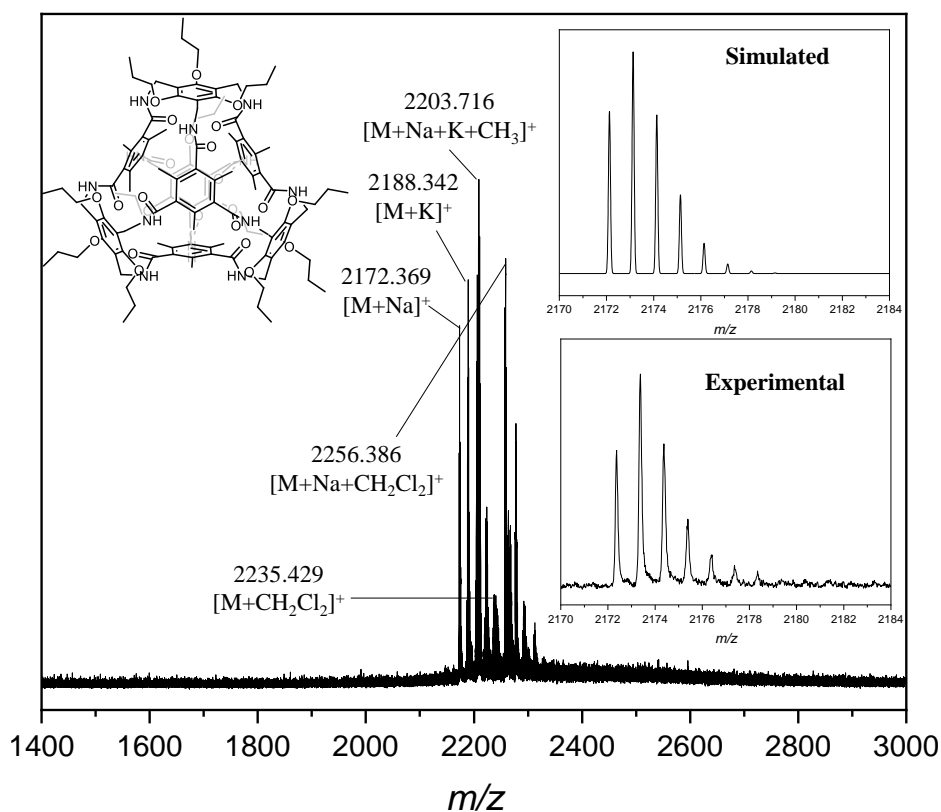
Figure 152. MALDI-TOF-MS (DCTB matrix, positive mode) spectrum of amide cage **B73-amide**.
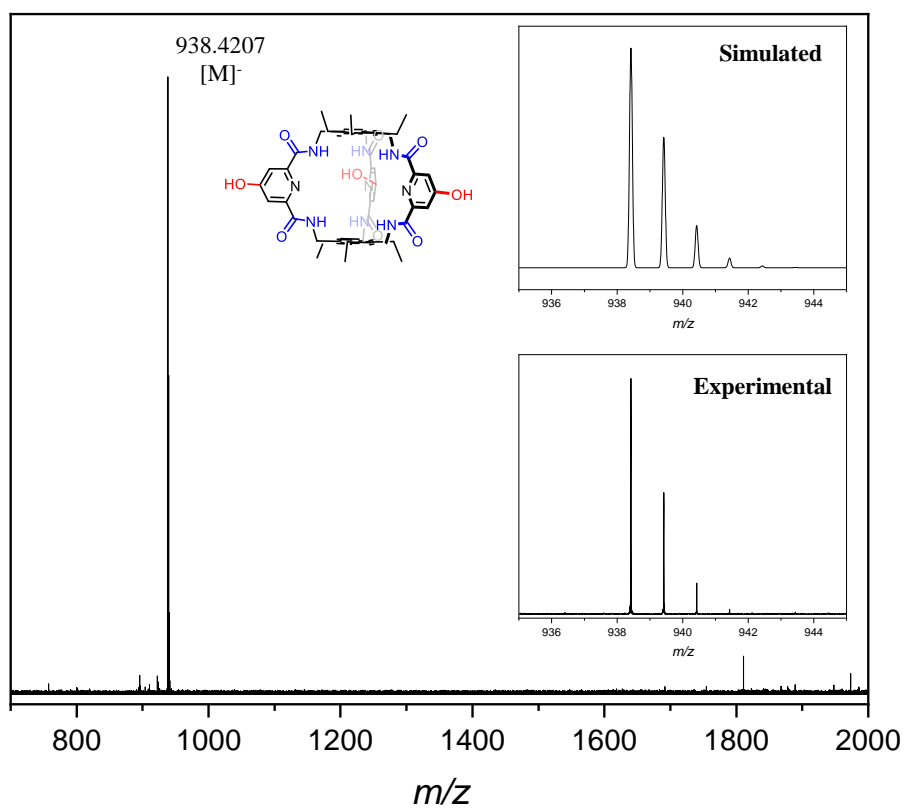
Figure 153. MALDI-MS (HR-MS, DCTB matrix, negative mode) spectrum of amide cage **76**.
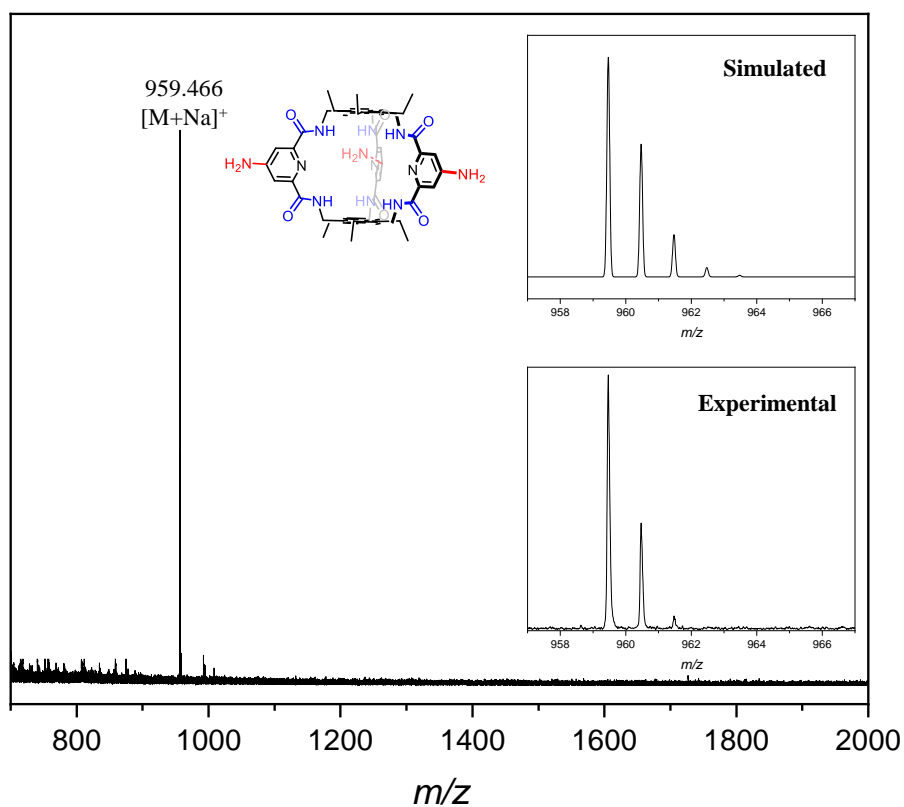
Figure 154. MALDI-TOF-MS (DCTB matrix, positive mode) spectrum of amide cage **77**.
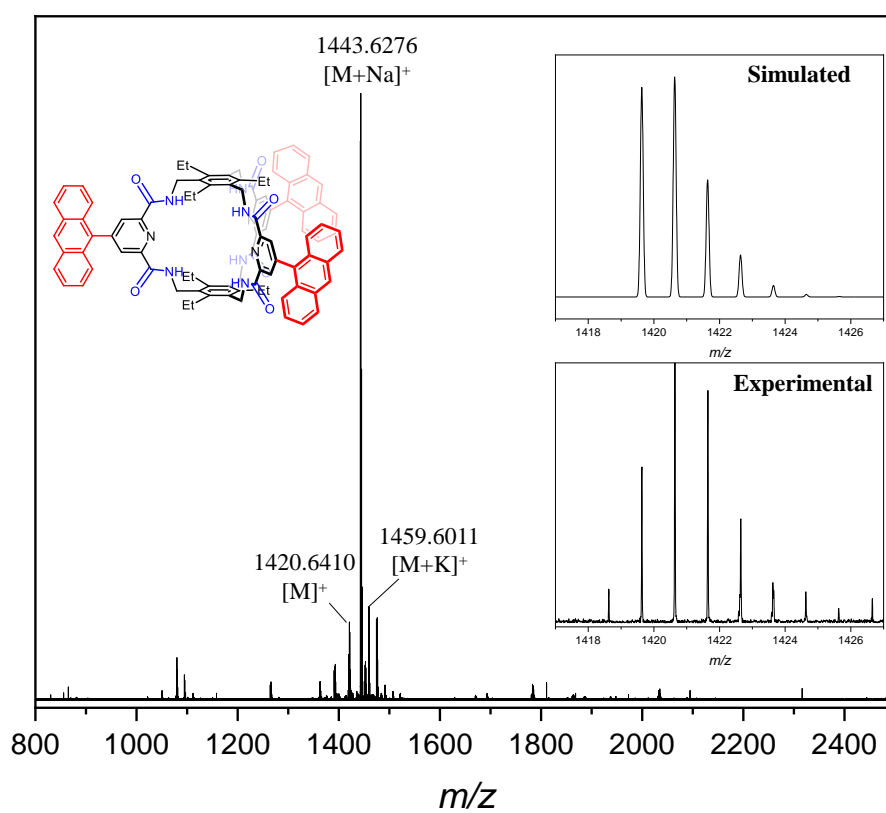
Figure 155. MALDI-MS (HR-MS, DCTB matrix, positive mode) spectrum of amide cage **78**.

2.1. Crude products (not isolated)
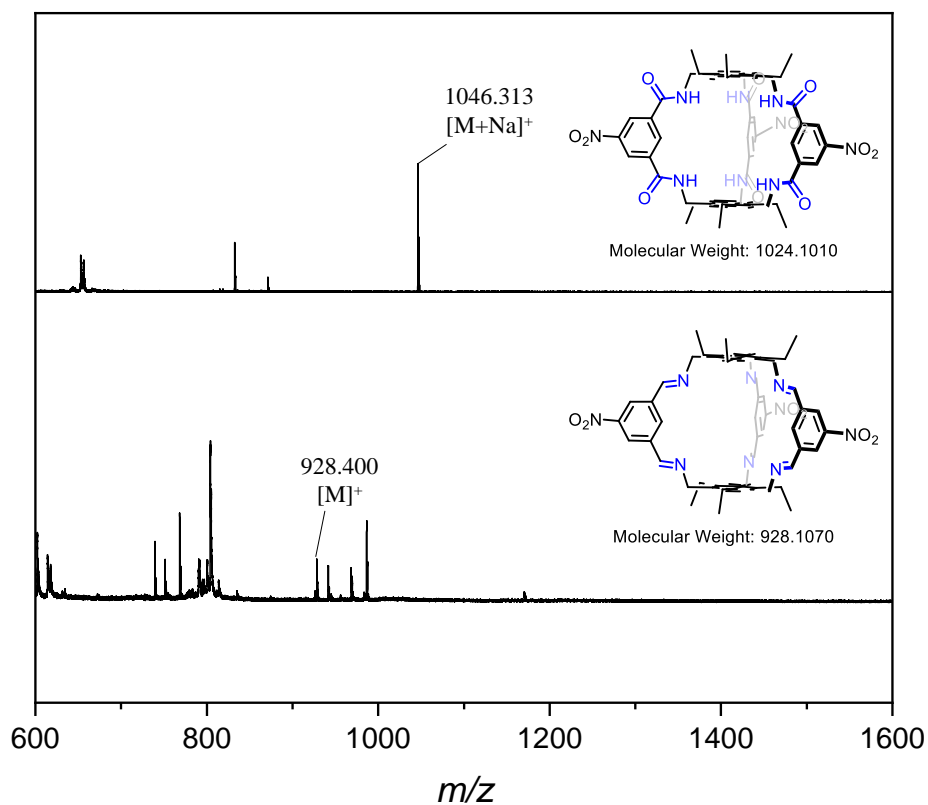
Figure 156. MALDI-TOF-MS (DCTB matrix, positive mode) spectrum comparison of imine cage **A66** (top) and amide cage **A66-amide** (bottom).
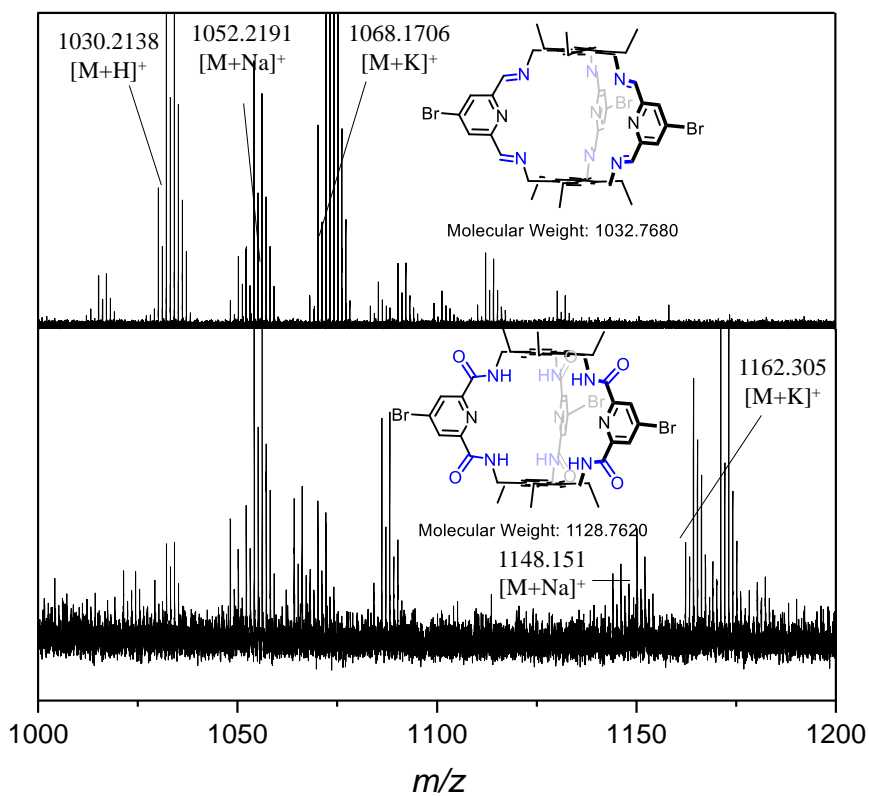
Figure 157. MALDI-TOF-MS (DCTB matrix, positive mode) spectrum comparison of imine cage **A65** (top) and amide cage **A65-amide** (bottom).

3. IR spectra
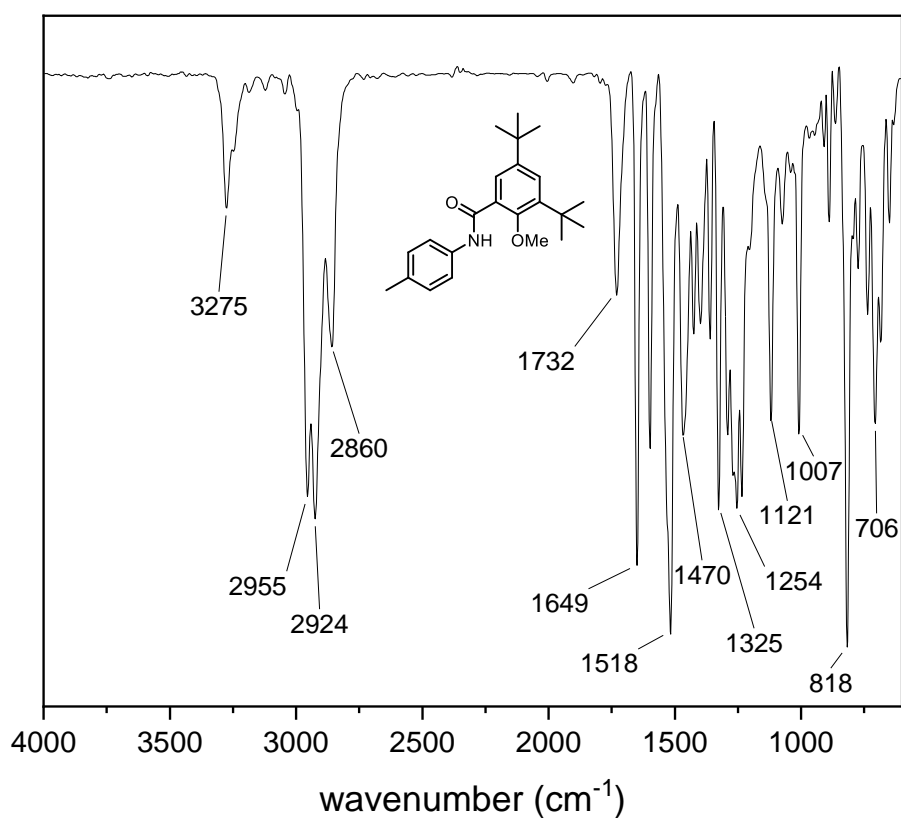
Figure 158. IR (ATR) spectrum of model compound **52'**.
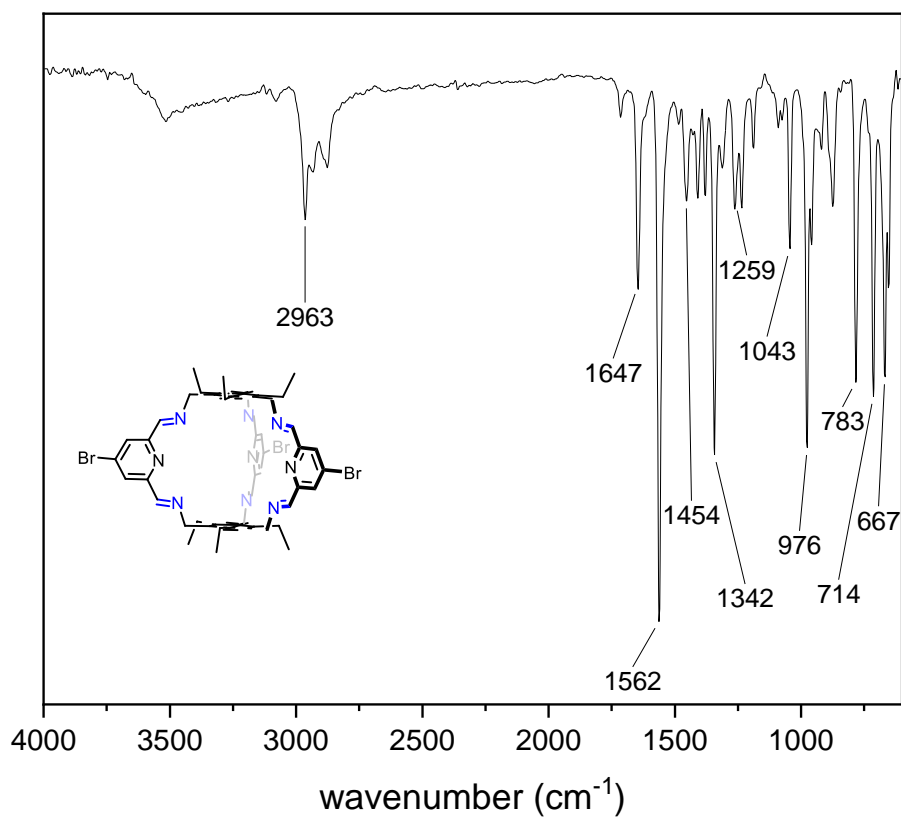
Figure 159. IR (ATR) spectrum of imine cage **A65**.
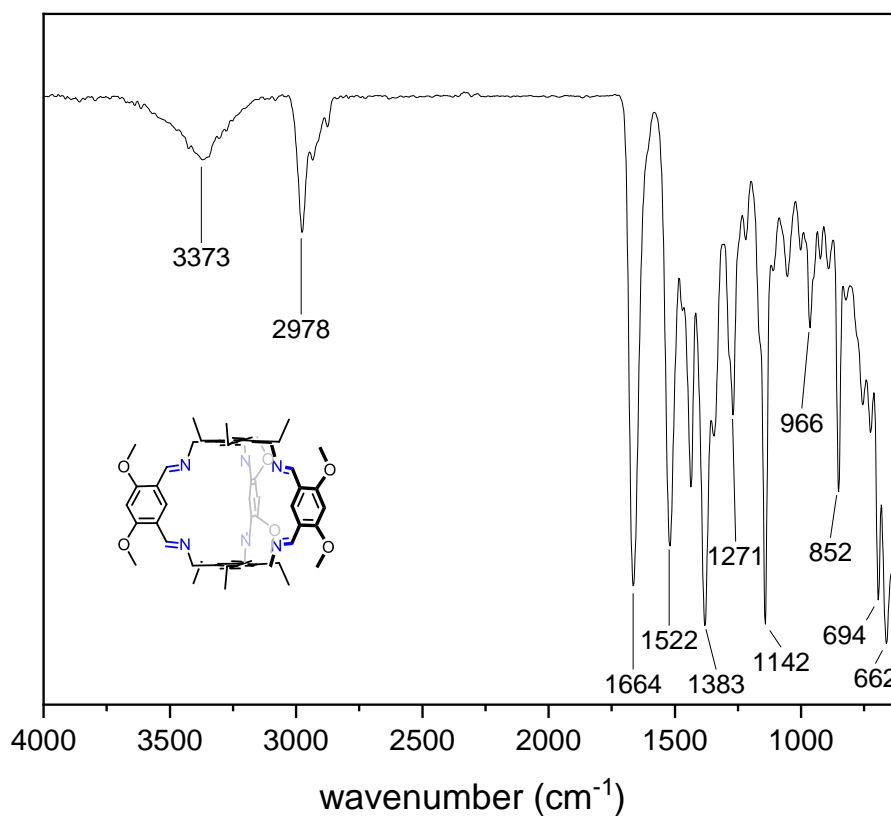
Figure 160. IR (ATR) spectrum of imine cage **A68**.
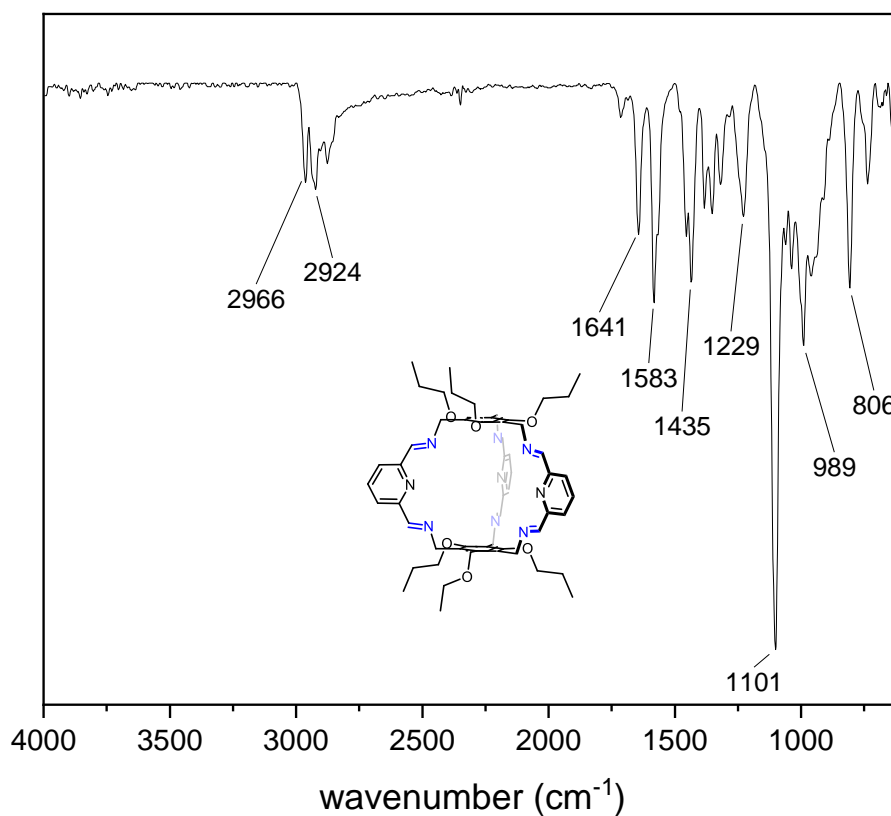
Figure 161. IR (ATR) spectrum of imine cage **B63**.
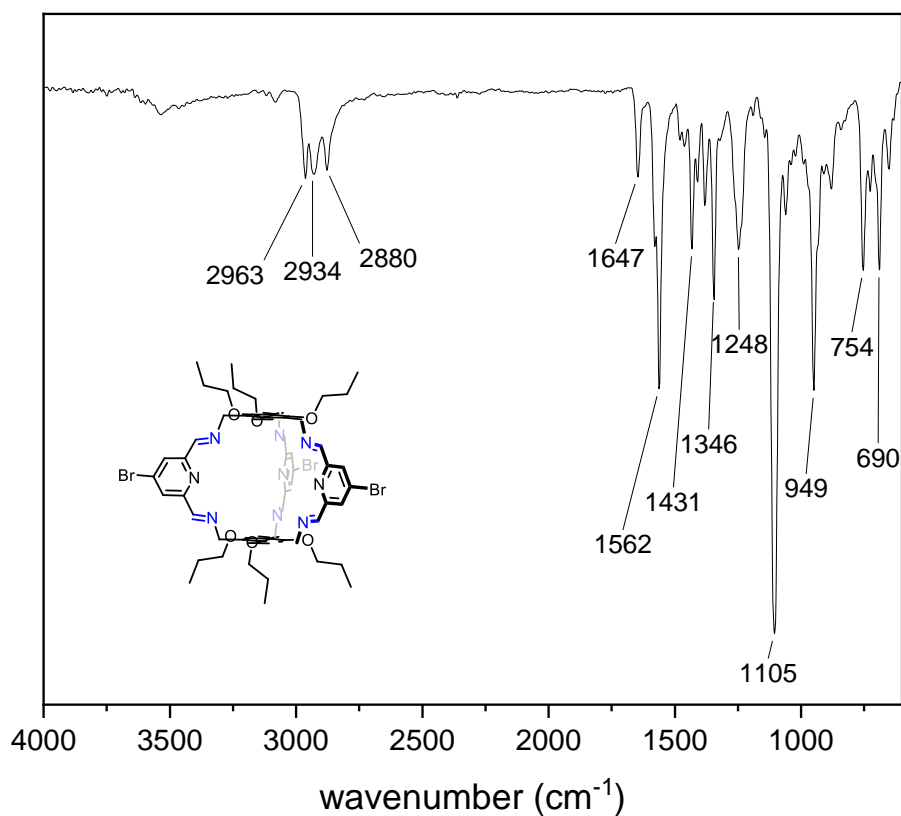
Figure 162. IR (ATR) spectrum of imine cage **B65**.
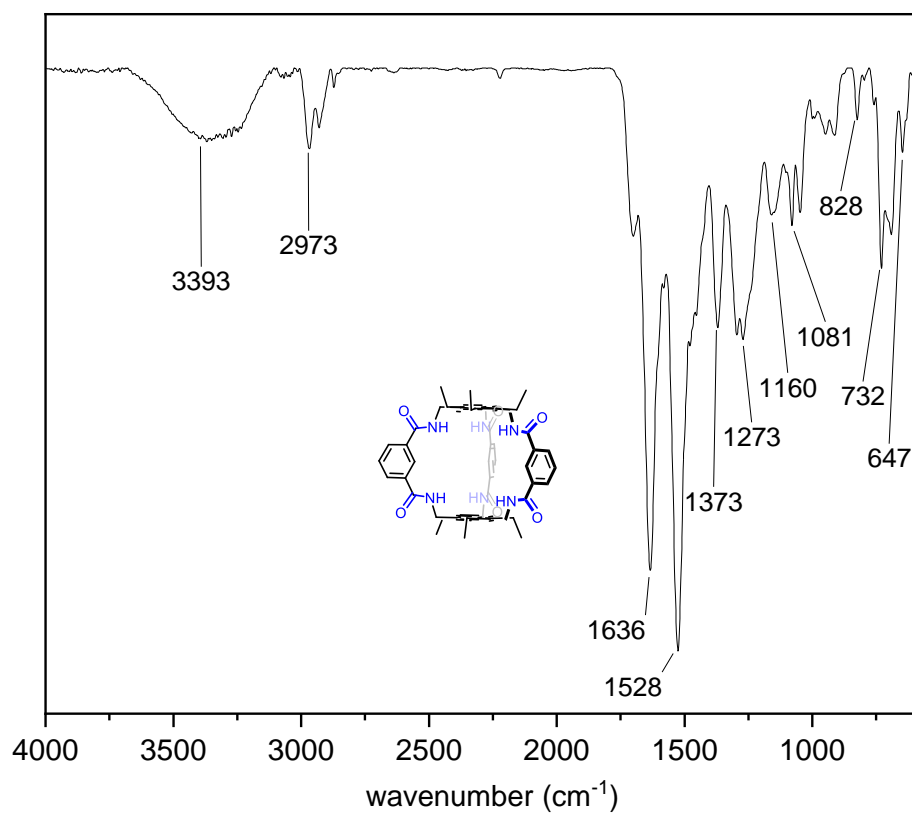
Figure 163. IR (ATR) spectrum of amide cage **A62-amide**.
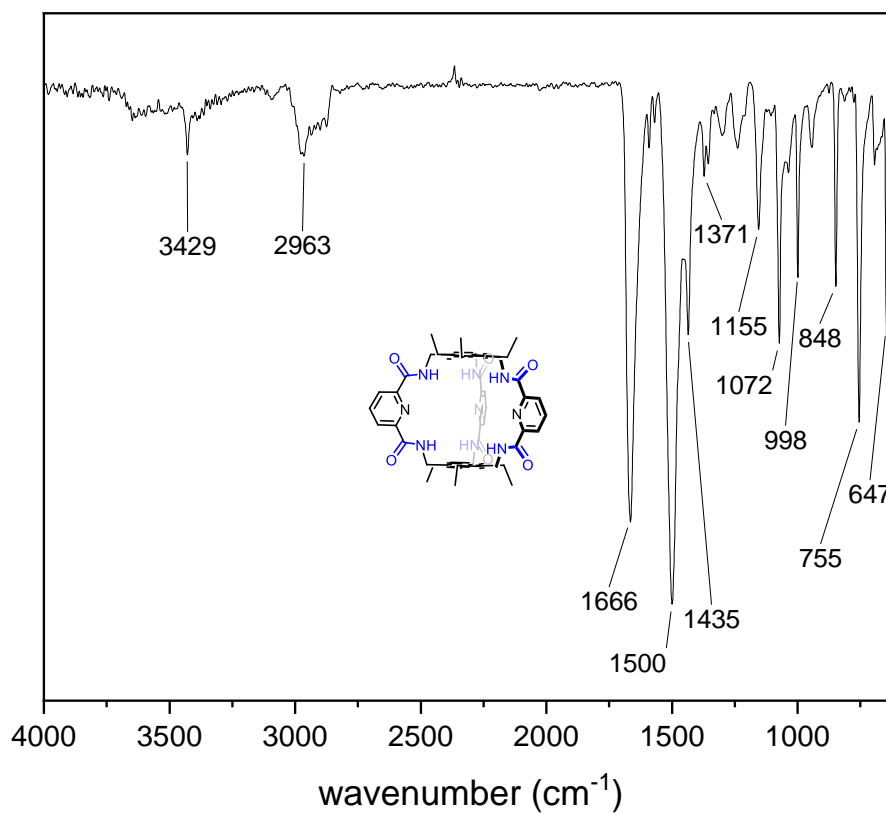
Figure 164. IR (ATR) spectrum of amide cage **A63-amide**.
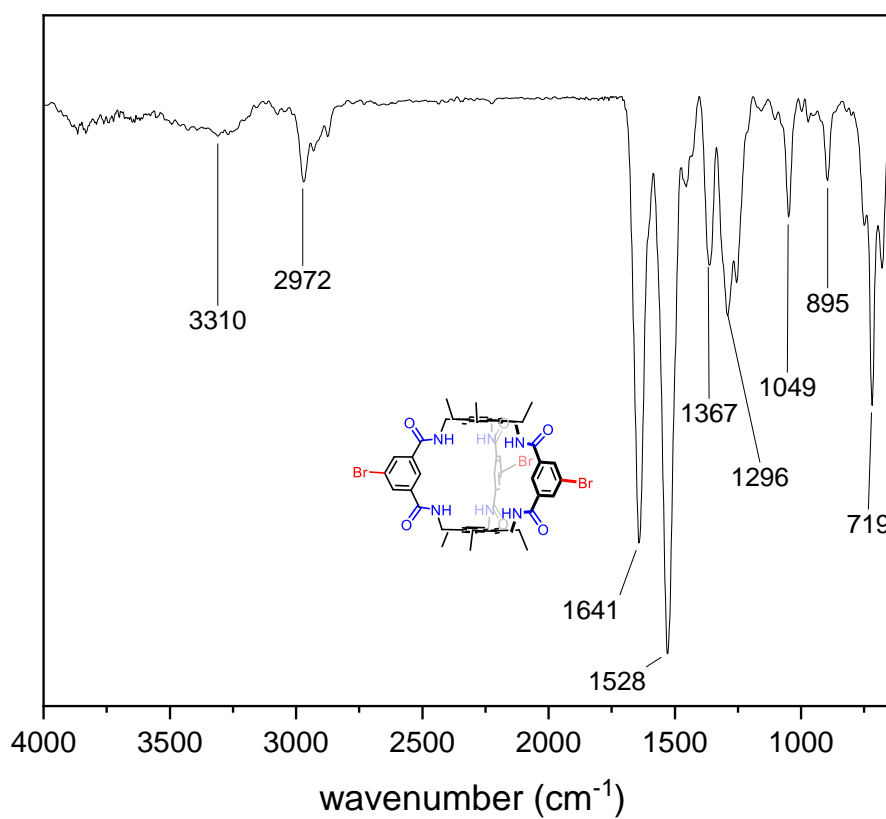
Figure 165. IR (ATR) spectrum of amide cage **A64-amide**.
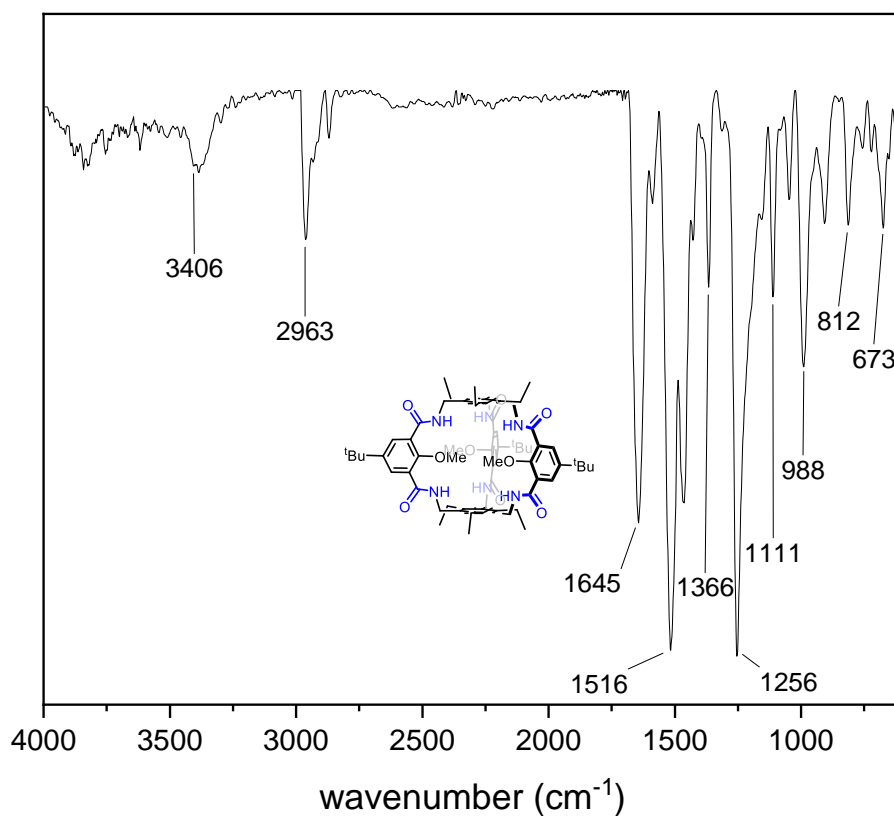
Figure 166. IR (ATR) spectrum of amide cage **A67-amide**.
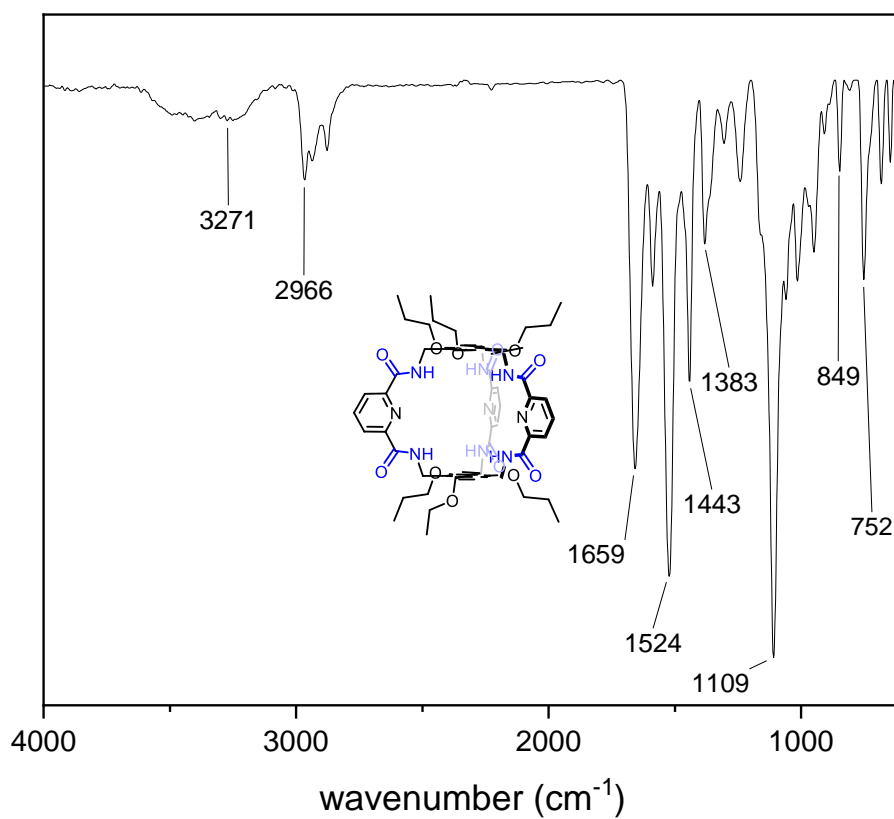
Figure 167. IR (ATR) spectrum of amide cage **B63-amide**.
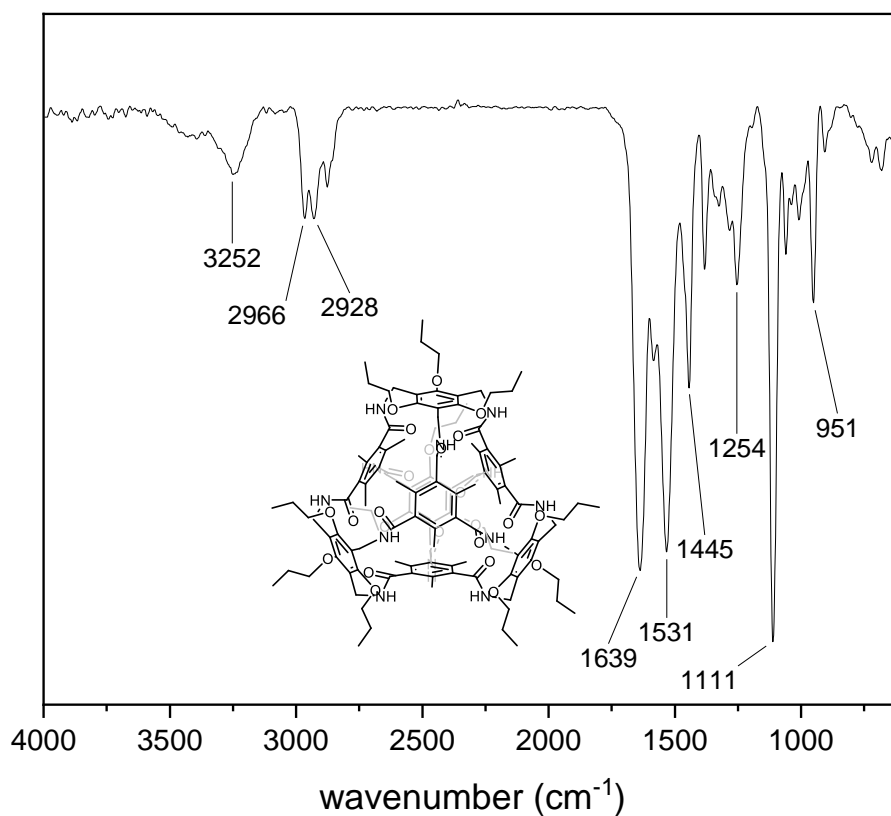
Figure 168. IR (ATR) spectrum of amide cage **B73-amide**.
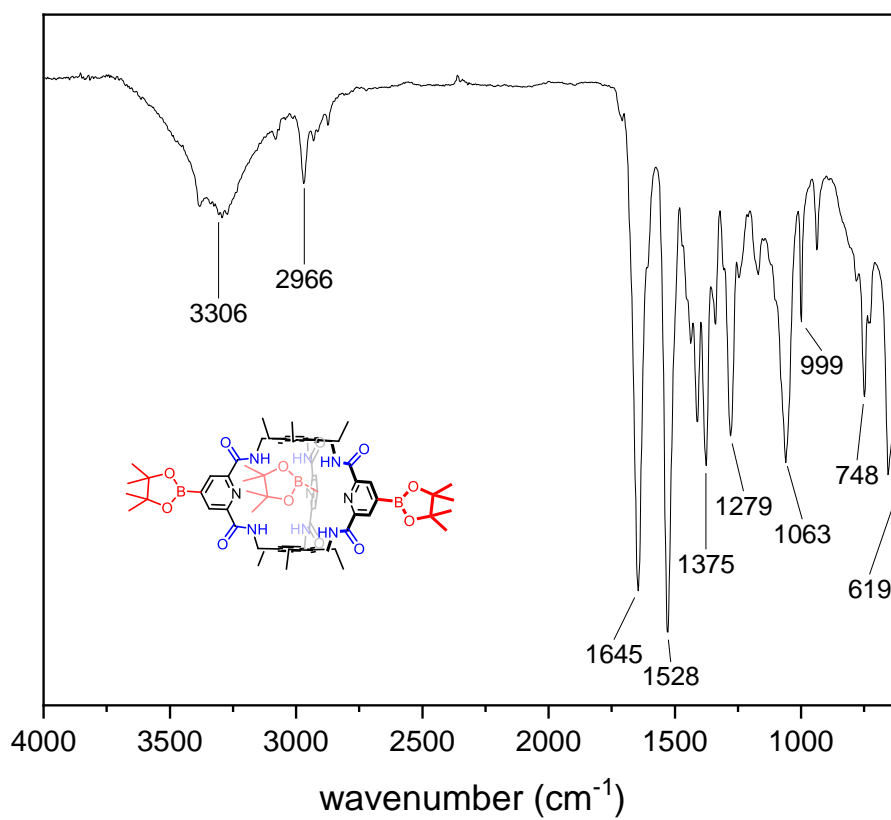
Figure 169. IR (ATR) spectrum of amide cage **74**.
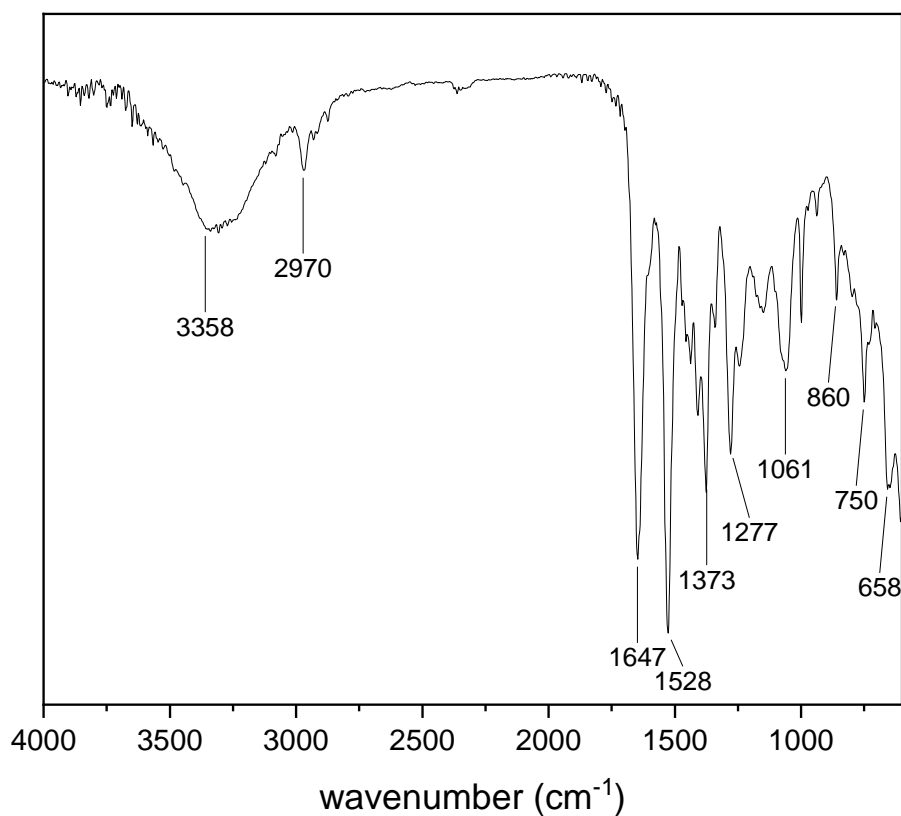
Figure 170. IR (KBr pellet) spectrum of amide cage **75**.
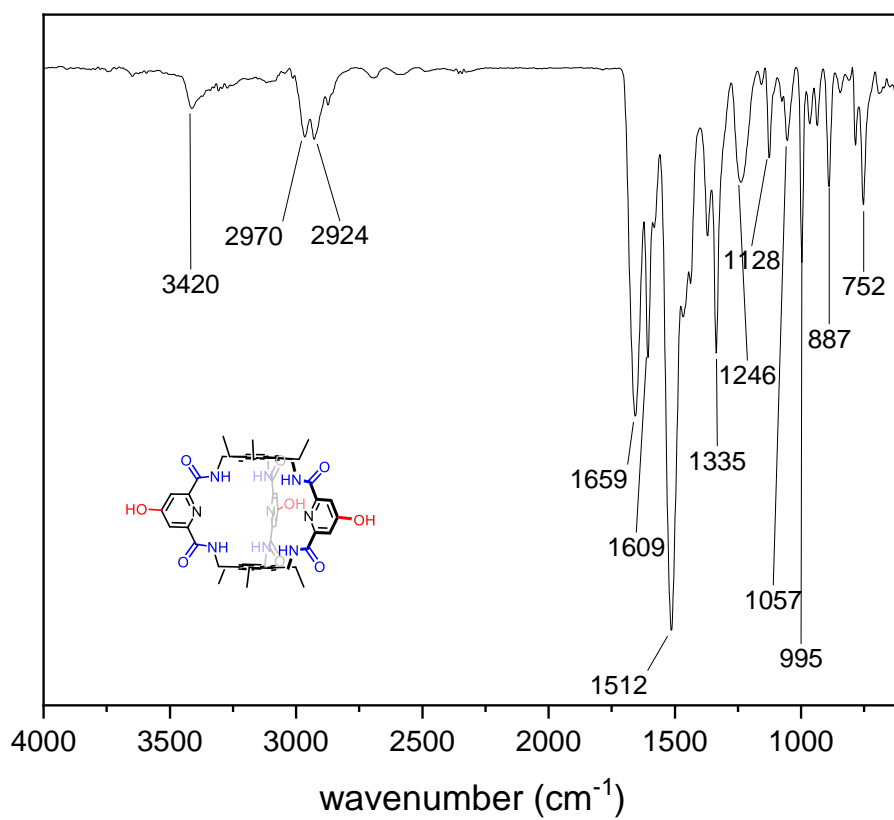
Figure 171. IR (ATR) spectrum of amide cage **76**.
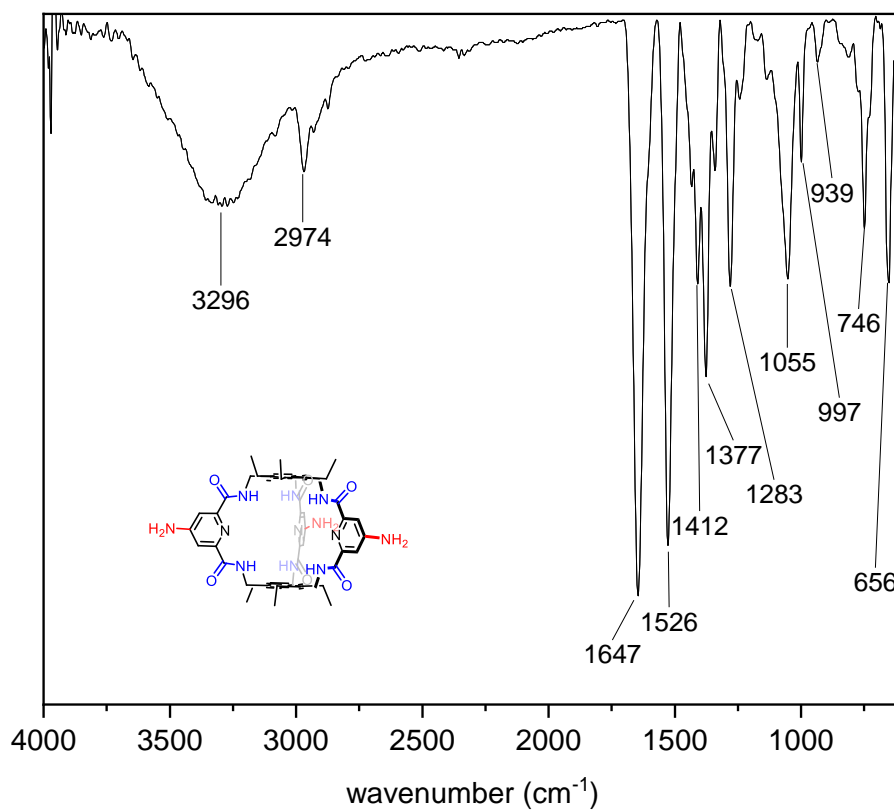
Figure 172. IR (ATR) spectrum of amide cage **77**.
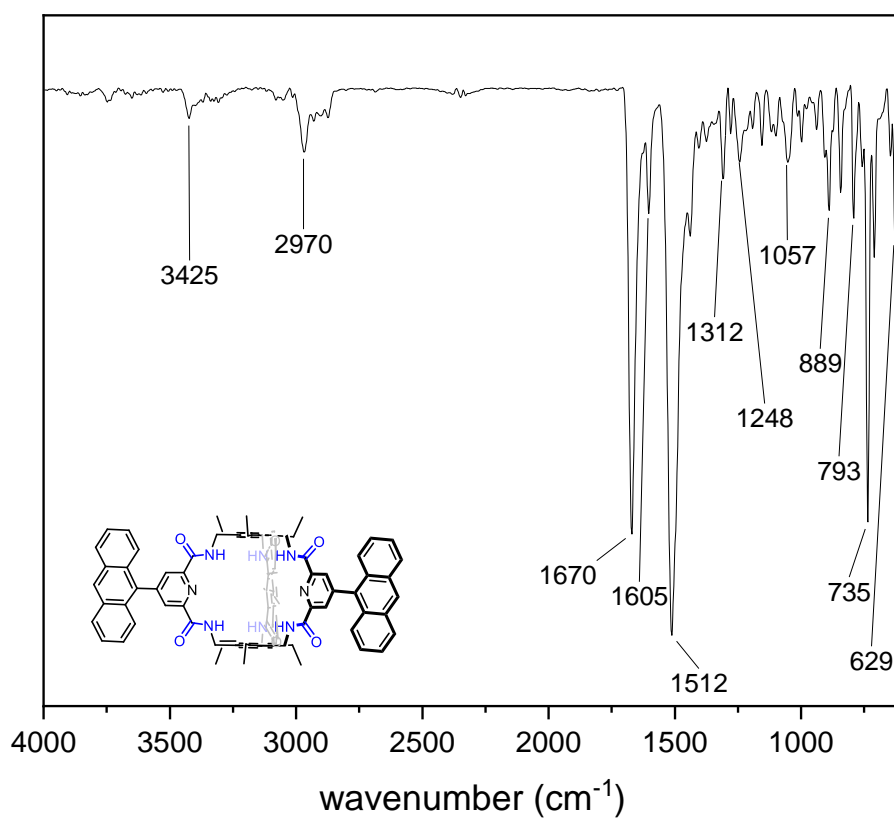
Figure 173. IR (ATR) spectrum of amide cage **78**.
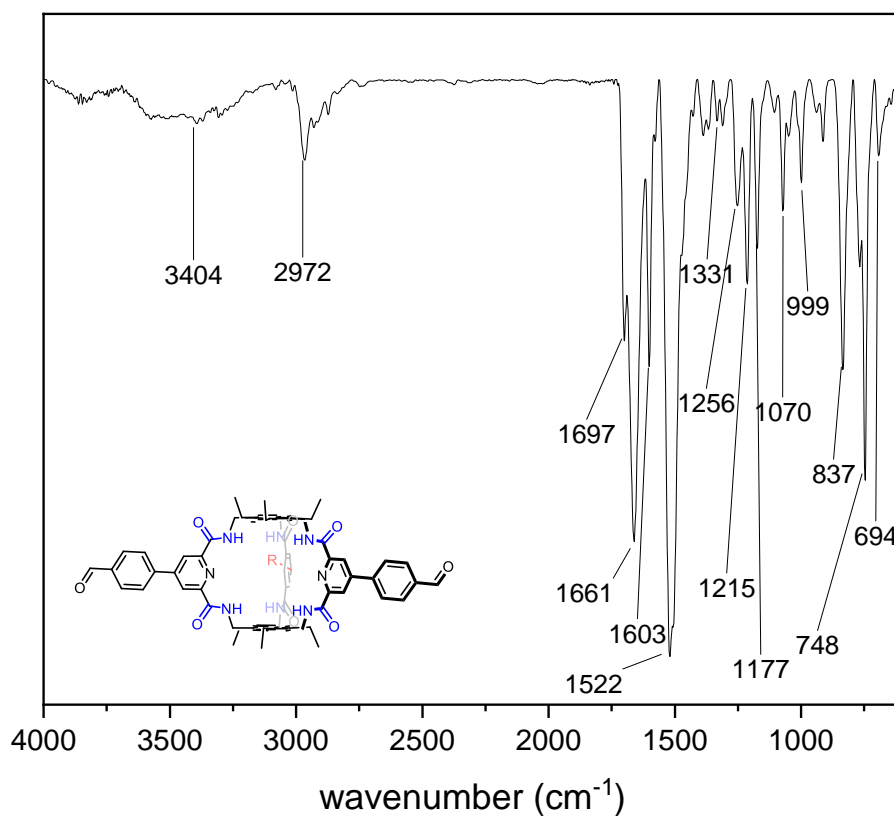
Figure 174. IR (ATR) spectrum of amide cage **79**.

4. Crystal structure data

4.1. Crystal structure of amide cage 61

Crystals suitable for SCXRD were obtained by slow evaporation of a solution of **61** in THF/water.
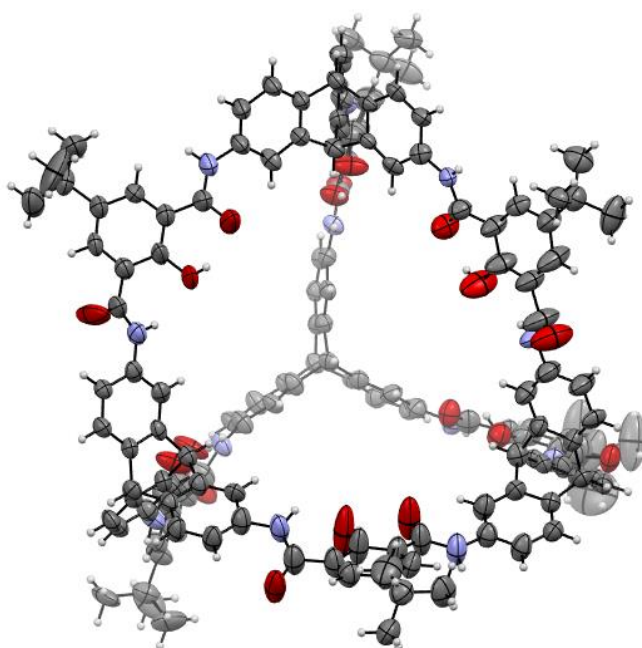
Identification code	avb7
Empirical formula	$C_{76}H_{64}N_6O_9$
Formula weight	1205.33
Temperature	110(2) K
Wavelength	1.54178 Å
Crystal system	triclinic
Space group	$P\bar{1}$
Z	4
Unit cell dimensions	a = 19.1852(8) Å α = 82.530(4) deg.
	b = 20.5440(11) Å β = 74.161(4) deg.
	c = 30.9823(16) Å γ = 82.259(4) deg.
Volume	11584.9(10) Å^3
Density (calculated)	0.69 g/cm^3
Absorption coefficient	0.37 mm^{-1}
Crystal shape	column
Crystal size	0.406 x 0.070 x 0.053 mm^3
Crystal colour	brown
Theta range for data collection	2.5 to 51.1 deg.
Index ranges	-12≤h≤19, -20≤k≤20, -31≤l≤31
Reflections collected	64800
Independent reflections	24118 (R(int) = 0.1117)
Observed reflections	13812 (I > 2σ (I))
Absorption correction	Semi-empirical from equivalents
Max. and min. transmission	2.24 and 0.56
Refinement method	Full-matrix least-squares on F^2
Data/restraints/parameters	24118 / 5877 / 1659
Goodness-of-fit on F^2	1.64
Final R indices (I>2sigma(I))	R1 = 0.148, wR2 = 0.434
Largest diff. peak and hole	0.48 and -0.44 eÅ^{-3}

4.2. Crystal structure of amide cage A62-amide

Crystals of amide cage **A62-amide** suitable for SCXRD were obtained by gradually cooling a hot saturated solution of **A62-amide** in methanol/diethyl ether.
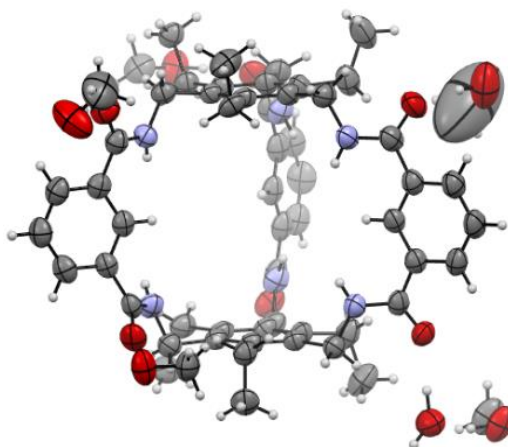
Identification number	avb8
Empirical formula	$C_{59}H_{82}N_6O_{12}$
Formula weight	1067.30
Temperature	200(2) K
Wavelength	1.54178 Å
Crystal system	triclinic
Space group	P$\bar{1}$
Z	2
Unit cell dimensions	a = 13.9033(8) Å α = 69.634(4) deg.
	b = 14.4499(8) Å β = 72.659(4) deg.
	c = 17.0983(9) Å γ = 68.413(4) deg.
Volume	2937.0(3) Å^3
Density (calculated)	1.21 g/cm^3
Absorption coefficient	0.68 mm^{-1}
Crystal shape	plate
Crystal size	0.157 x 0.067 x 0.016 mm^3
Crystal colour	colourless
Theta range for data collection	2.8 to 56.0 deg.
Index ranges	-14≤h≤14, -15≤k≤15, -13≤l≤18
Reflections collected	20023
Independent reflections	7595 (R(int) = 0.0565)
Observed reflections	4279 (I > 2σ (I))
Absorption correction	Semi-empirical from equivalents
Max. and min. transmission	1.36 and 0.61
Refinement method	Full-matrix least-squares on F^2
Data/restraints/parameters	7595 / 589 / 750
Goodness-of-fit on F^2	1.02
Final R indices (I>2sigma(I))	R1 = 0.068, wR2 = 0.156
Largest diff. peak and hole	0.27 and -0.29 eÅ^{-3}

4.3. Crystal structure of amide cage A63-amide

Crystals of **A63-amide** suitable for SCXRD were obtained by gradually cooling a hot saturated solution of **A63-amide** in methanol.
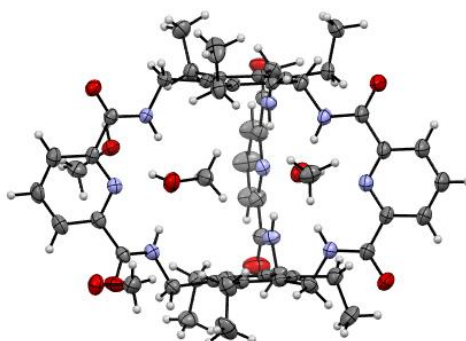
Identification code	avb14
Empirical formula	$C_{58}H_{85}N_9O_{14.50}$
Formula weight	1140.34
Temperature	200(2) K
Wavelength	0.71073 Å
Crystal system	triclinic
Space group	P$\overline{1}$
Z	4
Unit cell dimensions	a = 13.6868(9) Å α = 94.0110(16) deg.
	b = 16.5630(11) Å β = 92.9444(16) deg.
	c = 28.1253(18) Å γ = 90.1084(16) deg.
Volume	6351.7(7) Å^3
Density (calculated)	1.19 g/cm^3
Absorption coefficient	0.09 mm^{-1}
Crystal shape	brick
Crystal size	0.187 x 0.166 x 0.114 mm^3
Crystal colour	colourless
Theta range for data collection	0.7 to 24.1 deg.
Index ranges	-15≤h≤15, -19≤k≤19, -32≤l≤32
Reflections collected	76202
Independent reflections	20265 (R(int) = 0.0779)
Observed reflections	11342 (I > 2σ (I))
Absorption correction	Semi-empirical from equivalents
Max. and min. transmission	0.96 and 0.90
Refinement method	Full-matrix least-squares on F^2
Data/restraints/parameters	20265 / 1194 / 1522
Goodness-of-fit on F^2	1.03
Final R indices (I>2sigma(I))	R1 = 0.090, wR2 = 0.231
Largest diff. peak and hole	0.67 and -0.65 eÅ^{-3}

4.4. Crystal structure of amide cage A73-amide

Crystals of **B73-amide** suitable for SCXRD were obtained by gradually cooling a hot solution of **B73-amide** in DMSO.
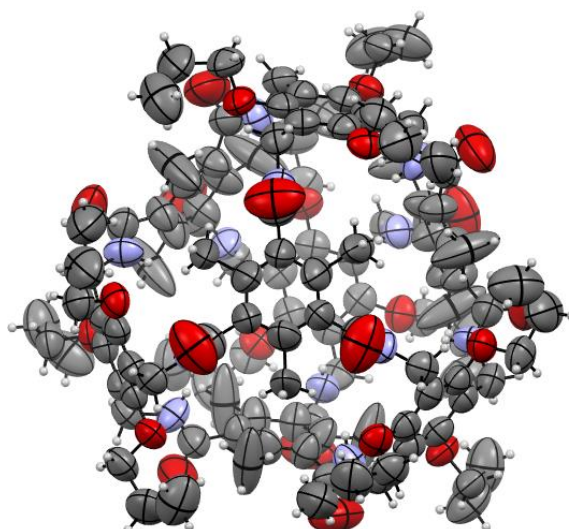
Identification code	avb13
Empirical formula	$C_{120}H_{156}N_{12}O_{24}$
Formula weight	2150.56
Temperature	200(2) K
Wavelength	1.54178 Å
Crystal system	cubic
Space group	$F\bar{4}3c$
Z	8
Unit cell dimensions	a = 34.0088(6) Å α = 90 deg.
	b = 34.0088(6) Å β = 90 deg.
	c = 34.0088(6) Å γ = 90 deg.
Volume	39335(2) Å^3
Density (calculated)	0.73 g/cm^3
Absorption coefficient	0.41 mm^{-1}
Crystal shape	cubic
Crystal size	0.190 x 0.135 x 0.115 mm^3
Crystal colour	colourless
Theta range for data collection	4.5 to 50.4 deg.
Index ranges	-33≤h≤33, -34≤k≤18, -27≤l≤34
Reflections collected	22821
Independent reflections	1717 (R(int) = 0.0484)
Observed reflections	1448 (I > 2σ (I))
Absorption correction	Semi-empirical from equivalents
Max. and min. transmission	2.56 and 0.55
Refinement method	Full-matrix least-squares on F^2
Data/restraints/parameters	1717 / 73 / 120
Goodness-of-fit on F^2	2.30
Final R indices (I>2sigma(I))	R1 = 0.100, wR2 = 0.279
Absolute structure parameter	0.3(3)
Largest diff. peak and hole	0.26 and -0.28 eÅ^{-3}

4.5. Crystal structure of amide cage 78

Crystals of **78** suitable for SCXRD were obtained by vapour diffusion of diethyl ether into a solution of **78** in DCM.
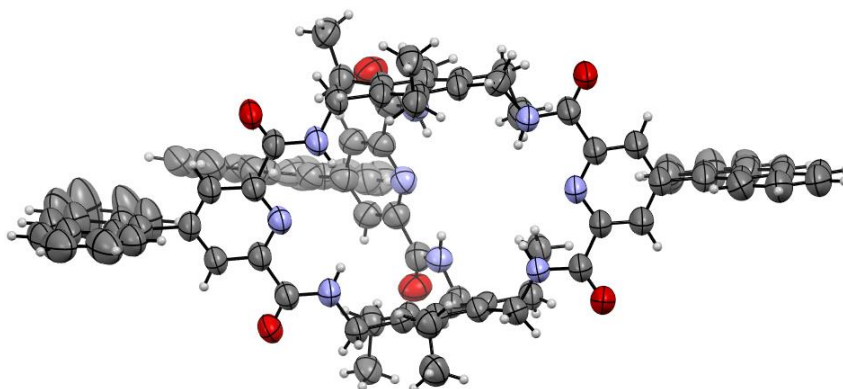
Identification code	AB556
Empirical formula	$C_{107.50}H_{116}Cl_5N_9O_9$
Formula weight	1855.34
Temperature	150(2) K
Wavelength	1.54178 Å
Crystal system	monoclinic
Space group	C2/c
Z	8
Unit cell dimensions	a = 31.8114(12) Å α = 90 deg.
	b = 25.1389(14) Å β = 104.027(3) deg.
	c = 25.3072(11) Å γ = 90 deg.
Volume	19634.8(16) Å^3
Density (calculated)	1.25 g/cm^3
Absorption coefficient	1.84 mm^{-1}
Crystal shape	brick
Crystal size	0.160 x 0.136 x 0.067 mm^3
Crystal colour	pale brown
Theta range for data collection	3.1 to 51.1 deg.
Index ranges	-32≤h≤31, -25≤k≤25, -25≤l≤20
Reflections collected	61661
Independent reflections	10574 (R(int) = 0.0796)
Observed reflections	6724 (I > 2σ (I))
Absorption correction	Semi-empirical from equivalents
Max. and min. transmission	1.61 and 0.69
Refinement method	Full-matrix least-squares on F^2
Data/restraints/parameters	10574 / 1709 / 1136
Goodness-of-fit on F^2	1.64
Final R indices (I>2sigma(I))	R1 = 0.140, wR2 = 0.384
Largest diff. peak and hole	1.15 and -0.61 eÅ^{-3}

4.6. Amide cage (A63-amide) zinc complex attempt

Crystals suitable for SCXRD were obtained while attempting to form a metal complex of cage **A63'** with $ZnCl_2$ using K_2CO_3 as a base. Reaction was conducted in MeOH under reflux for 16 hours. On cooling to rt, the reaction mixture was filtered, followed by exchanging the solvent with acetonitrile.
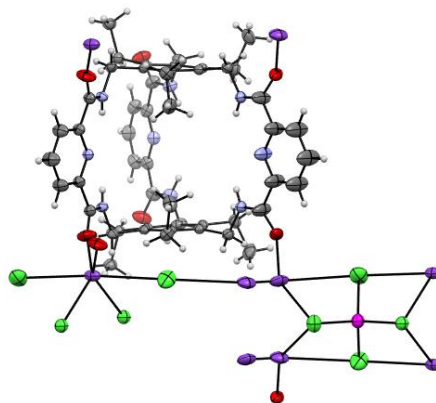
Identification code	avb10
Empirical formula	$C_{65}H_{78}Cl_4K_2N_{16}O_6Zn$
Formula weight	1464.80
Temperature	200(2) K
Wavelength	0.71073 Å
Crystal system	monoclinic
Space group	C2/m
Z	4
Unit cell dimensions	a = 34.7069(8) Å $\quad$ α = 90 deg.
	b = 14.0284(3) Å $\quad$ β = 91.670(1) deg.
	c = 14.7758(3) Å $\quad$ γ = 90 deg.
Volume	7191.0(3) Å^3
Density (calculated)	1.35 g/cm^3
Absorption coefficient	0.67 mm^{-1}
Crystal shape	brick
Crystal size	0.172 x 0.086 x 0.062 mm^3
Crystal colour	colourless
Theta range for data collection	1.2 to 30.5 deg.
Index ranges	-48≤h≤47, -20≤k≤20, -21≤l≤21
Reflections collected	47171
Independent reflections	11284 (R(int) = 0.0425)
Observed reflections	7360 (I > 2σ (I))
Absorption correction	Semi-empirical from equivalents
Max. and min. transmission	0.89 and 0.82
Refinement method	Full-matrix least-squares on F^2
Data/restraints/parameters	11284 / 556 / 544
Goodness-of-fit on F^2	1.03
Final R indices (I>2sigma(I))	R1 = 0.056, wR2 = 0.149
Largest diff. peak and hole	1.03 and -0.51 eÅ^{-3}

5. Gas sorption data

5.1. Theoretical background of gas sorption studies

In contrast to chemisorption (enthalpy of adsorption in the range of 40 – 500 kJ/mol), physisorption (enthalpy of adsorption in the range to 20 – 40 kJ/mol) occurs mostly due to weak dispersion interactions.[174] To conduct investigations in the range of physisorption, IUPAC recommends use of either Nitrogen (at 77K) or Argon (at 87K) as the adsorbates at cryogenic temperatures. In comparison to Argon, the measurement uncertainty with N_2 can go up to 20% due to its quadrupole moment.[128] However, due to practical reasons, with the availability of liquid nitrogen, the gas sorption experiments have been conducted with N_2 as the adsorbate. In 1985, IUPAC classified physisorption isotherms into six classes which was later updated explain the pore structures of the adsorbent.[128, 175] To further evaluate the surface area of the porous materials, BET (Brunauer-Emmett-Teller) method continues to be the most widely used procedure.[176]

While the use of the BET theory is easily applicable to macroporous and mesoporous adsorbents, applying it to microporous surfaces offers a bit of a challenge. Since the [4+6] amide cage materials primarily show microporous characteristics (see section 1.4.1), a useful procedure proposed by Rouquerol et al. helps finding the linear range of the BET plot.[177] This procedure is based on two main criteria:

i.   The y-intercept 'C' of the BET plot should always be positive.
ii. Application of the BET equation must be restricted to the range where $V(1 – P/P_0)$ continuously increases with P/P_0, where V is the adsorbed volume and P/P_0 is the relative pressure.

In addition to the specific surface area of these porous materials, it is useful to study pore sizes and their distribution. To understand the pore size distribution of microporous materials, methods based on density functional theory (DFT) and Monte-Carlo simulations (MC) have been used.[178] Though the non-local density functional theory (NLDFT) method proved to be particularly suitable for highly structured smooth surfaces (e.g. crystalline materials), amorphous materials deviate from this model. [179] Again, since some of the [4+6] amide cages appear to be amorphous in nature (see section 1.4.1), the quenched solid density functional theory (QSDFT) offers an alternate method to study the pore sizes of such heterogeneous surfaces.[178]

The methods described above are mostly used for the nitrogen adsorption isotherms. Further investigation of the adsorption of gases such as hydrogen, methane and carbon dioxide provide information for the prospective applications for the porous materials. Since the selective uptake of a certain gas from a binary gas mixture is of particular interest, several methods have been developed to study such a selectivity.[180] Two of those methods used in this study are the Henry selectivity method and the IAST selectivity method. Applying iterative approximation of the the non-linear Tóth equation (equation 1) to the experimentally obtained isotherms, the Henry constants can be calculated using equation 2.

$$q = \frac{q_s \cdot b^{1/n} \cdot p}{(1+(bp)^n)^{1/n}} \tag{1}$$

$$K_H = \lim_{p \to 0} \frac{dq}{dp} = b^{1/n} \cdot q_s \tag{2}$$

where, q is the adsorbed amount (in mmol/g), q_s is the saturation vapour pressure (in mmol/g) at pressure p (in bar), b and n are constants for specific adsorbent-adsorbate pairs.

The ratio of the Henry constants of gases A and B gives the Henry selectivity of gas A over gas B as shown in equation 3.

$$S_{A/B} = \frac{K_{H,A}}{K_{H,B}} \tag{3}$$

While the Henry selectivity method considers the co-efficients of two isolated gases, the IAST (*ideal adsorbed solution theory*) considers a binary system of gases. This method proposed by Myers et al. was used to calculated the selectivity of CO_2 over CH_4 using the [4+6] amide cages (see section 1.4.2).[181]

The strength of the interactions between the adsorbate and the adsorbate is estimated by calculating the isosteric heat of adsorption (Q_s). The adsorption isotherms of CO_2 and CH_4 was recorded at two different temperatures for all the amide cages and then fit iteratively to a virial-type equation (equation 4).

$$\ln p = \ln q + \frac{1}{T} \sum_{i=0}^{m} \left(a_i \cdot q^i \right) \sum_{i=0}^{m} b_i \cdot q^i \tag{4}$$

where, p is the pressure (in torr), q is the amount of gas adsorbed (in mol/g), T is the temperature (in K), a_i and b_i are a virial co-efficients, n and m are the number of coefficients required to adequately describe the isotherms.

The number of coefficients (*n* and *m*) were gradually increased until the contribution of extra added *a* and *b* coefficients was deemed to be statistically insignificant towards the overall fit, and the average value of the squared deviations from the experimental values was minimized (m≤6, n≤3). The values of the virial coefficients a_0 through a_m were then used to calculate the isosteric heat of adsorption using the following expression.[182]

$$Q_{st} = -R \sum_{i=0}^{m}(a_i \cdot q^i) \tag{5}$$

where: Q_{st} is the coverage-dependent isosteric enthalpy of adsorption (in J/mol), *R* is the universal gas constant (in $J \cdot K^{-1} \cdot mol^{-1}$), *q* is the amount of gas adsorbed (mol/g), a_i is a virial coefficient and *m* is the number of coefficients required to adequately describe the isotherms.

The heat of adsorption at zero-loading is taken as the value of the heat of adsorption since it best reflects the interactions between the adsorbate and the unloaded adsorbent (see section 1.4.2).

5.2. Nitrogen sorption at 77K

Cage 75 or possible boroxine COF
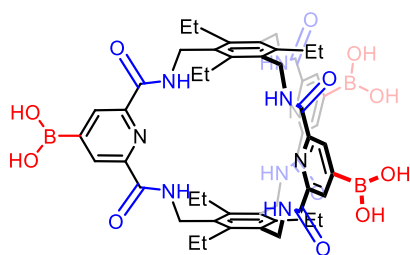
50 mg of the compound was suspended in isopropanol (30 mL) for 6 hours. It was filtered and washed with isopropanol (2 × 20 mL) (repeated 3 times) and then suspended in diethyl ether (30 mL) for 18 hours (repeated 3 times). It was filtered and washed with diethyl ether (2 × 20 mL) and dried under high vacuum (10^{-2} bar) at 100 °C for 16 hours.
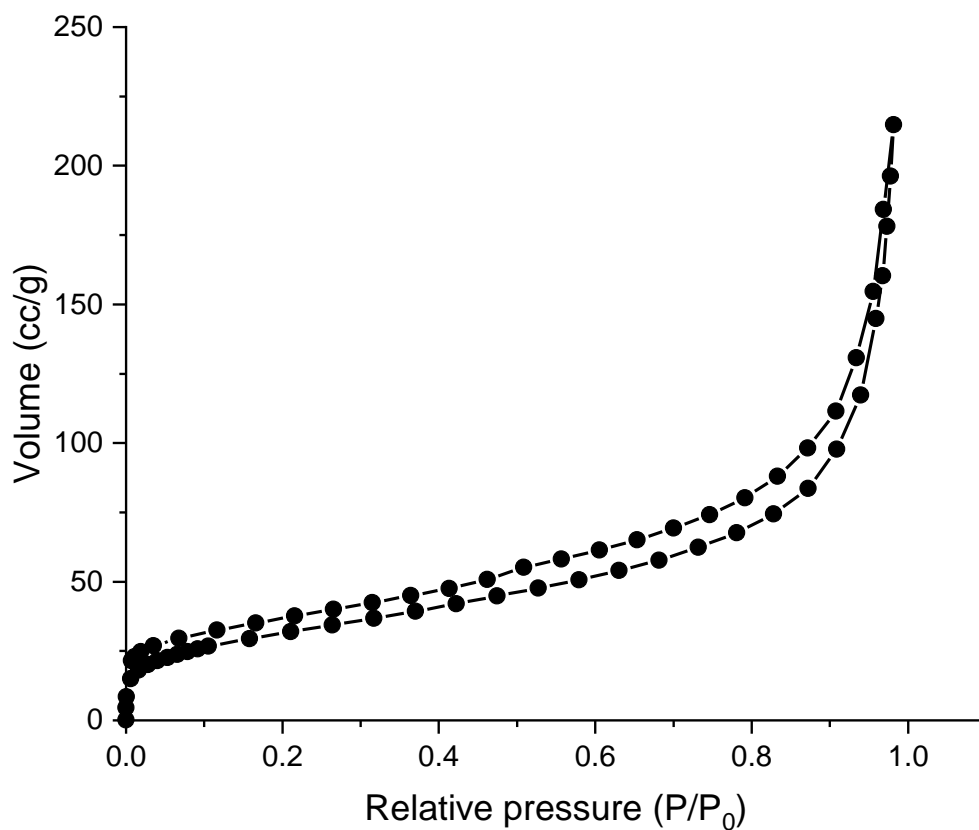
Figure 175. Nitrogen adsorption (black filled circles) and desorption (black hollow circles) isotherms of cage **75** at 77K.
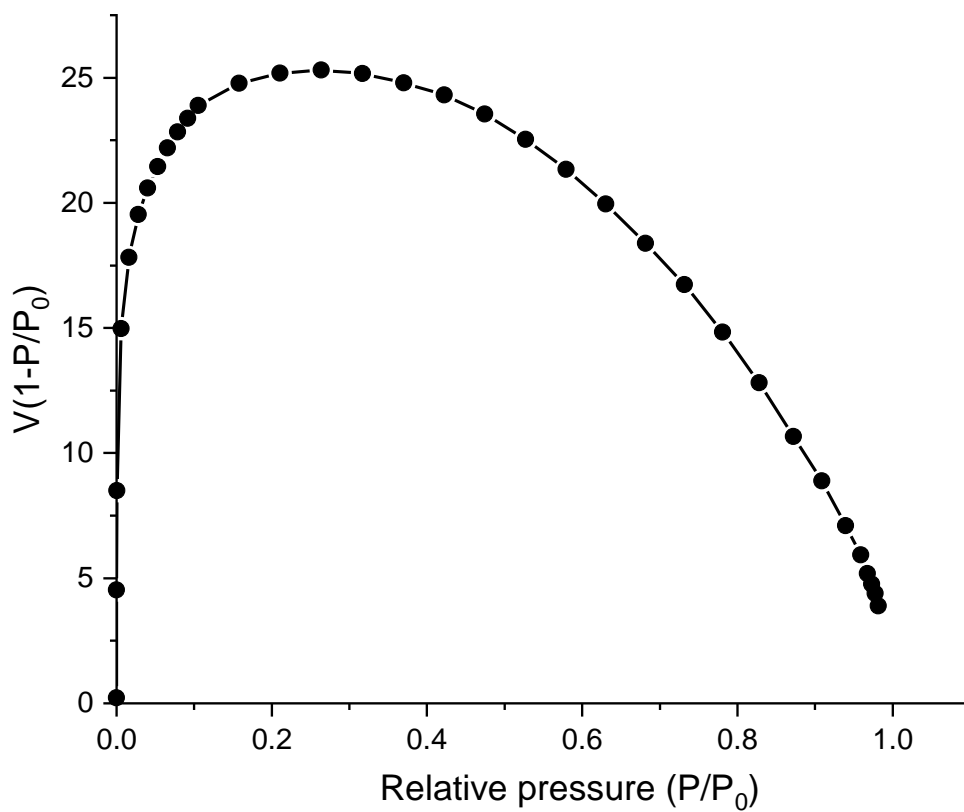
Figure 176. Rouquerol-plot for N_2 adsorption isotherm of cage **75.**
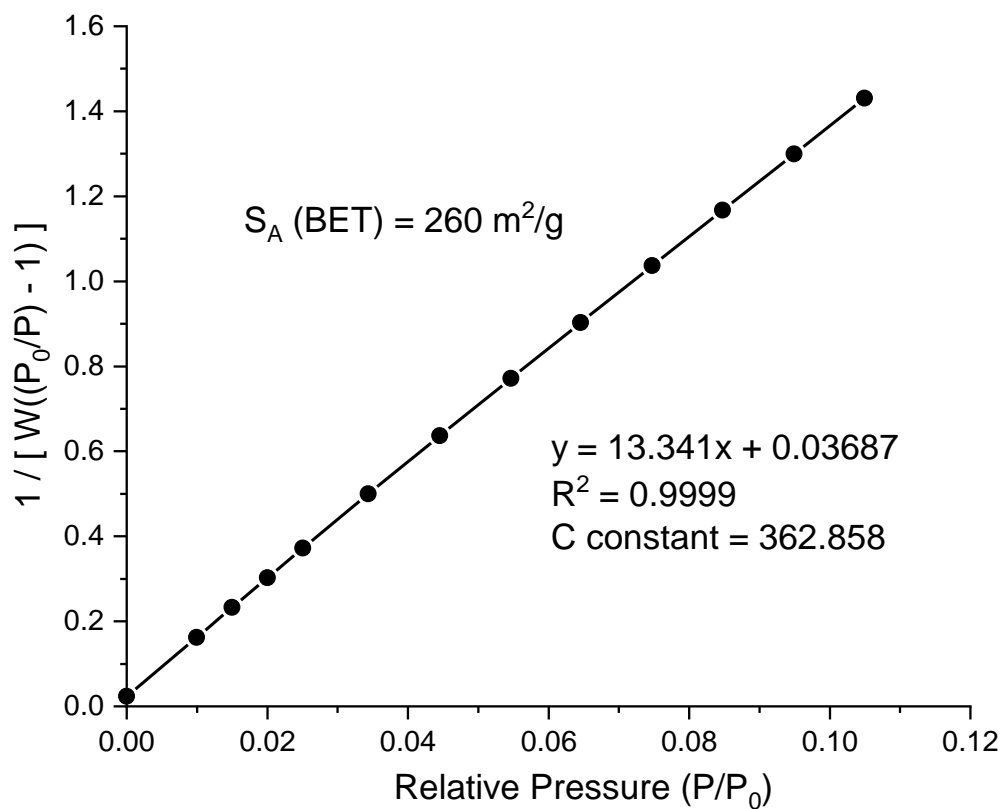
Figure 177. BET-plot corresponding to N_2 adsorption at 77K for cage **75**.
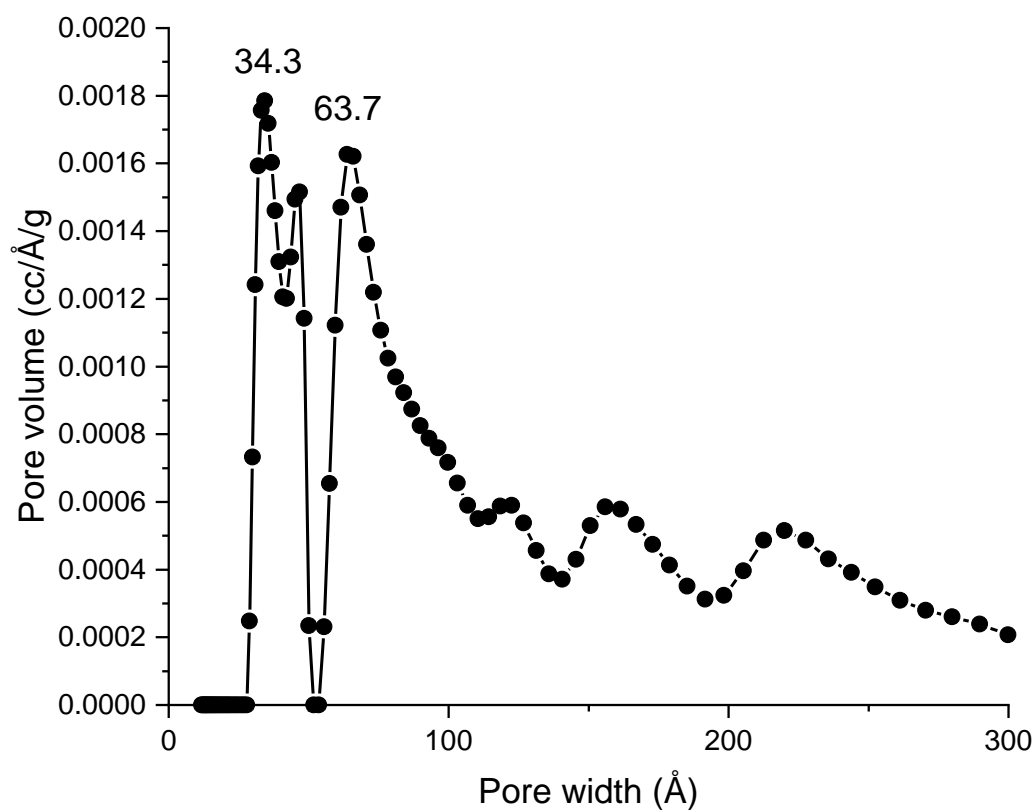
Figure 178. QSDFT (spherical/cylindrical pores, N_2 at 77 K on carbon) pore size distribution plot for cage **75**.

Cage 76
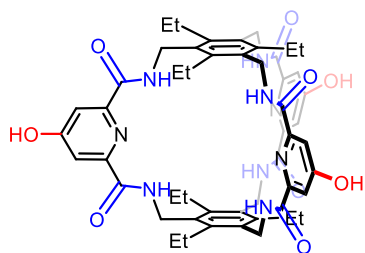
20 mg of the compound was suspended in diethyl ether (30 mL) for 18 hours. It was filtered and washed with diethyl ether (2×20 mL) (repeated 3 times) and dried under high vacuum (10^{-2} bar) at 100 °C for 3 hours.
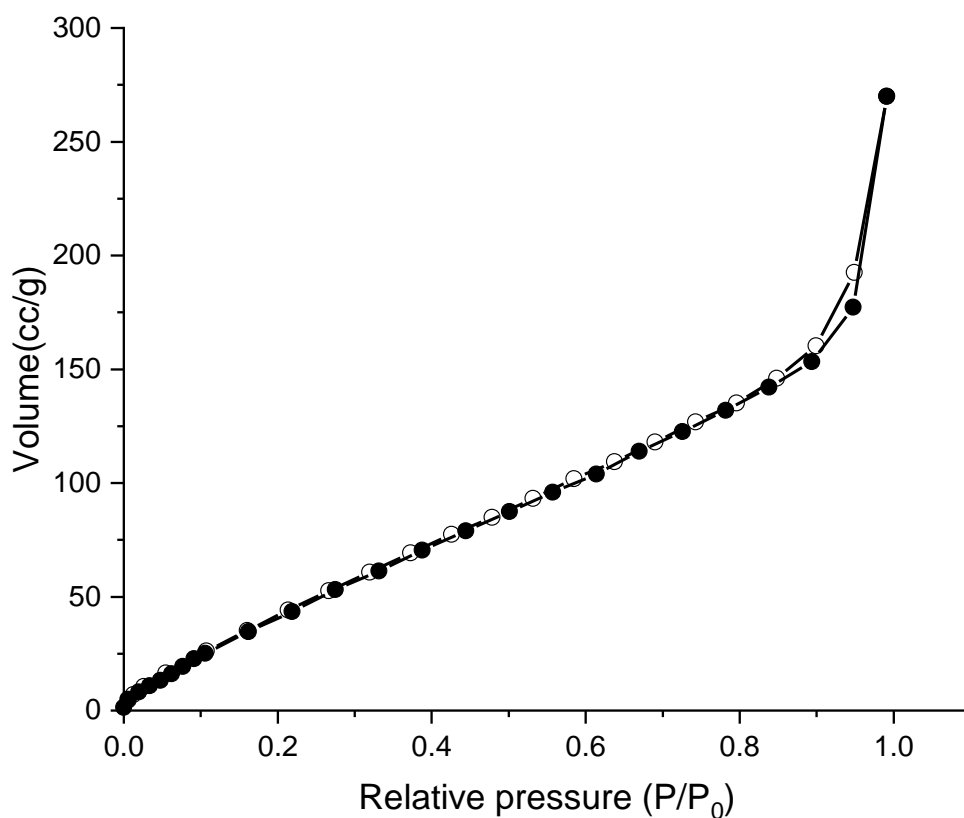
Figure 179. Nitrogen adsorption (black filled circles) and desorption (black hollow circles) isotherms of cage **76** at 77K.
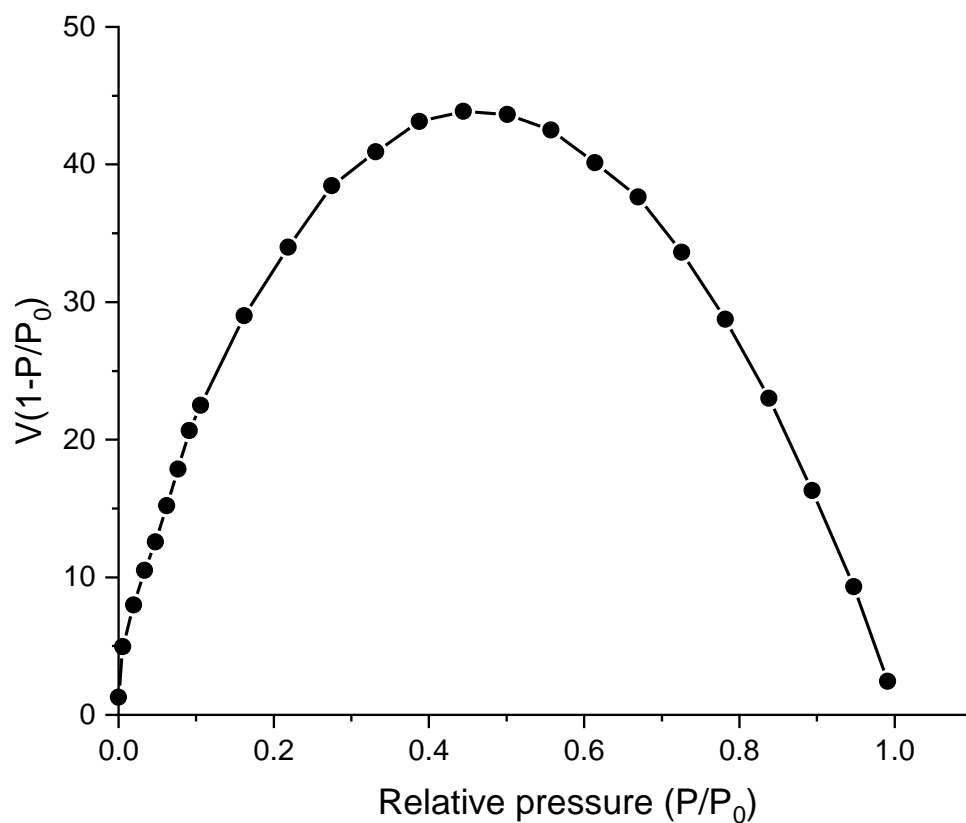
Figure 180. Rouquerol-plot for N_2 adsorption isotherm of cage **76**.

S_A (BET) = 129 m^2/g

y = 25.685x + 1.384
R^2 = 0.9238
C constant = 19.563
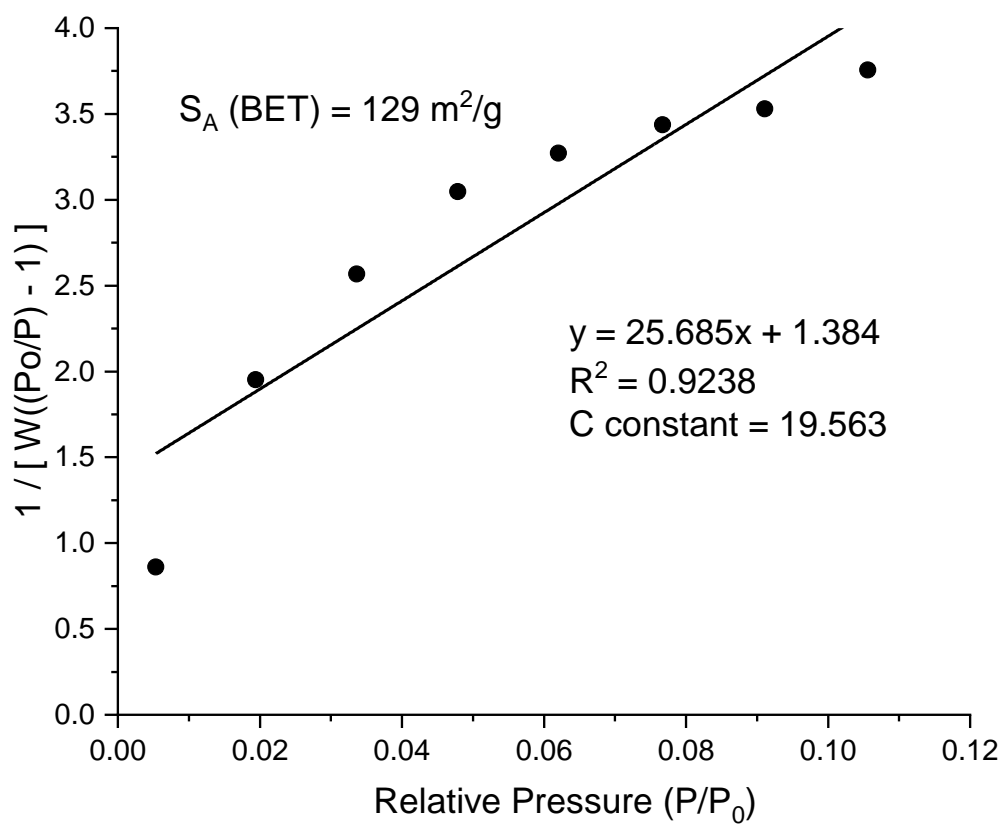
Figure 181. BET-plot corresponding to N_2 adsorption at 77K for cage **76**.
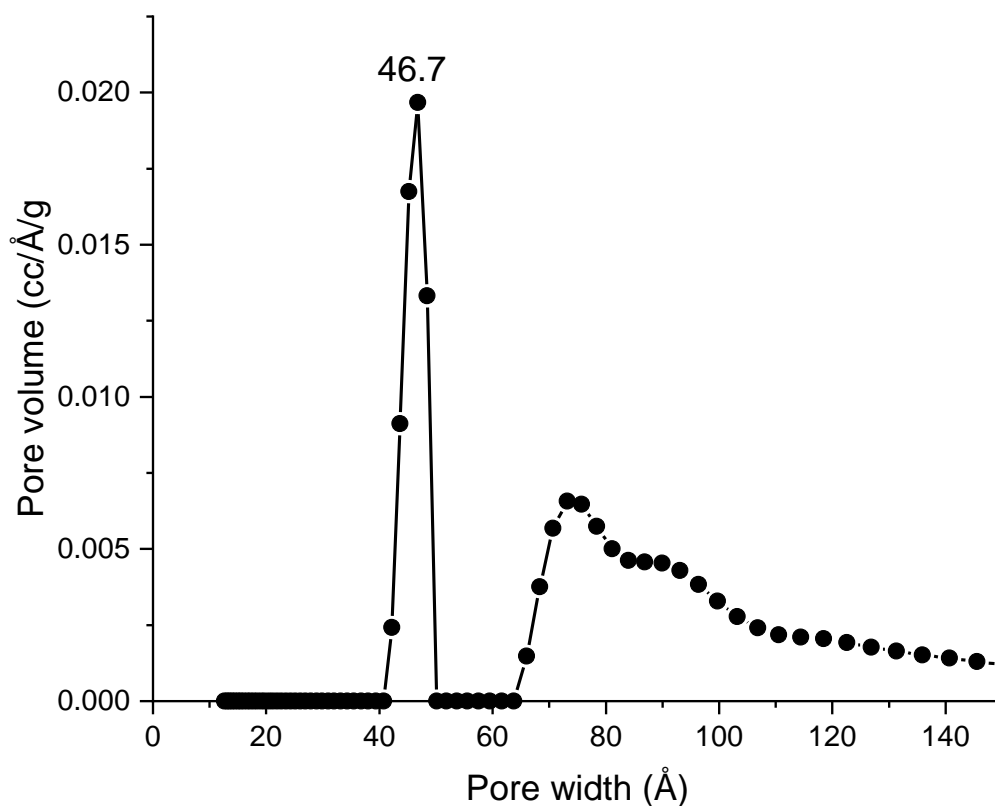
Figure 182. QSDFT (spherical/cylindrical pores, N_2 at 77 K on carbon) pore size distribution plot for cage **76**.

Cage 77
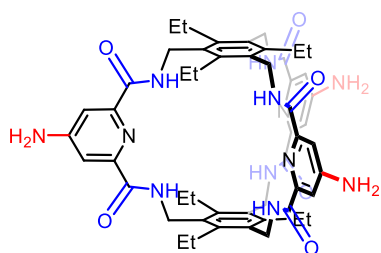
50 mg of the compound was suspended in isopropanol (30 mL) for 6 hours. It was filtered and washed with isopropanol (2×20 mL) (repeated 3 times) and then suspended in diethyl ether (30 mL) for 18 hours. It was filtered and washed with diethyl ether (2×20 mL) and dried under high vacuum (10^{-2} bar) at 100 °C for 3 hours.
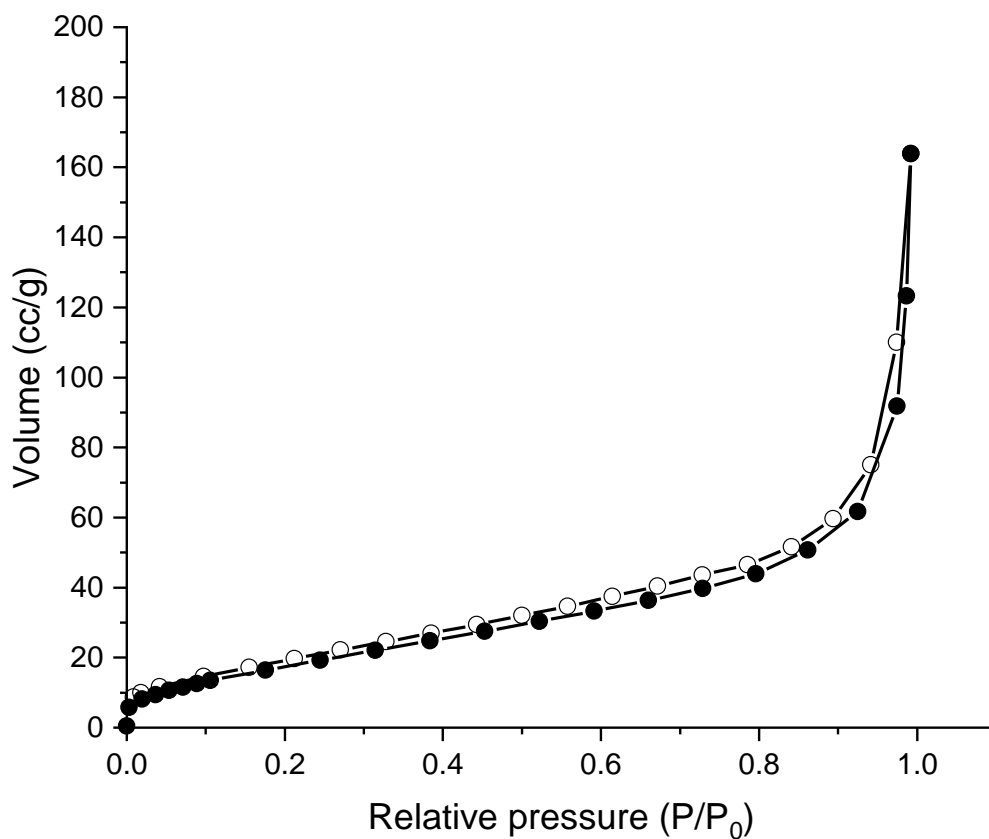
Figure 183. Nitrogen adsorption (black filled circles) and desorption (black hollow circles) isotherms of cage **77** at 77K.
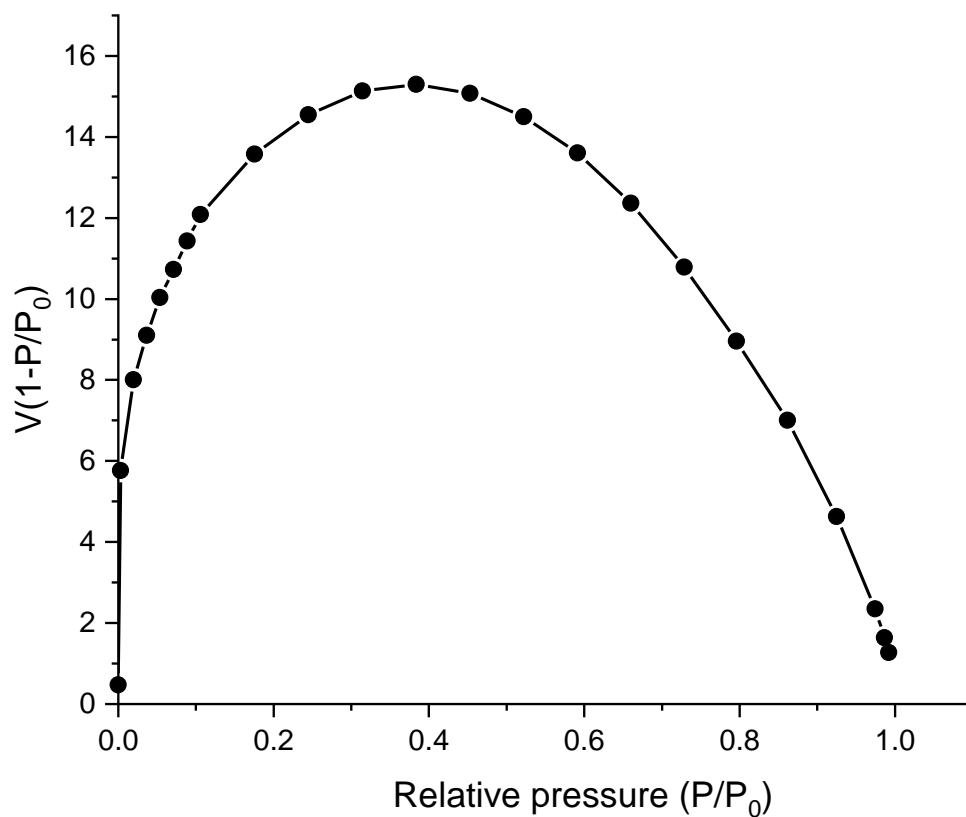
Figure 184. Rouquerol-plot for N_2 adsorption isotherm of cage **77**.
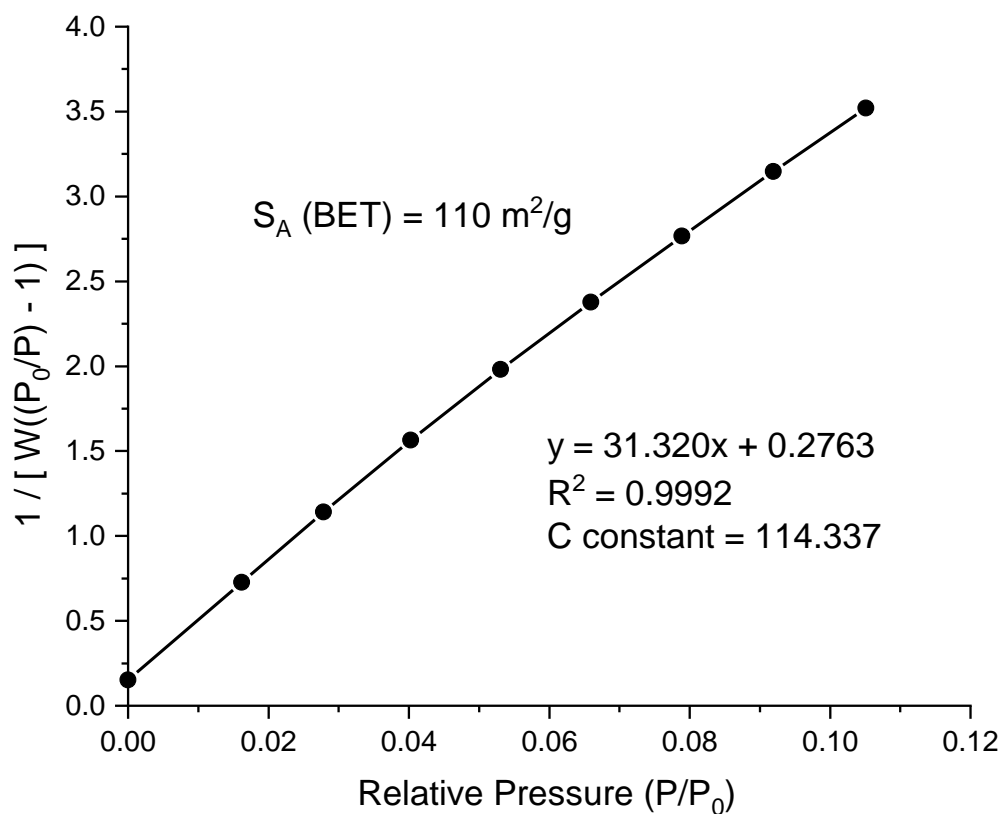
Figure 185. BET-plot corresponding to N_2 adsorption at 77K for cage **77**.
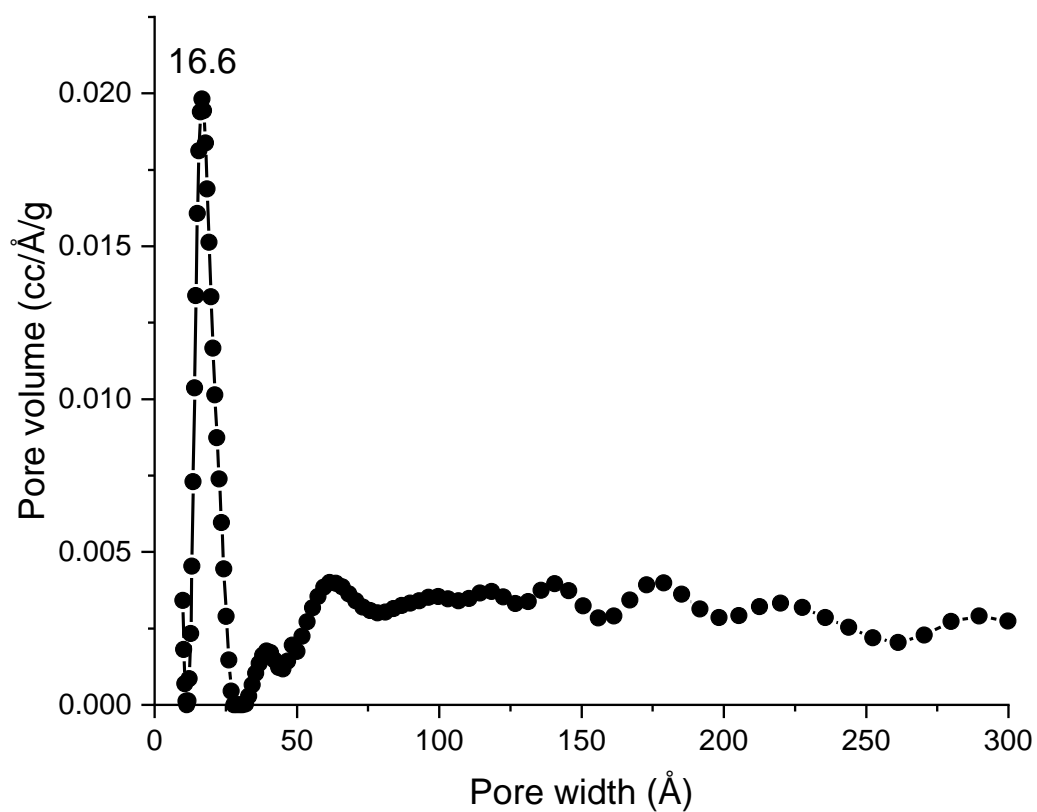
Figure 186. QSDFT (spherical/cylindrical pores, N_2 at 77 K on carbon) pore size distribution plot for cage **77**.

Cage **77** was subjected to imine condensation with terephthalaldehyde reaction in dioxane : mesitylene = 4:1 at 120 °C under acid catalysis (6M AcOH). Although it was found that the imine condensation did not take place, and the starting material was left unchanged, the gas sorption properties of the new material was different and is presented below:
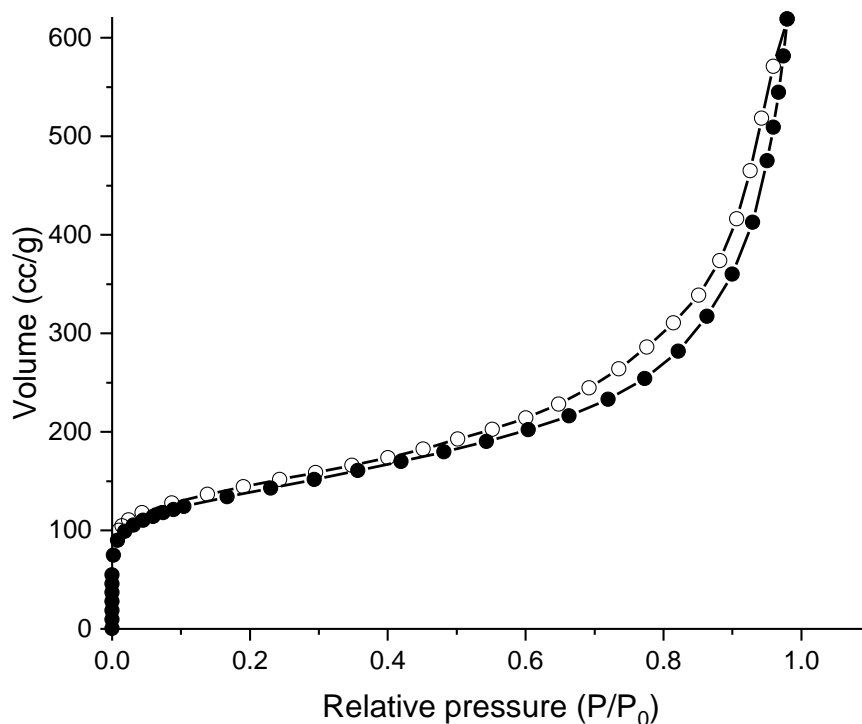
Figure 187. Nitrogen adsorption (black filled circles) and desorption (black hollow circles) isotherms of cage **77** after attempted imine condensation reaction at 77K.
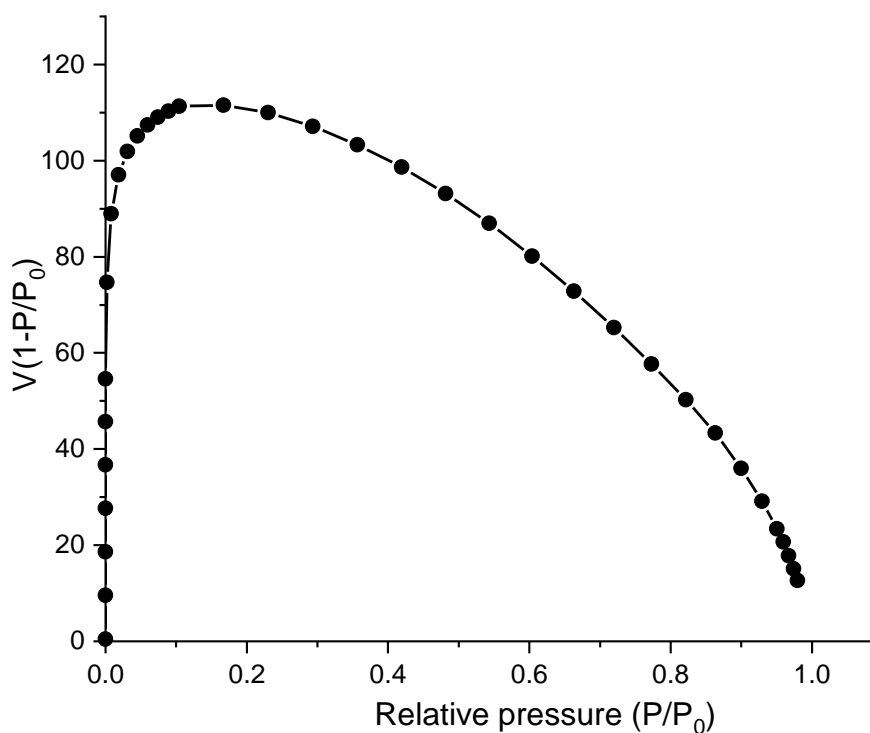
Figure 188. Rouquerol-plot for N_2 adsorption isotherm of cage **77** after attempted imine condensation reaction.
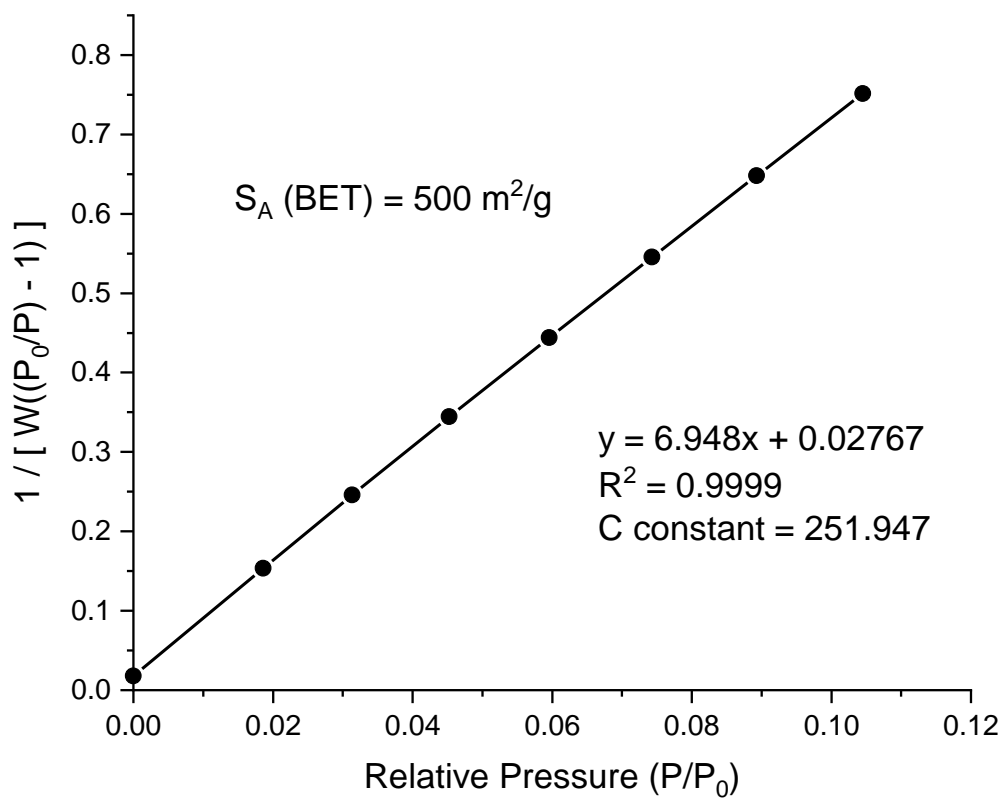
Figure 189. BET-plot corresponding to N_2 adsorption at 77K for cage **77** after the attempted imine condensation reaction.
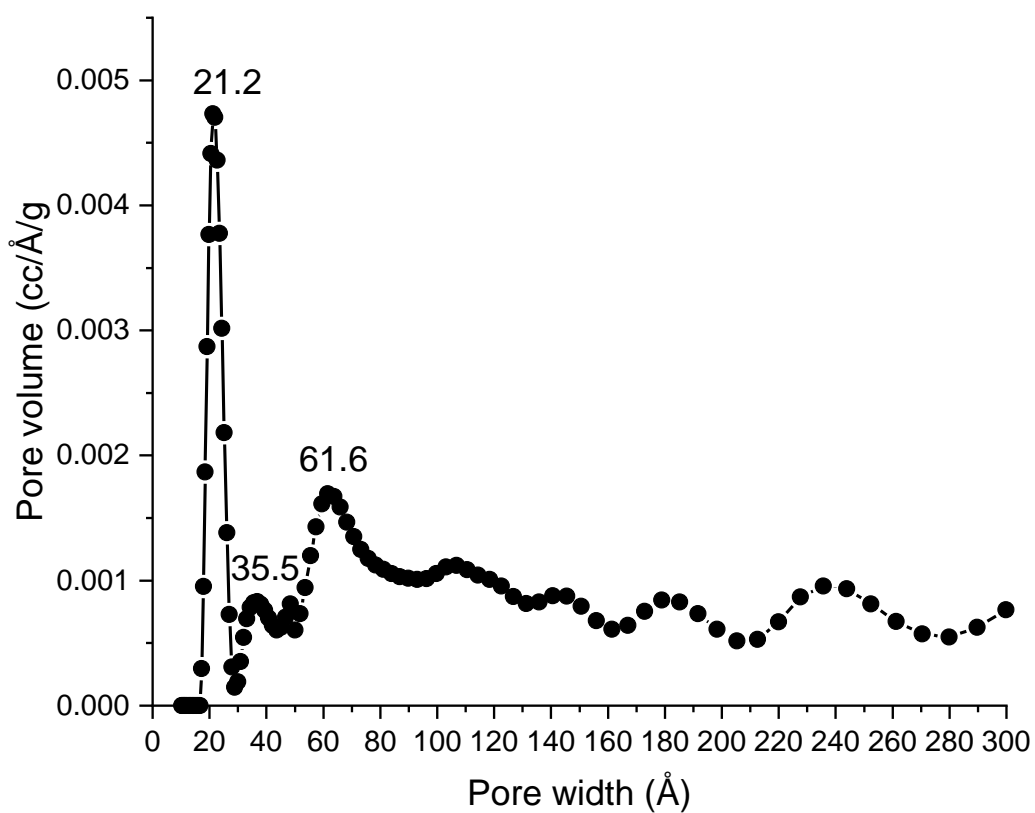
Figure 190. QSDFT (spherical/cylindrical pores, N_2 at 77 K on carbon) pore size distribution plot for cage **77** after attempted imine condensation reaction.

6. UPLC assay

6.1. Optimization of the Pinnick oxidation with model cage A62
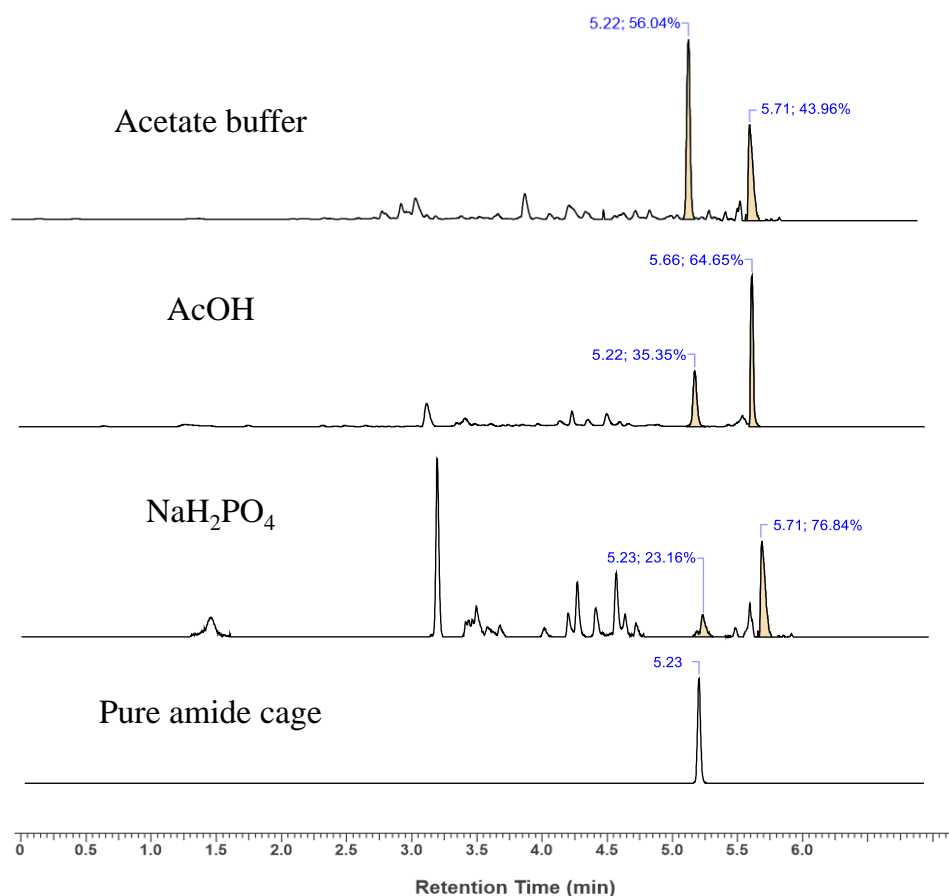
Figure 191. UPLC traces of the crude mixture of Pinnick oxidation and the internal standard (anthracene) with the peak integrations. See next section (6.2) for response factor calculation and determination of yield.

6.2. With acetic acid as the acid medium

1. Amide cage **A62-amide**:
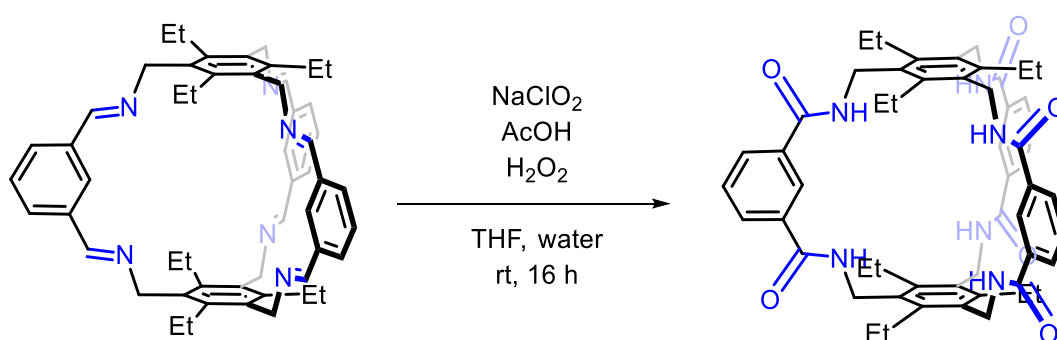
Imine cage **A62** (200 mg, 0.25 mmol, 1 eq.) in THF (20 mL), 35% w/w solution of hydrogen peroxide (1.8 mL, 18.75 mmol, 75 eq.), $NaClO_2$ (900 mg, 10 mmol, 40 eq.) and acetic acid (1M, 2.5 mL, 2.5 mmol, 10 eq.) was added dropwise over 10 minutes. 190 mg of the crude mixture was obtained which was dissolved in DMF (40 mL).
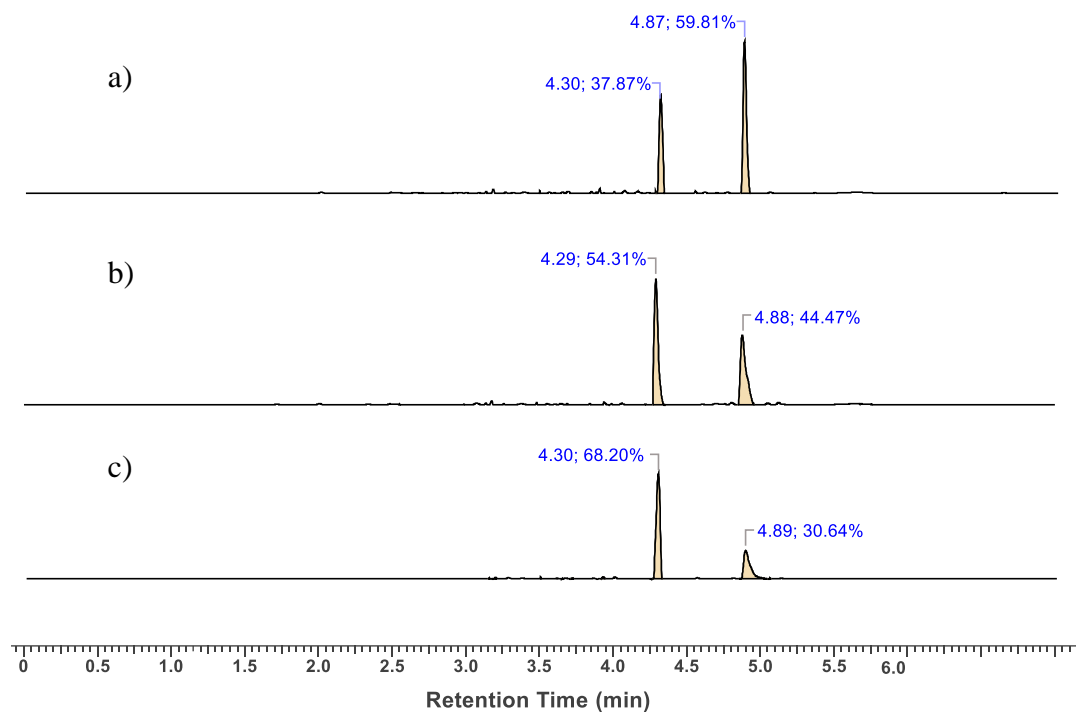
240

Determination of response factor:

UPLC method details: C8 column 1.7 µm BEH particles; column dimensions: 2.1 mm (diameter) $\times$ 50 mm (length); eluent: MeCN : H_2O = 10:90 to 50:50, 7 minute run, 0.6 mL/min.

Vial 1: 5mg of amide cage **A62-amide** in 1mL of DMF (5.6 mM solution).

Vial 2: 1mg of anthracene in 1mL of DMF (5.6 mM solution)

Vial 1 (µL)	Vial 2 (µL)	Ratio of conc. of anthracene to conc. of cage (C_{is}/C_s)	Area of antharacene peak (A_{is}) (in %)	Area of cage peak (A_s) (in %)	Ratio of the area of anthracene peak to cage peak (A_{is}/A_s)
90	30	0.33	34.22	65.78	0.52
60	60	1	58.95	41.01	1.44
30	90	3	78.12	24.88	3.13
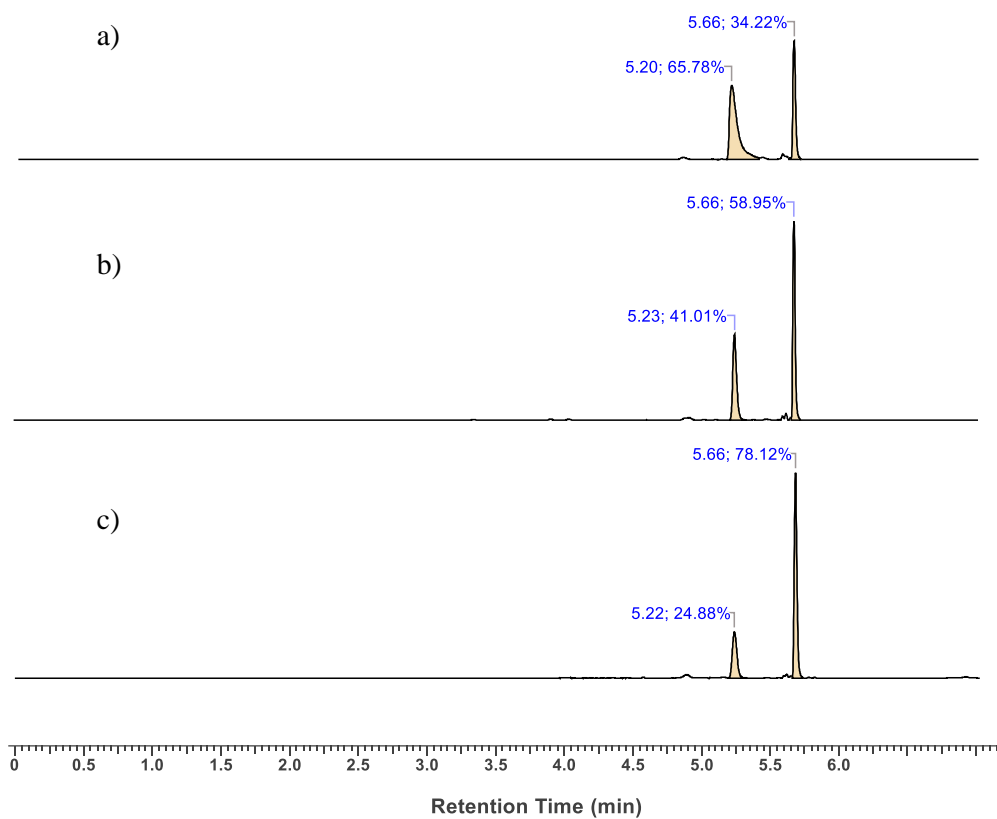
Figure 192. UPLC traces of the amide cage **A62-amide** and anthracene in varying concentrations: a) 90 µL from vial 1, 30 µL from vial 2; b) 60 µL from vial 1, 60 µL from vial 2; c) 30 µL from vial 1, 90 µL from vial 2.
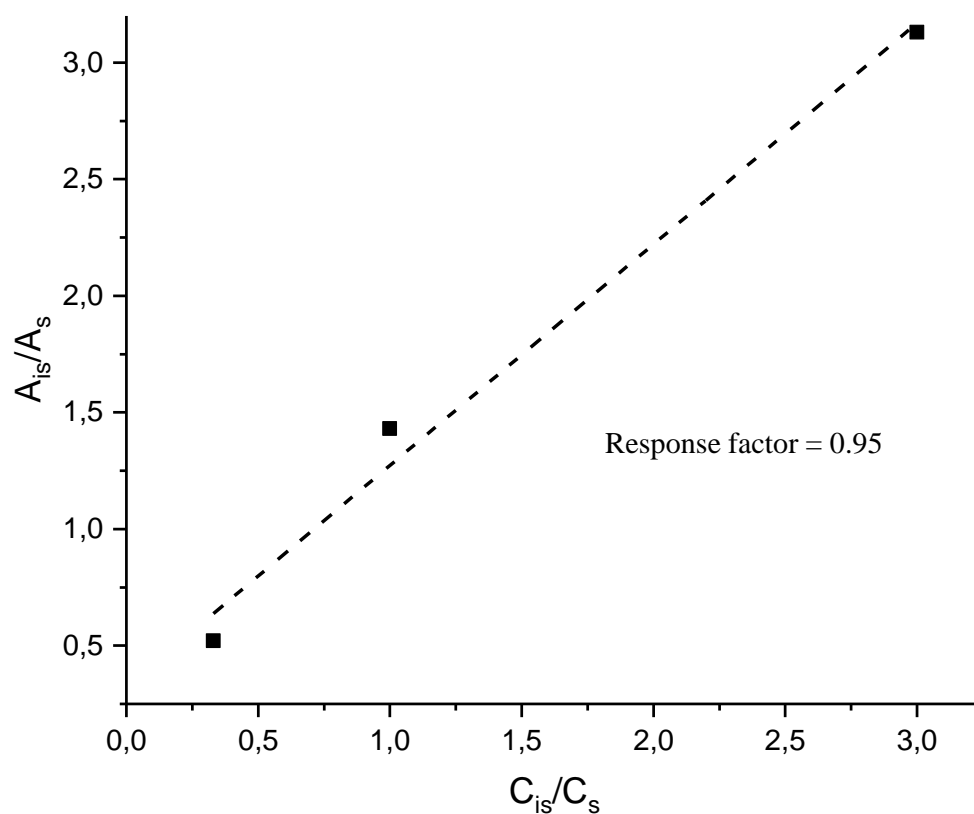
Figure 193. Graph of the ratio of concentrations on the X-axis and the ratio of the area on the Y-axis for the calculation of the response factor of amide cage **A62-amide**.

Determination of yield of the reaction:
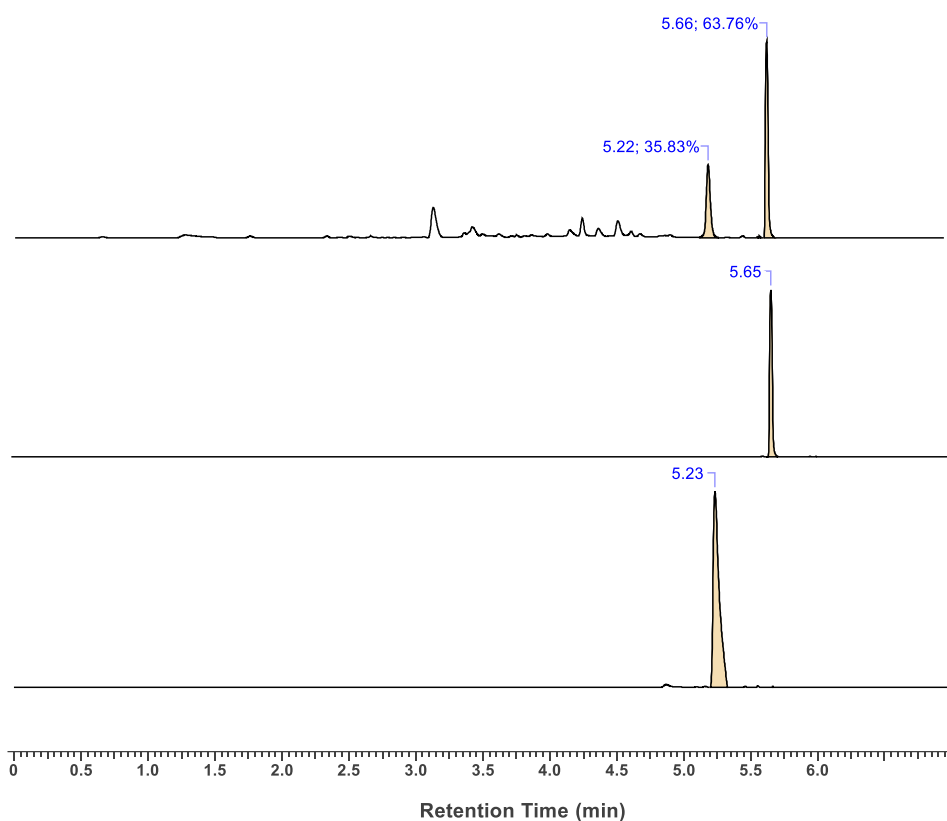
Figure 194. UPLC traces of: a) crude mixture and the internal standard; b) internal standard; c) pure amide cage.

$$\text{Amount of cage compound in the crude mixture} = \frac{(5.6)(35.83)(0.95)}{63.76}$$

$$= 2.98 \text{ mmoles/L}$$

Amount of amide cage in 40 mL of the crude mixture = 0.12 mmoles

$$\text{Yield} = \frac{0.12}{0.25} \times 100$$

$$= 48\%$$

2. Amide cage **A63-amide**:
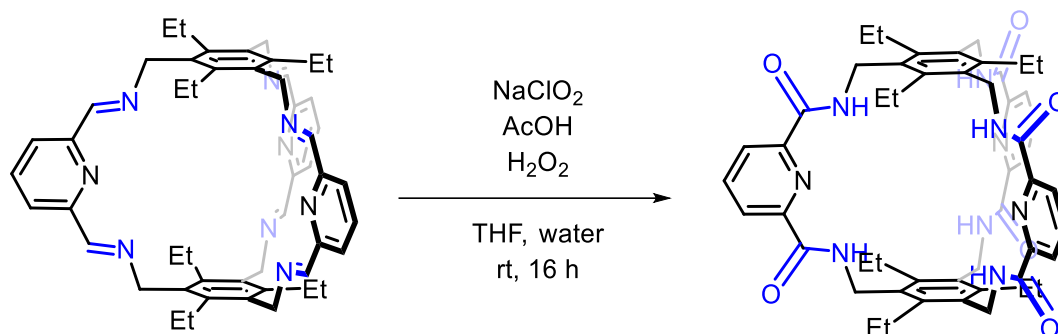
Imine cage **A63** (200 mg, 0.25 mmol, 1 eq.) in THF (20 mL), 35% w/w solution of hydrogen peroxide (1.8 mL, 18.75 mmol, 75 eq.), NaClO$_2$ (900 mg, 10 mmol, 40 eq.) and acetic acid (1M, 2.5 mL, 2.5 mmol, 10 eq.) was added dropwise over 10 minutes. 205 mg of the crude mixture was obtained which was dissolved in DMF (40 mL).

Determination of response factor:

UPLC method details: C8 column 1.7 µm BEH particles; column dimensions: 2.1 mm (diameter) × 50 mm (length); eluent: MeCN : H$_2$O = 10:90 to 80:20, 7 minute run, 0.6 mL/min.

Vial 1: 5mg of amide cage **A63-amide** in 1mL of DMF (5.6 mM solution).

Vial 2: 1mg of anthracene in 1mL of DMF (5.6 mM solution)

Vial 1 (µL)	Vial 2 (µL)	Ratio of conc. of anthracene to conc. of cage (C_{is}/C_s)	Area of antharacene peak (A_{is}) (in %)	Area of cage peak (A_s) (in %)	Ratio of the area of anthracene peak to cage peak (A_{is}/A_s)
90	30	0.33	26.88	73.12	0.36
60	60	1	53.51	46.49	1.15
30	90	3	77.87	22.13	3.51
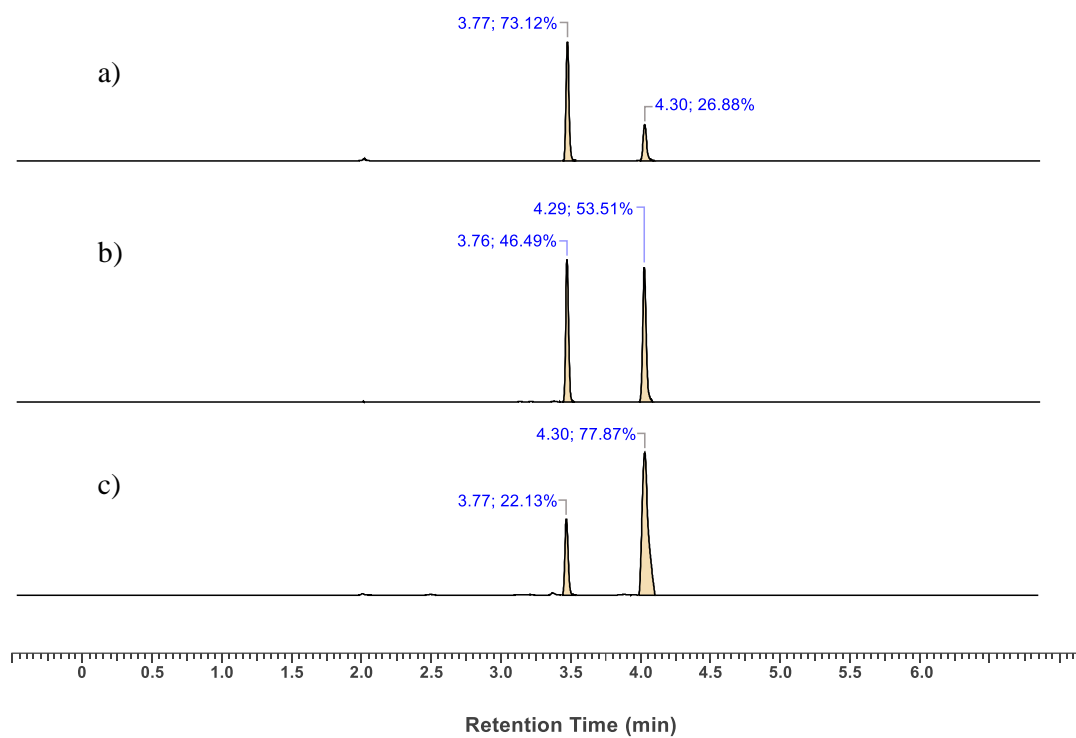
Figure 195. UPLC traces of the amide cage **A63-amide** and anthracene in varying concentrations: a) 90 µL from vial 1, 30 µL from vial 2; b) 60 µL from vial 1, 60 µL from vial 2; c) 30 µL from vial 1, 90 µL from vial 2.
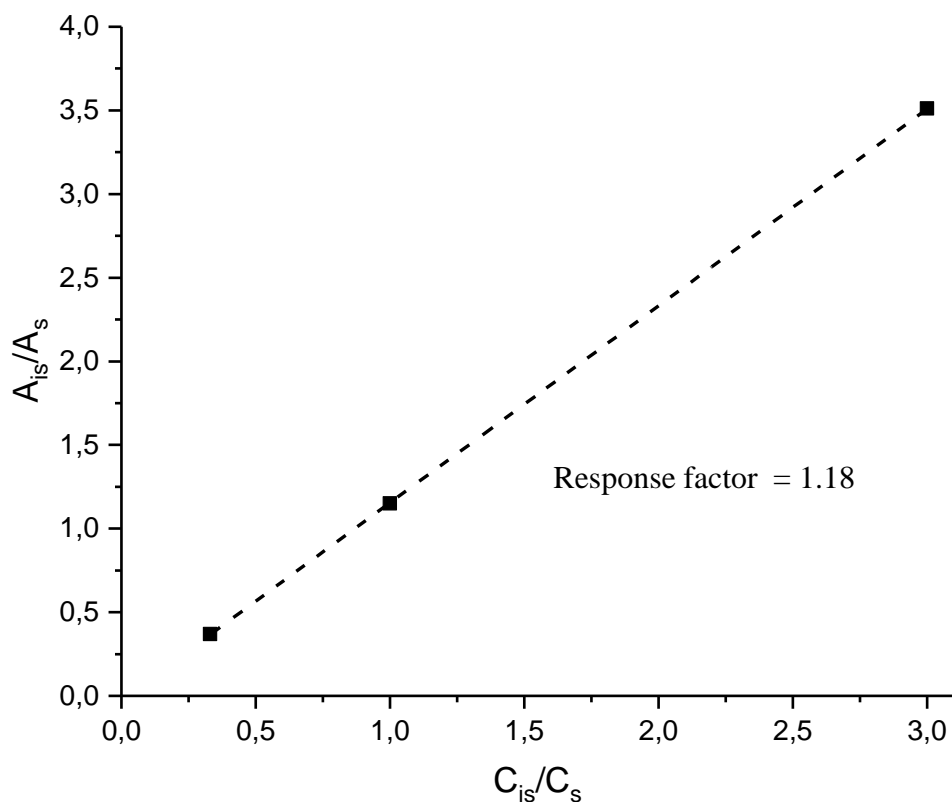
Figure 196. Graph of the ratio of concentrations on the X-axis and the ratio of the area on the Y-axis for the calculation of the response factor of amide cage **A63-amide**.

Determination of yield of the reaction:
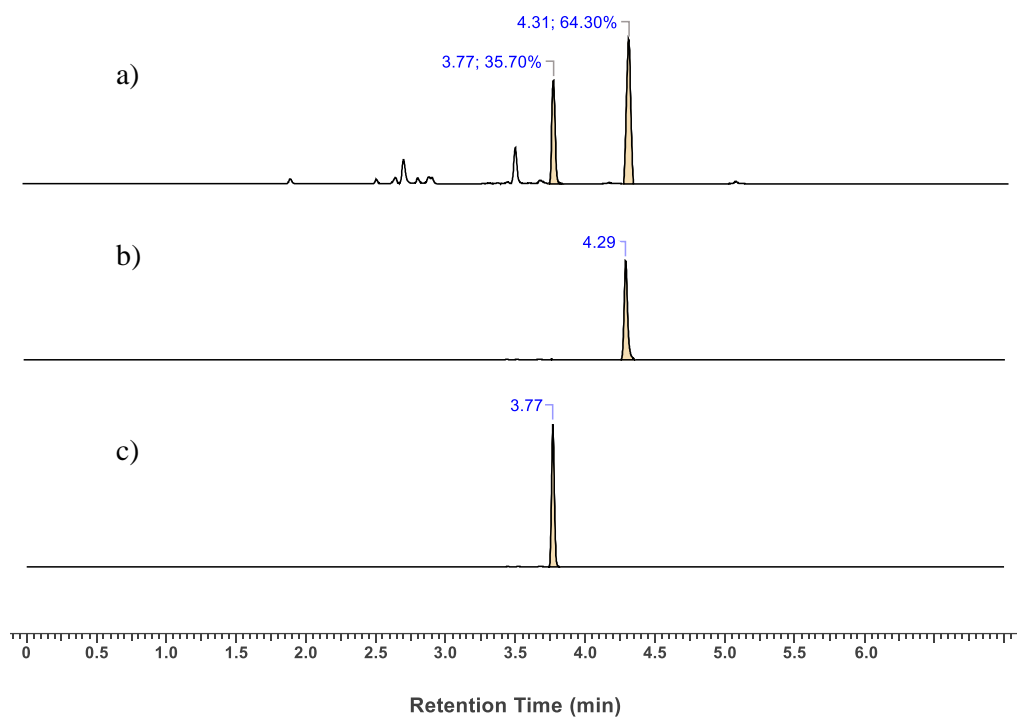
Figure 197. UPLC traces of: a) crude mixture and the internal standard; b) internal standard; c) pure amide cage.

$$\text{Amount of cage compound in the crude mixture} = \frac{(5.6)(38.70)(1.18)}{61.30}$$

$$= 4.17 \text{ mmoles/L}$$

Amount of amide cage in 40 mL of the crude mixture $= 0.17$ mmoles

$$\text{Yield} = \frac{0.17}{0.25} \times 100$$

$$= 67\%$$

3. Amide cage **A64-amide**:
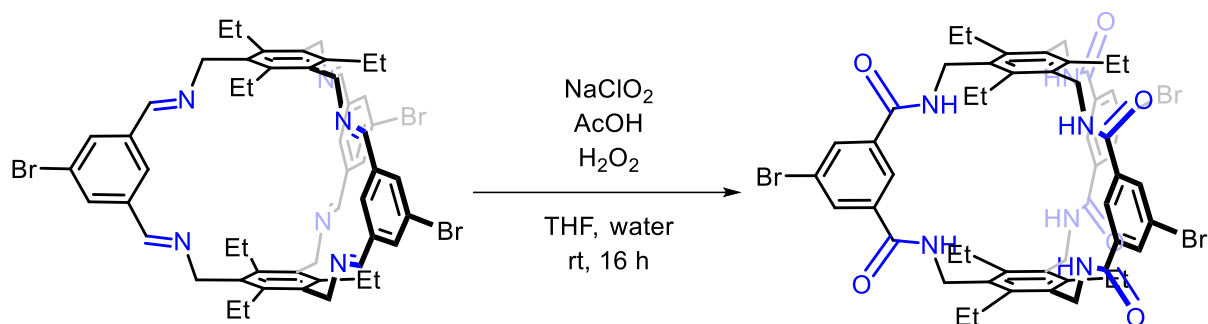
Imine cage **A64** (200 mg, 0.19 mmol, 1 eq.) in THF (20 mL), 35% w/w solution of hydrogen peroxide (1.4 mL, 14.25 mmol, 75 eq.), NaClO$_2$ (690 mg, 7.6 mmol, 40 eq.) and acetic acid (1M, 1.9 mL, 1.9 mmol, 10 eq.) was added dropwise over 10 minutes. The resulting solid was suspended in DMF (10 mL), sonicated for 10 minutes and then filtered (3 times). The DMF was removed to obtain 101 mg of the crude mixture which was dissolved in DMF (20 mL). Determination of response factor:

UPLC method details: C8 column 1.7 µm BEH particles; column dimensions: 2.1 mm (diameter) $\times$ 50 mm (length); eluent: MeCN : H$_2$O = 10:90 to 80:20, 7 minute run, 0.6 mL/min.

Vial 1: 6.5mg of amide cage **A64-amide** in 1mL of DMF (5.6 mM solution).

Vial 2: 1mg of anthracene in 1mL of DMF (5.6 mM solution)

Vial 1 (µL)	Vial 2 (µL)	Ratio of conc. of anthracene to conc. of cage (C_{is}/C_s)	Area of antharacene peak (A_{is}) (in %)	Area of cage peak (A_s) (in %)	Ratio of the area of anthracene peak to cage peak (A_{is}/A_s)
80	40	0.5	37.87	59.81	0.63
60	60	1	54.31	44.47	1.22
40	80	2	68.20	30.64	2.22

Figure 198. UPLC traces of the amide cage **A64-amide** and anthracene in varying concentrations: a) 80 µL from vial 1, 40 µL from vial 2; b) 60 µL from vial 1, 60 µL from vial 2; c) 40 µL from vial 1, 80 µL from vial 2.
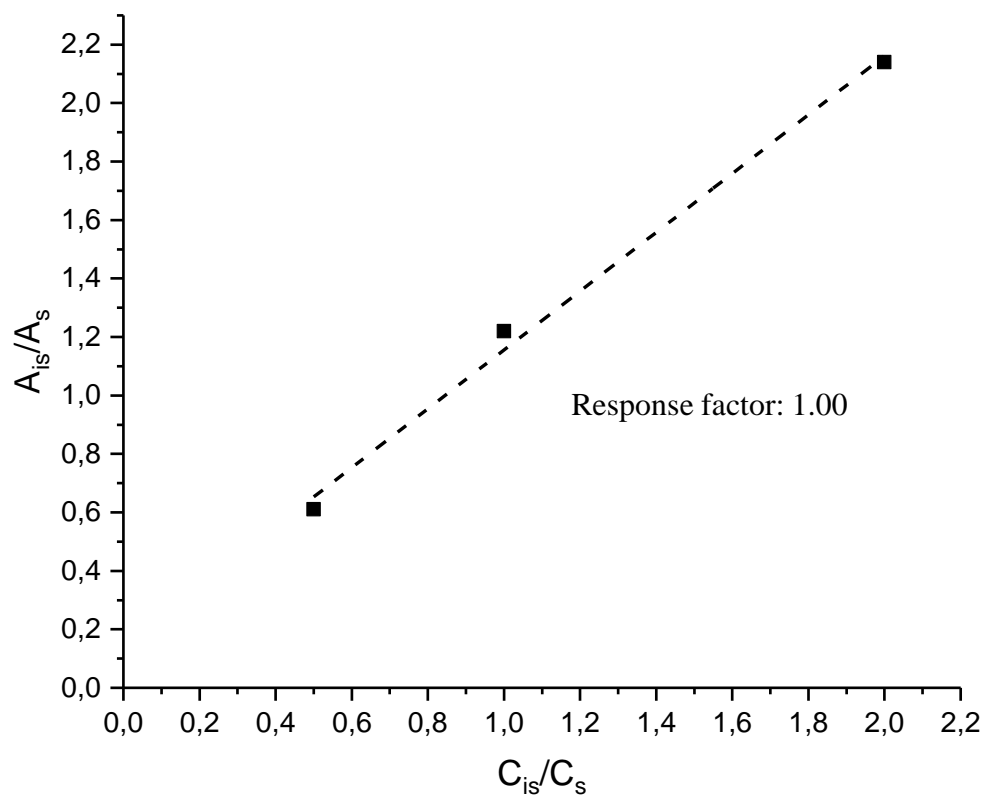
Figure 199. Graph of the ratio of concentrations on the X-axis and the ratio of the area on the Y-axis for the calculation of the response factor of amide cage **A64-amide**.
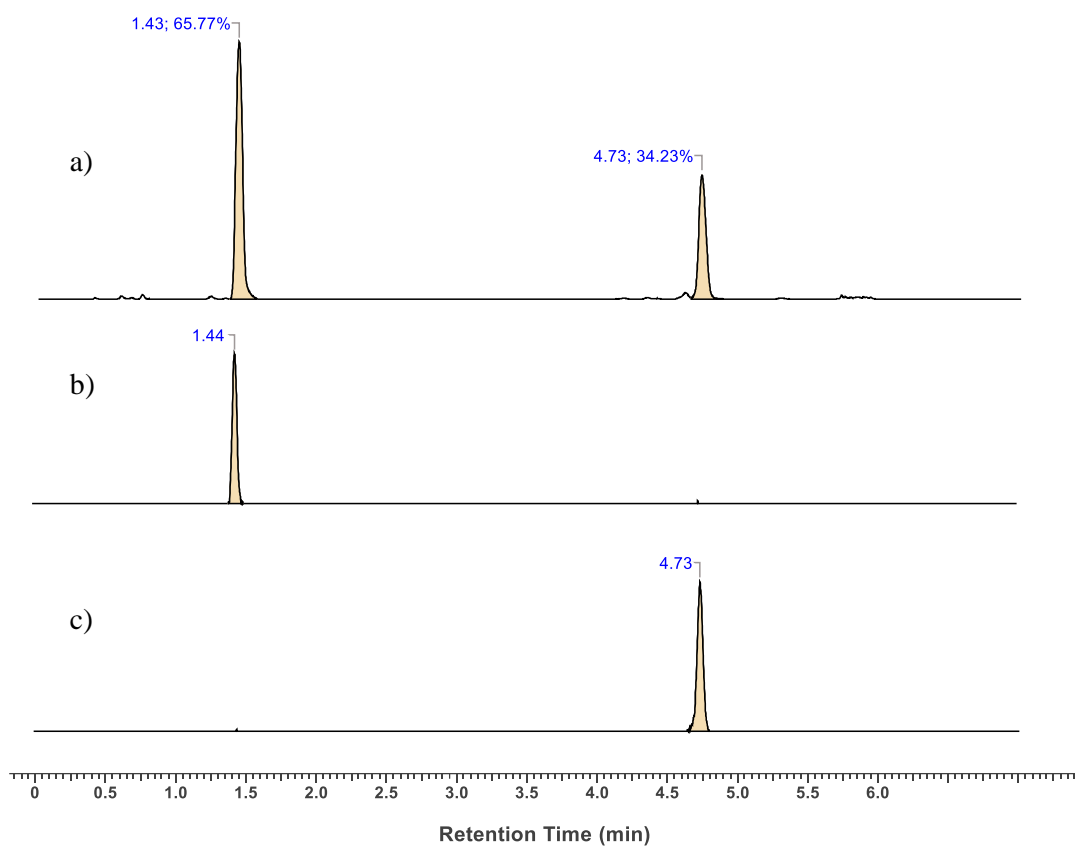
Determination of yield of the reaction:
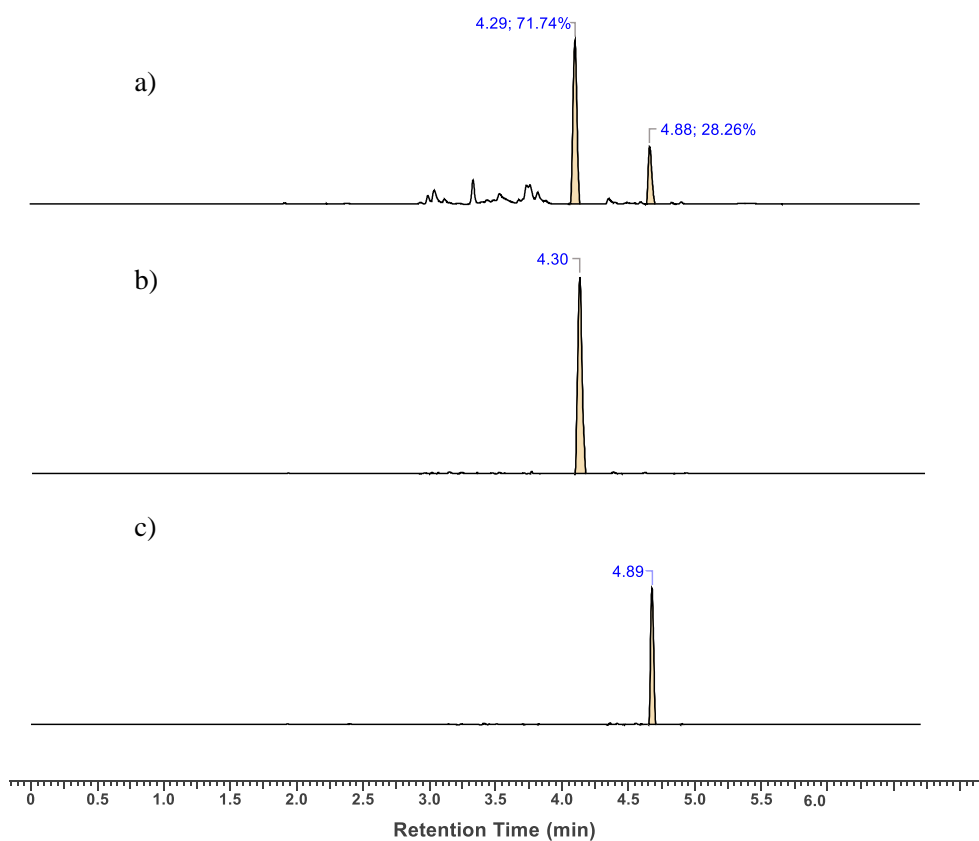
Figure 200. UPLC traces of: a) crude mixture and the internal standard; b) internal standard; c) pure amide cage.

$$\text{Amount of cage compound in the crude mixture} = \frac{(5.6)(28.21)(1)}{71.74}$$

$$= 2.2 \text{ mmoles/L}$$

Amount of amide cage in 20 mL of the crude mixture = 0.045 mmoles

$$\text{Yield} = \frac{0.044}{0.19} \times 100$$

$$= 23\%$$

4. Amide cage **A67-amide**:
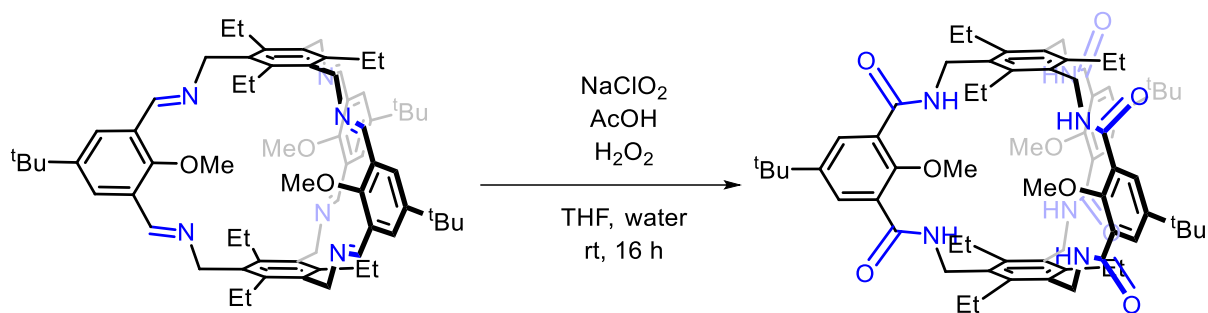
Imine cage **A67** (100 mg, 0.09 mmol, 1 eq.) in THF (10 mL), 35% w/w solution of hydrogen peroxide (0.7 mL, 7.12 mmol, 75 eq.), NaClO$_2$ (340 mg, 3.8 mmol, 40 eq.) and acetic acid (1M, 0.9 mL, 0.9 mmol, 10 eq.) was added dropwise over 10 minutes. 92 mg of the crude mixture was obtained which was dissolved in MeOH (15 mL).
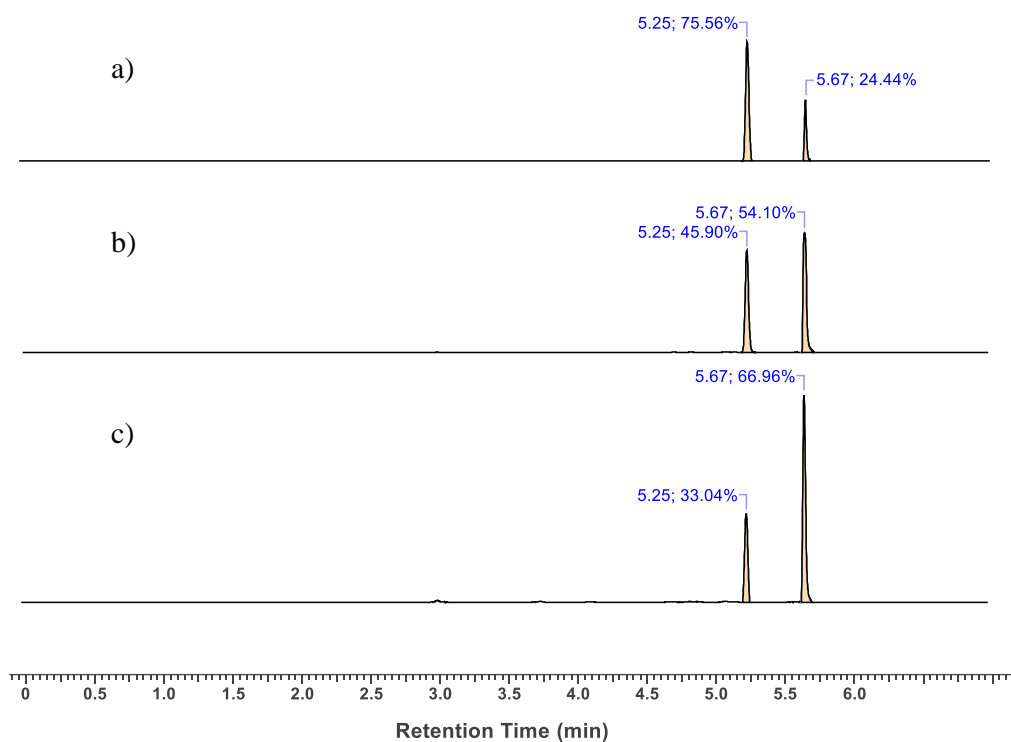
Determination of response factor:

UPLC method details: C8 column 1.7 µm BEH particles; column dimensions: 2.1 mm (diameter) × 50 mm (length); eluent: MeCN : H$_2$O = 50:50 to 70:30, 7 minute run, 0.6 mL/min.

Vial 1: 6.5mg of amide cage **A67-amide** in 1mL of DMF (5.6 mM solution).

Vial 2: 1mg of anthracene in 1mL of MeOH (5.6 mM solution)

| Vial 1 (µL)	Vial 2 (µL)	Ratio of conc. of anthracene to conc. of cage (C_{is}/C_s)	Area of antharacene peak (A_{is}) (in %)	Area of cage peak (A_s) (in %)	Ratio of the area of anthracene peak to cage peak (A_{is}/A_s)
80	40	0.5	40.29	59.71	0.67
60	60	1	59.14	40.86	1.45
40	80	2	72.29	27.71	2.61
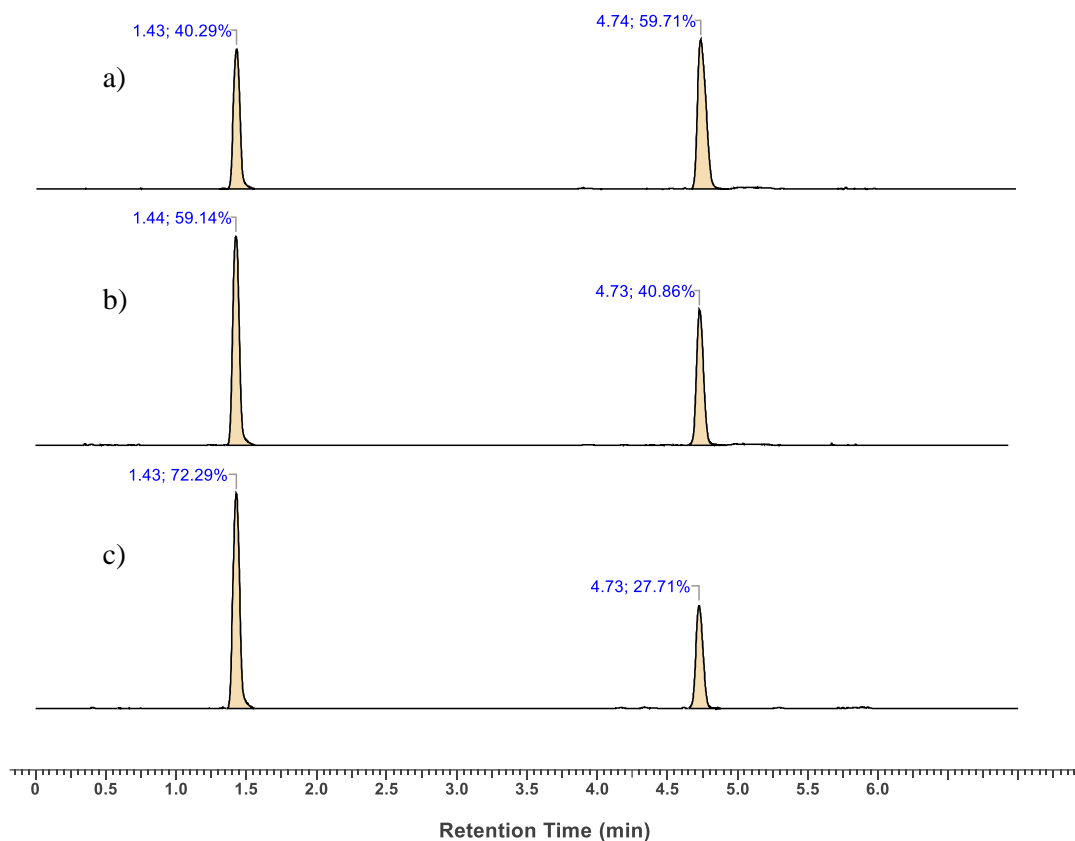
Figure 201. UPLC traces of the amide cage **A67-amide** and anthracene in varying concentrations: a) 80 µL from vial 1, 40 µL from vial 2; b) 60 µL from vial 1, 60 µL from vial 2; c) 40 µL from vial 1, 80 µL from vial 2.
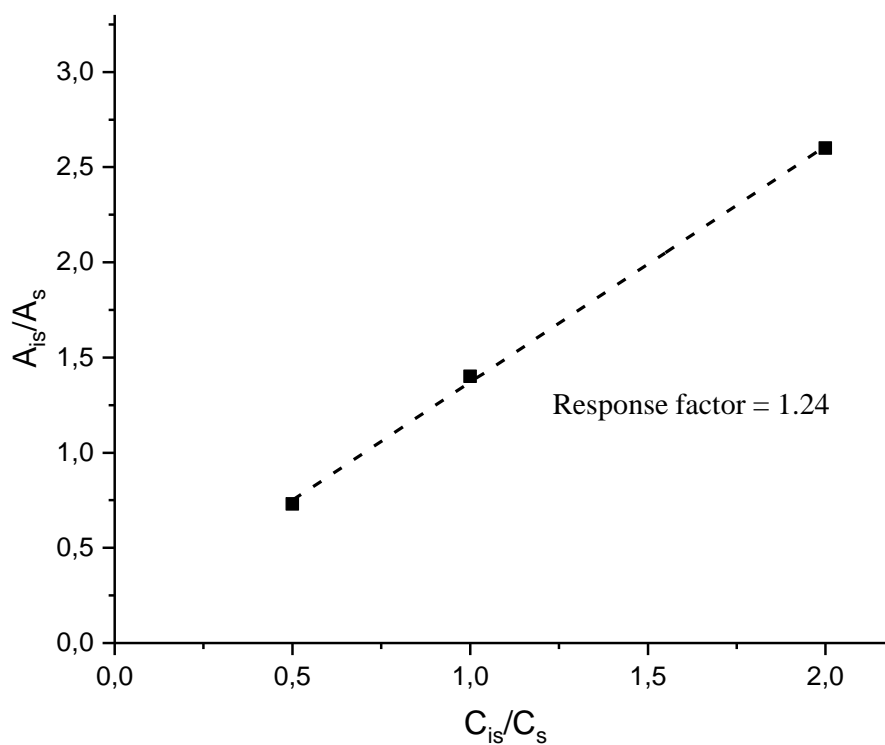
Figure 202. Graph of the ratio of concentrations on the X-axis and the ratio of the area on the Y-axis for the calculation of the response factor of amide cage **A67-amide**.

251

Determination of yield of the reaction:

Figure 203. UPLC traces of: a) crude mixture and the internal standard; b) internal standard; c) pure amide cage.

$$\text{Amount of cage compound in the crude mixture} = \frac{(5.6)(34.23)(1.24)}{65.77}$$

$$= 3.6 \text{ mmoles/L}$$

Amount of amide cage in 15 mL of the crude mixture = 0.054 mmoles

$$\text{Yield} = \frac{0.054}{0.095} \times 100$$

$$= 57\%$$

5. Amide cage **A70-amide:**
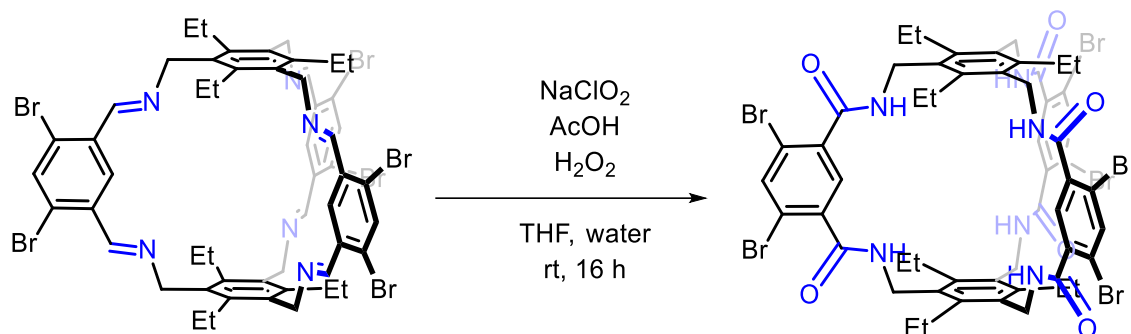
Imine cage **A70** (100 mg, 0.079 mmol, 1 eq.) in THF (10 mL), 35% w/w solution of hydrogen peroxide (10 M, 0.6 mL, 5.9 mmol, 75 eq.), $NaClO_2$ (286 mg, 3.16 mmol, 40 eq.) and acetic acid (1M, 0.8 mL, 0.79 mmol, 10 eq.) was added dropwise over 10 minutes. The resulting solid was suspended in DMF (5 mL), sonicated for 10 minutes and then filtered (3 times). The DMF was removed to obtain 41 mg of the crude mixture which was dissolved in DMF (10 mL).

Determination of response factor:

UPLC method details: C8 column 1.7 µm BEH particles; column dimensions: 2.1 mm (diameter) × 50 mm (length); eluent: $MeCN:H_2O = 20:80$ to 40:60, 7 minute run, 0.6 mL/min.

Vial 1: 6.5 mg of amide cage **A70-amide** in 1mL of DMF (5.6 mM solution).

Vial 2: 1mg of anthracene in 1mL of MeOH (5.6 mM solution)

Vial 1 (µL)	Vial 2 (µL)	Ratio of conc. of anthracene to conc. of cage (C_{is}/C_s)	Area of antharacene peak (A_{is}) (in %)	Area of cage peak (A_s) (in %)	Ratio of the area of anthracene peak to cage peak (A_{is}/A_s)
90	30	0.33	24.44	75.56	0.32
60	60	1	54.10	45.90	1.17
30	90	3	66.96	33.04	2.02

Figure 204. UPLC traces of the amide cage **A70-amide** and anthracene in varying concentrations: a) 80 µL from vial 1, 40 µL from vial 2; b) 60 µL from vial 1, 60 µL from vial 2; c) 40 µL from vial 1, 80 µL from vial 2.
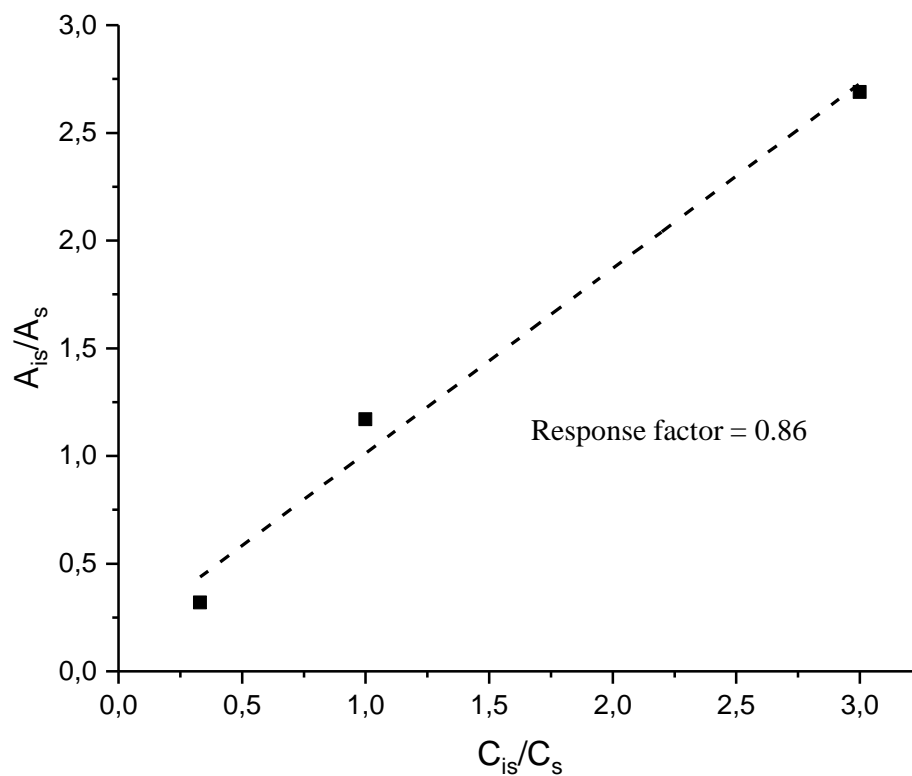
Figure 205. Graph of the ratio of concentrations on the X-axis and the ratio of the area on the Y-axis for the calculation of the response factor of amide cage **A70-amide**.

Determination of yield of the reaction:
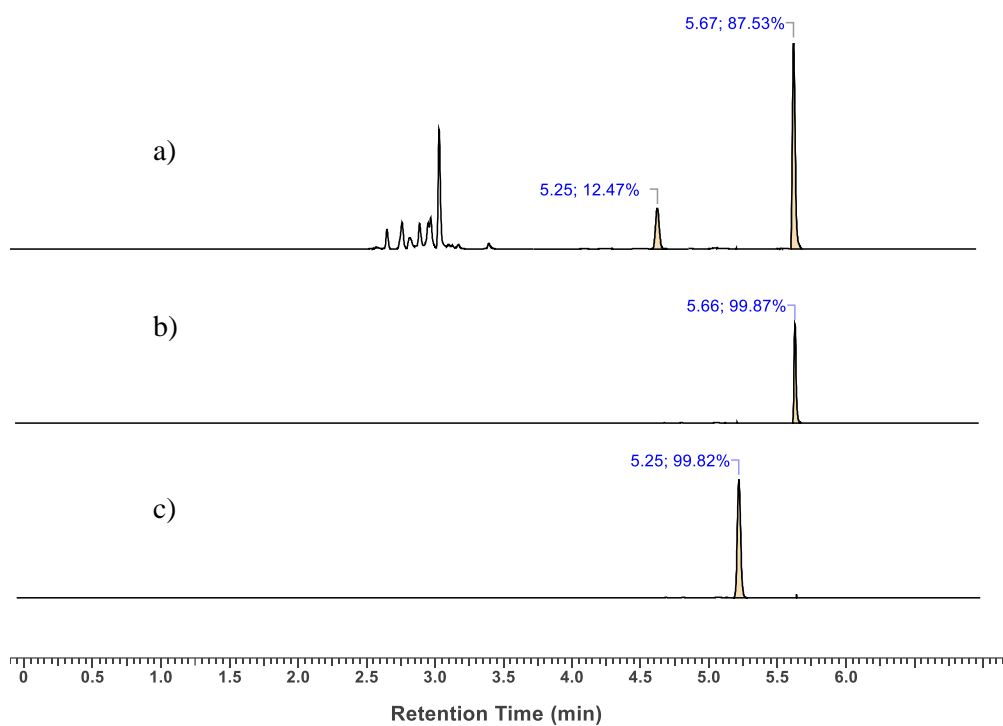
Figure 206. UPLC traces of: a) crude mixture and the internal standard; b) internal standard; c) pure amide cage.

$$\text{Amount of cage compound in the crude mixture} = \frac{(5.6)(12.47)(0.86)}{87.53}$$

$$= 0.69 \text{ mmoles/L}$$

Amount of amide cage in 10 mL of the crude mixture $= 0.007$ mmoles

$$\text{Yield} = \frac{0.007}{0.079} \times 100$$

$$= 9\%$$

6.3. Pinnick oxidation using acetate buffer (pH = 3.8)

All reactions described above were repeated with an acetate buffer containing acetic acid/sodium acetate (pH = 3.8) as the acid medium.

1. Amide cage **A62-amide**:
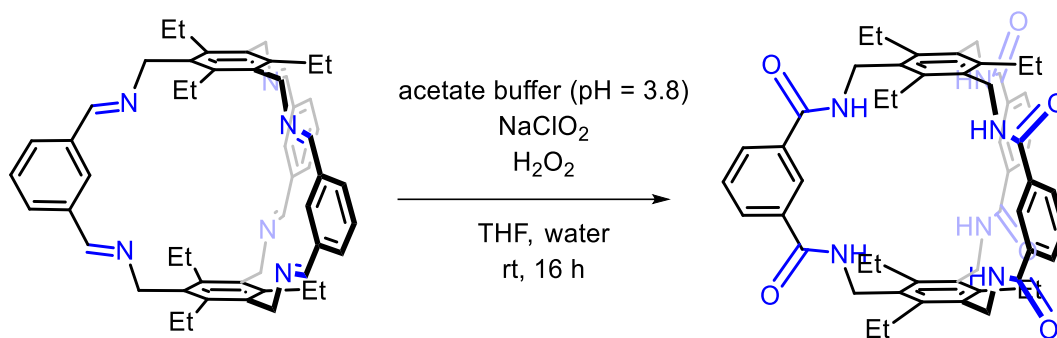
Imine cage **A62** (100 mg, 0.126 mmol, 1 eq.) in THF (10 mL), 35% w/w solution of hydrogen peroxide (1.8 mL, 9.45 mmol, 75 eq.), $NaClO_2$ (455 mg, 5 mmol, 40 eq.) and acetate buffer (2 mL) was added dropwise over 10 minutes. 92 mg of the crude mixture was obtained which was dissolved in DMF (10 mL).

UPLC method details: C8 column 1.7 µm BEH particles; column dimensions: 2.1 mm (diameter) $\times$ 50 mm (length); eluent: MeCN : H_2O = 10:90 to 50:50, 7 minute run, 0.6 mL/min.
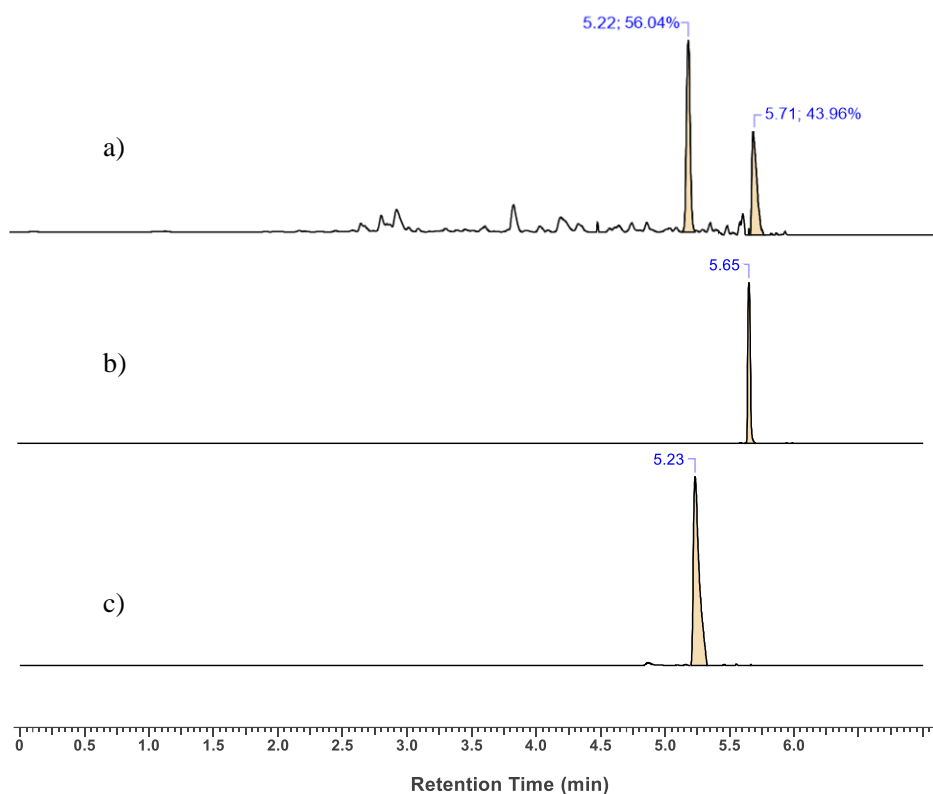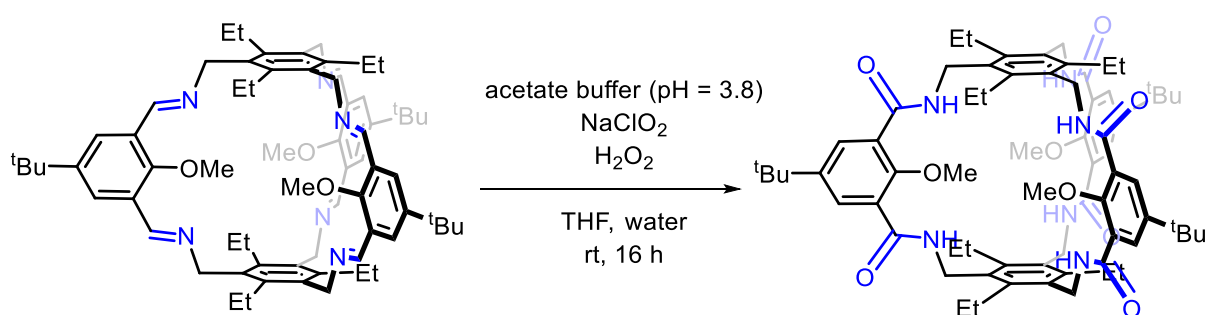
Figure 207. UPLC traces of: a) crude mixture and the internal standard; b) internal standard; c) pure amide cage.

$$\text{Amount of cage compound in the crude mixture} = \frac{(5.6)(56.04)(0.95)}{43.96}$$

$$= 6.8 \text{ mmoles/L}$$

Amount of amide cage in 10 mL of the crude mixture $= 0.068$ mmoles

$$\text{Yield} = \frac{0.068}{0.125} \times 100$$

$$= 54\%$$

2. Amide cage **A67-amide**:
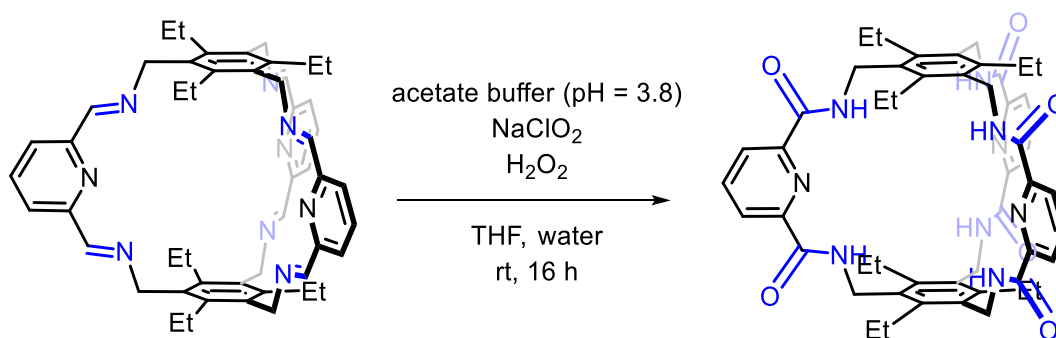
Imine cage **A67** (150 mg, 0.19 mmol, 1 eq.) in THF (20 mL), 35% w/w solution of hydrogen peroxide (1.5 mL, 14.25 mmol, 75 eq.), $NaClO_2$ (680 mg, 7.5 mmol, 40 eq.) and acetate buffer (2mL) was added dropwise over 10 minutes. 125 mg of the crude mixture was obtained which was dissolved in DMF (10 mL).

UPLC method details: C8 column 1.7 µm BEH particles; column dimensions: 2.1 mm (diameter) $\times$ 50 mm (length); eluent: MeCN : H_2O = 10:90 to 80:20, 7 minute run, 0.6 mL/min.
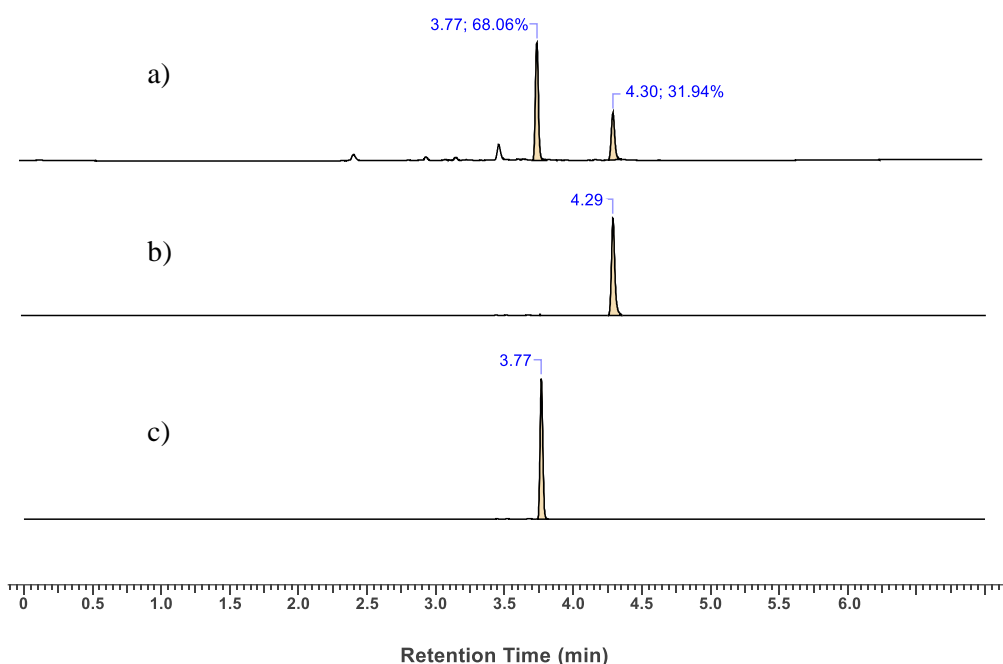
Figure 208. UPLC traces of: a) crude mixture and the internal standard; b) internal standard; c) pure amide cage.

$$\text{Amount of cage compound in the crude mixture} = \frac{(5.6)(68.06)(1.17)}{31.94}$$

$$= 13.96 \text{ mmoles/L}$$

$$\text{Amount of amide cage in 10 mL of the crude mixture} = 0.14 \text{ mmoles}$$

$$\text{Yield} = \frac{0.14}{0.19} \times 100$$

$$= 74\%$$

3. Amide cage **A64-amide**:
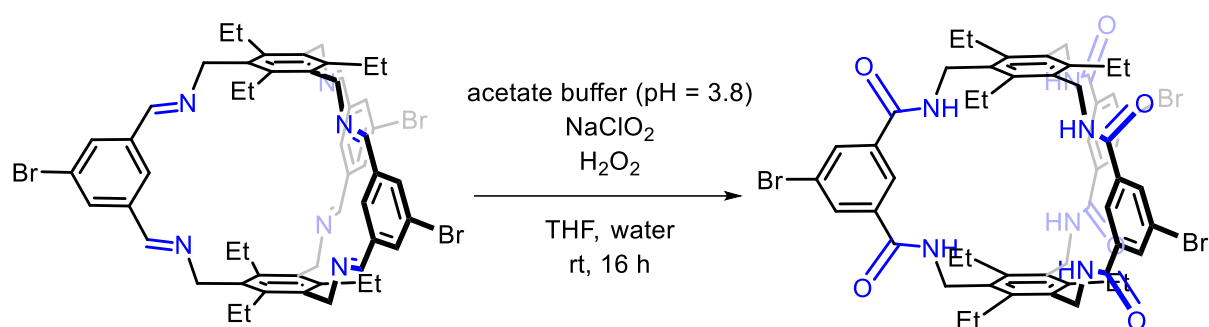
Imine cage **A64** (100 mg, 0.097 mmol, 1 eq.) in THF (20 mL), 35% w/w solution of hydrogen peroxide (7.3 mL, 7.29 mmol, 75 eq.), NaClO$_2$ (350 mg, 3.9 mmol, 40 eq.) and acetate buffer (2mL) was added dropwise over 10 minutes. The resulting solid was suspended in DMF (10 mL), sonicated for 10 minutes and then filtered (3 times). The DMF was removed to obtain 51 mg of the crude mixture which was dissolved in DMF (10 mL).

UPLC method details: C8 column 1.7 µm BEH particles; column dimensions: 2.1 mm (diameter) × 50 mm (length); eluent: MeCN : H$_2$O = 10:90 to 80:20, 7 minute run, 0.6 mL/min.
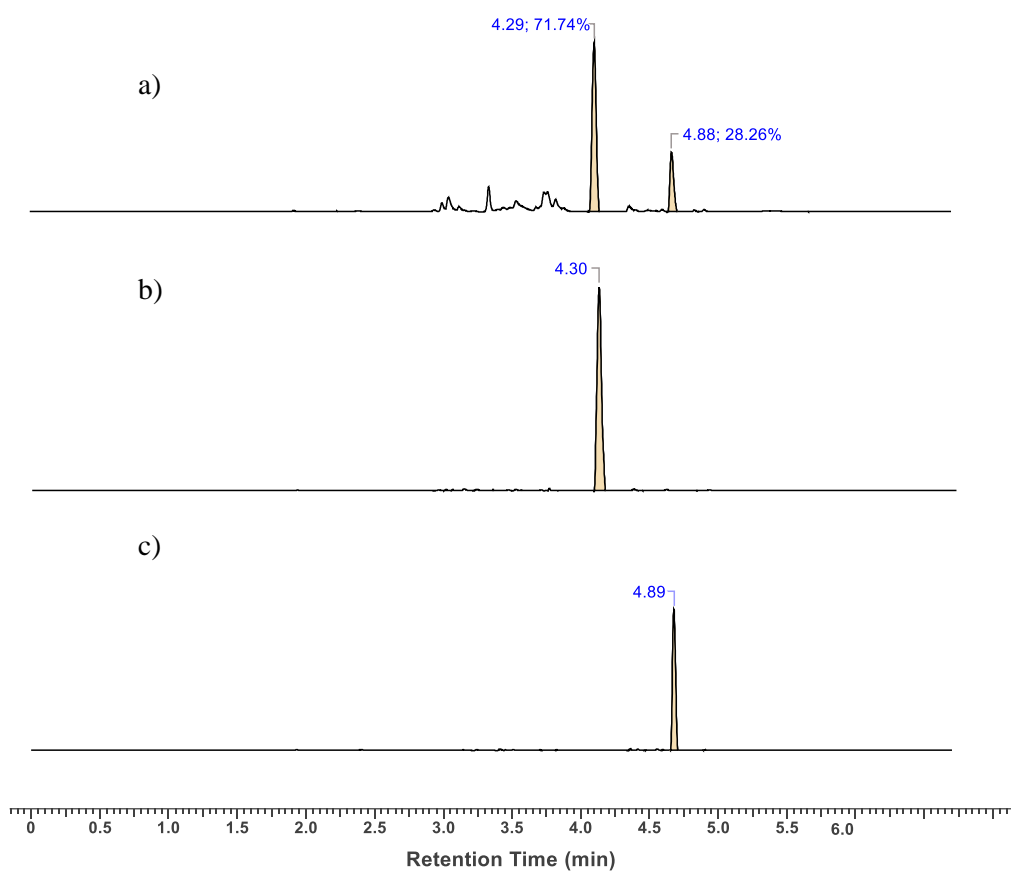
Figure 209. UPLC traces of: a) crude mixture and the internal standard; b) internal standard; c) pure amide cage.

$$\text{Amount of cage compound in the crude mixture} = \frac{(5.6)(45.92)(1)}{54.08}$$

$$= 4.75 \text{ mmoles/L}$$

Amount of amide cage in 10 mL of the crude mixture $= 0.047$ mmoles

$$\text{Yield} = \frac{0.047}{0.097} \times 100$$

$$= 48\%$$

4. Amide cage **A67-amide**:

Imine cage **A67** (200 mg, 0.19 mmol, 1 eq.) in THF (20 mL), 35% w/w solution of hydrogen peroxide (14 mL, 14.27 mmol, 75 eq.), NaClO$_2$ (688 mg, 7.6 mmol, 40 eq.) and acetate buffer (2mL) was added dropwise over 10 minutes. 188 mg of the crude mixture was obtained which was dissolved in MeOH (10 mL).

UPLC method details: C8 column 1.7 µm BEH particles; column dimensions: 2.1 mm (diameter) $\times$ 50 mm (length); eluent: MeCN : H$_2$O = 50:90 to 70:30, 7 minute run, 0.6 mL/min.
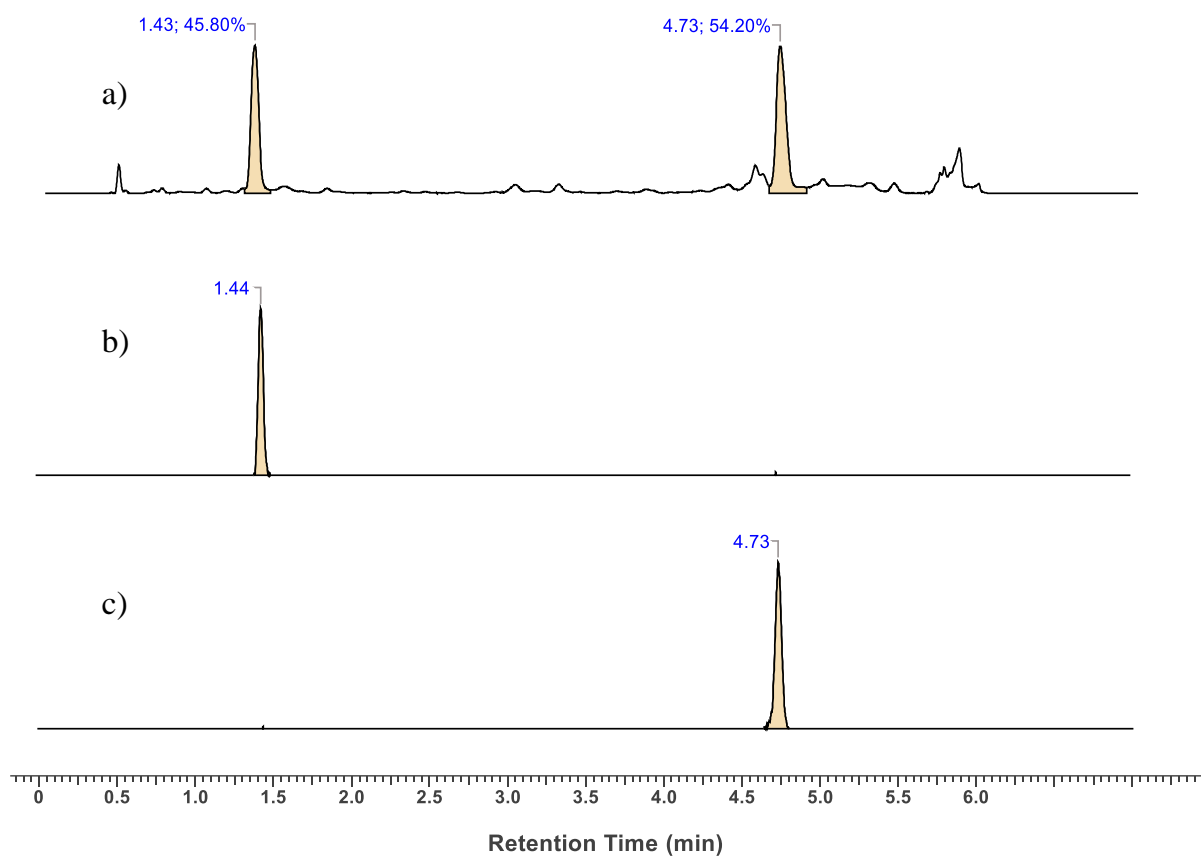
Figure 210. UPLC traces of: a) crude mixture and the internal standard; b) internal standard; c) pure amide cage.

$$\text{Amount of cage compound in the crude mixture} = \frac{(5.6)(54.20)(1.24)}{45.80}$$

$$= 8.22 \text{ mmoles/L}$$

Amount of amide cage in 10 mL of the crude mixture $= 0.08$ mmoles

$$\text{Yield} = \frac{0.08}{0.19} \times 100$$

$$= 43\%$$

Abbreviations

AcOH	acetic acid
APCI	atmospheric pressure chemical ionization
Ar	aryl
ATR	attenuated total refraction
BET	Brunauer, Emmett and Teller
^{t}Bu	tertiary butyl
CCDC	Cambridge Crystallographic Data Centre
COF	covalent organic framework
DCC	dynamic covalent chemistry
DCM	dichloromethane
DMF	N,N-dimethylformamide
DMSO	dimethylsulphoxide
EDG	electron donating group
eq.	equivalents
EtOH	ethanol
EWG	electron withdrawing group
FT-IR	Fourier transform-Infrared spectroscopy
g	grams
GPC	gel permeation chromatography
h	hours
HPLC	high-performance liquid chromatography
HR	high resolution
IAST	ideal adsorbed solution theory
MALDI	matrix-assisted laser desorption
MeCN	acetonitrile
MeOH	methanol
MS	mass spectrum
NBS	N-bromosuccinimide
nm	nanometers
NMR	nuclear magnetic resonance
ppm	parts per million
PXRD	powder X-ray diffraction
R_f	retention factor

rt	room temperature
SCXRD	single crystal X-ray diffraction
S_EAr	electrophilic aromatic substitution
SEC	size exclusion chromatography
SEM	scanning electron microscopy
TGA	thermogravimetric analysis
THF	tetrahydrofuran
TLC	thin layer chromatography
TOF	time of flight
TFA	trifluoroacetic acid
TREN	tris(2-aminoethyl)amine
UPLC	ultra-pressure liquid chromatography

Acknowledgements